VOL. 589 NOS. 1 + 2 JANUARY 10, 1992

COMPLETE IN ONE ISSUE

JOURNAL OF CHROMATOGRAPHY

INCLUDING ELECTROPHORESIS AND OTHER SEPARATION METHODS

ELSEVIER

JOURNAL OF CHROMATOGRAPHY

INCLUDING ELECTROPHORESIS AND OTHER SEPARATION METHODS

Scope. The *Journal of Chromatography* publishes papers on all aspects of chromatography, electrophoresis and related methods. Contributions consist mainly of research papers dealing with chromatographic theory, instrumental development and their applications. The section *Biomedical Applications*, which is under separate editorship, deals with the following aspects: developments in and applications of chromatographic and electrophoretic techniques related to clinical diagnosis or alterations during medical treatment; screening and profiling of body fluids or tissues with special reference to metabolic disorders; results from basic medical research with direct consequences in clinical practice; drug level monitoring and pharmacokinetic st clinical toxicology; analytical studies in occupational medicine.

Submission of Papers. Manuscripts (in English; *four* copies are required) should be submitted to: Editorial Office of *Jou Chromatography*, P.O. Box 681, 1000 AR Amsterdam, Netherlands, Telefax (+31-20) 5862 304, or to: The Editor of *Jo of Chromatography, Biomedical Applications*, P.O. Box 681, 1000 AR Amsterdam, Netherlands. Review articles are invite proposed by letter to the Editors. An outline of the proposed review should first be forwarded to the Editors for prelimina discussion prior to preparation. Submission of an article is understood to imply that the article is original and unpublished and is not being considered for publication elsewhere. For copyright regulations, see below.

Publication. The *Journal of Chromatography* (incl. *Biomedical Applications*) has 39 volumes in 1992. The subscription prices for 1992 are:

J. Chromatogr. (incl. *Cum. Indexes, Vols. 551–600*) + *Biomed. Appl.* (Vols. 573–611):
Dfl. 7722.00 plus Dfl. 1209.00 (p.p.h.) (total *ca.* US$ 4880.25)

J. Chromatogr. (incl. *Cum. Indexes, Vols. 551–600*) only (Vols. 585–611):
Dfl. 6210.00 plus Dfl. 837.00 (p.p.h.) (total *ca.* US$ 3850.75)

Biomed. Appl. only (Vols. 573–584):
Dfl. 2760.00 plus Dfl. 372.00 (p.p.h.) (total *ca.* US$ 1711.50).

Subscription Orders. The Dutch guilder price is definitive. The US$ price is subject to exchange-rate fluctuations and is given as a guide. Subscriptions are accepted on a prepaid basis only, unless different terms have been previously agreed upon. Subscription orders can be entered only by calender year (Jan.–Dec.) and should be sent to Elsevier Science Publishers, Journal Department, P.O. Box 211, 1000 AE Amsterdam, Netherlands, Tel. (+31-20) 5803 642, Telefax (+31-20) 5803 598, or to your usual subscription agent. Postage and handling charges include surface delivery except to the following countries where air delivery via SAL (Surface Air Lift) mail is ensured: Argentina, Australia, Brazil, Canada, China, Hong Kong, India, Israel, Japan*, Malaysia, Mexico, New Zealand, Pakistan, Singapore, South Africa, South Korea, Taiwan, Thailand, USA. *For Japan air delivery (SAL) requires 25% additional charge of the normal postage and handling charge. For all other countries airmail rates are available upon request. Claims for missing issues must be made within three months of our publication (mailing) date, otherwise such claims cannot be honoured free of charge. Back volumes of the *Journal of Chromatography* (Vols. 1–572) are available at Dfl. 217.00 (plus postage). Customers in the USA and Canada wishing information on this and other Elsevier journals, please contact Journal Information Center, Elsevier Science Publishing Co. Inc., 655 Avenue of the Americas, New York, NY 10010, USA, Tel. (+1-212) 633 3764, Telefax (+1-212) 633 3764.

Abstracts/Contents Lists published in Analytical Abstracts, Biochemical Abstracts, Biological Abstracts, Chemical Abstracts, Chemical Titles, Chromatography Abstracts, Clinical Chemistry Lookout, Current Contents/Life Sciences, Current Contents/Physical, Chemical & Earth Sciences, Deep-Sea Research/Part B: Oceanographic Literature Review, Excerpta Medica, Index Medicus, Mass Spectrometry Bulletin, PASCAL-CNRS, Pharmaceutical Abstracts, Referativnyi Zhurnal, Research Alert, Science Citation Index and Trends in Biotechnology.

See inside back cover for Publication Schedule, Information for Authors and information on Advertisements.

0021-9673/92/$05.00

Printed in the Netherlands

CONTENTS

(Abstracts/Contents Lists published in Analytical Abstracts, Biochemical Abstracts, Biological Abstracts, Chemical Abstracts, Chemical Titles, Chromatography Abstracts, Current Contents/Life Sciences, Current Contents/Physical, Chemical & Earth Sciences, Deep-Sea Research/Part B: Oceanographic Literature Review, Excerpta Medica, Index Medicus, Mass Spectrometry Bulletin, PASCAL-CRNS, Referativnyi Zhurnal, Research Alert and Science Citation Index)

(Continued overleaf)

(Continued overleaf)

Contents (continued)

In articles with more than one author, the name of the author to whom correspondence should be addressed is indicated in the article heading by a 6-pointed asterisk (*).

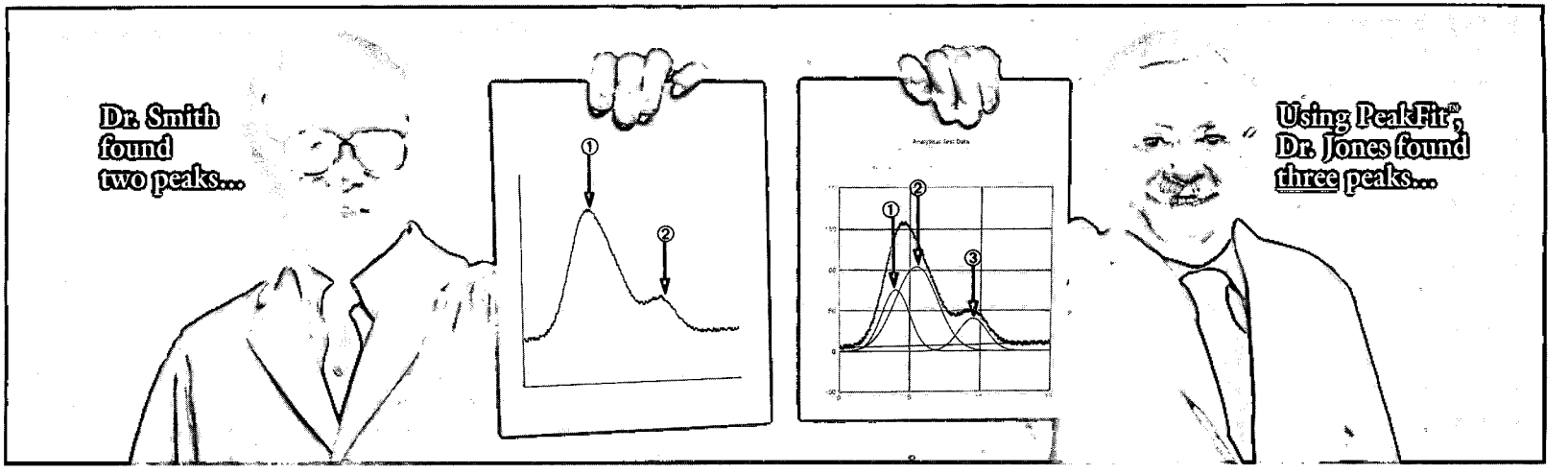

Guess who got the grant?

Because PeakFit™ uses sophisticated non-linear curve fitting techniques, it is far more effective than other data analysis tools in reducing noise and separating unresolved peaks! In fact, PeakFit is one of the most powerful software packages available today for chromatography and spectroscopy data analysis. For chromatographers, PeakFit extracts important system suitability information such as peak areas, asymmetries, and resolutions – plus column efficiency (number of theoretical plates) from raw data. For spectroscopists, PeakFit calculates peak amplitudes, areas, centers and widths – with complete uncertainty analysis, too!

Use PeakFit's 30 built-in peak functions (including Gaussian, Exponentially-Modified Gaussian,Voight and many others specifically suited for chromatography and spectroscopy) or input and use your own! Output both graphs and data to over 150 printers, including PostScript®. Of course we can't promise that PeakFit will win you a grant (your competition may already be using PeakFit!), but we can promise that PeakFit will enhance your current analysis methods. Order PeakFit today and see just how many peaks there <u>really</u> are in your data!

Manufacturers: Call for OEM info!

New Version 3.0!

PeakFit™

Peak Analysis Software for the IBM PC

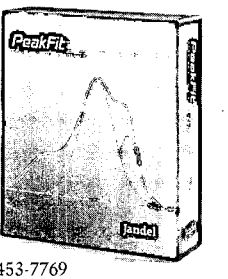

For free brochure:
800-874-1888 (U.S.)
415-453-6700 FAX 415-453-7769

From the makers of SigmaPlot®!

Jandel SCIENTIFIC

2591 Kerner Blvd
San Rafael, CA 94901

Europe: Schimmelbuschstr. 25
4006 Erkrath, Germany

Chromatography, 5th edition

Fundamentals and Applications of Chromatography and Related Differential Migration Methods

edited by **E. Heftmann**, *Orinda, CA, USA*

These are completely new books, organized according to the successful plan of the previous four editions. While avoiding repetition of material covered in the previous editions, the authors have succeeded in presenting a coherent and comprehensive picture of the state of each topic. The books provide beginners as well as experienced researchers with a key to understanding current activities in various separation methods. They will also serve as textbooks for graduate courses in technical, medical and engineering schools as well as all universities offering science courses.

Part A: Fundamentals and Techniques

Journal of Chromatography Library Volume 51A

Part A covers the theory and fundamentals of such methods as column and planar chromatography, countercurrent chromatography, field-flow fractionation, and electrophoresis. Affinity chromatography and supercritical-fluid chromatography are covered for the first time. Each topic is treated by one of the most eminent authorities in the field.

Contents Part A: 1. Theory of chromatography *(L.R. Snyder)*. 2. Countercurrent chromatography *(Y. Ito)*. 3. Planar chromatography *(S. Nyiredy)*. 4. Column liquid chromatography *(H. Poppe)*. 5. Ion-exchange chromatography *(H.F. Walton)*. 6. Size-exclusion chromatography *(L. Hagel and J.-C. Janson)*. 7. Affinity chromatography *(T.M. Phillips)*. 8. Supercritical-fluid chromatography *(P.J. Schoenmakers and L.G.M. Uunk)*. 9. Gas chromatography *(C.F. Poole and S.K. Poole)*. 10. Field-flow fractionation *(J. Janca)*. 11. Electrophoresis *(P.G. Righetti)*. Manufacturers and dealers of chromatography and electrophoresis supplies. Subject Index.

1992 xxxvi + 552 pages
Price: US $ 179.50 / Dfl. 350.00
ISBN 0-444-88236-7

Part B: Applications

Journal of Chromatography Library Volume 51B

Part B presents various applications of these methods. New developments are reviewed and summarized. Important topics such as environmental analysis and the determination of synthetic polymers and fossil fuels, are covered for the first time.

Contents Part B: 12. Inorganic species *(P.R. Haddad and E. Patsalides)*. 13. Amino acids and peptides *(C.T. Mant, N.E. Zhou and R.S. Hodges)*. 14. Proteins *(F.E. Regnier and K.M. Gooding)*. 15. Lipids *(A. Kuksis)*. 16. Carbohydrates *(S.C. Churms)*. 17. Nucleic acids, their constituents and analogs *(N-I Jang and P.R. Brown)*. 18. Porphyrins *(K. Jacob)*. 19. Phenolic compounds *(J.B. Harborne)*. 20. Drugs *(K. Macek and J. Macek)*. 21. Fossil fuels *(R.P. Philp and F.X. de las Heras)*. 22. Synthetic polymers *(T.H. Moury and T.C. Schunk)*. 23. Pesticides *(J. Sherma)*. 24. Environmental analysis *(K.P. Naikwadi and F.W. Karasek)*. 25. Amines from environmental sources *(H.A.H. Billiet)*. Manufacturers and dealers of chromatography and electrophoresis supplies. Subject Index.

1992 xxxii + 630 pages
Price: US $ 189.50 / Dfl. 370.00
ISBN 0-444-88237-5

Parts A & B Set
Set price: US $ 333.50 / Dfl. 650.00
ISBN 0-444-88404-1

Elsevier Science Publishers

P.O. Box 211, 1000 AE Amsterdam, The Netherlands
P.O. Box 882, Madison Square Station, New York, NY 10159, USA

New Developments in Ion Exchange

Materials, Fundamentals and Applications

Proceedings of the International Conference on Ion Exchange, ICIE '91, Tokyo, Japan, October 2-4, 1991

edited by **M. Abe**, Tokyo Institute of Technology, Tokyo, Japan,
T. Kataoka, University of Osaka Prefecture, Osaka, Japan and
T. Suzuki, Yamanashi University, Yamanashi, Japan

This volume contains the papers presented at the International Conference on Ion Exchange (ICIE '91). Included are reviews and original papers reflecting recent progress in new branches of science and technology based on novel ion-exchange materials and ion-exchange theory.

Topics covered include: Fundamentals (Ion exchange theory and process), Synthesis of New Materials, Chromatography (Ion and liquid chromatography, and associated techniques), Water Purification, Environmental, Membranes, Hydrometallurgy, Separation Science and Technology (Food, pharmaceutical, biological and others).

Contents:

1991 xlii + 636 pages
Price: US $ 218.00 / Dfl. 425.00
ISBN 0-444-98688-X

Co-edition with and distributed in Japan by Kodansha Scientific Ltd.

Elsevier Science Publishers

P.O. Box 211, 1000 AE Amsterdam, The Netherlands
P.O. Box 882, Madison Square Station, New York, NY 10159, USA

JOURNAL OF CHROMATOGRAPHY

VOL. 589 (1992)

JOURNAL of CHROMATOGRAPHY

INCLUDING ELECTROPHORESIS AND OTHER SEPARATION METHODS

ELSEVIER

AMSTERDAM — LONDON — NEW YORK — TOKYO

0021-9673/92/$05.00

Printed in the Netherlands

Journal of Chromatography, 589 (1992) V
Elsevier Science Publishers B.V., Amsterdam

Publisher's note

We are pleased to announce that Professor Udo Brinkman of the Free University, Amsterdam, has agreed to join the team of Editors of the *Journal of Chromatography*, as from January 1st, 1992.

Professor Brinkman's main research interests are in environmental analysis, sample preparation and detection for liquid chromatography, liquid chromatography–gas chromatography coupling and planar chromatography.

His personality, experience and knowledge will undoubtedly greatly contribute to the quality of the journal.

Journal of Chromatography, 589 (1992) 1–30
Elsevier Science Publishers B.V., Amsterdam

CHROM. 23 698

Review

Reaction kinetics and kinetic processes in modern liquid chromatographic reactors

Chawn-Ying Jeng and Stanley H. Langer*

Department of Chemical Engineering, University of Wisconsin, Madison, WI 53706 (USA)

(First received May 22nd, 1991; revised manuscript received August 20th, 1991)

ABSTRACT

The analysis and use of liquid chromatographic columns as chemical reactors are explained. Multifold applications of liquid chromatographic reactors with a wide range of materials are described and illustrated. Means for extracting chemical kinetic rate data from liquid chromatographic reactor experiments in the presence of other dynamic processes are emphasized. Techniques for controlling reactivity and selectivity are explained. It is also shown that useful information about the stationary phase and protein interaction with the stationary phase can be accessible from these experiments. Several explanations for multiple zone formation including results from interconversion studies are presented. It appears that a broader awareness of chromatographic reactor applications would be beneficial to workers in a variety of different fields. There are a number of additional possibilities for the future including the removal and detoxification through transformation of environmentally undesirable materials.

CONTENTS

0021-9673/92/$05.00

1. INTRODUCTION

During the past 15 years, liquid chromatography has emerged as one of the most powerful techniques available for the separation, identification and production of chemicals because of its versatility and freedom from the volatility requirement of gas chromatography. The merits of speed, efficiency, accuracy and ease of use have permitted modern liquid chromatography to be applied to compounds that range from simple organic species to complex macromolecular proteins. It was, however, the appreciation of similarities as well as differences between gas and liquid chromatography and the evolving understanding of gas chromatographic phenomena by a number of investigators that laid the foundation for the development of modern liquid chromatography. Much of the understanding was achieved through the analysis and interpretation of the physico-chemical components of chromatographic processes together with recognition of their dynamic character. Chromatographic equipment or procedures were altered so that information on the thermodynamics of solutions, gas–solid interactions, adsorption isotherms, diffusion and mass transfer processes all became available from gas chromatograms. It is now generally recognized that where applicable and suitable equipment is accessible, gas chromatographic techniques are among the most versatile for studying these phenomena [1–3].

Physico-chemical information can also be obtained from liquid chromatography although there are more complications from solution phenomena associated with the stationary phase, interaction between the mobile phase and the stationary phase and a wide assortment of solute–mobile phase interactions. Thus, liquid chromatographic processes are more complex than those of gas chromatographic systems and there have been stimulating disagreements about details of theory and the interpretation of pertinent physico-chemical phenomena [4–8]. Hence, some of the complications and their emphasis under selected experimental conditions provide an opportunity to study physico-chemical phenomena on surfaces, in the mobile phase and in the immobilized stationary phase [1,9,10].

The interpretation of the response to a pulse input in a catalytic microreactor equipped with a separate analytical chromatograph and similar equipment for kinetic and surface investigations has been common and extremely useful since the early days of gas chromatography [11,12]. However, the application of the column as a combined chemical reactor and separation device for studying and carrying out reactions has been utilized less, although there has been continuing, increased interest. This application is illustrated in Fig. 1, where a representative reaction chromatogram for a pulse of volatile reactant (cyclopentadiene dimer) dissociating to a more volatile product (cyclopentadiene) is shown. The relative positions of the reactant and product peaks would be reversed where the product is retained longer than the reactant. The column performs both reactor and chromatographic functions.

Earlier applications involving gas chromatographic systems led to several discussions of the advantages of chromatographic reactors relative to conventional static and flow reactors [2,3,13]. The attractive features of using chromatographic columns as chemical reactors with continuous mobile phase flow include the following: (a) the presence of concerted separation and reaction processes throughout the column; (b) the possibility of exceeding equilibrium conversions for reversible reactions as well as selective production of intermediate species with high purity in series reactions; (c) the capacity for quantitatively handling products and reactants readily without problems of transfer; (d) the ease of measuring the amount of reactant

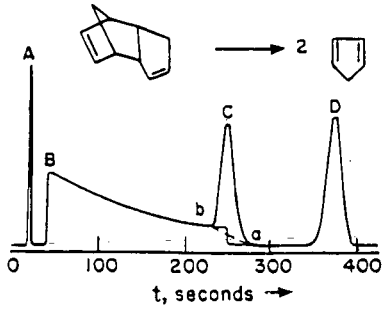

Fig. 1. Reaction chromatogram for the dissociation of dicyclopentadiene to cyclopentadiene. Column, 25% Apiezon L, 10 ft. × 0.25 in. I.D. at 209.6°C. A, air; B, cyclopentadiene; C, dicyclopentadiene reactant; D, inert standard. Carrier gas, helium. The line ba represents product formed during elution of the reactant peak.

introduced to the column and eluted from it and determining residence times in both the stationary phase and the mobile phase during passage through the column for each species; and (e) the ease of manipulation and control of chromatographic apparatus and associated detectors. Also, transport and sorption process rates frequently exceed those of chemical kinetic processes with gas chromatography so that only reaction rate is limiting and other effects frequently can be ignored.

While the possibility of carrying out reactions to advantage in gas chromatographic columns has been well realized in many instances [12–15], reaction kinetic studies and applications in liquid chromatographic columns have been less developed despite a number of incentives which can be envisioned for the future. In addition to the less ideal behavior inherent in the liquid, another factor is that many time-dependent processes such as mass transfer and sorption–desorption are much slower in the liquid phase than in the gas phase. This leads to complications in studying chemical reactions of comparable or faster rates because an additional category of kinetic processes must be considered. Since these relevant processes are slower, the chemical reactions studied in the column should also be slower in the best situations. Sometimes, modified chromatographic procedures can be invoked to compensate for slow chemical reaction, as will be illustrated later.

Until recently, many facets of liquid chromatographic reactors (LCR) have been unexploited although they have been gaining recognition [16–24]. However, much of the potential and many advantages of these systems are unrealized and unrecognized by many, awaiting further demonstration and investigation. Thus, a number of aspects of liquid chromatographic reactors and associated phenomena are appropriate for further study aided by continuing instrumental and theoretical developments. This is not to imply, however, that many of the virtues of liquid chromatographic reactor operations have not been discussed or utilized. Possibilities for exceeding equilibrium conversions through the elimination of reverse reactions by separation of products have been recognized and demonstrated by Wetherold *et al.* [25], Cho *et al.* [26,27] and Villermaux and co-workers [28,29]. Although application of the column as a reactor for preparative purposes has been infrequent, this potential is now being recognized [30–33]. On a much larger scale, Deans and co-workers [34,35] have even utilized ethyl acetate hydrolysis as a probe reaction in a subterranean oil reservoir together with chromatographic processes to obtain information on the reservoir bed. One major limitation for chromatographic reactor operations was the requirement that reactions proceed sufficiently fast for significant concentration changes during column residence. A means of compensating for slow reaction kinetics to provide for adequate changes is through "stopped flow", which can extend the range of kinetic studies in some instances [36–39]. A related technique involves immobilization on the surface followed by dissolution reactions, as explained later [40,41]. Pre- and post-column derivatization techniques for analysis and separation are, of course, well advanced and are discussed elsewhere [42–44].

With understanding and appreciation of liquid chromatographic reactor features, more opportunities for broader applications of modern liquid chromatographic systems should emerge, especially in environmental and biochemical related areas. For instance, one can ask whether or not there are possibilities for selectively reacting and removing small amounts of materials which are of environmental interest [45], whether reaction kinetic studies can assist the interpretation of chromatograms when some inadvertent biochemical reaction occurs [18,19,24] or the way in which interconversion reactions affect separations [20–23,46–48]. The purpose of this paper is to review recent work on liquid chromatographic reactor applications and related kinetics and, it is hoped, to provide some insights into the potential and limitations of LCR operations for other chromatographic investigators. An attempt is also made to show how common features and approaches have arisen among workers in diverse areas in hope that this recognition will benefit all. Because of space limitations the discussion has to be illustrative rather than comprehensive, although a broad range of topics and related literature are included together with leading references. The following section covers some fundamental principles of liquid chromatographic reactors and some strategy for handling models. LCR applications in chemical kinetics with chromatographic separation interactions are discussed in Section 3.

Section 4 presents a selection of recent studies on dynamic processes related to chemical reactions occurring in liquid chromatographic columns. Finally, some promising facets and developing potential applications of the LCR are discussed in Section 5.

2. THEORY

The chromatographic reactor of special interest here can be characterized as a chromatographic column–reactor system into which a reactant solute or reaction mixture is introduced and subsequently converted to products in the course of passage through the column. The hypothetical chromatogram in Fig. 2 resulting from a reactant pulse illustrates the behavior and consequences of concerted reaction, partitioning and separation in the column. Reactant and product materials are distributed between the mobile and stationary phases in a manner governed by characteristic partition coefficients. Where partition coefficients for reactants and products differ, separation occurs. Different types of chromatographic columns could be adapted for reactor use with either gas or liquid mobile phases; the stationary phase can be liquid coated on a solid support, one molecularly attached to the support or an adsorbent solid. Under proper conditions, reactant concentration changes and kinetic rate constants can be determined [13,47]. The ordinary chromatographic process results in constant dilution of eluites; thus, with the inherent presence of longitudinal diffusion and a significant pressure gradient (with gas chromatography), kinetic studies of first-order and pseudo-first-order reactions are most straightforward. However, special complex systems can be considered. For preparative applications and qualitative characterization purposes, requirements can be less stringent.

Many treatments of theory relevant to liquid chromatographic reactors are derived from the broad applications of gas chromatographic columns as chemical reactors. Gas chromatographic reactor behavior mainly involves a single-phase surface or two-phase homogeneous reaction in the case of heterogeneous catalytic reactor beds and gas–liquid partition columns, respectively. Analogous in the liquid chromatographic reactor are reaction systems in liquid–solid adsorption chromatography, and liquid–liquid partition or bonded-phase chromatography. With early theoretical treatments having focused on gas chromatographic reactors and related kinetic processes, a number of reviews are available with extensive coverage of these developments [12–15,49–51]. Although many concepts are not directly transferable, these studies have helped accelerate some understanding and more recent developments of liquid chromatographic reactors.

While there were discussions of mass transfer kinetic effects on band broadening and column efficiency in the early stages of modern liquid chromatographic development [52–56], studies of kinetic processes coupled with chemical reactions were limited. Recently, additional models of various complexities applicable to LCR kinetic studies have emerged [20,24,57–60]. Because of the complexity of the concerted reaction and separation processes in the chromatographic reactor, a number of problems remain, *e.g.*, solutions when all rate processes in both phases are considered, situations involving reactions of higher orders, and treatments involving stationary phase inhomogeneity.

Affinity chromatography has been among the popular liquid chromatographic techniques where considerable attention has been directed toward kinetic processes in the column because of the underlying chemical nature of interactions between solutes and ligands. Strictly, this type of system does not fall into the "chromatographic reactor" category as defined here, as no net chemical changes occur to the eluite between entering and leaving the column. Therefore, despite the increasing importance of affinity chromatography especially in biotechnology areas, it receives limited attention here with brief summaries of some important work in Section 4. Readers interested in the details of kinetic models describing affinity chromatography can refer to other reviews [61,62].

To provide a basis and perspective for discussing recent LCR developments, a chronological list of some of the significant progress of the past is presented by way of introduction. In Table 1, some important modelling efforts during the early development of gas chromatographic reactors are summarized, and in Table 2, some theoretical treatments more directly related to liquid chromatographic reactors are listed. In the section below, the limiting ideal reactor model is introduced first, followed by a

TABLE I

SOME MODELS FOR TREATING REACTIONS IN GAS CHROMATOGRAPHIC REACTORS

Reaction	Reaction phase(s)	Linearity of isotherm	Ideality assumption[a]	Solution	Ref.
A→B 1st irrev.	Stationary	Yes	No	Plate theory	63
A⇌B 1st rev.	Stationary	Yes	Yes	Number of ideal stages for reaction	64
A→B 1st irrev.	Gas and surface	Yes	A/D	Continuous-flow model	65
*n*th-order irrev.	Surface	Yes	Yes	Input pulse shape effect	66
A→B 1st irrev.	Gas and surface	Yes	AX	Continuous-flow model; limiting case	67
A→B 1st irrev.	Surface	Langmuir	A/D	Continuous-flow model	68
A→B 1st irrev.	Gas and surface	Yes	Yes	Continuous-flow model (ICR)	47
Multi-comp.	Stationary	No	MT	Moment analysis	69
A+B⇌2C 2nd rev.	Stationary	Yes	No	Plate model	70
A→B+C 1st irrev.	Surface	Yes	A/D	Moment analysis	71
A⇌B+C 1st and 2nd rev.	Surface	Langmuir	AX, A/D	Continuous-flow model	72
A→C or A+B→C 1st irrev.	Surface	Yes	AX, MT, A/D	Moment analysis	73
A→B 1st irrev.	Surface	Langmuir	AX, A/D	Moving bed	74
*n*th-order	Surface	Power law and Langmuir	Yes	Input pulse shape effect	75
A⇌B 1st rev.	Apparent for column	Yes	No	Plate theory	76
A⇌B 1st rev.	Apparent for column	No	No	Empirical equation for asymmetric peak	77
A→B 1st irev.	Surface	Yes	MT, A/D	Moment analysis	78
A→B→C 1st consec.	Surface	Yes	Yes	Moving bed	79
A⇌B+C	Apparent for column	Yes	No	Plate model	57
A→B 1st irrev.	Gas and surface	Yes	AX, MT	Moment analysis	80
A⇌B 1st rev.	Stationary	Yes	No	Plate model	81
A→B 1st irrev.	Stationary	Yes	AX, MT	Moment analysis	82
A⇌B 1st rev.	Surface	Langmuir	AX, A/D	Moving bed	83, 84

[a] A/D = Adsorption–desorption kinetics; AX = axial dispersion included; MT = interphase mass transfer or stationary phase (intraparticle) diffusion.

TABLE 2

KINETIC MODELS APPLICABLE TO LIQUID CHROMATOGRAPHIC REACTORS

Reaction	Column type	Reaction phase(s)[a]	Linearity	Ideality[b]	Approach	Ref.
$A \rightleftharpoons B$	General	Apparent	Yes	AX	Random walk model	46
$A \rightarrow B$	General	Both	Yes	AX, MT	Moment analysis	85
$A \rightleftharpoons B + C$	LC	Apparent	Freundlich	AX	Finite difference	25
$A + S \rightleftharpoons A \cdot S$	General	Stationary	Yes	AX, A/D	Steepest descent approximation	86, 87
$A + L \rightleftharpoons AL$	Affinity	Stationary	Yes	No	Moment analysis	88
Multi-comp. 1st irrev.	General	Both	Yes	AX, MT	Moment analysis	89
$A + B \rightleftharpoons AB$	LC	Mobile	Yes	MT, A/D	Moment analysis	90
$A + L \rightleftharpoons AL$	LC	Stationary	Yes	No	Plate model	56
General	General	Apparent	No	Yes	Vanishing species theorem	29
$A \rightleftharpoons B + C$	LC	Apparent	Freundlich	AX	Finite difference	26, 27
$A + L \rightleftharpoons AL$	Affinity	Both	Yes	No	Moment analysis	91
$A \rightarrow B$	LC	Surface	Yes	No	Plate model	92
$A \rightleftharpoons B$	LC	Both	Yes	Yes	Moment analysis	20, 93
Multi-comp. 1st rev.	LC	Both	Yes	No	Probability model	24
$A + B \rightarrow C$	LC	Both	Yes	AX, MT, A/D	Moment analysis	58
$A + L \rightleftharpoons AL$	Affinity	Stationary	No	No	Thomas theory	94
$A \rightarrow R \rightarrow S$	General	Both	Langmuir	No	Selectivity simulation	95
Multi-comp. 1st irrev.	General	Both	Yes	AX, MT	Fast Fourier transform	60
$A \rightarrow B$	LC	Surface	Yes	A/D	Moment analysis	59

[a] Apparent = Apparent (mobile and stationary) rate for column.
[b] See Table 1 for abbreviations.

discussion of some modifications which permit real operations to be described and a few case studies.

2.1. The ideal chromatographic reactor (ICR)

For understanding the features and advantages of chromatographic reactors, the limiting "ideal chromatographic reactor" (ICR) situation can be reviewed as a basis for comparison with conventional plug-flow (PFR) and continuous stirred-tank reactors (CSTR) [13,47]. Briefly, in such an ideal column reactor–separator:

(1) A reacting pulse is swept through the column with instantaneous separation from resulting products. The reaction and instant separation feature contrasts with the concept of instant mixing in the CSTR, and also differs from the uniform flow pattern in the PFR.

(2) The column is homogeneous in composition with respect to both the mobile phase and the stationary phase. In liquid chromatography, this treatment of the mobile phase is particularly valid, as the fluid is essentially incompressible.

(3) Distribution isotherms are linear, *i.e.*, the partition coefficients between the mobile and stationary phases for all reactants and products are independent of concentration.

(4) Peak spreading and axial dispersion are not important in the ideal case. For reactions other than first order, these effects must be minimal.

(5) The conversion process is controlled by chemical reaction, so that mass transfer and adsorption–desorption rates in the column are fast relative to chemical reaction rate.

(6) The column is isothermal; heats of reaction and solution are negligible with the types of small samples under consideration.

The simplified general material balance on a differential section of a chromatographic column

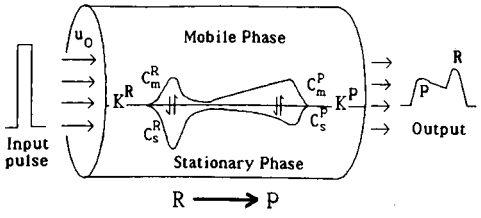

Fig. 2. Illustration of reactor chromatogram formation from concerted reaction and separation processes in a chromatographic column. K^R and K^P are the partition coefficients for the reactant (R) and the product (P). C_m and C_s represent concentrations in the mobile (m) and stationary (s) phases for the designated species [96].

with constant mobile phase velocity (Fig. 2) thus becomes

$$f_m\left(\frac{\partial C_m}{\partial t}\right) + f_s\left(\frac{\partial C_s}{\partial t}\right) = -u_0 f_m\left(\frac{\partial C_m}{\partial x}\right) - f_m r_m - f_s r_s \quad (1)$$

accumulation of reactant = net change of reactant due to flow + change in reactant due to chemical reaction in mobile and stationary phases

where

C_m, C_s = concentration of reactant in the mobile and stationary phase, respectively;

f_m, f_s = volume fraction of the mobile and stationary phase, respectively (for adsorption-type columns, the porosity ε can be used instead);

r_m, r_s = rate of reactant depletion in the mobile and stationary phase, respectively;

u_0 = linear velocity of the mobile phase;

t = time measured from injection;

x = position in the column measured from inlet.

From this equation, for first-order reactions with linear isotherms in a chromatographic column it is readily shown that [13,47]

$$\frac{W_{out}}{W_{in}} = \exp[-(k_m t_m + k_s t_s)] \quad (2)$$

where W_{in} and W_{out} are the total amounts of reactant entering and leaving the column, k_m and k_s are forward reaction rate constants in the mobile and stationary phase, respectively, and t_m and t_s are the corresponding residence times for the reactant.

Methods for determining reaction rate constants in chromatographic reactors have been reviewed [13,15]. Among them, the "inert standard" method is commonly used. If a known amount (W) of inert reference material (I) is added to a reactant (R) mixture before injection, then

$$\ln\left[\frac{A_R}{A_I}\right] = \ln\left(\frac{W_{R,in}/S_R}{W_I/S_I}\right) - k_{app} t_R \quad (3)$$

and

$$k_{app} \equiv \left(\frac{t_m}{t_R}\right) k_m + \left(\frac{t_s}{t_R}\right) k_s \quad (4)$$

where k_{app} is the apparent or composite rate constant in the column, t_R is the total column residence time for the reactant, A represents peak area and S represents detector sensitivity. With A_R/A_I and t_R measured experimentally from reactor chromatograms at varying flow-rates (Fig. 3), k_{app} can be evaluated.

It should be noted that k_m and k_s are the conventional kinetic rate constants in the mobile and stationary phase, respectively, not k_{app}. By

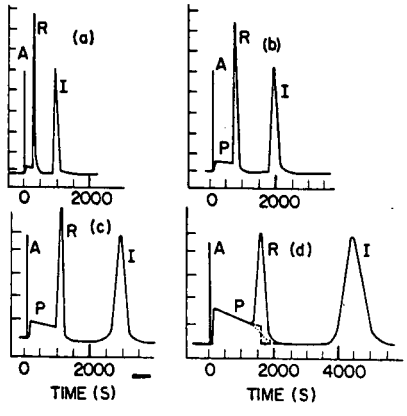

Fig. 3. Inert standard method for determining rate constants using gas chromatography. A methylcyclopentadiene dimer dissociating at 180.08°C in hexatriacontane–Gas Chrom Q (20:80), 122 cm × 0.48 cm I.D. column. A, air; P, product; R, reactant; I, inert (phenyl ether). (a) 15% conversion, flow-rate = 65.7 cm^3/min (corrected); (b) 25% conversion, flow-rate = 33.5 cm^3/min (corrected); (c) 34% conversion, flow-rate = 22.05 cm^3/min (corrected); (d) 50% conversion, flow-rate = 15.6 cm^3/min (corrected). (From ref. 126; reproduced with permission.)

measuring k_m in a batch reactor and k_{app} from the liquid chromatographic reactor, k_s can be evaluated with eqn. 4. Earlier investigations in gas–liquid systems were simplified by treatments of both phases as bulk fluids with the gas phase approximated as ideal [97]. For surface-catalyzed reactions, the reaction rate in the mobile phase is usually insignificant and can be neglected. In bonded-phase liquid chromatography, the stationary phase composition can be more complex and reaction kinetics in both phases can be studied through changes in experimental conditions [16,17,98].

ICR behavior can be approached experimentally by (a) using small, narrow pulses of reactant samples so that the isotherm linearity assumption is applicable, (b) utilizing slow flow-rates through the column to allow equilibrium to be established between two phases (however, for slow flow-rates the effects of axial diffusion can become more pronounced), (c) deliberately choosing a slow reaction to minimize possible complications from transport and adsorption processes, (d) selecting columns for study with packings of fine particles so that mass transfer effects can be neglected and (e) ensuring good temperature control for the entire column. Although some of the above considerations are not practical for large-scale operations, the ideal chromatographic reactor concept serves as a useful model for guiding and comparing reactor operations and provides a simple physical picture of the reactor system. With attention to the basic principles above, real reactors can be operated with features approaching those of the ICR where desired.

2.2. *Modifications of ICR assumptions*

Several modifications to the ideal reactor model have been made to accommodate some complications that affect real chromatographic systems. Non-equilibrium effects from the slow adsorption–desorption kinetics to compete with the reaction kinetics have been discussed [65,71,86,87]. Complications of chromatographic reactors with finite mass transfer rates involving longitudinal dispersion, intraparticle or stationary-phase diffusion and interfacial mass transfer between two phases also have received much attention [73,78,80,85,90]. In liquid chromatographic reactors, longitudinal dispersion is less serious than with gas chromatography because of low liquid diffusivity rates; however, this also can result in mass transfer and pore diffusion resistance. One attractive technique that can accommodate deviations from ideal chromatographic reactor behavior resulting from slow kinetic processes (*e.g.*, adsorption–desorption) is the stopped-flow method [36–39]. Isotherm non-linearity, which can be of special importance in adsorption chromatography and large-scale operations, results in another deviation from the ideal chromatographic reactor assumption [68,72,74,75,83,84].

The "discontinuous plate model" [99,100] and the "continuous flow model" [101,102] are two extremes frequently used to treat chromatographic dynamic processes. Comparisons between these two are shown in Table 3. While the plate model is generally simple and easy to use, plate-height values lose physical significance and become difficult to determine experimentally when chemical reactions confound

TABLE 3

COMPARISON OF THE CONTINUOUS-FLOW MODEL WITH THE PLATE (MIXING CELL) MODEL FOR CHROMATOGRAPHIC REACTORS

Treatment	Continuous-flow model	Plate (mixing cell) model
Description	Treat flow as continuous	Assume all processes occur stagewise (discontinuous)
Peak spreading	Introduce several physical parameters to describe spreading	Inherent spreading in treatment through introduction of the number of plates
System equations	A set of partial differential equations	A set of ordinary differential equations for each plate
Isotherm	Several types of non-linear isotherms can be incorporated	No satisfactory general expression incorporating non-linear effects
General solution	Analytical solutions difficult without simplifying assumptions	Plate number (N) used as the index parameter
First-order kinetics [13]	Ideal chromatographic reactor: $\frac{W_{in}}{W_{out}} = \exp(k_m t_m + k_s t_s)$	$N[1-(W_{out}/W_{in})]^{1/N} = k_m t_m + k_s t_s$ As $N \rightarrow \infty$, $\ln(W_{in}/W_{out}) = k_m t_m + k_s t_s$

other dynamic chromatographic processes. Therefore, solutions based on the continuous model are emphasized in this paper. A number of treatments emphasizing various aspects and complexities of reaction and kinetic processes and methods for solving the equations of proposed systems are summarized below.

2.2.1. Mathematical model. A general mathematical model for the LCR is employed here with consideration of axial dispersion (coefficient D_m), intraparticle or stationary phase diffusion (coefficient D_s) and adsorption–desorption processes (rate constants k_a and k_d) together with the reaction process [58]. A schematic representation of the rate processes considered in this model is shown in Fig. 4. Assuming first-order reactions in both phases, then for the reactant

$$f_m\left(\frac{\partial C_m}{\partial t}\right) + f_s\left(\frac{\partial \bar{C}_s}{\partial t}\right) = f_m \mathscr{D}_m\left(\frac{\partial^2 C_m}{\partial x^2}\right) - f_m\left\{\frac{\partial}{\partial x}[u(x)C_m]\right\} - f_m k_m C_m - f_s k_s \bar{C}_s \quad (5)$$

where $\bar{C}_s$ is the average reactant stationary phase concentration over a macroporous particle and $u(x)$ is the linear velocity of the mobile phase at position x in the column. The terms on the right-hand side include longitudinal diffusion, convection and reaction rate effects.

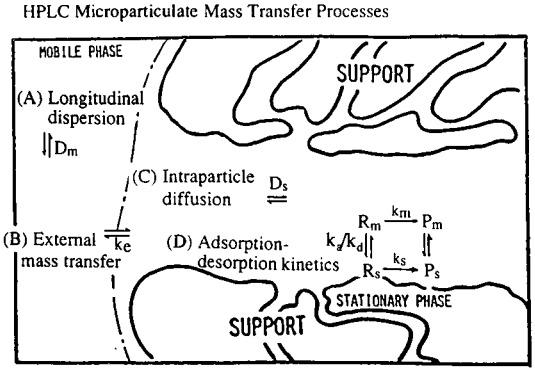

Fig. 4. Schematic representations of simple rate processes occurring in a section of a liquid chromatographic reactor. k_m and k_s, reaction rate constants in mobile and stationary phases; k_a and k_d, adsorption–desorption rate constants between mobile phase and stationary phase; k_e, mass transfer coefficient at the particle boundary; D_m and D_s, effective diffusion coefficients in mobile phase and pore [96].

For a spherical particle of packing in which reaction occurs [58],

$$\frac{\partial C_s}{\partial t} = \mathscr{D}_s\left(\frac{\partial^2 C_s}{\partial r^2} + \frac{2}{r}\cdot\frac{\partial C_s}{\partial r}\right) - k_s C_s \quad (6)$$

Here $\mathscr{D}_s$ is constant at low solute concentrations. For interfacial mass transfer in a dilute system,

$$\frac{\partial \bar{C}_s}{\partial t} = k_a C_m - (k_d + k_s)\bar{C}_s \quad (7)$$

For the model where radial uniformity is assumed, $\bar{C}_s$ is employed in eqns. 5 and 7 to eliminate any radial dependence of the $C_s(x,r,t)$ term used in eqn. 6. More complicated mathematical models dealing with stationary phase particle porosity and situations where external mass transfer across the particle boundary are important are also available [50,73].

2.2.2. Solution. With appropriate simplifications or modifications, this system can be solved or approximated using the following approaches:

(1) The ideal chromatographic reactor: by neglecting all diffusional and mass transfer resistances and assuming equilibrium distribution between two phases, the model simplifies to first-order differential equations (*e.g.*, eqn. 1) which can be solved analytically as shown previously [13,47,64,103].

(2) When the kinetics due to sorption–desorption are commensurate with chemical reaction rates, *i.e.*, distribution equilibrium is not established but all other ideal characteristics described above apply, then a solution can be obtained analytically [58,65] or statistically [71,86,87].

(3) When mass transfer processes are considered, then an analytical solution is difficult to obtain but a statistical moment approach [73,78,80,85,90] or a numerical solution [60,72,74] may be viable.

(4) Where non-linear equilibrium distributions are encountered, numerical methods usually have been utilized to solve particular situations such as those involving Langmuir and Freundlich isotherms [25–27,68,72,74,75].

(5) By varying the shapes and cycling periods of input pulses to screen and analyze responses, reactions other than first order can be studied; some kinetic parameters have been obtained for these circumstances with numerical methods [57,66,72,95, 104]. Continuous-flow feed operations in chromatographic reactors have also been studied in combi-

nation with additional parameters such as feed rate and feed position [26,27,74,78,83,84].

(6) By means of a theoretical plate treatment: this approach uses the number of plates as an adjustable parameter to incorporate all chromatographic processes that cause band broadening (Table 3). There is no direct clarification of the details of specific kinetic mechanisms for complex processes in the column. With the aid of rate theory which incorporates the contribution from each mechanism to the plate height, some kinetic parameters can be determined [63,70,76,81]. The use of a stirred tanks-in-series model with consideration of interactions at the local level also has been advocated by Villermaux to treat linear chromatography [105], with the claim that the complex phenomena involved can be represented by simple engineering concepts. Extensions to chemical reactions in both the mobile and stationary phases were illustrated.

(7) Most analyses above are based on information about reactant species only. Sometimes, it is difficult to identify the reactant peak within the overlapping elution curve which includes contributions from product concentration profiles (see Fig. 1). Then, general approaches dealing with overall elution profiles can be invoked. The statistical moment method has been applied both to the ideal situation [20,89,93,106] and some situations where non-ideal processes become important [59,82]. Alternatively, the random walk (stochastic probability) model has been utilized to treat multiple zones which appear because of interconverting species [24,46,107,108].

To illustrate and supplement some of the approaches described above, three case studies are considered below. However, the discussion is limited to a few principles and some simple results to provide an overview. Readers interested in the more detailed and involved mathematical treatments of chromatographic reactor modeling should consult the references of Tables 1 and 2.

2.2.3. Case 1. One of the most common deviations from ICR behavior stems from finite sorption kinetics for the reactant. For eqn. 7, adsorption and desorption rates are commensurate with chemical reaction rates. With a negligible dispersion effect in liquid columns, the second-order derivative term of eqn. 5 can be dropped so that a simple solution can be obtained by using proper initial and boundary conditions. For instance,

$$\text{at } x = 0, \quad C_m(0,t) = \phi(t) \tag{8}$$

$$\text{at } x = \infty, \quad C_m(\infty,t) = 0 \tag{9}$$

$$\text{at } t = 0, \quad C_m(x,0) = C_s(x,0) = 0 \tag{10}$$

where $\phi(t)$ is the reactant input function at the column inlet.

For pulse injections of reactant, the system can be solved by Laplace transformation together with the statistical moment method [58]. An expression similar to that of eqn. 3 is obtained when the inert standard method is used. However, then

$$\ln\left(\frac{A_R}{A_I}\right) = \ln\left(\frac{A_R}{A_I}\right)_{t=0} - k'_{app}t_m \tag{11}$$

and

$$k'_{app} \equiv k_m + \frac{f_s k_a k_s}{f_m(k_d + k_s)} \tag{12}$$

On comparison with eqn. 4 for the ideal chromatographic reactor, we see that eqn. 12 indicates how the measurements of the intrinsic reaction rate constant in the stationary phase can be affected by finite adsorption and desorption kinetic processes.

A more general expression for an overall elution profile which contains both reactant and product has been obtained in terms of the first absolute moment [59]. This approach overcomes difficulties in resolving reactant and product overlap in elution profiles and eliminates any need for either internal or external standards.

2.2.4. Case 2. When axial dispersion becomes important and the second-derivative term is significant, the system can be treated again with Laplace transformation and the statistical moment method. The following form can then approximate the solution [58]:

$$\ln\left(\frac{A_R}{A_I}\right) = \ln\left(\frac{A_R}{A_I}\right)_{t=0} + \frac{u_0 L}{2\mathscr{D}_m}\left\{1 - \left[1 + \left(\frac{4\mathscr{D}_m}{u_0 L}\right)\left(k_m t_m + \frac{k_s t_s}{1 + k_s/k_d}\right)\right]^{1/2}\right\} \tag{13}$$

More exact solutions for describing elution profiles are available in the form of statistical moments [73,89] or through numerical methods such as fast Fourier transformations [60]. However, evaluation of actual kinetic and dispersion parameters then becomes more difficult.

From eqn. 13, we can see that the axial dispersion influence on intrinsic kinetic evaluation is insignificant when

$$k_m t_m + \frac{k_s t_s}{1 + k_s/k_d} \ll \frac{u_0 L}{4\mathscr{D}_m} \quad (14)$$

If the column Peclet number ($u_0 L/\mathscr{D}_m$) is much greater than the reaction terms indicated in eqn. 14, one can neglect the effect of axial dispersion on LCR analysis, as eqn. 13 reduces to eqn. 11 after applying a binomial Taylor expansion. For modern liquid chromatography, this criterion is usually satisfactory as the dispersion coefficients of molecules in liquids are small and chemical reaction rates are relatively slow [58,59,93]. However, for situations involving very short columns, low flow-rates or fast reactions, this criterion should be examined carefully. When similar approaches for evaluating mass transfer effects from external film resistance and intraparticle diffusion have been used in the LCR their effects were also found to be insignificant [58,59].

2.2.5. Case 3. Although the linear distribution isotherm assumption is often valid for small pulse injections, it becomes questionable for large sample loadings and with frontal or displacement chromatography [109–111]. Therefore, several types of non-linear isotherms have been proposed for replacing the linear relationship between reactant concentrations in the two phases where LCR models are concerned.

Langmuir isotherms have often been used with gas–solid chromatographic reactors [68,72,74,75,83, 84] and sometimes for association behaviors in affinity chromatography [94,112]. They also have been incorporated in studies of the preparative chromatographic reactor [30]. For a multi-component system, they assume the form

$$C_{si} = \frac{\alpha_i C_{mi}}{1 + \sum_j \beta_j C_{mj}} \quad (15)$$

The solutions for LCR models have generally only been accessible with numerical methods. With a limited number of active sites, the Langmuir-type model gave a lower conversion than the linear-type model, especially at high reactant concentrations [30].

Although Langmuir isotherms describe non-linearity satisfactorily in many instances, they are not adequate for a highly heterogeneous surface or when strong interactions between solutes in the fluid phase occur. Because of this, the Freundlich isotherm has been used to treat multi-component, competitive adsorption LCR systems on several occasions [25–27]:

$$C_{si} = c_i C_{mi}^{\gamma_i} \quad (16)$$

In these studies, experimental data for multi-solute adsorption have given good least square fit of the parameters c_i and γ_i, with the reactor models being solved using the finite difference method.

Power law and other empirical equations can also be used to describe non-linear isotherm behavior [75,77]. In general, non-linear effects are less significant in the performance of the chromatographic reactor than chemical kinetics, even for preparative operations [30]. This is especially true when reaction features of the chromatographic reactors are a major focus. On the other hand, when separations or physico-chemical measurements are the main concern, a careful examination of this aspect is appropriate.

The utilization of the principles above both qualitatively and quantitatively in kinetic studies can be illustrated by reviewing their applications in several fields.

3. CHEMICAL KINETIC APPLICATIONS

Modern liquid chromatographic use for post-reaction sample analysis to obtain kinetic information has flourished over the last 10 years. The availability of fast separations with small sample requirements, ease of operation and accurate quantification has greatly facilitated conventional kinetic studies of chemical reactions. Examples of liquid chromatographic applications involving techniques such as spectrophotometric, conductive, electrochemical and radioactivity-monitoring methods for analysis of reaction mixtures to obtain kinetic parameters and mechanistic information abound. These encompass areas of biochemistry, especially pharmaceutical-related enzymatic reactions, and studies of organic and inorganic reactions, including photochemical-type reactions. Nevertheless, this area is still not included in the discussion of liquid chromatographic reactors that we have defined here

as reaction is not occurring inside the column and column use is really for the purpose of separation and analysis.

Although there was some general discussion of reaction and kinetic processes applicable to liquid chromatography by Keller and Giddings in 1960 [46,108], adaptation of the modern liquid chromatograph to chemical reactor use did not occur until the 1970s, and it is only in recent years that experimental applications in this area have witnessed significant progress. Detailed discussion on recent LCR developments is contained in this section. A distinction between two types of liquid chromatographic modes is made here because different reaction patterns and retention mechanisms are involved in each: (3.1) liquid–solid adsorption types and (3.2) bonded-phase types with emphasis on alkyl-bonded reversed-phase chromatography.

TABLE 4

REPRESENTATIVE REACTION KINETIC STUDIES IN LIQUID CHROMATOGRAPHIC REACTORS

Reaction	Mobile phase[a]	Stationary phase	Rate constant[b] (s^{-1})	Ref.
(A) Liquid–solid adsorption chromatography				
Hydrolysis of methyl formate to methanol and acetic acid	HCl–water	Activated charcoal	10^{-3}	25 26, 27
Ethanolic esterification of acetic acid to ethyl acetate	Dioxane–heptane Dioxane–water	Alumina–resin Cation-exchange resin	10^{-2} (70°C)	28 29
Hydroquinone oxidation to benzoquinone	*tert.*-Butanol–hexane	Iron-modified silica	10^{-3}	59, 113
(B) Bonded-phase liquid chromatography				
Base-catalyzed esterification of tetrachloroterephthaloyl chloride and its half-ester	Pyridine (4-picoline) in THF–CH_3OH	ODS	10^{-3}–10^{-4}	16, 17, 98
Papain/lysozyme/STI[c] denaturation	1-PrOH–H_3PO_4–water	C_4	10^{-3}	18, 19
Lysozyme/STI denaturation	1-PrOH–TFA–water	ODS	10^{-2}–10^{-3}	24
Lysozyme conformation	CH_3OH–H_3PO_4–water	C_4	10^{-2} (4°C)	114
α-Lactalbumin unfolding	Ammonium sulfate–water	C_1- and C_2-ether	10^{-2} (4°C)	115
Methoxyhydroquinone oxidation	Acetonitrile–water	C_8	10^{-3}	116
Base-catalyzed hydrolysis of *p*-nitrophenyl esters	NaOH in acetonitrile–water	Polymer-based PRP-1	10^{-2}–10^{-3}	41
(C) Interconversion and fast equilibria				
Cis–trans proline isomerization	Phosphate–water	ODs	10^{-3}	21, 106
RNase A refolding	1-PrOH–H_3PO_4–water	C_4	10^{-2}–10^{-3}	117, 118
RNase A denaturation–renaturation	GuHCl–water	Gel permeation, TSK-G2000SW	10^{-3}	93
Muramyldipeptide anomers	CF_3COOH–CH_3OH–water	ODS	10^{-3} (34°C)	119
Pyranose sugar anomer mutarotation	CH_3COOH–acetone–water	NH_2-silica	10^{-3}	120
Pd(II) dithiocarbamate intramolecular rotation	Isopropyl acetate–hexane	Silica	10^{-3} (0°C)	121
Carbon–nitrogen bond rotation of formanilide and *o*-substituted acetanilide	CH_3COOH–hexane–acetate or 1-PrOH	Silica	10^{-3} (−27.6°C) 10^{-3}–10^{-4} (−40°C)	122 22
Phenyl methylcarbamate intramolecular rotation	CH_3COOH–1-PrOH–hexane	OH	10^{-2}–10^{-3} (−30°C)	23

[a] THF = Tetrahydrofuran; 1-PrOH = *n*-propanol; TFA = trifluoroacetic acid; GuHCl = guanidinium chloride.

[b] First-order or pseudo-first-order kinetic assumption; room-temperature values except when noted otherwise in parentheses.

[c] STI = Soybean trypsin inhibitor.

In Section 3.3, interconversion and fast equilibria studies in liquid chromatographic columns are addressed separately because of the special nature of the reactions involved and the coupling with separation.

In Table 4 some representative reactions studied in modern liquid chromatographic reactors are summarized. Also illustrated in Table 4 is a rule of thumb for choosing a chemical reaction and proper operating conditions for LCR kinetics where rate constants apparently should be in the range between 10^{-2} and 10^{-4} s^{-1}. Reactions with rates below this range can still be studied by using special techniques such as stopped-flow methods. For preparative purposes, studies of reactions with faster rates are also common.

3.1. Liquid–solid (adsorption) chromatographic reactors

Liquid–solid adsorption chromatography received initial attention for reactor application because of a similarity to gas–solid chromatography and the availability of solid adsorbents with well characterized properties. Here, however, isotherm non-linearity and non-ideality due to adsorption kinetics often cannot be neglected. Varying isotherms and possible strong adsorption and slow desorption can be incorporated into models so that moment approaches and numerical procedures are usually required to obtain viable solutions for this type of reactor system.

A pioneering work in this area was the experimental and computational study by Wetherold *et al.* [25] in 1974 on the liquid-phase hydrolysis of methyl formate over an activated charcoal bed to form methanol and formic acid ($A \rightleftharpoons B + C$). A Freundlich isotherm with an empirical correction factor was chosen to treat the multi-component nature of the adsorption system. The possibility of overcoming thermodynamic conversion limitations, *i.e.*, the equilibrium value, was demonstrated. Specifically, because the two products had different affinities for the stationary phase there was sufficient separation to inhibit the reverse reaction. A similar reaction system was selected for study by Cho *et al.* [26,27] in a continuous-flow annular reactor configuration with a rotating feed injection port to achieve the same objective of exceeding the equilibrium conversion. An ideal chromatographic model modified for dispersion effects gave satisfactory agreement with experimental data. A simplified binary-component Freundlich adsorption isotherm was used in the numerical simulation when there was rapid disappearance of methyl formate reactant and no competitive adsorption between methanol and formic acid products.

The ethanolic esterification of acetic acid catalyzed by a cation-exchange resin to give ethyl acetate ($A + B \rightleftharpoons C$) was studied in a liquid–solid chromatographic reactor by Sardin and Villernaux [28]. A mixture of alumina acting as a sorbent and the cation-exchange resin was used for packing material, to separate the desired ethyl acetate product from water and from the reactants which travel at the same speed in a dioxane–heptane mobile phase. The 90% conversion attained far exceeded the 67% equilibrium conversion. Later, a general theoretical treatment of this system involving two shocks [29] was found to agree with experimental data; some deviations from isotherm linearity were discussed.

In addition to the above studies where product yield with reactor performance was the main concern, use of a liquid chromatographic column as a microcatalytic reactor for obtaining kinetic data was demonstrated by Melton *et al.* [123]. The lactase-catalyzed hydrolysis of α-nitrophenyl-β-D-galactopyranoside (ONPG) was used as a model reaction for studying immobilized enzyme activity on porous glass beads. Advantages of adapting a liquid chromatographic system to micro-reactor use for studying kinetics include speed, reproducibility, convenience for non-volatile samples, and the ready adaptation of equipment with little modification. Melton [124] also demonstrated the use of this micro-reactor and a factorial design approach involving nine system variables (see Table 5) to screen immobilized enzyme activity quickly and efficiently. The results from Melton's experiments indicated that the amount of enzyme initially present and the pH of immobilization were the most critical parameters, whereas the Mg^{2+} concentration, the temperature of immobilization and the support mesh size had little effect on immobilization effectiveness under his conditions.

The operation by Melton *et al.* actually resembles and utilizes some principles of the flow-injection analysis (FIA) technique [43,125]. FIA itself can

TABLE 5

VARIABLES IN FACTORIAL DESIGN EXPERIMENTS ON LACTASE-CATALYZED ONPG HYDROLYSIS

Variable No.	Variable	High value (+)	Low value (−)
1	Time of immobilization	90 min.	60 min
2	Sequence of anchoring agent[a] addition	Before enzyme	With enzyme
3	Length of anchor chain to glass bead	C_6	C_3
4	Mg^{2+} concentration	10^{-3} *M*	0
5	Temperature of immobilization	*ca.* 20°C (room temp.)	0°C
6	Amount of enzyme added	20 mg	10 mg
7	Mesh size of support	60–80	80–100
8	pH of immobilization	7	4
9	Anchoring agent[a] concentration	7.5%	2.5%

[a] Glutaraldehyde used as anchoring agent for this experiment.

provide rapid on-line determination of the complexing abilities of individual species. However, for mixtures of complexing species a high-performance liquid chromatographic (HPLC) system is needed [127]. FIA methods based on chemical reactions from the introduction of a continuous stream of reagent(s) and/or the stopped-flow technique are often adapted in post-column reaction detection for liquid chromatography, especially in enzyme kinetic studies. Excellent related studies of immobilized enzyme kinetics took place during the 1970s using HPLC and other types of equipment, some of which are referenced elsewhere [43,123]. However, because these are so well treated in more specialized texts, such as that by Carr and Bowers [181], they are not addressed further here.

Recently, catalytic activities in silica columns and related kinetic processes were examined by Jeng and Langer [113,128]. The oxidation of hydroquinone to form benzoquinone in an organic environment was used as a probe reaction to detect column activities resulting from contamination, probably from transition metal ions leached from the stainless-steel components of HPLC hardware [128]. Whereas flow-rate variation and direction reversal (Fig. 5) were applied to locate active sites in the column, their redox nature was characterized by column treatments with an appropriate oxidant or reductant. Later, the same reaction in a uniform column packed with iron(III)-modified silica was utilized to demonstrate the feasibility of using a statistical moment method based on the overall elution profile of reactant and product to evaluate reaction kinetic parameters [59]. Reactant adsorption kinetics were shown to be important factors in reaction-rate measurements for the low conversion situation occurring at lower temperatures and higher flow-rates. Further, LCR kinetic results were shown to complement retention behavior for the column to characterize the modified surface of the stationary phase [113]. A weaker adsorption effect was observed for the silica sample where strongly adsorbing, hydrogen-bonding surface silanol groups were eliminated during iron treatment. The foregoing group of publications illustrate the variety and kinds

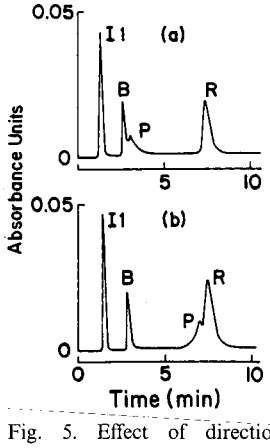

Fig. 5. Effect of direction of flow on liquid reactor chromatogram for 2.5 m*M* hydroquinone (R) oxidation; P = product formed in column, B = benzoquinone in injected sample. (a) Normal flow direction, (b) flow reversed. Column, Altex Ultrasil silica (10-μm); mobile phase, isopropanol–hexane (5:95); flow-rate, 1.76 cm^3/min (150 p.s.i.); sample size, 20 μl; wavelength, 254 nm. The active sites are distributed at the inlet of the column during normal flow direction. (From ref. 128; reproduced from the *Journal of Chromatographic Science* by permission of Preston Publications, a Division of Preston Industries, Inc.)

of information which can be obtained about the packing from diagnostic and kinetic studies where the column is used as a reactor.

3.2. Bonded-phase liquid chromatographic reactors

The stability and variety of available stationary phases and elution modes have been important factors in the growth and popularity of modern bonded-phase liquid chromatography as an analytical technique. Nevertheless, systematic studies using bonded-phase liquid chromatographic columns as chemical reactors did not occur until the 1980s. Some studies of solvolysis reactions of tetrachloroterephthaloyl chloride with alcohol (Fig. 6) by Langer and co-workers in a C_{18} reversed-phase liquid chromatographic reactor were directed toward demonstrating the feasibility of obtaining kinetic information and insights into stationary phase structure and retention mechanisms [16,129]. Specifically, pseudo-first-order rate constants for a base-catalyzed solvolysis were determined in the course of considering reaction in the stationary phase. The base catalysts, pyridine or 4-picoline, were present as homogeneous components in the mobile phase and were thereby also distributed in the stationary phase. The same reaction kinetics were subsequently utilized to attempt to characterize the nature of the chemically bonded stationary phase [17] and to evaluate the phase ratio in a bonded-phase column [130]. (The use of reaction kinetics as a tool for obtaining information on the stationary phase is discussed further in Section 5).

A series of LCR chromatograms from the work above is shown in Fig. 7 to illustrate further advantages of chromatographic reactors. These chromatograms result from the formation of a quaternary ammonium salt (M) initially in the course of the pyridine-catalyzed esterification of tetrachloroterephthaloyl chloride (R). In these chromatograms it can be seen that:

(a) impurities in injected reactant samples show up with characteristic retentions as peaks on the chromatogram and can be accommodated; here, H is the half methyl ester already formed before injection from a slow uncatalyzed reaction (Fig. 6);

(b) side-reactions can be detected on the chromatogram (additional product curves would be perceived [131]);

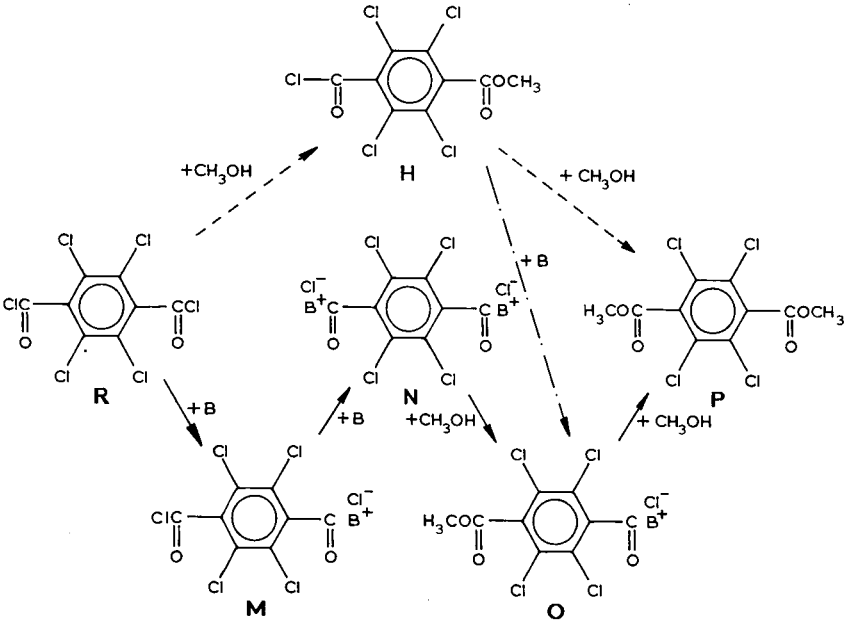

Fig. 6. Reaction sequence (solid arrows) for the base (B)-catalyzed methanolic esterification of tetrachloroterephthaloyl chloride ($TCTPCl_2$), R; uncatalyzed solvolysis sequence in parallel (dashed arrows). B is pyridine or 4-picoline; M, N and O are intermediate quaternary salts; H and P are the half-ester and di-ester products [129].

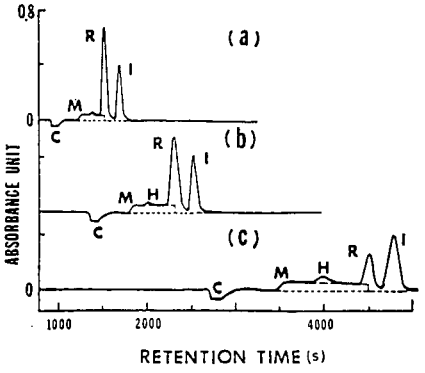

Fig. 7. Series of liquid chromatograms for the $TCTPCl_2$ esterification reaction catalyzed by 0.0075 *M* pyridine–0.123 *M* tetrahydrofuran (THF) in methanol at 35°C. R = reactant ($TCTPCl_2$); M = intermediate product (pyridinium, Cl-TCTP); H = half-ester impurity (methyl, Cl-TCTP); I = inert (1-phenylheptane); C = catalyst vacancy peak (pyridine). Flow-rate: (a) 0.32; (b) 0.21; (c) 0.11 cm^3/min [98]. Reproduced with permission.

(c) even if reverse reaction were to take place later in the column, any change would affect other parts of the chromatogram. With reacted material removed from the original eluting reactant peak, forward kinetic rates can still be ascertained.

As explained earlier, k_{app} can be calculated from eqn. 3 based on information obtained from Fig. 7; then, with a knowledge of k_m, it is possible to evaluate k_s using eqn. 4. Although k_m is usually measured from batch reactor information, a novel reactor configuration recently has been applied to the evaluation of rate constants in both phases simultaneously [98,132]. In this arrangement, a liquid chromatographic reactor was modified to incorporate a void column between two packed columns (Fig. 8). By simply varying the void-column size and the eluent flow-rate, which resulted in simultaneous changes of reactant residence (reaction) times in both mobile and stationary phases, rate constants in each phase could be determined through least-squares fitting of the following equation:

$$\frac{A_p + A_v}{A_I} = C_1 - C_2 \exp\left[-(k_{m,v}t_v + k_{m,c}t_m + k_s t_s)\right] \quad (17)$$

where A_p, A_v and A_I are the peak area of product, void product formation and inert standard, respectively, $k_{m,v}$ and $k_{m,c}$ represent the mobile phase rate constant in the void and packed column sections, t_v is the residence time in the void column and C_1 and C_2 are empirical constants [98,133]. A distinction between $k_{m,v}$ and $k_{m,c}$ can be used to examine the effects of liquid flow patterns on the rate of product formation. Another application of this type of approach to detect any inadvertent void zones and heterogeneities in a chromatographic column has been described [134].

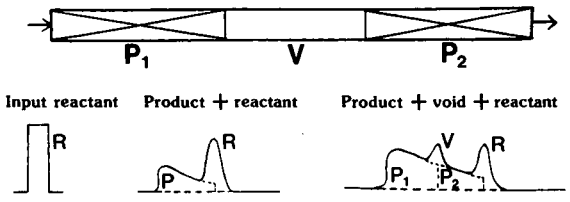

Fig. 8. Illustration of reaction chromatograms in the single void column (P_1–V–P_2) chromatographic reactor array [132]. In the void section, product (V) is formed and remains with reactant. It is separated from the reactant peak and superimposed on the product wave in the next packed column (P_2).

Additional potential for the use of chemically bonded liquid chromatographic reactors for kinetic studies was recognized by other researchers simultaneously with the investigations described above. Some interest arose through the observation of unexpected multiple peaks resulting from on-column reactions during chromatography. Special concerns emerged from studies on interactions between biochemical eluites and packing materials and possible adverse effects. These types of studies have provided *in situ* kinetic information about complex solute–surface interactions, which are otherwise difficult to obtain independently.

The examination of the reactive behaviors of proteins during separation in reversed-phase liquid chromatography by Karger and co-workers is a good example. Kinetics related to the unfolding of papain, soybean trypsin inhibitor (STI) and lysozyme on a hydrophobic *n*-butyl-bonded silica gel surface were studied [18,19]. The denaturation rate was estimated from the measurement of remaining native protein peak area relative to the "incubation" (reaction) time the species resided on the bonded-phase surface (Fig. 9). The suggested mechanistic model for the on-column unfolding process included two steps, one occurring rapidly upon contact of

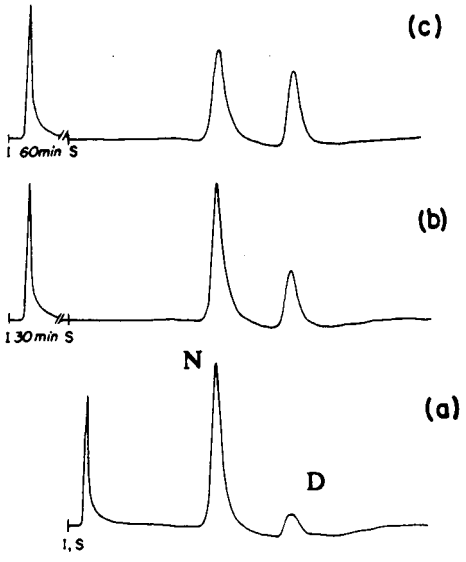

Fig. 9. Chromatographic behavior of papain as a function of on-column incubation time at mobile phase composition of 1-propanol–water (5.4:95.6, v/v) in which the total H_3PO_4 concentration is 10 m*M*. N = native peak; D = denatured papain peak. Conditions: column, C_4 bonded phase on 10-μm LiChrospher SI-500; gradient rate, 3% propanol/min, 15-min linear gradient; flow-rate, 1 ml/min; sample, 20 mg/ml papain, 6 μl injected; detection at 280 nm; column temperature, 5°C. I = Injection time; S = start of gradient. Incubation times: (a) 0; (b) 30; (c) 60 min. (From Ref. 18; reproduced with permission.)

proteins with the stationary phase and the other being a slow denaturation step.

More recently, intrinsic fluorescence has been used with liquid chromatography by Karger's group [114,115] to study the surface dynamics of proteins in contact with hydrophobic silica adsorbents. Grinberg *et al.* [135] have also reported another means beyond conformational changes by which multiple peaks arise. These were a result of protein aggregation during hydrophobic interaction chromatography of β-lactoglobulin A. Hearn *et al.* [136] have illustrated the application of (second) derivative spectroscopy and multi-wavelength detection for monitoring stationary phase-induced and/or mobile phase-mediated effects on protein conformational changes during reversed-phase and size-exclusion liquid chromatographic separation. In these types of kinetic studies, the flow was often interrupted and the eluite immobilized by mobile phase compositional changes to increase the chromatographic dwell ("incubation" or residence time in the column), followed by gradient elution (Fig. 9). Consequently, the reaction proceeded considerably further and the separation of products from reactants was also facilitated. This type of immobilization–gradient flow operation is in principle similar to the "stopped-flow" technique first suggested by Phillips *et al.* [36], which increased the residence time in a localized portion of the column. It is also used in the work of Jaeger and co-workers [40,41] described later.

Another early identification of solute–stationary phase interaction can be found in the study by Huang *et al.* of on-column redox reactions of methoxy-substituted hydroquinones and benzoquinones during reversed-phase chromatography [116]. They found that metal-catalyzed heterogeneous reactions that followed Langmuir–Hinshelwood kinetics occurred at the stationary phase surface. Good evidence that metal ions were acting as active catalytic sites on silica surfaces was also found in the investigation by Cramer *et al.* [137] of complexing reactions of deferoxamine in a similar chromatographic system. The use of probe reactions in liquid chromatographic columns as a diagnostic tool to study the stability of packing materials as well as the medium will probably expand in the future as HPLC is applied more frequently for specialized separations. This concept has been used with columns in connection with adsorption [128], ion-exchange [138] and ion-exclusion [139] chromatography and with preparative columns [140].

3.3. Interconversions and fast equilibria studies

Klinkenberg [64] and Keller and Giddings [46] very early recognized and attempted to analyze chromatographic profiles involving a first-order reversible reaction system where reaction rates are on about the same time scale as the column separation process. A hypothetical chromatogram for a mixture of interconverting species (R $\rightleftharpoons$ P) to simulate the situation is shown in Fig. 10. Here, an interference regime at the depression in the chromatogram where R and P are indistinguishable is the result of some conversion of each of the two species to the other in the course of passage through the column. Separation can be improved where the rate of the overall chromatographic process can be increased relative to the reaction process. This is illustrated in Fig. 11, where a simple *syn–anti*

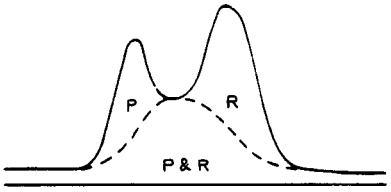

Fig. 10. Hypothetical chromatogram expected for a reversible first-order reaction R⇌P where reaction rates are commensurate with separation processes.

acetaldoxime ($CH_3C=NOH$) interconversion in polyethylene glycol was involved in the work by Yurchak and co-workers [47,141]. The separation of *syn* and *anti* forms was enhanced by effectively lowering the interconversion rate (by decreasing the temperature) and increasing the flow-rate (decreasing the reaction time). By controlling liquid chromatographic operating parameters such as flow-rate, temperature or mobile phase composition and pH with similar considerations, optimum conditions can be identified to achieve improved separations of rapidly interconverting species.

HPLC columns have now been applied as reactors a number of times with increasing understanding to study the kinetics of fast equilibria involving in isomerization, enantiomerization and intramolecular bond rotation [20–24,93,106]. A study by Melander *et al.* [142] reported peak splitting of proline-containing dipeptides in reversed-phase octadecylsilane (ODS) columns. This phenomenon was a result of the slow kinetics of *cis–trans* isomerization which were commensurate with the chromatographic separation process itself. Lowering the pH, increasing the temperature and decreasing the flow-rate all reduced peak splitting as the isomerization rate became fast relative to the separation rate in each instance. These results provide chromatographers and others with useful guidelines for optimizing isomer separations and have stimulated a number of subsequent studies. Lebl and Gut observed a similar plateau region between peaks for α- and β-anomers in the separation of muramyldipeptides in an ODS column [119]. Interconversion rate constants were determined using two experiments; however, these analyses may well have been oversimplified as no distinction was made between reactions occurring in the mobile phase and those occurring in the stationary phase as represented in the following simplified general scheme:

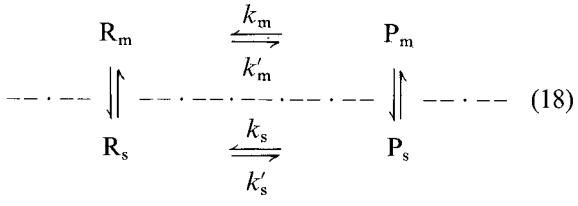

(18)

Additional studies of *cis–trans* proline isomerization in reversed-phase columns used as chromatographic reactors were reported later by Horváth and co-workers. Dynamic effects resulting from the simultaneous chromatographic movement and first-order reversible reactions in both phases as shown in eqn. 18 were investigated for a linear, ideal case by Melander *et al.* [20]. The dimensionless Damköhler number ($Da = kL/u_0$), representative of the ratio of time constants for bulk mass transport and chemical reaction, was used as a measure of the relative importance of these two competitive processes. The dependence of chromatographic profiles on the Damköhler number showed that the interplay of on-column reaction and chromatographic retention is important only in the range $10^{-3} < Da < 10^3$ in their study. In the limit of *Da* equal to zero, *i.e.*, no interconversion between the two isomers, a complete separation was obtained. At a sufficiently high *Da* value, the interconversion was so fast that no separation occurred and the two isomers eluted as a single merged peak (*e.g.*, see Fig. 11c). Expressions for the first and second moments of the elution profiles were also obtained as a function of *Da*.

Later, the first absolute moment (center of mass) and the second central moment (variance) of the entire concentration profile were measured experimentally during *cis–trans* proline isomerization in an ODS column using a phosphate-buffered aqueous mobile phase [21]. The forward and reverse

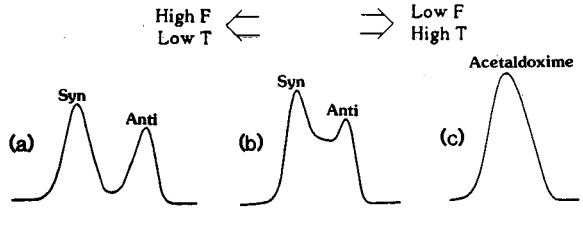

Fig. 11. Reactor chromatograms for reversible interconversion of *syn*- and *anti*-acetaldoxime [141]. T = temperature; F = flow-rate.

interconversion rate constants in the stationary phase could then be calculated. Because the estimated rate constant values in the stationary phase were higher than those in solution, it was suggested that the hydrocarbonaceous-bonded silica surface possessed special catalytic properties for the isomerization. Two recent papers by Hanai and coworkers have discussed an "elution-band relaxation method" to evaluate reversible isomerization kinetics in a linear, ideal liquid chromatographic reactor [93,106]. The theoretical approach was very similar to that of Melander *et al.* [20] and two reactions, denaturation–renaturation of ribonuclease A (RNase A) and *cis–trans* isomerization of proline, were examined experimentally. Plots of the measured first moment for the overall chromatographic profile of the two isomers *versus* inverse flow-rate were fitted with a least-squares analysis to give the "apparent" rate constants for the column.

Interconversion phenomena of the type discussed above have often been observed during separations of biomolecules. For example, Parente and Wetlaufer reported the reversible urea–thermal denaturation of α-chymotrypsinogen-A during ion-exchange chromatography [138]. Karger's group also studied unfolding–refolding effects in reversed-phase liquid chromatography of RNase A where reversible conformational kinetics occurred since the relaxation time for RNase A refolding was comparable to its mobile phase residence time [117,118]. The protein was denatured on adsorption in the bonded phase, and the reversible renaturation took place in the mobile phase in the course of elution down the column. In addition to flow and temperature variations, salt type and mobile phase composition have also been used as operating parameters to optimize chromatographic separations. These and other variables such as stationary phase hydrophobicity [143] and the presence of trace metals [116,137,144] are all important factors to consider when one attempts to understand and control conformational changes of complicated systems of this type during liquid chromatography. Hearn *et al.* have provided an excellent analysis and discussion on general systems involving polypeptides and proteins which undergo conformational changes in both mobile and stationary phases [24]. The observed multi-zoning phenomena can be traced to multi-phasic transitions of proteins during chromatography.

The advantages in understanding and elucidating these types of complicated kinetic effects in the LCR can be appreciated further by reviewing the interesting early work on separations of interconverting isomers at low temperatures in liquid chromatographic columns by Moriyasu and co-workers [120–122,145,146]. As indicated above, a similar approach had been applied in gas chromatography to study the dynamic isomer interconversion process [47,48,81,141]. The classical problem of interconverting dynamics was re-examined with modern liquid chromatography to measure some rates for reactions such as mutarotation [120], keto–enol interconversion [145], and intramolecular bond rotation [22,23,121,122]. In most experiments, the chromatographic systems were operated at unusually low temperatures to slow reactions and overcome the competition from fast interconversion so that the separation of the interconverting isomers could be achieved (*cf.*, Fig. 11). Only later was there an appreciation of complications from the catalytic effects of the acidic modifier (acetic acid) in the mobile phase and acidic groups on some silica packings. With appropriate changes in bonded columns and a more neutral mobile phase, they were able to raise the operating temperatures for isomer separation considerably [146]. Nevertheless, low-temperature LC operation was shown to offer advantages in the study of labile species and fast reactions [147,148]. Although lowering temperature gives some anticipated unfavorable effects on chromatographic efficiency because of slower mass transfer and adsorption kinetics, chemical kinetic effects are still more pronounced because of the relatively higher activation energy of the interconversion reactions.

Related to the above applications are chromatographic studies of secondary chemical equilibria in modern liquid chromatography. Examples of secondary chemical equilibria, in addition to the interconversions discussed above, include acid–base equilibria, ion pairing, complexation and solute–micelle interactions [10]. Liquid chromatography has made it possible to achieve some separations that are otherwise impossible. Several general reviews are available for discussion of physico-chemical aspects of these operations [9,149–151]. In general, few results for kinetic studies of secondary chemical equilibria occurring in liquid columns,

with the exception of interconversions, are available [46,49,149,152]. Hence the potential for applying the LCR to obtaining kinetic data for secondary chemical equilibria and the use of these phenomena with the LCR still await further exploration.

In this section, we illustrated applications of liquid chromatographic reactors to chemical kinetic studies of various types of reactions, such as reversible isomerizations and interconversions and also irreversible solvolyses and surface-catalyzed reactions. Whereas many theoretical solutions for problems in liquid chromatographic reactors have been obtained and some are described in Section 2, fewer experimental applications have been described in the literature. Moreover, assumptions of ideality and/or linearity have usually been used and distinctions between reaction rates in the mobile and stationary phases have sometimes not been addressed. Therefore, more detailed studies of the application of LCR systems to both irreversible and reversible reactions of different complexities are desirable and can be anticipated. Pertinent to this, a brief discussion of complications in LCR systems used for chemical kinetic studies which can originate with other dynamic processes is presented below.

4. KINETIC PROCESSES RELATED TO LCR APPLICATIONS

As indicated earlier, in addition to simple chemical reactions, other types of kinetic processes occurring in columns play important roles in studies of liquid chromatographic reactors. These include axial dispersion, interfacial mass transfer, intraparticle diffusion and sorption–desorption (Fig. 4). Where the rates of these processes are commensurate with chemical reaction rates, LCR systems can no longer be treated as ideal. As these phenomena can be complicated, only a limited number of examples can be examined here to illustrate the approach and the importance of careful analysis of non-ideal LCR systems. Also included in this section is a discussion of association–dissociation phenomena in liquid affinity chromatography. Although no net reaction occurs in most affinity columns, some relevant studies are reviewed below where the results indicate useful implications for non-ideal LCR systems.

4.1. Dynamic processes leading to non-ideal behavior

The development of the Van Deemter equation in 1956 [153] was the foremost, early systematic study of band broadening resulting from dynamic processes such as eddy diffusion, axial molecular diffusion and mass transfer. Subsequently, it has been extensively studied and modified, with consideration of processes such as surface diffusion and adsorption–desorption kinetics to provide better descriptions under various column operating conditions, by the groups of Giddings, Knox, Huber and Purnell, among others [52–54,154]. Recent views of band broadening mechanisms resulting from kinetic processes have been presented by other investigators (*e.g.*, [55,56,155,156]).

Band broadening observed in post-column reaction detectors in liquid chromatography is the result of a combination of contributions from normal spreading processes and chemical reaction. Nondek *et al.* [92,157] described reactor band broadening for a first-order, irreversible reaction. The Gaussian component of band broadening was distinguished from reaction broadening so that the results produced a quantitative relationship between the rate constant and the variance from reaction broadening. The influences of flow velocity, mobile phase composition and reaction temperature on band broadening from reaction were also examined to determine the optimum reactor operating conditions using carbamate hydrolysis catalyzed by a basic ion exchanger as a model reaction [157]. Shih and Carr also discussed a strategy for minimization of band broadening in post-column reactors which resulted from the presence of both dispersion and chemical reaction [158]. An approach to flow-rate and reactor size optimization was described to obtain sensitive reactor–detector performance.

Marshall *et al.* studied the contribution of sorption–desorption kinetics to band broadening in an octadecylsilica ion-pairing liquid chromatographic system [159]. The dynamics of sorption–desorption on several modified silica surfaces in liquid suspension were measured with experiments outside the column using a pressure-jump relaxation method. The results indicated that this process plays a significant role in the stationary phase performance. Higher column efficiencies were usually found with columns containing materials where relatively rapid sorption–desorption equilibration processes occur-

red. More recently, Lin and Ma studied the effects of pore diffusion and adsorption with both microporous and macroporous adsorbents in liquid chromatographic columns [160]. Adsorption importance relative to pore diffusion was found to be a function of adsorbent pore size. Their results indicated that both processes were important in describing macroporous adsorbents such as activated alumina, while a pore diffusion model was adequate for microporous silicalite adsorbents.

Conclusions from the studies described above should be applied with care to chromatographic reactor systems as the experiments were performed under conditions where no chemical reaction was occurring. Of course, studies of mass transfer and kinetic effects in the LCR have been limited since *in situ* estimations of transport and kinetic parameters become more elusive when these measurements are coupled with chemical reactions. Suzuki and Smith first examined moment solutions for a first-order surface reaction occurring in a chromatographic system in the presence of some non-ideal processes [50,73]. Wetherold *et al.* [25] and Cho *et al.* [26,27] modified the ideal reactor model by simulating axial dispersion effects to improve descriptions of experimental elution curves.

Recently, mass transfer effects on reaction rate evaluations in liquid chromatographic reactors were systematically examined in our group [58]; included were longitudinal diffusion, intraparticle diffusion and interfacial sorption–desorption. On applying some criteria based on dimensional analysis to recognize the onset of such effects, it was concluded that none of these processes significantly affected reaction kinetic measurements in the $TCTPCl_2$ solvolysis reaction study mentioned earlier. These criteria were used again with the iron-catalyzed hydroquinone oxidation in silica columns with similar conclusions, except that it was found that adsorption and desorption processes could exert some influence on the evaluation of intrinsic kinetics because of the adsorptive nature of the stationary silica bed [59]. A better fit of the kinetic data was obtained when the ideal reactor model was altered to incorporate consideration of finite adsorption kinetics to describe the LCR system. The approaches described here and other more advanced efforts to examine the significance of non-ideal processes relative to chemical reaction are likely to contribute to the future understanding and identification of governing dynamics in chromatographic reactor systems.

4.2. Association–dissociation kinetics and affinity chromatography

Miyawaki *et al.* [161] have described an interesting variation in the application of the chromatographic reactor concept with affinity chromatography. In contrast to most chromatographic reactor applications where reactants or products are adsorbed in the column, the design of their affinity chromatographic reactor took advantage of the strong retention of a cofactor which is a part of the biocatalyst system. Pyruvate and ethanol substrates for lactate production were supplied continuously into a hollow-fiber capillary reactor with an immobilized enzyme system of alcohol and lactate dehydrogenases, while the necessary cofactor, NAD, was supplied as a periodic pulse. The strong affinity of the cofactor for the immobilized enzyme led to NAD pulse retention times which were considerably longer than those of substrates or products. The consequence was very high cofactor turnover numbers. Further, the pulsing cofactor mode facilitated the recovery of expensive NAD, avoiding the instability and control problems of an alternative method where chemically modified NAD was bound and co-immobilized with the enzymes in a membrane reactor.

Association and dissociation dynamics involving solutes and ligands in affinity chromatography also might be considered illustrative of chemical kinetics occurring in the column. While such kinetics are pertinent, it can be noted again that they do not generally result in a net chemical change for the solute in the course of column passage. In 1975, Denizot and Delaage [88] developed a statistical treatment of affinity chromatography, based on the random walk model of Giddings and Eyring [107], to determine the rate constants for association and dissociation reactions involved in separations. Later, Weiss discussed the limitations of this approach for multiple binding sites [162]. In 1978, Horváth and Lin [56] developed a plate-height method for evaluating the association and dissociation kinetics for eluite molecules and the stationary phase in liquid chromatography. Hethcote and co-workers also presented a complete statistical

moment model for affinity chromatography which incorporated both physical and association kinetics [91,163,164]. These fundamental studies have accelerated applications of modern affinity chromatography to kinetic studies. One example is zone-interference chromatography based on the application of stochastic theory to the behavior of solute molecules to determine macromolecular kinetic constants [165].

Muller and Carr applied the theory developed by Horváth and Lin to study some thermodynamic and kinetic characteristics of the interaction between sugar eluites and silica-bound concanavalin A (Con A), a biospecific adsorbent in high-performance liquid affinity chromatography [166,167]. They showed that the observed large plate heights mainly resulted from the sluggish chemical kinetics of the Con A–sugar interaction rather than other mass transfer terms. It was also found that at high sugar concentrations the predominant effect on plate height was isotherm non-linearity [167]; however, no satisfactory quantitative plate theory was available to treat this effect. Subsequently, Anderson and Walters, studying a similar system [168], proposed that diffusion contributions could be larger than indicated by Muller and Carr. Moore and Walters also described a peak-decay method to determine the dissociation rate constant from the slope of the logarithm of the peak tailing response in affinity chromatography [169]. This approach was verified experimentally in the Con A–sugar system with addition of a competitive absorbate (mannose) to prevent re-association.

An interesting "split peak" phenomenon often observed in affinity chromatography has also been utilized in kinetic studies. First predicted by Giddings and Eyring in 1955 [107], the split-peak behavior of a single solute is characterized by a non-retaining peak and a strongly retained peak. This usually undesirable artifact is caused by slow adsorption kinetics or mass transfer of large molecules, and should not be confused with the peak splitting observed in the separation of interconverting species discussed earlier. The phenomenon was used to advantage in the evaluation of rate constants for the antibody–antigen complex formation reaction by Sportsman *et al.* [170]. Later, the theory was expanded by Walters and co-workers to systems where either slow diffusion or adsorption was rate-limiting [171,172]. Non-linear elution effects on measurements of diffusional and adsorption parameters resulting from large sample loads in split-peak chromatography also have been discussed recently [173,174].

Effects of non-linear isotherms on affinity chromatography performance have also received the attention. Chase used a non-linear, sorption rate-limited model to predict breakthrough curves in frontal analysis during preparative affinity chromatography and was able to measure binding kinetics for some biological macromolecular systems [112]. Arnold and Blanch developed a non-linear theory that allowed the effect of mass transfer to be separated from binding kinetics in both zonal and frontal affinity chromatography [94]. Later, Wade *et al.* [175] developed an impulse input method for making physico-chemical measurements in non-linear systems with some advantages over the above methods and discussed implications for the design of preparative-scale operations. With increasing interest in using affinity chromatography for preparative purposes, non-linear effects are likely to receive still more attention in the future.

5. SPECIAL APPROACHES AND APPLICATIONS

Liquid chromatographic features, including the capacity for handling heat-sensitive and non-volatile compounds which led to its widespread application, also make the development and understanding of liquid chromatographic reactors highly attractive. A number of kinetic applications of liquid chromatographic reactors and some of the complexity have already been addressed above. Thus, we see that direct and some indirect information on chemical reactions as well as other associated rate processes can frequently be extracted from reaction chromatograms.

Perhaps the most important conclusion from the work above is that the liquid chromatographic reactor is useful and operable but requires more extensive scrutiny and treatment in many instances than might be obvious at first glance. While implementations for chemical kinetic studies has been proven feasible, LCR systems also can be applied with advantage to other aspects of column operations such as characterizing the stationary phase bed or improving reactivity and/or selectivity for reac-

tions occurring in columns. LCR-type operations might well be feasible now for some preparative purposes. Some of these possibilities are developed further below to demonstrate the potential information available from LCR operations.

5.1. Characterization of column beds

Earlier, we alluded to the use of a chemical tracer method by Deans and co-workers [34,35] to determine residual oil saturation in reservoirs. The approach resembles the use of a liquid chromatographic reactor for characterizing a stationary bed, with flowing water funtioning as a mobile phase and the oil bed in porous strata serving as the stationary phase. Reactant tracer, ethyl acetate, was introduced as pulses into wells where unknown amounts of residual oils existed in the porous rock structure. The well was then sealed to allow some portion of the tracer to hydrolyze to form ethanol, the product reference material. While ethyl acetate is soluble in both water and oil phases, ethanol is most soluble in the water phase. Thus, on reversal of flow in the oil bed, the ethanol reached the well head first as it was retained significantly less within the oil phase than the unreacted ethyl acetate tracer. The difference in arrival times to the well head could then be correlated with residence in the oil phase and serve to measure the extent of residual oil saturation in the rock.

In Section 3, we introduced a few examples of surface-catalyzed liquid chromatographic reactions. The work of Karger, Horváth and others [18–24,116,137] has indicated further possibilities for stationary phase characterization and column design. In much of this work, increased reaction rates are a result of stationary phase surface activities. From the types and extent of reactions involved, one can characterize the catalytic nature of the column beds, *e.g.*, surface hydrophobicity [18,19,21,24,143], hydrogen bonding or acidic groups on silica surfaces [22,23,145,146], and metal ions associated with packing material or leached from the stainless-steel components of an HPLC system [116,128,137,144]. On the other hand, when reactions can occur in both homogeneously mobile and stationary phases, there are possibilities for determining the stationary phase composition through interpretation of kinetic data, as shown by Chu, Langer and co-workers in the course of characterizing a chemically bonded stationary phase with LCR reaction kinetics [16,17,130,176]. Thus, the kinetic data become tools for obtaining further information on the reaction environment rather than an end in themselves.

The statements above can probably best be understood by turning to an interpretation of reactor chromatograms with an octadecylsilyl phase (ODS, C_{18}) such as those in Fig. 7 together with eqn. 3. Our earlier study of $TCTPCl_2$ kinetics showed that the presence of methanol was required for initial reaction to form the quaternary salt intermediate, M [129]. Using the assumption that reaction occurred only in the methanolic mobile phase, calculated on-column solvolysis rates were found to be *ca.* 30% higher than those measured in bulk methanol [16]. The discrepancy could be explained by taking into account the possibility that reaction takes place in the stationary phase also with some associated methanol playing a role. A stationary phase rate constant, k_s, can be calculated from eqn. 4; this value is then compared with those estimated on the basis of two different bonded stationary phase models involving methanol and hydrocarbon ligands to gain information about the chemically derivatized phase.

With the methanol mobile phases employed in our work, one can consider two scenarios [17]: (1) solute molecules interact with an associated methanol "pseudo-layer" without the direct participation of the underlying hydrocarbon ligands [4] (model I); and (2) solute molecules interact with methanolic sheathed bonded hydrocarbon ligands, the sheaths being held by a dispersion type of interaction [6] (model II). The situation is broadly represented in Fig. 12. A stationary phase rate constant value can be calculated for each model for comparison with that obtained from experiments. The observed rates based on the chromatographic reactor results generally tended towards model II, although not completely. One can conclude that the "pseudo-phase" was of a composite type with contributions from both models I and II [17,176]. The approach outlined above, then, is illustrative of how reaction kinetic data can supplement spectroscopic and retention studies and contribute to elucidating the nature of the stationary phase atmosphere, and thus proposed retention mechanisms, in chemically bonded chromatographic systems.

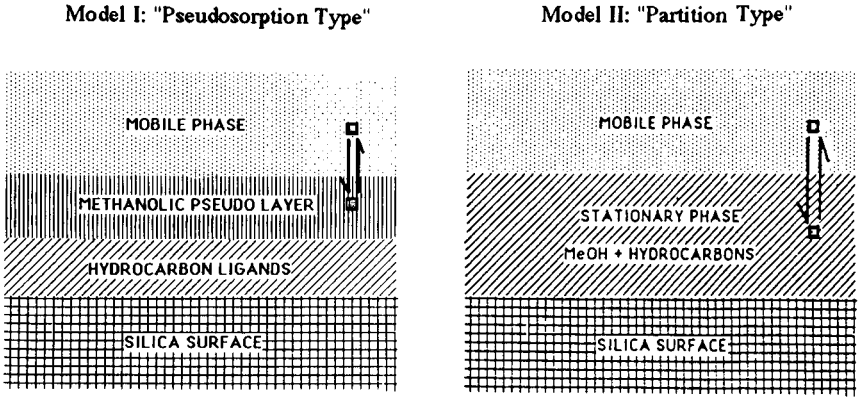

Fig. 12. Models for molecular retention in reversed-phase liquid chromatography with methanol solvent and hydrocarbon ligands. ◘ = Solute molecules [176].

Related to the above study is a determination of the phase ratio in bonded-phase liquid chromatographic systems. This determination is elusive owing to the nature of the composite chemically derivatized stationary phase, modelled above, and problems in interpreting solute retention behavior. The phase ratio (φ) for a column is defined as V_s/V_m, where V_s and V_m are the stationary phase and mobile phase volumes, respectively. Because the boundary between these two phases in bonded-type chromatography is often ill-defined and dependent on mobile phase composition, phase ratio determinations have been limited. Continuing the above study, an equation was derived to obtain a value for the phase ratio of the chemically bonded ODS system on the basis of measured LCR kinetics [130]. Thus,

$$\varphi = \sqrt{\frac{k_c' \; k_m}{k_s} \; \frac{V_{s,CH_3OH}}{V_m}} \tag{19}$$

where k_c' is the catalyst capacity factor and V_{s,CH_3OH} is the volume of associated methanol pseudo-layer which is determined from an adsorption isotherm experiment. With known kinetic data for both phases, the phase ratio can be determined. Then, solute retention can be treated on a quantitative basis in the chemically bonded chromatographic system.

The approach utilizing LCR kinetics as described above is an operational one. The calculated phase-ratio values were fairly consistent for different catalyst solutes (pyridine or picoline). Although this result might seem satisfying, it is desirable to carry out additional measurements using other reaction kinetics. Such agreement is required if this method is to be utilized in the future with confidence. Most important here, however, is noting how simple LCR kinetic experiments can provide a basis for interpreting stationary phase characteristics.

5.2. Modifications of reactivity and selectivity

The potential for using chromatographic reactors to enhance both production and selectivity during chemical reactions has created further interest. In principle, the operation is advantageous only for certain reaction systems. In the case of reversible reactions such as $A \rightleftharpoons B + C$ or $A + E \rightleftharpoons R + S$, the reactant conversion can be driven well beyond equilibrium conversion limits of conventional reactors because the possibilities for reverse reactions are minimized through product separation or removal. Some applications have been reviewed by Villermaux [51]. Examples pertaining to liquid chromatographic reactors [25–29] already have been discussed.

Chromatographic reactor operation can also be employed advantageously for reactant conversions where consecutive reactions are involved. For instance, if we consider

$$R \xrightarrow{+B,k_1} M \xrightarrow{+B,k_2} N \tag{20}$$

the goal might well be to improve the yield of intermediate species, M. Indeed, it has been shown that the selectivity and yield of intermediate products for consecutive reactions can be improved in

pulse or moving-bed chromatographic reactors compared with fixed-bed reactors [79,95,177]. Further, intermediates can be recovered with enhanced purity because of the chromatographic separation features involved in intermediate removal with retardation of reactant in the column. One example is in the sequence of reactions for catalyzed $TCTPCl_2$ solvolysis shown in Fig. 6; here, the early elution of the first intermediate, pyridinium, Cl-TCTP (M), eliminates the possibility of further reaction to other products in the column (Fig. 7). On the other hand, the pulsed chromatographic reactor may not be adequate for separating M from B effectively to give yield improvement unless R and B are eluted at the same time [30,51,95].

For other irreversible reactions operating in chromatographic reactors, the separation features above normally give no advantage for achieving higher production. For slow reactions, enhancement of conversion can be achieved through increase of reactant contact time with catalysts in the reactor bed. This effectively lengthens the column to provide increased volume for reactions. An example of utilizing this concept in LCR operation is the affinity chromatographic reactor of Miyawaki *et al.* [161] reviewed earlier, where the high catalyst turnover was a result of relatively selective retention of the cofactor on the immobilized enzyme. The stopped-flow technique adapted for measurements of slow kinetics as mentioned earlier also has potential for enhancing reaction productivity, especially in the LCR because sample dispersion during the stopped-flow interval is minimal in liquids [178]. For example, a chromatographic stopped-flow method combined with varying eluent strength was used to overcome the slow dissociation kinetics of the sugar–Con A complex [38]. This resulted in a larger peak area (*i.e.*, fractional recovery) and diminished peak tailing.

Beyond the utilization of some special concerted separation and reaction features, reactivity and/or selectivity in chromatographic reactors can be enhanced through modification of stationary phase properties. Whereas LCR applications to heterogeneous catalysis are conceptually simple and have ample precedent, the utilization of interfacial hydrophobic and hydrophilic properties to enhance the reactivity and selectivity of liquid chromatographic reactions is more complex and less familiar at present. For slow biphase reactions involving miscibility problems between organic substrates and water-soluble reagents, there is the possibility of altering reactivity and selectivity in designed chromatographic reactors through utilization of the principles of phase-transfer catalysis or the action of surface-active agents. This can be illustrated by the work of Tanaka *et al.* [179] and Jaeger and co-workers [40,41] described below on reactions which are interfacial in nature and involve both organic and aqueous species.

The utilization of interfacial properties in HPLC was first directed toward strengthening its separation potential, as with most other aspects of HPLC development. One prominent example involved the application of micellar liquid chromatography [10]. The potential for utilizing associated principles for enhancing reactivity and/or selectivity of reactions in HPLC columns was described first by Tanaka *et al.* in 1984 [179]. Two nucleophilic displacement reactions were studied at phase boundaries between an aqueous nucleophile (sodium iodide or sodium acetate) and an alkyl halide (*n*-octyl bromide or benzyl chloride) associated with alkylsilylated silica surfaces through hydrophobic interactions. Higher reaction rates and improved selectivity for product formation resulted from using immobilized organic phases in the column, as compared with reacting the halides in a conventional liquid–liquid biphase system. The results suggested that the nucleophilic displacement reactions involved took place at the interface.

Other selectivity studies of liquid chromatographic reactions with polymer-based reversed-phase columns have been reported by Jaeger and co-workers on several occasions. For reactions of compounds with similar intrinsic reactivity (in solution) but different relative hydrophilic/lipophilic character, reaction selectivity could be altered using interrupted flow procedures involving adsorption followed by selective reaction on desorption. For chlorination of *n*-alkyl phenyl ethers, for example, the ether reactant was first introduced and immobilized on a C_{18} column; on introduction of a chlorine–water mobile phase followed by acetonitrile–water gradient elution, selective chlorination favoring *para* over *ortho* positions was observed [40]. The organic-bonded phase and/or the bonded phase–aqueous mobile phase interface were hypothesized to be the

reactive environment and critical to determining the observed selectivity. Another variation of this approach involving an ionic, inorganic reagent reacting with competitive organic substrates was demonstrated in a study of base-catalyzed hydrolyses of *p*-nitrophenyl esters [41]. In the procedure, acetate and hexanoate esters were adsorbed on polystyrene–divinylbenzene-type packings. This was followed by aqueous base, mobile phase treatment and acetonitrile gradient elution. Saponification of the acetate ester was favored relative to the hexanoate, presumably because of the order of desorption of these materials. This type of selectivity was less pronounced at lower ratios of acetonitrile to water where retention differences between the two ester substrates were less pronounced. From the above discussion, it can be seen that there are opportunities for the development of selective reaction schemes here for the small-scale preparation of valuable materials and for reaction of compounds present in trace amounts in the mobile phase.

5.3. Large-scale application

The actual use of an LCR on a production scale has been addressed only recently and is still in an early stage of development. Where an aqueous mobile phase can be employed some procedures already look attractive. Examples from earlier papers [25–30] addressed situations where enhanced product yield for reversible reactions was a major concern. As explained earlier, applications of the LCR are also compatible with a strategy for improving the yields of intermediates where sequential reactions are involved through selective elution. The potential for reduction of downstream purification costs where the LCR is applied is another positive aspect where economics are important. With these features, the chromatographic reactor becomes a prominent candidate for consideration when significant production of costly chemicals involves either reversible or consecutive reactions [51]. For example, Schweich and Villermaux carried out a feasibility study of preparative chromatographic reactors in 1982 [30]. In evaluating their potential, they concluded that broad injections and poor column efficiency were tolerable and that chemical kinetic rate limitations were probably the most important hindrance to efficient chromatographic reactor utilization. Further, they emphasized that extent of reaction with the separation feature, beyond mere conversion alone, is important for an LCR operation to become attractive. A major trend in adapting chromatographic reactor strategies has involved studies of possibilities for using rotating annular beds or moving beds to provide what is effectively continuous chromatographic reactor operations [26,27,74,83,84].

Only a few LCR-type preparative applications of practical industrial interest have been seriously considered. One is a process for producing a high-fructose syrup from glucose reported by Hashimoto *et al.* [31]. A series of stationary immobilized glucose isomerase reactors were arranged alternately with Y zeolite adsorption columns in an array where the inlets were continuously advanced. As all other inlets and outlets were fixed, the columns selectively adsorbed fructose to simulate continuous countercurrent contact of the liquid stream with the stationary bed without actual movement of the solid adsorbent. This process tends to consume less desorbing material than processes involving a separate reactor coupled with either fixed-bed or moving-bed adsorbers, while producing an aqueous syrup with a 45–65% fructose content.

The biosynthesis of a dextran polymer of higher molecular weight from sucrose has been studied recently in a chromatographic reactor by Zafar and Barker [32]. The byproduct, fructose, was retarded through complexation with the calcium ions of the immobilized resin, while the desired dextran product and the sucrose substrate were size excluded and eluted in order. Owing to the substantial denaturation rates of the dextransucrase catalyst, it was necessary to add enzyme continuously to the mobile phase, thus increasing production costs. The separation of the reaction mixture components, however, can result in downstream product purification cost savings while facilitating reactant recycling. Recently, Barker and Ganetsos prepared a stimulating review describing some principles and identifying some potential applications of the LCR in biotechnology [33].

As non-linear and non-ideal processes may not be important in obtaining analytical-scale data, such data cannot be used with confidence for predicting the performance of a preparative chromatographic reactor during scale-up [109–111,178]. Experience together with the elucidation and understanding of

important features of liquid chromatographic reactor operation as suggested here should help to solve the problem in many instances.

6. CONCLUSIONS

Starting with some well defined concepts and the ideal chromatographic reactor, we have seen how operational and equipment modifications can be made to encompass a range of applications, approaches and interfacial situations. Because of this range, only a few illustrative examples of the utilization of the liquid chromatographic reactor could be presented in each area. Earlier extensive gas chromatographic reactor studies helped accelerate applications of liquid chromatographic reactors. However, more complicated processes in the liquid system have often caused some difficulty when one wants to characterize reactor behavior. Further, there has been some compartmentalization of research in several areas so that related techniques have tended to be developed independently (*e.g.*, "stopped flow" and "surface incubation"). Therefore, knowledge of liquid chromatographic reactors compared with gas chromatographic reactors is less advanced at this time, so that further application and understanding emerge as a special challenge for the future. Interesting and attractive possibilities exist. We hope that this review will foster the more widespread use of the LCR in simple situations and improved integration of efforts from multifold investigations in more complex situations.

One unexploited area so far has been in large-scale LCR applications to the treatment and perhaps removal of undesirable materials. This could be from bulk chemicals, physiological fluids or the environment as a whole [41,45,180]. Up to now, the major contribution of chromatography to these types of problems has been as an analytical tool for the identification of undesired or dangerous species. Standard chemical treatments involving fixed-bed adsorbers and reactors have had only limited use for the removal or destruction of toxic materials where complete conversions or selectivity are desired. Alternative incineration techniques are expensive, sometimes difficult to operate and questionable for removing low concentrations of material from fluid wastes. In many situations, concentration of wastes is necessary before treatment and the separation of small amounts of materials from bulk non-toxic fluids can be difficult with high costs. Chromatographic reactors might be applied in a variety of ways to solve these problems. Providing the advantages of higher (sometimes 100%) product or intermediate yields in reversible or consecutive reactions and possibly lower separation costs with the development of large-scale operation, liquid chromatographic reactors can become an additional tool available to environmental engineers. This is particularly true where only a small amount of material must be removed from large amounts of bulk fluid or only limited chemical transformation is needed to detoxify or start the detoxification process.

Taking a wider view, we can recognize that we are dealing with the elucidation of broad, varied situations involving concerted reactions with separation during two-phase flow. This can cover many types of operations that range in scale and type from flow through capillary veins to subterranean terrestrial beds. The treatment of the phase boundary and surface variations and defining interfacial structure are problems in these areas as they are with liquid chromatographic reactors. Sometimes these or combinations of conditions can be altered to advantage to attain more insight or a particular conversion. Further research and advances with an integration of knowledge among investigators should be forthcoming and can be expected to be beneficial to progress in many areas.

7. ACKNOWLEDGEMENTS

We thank the United States Army Research Office for their support of this work. This review was initiated as a result of earlier suggestions and encouragement by Dr. Robert Shaw and Dr. Frank Paur of that office. We also appreciate many stimulating conversations with Dr. Alexander Chu and Mr. Brian S. Ludolph.

REFERENCES

1 D. C. Locke, *Adv. Chromatogr.*, 14 (1975) 87.
2 R. J. Laub and R. L. Pecsok, *Physicochemical Applications of Gas Chromatography*, Wiley, New York, 1978.
3 J. R. Conder and C. L. Young, *Physicochemical Measurements by Gas Chromatography*, Wiley, New York, 1979.
4 J. H. Knox and A. Pryde, *J. Chromatogr.*, 112 (1975) 171.

5 R. P. W. Scott and P. Kucera, *J. Chromatogr.*, 142 (1977) 213.
6 C. R. Yonker, T. A. Zwier and M. F. Burke, *J. Chromatogr.*, 241 (1982) 257 and 269.
7 P. Jandera, H. Colin and G. Guiochon, *Anal. Chem.*, 54 (1982) 435.
8 R. K. Gilpin, *J. Chromatogr. Sci.*, 22 (1984) 371.
9 W. R. Melander and Cs. Horváth, in Cs. Horváth (Editor), *High-Performance Liquid Chromatography —Advances and Perspectives*, Vol. 2, Academic Press, New York, 1980, p. 113.
10 J. G. Dorsey, J. P. Foley, W. T. Cooper, R. A. Barford and H. G. Barth, *Anal. Chem.*, 62 (1990) 324R.
11 W. K. Hall, D. S. MacIver and H. P. Weber, *Ind. Eng. Chem.*, 52 (1960) 421.
12 V. R. Choudhary and L. K. Doraiswamy, *Ind. Eng. Chem., Prod. Res. Dev.*, 10 (1970) 218.
13 S. H. Langer and J. E. Patton, in J. H. Purnell (Editor), *New Developments in Gas Chromatography*, Wiley, New York, 1973, p. 293.
14 N. C. Saha and D. S. Mathur, *J. Chromatogr.*, 81 (1973) 207.
15 J. Coca and S. H. Langer, *CHEMTECH*, 13 (1983) 682.
16 M. W. Bolme and S. H. Langer, *J. Phys. Chem.*, 87 (1983) 3363.
17 A. H. T. Chu and S. H. Langer, *Anal. Chem.*, 57 (1985) 2197.
18 K. Benedek, S. Dong and B. L. Karger, *J. Chromatogr.*, 317 (1984) 227.
19 S. A. Cohen, K. Benedek, S. Dong, Y. Tapuhi and B. L. Karger, *Anal. Chem.*, 56 (1984) 217.
20 W. R. Melander, H.-J. Lin and Cs. Horváth, *J. Phys. Chem.*, 88 (1984) 4527.
21 J. Jacobson, W. Melander, G. Vaisnys and Cs. Horváth, *J. Phys. Chem.*, 88 (1984) 4536.
22 M. Moriyasu, K. Kawanishi, A. Kato, Y. Hashimoto, M. Sugiura and T. Sai, *Bull. Chem. Soc. Jpn.*, 58 (1985) 3351.
23 M. Moriyasu, C. Yamagami, A. Kato, Y. Hashimoto and N. Takao, *Bull. Chem. Soc. Jpn.*, 59 (1986) 1539.
24 M. T. W. Hearn, A. N. Hodder and M. I. Aguilar, *J. Chromatogr.*, 327 (1985) 47.
25 R. G. Wetherold, E. H. Wissler and K. B. Bischoff, *Adv. Chem. Ser.*, 133 (1974) 181.
26 B. K. Cho, R. W. Carr, Jr. and R. Aris, *Chem. Eng. Sci.*, 35 (1980) 74.
27 B. K. Cho, R. W. Carr, Jr. and R. Aris, *Sep. Sci. Technol.*, 15 (1980) 679.
28 M. Sardin and J. Villermaux, *Nouv. J. Chim.*, 3 (1979) 255.
29 D. Schweich, J. Villermaux and M. Sardin, *AIChE J.*, 26 (1980) 477.
30 D. Schweich and J. Villermaux, *Chem. Eng. J.*, 24 (1982) 99.
31 K. Hashimoto, S. Adachi, H. Noujima and Y. Ueda, *Biotechnol. Bioeng.*, 25 (1983) 2371.
32 I. Zafar and P. E. Barker, *Chem. Eng. Sci.*, 43 (1988) 2369.
33 P. E. Barker and G. Ganetsos, in A. E. Rodrigues, M. D. Levan and D. Tondeur (Editors), *Adsorption: Science and Technology*, Kluwer, Dordrecht, 1989, p. 491.
34 H. A. Deans, *US Pat.*, 3 623 842 (1971).
35 J. F. Tomich, R. L. Dalton, H. A. Deans and L. K. Shallenberger, *J. Pet. Technol.*, (1973) 211.
36 C. S. G. Phillips, A. J. Hart-Davis, R. G. L. Sauland and J. Wormald, *J. Gas Chromatogr.*, 5 (1967) 424.
37 N. A. Katsanos, *Flow Perturbation Gas Chromatography*, Marcel Dekker, New York, 1988, p. 41.
38 A. J. Muller and P. W. Carr, *J. Chromatogr.*, 294 (1984) 235.
39 J. **B.** Powell, C. Y. Jeng and S. H. Langer, *Chem. Eng. Sci.*, 42 (**19**87) 1797.
40 D. **A.** Jaeger, M. W. Clennan, D. E. Leyden and R. S. S. **Murthy**, *Tetrahedron Lett.*, 28 (1987) 4805.
41 D. A. Jaeger and M. W. Clennan, *J. Org. Chem.*, 53 (1988) 3985.
42 J. F. Lawrence and R. W. Frei, *Chemical Derivatization in Liquid Chromatography*, Elsevier, Amsterdam, 1976.
43 L. D. Bowers and W. D. Bostick, in R. W. Frei and J. F. Lawrence (Editors), *Chemical Derivatization in Analytical Chemistry*, Vol. 2, Plenum Press, New York, 1982, Ch. 3.
44 I. S. Krull (Editors), *Reaction Detection in Liquid Chromatography*, Marcel Dekker, New York, 1986.
45 J. G. Ekerdt, K. J. Klabunde, J. R. Shapley, J. M. White and J. T. Yates, Jr., *J. Phys. Chem.*, 92 (1988) 6182.
46 R. A. Keller and J. C. Giddings, *J. Chromatogr.*, 3 (1960) 205.
47 S. H. Langer, J. Y. Yurchak and J. E. Patton, *Ind. Eng. Chem.*, 61 (1969) 10.
48 P. J. Marriott and Y.-H. Lai, *J. Chromatogr.*, 447 (1988) 29.
49 M. van Swaay, *Adv. Chromatogr.*, 8 (1968) 363.
50 M. Suzuki and J. M. Smith, *Adv. Chromatogr.*, 13 (1975) 213.
51 J. Villermaux, in A. E. Rodrigues and D. Tondeur (Editors), *Percolation Processes: Theory and Applications*, Sijthoff and Noordhoff, Alphen aan den Rijn, 1981, p. 539.
52 J. C. Giddings, *Dynamics of Chromatography*, Marcel Dekker, New York, 1965.
53 J. H. Knox, *Anal. Chem.*, 38 (1966) 253.
54 J. F. K. Huber, *J. Chromatogr. Sci.*, 7 (1969) 85.
55 Cs. Horváth and H.-J. Lin, *J. Chromatogr.*, 126 (1976) 401.
56 Cs. Horváth and H.-J. Lin, *J. Chromatogr.*, 149 (1978) 43.
57 D. Schweich and J. Villermaux, *Ind. Eng. Chem., Fundam.*, 17 (1978) 1.
58 A. H. T. Chu and S. H. Langer, *Anal. Chem.*, 58 (1986) 1617.
59 C. Y. Jeng and S. H. Langer, *Ind. Eng. Chem. Res.*, 30 (1991) 1489.
60 J. T. Hsu and U. P. Ernst, *Chem. Eng. Sci.*, 45 (1990) 1017.
61 A. F. Bergold, D. A. Hanggi, A. J. Muller and P. W. Carr, in Cs. Horváth (Editor), *High-Performance Liquid Chromatography —Advances and Perspectives*, Vol. 5, Academic Press, San Diego, 1988, p. 95.
62 A. Jaulmes and C. Vidal-Madjar, *Adv. Chromatogr.*, 28 (1989) 1.
63 J. Kallen and E. Heilbronner, *Helv. Chim. Acta*, 43 (1960) 489.
64 A. Klinkenberg, *Chem. Eng. Sci.*, 15 (1961) 255.
65 S. Z. Roginskii and A. L. Rozental, *Dokl. Akad. Nauk SSSR*, 146 (1962) 152.
66 G. A. Gaziev, V. Y. Filanovskii and M. I. Yanovskii, *Kinet. Katal.*, 4 (1963) 668.
67 S. Z. Roginskii and A. L. Rozental, *Kinet. Katal.*, 5 (1964) 104.

68 T. Hattori and Y. Murakami, *J. Catal.*, 12 (1968) 166.
69 H. A. Deans, F. J. M. Horn and G. Klauser, *AIChE J.*, 16 (1970) 426.
70 L. G. Harrison and Y. Koya, *J. Chromatogr.*, 52 (1970) 31.
71 A. D. Berman and M. I. Yanovskii, *Dokl. Akad. Nauk SSSR*, 197 (1971) 369.
72 C. Chu and L. C. Tsang, *Ind. Eng. Chem., Process Des. Dev.*, 10 (1971) 47.
73 M. Suzuki and J. M. Smith, *Chem. Eng. Sci.*, 26 (1971) 221.
74 S. Viswanathan and R. Aris, *Adv. Chem. Ser.*, 133 (1974) 191.
75 D. Duprez, M. Bastick and J. Bastick, *J. Chim. Phys.*, 71 (1974) 278.
76 R. Kramer, *J. Chromatogr.*, 107 (1975) 241.
77 E. Cremer and R. Kramer, *J. Chromatogr.*, 107 (1975) 253.
78 K. Takeuchi and Y. Uraguchi, *J. Chem. Eng. Jpn.*, 9 (1976) 164.
79 K. Takeuchi, T. Miyauchi and Y. Uraguchi, *J. Chem. Eng. Jpn.*, 11 (1978) 216.
80 J.-C. Huang, D. Rothstein and R. Madey, *J. Chromatogr.*, 261 (1983) 1.
81 W. Burkle, H. Karfunkel and V. Schurig, *J. Chromatogr.*, 288 (1984) 1.
82 R. Thede, H. Pscheidl and D. Haberland, *Z. Phys. Chem.*, 266 (1985) 1089.
83 T. Petroulas, R. W. Carr, Jr., and R. Aris, *Chem. Eng. Sci.*, 40 (1985) 2233.
84 B. B. Fish and R. W. Carr, Jr., *Chem. Eng. Sci.*, 44 (1989) 1773.
85 M. Kocirik, *J. Chromatogr.*, 30 (1967) 459.
86 K.-P. Li, D. L. Duewer and R. S. Juvet, *Anal. Chem.*, 46 (1974) 1209.
87 K.-P. Li and Y.-Y. H. Li, *Anal. Chem.*, 48 (1976) 737.
88 F. C. Denizot and M. A. Delaage, *Proc. Natl. Acad. Sci. U.S.A.*, 72 (1975) 4840.
89 K. Yamaoka and T. Nakagawa, *J. Chromatogr.*, 117 (1976) 1.
90 A. T. Melenevskii, G. E. El'kin and G. V. Samsonov, *J. Chromatogr.*, 148 (1978) 299.
91 H. W. Hethcote and C. DeLisi, *J. Chromatogr.*, 248 (1982) 183.
92 L. Nondek, *Anal. Chem.*, 56 (1984) 1192.
93 R. Hanai, S. Endo and A. Wada, *Biophys. Chem.*, 25 (1986) 27.
94 F. H. Arnold and H. W. Blanch, *J. Chromatogr.*, 355 (1986) 13.
95 G. Liden and L. Vamling, *Chem. Eng. J.*, 40 (1989) 31.
96 C. Y. Jeng, *Ph.D. Thesis*, University of Wisconsin, Madison, WI, 1991.
97 S. H. Langer and J. E. Patton, *J. Phys. Chem.*, 76 (1972) 2159.
98 A. H. T. Chu and S. H. Langer, *J. Chromatogr.*, 384 (1987) 231.
99 A. T. James and A. J. P. Martin, *Biochem. J.*, 50 (1952) 679.
100 A. J. P. Martin and R. M. L. Synge, *Biochem. J.*, 35 (1941) 1358.
101 E. Glueckauf, *Trans. Faraday Soc.*, 51 (1955) 34.
102 L. Lapidus and N. R. Amundson, *J. Phys. Chem.*, 56 (1952) 984.
103 E. M. Magee, *Ind. Eng. Chem., Fundam.*, 2 (1963) 32.
104 E. F. Gore, *Ind. Eng. Chem., Process Des. Dev.*, 6 (1967) 10.
105 J. Villermaux, *J. Chromatogr.*, 406 (1987) 11.
106 R. Hanai and A. Wada, *J. Chromatogr.*, 394 (1987) 273.
107 J. C. Giddings and H. Eyring, *J. Phys. Chem.*, 59 (1955) 416.
108 J. C. Giddings, *J. Chromatogr.*, 3 (1960) 443.
109 J. R. Conder, in J. H. Purnell (Editors), *Progress in Gas Chromatography*, Wiley-Interscience, New York, 1973, p. 137.
110 J. Frenz and Cs. Horváth, in Cs. Horváth (Editor), *High-Performance Liquid Chromatography —Advances and Perspectives*, Vol. 5, Academic Press, San Diego, 1988, p. 211.
111 S. Golshan-Shirazin, B. Lin and G. Guiochon, *Anal. Chem.*, 61 (1989) 1960.
112 H. A. Chase, *J. Chromatogr.*, 297 (1984) 179.
113 C. Y. Jeng and S. H. Langer, *J. Chromatogr.*, 556 (1991) 383.
114 X. M. Lu, A. Figueroa and B. L. Karger, *J. Am. Chem. Soc.*, 110 (1988) 1978.
115 P. Oroszlan, R. Blanco, X. M. Lu, D. Yarmush and B. L. Karger, *J. Chromatogr.*, 500 (1990) 481.
116 J.-X. Huang, J. D. Stuart, W. R. Melander and Cs. Horváth, *J. Chromatogr.*, 316 (1984) 151.
117 S. A. Cohen, K. Benedek, Y. Tapuhi, J. C. Ford and B. L. Karger, *Anal. Biochem.*, 144 (1985) 275.
118 X. M. Lu, K. Benedek and B. L. Karger, *J. Chromatogr.*, 395 (1986) 19.
119 M. Lebl and V. Gut, *J. Chromatogr.*, 260 (1983) 478.
120 M. Moriyasu, A. Kato, M. Okada and Y. Hashimoto, *Anal. Lett.*, 17 (1984) 1533.
121 M. Moriyasu, Y. Hashimoto and M. Endo, *Bull. Chem. Soc. Jpn.*, 56 (1983) 1972.
122 M. Moriyasu, K. Kawanishi, A. Kato and Y. Hashimoto, *Bull. Chem. Soc. Jpn.*, 57 (1984) 1766.
123 H. R. Melton, D. C. Bailey and S. H. Langer, *J. Chem. Technol. Biotechnol.*, 31 (1981) 44.
124 H. R. Melton, *Ph.D. Thesis*, University of Wisconsin, Madison, WI, 1976.
125 J. Růžička and E. H. Hansen, *Flow Injection Analysis*, Wiley, New York, 2nd ed., 1988.
126 S. H. Langer, H. R. Melton, T. D. Griffith and J. Coca, *J. Chromatogr.*, 122 (1976) 487.
127 N. Yoza, T. Shuto, Y. Baba, A. Tanaka and S. Ohashi, *J. Chromatogr.*, 298 (1984) 419.
128 C. Y. Jeng and S. H. Langer, *J. Chromatogr. Sci.*, 27 (1989) 549.
129 S. H. Langer, A. H. T. Chu, M. W. Bolme, M. S. Turner and G. R. Quinting, *J. Chem. Res. (S)*, (1985) 342.
130 A. H. T. Chu and S. H. Langer, *J. Chromatogr.*, 389 (1987) 11.
131 J. E. Patton, H. Kung and S. H. Langer, *J. Chromatogr.*, 104 (1975) 73.
132 A. H. T. Chu, *Ph.D. Thesis*, University of Wisconsin, Madison, WI, 1984.
133 T. D. Griffith, A. H. T. Chu and S. H. Langer, *Chem. Eng. J.*, 36 (1987) 73.
134 J. E. Patton and S. H. Langer, *Anal. Chem.*, 42 (1970) 1449.
135 N. Grinberg, R. Blanco, D. M. Yarmush and B. L. Karger, *Anal. Chem.*, 61 (1989) 514.

136 M. T. W. Hearn, M. I. Aguilar, T. Nguyen and M. Fridman, *J. Chromatogr.*, 435 (1988) 271.
137 S. M. Cramer, B. Nathanael and Cs. Horváth, *J. Chromatogr.*, 295 (1984) 405.
138 E. S. Parente and D. B. Wetlaufer, *J. Chromatogr.*, 314 (1984) 337.
139 M. A. Gattrell and D. K. Kirk, *J. Chromatogr.*, 409 (1987) 404.
140 R. Viville, A. Scarso, J. P. Durieux and A. Loffet, *J. Chromatogr.*, 262 (1983) 411.
141 J. Y. Yurchak, *M. S. Thesis*, University of Wisconsin, Madison, WI, 1966.
142 W. R. Melander, J. Jacobson and Cs. Horváth, *J. Chromatogr.*, 234 (1982) 269.
143 S. L. Wu, K. Benedek and B. L. Karger, *J. Chromatogr.*, 359 (1986) 3.
144 J. Nawrocki, D. L. Moir and W. Szczepaniak, *J. Chromatogr.*, 467 (1989) 31.
145 M. Moriyasu, A. Kato and Y. Hashimoto, *J. Chem. Soc., Perkin Trans. 2*, (1986) 515.
146 M. Moriyasu, A. Kato and Y. Hashimoto, *J. Chromatogr.*, 400 (1987) 143.
147 D. E. Henderson and D. J. O'Connor, *Adv. Chromatogr.*, 23 (1984) 65.
148 D. E. Henderson and Cs. Horváth, *J. Chromatogr.*, 368 (1986) 203.
149 B. L. Karger, J. N. LePage and N. Tanaka, in Cs. Horváth (Editor), *High-Performance Liquid Chromatography —Advances and Perspectives*, Vol. 1, Academic Press, New York, 1989, p. 113.
150 E. Tomlinson, *Chem. Ind. (London)*, (1981) 687.
151 J. P. Foley, *Chromatogr. Forum*, 2, June (1987) 43.
152 G. Klein, in A. E. Rodrigues and D. Tondeur (Editors), *Percolation Processes: Theory and Applications*, Sijthoff and Noordhoff, Alphen aan de Rijn, 1981, p. 363.
153 J. J. van Deemter, F. J. Zuiderweg and A. Klinkenberg, *Chem. Eng. Sci.*, 5 (1956) 271.
154 J. H. Purnell, *Gas Chromatography*, Wiley, New York, 1962.
155 R. W. Stout, J. J. DeStefano and L. R. Snyder, *J. Chromatogr.*, 282 (1983) 263.
156 S. J. Hawkes, *J. Chem. Educ.*, 60 (1983) 393.
157 L. Nondek, U. A. Th. Brinkman and R. W. Frei, *Anal. Chem.*, 55 (1983) 1466.
158 Y. T. Shih and P. W. Carr, *Anal. Chim. Acta*, 167 (1985) 137.
159 D. B. Marshall, J. W. Burns and D. E. Connolly, *J. Chromatogr.*, 360 (1986) 13.
160 Y. S. Lin and Y. H. Ma, *Ind. Eng. Chem. Res.*, 28 (1989) 622.
161 O. Miyawaki, K. Nakamura and T. Yano, *Agric. Biol. Chem.*, 49 (1985) 2063.
162 G. H. Weiss, *Sep. Sci. Technol.*, 16 (1981) 75.
163 H. W. Hethcote and C. DeLisi, *J. Chromatogr.*, 240 (1982) 269.
164 C. DeLisi, H. W. Hethcote and J. W. Brettler, *J. Chromatogr.*, 240 (1982) 283.
165 S. Endo and A. Wada, *Biophys. Chem.*, 18 (1983) 291.
166 A. J. Muller and P. W. Carr, *J. Chromatogr.*, 284 (1984) 33.
167 A. J. Muller and P. W. Carr, *J. Chromatogr.*, 357 (1986) 11.
168 D. J. Anderson and R. R. Walters, *J. Chromatogr.*, 376 (1986) 69.
169 R. M. Moore and R. R. Walters, *J. Chromatogr.*, 384 (1987) 91.
170 J. R. Sportsman, J. D. Liddil and G. S. Wilson, *Anal. Chem.*, 55 (1983) 771.
171 D. S. Hage, R. R. Walters and H. W. Hethcote, *Anal. Chem.*, 58 (1986) 274.
172 L. A. Larew and R. R. Walters, *Anal. Biochem.*, 164 (1987) 537.
173 D. S. Hage and R. R. Walters, *J. Chromatogr.*, 436 (1988) 111.
174 J. L. Wade and P. W. Carr, *J. Chromatogr.*, 449 (1988) 53.
175 J. L. Wade, A. F. Bergold and P. W. Carr, *Anal. Chem.*, 59 (1987) 1286.
176 B. S. Ludolph, personal communication, M.S. Report, Department of Chemical Engineering, University of Wisconsin, Madison, WI, 1989.
177 T. Hattori and Y. Murakami, *J. Catal.*, 10 (1968) 114.
178 J. Coca, G. Adrio, C. Y. Jeng and S. H. Langer, in G. Ganetsos and P. E. Barker (Editors), *Preparative and Production Scale Chromatographic Processes and Applications*, Marcel Dekker, New York, 1991, in press.
179 N. Tanaka, K. Hosoya, K. Iwaguchi and M. Araki, *J. Am. Chem. Soc.*, 106 (1984) 3057.
180 N.-H. L. Wang and M. R. Smith, *Chem. Eng. Commun.*, 29 (1984) 209.
181 P. W. Carr and L. D. Bowers, *Immobilized Enzymes in Analytical and Clinical Chemistry*, Wiley, New York, 1980.

Journal of Chromatography, 589 (1992) 31–43
Elsevier Science Publishers B.V., Amsterdam

CHROM. 23 691

Feasibility study for the construction of an integrated expert system in high-performance liquid chromatography

T. Hamoir, M. De Smet, H. Pyrins, P. Conti☆, N. Vanden Driessche and D. L. Massart*

Pharmaceutical Institute, Vrije Universiteit Brussel, Laarbeeklaan 103, B-1090 Brussels (Belgium)

F. Maris and H. Hindriks

Analytical R & D Laboratories, Organon International BV, P.O. Box 20, 5340 BH Oss (Netherlands)

P. J. Schoenmakers

Philips Research Laboratories, P.O. Box 80 000, 5600 JA Eindhoven (Netherlands)

(First received February 18th, 1991; revised manuscript received June 4th, 1991)

ABSTRACT

An integrated expert system consisting of several stand-alone expert systems was developed to assist the chromatographer in the determination of optimum high-performance liquid chromatographic conditions, *i.e.*, after a good "first guess", an elution within a reasonable analysis time and with adequate resolution. The implementation and linking of the systems were performed by means of the expert system building tool KES. The knowledge incorporated in this expert system is described.

INTRODUCTION

The selection of initial conditions ("first guess"), retention optimization and selectivity optimization are steps that need to be performed during high-performance liquid chromatographic (HPLC) method development. Expertise is required to perform these steps within a certain time constraint, and these constraints surely exist in the pharmaceutical world. In this field, the application of expert systems was investigated within ESPRIT (European Strategic Programme for Research and Development in Information Technology). The ESCA (Expert Systems in Chemical Analysis) project was supported by the EEC to study the feasibility of building complex expert systems for HPLC method development. Such expert systems would contain the experts' chemical knowledge, which could then be applied by (pharmaceutical) analysts less experienced in the field. Prior to the building of an expert system, the knowledge was acquired for each of the above steps. Once the knowledge acquisition was completed, stand-alone expert systems were developed for each of these steps. Then, in a later stage, these stand-alone expert systems were linked together. Of course, this latter process required additional knowledge to direct the user through the integrated system. Our aim in this paper is to describe the results of the feasibility study for the construction of an integrated system from stand-alone systems and, in particular, the chemical knowledge incorporated in this integrated system. The integration strategy from the software point of view has already been described

☆ On leave from the University of Camerino, Italy.

0021-9673/92/$05.00

elsewhere [1]. It is stressed that this is a feasibility study and that much more work would be needed to achieve a complete operational system.

OVERALL STRUCTURE OF THE INTEGRATED SYSTEM

The first task in the development of an HPLC method is the selection of initial chromatographic conditions. In the present integrated system, such first-guess conditions are selected by the expert systems LABEL, DASH and LIT, depending of the application field. After carrying out the first experiment, the retention time range of the solutes is evaluated. If there are solutes with capacity factors (k') outside the desired range, the retention optimization expert systems LABEL', DASH' and LIT' are consulted. At this level, a chromatogram is obtained in which all solutes elute within a reasonable time. However, two or more peaks may still overlap. The selectivity optimization expert system SLOPES is then consulted. The strategic knowledge necessary to route the end user to the different expert systems during the method development is incorporated in the SUPERVISOR expert system. A survey of the integrated system is presented in Fig. 1.

EXPERT SYSTEM BUILDING TOOL

The implementation of the different stand-alone expert systems was performed in KES (Knowledge Engineering System; release 2.5), written in C-language and based on the use of production rules. The tool reasons by backward and by forward chaining. External links to databases, spreadsheets and other processes are provided within KES. KES is embedded in C and this feature was used to link the different stand-alone expert systems without modification of the knowledge bases.

DESCRIPTION OF THE CHEMICAL KNOWLEDGE

LABEL–LABEL'

The expert system LABEL selects initial chromatographic conditions for the label claim analysis of pharmaceutical formulations on a cyanopropyl column used in different chromatographic modes. The knowledge incorporated in LABEL has already been described [2,3].

The main task of the expert system LABEL' is to situate the capacity factor in a suitable range. The retention optimization is performed by increasing or decreasing the percentage of organic modifier in the mobile phase, starting from the first-guess composition. As three different chromatographic modes are applied on the cyanopropyl column, three sets of rules for retention optimization are incorporated in LABEL'. An example of the rules for the "reversed-phase (RP) with buffer" chromatographic mode is given in the Appendix. The other sets of rules, namely for the "reversed-phase with water" and the normal-phase (NP) chromatographic mode, are similar. However, different rates of increase or decrease in the percentage of organic modifier are applied. In the RP chromatographic mode methanol is used as the modifier, while in the NP mode dichloromethane–hexane mixtures are used.

DASH–DASH'

The expert system DASH (Drug Analysis System

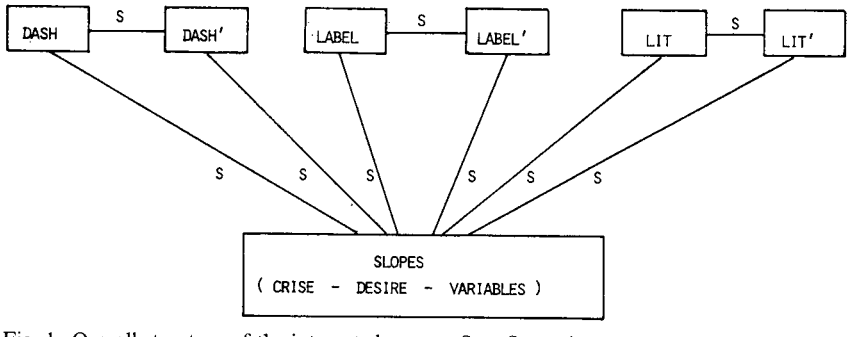

Fig. 1. Overall structure of the integrated system. S = Supervisor.

in HPLC) was originally developed for the purity control of basic compounds, namely CNS (central nervous system)-active and cardiovascular drugs. This expert system determines the initial chromatographic conditions to obtain a capacity factor between 3 and 10. The chemical knowledge incorporated in the expert system DASH has been described in the literature [4]. In more than 75% of all cases, correct predictions were obtained for the original family of substances. However, such a result cannot be expected for a wider range of pharmaceutical compounds. Therefore, the expert system DASH′ was introduced, which performs retention optimization on the basis of the first guess result [5].

LIT–LIT′

The expert system LIT deals with HPLC methods selected from the literature by the end user for application in practice. This expert system functions in fact as a kind of filter to use only methods which can be treated further by the other expert system modules, more specifically the retention optimization expert system LIT′ and the selectivity optimization expert system SLOPES. The system therefore checks a number of parameters. With regard to the knowledge in SLOPES, for example, all columns used in reversed-phase chromatography are admitted, whereas in normal-phase chromatography only the LiChrosorb cyanopropyl column can be used. This is not due to a lack of quality of other columns, but to the available knowledge in the team. In addition, several other restrictions were imposed (Table I).

TABLE I

PARAMETERS ADMITTED WITHOUT RESTRICTIONS (A) AND NON-ADMITTED (NA) BY THE EXPERT SYSTEM LIT

Parameter	A	NA
Mol.wt. < 1500	*	
Amino acids		*
Peptides		*
Proteins		*
Sugars		*
Inorganic cations/anions		*
Chiral separations		*
Ion-pair chromatography		*
Ion chromatography		*
Gel-permeation chromatography		*
Peak-shape additives	*	
HPLC instrumentation	*	
Detection	*	
Matrices	*	

The knowledge for the retention optimization is incorporated in the expert system LIT′. This step is carried out by comparing the experimental and the literature chromatograms. Three different cases for consulting LIT′ have to be distinguished (Table II). In the first case the concentration organic modifier in the mobile phase will be decreased and in the second case it will be increased; in the third case the expert system will advise another brand of the particular type of column tested and the same strategy as mentioned above is followed. If the same elution pattern (case 3) persists, then the expert system will surrender. In all cases the end user has the possibility of stopping consulting the retention optimization expert system, once the experimental result is satisfactory.

SLOPES

The expert system for selectivity optimization consists of three different modules, namely VARIABLES, DESIRE and CRISE. In VARIABLES, the relevant optimization parameters and their boundaries are selected. Thereafter, the type of the experimental design and the location of the experiments are determined in DESIRE. Finally, the most suitable optimization criterion to describe the quality of a chromatogram is selected in CRISE. The stand-alone expert system CRISE has already been described [6]. Therefore, only the chemical knowledge incorporated in VARIABLES and DESIRE will be discussed.

TABLE II

DIFFERENT CASES FOR THE CONSULTATION OF THE EXPERT SYSTEM LIT

1. At least one relevant peak elutes with a significantly smaller retention time in comparison with the expected result
2. At least one relevant peak elutes with a significantly larger retention time in comparison with the expected result
3. At least one of the early-eluting peaks has a smaller retention time, and at least one of the late-eluting peaks is retained more strongly, in comparison with the expected result

VARIABLES

This expert system selects the optimization variables and the boundaries within which the optimization will be carried out. This depends of the chromatographic mode: in NPLC and RPLC with water the only possible variable is the solvent selectivity. In RPLC with buffer there are two possibilities: one can attempt to use the solvent selectivity or one can optimize the solvent strength and the pH simultaneously. The selection of the variables in RPLC with buffer is performed by determining the acid–base status of the components [2]. Once the acid–base characteristics of the compounds have been determined, the optimization variables and their boundaries are selected. This knowledge is outlined in Fig. 2.

The user is also asked whether solute/sample degradation can occur owing to one of the organic modifiers. In NPLC this leads to discarding one organic modifier, *i.e.*, carrying out the optimization with the base solvent (hexane) and the remaining modifier(s). In RPLC the organic modifier can be replaced. In RPLC with buffer, for example, methanol can be replaced with acetonitrile.

DESIRE

In the expert system DESIRE the most suitable experimental design is selected first. The possibilities considered in the integrated expert system are as follows.

(i) A simplex design, which belongs to the group of the sequential designs. In a sequential design only a few experiments are defined initially. The following experiments are based on the results of the first experiments [7–9].

(ii) A Doehlert design, which belongs to the group of factorial or simultaneous designs. In contrast to the sequential designs, all the experiments are defined before performing the experiments. In comparison with some of the common factorial designs, such as the central composite design, the Doehlert design is very economical. Only seven experiments are required for two optimization parameters. In this case the design takes the form of a centred

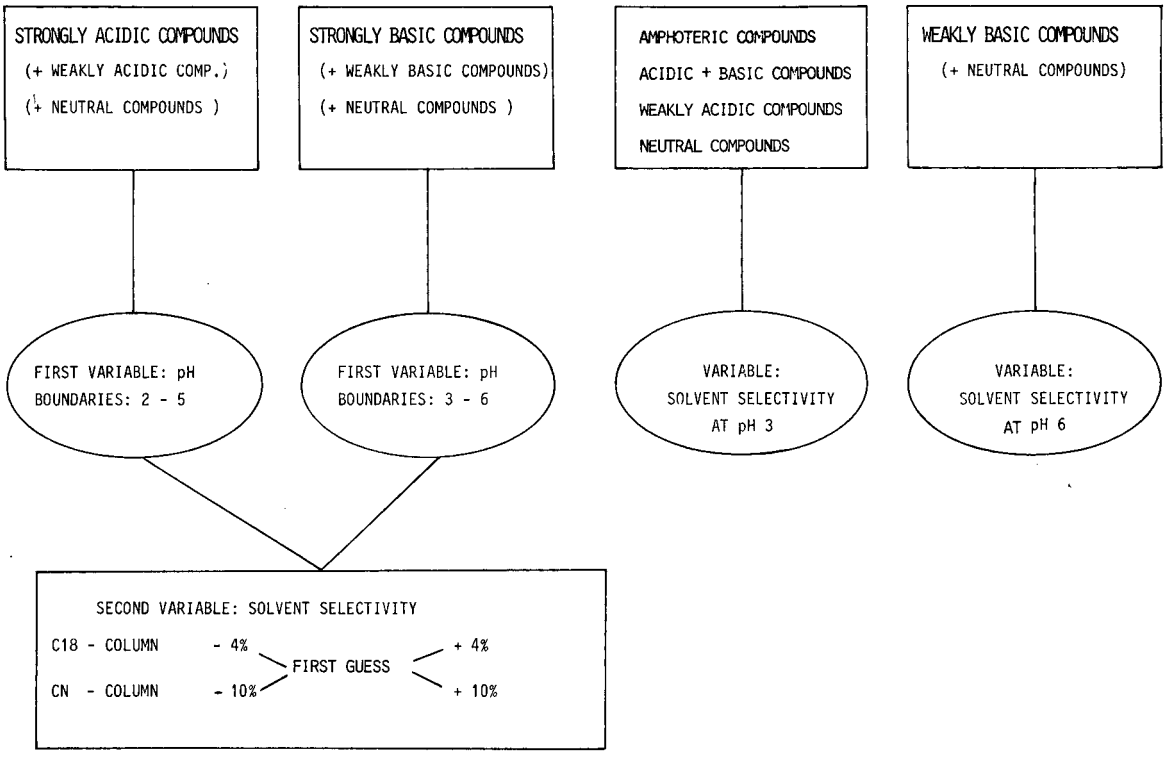

Fig. 2. Selection of the optimization variables and their boundaries.

hexagon. Such a design permits a uniform description of the parameter space [10].

(iii) A mixture design, which is a special factorial design due to a constraint on the variables, *i.e.*, the sum of the selected parameters is constant. This approach was originally developed by Glajch *et al.* [11].

The algorithm for each design was implemented as a separate computer program. Knowledge concerning the selection of the appropriate design was included in the expert system but, as this is only a study designed to investigate whether integration is feasible, only the Doehlert design was actually included in the integrated system. The Doehlert design was selected from the three above, as it is more novel and it is therefore more interesting to obtain information about its use. The necessary connections for the inclusion of the other algorithms are already provided in the integrated expert system.

Once a design has been selected, the number and the location of the experiments to be carried out are determined. Thereafter the correctness of the approach is investigated. Finally, the response function is predicted and the optimum located.

Selection of the design

Generally, a factorial approach is preferred to a simplex procedure. Only when more than two variables have to be optimized simultaneously is the simplex design selected. VARIABLES recommends a maximum of two optimization parameters. The option of a simplex design is provided for further extension in the future, because in a few cases (*e.g.*, ion-pair chromatography) for which the knowledge is not yet incorporated in this system, more than two variables may be selected. When there are one or two optimization parameters different situations arise (Fig. 3).

Because only the Doehlert design was actually implemented, only this one will be discussed in more detail.

Optimization strategy

The Doehlert design is constructed knowing the boundaries of both variables. The variable with the largest effect on the response, the pH, is tested on five levels and the other variable, the solvent strength, on three levels. The experiments are listed in Table III.

The Doehlert design is a simultaneous approach where all the experiments are defined before performing the first one. Within the expert system, the user may carry out the experiments in a sequential way. One may start with four experiments (Nos. 1, 2, 3 and 4 in Table III). After these four experiments, the user may then decide that one of them gives sufficiently good results and stop. Afterwards, if still necessary, the remaining experiments can be carried out. The knowledge for this part of the system is represented in Fig. 4.

General evaluation

The module of the expert system that deals with the evaluation of the experimental results consists of two parts. First, the system checks whether the capacity factors of the compounds are situated in an acceptable range for at least four experiments. If not, the boundaries for the optimization parameters recommended by VARIABLES are incorrect. New upper and lower limits must be selected in the area of optimum retention times. This knowledge is also outlined in Fig. 4. The second part of the evaluation concerns the effect of the variables on the selectivity coefficient α. If neither the pH nor the solvent strength has an effect on α, the parameters have not been selected correctly. The system then advises to optimize solvent selectivity and to use a mixture design. In all other situations the optimization procedure can be continued. Depending on the user's choice between the sequential and the simultaneous approach, different paths will be followed. A survey of this part of the system is presented in Fig. 5.

Location of the optimum

After selection of the optimization criterion with CRISE and entering all experimental data [retention time (t_r), dead time (t_0) and peak width at half height ($W_{1/2}$)] for each solute at each of the data points, the response function is modelled. The model used is a quadratic relationship between log k' (or log $W_{1/2}$) and the variables. The following model equation is used:

$$Y = \beta_0 + \beta_1 X_1 + \beta_2 X_2 + \beta_{11} X_1^2 + \beta_{22} X_2^2 + \beta_{12} X_1 X_2$$

where Y represents log k' or log $W_{1/2}$, and X_1 and X_2 are the pH and the concentration organic modifier, respectively. The β-coefficients are calculated by

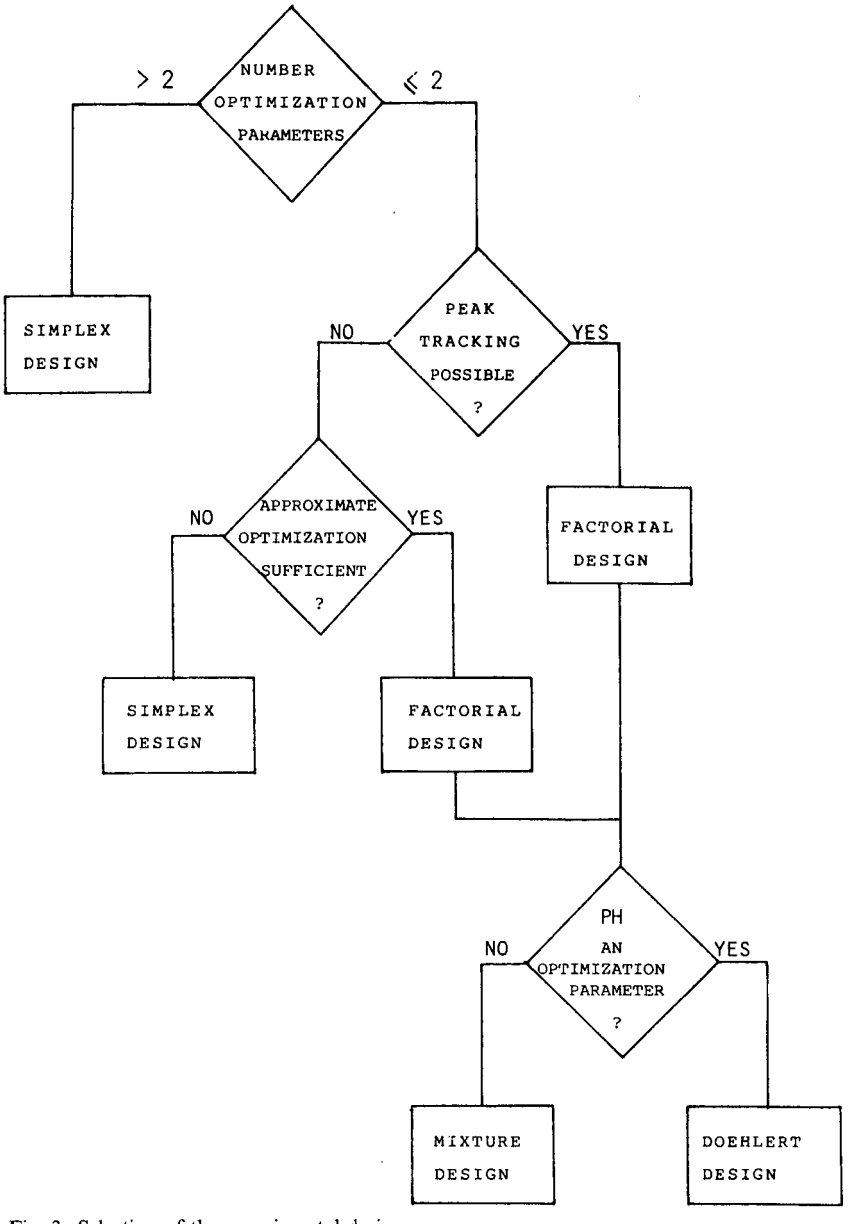

Fig. 3. Selection of the experimental design.

regression. Once these coefficients are known for all solutes, the response can be predicted and the optimum located. If the experimental result differs significantly from the predicted value, a recalculation of the optimum response is carried out, taking the results of the experiment at the initially predicted optimum into account. Once there is no significant difference between the predicted and the experimental results, the user has the possibility either of stopping or of predicting the response under other experimental conditions (Fig. 6). The latter may be useful, for example, if the optimum is situated on the low pH boundary and the user prefers a higher pH.

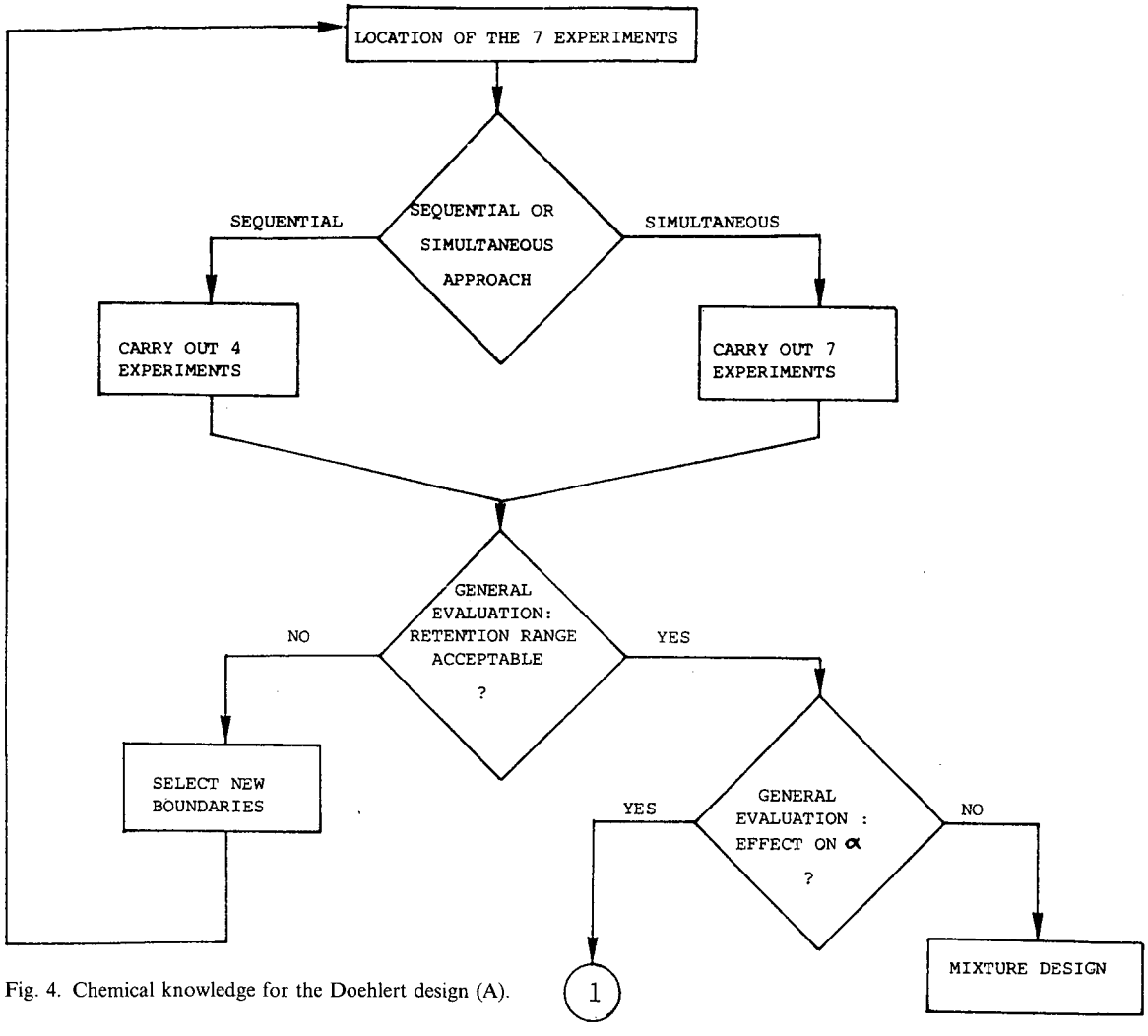

Fig. 4. Chemical knowledge for the Doehlert design (A).

TABLE III

LOCATION OF THE EXPERIMENTS IN THE DOEHLERT MATRIX DESIGN (IN NORMALIZED UNITS)

The upper and lower values for both parameters are +1 and −1, respectively.

No.	X_1 (=pH)	X_2 (=% organic modifier)
1	+0.5	−0.866
2	−0.5	−0.866
3	+0.5	+0.866
4	−0.5	+0.866
5	+1	0
6	0	0
7	−1	0

SUPERVISOR

The SUPERVISOR expert system contains the strategic knowledge necessary to route the end user to the different expert systems. The SUPERVISOR starts by soliciting a problem statement from the user and identifying the problem as belonging to LABEL, DASH or LIT. The link from LABEL, DASH or LIT to the SUPERVISOR is unidirectional, *i.e.*, once the problem statement is transmitted to one of the expert systems, a complete advice is given (Table IV) and afterwards the system will not be addressed again. Once the first-guess experiment has been carried out, the results are communicated to the SUPERVISOR for evaluation.

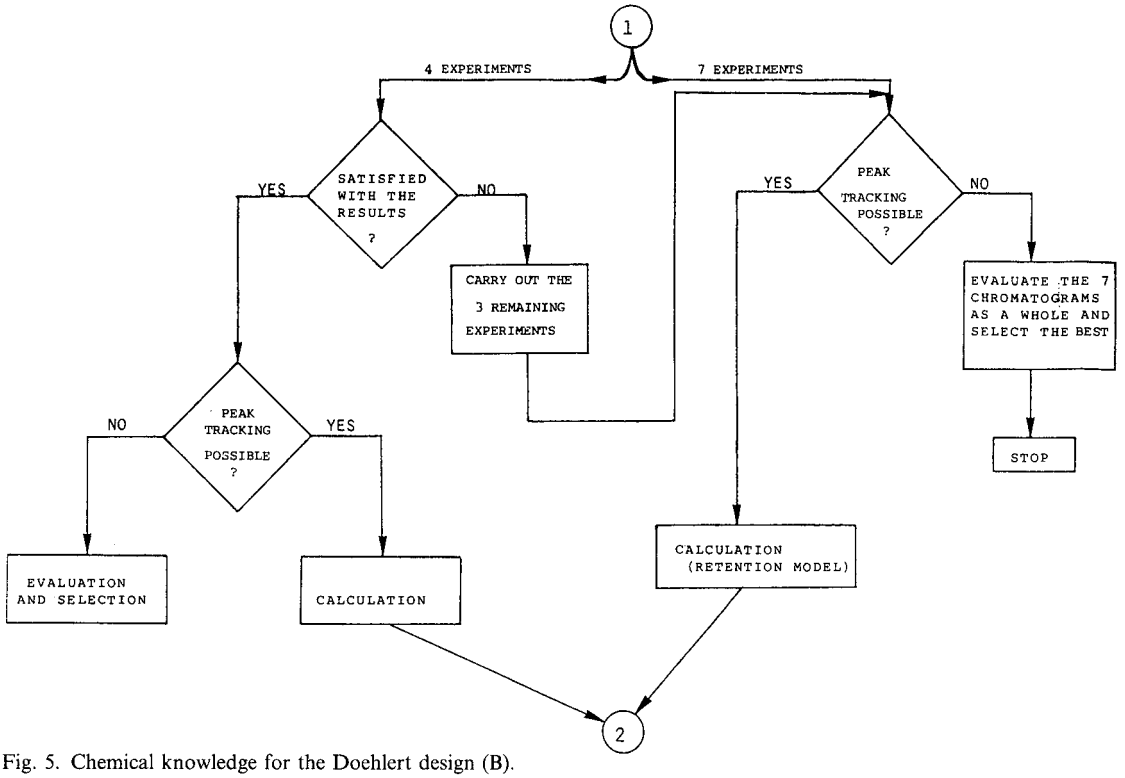

Fig. 5. Chemical knowledge for the Doehlert design (B).

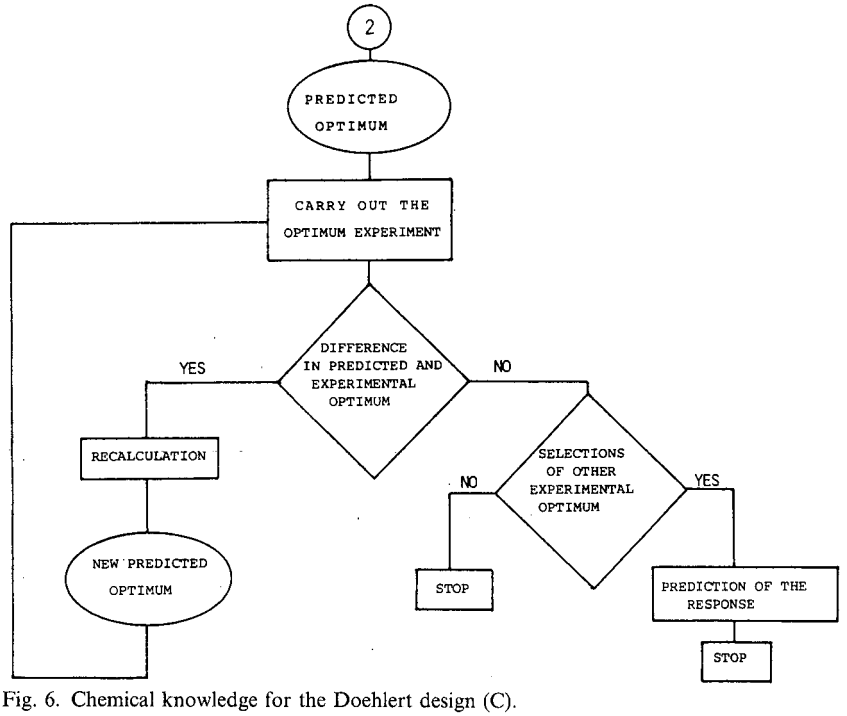

Fig. 6. Chemical knowledge for the Doehlert design (C).

For this purpose default values are applied (Table V). The conclusion of this evaluation is always submitted to the user, who has the possibility of overruling the decision of the SUPERVISOR. If the user agrees with the decision of the SUPERVISOR, then one is routed to the retention optimization expert systems.

The philosophy of the further interaction between LABEL′ and the SUPERVISOR is represented in Fig. 7. Second and third guesses are permitted, but not a fourth. The second and third guesses are obtained from LABEL′. If the third guess is unsuccessful, then the SUPERVISOR routes back to the advice obtained from LABEL and the second preference is tried out in the same way as the first approach. This process continues until either a satisfactory result is obtained or all possibilities have been exhausted. In the latter instance the retention optimization failed and the user has to find another way to solve the problem.

When gradient elution is recommended by LABEL (as a possible, but not a preferred approach) and the third guess is still unsuccessful, the user is advised to perform a gradient elution. The knowledge on gradient optimization is, however, not incorporated in the integrated system.

The rules to route to the retention optimization system DASH′ have already been described [4].

When LIT is used, the user has to compare the experimental result with the published result in the literature method. If the user is satisfied, no retention optimization with LIT′ is suggested by the SUPERVISOR. If the result is unsatisfactory, the SUPERVISOR routes to LIT′.

After successful application of LABEL′, DASH′ or LIT′, the retention times are situated in an acceptable range. However, the resolution may need to be enhanced for partially or completely overlapping peaks. For this purpose the selectivity optimization expert system can be consulted. To decide whether or not selectivity optimization is required,

TABLE IV

ADVICE FROM THE FIRST-GUESS EXPERT SYSTEMS LABEL, DASH AND LIT

LABEL	→ RP with water
	→ RP with buffer
	→ NP
	→ Gradient elution
	→ Three approaches in order of decreasing preference, for instance: first approach: RP with water; second approach: RP with buffer; third approach: NP
DASH	→ a single approach
LIT	→ one literature system at one time

TABLE V

DEFAULT VALUES APPLIED BY THE SUPERVISOR FOR THE CONSULTATION OF THE EXPERT SYSTEM LABEL′

$1 < k' < 3$ (for $n = 1$ or 2; n = number of substances)
$1 < k' < 5$ (for $n = 3$ or 4)
$1 < k' < 10$ (for $n > 4$)

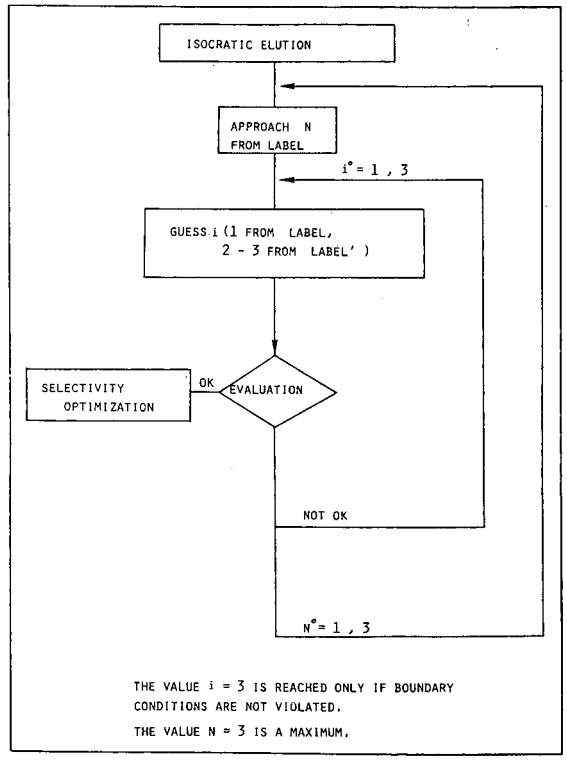

Fig. 7. Interaction between LABEL′ and the SUPERVISOR.

TABLE VI

RULES FOR THE CONSULTATION OF THE SELECTIVITY OPTIMIZATION EXPERT SYSTEM SLOPES

If $N_{found} \geqslant N_{exp}$, which means that all relevant peaks have been detected (case of LABEL, $N_{found} = N_{exp}$) or that an impurity has been found (case of DASH, $N_{found} > N_{exp}$), the selectivity optimization is not required
If $N_{found} < N_{exp}$, then the SUPERVISOR will route to the selectivity optimization expert system

TABLE VII

CHARACTERISTICS OF THE TEST COMPOUNDS

Compound	Acid/base status	Functional group
(1) Org 9731	Neutral/slightly basic	NH_2–C=N–OH
(2) Acid	Acidic	–COOH
(3) Amide	Neutral	NH_2–C=O
(4) Amidine	Basic	NH_2–C=NH

the SUPERVISOR applies rules, which compare the number of peaks in the experimentally obtained chromatogram (N_{found}) with the expected number of peaks (N_{exp}). These rules are listed in Table VI.

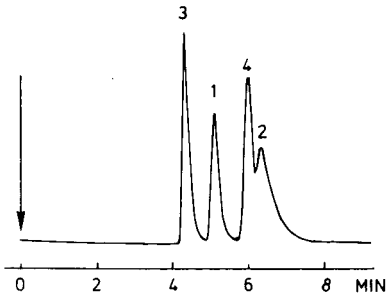

Fig. 8. Chromatogram of Org 9731 and related compounds after consultation of LABEL. Drugs as in Table VII. For experimental conditions, see Table VIII.

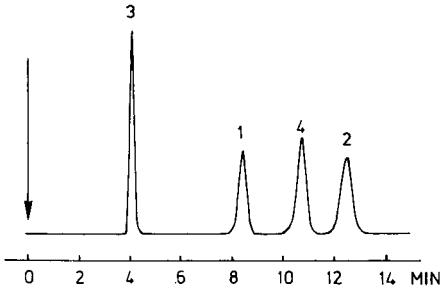

Fig. 9. Chromatogram of Org 9731 and related compounds after consultation of LIT. Drugs as in Table VII. For experimental conditions, see Table VIII.

EXAMPLE OF AN APPLICATION

A separation method was developed for Org 9731 and three related compounds. Some characteristics of the test compounds are shown in Table VII. In a first step the first-guess expert systems were consulted. As the fluorine atom in Org. 9731 was not present in the list of structural elements in DASH,

TABLE VIII

CHARACTERISTICS OF THE LABEL AND LIT METHODS

Parameter	LIT	LABEL
Column (dimensions, particle size)	μBondapak C_{18} (300 × 3.9 mm I.D., 10 μm)	LiChrosorb CN (250 × 4.0 mm I.D., 5 μm)
Basic solvent (%) (pH, μ)	Aqueous buffer (60%) (pH 3.5, μ = 0.1)	Phosphate buffer (80%) (pH 3.0, μ = 0.05)
Modifier (%)	Methanol (40%)	Methanol (20%)
Additive (%)	Amine (10%)	–
Flow-rate	1.5 ml/min	1.0 ml/min
Detector	Diode-array	UV–VIS
Temperature	30°C	Ambient

the consultation of this expert system was impossible. Concerning the expert system LIT, a method from the literature was available, which was in this case a method developed within Organon. The expert system LABEL was also consulted. The chromatograms obtained after carrying out the advice of LABEL and LIT (Table VIII) are shown in Figs. 8 and 9, respectively. In both instances acceptable retention times were obtained and further retention optimization was therefore unnecessary. At this level the best method was selected. As the separation selectivity and also the chromatographic performance, such as peak shapes and plate counts, were found to be better with the LIT method, this was selected for further selectivity optimization. The Org 9731 mixture consisted of an acidic, a basic and two neutral solutes. In such a situation the expert system advises an optimization at constant pH. However, in order to continue with the selectivity optimization the mixture was considered to consist of only basic and neutral solutes.

The Doehlert design was performed in a sequential way. As the mixture was not so complex, four experiments for the description of a first-order model were expected to be sufficient. The experiments are listed in Table IX (Nos. 1, 2, 3 and 4). The experimental results were evaluated. The variables and their boundaries were found to be correctly selected. Subsequently the optimization criterion was selected in CRISE. This expert system advised a threshold criterion (resolution) with an *a priori* value of 1.5. The optimum was predicted and then verified experimentally. As shown in Fig. 10, the predicted optimum was unsatisfactory. Resolution between compounds 2 and 3 was moderate, with a value of 0.87. The predicted retention times and peak widths were not in agreement with the experimental results. The result obtained with the input method (LIT) was clearly better. This illustrates that the first-order model was not accurate enough for the description of the response surface. For this reason the three remaining experiments were performed (Nos. 5, 6 and 7 in Table IX).

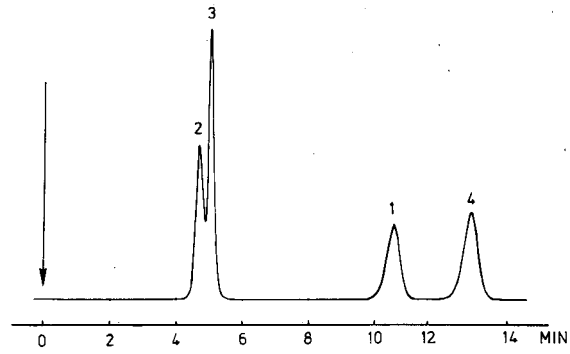

Fig. 10. Optimum for Org 9731 and related compounds after four experiments in the Doehlert design, using a threshold criterion as global optimization criterion. Mobile phase: aqueous buffer (pH 5.7)–methanol (61:39). Drugs as in Table VII. For other experimental conditions, see Table VIII.

The same route as described for the four experiments was followed for further consultation. Depending on the criterion selected, different optima can be obtained. Two optimization criteria were

TABLE IX

LOCATION OF THE EXPERIMENTS IN THE DOEHLERT MATRIX DESIGN FOR THE ORG 9731 MIXTURE

No.	X_1 (=pH)	X_2 (=% organic modifier)
1	5.2	36
2	3.7	36
3	5.2	44
4	3.7	44
5	6.0	40
6	4.5	40
7	3.0	40

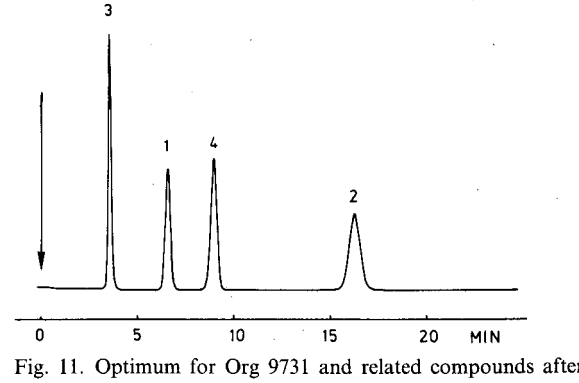

Fig. 11. Optimum for Org 9731 and related compounds after seven experiments in the Doehlert design, using required analysis time as global optimization criterion. Mobile phase: aqueous buffer (pH 3.0)–methanol (57:43). Drugs as in Table VII. For other experimental conditions, see Table VIII.

investigated, namely a threshold criterion (resolution) and also the required analysis time at constant pressure drop. In the first instance the separation is performed on the same column, whereas in the second the column length and/or particle size may be optimized in a later stage. The predicted retention time was 7.3 min (minimum resolution of 1.5) and 16.3 min (minimum resolution of 4.2), respectively. As shown in Fig. 11, the experimental results are in reasonable agreement with the predicted values. In the second instance the system was reconsulted to investigate whether the optimum was correctly selected. The difference between the "old" and the new optima was very small, so the supplementary experimental data point fitted very well in the calculated response surface.

CONCLUSIONS

This study was carried out to investigate the feasibility of building complex expert systems for method development in HPLC. It can be concluded that such a complex expert system can be developed by first dividing the problem into several smaller sub-problems. For instance, one can first investigate separately the first-guess stage, retention optimization and selectivity optimization. The knowledge acquisition and implementation for these sub-problems result in several smaller expert systems. In a later stage these systems can be linked.

The system developed here is not a complete system for HPLC method development in the sense that many application areas and many types of HPLC methods are not covered. However, the example demonstrates that the present system can be applied to many real problems.

We believe that using the approach described in this paper, one should be able to develop complete systems for specific areas, such as reversed-phase HPLC for basic drugs in biological media. It seems too ambitious to envisage building an expert system for the whole of HPLC. The main difficulty is that technology changes rapidly, so that the knowledge incorporated in expert systems should also change. It is feasible to adapt expert systems in a restricted area to these changes, but it seems nearly impossible (at least at an acceptable cost) to do so for a system covering the whole area.

ACKNOWLEDGEMENTS

This research was financially supported by the European Commission as part of ESPRIT Project 1570 (ESCA), FGWO and NFWO. The authors also thank Philips Scientific, who ensured the coordination of the ESPRIT project.

APPENDIX: EXAMPLE OF RULES FOR LABEL' (FOR THE RP + BUFFER MODE)

(I) $n = 1$

If $k' < 0.5$, then use -20% methanol in the mobile phase.

If $0.5 < k' < 1$, then use -10% methanol in the mobile phase.

If $k' > 5$, then use $+20\%$ methanol in the mobile phase.

If $3 < k' < 5$, then use $+10\%$ methanol in the mobile phase.

(II) $n = 2$

If $k'_1, k'_2 < 1$, then use -20% methanol in the mobile phase.

If $k'_1 < 0.5$ and $1 < k'_2 < 3$, then use -10% methanol in the mobile phase.

If $k'_1 < 0.5$ and $k'_2 > 3$, then the user decides if -10% methanol in the mobile phase is applied.

If $1 < k'_1 < 3$ and $k'_2 > 3$, then use $+10\%$ methanol in the mobile phase.

If $k'_1, k'_2 > 5$, then use $+20\%$ methanol in the mobile phase.

(III) $n = 3$ or 4

If k' of all compounds < 1, then use -30% methanol in the mobile phase.

If k' of all compounds > 10, then use $+30\%$ methanol in the mobile phase.

If k' of all compounds is between 5 and 10, then use $+20\%$ methanol in the mobile phase.

If the number of compounds with $k' < 1$ is larger than the number of compounds with $k' > 1$, then use -20% methanol in the mobile phase.

If the number of compounds with $k' < 1$ is smaller than or equal to the number of compounds with $k' > 1$, then use -10% methanol in the mobile phase.

If the number of compounds with $k' > 5$ is larger than the number of compounds with $k' < 5$, then use $+20\%$ methanol in the mobile phase.

If the number of compounds with $k' > 5$ is smaller than or equal to the number of compounds with $k' < 5$, then use $+10\%$ methanol in the mobile phase.

If there are compounds with $k' < 1$ and $k' > 5$, then the user decides if -10% methanol in the mobile phase is applied.

(IV) $n > 4$

If k' of all compounds < 1, then use -40% methanol in the mobile phase.

If k' of all compounds > 20, then use $+40\%$ methanol in the mobile phase.

If k' of all compounds is between 10 and 20, then use $+20\%$ methanol in the mobile phase.

If the number of compounds with $k' < 1$ is larger than the number of compounds with $k' > 1$, then use -20% methanol in the mobile phase.

If the number of compounds with $k' < 1$ is smaller than or equal to the number of compounds with $k' > 1$, then use -10% methanol in the mobile phase.

If the number of compounds with $k' > 10$ is larger than the number of compounds with $k' < 10$, then use $+20\%$ methanol in the mobile phase.

If the number of compounds with $k' > 10$ is smaller than or equal to the number of compounds with $k' < 10$, then use $+10\%$ methanol in the mobile phase.

If there are compounds with $k' < 1$ and $k' > 10$, then the user decides if -10% methanol in the mobile phase is applied.

REFERENCES

1 P. Conti, T. Hamoir, H. Piryns, N. Vanden Driessche, M. De Smet, F. Maris, H. Hindriks, P. J. Schoenmakers and D. L. Massart, *Chemometr. Intell. Lab. Syst.*, 11 (1991) 27.
2 M. De Smet, G. Musch, A. Peeters, L. Buydens and D. L. Massart, *J. Chromatogr.*, 485 (1989) 237.
3 M. De Smet, A. Peeters, L. Buydens and D. L. Massart, *J. Chromatogr.*, 457 (1988) 25.
4 H. Hindriks, F. Maris, J. Vink, A. Peeters, M. De Smet, D. L. Massart and L. Buydens, *J. Chromatogr.*, 485 (1989) 255.
5 F. Maris, H. Hindriks, J. Vink, A. Peeters, N. Vanden Driessche and D. L. Massart, *J. Chromatogr.*, 506 (1990) 211.
6 A. Peeters, L. Buydens, D. L. Massart and P. J. Schoenmakers, *Chromatographia*, 26 (1988) 101.
7 P. J. Schoenmakers, *Optimization of Chromatographic Selectivity*, Elsevier, Amsterdam. 1986.
8 J. C. Berridge, *Techniques for the Automated Optimization of HPLC Separations*, Wiley, New York, 1985.
9 A. G. Wright, A. F. Fell and J. C. Berridge, *Chromatographia*, 24 (1987) 533.
10 Hu Yuzhu and D. L. Massart, *J. Chromatogr.*, 485 (1989) 311.
11 J. L. Glajch, J. J. Kirkland, K. M. Squire and J. M. Minor, *J. Chromatogr.*, 199 (1980) 57.

Journal of Chromatography, 589 (1992) 45–51
Elsevier Science Publishers B.V., Amsterdam

CHROM. 23 720

Effect of superfluous remote polar functionality on chiral recognition

William H. Pirkle* and Christopher J. Welch

School of Chemical Sciences, University of Illinois, Urbana, IL 61801 (USA)

(First received July 30th, 1991; revised manuscript received September 2nd, 1991)

ABSTRACT

During the liquid chromatographic separation of enantiomers on chiral stationary phases (CSPs), non-specific adsorption processes diminish the observed enantioselectivity. The role of those polar groups in the analyte which are not specifically required for chiral recognition was investigated. A series of racemic analytes bearing various non-essential polar groups spatially removed from the sites of chiral recognition were synthesized and chromatographically evaluated. Four scenarios for the interaction of these remote polar groups with the CSP were considered and used to rationalize experimental findings. Cases were observed where enantioselectivity decreased, increased or remained the same on incorporation of a remote polar group.

INTRODUCTION

The separation of enantiomers on chiral stationary phases (CSPs) is dependent on the formation of transient diastereomeric adsorbates with different free energies (Fig. 1). Although this process can be conveniently represented as the formation of a more and a less stable adsorbate pair as in Fig. 1, the actual situation represents the contribution of a number of different adsorbate structures. Nevertheless, we have found that by considering the most probable adsorbate structures, reasonably accurate predictions concerning CSP performance and enantiomer elution order can be made. Using this approach, we have successfully designed and produced a number of CSPs with both broad scope and high enantioselectivity, achieving separation factors (α) greater than 50 in some instances [1].

On these CSPs, enantiomer separation requires that the analyte contain an appropriate combination of suitably located functionality for interaction with complementary sites in the CSP. However,

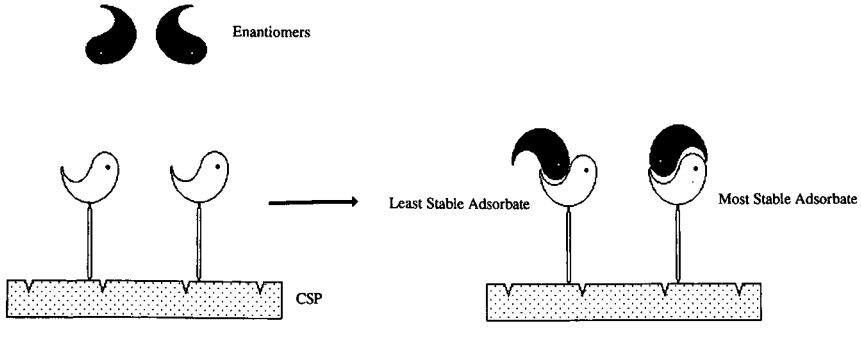

Fig. 1. Formation of transient diastereomeric adsorbates with different free energies permits enantiomer separation on CSPs.

0021-9673/92/$05.00

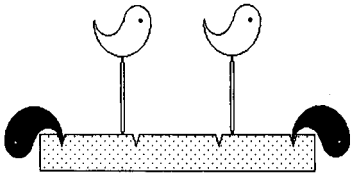

Fig. 2. Achiral retention, illustrated here as an interaction with the underlying chromatographic support, typically increases retention and decreases enantioselectivity.

many analytes which do possess such an arrangement also contain interaction sites not required in the chiral recognition process. In this investigation, we focused on the influence of these superfluous polar groups on chiral recognition. To investigate this phenomenon, a series of derivatives of the well studied N-(3,5-dinitrobenzoyl)leucine were studied chromatographically using several different CSPs.

BACKGROUND

Non-specific adsorption stemming from sites on the CSP

Non-specific adsorption stemming from superfluous sites on a CSP is known to lead to diminished enantioselectivity (Fig. 2). For example, it is well known that end-capping residual silanol groups on the underlying silica support often decreases retention and increases enantioselectivity [2].

Tandem column experiments such as the example shown in Fig. 3 clearly illustrate this principle. When a racemate such as β-binaphthol is chroma-

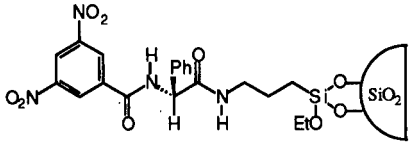

CSP 1

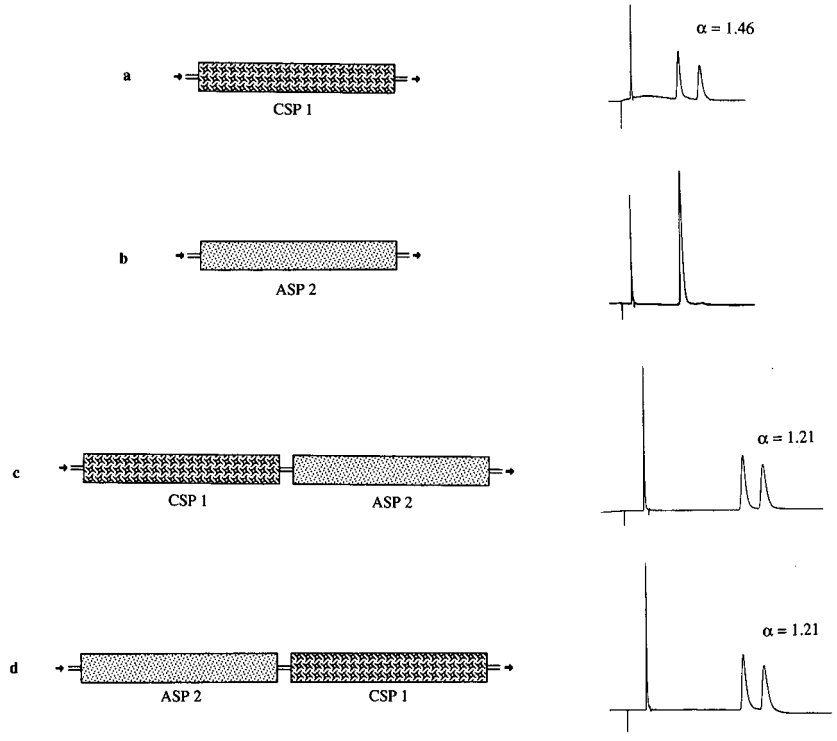

Fig. 3. Tandem column experiment illustrating decrease in enantioselectivity due to achiral retention. CSP 1 = Regis (*R*)-DNB-phenylglycine; ASP 2 = DNB-aminobutyl; mobile phase = 2-propanol–hexane (5:95); flow-rate = 2.00 ml/min; void volume indicator = tri-*tert.*-butylbenzene [5].

tographed on CSP 1 [3], the enantiomers are resolved (Fig. 3a), the separation factor being derived from their relative retention. An achiral stationary phase (ASP) such as ASP 2 gives retention, but no

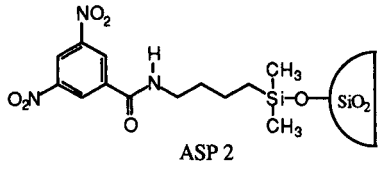

ASP 2

separation of enantiomers (Fig. 3b). When racemic β-binaphthol is chromatographed on a tandem column arrangement such as that shown in Fig. 3c or d, increased retention is observed. However, the interval between the elution of the enantiomer peaks remains the same. Hence the observed separation factor (α) decreases relative to the single column experiment.

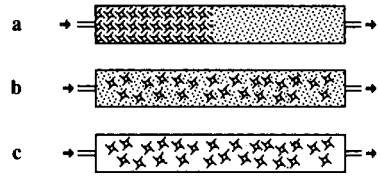

Fig. 4. Tandem column arrangement is equivalent to a single column containing regions of chiral and achiral packing (a), or to a column where these regions are intermingled (b). Elimination of sites for non-specific retention leads to improved CSPs (c).

The tandem column arrangement shown in Fig. 3c or d is conceptually identical with a single column having either separate or intermingled regions of chiral and achiral packing (Fig. 4a and b). Elimination of sites of non-specific analyte adsorption (Fig. 4c) leads to CSPs with improved enantioselectivites, as seen in the end-capping studied cited pre-

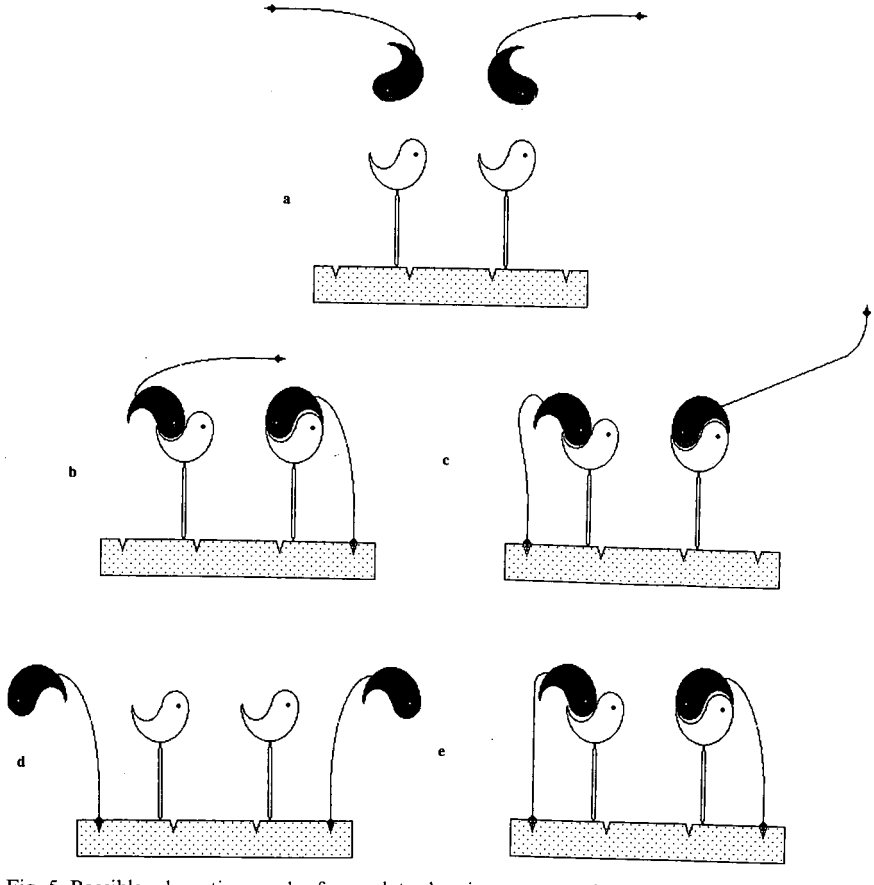

Fig. 5. Possible adsorption modes for analytes bearing remote polar groups.

viously. Although this message may seem obvious, its importance is not generally appreciated even though it has profound implications regarding CSP design. Many CSPs reported in the literature (or offered for sale) contain adsorption sites in excess of those required for chiral recognition. A forthcoming paper will deal specifically with the design of improved CSPs by deleting sites of non-productive adsorption. This study focuses on the effect of non-essential interaction sites present in the analyte.

Non-specific adsorption stemming from sites in the analyte

A racemic analyte bearing a remote polar group can be imagined to interact with a CSP in several different ways, all of which contribute to the observed retention (Fig. 5). Fig. 5 specifically illustrates the remote polar group interacting with the underlying chromatographic support. However, the remote polar group might also interact at sites in the selector or in the connecting tether. The consequences of these interactions will be similar regardless of their sites provided the interaction site is not one required for chiral recognition. Fig. 5a depicts the analyte enantiomers prior to adsorption by the CSP. Fig. 5b depicts the more strongly adsorbed enantiomer being selectively stabilized owing to an additional interaction between its remote polar group and the CSP. In the absence of a similar interaction for the less retained enantiomer, enantioselectivity is increased. Fig. 5c shows the converse of this situation where it is now the less stable diastereomeric adsorbate which is selectively stabilized by interaction of the remote polar group. This situation leads to a decrease in the observed enantioselectivity. In an extreme case, the elution order might even be reversed as the formerly less stable diastereomeric adsorbate becomes the most stable. Fig. 5d illustrates the situation where both enantiomers interact solely through the remote polar group. These achiral processes compete with those which afford chiral recognition, attenuating the observed enantioselectivity. The situation pictured in Fig. 5d is analogous to the tandem column and pre-end-capping situations described earlier, situations which were shown to afford a decrease in enantioselectivity. The final example (Fig. 5e) depicts the remote polar group of each enantiomer interacting equally well with the CSP during the normal chiral recognition process. This situation is expected to give rise to increased retention but no change in enantioselectivity as it increases binding energies but does not alter the difference in the binding energies.

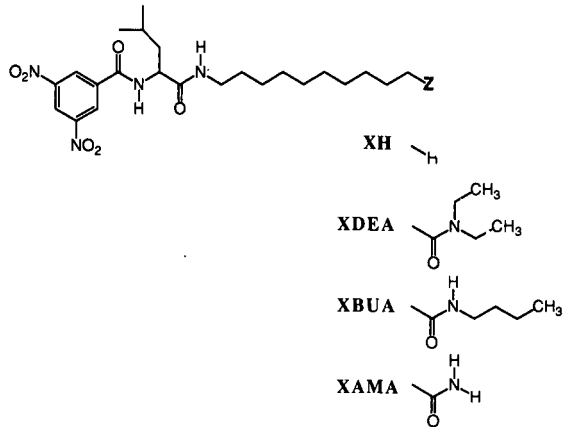

Fig. 6. The group of four N-(3,5-dinitrobenzoyl)leucine derivatives used in the study.

In an effort to assess the contribution of the various adsorption modes to actual chiral separations, four derivatives of the well-studied N-(3,5-dinitrobenzoyl)leucine system were prepared and analyzed on several CSPs. The four analytes, shown in Fig. 6, contain groups of varying polarity at Z. Using the symbol X to designate the DNB-leucine moiety containing ten methylene units, the four derivatives are termed XH, XDEA, XBUA and XAMA. The last three terminal groups are amides, good hydrogen bond acceptors having sizable dipole moments. These have, respectively, no, one and two acidic hydrogen bond donor sites as well.

EXPERIMENTAL

Apparatus

Chromatographic analysis was performed using a Beckman-Altex Model 100-A pump, a Rheodyne Model 7125 injector with a 20-μl sample loop, a Beckman 153A UV absorbance monitor (254 nm) and a Hewlett-Packard HP 3394A integrating recorder.

Materials

Solvents used were of HPLC grade or distilled

prior to use. The four N-(3,5-dinitrobenzoyl)leucine derivatives were prepared by addition of the appropriate amine to the corresponding N-hydroxysuccinimide active ester in acetonitrile solvent, followed by purification of the derivative by flash chromatography on silica. All were satisfactorily characterized by ^{1}H NMR spectrometry.

CSPs 1, 3, 4 and 6 are the commercial versions (Regis Chemical, Morton Grove, IL, USA) of CSPs developed in our laboratories. CSPs 2, 5 and 7 were produced in our laboratories and will be described in subsequent publications. CSPs 8 and 9 were available from a previous study [4].

Methods

All chromatographic experiments were carried out at a nominal flow-rate of 2.00 ml/min. The void time was determined by injection of 1,3,5-tri-*tert.*-butylbenzene [5].

RESULTS AND DISCUSSION

We have previously reported [6] that the N-(2-naphthyl)alanine-based CSP 3, affords high enantioselectivities for the separation of the enantiomers of N-3,5-dinitrobenzoyl (DNB) derivatives of amino acids. The data concerning the separation of the enantiomers of the four remote polar group analytes on this CSP are given in Table I. The compounds undergo a dramatic increase in retention as the polarity of the Z group is increased. However, the separation factor remains relatively unchanged throughout the series, indicating a predominant mode of interaction such as that shown in Fig. 5e.

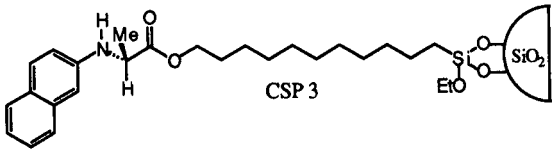

The recently developed N-(1-naphthyl)leucine CSP 4 is mechanistically similar to CSP 3 but has been shown to afford greater enantioselectivity in some instances [1]. Data pertinent to the separation of the enantiomers of three of the four remote polar group analytes on this CSP are given in Table I. A dramatic increase in retention occurs as the polarity of the Z group is increased with α remaining more or less constant throughout the series, again indicating an interaction mode such as that shown in Fig. 5e.

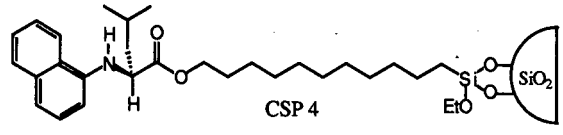

The recently developed CSP 5 represents an alternative anchoring scheme for the selector shown in CSP 3. Owing to the greater electron density on the carbonyl oxygen in this CSP, increased enantio-

TABLE I

CHROMATOGRAPHIC DATA FOR THE SEPARATION OF THE FOUR REMOTE POLAR GROUP ANALYTES ON DIFFERENT CSPs

CSP	Mobile phase[a]	XH			XDEA			XBUA			XAMA		
		k'_1	k'_2	α	k'_1	k'_2	α	k'_1	k'_2	α	k'_1	k'_2	α
CSP 3	A	1.35	17.45	12.93	5.09	68.40	13.44	4.04	51.19	12.67	6.60	83.19	12.66
CSP 4	A	1.11	26.56	23.93	2.92	68.38	21.71	2.39	51.19	21.67	–	–	–
CSP 5	A	1.07	33.72	31.51	2.43	67.34	27.71	3.02	78.11	25.86	4.81	115.6	24.04
CSP 3	B	2.15	10.95	5.09	2.08	10.08	4.85	1.29	6.05	4.69	0.95	4.40	4.63
CSP 6	A	0.87	1.30	1.49	4.59	6.75	1.47	3.97	5.87	1.48	8.99	13.13	1.46
CSP 7	A	0.58	1.20	2.07	2.05	3.83	1.87	2.11	3.81	1.81	5.08	9.01	1.77
CSP 8	A	1.77	1.77	1.00	7.65	10.48	1.37	9.53	11.67	1.22	23.44	37.26	1.59
CSP 9	A	0.73	1.34	1.84	3.79	4.94	1.30	4.35	5.75	1.32	13.37	13.37	1.00

[a] Mobile phase: (A) 2-propanol–hexane (20:80); (B) methanol–water (80:20).

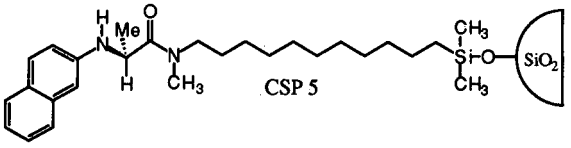

CSP 5

selectivity relative to CSP 3 is often noted for analytes using this carbonyl oxygen as an essential interaction site. Data for the separations of the enantiomers of the four remote polar groups analytes on CSP 5, given in Table I, show greatly increased retention and relatively constant α throughout the series. The slight decrease in enantioselectivity observed as the polarity of the Z group is increased may reflect some contribution to retention by adsorbates such as that shown in Fig. 5d. As Z groups of increased polarity decrease enantioselectivity more dramatically on CSP 5 than on either CSP 3 or 4, one presumes that the amide carbonyl oxygen of the CSP may be involved in additional achiral interaction.

Reversed-phase separation of the enantiomers of the four remote polar group analytes on CSP 3 is also shown in Table I. As is frequently the case, enantioselectivities are reduced relative to those obtained under normal-phase conditions [6,7]. Not unexpectedly, the retentions decrease with increasing Z group polarity, reflecting the increased solvation of the more polar Z groups. Again, a slight decrease in α with increasing Z group polarity is noted, perhaps indicating the contribution of adsorbates such as that shown in Fig. 5d.

An interesting property of DNB-amino acid derivatives is their modest capacity for self-recognition. Thus, a DNB-leucine CSP such as CSP 6 is

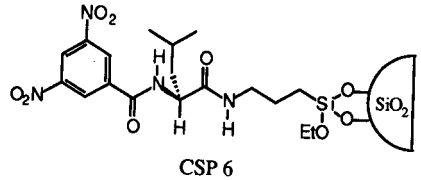

CSP 6

capable of serparating the enantiomers of racemic DNB-leucine derivatives. Data for the separation of the four analytes on CSP 6, given in Table I, again exhibit a dramatic increase in retention with increasing Z group polarity. However, α remains constant throughout the series, indicating that the predominant adsorbate may be represented as shown in Fig. 5e.

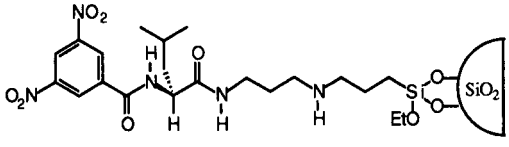

CSP 7

In CSP 7, an analogue of CSP 6, a superfluous amino group has been incorporated into the linking tether. Although this CSP shows the typical increase in retention with increasing Z group polarity, its enantioselectivity decreases for those analytes having more polar Z groups. This result may be indicative of the contribution of adsorbate structures (such as that shown in Fig. 5d) where the polar Z groups are capable of achiral interaction with the superfluous amine moiety.

Perhaps the most interesting observations come from the analysis of the remote polar group analytes on CSPs 8 and 9. These CSPs are very similar except for their mode of attachment to silica. When used to separate the enantiomers of DNB derivatives of a homologous series of α-arylaminoalkanes, the alkyl-linked CSP 8 shows increased enantioselectivity as the length of the alkyl substituent of the analyte is increased, whereas the acyl-linked CSP 9 shows decreased enantioselectivity [4]. This behavior was explained in terms of differential intercalation of the alkyl substituents of analyte enantiomers between strands of bonded phase. Differential intercalation influences enantioselectivity and the mode of attachment of the chiral selector to the silica determines whether it is the initially eluted or the more retained enantiomer which has the more severe intercalation problem. Differential intercalation also seems to explain the behavior of the remote polar group analyte enantiomers when chromatographed on CSPs 8 and 9.

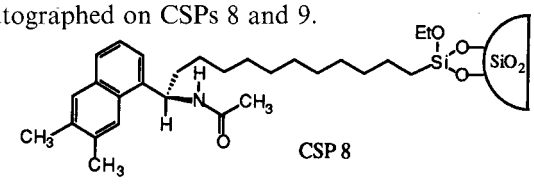

CSP 8

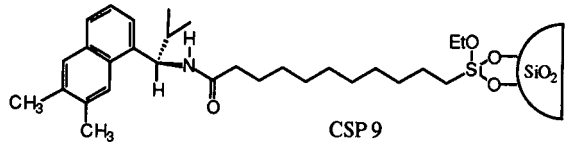

CSP 9

Data pertinent to the separation of the enantiomers of the remote polar group analytes on CSPs 8 and 9 are presented in Table I. On the alkyl-linked CSP 8, an increase in enantioselectivity occurs with an increase in Z group polarity, whereas on the acyl-linked CSP 9, enantioselectivity decreases as Z becomes more polar. Although the chain of ten methylene units causes intercalation difficulties, a polar group at its end makes possible a bonding interaction with (presumably) the underlying silica support. The mode of attachment of the selector to the silica support determines which enantiomer most effectively intercalates its Z group. This situation is depicted in Fig. 5b and c for CSPs 8 and 9, respectively. Consistent with this interpretation, when a homologous series of DNB-leucine *n*-alkylamides is chromatographed on CSPs 8 and 9, an increase in the length of the *n*-alkyl group causes a decrease in enantioselectivity on CSP 8 but an increase on CSP 9. Moreover, the elution orders noted (an *R* CSP selectively retains the *R* analyte enantiomer) are consistent with this mechanistic picture.

CONCLUSIONS

Four racemic derivatives of N-(3,5-dinitrobenzoyl)leucine bearing non-essential polar functionalities remote from those sites essential for chiral recognition have been examined on several CSPs. Four possible scenarios for the interaction of these remote polar groups with the CSP and the consequences thereof (in terms of the effect on enantioselectivity) have been considered and used to rationalize the experimental observations. The case in which the retention increases dramatically and the enantioselectivity remains more or less constant on incorporation of a remote polar group seems to be common. Such cases, owing to the greatly increased retentions, would commonly necessitate the use of more polar mobile phases to achieve reasonable analysis times. As enantioselectivity generally diminishes with increasing mobile phase polarity [7], the remote polar groups may have the effect of indirectly reducing enantioselectivity.

ACKNOWLEDGEMENTS

This material was presented in part at the *17th Annual Meeting of the Federation of Analytical Chemistry and Spectroscopy Societies, Cleveland, OH, October 1990.* This research was funded in part by a Department of Education Advanced Opportunities in Chemistry Graduate Fellowship. Special thanks are due to Qing Yang for the preparation of CSP 7.

REFERENCES

1 W. H. Pirkle, K. C. Deming and J. A. Burke, *Chirality*, 3 (1991) 183.
2 W. H. Pirkle and R. S. Readnour, *Chromatographia*, 31 (1991) 129.
3 W. H. Pirkle and J. L. Schreiner, *J. Org. Chem.*, 46 (1981) 4988.
4 W. H. Pirkle, M. H. Hyun and B. Bank, *J. Chromatogr.*, 316 (1984) 585.
5 W. H. Pirkle and C. J. Welch, *J. Liq. Chromatogr.*, 14 (1991) 1.
6 W. H. Pirkle and T. C. Pochapsky, *J. Am. Chem. Soc.*, 108 (1986) 352.
7 W. H. Pirkle and C. J. Welch, *J. Liq. Chromatogr.*, 14 (1991) 2027.

Journal of Chromatography, 589 (1992) 53–59
Elsevier Science Publishers B.V., Amsterdam

CHROM. 23 726

Silica-bonded chiral stationary phases with structurally simple π-donor chiral selectors for high-performance liquid chromatography

Laureano Oliveros* and Cristina Minguillón☆

Conservatoire National des Arts et Métiers, Laboratoire de Chimie Générale (CNRS URA 1103), 292 Rue Saint-Martin, 75141 Paris Cédex 03 (France)

Bernard Desmazières and Paul-Louis Desbène

URA 455, Université P. et M. Curie, Laboratoire de Chimie Organique Structurale, 4 Place Jussieu, 75230 Paris Cédex 05, and Université de Rouen, LASOC, 43 Rue Saint Germain, 27000 Evreux (France)

(First received June 19th, 1991; revised manuscript received September 3rd, 1991)

ABSTRACT

Seven new chiral stationary phases obtained from (*S*)-phenylalanine derivatives, (*R*)-Mosher's acid and (*S*)-naproxen were prepared and evaluated. The racemic substances used to test them contained either π-acidic or π-basic sites. The best results were observed when the chiral entity bonded to γ-aminopropylsilica gel was 3,5-dimethylanilido-, 3,5-dimethylbenzoyl- or 3,5-dimethoxybenzoyl-(*S*)-phenylalanine and -(*S*)-naproxen.

INTRODUCTION

Although silica gel bonded to optically active compounds has a relatively limited scope of application, it constitutes an important kind of stationary phase for the resolution of racemic compounds by high-performance liquid chromatography (HPLC) [1]. The main advantage of such stationary phases is their ease of preparation when compared with macromolecular supports such as proteins, polysaccharides or synthetic polymers whose range of application is wider than that of silica-bonded chiral stationary phases [2].

Many of the chiral molecules used for bonding on silica gel have either π-donor or π-acceptor radicals. Chiral entities described in π-acceptor stationary phases are almost always 3,5-dinitrobenzoyl derivatives of amino acids. However, π-donor stationary phases have several kinds of chiral entities, most of which bear a naphthyl radical [3]. This structural diversity on π-donor chiral entities shows that a suitable family of π-donor chiral selectors has not yet been found.

New silica-bonded stationary phases with the naphthylethylamine group, either isolated or associated with amino acids, as chiral entity have recently been described, with a relatively wide range of application [4,5]. However, the general use of chiral stationary phases having π-donor character is only recommended for the resolution of racemic compounds bearing a 3,5-dinitrobenzoyl group.

In this context, we considered the utility of

☆ Present address: Laboratorio de Química Farmacéutica, Facultad de Farmacia, Universidad de Barcelona, Avd. Diagonal s/n, 08028-Barcelona, Spain.

0021-9673/92/$05.00

searching for new π-donor chiral selectors, taking into account the good performances of stationary phases with a naphthyl or a 3,5-disubstituted phenyl radical [3,6]. According to the literature, the performances of π-donor stationary phases are not improved if the structure of the chiral entity becomes more complex, so we chose easily accessible, structurally simple molecules.

In a previous paper [7] we showed that the coexistence of two different chiral centres on the same silica gel can prevent the resolution of certain racemic compounds. Therefore, we utilized optically active molecules with only one asymmetric centre to be bonded on γ-aminopropylsilanized silica gel.

We describe the preparation of seven new chiral stationary phases, six of which have a π-donor character. These stationary phases were obtained by covalently bonding either optically active acids or (*S*)-phenylalanine derivatives on γ-aminopropylsilanized silica gel. The structures of all of them are given in Figs. 1 and 2.

Chiral silica bonded phases were tested with several racemic compounds, also used in our previous study [7] (Fig. 3).

EXPERIMENTAL

NMR spectra were measured using a Bruker AC200 spectrometer. Tetramethylsilane (TMS) was used as the internal standard with chemical shifts measured in ppm. Rotatory power was measured with a Perkin-Elmer Model 241 polarimeter. Elemental analyses were performed by the Service Central de Microanalyse du CNRS (Vernaison, France). The chromatographic experiments were carried out on an HP 1090 liquid chromatograph (Hewlett-Packard, Palo Alto, CA, USA) equipped with a PU 4020 UV detector (Philips, Cambridge, UK). The chiral stationary phases were packed into stainless-steel tubes (100 × 4.6 mm I.D.) by the slurry method according to Coq *et al.* [8]. The volume of sample injected was 5 μl, the flow-rate of the pump was 1 ml/min, the detection wavelength was 254 nm and the mobile phases consisted of various mixtures of *n*-heptane, chloroform and methanol.

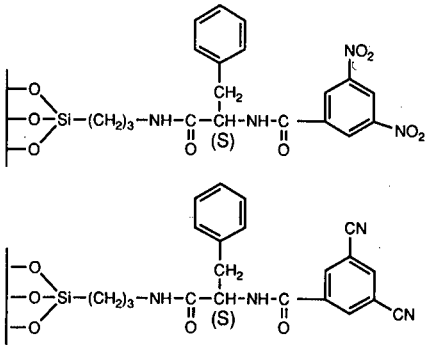

Fig. 1. Structures of chiral stationary phases with a π-acceptor character.

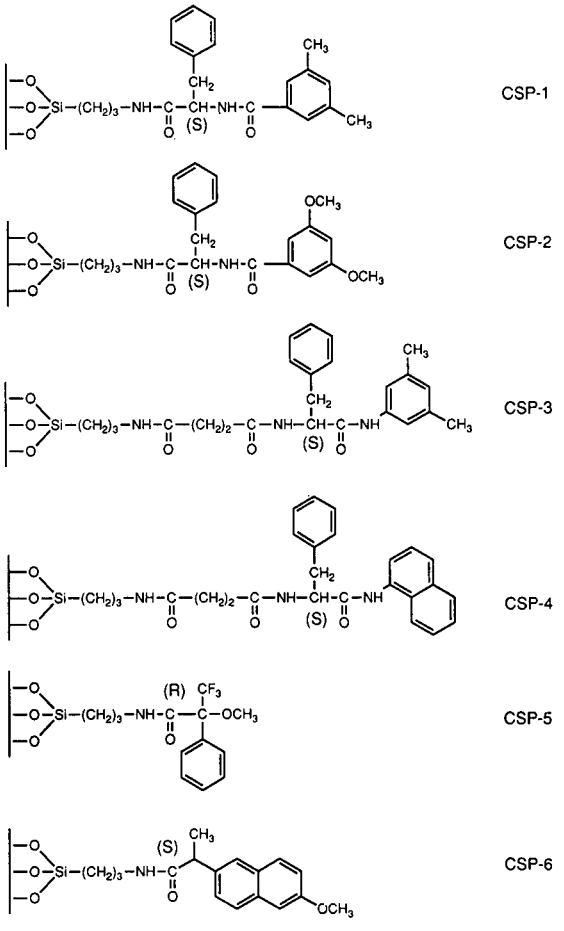

Fig. 2. Structures of chiral stationary phases with a π-donor character.

Chemicals and reagents

Compounds **1–3** (Fig. 3) were obtained by treating the methyl ester of each amino acid with 3,5-dinitrobenzoyl chloride. Compound **6** was prepared

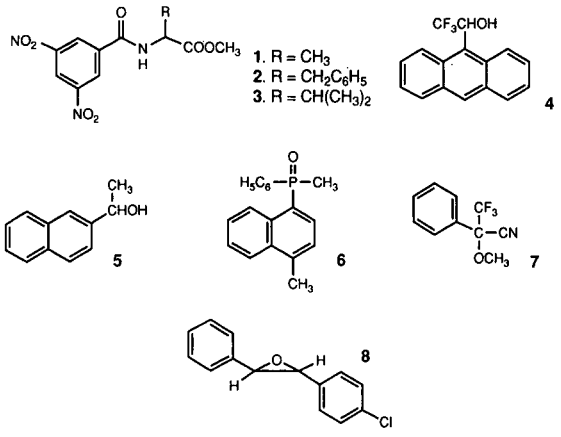

Fig. 3. Structures of test compounds.

by the method described previously [9]. All were identified by their ^{1}H NMR spectra and elemental analysis. Compounds **4**, **5**, **7** and **8** were purchased from Aldrich.

*(S) - tert. - Butoxycarbonylphenylalanyl - 3,5 - dimethylanilide (**9**) and (S)-tert.-butoxycarbonylphenylalanyl-1-naphthylamide (**10**) (Fig. 4).* To a solution of 3.6 g (13.6 mmol) of L-N-Boc-phenylalanine and 14.0 mmol of the appropriate amine in 50 ml of tetrahydrofuran (THF), a solution of 3.46 g (14.0 mmol) of 2-ethoxy-1-ethoxycarbonyl-1,2-dihydroquinoline (EEDQ) in 30 ml of THF was added. The mixture was allowed to react overnight at room temperature, then the solution was evaporated. The residue was diluted with dichloromethane and washed with 1% orthophosphoric acid, 0.2 *M* potassium hydroxide and distilled water. After drying over sodium sulphate, the solution was evaporated and the residual solid collected.

When 3,5-dimethylaniline was used, recrystallization from toluene–heptane gave 3.8 g (76%) of a white solid, m.p. 142°C. ^{1}H NMR (200 MHz): δ (C^2HCl_3) 1.41 (s, 9H, *tert.*-butyl), 2.21 (s, 6H, CH_3Ar^a), 3.13 (m, 2H, CH_2Ar'), 4.61 (m, 1H, CH), 5.55 (d, 1H, N*H*CH), 6.71 (s, 1H, C^4H), 7.03 (s, 2H, C^2H and C^6H), 7.26 (s, 5H, Ar'H), 8.36 (m, 1H, NHAr). ^{13}C NMR (50.3 MHz): δ (C^2HCl_3) 21.2 (CH_3Ar), 28.2 [$(CH_3)_3$], 38.6 (CH_2), 56.7 (CH), 80.4, (Cq = quaternary carbon atom), 117.8 (C^2H and C^6H), 126.0 and 126.9 (C^4H and $C^{4'}H$), 128.6 and 129.3 ($C^{2',6'}H$ and $C^{3',5'}H$), 136.7 and 137.2 (C^1 and $C^{1'}$), 138.4 ($C^{3,5}$), 155.8 (OCON), 169.7 (CON). $[\alpha]_D^{23} = -13.7°$ (c = 1.4, chloroform). Analysis: calculated for $C_{22}H_{28}N_2O_3$, C 71.71, H 7.66, N 7.60; found, C 71.79, H 7.56, N 7.46%.

When 1-naphthylamine was used, recrystalliza-

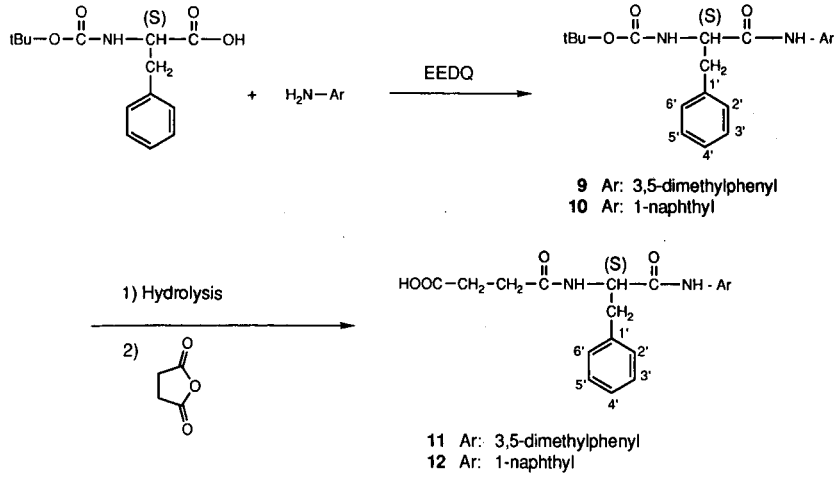

Fig. 4. Scheme for the preparation of **11** and **12**. tBu = *tert.*-Bu

[a] Ar and Ar' refer to the formulae in Figs. 4 and 5. Ar represents the disubstituted phenyl radical, symbolized by Ar and numbered 1, 2 .... and also the naphthyl radical of compounds 10 and 12. Ar' represents the phenyl radical C_5H_6 the positions of which are numbered 1', 2', etc.

tion from toluene gave 5 g (94.5%) of a white solid, m.p. 139°C. ^{1}H NMR (200 MHz): δ (C^2HCl_3) 1.46 (s, 9H, *tert.*-butyl), 3.24 (d, 2H, CH_2Ar'), 4.68 (m, 1H, CH), 5.39 (m, 1H, N*H*CH), 7.3–7.9 (m, 12H, ArH and Ar'H), 8.44 (m, 1H, NHAr). ^{13}C NMR (50.3 MHz): δ (C^2HCl_3) 27.7 [$(CH_3)_3$], 37.5 (CH_2), 56.2 (CH), 80.0 (Cq *tert.*-butyl), 120–136 (CH and Cq aromatic), 155.3 (OCON), 169.6 (CON). $[\alpha]_D^{23} = -33.6°$ (c = 1.5, chloroform). Analysis: calculated for $C_{24}H_{26}N_2O_3$, C 73.82, H 6.71, N 7.17; found, C 73.64, H 6.91, N 7.05%.

*Succinyl (S)-phenylalanyl-3,5-dimethylanilide (**11**).* A 2-g (5.4-mmol) amount of **9** was dissolved in glacial acetic acid (36 ml) and cooled in an ice-bath. Hydrogen chloride was passed through for 40 min and the solution was left to stand at room temperature for 3 h. The solvent was removed *in vacuo* and the residual solid was washed in diethyl ether. The solid was dissolved in pyridine (25 ml) and succinic anhydride (2.7 g, 27 mmol) was added. After stirring for 24 h at room temperature, the mixture was evaporated and the residue treated with 5% orthophosphoric acid and distilled water. Recrystallization from ethanol–water gave 1.7 g (84%) of a white solid, m.p. 178°C. ^{1}H NMR (200 MHz): δ {[$^2H_6$]dimethyl sulphoxide (DMSO-d_6)} 1.83 (s, 6H, CH_3Ar), 2.00–2.12 (m, 4H, CH_2CH_2), 2.56–2.75 (AB zone of ABX system, 2H, CH_2Ar'), 4.35 (m, 1H, CH), 6.27 (m, 1H, NHAr), 6.73–6.84 (m, 8H, ArH and Ar'H), 7.40 (d, 1H, N*H*CH), 8.91 (s, 1H, COOH). ^{13}C NMR (50.3 MHz): δ (DMSO-d_6) 19.9 (CH_3Ar), 28.1 and 29.2 (CH_2CH_2), 36.5 (CH_2Ar'), 53.5 (CH), 116.4 (C^2H and C^6H), 124.1 and 125.1 (C^4H and $C^{4'}H$), 126.8 and 127.9 ($C^{2',6'}H$ and $C^{3',5'}H$), 136.1 and 136.8 (C^1 and $C^{1'}$), 136.6 (C^3 and C^5), 168.4, 170.5 and 173.1 (CO). $[\alpha]_D^{23} = -18.5°$ (c = 1.3, pyridine). Analysis: calculated for $C_{21}H_{24}N_2O_4$, C 68.46, H 6.56, N 7.60; found, C 68.80, H 6.72, N 7.58%.

*Succinyl (S)-phenylalanyl-1-naphthylamide (**12**).* Analogously to **11**, **12** was obtained from **10** (2 g, 5.12 mmol). Recrystallization from ethanol–water gave 1.7 g (85%) of a white solid, m.p. 170°C. ^{1}H NMR (200 MHz): δ (DMSO-d_6) 2.44 (m, 4H, CH_2CH_2), 2.88–3.30 (AB zone of ABX system, 2H, CH_2Ar'), 4.87 (m, 1H, CH), 7.18–8.04 (m, 12H, ArH and Ar'H), 8.43 (d, 1H, N*H*CH), 10.0 (s, 1H, NHAr), 11.6–12.4 (ba, 1H, COOH). ^{13}C NMR (50.3 MHz): δ (DMSO-d_6) 29.0 and 29.8 (CH_2CH_2), 37.7 (CH_2Ar), 54.6 (CH), 122–130 (CH aromatic), 127.9, 133.1, 133.5 and 137.6 (Cq aromatic), 170.7, 171.2 and 173.8 (CO). $[\alpha]_D^{23}$ −23.7° (c = 1.4, pyridine). Analysis: calculated for $C_{23}H_{22}N_2O_4$, C 70.76, H 5.68, N 7.17; found, C 70.68, H 5.95, N 7.01%.

3,5-Dicyanobenzoic acid. 3,5-Dicyanotoluene (5 g, 35 mmol) was dissolved in 30 ml of acetic acid and 5 ml of concentrated sulphuric acid and cooled in an ice-bath. Chromic oxide (9 g, 90 mmol) dissolved in 90 ml of acetic acid was added while stirring. The solution was stirred at room temperature for 14 h and poured on ice. The resulting solid was filtered and dissolved in aqueous sodium carbonate solution. The solution was filtered and acidified with hydrochloric acid. The solid was collected by filtration and washed with water. Recrystallization from water gave 1.5 g (25%) of a white solid, m.p. 228°C. ^{1}H NMR (200 MHz): δ (C^2HCl_3–DMSO-d_6) 7.74 (d, 1H, C^4H), 7.81 (d, 2H, C^2H and C^6H). ^{13}C NMR (50.3 MHz): δ (C^2HCl_3–DMSO-d_6) 112.4 and 114.7 (CN and $C^{3,5}$), 132.3 (C^1), 135.2 ($C^{2,6}H$), 137.5 (C^4H), 162.7 (COOH). Analysis: calculated for $C_9H_4N_2O_2$, C 62.80, H 2.34, N 16.27; found, C, 62.27, H 2.36, N 16.27%.

*N-Acyl-(S)-phenylalanines (**13–16**) (Fig. 5).* (*S*)-Phenylalanine (4.13 g, 25 mmol) was dissolved in 45 ml of 1 *M* sodium hydroxide solution and

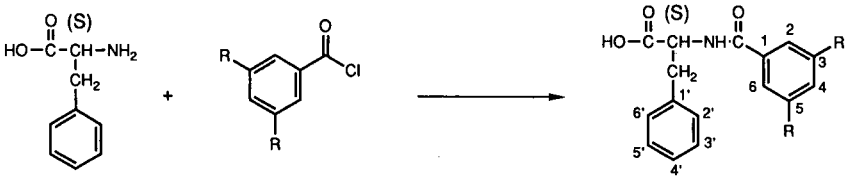

13 R: NO_2 **15** R: CH_3
14 R: CN **16** R: OCH_3

Fig. 5. Scheme for the preparation of **13–16**.

cooled in an ice-bath. The appropriate acyl chloride (25 mmol), obtained by treating the corresponding acid with thionyl chloride, and 50 ml of 1 *M* sodium hydroxide solution were added simultaneously, with magnetic stirring, over a period of 20 min. The solution was stirred at room temperature for 90 min and acidified with concentrated hydrochloric acid (pH 2–3). The resulting solid was collected by filtration and washed with water. Recrystallization from ethanol yielded the corresponding N-acyl-phenylalanine.

N-(3,5-Dinitrobenzoyl)-(*S*)-phenylalanine (**13**) was described previously [10].

N-(3,5-Dicyanobenzoyl)-(*S*)-phenylalanine (**14**) could not crystallized, so it was dissolved in methanol and boiled with charcoal, filtered and evaporated; yield 42%, m.p. 110°C. ^{1}H NMR (200 MHz): δ (C^2HCl_3–DMSO-d_6) 2.60–3.05 (m, 2H, CH_2), 4.47 (m, 1H, CH), 6.85 (s, 5H, phenyl), 7.73 (s, 1H, C^4H), 8.10 (s, 2H, C^2H and C^6H), 8.50 (d, 1H, NH). ^{13}C NMR (50.3 MHz): δ (C^2HCl_3–DMSO-d_6) 36.1 (CH_2), 53.5 (CH), 112.7 (C^3 and C^5), 115.4 (CN), 125.6 ($C^{4'}H$), 127.3 and 128.1 ($C^{2',6'}H$ and $C^{3',5'}H$), 129.8 ($C^{1'}$), 134.5 ($C^{2,6}H$), 135.4 (C^1), 136.3 (C^4H), 162.0 (CONH), 172.0 (COOH). $[\alpha]_D^{23} = -32.9°$ (c = 1,3, pyridine). Analysis: calculated for $C_{18}H_{13}N_3O_3$. H_2O, C 64.10, H 4.48, N 12.46; found, C 64.19, H 4.41, N 12.63%.

N-(3,5-Dimethylbenzoyl)-(*S*)-phenylalanine (**15**) was obtained in 86% yield, m.p. 139°C. $[\alpha]_D^{23} = -31.5°$ (c = 1.4, pyridine). ^{1}H NMR (200 MHz): δ ($CDCl_3$) 2.33 (s, 6H, CH_3), 3.32 (m, 2H, CH_2), 5.09 (m, 1H, CH), 6.61 (d, 1H, NH), 7.14–7.31 (m, 8H, ArH), 8.65 (bb, 1H, COOH). ^{13}C NMR (50.3 MHz): δ (C^2HCl_3) 21.1 (CH_3), 37.2 (CH_2), 55.5 (CH), 124.7 ($C^{2,6}H$), 127.2 ($C^{4'}$), 128.6 and 129.4 ($C^{2',6'}H$ and $C^{3',5'}H$), 133.2 and 135.5 (C^1 and $C^{1'}$), 133.3 (C^4H), 138.3 ($C^{3,5}$), 168.1 (CONH), 175.0 (COOH). Analysis: calculated for $C_{18}H_{19}NO_3$, C 72.72, H 6.40, N 4.71; found, C 72.99, H 6.30, N 4.74%.

N-(3,5-Dimethoxybenzoyl)-(*S*)-phenylalanine (**16**) was obtained in 80% yield, m.p. 146°C. ^{1}H NMR (200 MHz): δ (C^2HCl_3–DMSO-d_6) 2.74 (m, 2H, CH_2), 3.34 (s, 6H, CH_3O), 4.36 (m, 1H, CH), 6.10 (d, 1H, C^4H), 6.50 (d, 2H, C^2H and C^6H), 6.82 (m, 5H, phenyl), 7.83 (d, 1H, NH). ^{13}C NMR (50.3 MHz): δ (C^2HCl_3–DMSO-d_6) 35.7 (CH_2), 52.9 (CH), 54.0 (CH_3O), 102.1 (C^4H), 104.0 ($C^{2,6}H$), 125.5 ($C^{4'}H$), 126.9 and 127.8 ($C^{2',6'}H$ and $C^{3',5'}H$), 134.7 and 135.8 (C^1 and $C^{1'}$), 159.1 ($C^{3,5}$), 165.5 (CONH), 170.4 (COOH). $[\alpha]_D^{23} = -30.8°$ (c = 1.3, pyridine). Analysis: calculated for $C_{18}H_{19}NO_5$, C 65.65, H 5.81, N 4.25; found, C 65.60, H 5.75, N 4.06%.

Chiral stationary phases

All chiral stationary phases were obtained from the appropriate chiral acidic compound according to the procedure described previously [7]. Elemental analyses are given in Table I.

RESULTS AND DISCUSSION

Chromatographic behaviour of stationary phases

Chromatographic results are given in Table II. We have also included results obtained from two π-acceptor stationary phases bearing N-(3,5-dinitrobenzoyl)-(*S*)-phenylalanine or N-(3,5-dicyanobenzoyl)-(*S*)-phenylalanine as chiral selectors (CSP-A1 and CSP-A2, respectively). CSP-A1 has already been described [10] and the corresponding results come from ref. 7. CSP-A2 was prepared in order to compare the efficacy of the 3,5-dicyanobenzoyl radical with that of the 3,5-dinitrobenzoyl radical, both being π-acceptors. Although the chromatographic behaviours of these two stationary phases are similar, the performance of CSP-A1 is better than that of CSP-A2. This is a new illustration of the efficacy of the 3,5-dinitrobenzoyl radical in the resolution of racemic compounds by means of silica-bonded chiral stationary phases, either when belonging to the chiral selector in the stationary phase or being borne by the racemic compound [7].

Enantiomers of racemic test compounds, except **5** and **6**, and to a lesser extent **4**, are well resolved by four of the six π-donor stationary phases, *viz.*, CSP-1, CSP-2, CSP-3 and CSP-6, whose chiral entities are 3,5-dimethylbenzoyl-(*S*)-phenylalanine, 3,5-dimethoxybenzoyl-(*S*)-phenylalanine, (*S*)-phenylalanyl-3,5-dimethylanilide and (*S*)-naproxen, respectively. The choice of chiral entities constituted by a substituted phenyl radical with electron-donating groups seems to be correct. On the other hand, with respect to the naphthyl group, our results are not conclusive. Although CSP-6 [(*S*)-naproxen] gives good results, like those of chiral sta-

TABLE I

ELEMENTAL ANALYSES OF CHIRAL STATIONARY PHASES

Chiral stationary phase	Elemental analysis (%)			Ratio of carbon atoms per nitrogen atom		Bonded chiral moieties per gram of stationary phase[a] (mmol)	
	C	H	N	Analytical	Theoretical[a]	From %C	From %N
CSP-A1	10.93	1.76	2.69	4.74	4.75	0.48	0.48
CSP-A2	9.45	1.45	2.28	4.84	4.75	0.41	0.41
CSP-1	11.54	1.48	1.74	7.74	10.50	0.46	0.62
CSP-2	13.69	1.93	2.00	7.99	10.50	0.54	0.71
CSP-3	12.99	1.95	2.16	7.01	8.00	0.45	0.51
CSP-4	12.28	1.87	1.67	8.58	8.67	0.39	0.40
CSP-5	7.56	1.16	1.02	8.65	13.00	0.48	0.73
CSP-6	9.42	1.56	1.04	10.57	17.00	0.46	0.74

[a] Calculations made with regard to organic moiety structures in each stationary phase. The remaining free NH_2 groups were not considered.

TABLE II

CAPACITY FACTORS, k'_1, OF FIRST-ELUTED ENANTIOMER AND SELECTIVITY FACTORS, α, IN THE COLUMNS TESTED

Chiral stationary phase	**1**		**2**		**3**		**4**		**5**		**6**		**7**		**8**	
	k'_1	α	k'_1	α	k'_1	α	k'_1	α	k'_1	α	k'_1	α	k'_1	α	k'_1	α
CSP-A1	1.84 (*R*)[a]	1.19	1.27 (*R*)	1.21	1.03 (*R*)	1.22	2.18 (*S*)	1.19	8.10	1.06	19.17	1.13	0.35	1.27	0.52	1.60
CSP-A2	2.15 (*R*)	1.13	1.38 (*R*)	1.18	1.22 (*R*)	1.13	1.79	1.03	6.28	1.00	16.81	1.05	0.31	1.00	0.63	1.43
CSP-1	2.02 (*R*)	1.63	0.90 (*R*)	1.90	0.62 (*R*)	1.81	2.91	1.00	2.73	1.00	1.64	1.00	0.19	14.86	0.14	1.50
CSP-2	1.66 (*R*)	2.29	0.75 (*R*)	2.21	0.56 (*R*)	2.00	2.06	1.00	2.12	1.00	0.39	1.00	0.18	23.00	0.04	3.33
CSP-3	1.90 (*R*)	2.32	0.91 (*R*)	2.10	0.65 (*R*)	2.47	1.50	1.00	2.48	1.00	2.33	1.00	0.14	3.55	0.14	1.70
CSP-4	2.86 (*R*)	1.13	1.51 (*R*)	1.17	1.15 (*R*)	1.19	1.54	1.00	4.37	1.00	7.45	1.00	0.20	1.00	0.20	1.80
CSP-5	0.72	1.00	0.31	1.00	0.26	1.00	0.85	1.00	3.26	1.06	2.16	1.00	0.24	2.17	0.10	1.50
CSP-6	5.53 (*S*)	1.34	2.37 (*R*)	1.51	1.37 (*S*)	1.51	2.10	1.03	6.00	1.00	5.93	1.00	0.26	4.20	0.22	1.50
Mobile phase chloroform + 0.5% methanol–heptane	70:30		70:30		70:30		70:30		25:75		50:50		10:90		25:75	

[a] Absolute configuration of first-eluted enantiomer.

tionary phases with a naphthylethylamine group [7,11], CSP-4, with a 1-naphthylamido group, shows mediocre performance.

The elution order of enantiomers is the same on all stationary phases in which (*S*)-phenylalanine is the chiral moiety in the chiral selector. However, the radical responsible for π–π interaction is bonded to the acidic group of (*S*)-phenylalanine in CSP-3 and CSP-4 and to the amino group in CSP-1 and CSP-2. Hence, the order of elution of enantiomers does not seem to be affected by the direction of fixing of the π-donor or π-acceptor groups on the amino acid. This observation is not in accordance with the three-point attachment recognition model in which the π-π interaction is the most important [12].

As we have already shown [7], the resolution of **7** is in general particularly good. The behaviour of this compound led us to prepare CSP-5 in which (*R*)-Mosher's acid is the chiral entity. We hypothesized that a certain reciprocity could be applied to the chiral recognition in this chiral moiety, but the performance of CSP-5 is the worst of the group of stationary phases tested.

Importance of the classification of stationary phases as π-donors and π-acceptors

As expected, π-acceptor racemic compounds, 3,5-dinitrobenzoyl derivatives of methyl esters of amino acids (compounds **1–3**), are well resolved by all the new stationary phases (except CSP-5). On the other hand, their ability to resolve **4**, **5** and **6**, which are π-donors, is obviously limited. However, this must be qualified, given that such compounds are poorly resolved by CSP-A1 and especially CSP-A2, which are π-acceptors. In general, however, racemic compounds bearing a 3,5-dinitrobenzoyl group are well resolved by either π-acceptor or π-donor chiral stationary phases.

The foregoing would seem to indicate that the classification of π-donor and π-acceptor chiral silica-bonded stationary phases is not sufficiently justified if it refers to the nature of the principal solute–stationary phase interactions in the enantiomeric recognition. More probably the whole chiral moiety should be taken into account instead of individual interactions, in the search for a hypothetical chiral recognition mechanism. However, this classification is convenient to distinguish two fairly different kinds of HPLC chiral stationary phases: those with a 3,5-dinitrobenzoyl radical (π-acceptors) and those without (π-donors).

CONCLUSIONS

Of the seven chiral stationary phases described here, four gave good results in the resolution of racemic compounds possessing either π-acidic or π-basic sites. This study has shown that chiral entities with a relatively simple structure can give efficient chiral stationary phases.

ACKNOWLEDGEMENTS

Cristina Minguillón thanks the Dirección General de Investigación Científica y Técnica del Ministerio de Educación y Ciencia of Spain and the Direction de Coopération Scientifique et Technique du Ministère des Affaires Etrangères of France for a fellowship in the Mercure programme.

REFERENCES

1 W. H. Pirkle and T. C. Pochapsky, *Chem. Rev.*, 89 (1989) 347.
2 S. G. Allenmark, *Chromatographic Enantioseparation: Methods and Applications*, Ellis Horwood, Chichester, 1988.
3 T. D. Doyle, in W. J. Lough (Editor), *Chiral Liquid Chromatography*, Blackie, London, 1989, Ch. 6.
4 N. Ôi, H. Kitahara and R. Hira, *J. Chromatogr.*, 515 (1990) 441.
5 N. Ôi, H. Kitahara and R. Hira, *J. Chromatogr.*, 535 (1990) 213.
6 Y. Okamoto, R. Aburatani and K. Hatada, *Bull. Chem. Soc. Jpn.*, 63 (1990) 955.
7 L. Oliveros, C. Minguillón, B. Desmazières and P.-L. Desbène, *J. Chromatogr.*, 543 (1991) 277.
8 B. Coq, C. Gonnet and J. L. Rocca, *J. Chromatogr.*, 106 (1975) 249.
9 P. Pescher, M. Caude, R. Rosset, A. Tambuté and L. Oliveros, *Nouv. J. Chim.*, 9 (1985) 621.
10 L. Oliveros and M. Cazau, *J. Chromatogr.*, 409 (1987) 357.
11 N. Ôi, M. Nagase and T. Doi, *J. Chromatogr.*, 257 (1983) 111.
12 L. Oliveros, C. Minguillón, B. Desmazières and P.-L. Desbène, *J. Chromatogr.*, submitted for publication.

Journal of Chromatography, 589 (1992) 61–70
Elsevier Science Publishers B.V., Amsterdam

CHROM. 23 680

Simple test for determination of the degree of distortion of the liquid-phase flow profile in columns for preparative liquid chromatography☆

Marian Kamiński

Technical University of Gdańsk, Institute of Inorganic Chemistry and Technology, PL 80-952 Gdańsk (Poland)

(First received November 8th, 1990; revised manuscript received July 16th, 1991)

ABSTRACT

A simple method for the determination of the degree of distortion of the flow profile in a well designed preparative liquid chromatographic column is presented. The method consists in carrying out two test chromatographic analyses, one standard and one bidirectional elution. It was experimentally verified that similarity of the results of the two tests confirms a virtually plug flow profile of the mobile phase in a column. On the other hand, differences in the results of the two tests demonstrate that the mobile phase flow profile in a column bed is of non-plug character. In such instances mass dispersion in a packed bed is then much better characterized by the HETP value calculated on the basis of bidirectional column test.

INTRODUCTION

Liquid chromatography (LC) is being used increasingly often for obtaining pure, particularly biologically active, substances [1–9]. There is also growing interest in preparing preparative columns for one's own purposes. The number of published preparative column packing procedures is small [7,10–17]. In addition, it often happens that repetition of a procedure under different conditions, *e.g.*, different column geometry, sorbent type (particularly irregular particle shape and greater Δd_p) and instrumentation used for packing the column, yields much worse results. Preparative columns prepared under such conditions often reveal unsatisfactory efficiency and poor peak shapes, far from Gaussian even without overloading during efficiency testing.

This does not only happen with columns prepared and packed by the user, as commercial preparative columns also usually reveal tailing near the baseline [12,17,18]. This tailing can be avoided only when the columns are operated under "infinite diameter" conditions [12,18–22]. Hence is difficult or even impossible to obtain very pure substances (99.99% or more) when using the entire cross-section of the column during separation [18]. It seems, therefore, that it is necessary to continue investigations on the problems of the reproducible packing of efficient and stable preparative columns for LC.

Poor efficiency of preparative columns can be due in general to the following reasons: (1) poor structure of the column packing resulting from the deficiencies of the described packing methods: (a) non-plug flow profile of the mobile phase in the column bed, resulting from an irregular radial distribution of particles of various size, or an irregular radial distribution of the degree of packing of the particles [12,13,18,19,21,22]; these problems are often encountered in practice; (b) insufficiently stable packing of the particles or irregularities of the packing bed —large intergranular spaces, splitting of the packing bed in the column or a large dead space between the upper distribution head and the packing layer, resulting from settlement of the

☆ This work was presented in part at the *2nd International Symposium on Preparative and Up-scale Liquid Chromatography, Baden-Baden, February 1–4, 1988.*

0021-9673/92/$05.00

packing bed [12,13,18–21]; these problems rarely occur when the columns are provided with axial packing compression systems [10,12,13]. (2) Incorrect design of the distribution heads, resulting in: (a) distortion of the zone of the injected substances directly below the head outlet owing to a too great resistance of radial flow of the liquid in the head [23]; (b) a significant broadening of the zone of the sampled substances resulting from diffusion in the excessively large space in the distribution or the outlet head [21], or from the presence of a void volume and blockage of frits in the column heads.

There are a few methods that permit the diagnosis of the reasons for unsatisfactory peak shapes and poor efficiency of preparative LC columns with particle sizes ranging from 5 to 100 μm [12,13,21–27]. These methods, however, cause the destruction of the column packing [12,13,23–25] or are very complicated and require the application of special expensive equipment [22,26,27].

The need for the development of a simple method allowing the diagnosis of the major reasons for unsatisfactory column efficiency has stimulated rational investigations on the technology of column packing. The determination of the potentially attainable column efficiency for a particular sorbent, mobile phase flow-rate and separated substances is also important, particularly when looking for the optimum conditions of column packing with new sorbents. Under the conditions of a standard column efficiency test, such information can be obtained only when the profile of the mobile phase flow in the column bed is truly plug.

Calculations of the attainable column efficiency according to Knox *et al.* [22] are not reliable when the packing particles are irregular and the fraction of the particle size is relatively broad.

The paper presents a simple, two-stage test, which enables some conclusions to be drawn regarding the reasons for unsatisfactory column performance and/or the determination of the potentially attainable efficiency of a preparative LC column, provided that the column is correctly designed and packed in an optimum manner (the mobile phase flow profile in the column bed should be of the plug type). The proposed test can be also useful for the determination of the extra-column broadening of the bands of separated substances in analytical LC or with the use of microcolumns.

PRINCIPLE OF THE TEST

The test consists of two stages (see Fig. 1). The first stage is a standard test of the column efficiency, *i.e.*, a test chromatogram of a single substance or an easily separable mixture under the conditions when no overloading occurs (Fig. 1a and item 1 in the table of the positions of the six-port valve). The second stage involves bidirectional elution of a single test substance, initially as in the first stage, but only until a certain fraction of the column length

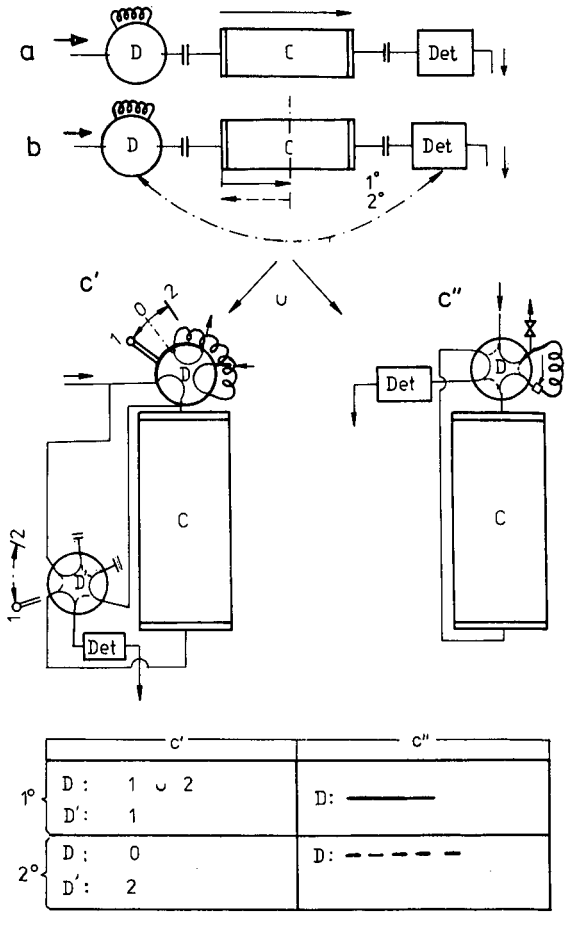

Fig. 1. Illustration of the principle of the two-stage test [(a) conventional test; (b) bidirectional test] and instrument set-up facilitating the performance of the bidirectional test (c', c"): the asterisk denotes sampling of tracer to the sampling loop without the eluent flow. C = chromatographic column; D = six-port sampling valve; Det = chromatograpahic detector; D' = auxiliary six-port valve; 1, 0, 2 = positions of the valve lever, → and - - - → denote directions of liquid flow.

(one to three quarters) has been reached. Next the direction of the eluent flow is reversed and the tracer is eluted back to the column inlet. The reversal of the eluent flow and the recording of the chromatogram during the reversed elution of the tracer are possible owing to an exchange of the positions of the sampling valve and the detector (Fig. 1b and item 2 in the table of the positions of the six-port valve). The exchange can be accomplished by a real reversal of the column (Fig. 1c) with respect to the sampling valve (D) and the detector (Det); application of a set of two six-port valves connected to the column and the detector according to scheme c′ in Fig. 1; or application of the system c″ in Fig. 1, introducing the tracer solution to the "sampling loop" through a membrane.

Both stages of the test are carried out properly only when a small amount of the tracer is introduced into the column in the form of a narrow rectangular pulse. The maximum volume of the tracer solution can be calculated from the equation

$$V_i^{max} \approx 0.7\, d_c^2\, L_c^{1/2}\, d_p^{1/2} \qquad (1)$$

In the case of application of the bidirectional test for the quantitative determination of the extra-column dispersion of the bands of the separated substances ($\Sigma\sigma_{vex}^2$), it is necessary to perform a series of experiments with bidirectional elution of the smallest possible amount of a non-retained substance. The elution should be carried out for various distances of elution of the tracer band in the column (*e.g.*, for a distance of one, two or three quarters of the column length). Next it is necessary to prepare a diagram of the $\sigma_v^2 = f(l')$ dependence (see Fig. 2 and the list of symbols) and to extrapolate the value of σ_v^2 for $l' = 0$ (best of all using the linear regression method).

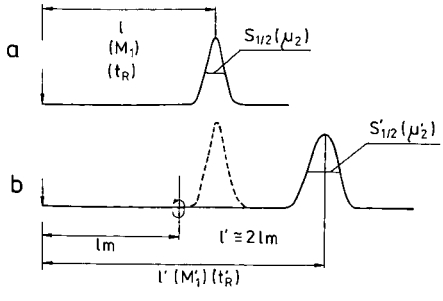

Fig. 2. Chromatograms obtained from (a) the conventional and (b) the bidirectional column test: illustration of eqns. 2 and 3.

PRINCIPLES OF CALCULATION OF THE DISPERSIVE PARAMETERS OF A COLUMN

According to the outline in Fig. 2, on the basis of the chromatograms obtained it is possible to calculate the dispersive parameters of the column separately for stages I and II of the test. Both the HETP (H) and the dispersion coefficient (D) can be used for this purpose. The calculations can be performed on the basis of peak width at half-height ($S_{1/2}$), or on the basis of statistical moments, which, according to Carbonell and McCoy [28], is more objective.

The following dependence for the bidirectional test can be written on the basis of definitions of H or D values [21,22,29], and taking into account the scheme in Fig. 2:

$$H = L_c \cdot \frac{\mu_2'}{M_1 M_1'} \qquad (2)$$

In cases when the peak width at half-height and the l and l' segments are measured on the chromatograms, this equation is simplified to

$$H = \frac{L_c}{5.54} \cdot \frac{(S_{1/2})^2}{l'} \qquad (3)$$

After calculating H, also the longitudinal dispersion coefficient D and the dispersive Peclet number can be calculated. The results can therefore be presented as $H = f(u_0)$ or $Pe_D^{-1} = f(ReSc)$, and hence as $h/2 = f(v)$.

MODELS OF DISPERSION OF TRACER ZONES IN MICROGRANULAR POROUS BEDS

Fig. 3 shows the models of possible mass dispersion conditions in a microgranular bed of a chromatographic column. Extreme conditions have been taken into account: from a bed containing a large plate number and characterized by a plug flow profile (Fig. 3, 1), through dense beds of irregular radial permeability distribution (Fig. 3, 2), to poorly packed beds (mainly as a result of excessive electrostatic interaction between the particles) of plug (Fig. 3, 3) and non-plug (Fig. 3, 4) permeability profiles. Apart from the column cross-sections, part a in Fig. 3 presents the local tracer concentration distribu-

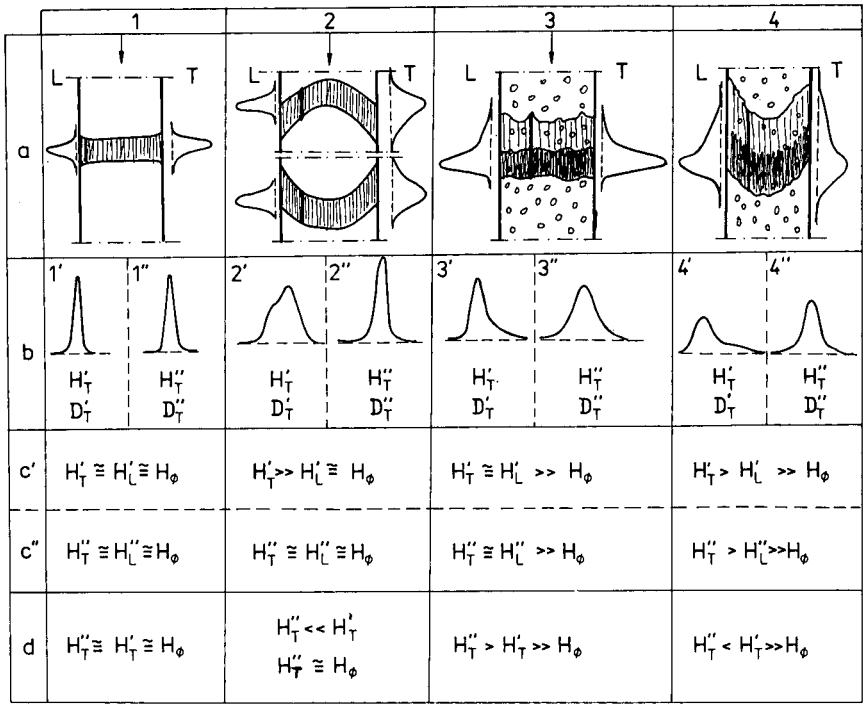

Fig. 3. Comparison of mass dispersion conditions in a microgranular layer (a) with the results of the conventional (b, 1', 2', 3', 4', c') and the bidirectional (b, 1", 2", 3", 4", c") column efficiency test. L = locally observed tracer concentration distributions; T = tracer concentration distributions averaged for the entire column cross-section (measured at the column outlet). Part d presents the dependences allowing the evaluation of the packing bed structure, based on a comparison of the results from both the stages of the test. Single prives denote results of the conventional test and double primes the results of the bidirectional test.

tions (L) and distributions averaged for the column cross-section (T). Part b illustrates the approximate peak shapes for the conventional test (denoted by single primes) and for the bidirectional test (denoted by double primes). Part c of Fig. 3 presents the expected dependences between the HETP values determined locally and at the column outlet for the conventional (c') or the bidirectional test (c"). Part d of Fig. 3 presents the theoretically predicted dependence between the HETP values from the conventional and the bidirectional tests, determined for the mentioned above four different dispersion conditions. The HETP values in Fig. 3c and d have also been related to the minimum attainable dispersion in the examined column (H_ϕ).

It can be expected from the comparison of the dependences between H''_T, H'_T and H_ϕ shown in part d of Fig. 3 that the comparison of the HETP values from the conventional and bidirectional tests, taking additionally into account the approximate HETP values calculated from theoretical dependences (*e.g.*, using the Knox equation [22]), should allow the prediction of the type of flow profile in the column and the degree of packing of the column bed.

At the same time the bidirectional test should allow the determination of the maximum attainable column efficiency (H_ϕ) for columns of a dense packing bed (Fig. 3, 1 and 2) in spite of a non-plug flow profile, as in Fig. 3, 2. It also follows from Fig. 3, 2 that the conventional test allows the determination of the HETP value describing the radial dispersion in the column packing only when the flow profile in the column is of a truly plug-type.

The above conclusions arising from the analysis of the model presented in Fig. 3 have been drawn assuming that the effect of radial dispersion on the results of the bidirectional test is negligible. Based on the results of Knox *et al.* [22], this assumption is

more valid the smaller is d_p and the higher is u_0. However, in cases of a strongly distorted flow profile in the column, the radial dispersion can cause a certain broadening of peaks obtained in the bidirectional test, particularly in the peak base region. In such cases the values of HETP determined on the basis of peak width at half-height in chromatograms obtained by the bidirectional test should be more useful for the calculation of H and D than values calculated on the basis of statistical moments.

EXPERIMENTAL

Materials

The column packings were silica gel 60 Å of mean particle diameter d_p = 17, 22, 33, 50 and 124 μm and with the particle size distribution given previously [13], LiChrosorb RP-18 (d_p = 10 μm), LiChroprep Si 60 (d_p = 25–40 μm) (E. Merck, Darmstadt, Germany) and Nucleosil C_{18} (d_p = 7 μm) (Macherey, Nagel & Co., Düren, Germany).

Methanol, methanol–water (8:2, v/v), hexane–dioxane (85:15, v/v) were used as mobile phases with reagents from POCh (Gliwice, Poland) and demineralized water.

Instrumentation

Columns of I.D. 17, 25, 33, 44 and 52 mm and length varying from 100 to 450 mm (stainless steel), equipped with moveable distribution heads with mechanical axial compression of the packing, were used. The design of the heads has been described [30]. Proper operation of the distribution heads of these columns has been checked previously [13].

A Model CHP 02 preparative chromatograph for column testing (Elkor, Gdańsk, Poland) was used, equipped with a two-head piston pump (5–300 ml/min, P_{max} = 150 bar), pulse damper, six-port sampling valve (20 μl–20 ml), a UV detector (254 nm), a refractive index (RI) detector (5 μl) connected to a split at the column outlet and a y–t recorder.

The columns were dry [13,15] or slurry packed [12,17] under both optimum and unfavourable conditions.

Methods

Preparative column tests were carried out according to the procedure described under Principle of the Test. The Model CHP 02 preparative chromatograph was modified for this purpose according to scheme c″ in Fig. 1.

Solutions of benzene and *o*-nitroaniline in hexane–dioxane (85:15) were sampled in the case of columns packed with silica gel in the first stage of the test (conventional test). The RP-18 columns were examined using benzene and naphthalene in methanol–water. Sample sizes were 20, 200, 400 and 500 μl for the columns of 17, 33, 44 and 50 mm I.D., respectively.

During the second stage (bidirectional test), samples of the same size, but containing one of the test substances dissolved in the mobile phase, were injected. For the determination of the dead volume of the column pure methanol was used as the mobile phase for benzene as the solute.

On the basis of the chromatograms obtained, the value of H was calculated as the measure of HETP taking into account the peak width at half-height.

In addition, two or three "bands" of Sudan I dye dissolved in dioxane (10%, w/v) were injected into some of the columns (without eluting them from the column). Owing to this, after pushing the packing out of the column it was possible to photograph the shape of the zones of the eluted substances in the axial cross-section of the column packing and to observe the changes in the zone shape during the elution of the dye bands along the column [12,13,23]. The illustrations in Fig. 6 (column C) were drawn on the basis of these photographs.

For the purposes of this paper, specially prepared distribution heads were also additionally used, *viz.*, heads with an enlarged volume of the space between the liquid inlet and the frit and heads with zero volume of this space (radial distribution plate removed), in which the radial flow of the liquid was virtually impossible.

RESULTS AND DISCUSSION

Figs. 4 and 5 present examples of chromatograms obtained during testing the columns by the conventional and the bidirectional tests (for benzene as the test substance). Fig. 4 presents the chromatograms obtained for two columns of 50 mm I.D., dry packed with LiChroprep Si 60 (d_p = 25–40 μm), and Fig. 5 the chromatograms obtained for two columns of 32 mm I.D., slurry packed with Nucleosil C_{18} (d_p = 7 μm). The columns were packed under the previously

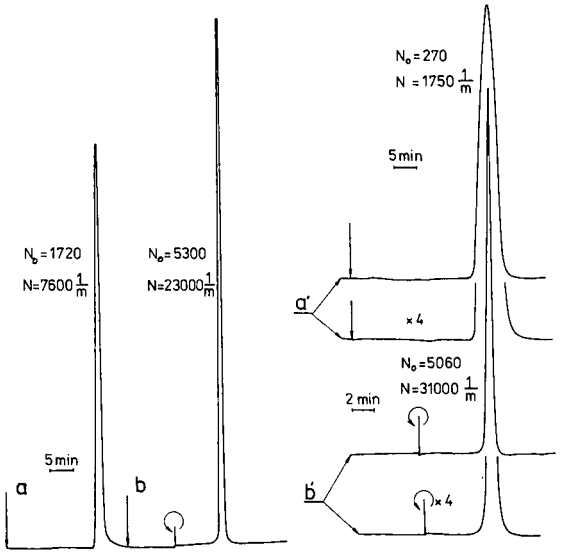

Fig. 4. Examples of test chromatograms of two preparative columns, d_c = 50 mm, L_c = (I) 22 cm and (II) 16 cm, dry packed with silica gel LiChroprep SI 60, d_p = 20–40 μm. a, a', Conventional test; b, b', bidirectional test; a, b, column I; a', b', column II. Parts a' and b' also present the bottom fragments of the respective peaks obtained at four times higher detector sensitivity. Flow-rate, 19 ml/min; mobile phase, methanol; test substance, *o*-nitroaniline.

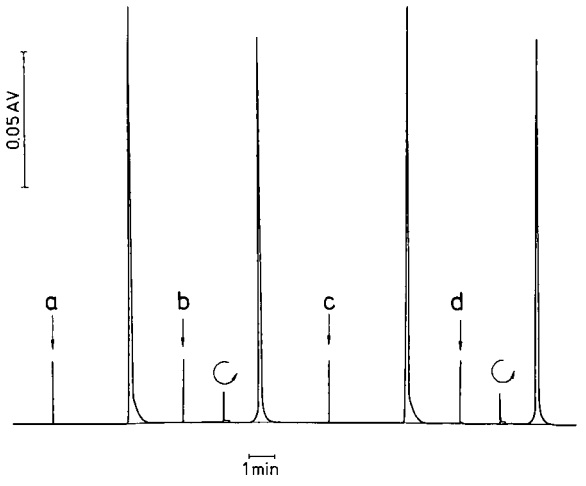

Fig. 5. Chromatograms obtained during (a, c) conventional and (b, d) bidirectional testing of efficiency of a 250 × 16 mm I.D. column packed by slurry method with Nucleosil C_{18} (7 μm). Mobile phase, methanol–water (8:2, v/v); sample, benzene; mobile phase velocity, u = 1.3 mm/s.

described conditions [12,13]. The results obtained are summarized in Fig. 6.

Column A in Fig. 6 presents typical examples of the results obtained in the first stage of testing the preparative columns packed with various methods under various conditions, and column B the results obtained in the second stage. Column C shows the shapes of two Sudan I zones retained during elution in the cross-section of the packing. Column D lists the dimensions of the columns (d_c, L_c) and packing particle sizes (d_p). The values of $h = H/d_p$ and $\upsilon = u_0 d_p/D_m$, obtained in the first and second stages, and the values of h_t calculated using the Knox equation [22] are listed by the respective chromatograms (values of A, B and C for these calculations are given at the bottom of Fig. 6). Arrows on the chromatograms indicate unsatisfactory peak shapes.

The results illustrated in Figs. 4–6, and other results obtained previously, lead to the following considerations. It is very difficult in practice to obtain preparative LC columns that produce ideal Gaussian peaks and at the same time have similar HETP values in the conventional and the bidirectional tests. Such a similarity often occurs for columns packed with the most reproducible slurry method when the peak width is measured at half-height. However, such preparative columns usually reveal tailing at the baseline when tested conventionally. Under the conditions of the bidirectional test this tailing appears on both sides of a peak at about half the width of the tailing part of a peak obtained during conventional testing. Tailing does not occur only in cases when the columns are tested under "infinite diameter" conditions (Fig. 6, 1, b; split = 50%, V_i = 50 μl). The results obtained are consistent with previous investigations [12,18]. It seems that slower migration of bands in the vicinity of the column walls results from excessive packing of the near-wall packing layer compared with the remaining part of less dense packing, not "leaning" against the rigid column walls.

Unsatisfactory peak shapes and poor column efficiencies are often observed in the conventional test also with columns dry-packed using the pre-

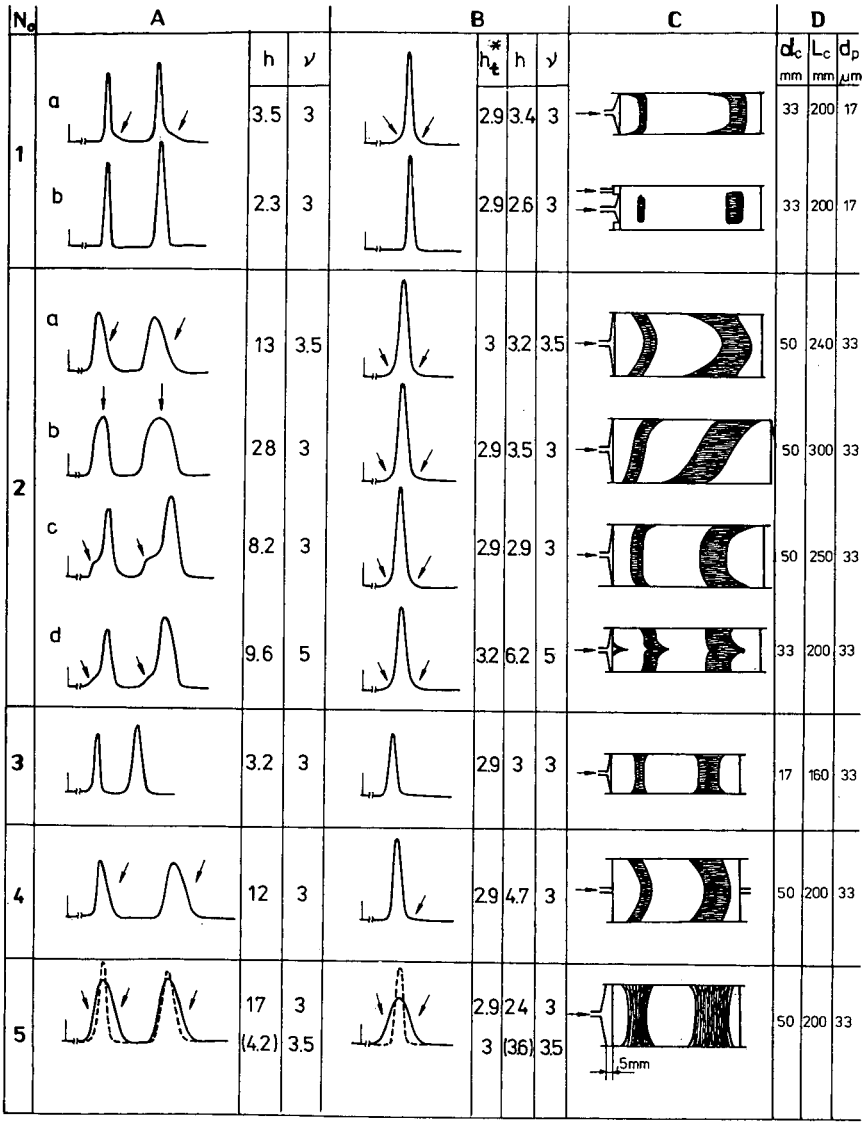

Fig. 6. Comparison of examples of typical results of the (A) conventional and (B) bidirectional tests of various preparative columns packed by the slurry method [12,17] (No. 1) and the impact method [13,15] (Nos. 2–5), under various conditions of application of the impact method, both optimum (Nos. 3, 4 and 5) and unfavourable (Nos. 2a–d). Column efficiency characterized by h for a given v. Arrows indicate unfavourable fragments of the chromatographic peaks. Distribution heads of an incorrect design were used for testing columns. Nos. 4 and 5. Experiments with column 1B were carried out under "infinite diameter" conditions (S = 50%, 50-μl sample). The dashed line in the case of column No. 5 illustrates testing with a proper distribution head (the respective values of h are given in parentheses). Column C illustrates the shapes of the zones of Sudan I dye retained during elution in a column (axial cross-section). * B = 1.6; A = 1.5; C = 0.06; $h_t = B/v + A \cdot v^{0.33} + C \cdot v$.

viously described impact method [13]. This method was used with mean packing particle diameter d_p > 25–30 μm (Figs. 5 and 6, 2–5). The above statement particularly concerns long columns (L_c > 25 cm) packed with an irregular packing material of a relatively broad particle size range (1.5 <

$d_{p\ max}/d_{p\ min} < 2$). Columns of poor efficiency are obtained particularly often when the packing material is introduced too slow (Fig. 6, 2, c) or too fast (Fig. 6, 2, a), or when a slant surface of the packing material is formed during packing (Fig. 6, 2, b). These difficulties are usually due to a non-plug liquid flow profile in the prevailing part or in the entire column cross-section (Fig. 6, 2, a–c). In spite of a wrong flow profile, under such conditions the bidirectional test yields HETP values that are very close to the theoretical values (column 2, B in Fig. 6).

Previous investigations [13] demonstrated that these phenomena are due either to spontaneous segregation of the packing particles during packing, intensified by the vibration of the column walls and of the packing (*i.e.*, too long packing time), or to a non-uniform radial interparticle porosity distribution of the packing bed [13] (*i.e.*, too short packing time). In the second case, the degree of packing density of the bed decreases with distance from the column wall owing to the vibrations of the walls and the resistance offered by them. Beds that are insufficiently packed and at the same time are not stabilized by the pressure of the heads, or dried beds, undergo splitting (Fig. 6, 2, d).

The bidirectional test almost completely eliminates these effects (Fig. 6, 2, a–d), as the molecules cover a similar route in the column in both directions. The certain broadening of peaks observed in this method mainly at the peak base is due to radial dispersion of mass in the column packing. Peak shapes (particularly at the base) and HETP values obtained from the conventional test were similar to those from the bidirectional test only in the very rare cases of a truly plug flow profile. This indicates that the unsatisfactory preparative LC column efficiency observed in practice is mainly due to a non-plug profile of liquid flow in the column (case 2 in Fig. 3).

Unfortunately, the results can be non-explicit and can lead to a conclusion that the liquid flow profile is incorrect also when the distribution head is incorrectly designed (too large radial flow resistance) (see Fig. 6, 4). However, an unnaturally rapid increase in the column operating pressure accompanying the increase in the mobile phase flow-rate is simultaneously observed in such instances, which helps in giving a proper diagnosis [an increase in the reduced permeability (Φ) ranging from 1300 for $v = 3$ to 3600 for $v = 78$ was observed for column 4 in Fig. 6; the decrease in permeability accompanying the flow-rate increase was eliminated by moving the upper head 2 mm away from the column packing].

On the other hand, when the distribution heads operate incorrectly owing to the so-called diffusional dead spaces inside the heads, the results of the bidirectional test with a well packed column are often worse than the results of the conventional test. In such cases the results of the bidirectional test can be better than the results of the conventional test when band broadening in the head is accompanied by a poor liquid flow profile in the column. Such a phenomenon occurs during conventional testing when the poor liquid flow profile influences the column efficiency to a larger extent than the diffusive broadening of the band in the head. Such effects have been observed, for example, when the head of column 5 (Fig. 6) was used for column 2b (Fig. 6). However, the value of h obtained from the bidirectional test, equal to *ca.* 25 ($v = 3$), although close to the value obtained from conventional testing ($h = 28$), is far from theoretical expectations ($h_t = 2.9$).

Examination of the proper operation of the distribution heads is nowadays less important, as commercial preparative LC columns usually have properly designed systems of radial distribution of the mobile phase to/from the packing surface and they do not have excessive dead spaces.

It is very important to check whether the column is completely packed and both the heads contact the packing bed before carrying out the bidirectional test, otherwise it is possible that the structure of the column packing bed will be destroyed owing to particle movement during the backward flow of the liquid phase. This statement means that the proposed bidirectional column test can be applied only for preparative columns with axial compression of the packing, achieved by mechanical, pneumatic or hydraulic pressing of the heads to the packing during column operation. It has been established experimentally that in such columns the packing bed was not destroyed by the reverse flow of the mobile phase. For instance, the HETP values determined for both directions of the mobile phase flow are similar provided that the heads are presented sufficiently strongly to the packing bed.

CONCLUSIONS

The described simple two-stage column test, consisting of a conventional test and a bidirectional test, produces repeatable results. It can yield a few practical benefits when it is performed on well designed columns (when proper operation of the distribution heads is certain and when the heads are strongly pressed to the packing bed), as follows.

(1a) The differences between the HETP values, and between the shapes of peaks obtained during the conventional testing (broad peaks) and bidirectional testing (narrow peaks), prove that the flow profile in the column is non-plug. The greater the difference between the peak widths from both tests, the further is the flow profile from plug flow. The HETP value obtained from the bidirectional test characterizes in such instances the potentially attainable column efficiency in the applied chromatographic system, while the HETP value calculated from the conventional test chromatogram has no simple physical sense, as it is influenced by the flow profile in the column, which is assumed to be plug flow in all definitions of HETP.

(1b) A similarity of peak shapes and HETP values obtained from both tests proves a satisfactory profile of liquid flow in the column. Should the HETP value be additionally close to the value calculated from the Knox equation, the structure of the column packing is satisfactory and the extra-column effects are negligible.

(2) When the liquid flow profile in the column is non-plug, the results of the bidirectional test characterize well the attainable column efficiency. This is very important when testing the applicability of new sorbents for preparative purposes.

(3) The bidirectional test permits the examination of the dependence of HETP on k', d_p, u_0 and other parameters, even when one cannot be sure whether the flow profile in the column is truly plug.

(4) The bidirectional test performed on analytical or microcolumns with a few elution distances can be one of the methods for the experimental determination of the extra-column broadening of bands of the separated substances.

In cases when proper operation of the distribution heads is doubtful:

(1) When it is certain that the structure of the packing and the flow profile are satisfactory, the differences between the HETP values in favour of the conventional test confirm the existence of large diffusion spaces in column heads, or large extra-column (out of the bed) band-broadening effects (*e.g.*, the existence of void volumes and/or blockage of the frit). On the other hand, a difference between the HETP values in favour of the bidirectional test can indicate excessive resistance of radial flow in the distribution head.

(2) When the occurrence of an incorrect liquid flow profile cannot be excluded, the comparison of the results of the conventional and the bidirectional test yields limited diagnostic data, and hence the application of additional methods of quantitative evaluation of the structure of the column packing is necessary in such instances in order to determine unequivocally the reasons for the observed poor column efficiency.

SYMBOLS

a'	value determined in the conventional test
a''	value determined in the bidirectional test
a	one of the following symbols: H_T, H_L, D_T (see Fig. 3)
A, B, C	constants in the Knox equation
d_c	column diameter
D	coefficient of axial dispersion in the column; $D \equiv \frac{1}{2} \cdot \frac{d\sigma_L^2}{dt} = \frac{1}{2} \cdot \frac{HL_c}{t_R}$
d_p	particle diameter (mm)
D_m	diffusion coefficient of sample substance in the mobile phase
H	height equivalent to a theoretical plate (HETP)
H_Φ	HETP attainable in the given column
H_T	HETP at the outlet of the column
H_L	HETP calculated on a basis of a local width of a band "stopped" in the column
h	reduced HETP ($h = H/d_p$)
L	elution distance along the column
L_c	column length
L_m	length of migration path of a sample in the column in one direction
l_0	retention distance for a non-retained substance on a conventional test chromatogram

l, l'	distance between the start and the peak maximum on a chromatogram (see Fig. 2)
l_m	distance between the start and the moment of flow direction reversal, measured on a chromatogram from the two-stage test
M_1, M_1'	first ordinary statistical moment of a chromatographic peak
Pe_D	dispersive Peclet number, $Pe_D = (ud_p)/D$
Re	Reynold's number, $Re = (u_o d_p \rho)/\eta$
Sc	Schmidt's number (diffusive), $Sc = \eta/(D_m\rho)$
$S_{1/2}$, $S_{1/2}'$	peak width at half-height (see Fig. 2)
t_0	retention time of a non-retained substance in the conventional test
t_R, t_R'	retention time of the test substance (see Fig. 2)
u_0	mobile phase linear flow velocity, $u_0 = L_c/t_0$
u	apparent rate of tracer migration along the column axis
V_R	retention volume
η	mobile phase viscosity
ρ	mobile phase density
v	reduced mobile phase flow velocity, $v = u\, d_p/D_M$
μ_2, μ_2'	second central moment of a chromatographic peak
σ_v^2	variance of the concentration distribution in a peak, calculated in terms of volume
$\Sigma\sigma_{vex}^2$	tracer extra-column dispersion, calculated in terms of volume
σ_L^2	variance of tracer band broadening, calculated along the column

REFERENCES

1 M. Verzele and E. Geeraet, *J. Chromatogr. Sci.*, 18 (1980) 559–570.
2 K. Jones, *Chromatographia*, 25 (1988) 437–442, 443–446, 487–492 and 577–581.
3 K. Jones, *Chromatographia*, 25 (1988) 547–559.
4 K. Hostettman, *Preparative Chromatographic Techniques: Applications in Natural Product Isolation*, Springer, Berlin, 1986.
5 G. Guiochon and A. Katti, *Chromatographia*, 24 (1987) 165–189.
6 E. Katz, K. L. Ogan and R. P. W. Scott, *J. Chromatogr.*, 289 (1984) 65–83.
7 H. Collin, P. Hilaireau and J. de Tournemire, *LC · GC Int.*, 3, No. 4 (1990) 40–48.
8 S. Golshan-Shirazi and G. Guiochon, *Anal. Chem.*, 61 (1989) 1368–1382.
9 J. H. Knox and H. M. Pyper, *J. Chromatogr.*, 363 (1986) 1–30.
10 E. Godbille and P. Devaux, *J. Chromatogr. Sci.*, 12 (1974) 564–569.
11 I. Halasz and G. Meldener, *Anal. Chem.*, 55 (1983) 1842–1847.
12 M. Kamiński, J. Klawiter and J. S. Kowalczyk, *J. Chromatogr.*, 243 (1982) 225–244.
13 J. Klawiter, M. Kamiński and J. S. Kowalczyk, *J. Chromatogr.*, 243 (1982) 207–224.
14 W. Beck and I. Halasz, *Fresenius' Z. Anal. Chem.*, 291 (1978) 312–318 and 340–348.
15 Th. Leutert and E. von Arx, *J. Chromatogr.*, 292 (1984) 333–344.
16 T. Wang, R. A. Hartwig, N. T. Miller and D. C. Shelly, *J. Chromatogr.*, 523 (1990) 23–34.
17 C. W. Martin and Y. Shalon, *LC Mag.*, 3, No. 6 (1985).
18 M. Kaminski and J. F. Reusch, in L. Kerecsen and H. Kalász (Editors), *Proceedings of the 6th Annual American Eastern European Colloquium and Symposium on Chromatography: New Advances in Liquid Chromatography, Balatonszéplak, Hungary, September 27–30, 1986*, Department of Pharmacology, Semmeweis University of Medicine, Budapest, 1986, p. 43.
19 A. W. J. De Jong, H. Poppe and J. C. Kraak, *J. Chromatogr.*, 148 (1978) 127–141.
20 B. Coq, G. Cretier and J. L. Rocca, *J. Chromatogr.*, 186 (1979) 457–473.
21 J. J. Kirkland, W. W. Yau, H. J. Stoklosa and C. H. Dilks, Jr., *J. Chromatogr. Sci.*, 15 (1977) 303–316.
22 J. H. Knox, G. R. Laird and P. A. Raven, *J. Chromatogr.*, 122 (1976) 129–145.
23 B. Coq, G. Cretier, J. L. Rocca and R. Kastner, *J. Chromatogr.*, 178 (1979) 41–61.
24 R. F. Benenati and C. B. Brosilow, *AIChE J.*, 8 (1962) 359.
25 R. H. S. Roblee, R. M. Baird and J. W. Tierney, *AIChE J.*, 4 (1958) 460.
26 M. Ilg, J. Maier-Rosenkranz, W. Mueller and E. Bayer, *J. Chromatogr.*, 517 (1990) 263–268.
27 S. A. Volkov, V. J. Reznikow, V. J. Smirnov, V. Yu. Zelvensky, B. S. Rinkevichus, K. J. Sakodynski and F. Ya. Frolov, *J. Chromatogr.*, 156 (1978) 225–232.
28 R. G. Carbonell and B. J. McCoy, *Chem. Eng. J.*, 9 (1975) 115.
29 J. R. Cluff and S. J. Hawkes, *J. Chromatogr. Sci.*, 14 (1976) 248–255.
30 J. S. Kowalczyk, M. Kamiński and J. Klawiter, *Pol. Pat.*, 138838, *Eur. Pat. Appl.*, EP 108242, 1984.

Journal of Chromatography, 589 (1992) 71–85
Elsevier Science Publishers B.V., Amsterdam

CHROM. 23 701

Predictability of chromatographic protein separations

Study of size-exclusion media with narrow particle size distributions

Atul M. Athalye, Stephen J. Gibbs☆ and Edwin N. Lightfoot*

Department of Chemical Engineering, University of Wisconsin–Madison, 1415 Johnson Drive, Madison, WI 53706 (USA)

(First received May 1st, 1991; revised manuscript received August 23rd, 1991)

ABSTRACT

It is shown that existing models of differential chromatography are capable of predicting the behavior of polydisperse packings in commercially available columns in terms of separately determined transport and equilibrium properties. Experiments conducted using proteins on size-exclusion media with a narrow particle size distribution indicate that such packings perform as well as predicted by theory of their more expensive monodisperse counterparts. These results confirm theoretical studies and previous data suggesting that a modest degree of polydispersity has no significant effect on separation efficiency, thus allowing the direct design of large columns from basic transport and equilibrium data.

INTRODUCTION

The purpose of the work described here was to test the utility of currently available one-dimensional lumped-parameter models of differential chromatography for describing the performance of commercially available columns and packing materials. The model used for this purpose is essentially that of Gibbs and Lightfoot [1], but it differs only in detail from those of others (see, for example, the books by Giddings [2], Ruthven [3] and Jönsson [4] and the papers by Lenhoff [5] and Weber and Carr [6]). The experimental results are shown later as Van Deemter plots [7] in Figs. 3–5. Both glass (Omnifit) and stainless-steel (Alltech) columns were used in the study. The packings employed were macroporous TSK-GEL Toyopearl HW65 size-exclusion beads (TosoHaas; mean diameters 30 and 75 μm), selected for study because of their importance as support materials or base matrices that are derivatized with ion exchange, hydrophobic interaction and affinity functionalities.

Size-exclusion chromatography was chosen for this work because of its simplicity, in that the only rate parameters needed for *a priori* prediction of peak widths are intraparticle diffusivities, convective dispersion coefficients and, to a secondary degree, fluid-phase mass-transfer coefficients. As will be shown later, sufficient information of this type is available to provide a meaningful comparison between observations and *a priori* predictions of plate heights. On the other hand, accurate estimates of geometric and thermodynamic parameters (collectively called equilibrium parameters) such as the inclusion porosity of a species, which determine the peak position in the differential mode of operation,

☆ Present address: University of Cambridge School of Clinical Medicine, Herchel Smith Laboratory for Medicinal Chemistry, University Forvie Site, Robinson Way, Cambridge CB2 2PZ, UK.

0021-9673/92/$05.00

are best obtained directly from experiment, and no attempt is made here to predict them.

Our interest centered on two specific practical questions: (i) are existing lumped-parameter models adequate to describe the behavior of commercially available chromatographic media?, and (ii) is monodispersity of the packing material necessary to achieve maximum separation efficiency?

Before turning to our results and their significance, we summarize the model used for differential chromatography, then briefly review the pertinent literature in the context of the model and outline our experimental procedure.

CHROMATOGRAPHIC MODEL

We deal here with linear chromatography in which the equilibrium constant for adsorption and the fluid properties are considered to be independent of concentration, a reasonable assumption for dilute samples or low loadings. The model is formulated for an adsorptive system, with size-exclusion chromatography treated as a special case. The details of the problem statement are given in the Appendix in order to clarify our notation, which differs slightly from that of Gibbs and Lightfoot [1]. In this section, we first present a solution to the model equations valid for long columns, then provide an overview of available information on the transport parameters which appear in the model and finally discuss the issue of predictability of chromatographic performance.

Asymptotic long-time solution

Some of the earliest solutions of the pseudo-continuum equations of linear chromatography for specific cases of the dominant broadening mechanisms were obtained by, among others, Lapidus and Amundson [8] and Rosen [9]. Rasmuson [10] later derived a general solution which includes the effects of convective axial dispersion, fluid-phase mass transfer, intraparticle diffusion and linear adsorption kinetics. The expression being tested here is a convenient lumped-parameter approximation to these solutions, developed by Reis *et al.* [11] for rapid adsorption and extended by Gibbs and Lightfoot [1] to include the effects of adsorption kinetics and to treat gradient elution. It has been shown that this solution combines simplicity with a surprising degree of accuracy and that it should be adequate for most purposes in liquid chromatography [1,5].

Differential chromatography involves the application of a short feed pulse into the mobile phase of a column previously devoid of solute. The initial conditions for the concentrations in the fluid and stationary phases can then be written as

$$c_f(z,t=0) = \frac{m_0}{A_0\varepsilon_b}\delta(z) \quad \text{and} \quad c_b(z,t=0) = 0 \tag{1}$$

respectively, where A_0 is the column cross-sectional area, m_0 is the mass (or moles) of solute initially injected, ε_b is the interstitial void fraction and $\delta(\cdot)$ is the Dirac delta function. Columns of interest for practical separations are typically long in the sense that the boundary conditions have little effect on the peak shape [5]. It is hence convenient to use the simplest type of physically reasonable boundary conditions, and here we choose the long-column form, which assumes that the concentration field decays rapidly at long distances:

$$\lim_{z\to\pm\infty} c_f = \lim_{z\to\pm\infty} c_b = 0 \tag{2}$$

In order to test the utility of the model, we need only consider isocratic operation, in which case the long-time solution to the equations of linear chromatography is a Gaussian function [11] of the axial coordinate z in the column:

$$c_f(z,t) = \frac{m_0 u}{A_0\varepsilon_b\sqrt{2\pi H z_0}} \exp\left[\frac{-(z-z_0)^2}{2Hz_0}\right] \tag{3}$$

with

$$z_0 \equiv uvt \quad \text{and} \quad u \equiv \frac{\varepsilon_b}{\varepsilon_b + (1-\varepsilon_b)\varepsilon_p^*(1+K_d)} \tag{4}$$

where v is the interstitial fluid velocity and the quantity u represents the fraction of solute in the moving fluid phase at long times. Here K_d is the equilibrium constant for adsorption, defined as the ratio of the mass of adsorbed solute to that of unadsorbed solute *within a particle* at equilibrium, while ε_p^* is a species-dependent inclusion porosity which represents the fractional volume of stationary phase that is effectively accessible to a solute. (We note as an aside that a simplification results for size-exclusion chromatography, where $K_d = 0$).

Both the variance and mean of the Gaussian function in eqn. 3 vary linearly in time and hence their ratio H, the height equivalent to a theoretical plate (HETP or plate height) [12], is a useful time-independent measure of column performance. It follows that a small plate height implies a relatively narrow peak, and hence better separation performance. Note that solutions for other initial conditions can be written in terms of the Gaussian expression above by means of a superposition [13].

The present description of linear chromatography allows us to express the plate height in terms of the lumped parameters which characterize the different mechanisms of peak broadening in a packed bed [1,5,11]. It is instructive and convenient to write the explicit expression for plate height in dimensionless terms by defining a reduced plate height, $h \equiv H/2R$. We then have the following extension of the Van Deemter equation [7]:

$$h = \frac{2}{Pe_{\mathscr{E}}} + \frac{(1-u)^2}{3(1-\varepsilon_b)}(ReSc)\left[\frac{1}{Nu} + \frac{m}{10} + \frac{m'}{Da}\right] \quad (5)$$

Here the dispersion Péclet number $Pe_{\mathscr{E}}$ and the Nusselt number Nu are simply scaled representations of the convective axial dispersion coefficient $\mathscr{E}$ and the fluid-phase mass-transfer coefficient k_c, as defined below:

$$Pe_{\mathscr{E}} \equiv \frac{2Rv}{\mathscr{E}} \quad \text{and} \quad Nu \equiv \frac{2Rk_c}{\mathscr{D}_f} \quad (6)$$

Both these dimensionless numbers are functions of the interstitial void fraction ε_b and the reduced velocity $ReSc \equiv 2Rv\varepsilon_b/\mathscr{D}_f$, as discussed later. The typical velocity range of interest in liquid chromatographic practice is $1 < ReSc < 200$, with size-exclusion chromatography usually conducted below $ReSc = 50$. The terms involving the quantities m and m', defined as

$$m \equiv \frac{\mathscr{D}_f}{\varepsilon_p^* \mathscr{D}_p} \quad \text{and} \quad m' \equiv \frac{3}{2}m\left(\frac{K_d}{1+K_d}\right)^2 \quad (7)$$

are respectively the contributions of the intraparticle diffusion resistance and sorption kinetics to peak broadening; the Damköhler number $Da \equiv R^2 k_a/\mathscr{D}_p$.

We shall henceforth be concerned with size-exclusion chromatography, where K_d and m' vanish, so that the term involving Da in eqn. 5 will not be needed any further in our discussion. The reduced plate height is commonly displayed as a function of the dimensionless velocity $ReSc$ in a Van Deemter plot [7] which, it may be observed, does not depend explicitly on particle size.

Description of transport parameters

In this section, we provide information available in the literature on the three transport parameters needed to characterize the performance of size-exclusion chromatography, namely, the intraparticle diffusivity, the convective dispersion coefficient and the fluid-phase mass-transfer coefficient.

We begin by noting that at the low concentrations encountered in linear chromatography, the diffusivity of a solute can be assumed to be independent of concentration, as done in the analysis above. It is also adequate to follow the commonly used practice of considering the intraparticle diffusivity to be proportional to that in free solution, with the proportionality constant depending on the size of the pores relative to that of the solute and on the shape and tortuosity of the pores [14]. Expressions for this proportionality constant, derived from a simplified hydrodynamic model of pore-wall effects and written in terms of the solute-to-pore size ratio, have been used successfully in the literature [14–16] for both correlative and predictive purposes. However, our particular experimental system allows us to proceed without this detailed information, a point we shall pursue further in the section on plate-height predictions.

We now present what we consider to be the most reliable correlations available in the literature for the lumped parameters $Pe_{\mathscr{E}}$ and Nu defined above. It is known from the continuum form of the equations of change [17] that for transport in forced convective flow, the scaled state variables of a system, and hence dimensionless quantities derived from them (such as $Pe_{\mathscr{E}}$ and Nu), depend parametrically on system geometry and the Reynolds and Schmidt numbers, given respectively as

$$Re \equiv \frac{2Rv\varepsilon_b\rho}{\mu} \quad \text{and} \quad Sc \equiv \frac{\mu}{\rho\mathscr{D}_f} \quad (8)$$

where ρ and μ are the density and viscosity of the fluid. It turns out that modern liquid chromatography is almost always conducted in the creeping flow regime, defined for packed beds by the Reynolds number being of the order of unity or

smaller. This fact is of significance because creeping flow is qualitatively different in nature from high-*Re* flow (of which turbulent flow is a special case), owing to the dominance of viscous effects over inertial effects at low Reynolds numbers. Under these conditions, it can be shown on purely dimensional grounds [17] that the dimensionless transport coefficients should depend on *Re* and *Sc* only through their product, the reduced velocity *ReSc*, which is also called the diffusion Péclet number. The correlations given below satisfy this requirement. Moreover, experience suggests that the most important determinant of the flow geometry in a well-packed, random bed of spheres is the interstitial void fraction ε_b. It is hence customary to express the dimensionless transport parameters as functions of *ReSc* and ε_b in creeping flow.

We proceed first to an overview of available information on convective dispersion coefficients, and we begin by examining behavior under limiting conditions. Several investigations [18,19] have confirmed that for $ReSc \ll 1$, the dispersion coefficient is simply $\mathscr{D}_f/\tau$, indicating purely diffusive axial spreading; here τ is the interstitial tortuosity factor, about 1.4 for a packed bed of spheres (for simplicity, however, we retain the term "convective dispersion" even in this diffusion-dominated regime). On the other hand, for very high *ReSc* values, the dispersion Péclet number approaches an asymptotic value which depends only on the Reynolds number [20–22], corresponding to the limit of purely hydrodynamic dispersion [23]. Gunn [24] has correlated this high-*ReSc* limit in the form

$$Pe_{\mathscr{g}} \approx \frac{2p}{(1-p)} \quad \text{for very high } ReSc \tag{9}$$

where the adjustable parameter p for a column packed with spheres is found from experiment to be

$$p \equiv 0.17 + 0.33\exp(-24/Re) \tag{10}$$

Thus p is constant at 0.17 in creeping flow, giving a limiting $Pe_{\mathscr{g}}$ of about 0.4.

The behavior for intermediate values of reduced velocity has been analyzed by several workers [2,24,25]. Of these, Gunn [24,26] has carried out a semi-theoretical treatment which involves the adjustable parameter p given above, leading to the development of a correlation capable of predicting convective axial dispersion coefficients reasonably well over a wide range of conditions for both gases and liquids:

$$\frac{1}{Pe_{\mathscr{g}}} = \frac{(1-p)}{p}\left[Y + Y^2\left(\exp(-1/Y) - 1\right)\right] + \frac{\varepsilon_b}{\tau ReSc} \tag{11}$$

where

$$Y \equiv \frac{p(1-p)ReSc}{4\alpha_1^2(1-\varepsilon_b)} \tag{12}$$

Here α_1 is the smallest positive zero of the Bessel function $J_0(\cdot)$ and is approximately 2.405, p is given by eqn. 10 and τ is as mentioned above. It is easy to see that this expression for $Pe_{\mathscr{g}}$ depends only on the product *ReSc* when attention is restricted to creeping flow (with $p = 0.17$) and that it reduces to the widely accepted asymptotic results quoted in the preceding paragraph. Gunn [26] has also provided an extension of the above correlation to account for macroscopically non-uniform flow and wall effects.

It should be emphasized that no empirical correlation is perfect, especially when the objective of the correlation is to fit data over a wide range of variables, and caution is recommended in the use of such results. For example, large discrepancies are seen between Gunn's correlation and the dispersion coefficients measured by Miller and King [22] for reduced velocities between 7 and 50 in creeping flow. We hence seek a description which provides a reasonable upper bound on dispersion coefficients (or a lower bound on $Pe_{\mathscr{g}}$) for intermediate *ReSc* values in creeping flow.

Among data available in the literature [27,28] for the creeping flow regime are those of Rifai *et al.* [29], Hiby [23], Miller and King [22], Knox and Parcher [30] and Han *et al.* [28]. Some of this work does not appear to be reliable, either because narrow columns were used [30] or because the methods of analysis seem to have introduced large errors in the measured dispersion coefficients [29]. Also, the data sets of Han *et al.* and Hiby do not exhibit the limiting behavior at high *ReSc* observed by others, as will be seen shortly.

We therefore considered the data of Miller and King for obtaining a conservative upper estimate for the convective dispersion coefficient. The data points chosen for an empirical fit over intermediate reduced velocities ($7 < ReSc < 320$) and for $Re <$

1 correspond to eight runs (tabulated and numbered 12–16, 22, 24 and 25 in ref. 31) which show the most reproducibility in repeated experiments. The coordinates chosen for the fit, displayed in Fig. 1, are those suggested by Gunn's expression, namely $Pe_{\mathscr{E}}$ and $ReSc/(1-\varepsilon_b)$, and the following result then summarizes the data of Miller and King:

$$Pe_{\mathscr{E}} = \left(\frac{ReSc}{1-\varepsilon_b}\right)^{-1/6} \tag{13}$$

Also shown in Fig. 1 for comparison are the predictions of Gunn's correlation, the fit for the data of Han *et al.* (Fig. 9 or 15 in ref. 28) and the correlation given by Hiby. The fit from Han *et al.* for $10^2 < ReSc/(1-\varepsilon_b) < 10^3$ is given by

$$Pe_{\mathscr{E}} = 4.36\left(\frac{ReSc}{1-\varepsilon_b}\right)^{-0.262} \tag{14}$$

and Hiby's correlation [23] is

$$\frac{1}{Pe_{\mathscr{E}}} = \frac{0.65}{1.0 + 7.0\sqrt{\varepsilon_b/ReSc}} + \frac{0.67\varepsilon_b}{ReSc} \tag{15}$$

As seen in Fig. 1, the discrepancy between the fit to the Miller and King data and Gunn's predictions becomes markedly small towards high *ReSc*. However, the other two curves, corresponding to eqns. 14 and 15, are seen to predict dispersion coefficients much less than the first two. The discrepancies observed in Fig. 1 elude explanation, and we shall return to this point in the discussion of our results. We stress that eqn. 13 is not to be interpreted as any more than a convenient analytical representation of one particular data set. The comparison in Fig. 1, however, serves to underscore the existing uncertainty in the estimation of convective dispersion over the intermediate range of reduced velocities. It is generally believed that the typical behavior, if such a notion makes sense for convective dispersion in packed beds, probably lies between the limits given by the expression of Gunn and the data of Miller and King ($Pe_{\mathscr{E}}$ between 0.5 and 1.0 over the range of interest [32,33]). In any case, it is clear that more work is necessary to rectify the dearth of reliable data and thus obtain a better understanding of convective dispersion in granular beds.

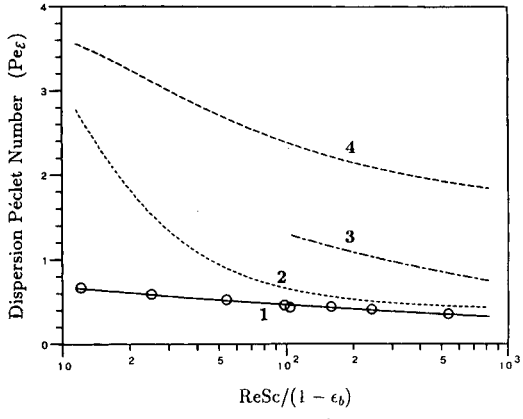

Fig. 1. Comparison of dispersion Péclet numbers ($Pe_{\mathscr{E}} \equiv 2Rv/\mathscr{E}$) from various sources. The data points are those of Miller and King (see text) and the solid line (curve 1) is the fit given by eqn. 13; curve 2 depicts the correlation of Gunn (eqn. 11); curve 3 shows the fit from the work of Han *et al.* (eqn. 14); and curve 4 is the correlation of Hiby (eqn. 15) with $\varepsilon_b = 0.4$.

On the theoretical side, Koch and Brady [34] have carried out an asymptotic analysis of dispersion, valid for low volume fractions of randomly configured spheres held fixed in a creeping ambient flow. Their prediction of the convective axial dispersion coefficient, derived for $ReSc \gg 1$, does capture the general trend of the experimental measurements taken from the literature, but severely underestimates the data over *ReSc* values between 1 and 200. (For the sake of completeness, we mention that the diffusion Péclet number in the original expression of Koch and Brady has been erroneously transcribed elsewhere in the literature [6,35].)

We hence restrict ourselves to the use of eqn. 11 and 13 as two representative limits of convective dispersion for predictive purposes later.

Having discussed the available information on convective axial dispersion, we turn now to transport between the mobile fluid far from a spherical particle and the fluid at the particle surface. As noted earlier, the fluid-phase mass-transfer coefficient k_c which characterizes the mass flux at the particle surface can be expressed in terms of a Nusselt number *Nu*. Boundary-layer theory predicts the asymptotic functional dependence of *Nu* for large values of *ReSc* [36] in creeping flow to be of the form

$$Nu = \gamma(ReSc)^{1/3} \quad (\text{for } ReSc \gg 1) \tag{16}$$

Wilson and Geankoplis [37] found their measurements from electrochemical experiments to follow this dependence fairly accurately, and obtained $\gamma =$

$1.09/\varepsilon_b$. As far as the behavior at low values of *ReSc* is concerned, there appears to have been some uncertainty in the literature [38], but both analysis [39,40] and experiment [41,42] suggest that the Nusselt number approaches a constant value β as $ReSc \rightarrow 0$, much as with an isolated sphere in a stagnant fluid [17].

Following the procedure employed in ref. 43 for patching up asymptotic results, we used this limiting information to develop the following expression:

$$Nu \approx [\beta^3 + \gamma^3(ReSc)]^{1/3} \tag{17}$$

where γ is as above and β is conservatively chosen [39] to be 4.0. This cube-averaged form has been selected because it conforms to the limiting behavior mentioned above and gives uniformly good agreement (within 10%) with the numerical results of Sørensen and Stewart [39] over five decades of *ReSc*. It can be shown that the large *ReSc* limit is adequate for most practical purposes because the contribution of fluid-phase mass-transfer resistance to plate height is negligibly small at low *ReSc*, so that the plate height is not particularly sensitive to the choice of β.

This completes the description of the chromatographic model used in this study.

Predictability of chromatographic performance

At this juncture, it is worth pointing out that a number of empirical relationships for the dependence of the reduced plate height have emerged in the literature. Perhaps the most successful of these is the so-called Knox equation [44,45], given here in a general form:

$$h = A(ReSc)^{1/3} + \frac{B}{ReSc} + CReSc + D \tag{18}$$

where A, B, C and D are empirical constants for a given column, eluent and solute. This equation, however, may not be very useful for process design when extrapolating from laboratory conditions, inasmuch as the empirical constants here are not directly related to independently measurable quantities such as those in eqn. 5. Although the C-term above, for example, can be related to an effective stationary-phase diffusion coefficient [46], it is desirable for design purposes to retain a distinction between the individual contributions, as done in eqn. 5. Weber and Carr [6] have reviewed the origins and validity of eqn. 18 and its competitors.

We now consider the issue of predictability of chromatographic separations using the lumped-parameter model outlined in the preceding sections. We shall shortly see that the Gaussian solution and the plate-height expression given above yield accurate descriptions of (linear and isocratic) size-exclusion chromatography in the differential mode, *given reliable values of the transport parameters involved.* The correlations for convective axial dispersion and fluid-phase mass transfer quoted from the literature are adequate for most purposes, except at low reduced velocities where convective dispersion is poorly understood. However, in order to use the above model for design predictions, transport parameters such as the factor m (which involves the intraparticle diffusivity) in eqn. 5 must still be obtained by other means, because these parameters cannot be determined reliably using the plate-height equation as a basis for analyzing experimental data [5,47].

Such a situation is not unusual in engineering practice, and a simple example in point concerns the extraction of intraparticle diffusion coefficients from the plate height measured in a single size-exclusion experiment at a relatively low velocity and its use for predicting chromatographic behavior at high velocities. At low velocities, convective axial dispersion dominates the plate height, but the considerable uncertainty in its prediction (as indicated in the previous section) can lead to an uncertainty in the value of intraparticle diffusivity extracted. As a result, the plate height predicted at high velocities, where intraparticle diffusion is the dominant resistance, on the basis of the low-velocity data would likely be in error by a significant amount. Another illustration is afforded by the work of Nakanishi *et al.* [48] on size-exclusion chromatography. They found that the diffusivity ratio calculated from the slope of the measured Van Deemter plot was about half of that determined from experiments conducted on single gel beads, suggesting that there was significant bypassing or channelling in the columns used.

We have therefore concentrated in our program on reliable means for estimating the parameters appearing in the above description in isolation from each other, using separate, well-defined experiments

[35,49]. Some of our results to date are used later in this study.

Before moving to a description of our experiments and predictions, we briefly summarize prior work published in the literature on the effect of polydispersity of packing material on performance.

PRIOR WORK ON THE EFFECT OF POLYDISPERSITY

In this section, we review the effect of particle size distribution (PSD) on three interrelated factors: the plate height or separation performance, the packing quality and the pressure drop in a fixed bed.

The effect of polydispersity of packing media on chromatographic performance has been studied experimentally by only a few investigators. Dawkins *et al.* [50] published one of the early studies on PSD in gel permeation chromatography using cross-linked polystyrene gels, but for the most part only compared distributions with different mean sizes. A careful examination of their data reveals, however, that for a completely excluded solute, the plate heights of narrowly distributed and monodisperse media (with the same mean size) were similar. Moreover, the observed limiting behaviour of the plate height for high values of the dimensionless group *ReSc* appears to be consistent with the prediction from Gunn's correlation for the convective dispersion coefficient (eqn. 11).

Later, Nakanishi *et al.* [48], in a series of papers on dispersion mechanisms in size-exclusion chromatography, investigated the performance of Sephadex (Pharmacia) gels, with sodium chloride and myoglobin as solutes. They found that for each solute, the dimensionless Van Deemter plots for different sieve fractions did collapse into a single line as expected from eqn. 5, but only when the particle size used for scaling was chosen as the volume-averaged root-mean-square diameter calculated from the PSD of each sieve fraction. From eqn. 5, this result is seen to be consistent with the intraparticle diffusion resistance dominating the plate height.

Most recently, Han *et al.* [28] studied two sets of non-porous particles with a discrete distribution of sizes and compared their convective dispersion coefficients with those obtained from monodisperse beads, with all three sets having the same area-averaged mean particle diameter. It was observed that the narrower distribution and the uniform set behaved almost identically, whereas the particles which were broadly distributed gave dispersion coefficients higher by a factor of two.

As far as theoretical analyses on this topic are concerned, a few workers have carried out numerical solutions of special cases of the equations of change to investigate the effect of PSD on performance in chromatography [51–55] and in stirred batch systems [56]. The general consensus from all these investigations is that polydispersity may have an adverse impact on the broadening of a peak or a front only for very broad or asymmetric PSD in a short bed. For columns with the large number of plates typically necessary for protein separations, it appears adequate to use chromatographic media with a symmetric size distribution of modest breadth. This conclusion also seems to imply that the use of a mean diameter is reasonable for design calculations under the conditions noted above, an important point we shall use in our predictions.

We next come to the issue of packing quality in relation to polydispersity. The most recent experimental work on this subject is that of Kulin *et al.* [57], who prepared remarkably monosized poly (styrene–divinylbenzene) particles of 5, 10 and 20 μm diameter for size-exclusion chromatography. They encountered a lack of reproducibility in experiments on columns packed with 5-μm beads, and found that two identically sized columns with 10- and 20-μm particles had interstitial voidages as high as 0.58 and 0.47, respectively. These observations cast doubts on the reliability of the slurry packing method used and on the resulting packing quality using such monodisperse media, and preclude any definitive conclusions on this topic.

The last consideration regarding PSD is its effect on the pressure drop in a packed bed, and two representative studies are cited here. Dewaele and Verzele [58] worked with silica-based reversed-phase sorbent materials (Alltech) made as mixtures of two narrowly distributed fractions and showed that the pressure drop in columns packed with mixtures of very different size fractions was well above that predicted by using the arithmetic mean diameter in the Blake–Kozeny equation [17]. In contrast, Yamamoto *et al.* [59] found that the Blake–Kozeny equation was satisfactory for their columns packed with Toyopearl HW55 media (TosoHaas), which have a reasonably narrow size distribution.

Having discussed the reported effects of polydispersity on chromatography, we now proceed to a description of the experimental work undertaken.

EXPERIMENTAL OBSERVATIONS

As a part of the larger goal of separately measuring transport parameters and using these estimates for the design and scale-up of chromatographic separations, the work described in this section involved the use of size-exclusion column experiments for assessing the general performance of the Toyopearl HW65 media.

Experiments on differential chromatography were conducted on two sets of columns. (i) One set consisted of two glass columns (Omnifit) with the same I.D.(2.50 cm) and bed lengths of 11.5 and 46.5 cm (chosen so as to study the dispersion from column ancillaries). This pair of columns was packed at TosoHaas by the constant-pressure method at 2 bar with a 30% slurry of the vinyl polymer-based, macroporous size-exclusion medium Toyopearl HW65C, which has a particle size range of 50–100 μm. (ii) The other consisted of a 25.0 $\times$ 2.25 cm I.D. stainless-steel column (Alltech) packed with Toyopearl HW65S, nominally the same medium as above, but with a size range of 20–40 μm. This column was packed by adding a slurry of the gel particles under gravity-induced flow. The bed was then allowed to settle under a flow of 5 ml/min. Finally, a small amount of additional packing was added to fill voids at the top of the column resulting from the settling.

For the glass columns, injections of *ca.* 0.1 ml of bovine hemoglobin (Sigma; No. H 2500) at concentrations of 10, 50 and 100 mg/ml were applied, whereas for the stainless-steel column, the samples were 20 mg/ml ovalbumin (Sigma; No. A 5503) in volumes of about 0.02 ml for the first set of data and 0.1 ml for data taken 2 months later. In all instances, the samples were made up in 0.1 *M* Tris–HCl buffer (pH 8) and applied using a Rheodyne (Model 7125) valve. The pulse response experiments were run at a series of flow-rates with elution by the above buffer, filtered and degassed, using Gilson Model 303 pumps. The column effluent concentration was monitored by measuring the UV absorption at 254 or 280 nm across 2- or 10-mm flow cells for hemoglobin and at 280 nm across a 10-mm flow cell for ovalbumin, both in a Gilson Holochrome detector (cell volumes under 11 μl). The output was acquired digitally and stored using a PDP 11/75 computer (Digital Equipment). All the work described here was carried out at room temperature (20°C).

Two preliminary experiments were conducted to measure the interstitial void volume in the columns and to quantify the effects of extracolumn fittings including the injection valve, tubing and detector on measured effluent chromatograms. For the former experiment, both blue dextran (Sigma; No. D 5751) and calf thymus DNA (Calbiochem) [60] were used individually, but were found to have broad molecular weight distributions. For the short glass column, the least retained component of blue dextran, which was isolated and eluted separately, repeatedly indicated an interstitial void fraction of about 0.36, as did the runs with DNA, whereas DNA elution on the long glass column suggested a voidage close to 0.39. For the stainless-steel column, experiments with DNA gave a void fraction of about 0.31. The other set of preliminary runs for studying the additional dispersion from extra-column fittings consisted of disconnecting the columns from the flow path and carrying out pulse response measurements. It was determined that these contributions to the broadening of a pulse sent to the column were negligible enough to cause less than a 1% change in the plate height of the shortest column used here even when operated at its most efficient.

The elution curve for each run was fitted to the long-column Gaussian solution (eqn. 3 with z held constant at the column length) by a non-linear least-squares fitting routine developed at the University of Wisconsin [61]. We eschewed the use of methods based on tangents or moments or on information derived from isolated points on the chromatogram, as these procedures are generally unreliable or prone to numerical errors [5]. A sample chromatogram with the best fit is shown in Fig. 2. As the peak in each experiment was digitally sampled in a set of 150–300 points, the fitting code provided confidence limits of better than 3% on the three parameters estimated *in each run*, namely, the inclusion porosity, the plate height and a measure of the mass of solute injected. (The solute mass was left as a quantity to be estimated because the injection volumes and sample concentrations were not con-

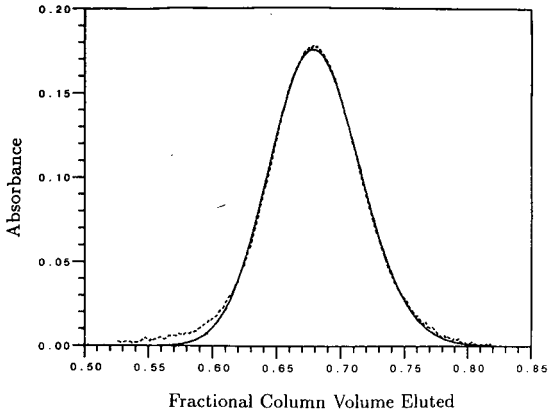

Fig. 2. Comparison of an effluent chromatogram shape with a least-squares best fit (solid line) based on the Gaussian expression in eqn. 3. A 0.1-ml sample of 10 mg/ml hemoglobin was eluted at 0.6 ml/min in an 11.5-× 2.5 cm I.D. glass column packed with Toyopearl HW65C; absorbance was measured at 280 nm across a 10-mm path length. Parameter values estimated: $\varepsilon_p = 0.498$ and $h = 4.16$. The number of data points on the digitized chromatogram used for fitting was 246 in this instance. Other details are given in the text.

trolled to the same degree of accuracy as reflected in the confidence limits given by the fitting routine; from eqn. 3 it is clear that doing so should not affect the estimation of the other two parameters.)

The estimates obtained for the inclusion porosity ε_p^* were as follows: a mean value of 0.503 for hemoglobin in HW65C in the 11.5-cm glass column, based on 39 separate runs over a range of flow-rates [relative standard deviation (R.S.D.), 1.4% of the mean]; 0.491 for hemoglobin in HW65C in the 46.5-cm glass column, based on 19 runs (R.S.D., 1.2%); and 0.454 for ovalbumin in HW65S in the stainless-steel column, based on 17 runs (R.S.D., 1.9%). The value for ovalbumin in HW65S is consistent with that measured by Germershausen *et al.* [60] in Toyopearl HW65F (size range 30–60 μm). Also, the values of ε_p^* for hemoglobin in HW65C are seen to agree fairly closely with each other when measured on two columns of different length. However, this value for hemoglobin (molecular weight 64 kilodalton) in HW65C is larger than that for the slightly smaller protein ovalbumin (45 kilodalton) by about 10%, with the latter porosity measured in HW65S, which is putatively the same medium as HW65C but has a different particle size. In a macroporous gel such as HW65 with a reported protein exclusion limit of 5 megadalton [62], these two molecules are expected to have roughly the same degree of partition, and the discrepancy of 10% is then not practically significant for this medium.

This observation suggests to us that our measurements of interstitial voidage are probably not completely accurate. Indeed, from the form of eqn. 4, it is clear that the parameter ε_p^* in size-exclusion chromatography is very sensitive to ε_b and the elution volume, so that small errors in the measurement of the solute mean residence time and void fraction can become magnified into large errors in the estimates of the inclusion porosity. As an illustration of this sensitivity and the concomitant tendency for error in parameter estimation, we point out that Yamamoto *et al.* [63] and Germershausen *et al.* [60] obtained results that give inclusion porosities differing by 20–25% *for a given protein in the same medium.* These two groups worked with Toyopearl HW55F, each using both ovalbumin and bovine serum albumin (69 kilodalton), but with different buffers (Tris–HCl and KCl–phosphate, respectively).

We shall return to the effect of the small uncertainty in the estimation of the inclusion porosity briefly in the next section. To summarize, we obtained an average inclusion porosity of the medium in each column for the respective proteins, and also measured values of plate height as a function of velocity for different samples sizes and concentrations. The maximum interstitial velocities used in this study were 1.6 and 1.1 cm/min for the short and long glass columns, respectively, and 4.0 cm/min for the stainless-steel column, corresponding to a range of *ReSc* values between 0.7 and 110. Our data therefore covered the normal velocity range of operation of size-exclusion columns, namely 0.5–1.5 cm/min.

PLATE-HEIGHT PREDICTIONS

Our goal now is to calculate the plate height as a function of interstitial velocity essentially *a priori*, using only the values of void fraction and inclusion porosity determined from experiment. The two major hurdles in this approach are the lack of knowledge of the intraparticle diffusivity and of a mean particle size for use in the reduced plate-height equation given previously.

As mentioned earlier, it is convenient and ade-

quate to assume that the intraparticle diffusivity of a solute is proportional to its free-solution diffusivity, with the effective tortuosity factor $\mathscr{D}_f/\mathscr{D}_p$ dependent on the relative sizes of the solute and the pores. Gibbs and co-workers [64,65] measured ovalbumin diffusivities by pulsed field gradient NMR in solution and inside Toyopearl HW65 media at 20°C and found that the ratio $\mathscr{D}_f/\mathscr{D}_p$ is between 2.2 and 2.4 over the concentration range 1–200 mg/ml. This effective tortuosity factor can be expected to apply also to hemoglobin, inasmuch as the hemoglobin and ovalbumin molecules are comparable in size (radii of gyration 25 and 22 Å, respectively [66]) and both much smaller than the pores of the HW65 media (protein exclusion limit 5 megadalton) [62]. We hence do not need explicitly to use any predictive expression for the pore-wall effect [14], as indicated in the section on the description of transport parameters. The free-solution diffusivity of hemoglobin at 20°C is available in the literature [66,67]. For the purposes of prediction, it was assumed that the intraparticle diffusivity for hemoglobin differs from the free-solution value simply by a factor of about 2.3 for the HW65 media. As an aside, we mention that the slope of the plate-height data of Yamamoto *et al.* [63] yields a high diffusivity ratio of about 7.0 for myoglobin (16 kilodalton) in the Toyopearl HW55 media, which have an exclusion limit of 700 kilodalton and pores presumably narrower than those of HW65.

A study of the particle size distribution of the HW65 media (conducted at Rohm and Haas Research Labs. using a Malvern laser light-scattering device) indicates that the bead diameters are narrowly distributed about the arithmetic mean of the upper and lower size limits quoted by the manufacturer, with a d_{90}/d_{10} ratio of only 1.2 (d_{90} and d_{10} refer to the sizes below which 90% and 10% of the particles are found). Moreover, the number-, area- and volume-averaged particle diameters are found to be close to the arithmetic mean size. Then, in accordance with the discussion of prior work on the effect of polydispersity, it appears reasonable to use the arithmetic mean particle diameter for both the size fractions used here.

The system properties assumed for predicting plate heights from eqn. 5 are summarized in Table I. From information available in the original sources cited, the diffusivity values shown are considered accurate to about 10% or better. The predictions for the convective dispersion coefficients were made using Gunn's semi-empirical correlation (eqn. 11) and the Miller and King fit (eqn. 13) (although the latter is based on data for $ReSc > 7$, we have used it down to $ReSc = 2$ for clarity). The mobile phase mass-transfer coefficient was obtained using eqn. 17. The predictions are accurate to about 5% on the basis of the diffusivity values used. Finally, we mention that the calculated plate-height curves were found to be insensitive to variations of 10% in the value of the inclusion porosity, which corresponds to the extent of discrepancy in our observations mentioned in the previous section.

RESULTS AND DISCUSSION

The observations and predictions of plate height in size-exclusion chromatography are compared in Figs. 3, 4 and 5 for the three columns used with the two proteins and the two particle sizes noted above. As expected for the small loadings used here, the plate height is not particularly sensitive to the injected solute concentration in the case of the professionally packed glass columns. With the stain-

TABLE I

PARAMETER VALUES USED FOR PLATE-HEIGHT PREDICTIONS IN FIGS. 3–5

Parameter	Fig. 3	Fig. 4	Fig. 5
Particle radius (R, μm)	37.5	37.5	15.0
Solution diffusivity ($\mathscr{D}_f$, cm^2/s)	$6.9 \cdot 10^{-7}$	$6.9 \cdot 10^{-7}$	$7.9 \cdot 10^{-7}$
Pore diffusivity ($\mathscr{D}_p$, cm^2/s)	$3.0 \cdot 10^{-7}$	$3.0 \cdot 10^{-7}$	$3.3 \cdot 10^{-7}$
Bed void fraction (ε_b)	0.36	0.39	0.31
Inclusion porosity (ε_p^*)	0.503	0.491	0.454

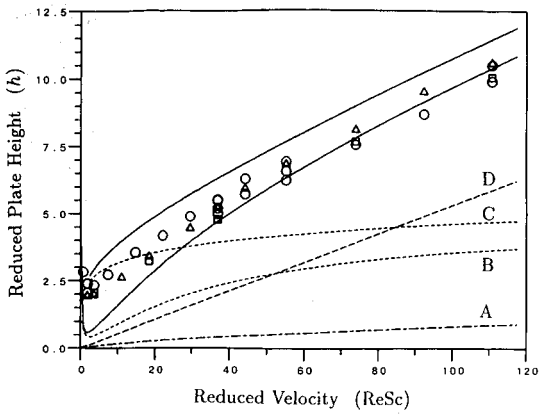

Fig. 3. Plate-height data for an 11.5 × 2.5 cm I.D. glass column packed with Toyopearl HW65C obtained from the elution of 0.1-ml bovine hemoglobin samples with concentrations of (○) 10, (△) 50 and (□) 100 mg/ml. The contributions to the reduced plate height from individual broadening mechanisms, predicted by means of eqn. 5 and the parameter values in Table I, are as follows: (A) mobile phase mass-transfer term (eqn. 17); (B) axial dispersion prediction using Gunn's correlation (eqn. 11); (C) axial dispersion prediction from the Miller and King fit (eqn. 13); and (D) intraparticle diffusion resistance. The lower and upper solid lines represent the total reduced plate height based on curves B and C, respectively. Note that an *ReSc* value of 100 corresponds to a velocity of about 1.5 cm/min.

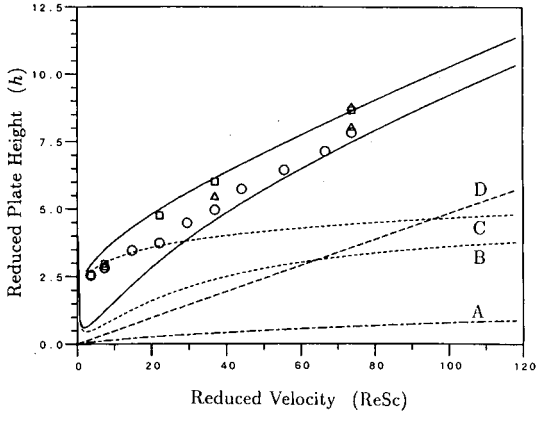

Fig. 4. Plate-height data for a 46.5 × 2.5 cm I.D. glass column packed with Toyopearl HW65C obtained from the elution of 0.1-ml bovine hemoglobin samples with concentrations of (○) 10, (△) 50 and (□) 100 mg/ml. The predictions of plate height and the break-up into its constituent contributions are as in Fig. 3. To allow comparison between the long and short columns, the scale used is as in Fig. 3. Note that an *ReSc* value of 100 corresponds to a velocity of about 1.4 cm/min.

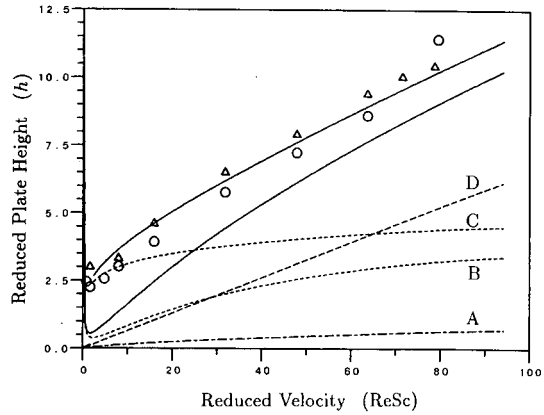

Fig. 5. Plate-height data for the 25.0 × 2.25 cm I.D. stainless-steel column packed with Toyopearl HW65S, obtained from the elution of 20 mg/ml ovalbumin samples. Injected volumes were (○) 0.02 and (△) 0.1 ml, with the latter data taken 2 months after the former. The predictions of plate height and the break-up into its constituent contributions are as in Fig. 3. Note that an *ReSc* value of 20 corresponds to a velocity of about 1.0 cm/min.

less-steel column which was slurry-packed in our laboratory without any specialized equipment, the slight discrepancy between data sets acquired 2 months apart using different sample volumes was most likely caused by bed settling, leading to a small additional dispersion, rather than by loading effects. It should be noted that the plate heights for the 11.5-cm glass column do not uniformly exceed those from the 46.5-cm column even at low velocities (where the separation efficiency is highest and hence most susceptible to extraneous broadening). We also estimated the effect of the pair of headers on the broadening by using a liquid hold-up in each end-piece of 0.055 ml (as obtained from Omnifit) and by assuming each header to be a well-stirred tank (a single plate), as a worst-case limit; this contribution to the reduced plate height was found to be 0.006 for the short column. Hence the dispersion due to the headers is negligible and well within the scatter in the data.

The major ambiguity in the prediction of plate height concerns the estimates of convective dispersion made using Gunn's correlation and the Miller and King data. As seen from the figures, the two sets of predictions appear to bracket the data over most of the range of velocities. At the lower end of reduced velocities, where convective axial dispersion is the dominant contributor to the plate height, the

agreement between our data and the predictions based on the Miller and King fit is much better than that with the Gunn correlation. Note that, contrary to some claims [5], the dispersive contribution to reduced plate height resulting from mixing in the headers or extra-column hold-up is too small to explain the discrepancy between our low-velocity data and those of Hiby [23] (recall the discussion regarding Fig. 1). Hence the discrepancies between prediction and observation are not very large and would probably be of little consequence for design purposes: neither equilibrium nor transport parameters are likely to be known with sufficient accuracy in practice to allow such small distinctions to be made meaningfully.

It is then reasonable to state that for the systems investigated here, *a priori* prediction of the performance of well-packed columns *based on independent estimates of transport parameters* is, for almost all practical purposes, as good as direct measurement via chromatographic experiments. (It is important to reiterate that the *a priori* predictions mentioned here refer only to plate heights and not to equilibrium parameters such as inclusion porosities, an accurate determination of which is best left to measurement.)

This conclusion is important for several reasons. (1) It suggests that both the design of and the packing procedure for the columns used here were adequate to give maximum performance for the media considered, and that further design refinements are not essential for these types of separations, at least at low loadings. (2) It is not necessary, or indeed desirable, to go to the expense of obtaining monodisperse packings: there would be no significant gain in separation effectiveness by making such a change, and there is in fact reason to believe that a moderate degree of polydispersity may be helpful. It is well known, for example, that polydispersed particles give higher packing densities, and it appears that monodisperse packings can give rise to long-range wall effects [30,68]. The spherical symmetry of the particles, combined with the cylindrical symmetry of the wall, decreases the local packing density near the wall significantly, and the tendency towards long-range order in monodisperse packings can cause wall-induced irregularities to persist for long distances. Polydispersity, on the other hand, tends to break up such long-range effects. Moreover, as mentioned before, packings with a modest size distribution do not produce major increases in pressure drop over what is expected of their monodisperse counterparts for a given interstitial void fraction [59]. (3) These results suggest that simulation studies *based on accurate transport and equilibrium parameters* can be both useful and inexpensive for optimizing separations. Moreover, as both diffusivities and dispersion coefficients can usually be estimated fairly easily, it should be possible to guide the beginning stages of experimental investigations, thus obtaining attractive process specifications at a very early step in the process development. This consideration is particularly important for modern pharmaceutical production where process specifications tend to be frozen fairly early. (4) The success of simple transport models for predicting the behavior of chromatographic columns suggests the possibility of developing alternate types of contactors, such as true counterflow devices [69], on a rational basis.

Although the experiments described here were carried out on non-adsorptive systems, the above conclusions can be extended with some confidence to more complex situations. For example, the results on the effect of particle size distribution should also apply to adsorptive media, as the contribution to the plate height due to the finite rate of adsorption is independent of particle size. Finally, we feel that more work needs to be undertaken to characterize better the convective dispersion in packed beds for reduced velocities between 1 and 100 where there is an acute paucity of reliable information.

ACKNOWLEDGEMENTS

We gratefully acknowledge financial and material assistance from Rohm and Haas Company (Philadelphia, PA, USA). We appreciate the several valuable discussions with Drs. Edward Firouztale, Peter G. Cartier and Robert A. Albright of Rohm and Haas, and the help received from Dr. Michael Byers of TosoHaas who generously provided the packed glass columns. S.J.G. and E.N.L. thank the National Science Foundation for a Fellowship and for NSF Grant CBT-8901406, respectively. We also thank the State of Wisconsin for making possible the purchase of the Gilson apparatus used in this work.

SYMBOLS

A_0 column cross-sectional area (cm^2)
c_b volume-averaged solute concentration in a sorbent particle (mg/ml)
c_f solute concentration in moving fluid phase (mg/ml)
Da Damköhler number, defined as $R^2k_a/\mathscr{D}_p$
$\mathscr{D}_f$ effective solute diffusivity in unbounded solution (cm^2/s)
$\mathscr{D}_p$ effective solute diffusivity in pore liquid (cm^2/s)
$\mathscr{E}$ convective axial dispersion coefficient (cm^2/s)
$\mathscr{F}$ local sorption rate in the stationary phase (mg/ml·s)
H height equivalent to a theoretical plate (HETP) or plate height (cm)
h reduced plate height, $H/2R$
K_d ratio of masses of adsorbed and pore-liquid solutes at equilibrium
k_a (forward) rate constant of adsorption (s^{-1})
k_c concentration-based fluid-phase mass-transfer coefficient (cm/s)
m,m' parameters in the reduced plate height expression, defined in eqn. 7
m_0 mass of solute fed to column in a pulse (mg)
Nu fluid-phase Nusselt number, defined as $2Rk_c/\mathscr{D}_f$
$Pe_{\mathscr{E}}$ dispersion Péclet number, defined as $2Rv/\mathscr{E}$
p empirical parameter in Gunn's correlation, defined in eqn. 10
R radius of a stationary-phase particle (cm or μm)
r radial coordinate inside a spherical particle (cm or μm)
Re Reynolds number, defined as $2Rv\varepsilon_b\rho/\mu$
$ReSc$ reduced velocity or diffusion Péclet number, defined as $2Rv\varepsilon_b/\mathscr{D}_f$
Sc Schmidt number, defined as $\mu/\rho\mathscr{D}_f$
t time (s or min)
u fraction of solute in the moving fluid phase at long times, defined in eqn. 4
v interstitial fluid velocity, based on the area $\varepsilon_b A_0$ (cm/s or cm/min)
w_p concentration in pore liquid, based on unit volume of stationary phase (mg/ml)
w_s concentration of adsorbed solute, based on unit volume of stationary phase (mg/ml)
Y dimensionless group in Gunn's correlation, defined in eqn. 12
z axial coordinate in a packed bed (cm)
z_0 mean position of a solute peak at a given time, defined as uvt (cm)

GREEK LETTERS

α_1 smallest zero of the Bessel function $J_0(\cdot)$; *ca.* 2.405
β low *ReSc* asymptote of the Nusselt number (eqn. 17)
γ parameter in the correlation for Nu (eqn. 16), defined as $1.09/\varepsilon_b$
ε_b interstitial (interparticle) void fraction in a packed bed
ε_p^* (intraparticle) inclusion porosity of a solute
μ fluid viscosity (g/cm·s)
ρ fluid density (g/cm^3)
τ bed tortuosity factor in Gunn's correlation; value 1.4

APPENDIX

Here we provide a formulation of the chromatographic equations to which the asymptotic solution has been presented in the section Chromatographic Model. The problem statement given below has been included in order to explain the notation used in this paper, which is different from that in the original source of this model [1].

The convective transport of solute by the mobile fluid phase in a granular bed is commonly described by a one-dimensional, pseudo-continuum model in which one neglects non-uniformities within the bed to write

$$\varepsilon_b\left(\frac{\partial c_f}{\partial t} + v\cdot\frac{\partial c_f}{\partial z} - \mathscr{E}\cdot\frac{\partial^2 c_f}{\partial z^2}\right) = -(1-\varepsilon_b)\frac{\partial c_b}{\partial t} \qquad \text{(A1)}$$

where c_f and c_b refer to the concentrations of a solute in the mobile and stationary phases, respectively, v is the interstitial velocity and ε_b is the interstitial void fraction of the bed (see Symbols). Here, we have assumed dispersed plug flow in the bed, with the convective axial dispersion coefficient $\mathscr{E}$ used to account for axial molecular diffusion and the hydrodynamic broadening effects associated with the local non-uniformities in the interstitial fluid velocity that

are caused by the complicated flow paths around sorbent particles. The use of a second-derivative (pseudo-Fickian) term to capture the effect of convective axial dispersion is justified for long, linear systems because the resulting Gaussian solution to a pulse input agrees well with observations on such systems.

The governing equations for solute transport inside a porous sorbent particle, assuming spherical symmetry and neglecting surface diffusion, are as follows:

$$\frac{\partial w_p}{\partial t} = \frac{\mathscr{D}_p}{r^2} \cdot \frac{\partial}{\partial r}\left(r^2 \cdot \frac{\partial w_p}{\partial r}\right) - \mathscr{F}(w_p, w_s) \qquad \text{for } 0 \leqslant r \leqslant R \tag{A2}$$

$$\frac{\partial w_s}{\partial t} = \mathscr{F}(w_p, w_s) \qquad \text{for } 0 \leqslant r \leqslant R \tag{A3}$$

$$\frac{\partial w_p}{\partial r} = 0 \qquad \text{for } r = 0 \tag{A4}$$

Here the local concentrations of solute present in the pore fluid (w_p) and adsorbed on the internal surfaces (w_s) are based on a unit volume of stationary phase (*i.e.*, the solid matrix and the pore space) rather than on the respective phase volumes within a particle. The assumption of linear adsorption kinetics allows us to express the local sorption rate $\mathscr{F}$ as

$$\mathscr{F}(w_p, w_s) = k_a\left(w_p - \frac{w_s}{K_d}\right) \tag{A5}$$

where k_a is the forward rate constant of adsorption, and the equilibrium constant K_d is simply the ratio of the mass of adsorbed solute to that of unadsorbed solute within a particle at equilibrium. The overall stationary-phase concentration of solute, c_b, is defined as

$$c_b \equiv (4\pi R^3/3)^{-1} \int_0^R (w_p + w_s) 4\pi r^2 dr \tag{A6}$$

The link between the mobile phase and stationary phase descriptions is provided by the matching condition of flux continuity at the particle surface:

$$-\mathscr{D}_p \cdot \frac{\partial w_p}{\partial r} = k_c\left(\frac{1}{\varepsilon_p^*} \cdot w_p - c_f\right) \quad \text{for } r = R \tag{A7}$$

where k_c is the fluid-phase mass-transfer coefficient. We distinguish here between the absolute intraparticle porosity of the stationary phase, which does not appear explicitly in our model, and the solute-dependent inclusion porosity (or an overall rejection factor) ε_p^* which, as seen from eqn. 4, gives the effective volume fraction of the stationary phase that is accessible to the solute. The advantage of using such an inclusion porosity is that we do not need to consider the intraparticle porosity and the rejection factor as separate geometrical parameters [5], which, in any event, are difficult to measure individually. This notation also couches the concentrations of the pore fluid and adsorbed solute, and thus the equilibrium distribution constant K_d, in experimentally meaningful and hence more practically useful terms.

The model formulation is now complete except for the initial and boundary conditions, which are discussed in the main text.

REFERENCES

1 S. J. Gibbs and E. N. Lightfoot, *Ind. Eng. Chem. Fundam.*, 25 (1986) 490–498.
2 J. C. Giddings, *Dynamics of Chromatography. Part I: Principles and Theory* (*Chromatographic Science Series*, Vol. 1), Marcel Dekker, New York, 1965.
3 D. M. Ruthven, *Principles of Adsorption and Adsorption Processes*, Wiley, New York, 1984.
4 J. Å. Jönsson in J. Å. Jönsson (Editor), *Chromatographic Theory and Basic Principles* (*Chromatographic Science Series*, Vol. 38), Marcel Dekker, New York, 1987, Ch. 2, pp. 27–102.
5 A. M. Lenhoff, *J. Chromatogr.*, 384 (1987) 285–299.
6 S. G. Weber and P. W. Carr, in P. R. Brown and R. A. Hartwick (Editors), *High Performance Liquid Chromatography* (Chemical Analysis Series, Vol. 98), Wiley, New York, 1989, Ch. 1, pp. 1–115.
7 J. J. van Deemter, F. J. Zuiderweg and A. Klinkenberg, *Chem. Eng. Sci.*, 5 (1956) 271–289.
8 L. Lapidus and N. R. Amundson, *J. Phys. Chem.*, 56 (1952) 984–988.
9 J. B. Rosen, *J. Chem. Phys.*, 20 (1952) 387–394.
10 A. Rasmuson, *AIChE J.*, 27 (1981) 1032–1035.
11 J. F. G. Reis, E. N. Lightfoot, P. T. Noble and A. S. Chiang, *Sep. Sci. Technol.*, 14 (1979) 367–394.
12 A. Klinkenberg and F. Sjenitzer, *Chem. Eng. Sci.*, 5 (1956) 258–270.
13 I. Stakgold, *Green's Functions and Boundary Value Problems*, Wiley, New York, 1979.
14 C. N. Satterfield, C. K. Colton and W. H. Pitcher, *AIChE J.*, 19 (1973) 628–635.
15 R. R. Walters, *J. Chromatogr.*, 249 (1982) 19–28.
16 B. F. D. Ghrist, M. A. Stadalius and L. R. Snyder, *J. Chromatogr.*, 387 (1987) 1–19.
17 R. B. Bird, W. E. Stewart and E. N. Lightfoot, *Transport Phenomena*, Wiley, New York, 1960.

18 M. F. Edwards and J. F. Richardson, *Chem. Eng. Sci.*, 23 (1968) 109–123.
19 D. J. Gunn and C. Pryce, *Trans. Inst. Chem. Eng.*, 47 (1969) T341–T350.
20 E. A. Ebach and R. R. White, *AIChE J.*, 4 (1958) 161–169.
21 G. L. Jacques, A. Hennico, J. S. Moon and T. Vermeulen, *Lawrence Radiation Lab. Rep.*, UCRL-1069, Part II, 1964.
22 S. F. Miller and C. J. King, *AIChE J.*, 12 (1966) 767–773.
23 J. W. Hiby, in A. Rottenburg (Editor), *Proceedings of Symposium on Interaction between Fluids and Particles*, Institution of Chemical Engineers, London, 1962, pp. 312–325.
24 D. J. Gunn, *Trans. Inst. Chem. Eng.*, 47 (1969) T351–T359.
25 C. L. De Ligny, *J. Chromatogr.*, 49 (1970) 393–401.
26 D. J. Gunn, *Chem. Eng. Sci.*, 42 (1987) 363–373.
27 J. R. Cluff and S. J. Hawkes, *J. Chromatogr. Sci.*, 14 (1976) 248–255.
28 N. W. Han, J. Bhakta and R. G. Carbonell, *AIChE J.*, 31 (1985) 277–288.
29 M. N. E. Rifai, W. J. Kaufman and D. K. Todd, *Sanitary Eng. Res. Lab. Rep.*, No. 3, IER Series 90, Berkeley, CA, 1956.
30 J. H. Knox and J. F. Parcher, *Anal. Chem.*, 41 (1969) 1599–1606.
31 S. F. Miller and C. J. King, *Lawrence Radiation Lab. Rep.*, UCRL-11951, 1965.
32 D. S. Horne, J. H. Knox and L. McLaren, *Sep. Sci.*, 1 (1966) 531–554.
33 S. Yamamoto, K. Nakanishi and R. Matsuno, *Ion-Exchange Chromatography of Proteins (Chromatographic Science Series*, Vol. 43), Marcel Dekker, New York, 1988, Ch. 5, pp. 161–170.
34 D. L. Koch and J. F. Brady, *J. Fluid Mech.*, 154 (1985) 399–427.
35 S. J. Gibbs, *Ph.D. Thesis*, University of Wisconsin–Madison, 1989.
36 W. E. Stewart, *AIChE J.*, 9 (1963) 528–535.
37 E. J. Wilson and C. J. Geankoplis, *Ind. Eng. Chem. Fundam.*, 5 (1966) 9–14.
38 H. Martin, *Chem. Eng. Sci.*, 33 (1978) 913–919.
39 J. P. Sørensen and W. E. Stewart, *Chem. Eng. Sci.*, 29 (1974) 811–837.
40 P. Fedkiw and J. Newman, *Chem. Eng. Sci.*, 33 (1978) 1043–1048.
41 D. J. Gunn and J. F. C. DeSouza, *Chem. Eng. Sci.*, 29 (1974) 1363–1371.
42 T. Miyauchi, T. Kikuchi and K.-H. Hsu, *Chem. Eng. Sci.*, 31 (1976) 493–498.
43 A. J. Karabelas, T. H. Wegner and T. J. Hanratty, *Chem. Eng. Sci.*, 26 (1971) 1581–1589.
44 J. H. Knox, *J. Chromatogr. Sci.*, 10 (1972) 549–556.
45 J. H. Knox, *J. Chromatogr. Sci.*, 15 (1977) 352–365.
46 J. H. Knox and H. P. Scott, *J. Chromatogr.*, 282 (1983) 297–313.
47 E. N. Lightfoot, S. J. Gibbs, A. M. Athalye and T. H. Scholten, *Isr. J. Chem.*, 30 (1990) 229–237.
48 K. Nakanishi, S. Yamamoto, R. Matsuno and T. Kamikubo, *Agric. Biol. Chem.*, 42 (1978) 1943–1945.
49 T. H. Scholten, *Ph.D. Thesis*, University of Wisconsin–Madison, Madison, WI, 1990.
50 J. V. Dawkins, T. Stone and G. Yeadon, *Polymer*, 18 (1977) 1179–1184.
51 A. S. Moharir, D. Kunzru and D. N. Saraf, *Chem. Eng. Sci.*, 35 (1980) 1795–1801.
52 A. S. Moharir, D. N. Saraf and D. Kunzru, *Chem. Eng. Commun.*, 11 (1981) 377–386.
53 A. Rasmuson, *Chem. Eng. Sci.*, 40 (1985) 621–629.
54 G. Carta and J. S. Bauer, *AIChE J.*, 36 (1990) 147–150.
55 Y. S. Lin and Y. H. Ma, *AIChE J.*, 36 (1990) 1569–1576.
56 D. O. Cooney, B. A. Adesanya and A. L. Hines, *Chem. Eng. Sci.*, 38 (1983) 1535–1541.
57 L.-I. Kulin, P. Flodin, T. Ellingsen and J. Ungelstad, *J. Chromatogr.*, 514 (1990) 1–9.
58 C. Dewaele and M. Verzele, *J. Chromatogr.*, 260 (1983) 13–21.
59 S. Yamamoto, M. Nomura and Y. Sano, *J. Chem. Eng. Jpn.*, 19 (1986) 227–231.
60 J. Germershausen, R. Bostedor, R. Liou and J. D. Karkas, *J. Chromatogr.*, 270 (1983) 383–386.
61 W. E. Stewart, M. Caracotsios and J. P. Sørensen, *Computational Modelling of Reactive Systems*, Butterworths, London, 1992, in preparation.
62 TosoHaas Technical Service Center, Woburn, MA, personal communication, 1990.
63 S. Yamamoto, M. Nomura and Y. Sano, *J. Chromatogr.*, 394 (1987) 363–367.
64 S. J. Gibbs, A. C. Chu, E. N. Lightfoot and T. W. Root, *J. Phys. Chem.*, 95 (1991) 467–471.
65 S. J. Gibbs, E. N. Lightfoot and T. W. Root, in preparation.
66 M. T. Tyn and T. W. Gusek, *Biotechnol. Bioeng.*, 35 (1990) 327–338.
67 C. R. Jones, C. S. Johnson and J. T. Penniston, *Biopolymers*, 17 (1978) 1581–1593.
68 R. C. Dean, presented at the *American Society of Mechanical Engineers Seminar on Process Equipment Technology for the Manufacture of Biopharmaceuticals, University of Virginia, September 26, 1989*, lecture 5.
69 E. N. Lightfoot, A. M. Athalye and D. K. Roper, in preparation.

Journal of Chromatography, 589 (1992) 87–91
Elsevier Science Publishers B.V., Amsterdam

CHROM. 23 690

Phosphorylated polystyrene resins in high-performance ion-exchange chromatography

D. Letourneur*, V. Migonney, D. Muller and M. Jozefowicz

LRM, CNRS URA 502, University Paris XIII, Avenue J. B. Clément, 93430 Villetaneuse (France)

(First received November 28th, 1990; revised manuscript received August 6th, 1991)

ABSTRACT

Non-porous polystyrene beads were highly substituted with phosphate groups, grafted via spacers on hydroxylated polystyrene. The phosphorylated polystyrene resins exhibit ion-exchange properties that are different to those of the usual stationary phases containing carboxymethyl or sulphopropyl groups. Moreover, the substituted polymers possess high mechanical and chemical stability, hydrophilicity and ion-exchange capacity. Various proteins were fractionated with these phosphorylated resins, packed in high-performance liquid chromatographic columns. The chromatographic separation occurred according to an ion-exchange mechanism; the adsorption of biomolecules was controlled by the pH and ionic strength of the eluent.

INTRODUCTION

The stationary phases used in ion-exchange chromatography (IEC) for protein separations are generally functional polymers substituted with carboxymethyl or sulphopropyl groups in the case of cationic proteins and aminoethyl or diethyl aminoethyl groups in the case of anionic proteins. However, these stationary phases, generally based on polysaccharides, usually have poor mechanical properties which prevent their use in high-performance liquid chromatography (HPLC) and limit scaling up of the separation.

Therefore, great effort [1–3] has been devoted to the development of new phases based on silica or cross-linked synthetic polymers with better mechanical properties, which would allow their use in HPLC. Cross-linked polystyrene (PS) has recently been shown to perform well at high pressure when substituted with L-arginyl methyl ester [4] or when substituted with sulphonyl groups followed by coating with polyethyleneimine [5].

Little attention has been paid to phosphorylated stationary phases despite their potential interest for both IEC and affinity chromatography, and no phosphorylated PS resins have been described. Therefore, we decided [6] to synthesize phosphorylated PS derivatives via a multi-step procedure.

This paper describes the synthesis of these new phases and their use as stationary phases in the chromatography of proteins.

EXPERIMENTAL

Preparation of phosphorylated polystyrene resins

Polystyrene beads cross-linked with 2% divinylbenzene were obtained from Fluka (Buchs, Switzerland). These are nearly spherical and are about 50 μm in diameter (200–400 mesh). The substitution of PS was performed in a multi-step reaction with analytical-reagent grade reagents.

In the first step, PS was chloromethylated in more than 90% yield as described previously [7,8]. Starting from this material poly(hydroxypropylstyrene) was then prepared [7] (Fig. 1): 4 g of chloromethylated PS were heated at 80°C for 24 h with 30 ml of diethyl malonate, 10 g of potassium carbonate and 1 g of tetrabutylammonium hydrogensulphate. After filtration, the polymer was successively suspended for 12 h in 200 ml of 6 *M* sodium hydroxide,

0021-9673/92/$05.00

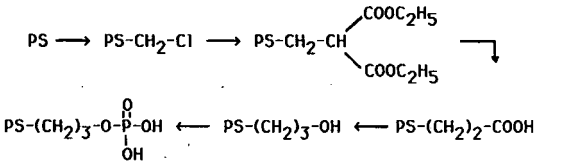

Fig. 1. Synthesis of insoluble phosphorylated polystyrene (PS) derivatives.

then in a mixture of 200 ml of water and 200 ml of 6 *M* hydrochloric acid for 24 h at 110°C. The resulting poly(carboxyethylstyrene) was resuspended in 45 ml of di(2-methoxyethyl) ether, 75 ml of 1 *M* sodium borohydride and 18 ml of boron trifluoride etherate for 12 h at room temperature, leading to poly(hydroxypropylstyrene). Finally, 4.1 g of poly(hydroxypropyl)styrene in 25 ml of trimethyl phosphate were reacted with 3 ml of phosphorus oxychloride at 60°C for 12 h; the phosphorylated resin was stirred for 2 h in 250 ml of water, then washed with water, dioxane, methanol and dichloromethane and dried at 80°C under vacuum.

Chemical characterization

Acid–base titrations of phosphoester derivatives of polystyrene were performed [7] under a flow of nitrogen with an Tacussel TT100 + TT300 automatic titrator in freshly distilled water containing 0.2 *M* NaCl; small amounts of titration solution (10^{-3} ml of 0.1 *M* NaOH) were added with automatic monitoring which allowed the thermodynamic equilibrium to be approached; thus, the rate of addition was about 0.5 ml/day.

Infrared spectra were recorded with a Perkin-Elmer Model 580 spectrophotometer, the polymeric samples being dispersed in KBr pellets.

Elemental microanalyses were carried out by the Service Central d'Analyse (CNRS, Vernaison, France).

Chromatographic experiments

The chromatographic system consisted of a three-headed (120°) pump (Merck LC219), connected to a Rheodyne Model 7126 injection valve (sample loop 200 μl), a 25 x 0.4 cm I.D. stainless-steel column (Merck–Clevenot) in which about 2 g of phosphorylated polystyrene beads were packed by a slurry method, a variable-wavelength UV–visible detector (Merck LC313) and the gradient system. The system was controlled by an Epson QX-10 computer. Experiments were performed at room temperature.

The eluents were prepared with freshly distilled water and were filtered (0.22-μm Millipore GS membrane) and degassed. Analytical-reagent grade reagents were used in these experiments.

Samples

The proteins examined were myoglobin, bovine serum albumin (BSA), transferrin and horse cytochrome *c* purchased from Sigma (La Verpillière, France). Buffered protein solutions (2 mg/ml) in the starting mobile phase were stored at 4°C before use.

RESULTS AND DISCUSSION

Synthesis and characterization

The synthesis described under Experimental results in a three-carbon spacer between the aromatic styrene nucleus and a phosphomonoester group (Fig. 1). Elemental analysis (Table I) indicates a substitution ratio of 2.6 mequiv. of phosphate groups per gram of dry resin. Thus, on the macromolecular chains, 62% of the monomer units bear phosphate groups, randomly distributed along the polymer chains [6,9,10]. The other substituents are mainly hydroxyl groups. Less than 10% of the styrene units are unsubstituted.

As shown in Fig. 2, the acid–base titration curve

TABLE I

CHARACTERISTICS OF THE STATIONARY PHASE

Elemental analysis of the phosphorylated polystyrene

C (%)	H (%)	O (%)	P (%)	Phosphate groups
61.7	6.7	19.2	8.0	2.6 mequiv./g

Elemental analysis of the precursors

C (%)	H (%)	O (%)	Cl (%)	Precursors
79.1	8.1	10.2	–	PS–$(CH_2)_3OH$
74.3	6.8	16.2	–	PS–$(CH_2)_2COOH$
72.3	7.1	17.2	<0.2	PS–$CH_2CH(COOC_2H_5)_2$
72.0	6.1	–	20.8	PS–CH_2Cl
90.4	7.6	0.2	0.09	PS

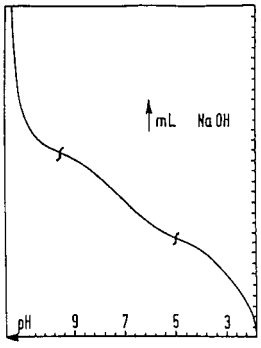

Fig. 2. Titration curve of phosphorylated polystyrene resin with 0.1 *M* sodium hydroxide.

showed evidence of phosphomonoester groups characterized by their acidic properties. Fig. 2 exhibits two inflection points, one strong and one weak acid, with apparent pK_a values of *ca.* 4 and 8.

The chemical and physical characteristics of the resin remained unchanged after treatment for several weeks at a temperature of 160°C, with aqueous solutions with pH values ranging between 1 and 14 and at pressures as high as 200 bar. Moreover, the swelling ratio of the phosphorylated polymer in aqueous solutions was about 200% compared with the dry resin, indicating the high hydrophilicity of this material. From these results, it can be concluded that the syntheses are easily reproducible and well characterized and that the chemical and physical stabilities of the hydrophilic resin are excellent even under extreme temperature, pressure and acidic and basic conditions. Moreover, depending on the $POCl_3$ volume of phosphorus oxychloride added, the range of substitution ratios was from 0 to 80% of phosphate groups [7,11].

Chromatographic experiments

We assessed the applicability of phosphorylated PS resins in the ion exchange of proteins by performing HPLC experiments with solutions of albumin, myoglobin and cytochrome *c* and mixtures of these proteins, the molecular weights (MW) and isoelectric points (p*I*) [12] of which are reported in Table II.

Hydrophilic behaviour. Albumin is a highly hydrophobic protein [13] and near the top of the hydrophobic chromatographic scale, and would be expected to adsorb on the hydrophobic stationary phases. To demonstrate the hydrophilic behaviour of phosphorylated PS resins, isocratic elution of BSA was performed at pH 7.4 in 5 m*M* phosphate buffer–0.1 *M* NaCl, or in 5 m*M* Tris–HCl buffer–0.1 *M* NaCl, and at pH 7 in 5 m*M* Tris–HCl buffer–0.01 *M* NaCl, as shown in Fig. 3. Even at low salt concentrations (at physiological pH), BSA was eluted in the void volume of the column whatever the buffer used. This result confirmed the hydrophilic character of these stationary phases be-

TABLE II

ANION-EXCHANGE CHROMATOGRAPHY OF PROTEINS AT pH 7.6 ON A PHOSPHORYLATED POLYSTYRENE COLUMN (250 × 4 mm I.D.)

Conditions: 3.5-ml linear A–B gradient following 4.2-ml isocratic elution with buffer A, where buffer A is 5 m*M* Tris–HCl (pH 7.6) and buffer B is buffer A + 2 *M* NaCl; flow-rate, 0.1 ml/min; injection volume, 50 µl (2 mg/ml).

Protein	MW	p*I*	Elution volume (ml)
Cytochrome *c*	12 400	9.2	6.84
Myoglobin	17 400	7.1	1.42
Bovine serum albumin	66 000	5	1.44
Transferrin	80 000	5–7	1.45

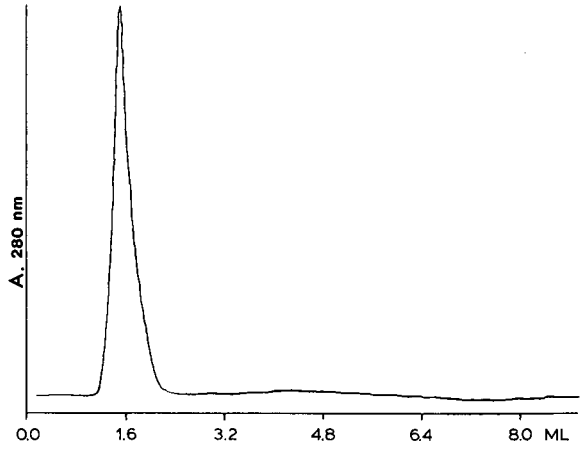

Fig. 3. Isocratic elution of BSA on a phosphorylated PS column (250 × 4 mm I.D.). Sample, 35 µl at 2 mg/ml; flow-rate, 0.1 ml/min; eluent, 50 m*M* phosphate buffer (pH 7.4)–0.1 *M* sodium chloride.

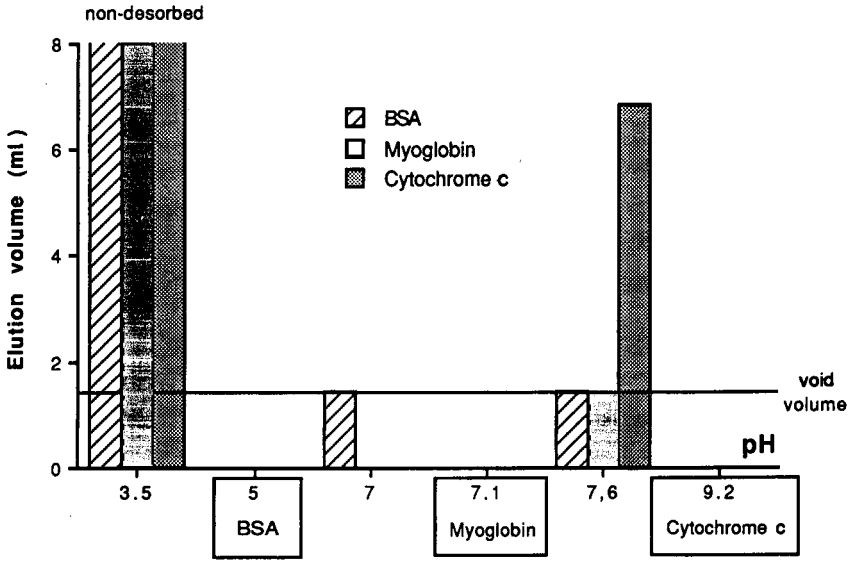

Fig. 4. Anion-exchange chromatography of proteins on a phosphorylated PS column (250 × 4 mm I.D.) at various pH values. Mobile phase, 3.5 ml linear A–B gradient following 4.2-ml isocratic elution with buffer A, where buffer A is 0.16 *M* citrate–sodium phosphate at pH 3.5, 0.05 *M* Tris–HCl–0.01 *M* NaCl at pH 7.0 and 0.05 *M* Tris–HCl at pH 7.6 and buffer B is buffer A plus 2 *M* sodium chloride; flow-rate, 0.1 ml/min; temperature, 20°C; injection volume, 50 μl at 2 mg/ml.

cause BSA is well known [13,14] to adsorb strongly on hydrophobic surfaces.

Influence of pH. Elutions of proteins were performed at various pH values in order to check whether the resins behaved as ion-exchange stationary phases. At pH 3.5 (0.16 *M* citrate–sodium phosphate buffer), *i.e.*, below the p*I* of the proteins under study, the proteins were strongly adsorbed by the resins and could not be eluted even with the use of 2 *M* sodium chloride as eluent. At pH 7, BSA (p*I* = 5.0) was eluted without retention on the stationary phase, as mentioned above. At pH 7.6 in 5 m*M* Tris–HCl without NaCl, elution of myoglobin, BSA and transferrin also occurred in the void volume, as reported in Table II. All these proteins with a p*I* lower than 7.6 did not interact, as expected, with the negatively charged phosphorylated resin, whereas cytochrome *c* (p*I* = 9.2) was desorbed at an NaCl concentration of 1.8 *M*.

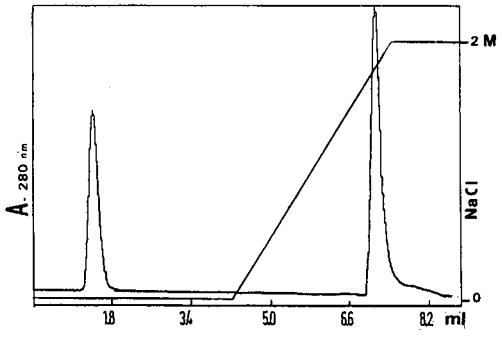

Fig. 5. Separation of myoglobin and cytochrome *c* mixture on a non-porous phosphorylated PS column (250 × 4 mm I.D.). Sample in 150 μl injection volume, 100 μg of myoglobin and 200 μg of cytochrome *c*; linear A–B gradient (100 m*M* salt/ml following 4.2-ml isocratic elution with buffer A), where buffer A is 5 m*M* Tris–HCl (pH 7.6) and buffer B is buffer A plus 2 *M* sodium chloride; flow-rate, 0.1 ml/min; temperature, 20°C.

The results of the studies are summarized in Fig. 4: at pH below the p*I* of the proteins, they are adsorbed on the anionic stationary phase, whereas at pH above the p*I* the proteins are eluted in the void volume. When a protein is retained on the stationary phase, elution occurs at high ionic strength. This implies that the "hydrophobic" contribution to the chromatographic mechanism is minimal, and interaction is primarily though an ion-exchange mechanism. Moreover, the molecular weight does not affect the elution of proteins (Table II), which

shows that the chromatographic mechanism is not one of size exclusion. In all instances, the recovery of the proteins after elution was quantitative.

Fractionation of protein mixtures

The above conclusions are supported by the results of fractionation of a myoglobin and cytochrome *c* mixture. HPLC experiments at pH 7.6 indicate a complete resolution (Fig. 5) of the two proteins when a linear salt gradient is used: myoglobin was first eluted at the initial ionic strength and cytochrome *c* was only eluted with 1.8 *M* NaCl in the eluent.

CONCLUSIONS

Phosphorylated derivatives of cross-linked PS were synthesized and characterized. They are fairly reproducible and of high ion-exchange capacity. These polymeric materials, in the form of beads 50 μm in diameter, were demonstrated to be essentially hydrophilic for proteins such as albumin.

As stationary phases in HPLC they exhibited excellent mechanical properties. Phosphorylated resins are stable in strongly acidic or alkaline solutions. They can also be autoclaved. Experiments performed under HPLC conditions indicated that the elution of the biomolecules is controlled by the pH and ionic strength of the eluent, involving an ion-exchange mechanism. These new synthetic ionized stationary phases allowed the ion-exchange chromatography of protein mixtures.

In ion-exchange chromatography, phosphorylated polystyrene permitted polycationic proteins to be adsorbed at relatively low pH. Moreover, phosphoric acid is an important tool for affinity chromatography because phosphate esters dominate the living world. Thus, phosphorylated resins can be used for the purification of proteins or enzymes interacting with the phosphate groups of biological molecules, including nucleic acids.

REFERENCES

1 L. R. Snyder and J. J. Kirkland, *Introduction to Modern Liquid Chromatography*, Wiley-Interscience, New York, 1979.
2 A. J. Alpert, *J. Chromatogr.*, 266 (1983) 23.
3 W. Kopaciewicz and F. E. Regnier, *J. Chromatogr.*, 358 (1986) 107.
4 X. J. Yu, A. M. Fischer, D. Muller, A. Bros, J. Tapon-Bretaudiere and J. Jozefonvicz, *J. Chromatogr.*, 376 (1986) 429.
5 M. A. Rounds and F. E. Regnier, *J. Chromatogr.*, 443 (1988) 73.
6 D. Letourneur, C. Douzon, V. Migonney, D. Muller and M. Jozefowicz, *US Pat.*, 7 235 113 (1988).
7 D. Letourneur, C. Douzon and M. Jozefowicz, *J. Polym. Sci.*, 29 (1991) 1367.
8 J. M. J. Frechet, M. D. De Smet and M. J. Farall, *J. Org. Chem.*, 44 (1979) 1774.
9 D. Letourneur, V. Migonney and M. Jozefowicz, *Clin. Exp. Rheum.*, 8 (1990) 208.
10 D. Letourneur, M. Jozefowicz, *Biomaterials*, in press.
11 D. Letourneur, *Ph. D. Thesis*, Paris-Nord University, Paris, 1988.
12 W. G. Burton, K. D. Nugent, T. K. Slattery, B. R. Summers and L. R. Snyder, *J. Chromatogr.*, 443 (1988) 363.
13 J. D. Andrade, *Surface and Interfacial Aspects of Biomedical Polymers*, Vol. 2, Plenum Press, New York, 1985, p. 51.
14 R. C. Eberhart, M. S. Munro, J. R. Frautschi, V. I. Sevastianov, in J. L. Brash and T. A. Horbett (Editors), *Proteins at Interfaces (ACS Symposium Series*, Vol. 343), American Chemical Society, Washington, DC, 1987. Ch. 24, p. 378.

Journal of Chromatography, 589 (1992) 93–100
Elsevier Science Publishers B.V., Amsterdam

CHROM. 23 689

Cellulose beads: a weak leaking affinity support

M. Baeseler and H.-F. Boeden*

Central Institute of Molecular Biology, Robert-Rössle-Strasse 10, O-1115 Berlin (Germany)

R. Koelsch and J. Lasch

Institute of Biochemistry, Medical Faculty, Martin Luther University, O-4020 Halle/Saale (Germany)
(First received April 9th, 1991; revised manuscript received August 14th, 1991)

ABSTRACT

The release of immobilized ligands from cellulose beads was studied by solvolytic detachment of glycine, DL-leucine, azocasein and leucine aminopeptidase, which were coupled to carbonochloridate-activated supports. It is demonstrated with immobilized glycine and leucine that the urethane linkage formed between the matrix and ligands is very stable in the pH range 2–10. Comparison of the leakage with corresponding Sepharose conjugates shows the superiority of conjugates based on cellulose beads. The release of immobilized amino acids from bead cellulose was less than 1% for 1000 h at room temperature. For the immobilized proteins it is shown that the initial leakage is due to the desorption of a small amount of non-covalently bound protein (< 10%). Leakage of the proteins multivalently bound to the matrix by the urethane bond was not detectable.

INTRODUCTION

Immobilized enzymes or other biologically active compounds are of growing interest for biotransformation processes, *e.g.*, in enzyme reactors, for the chromatographic purification of biomacromolecules, *e.g.*, in affinity chromatography of antibodies, lectins and enzymes, and for desorption processes in clinical medicine, *e.g.*, extracorporeal detoxification. The application of supports with covalently bound ligands for these purposes depends on the stability of the matrix, their binding capacities and an unimpaired manifold reuse. Moreover, it is essential to check their liability to leakage because the detached ligand may contaminate the purified product or decrease the binding capacity in the further employment of the adsorbent.

In addition to attrition of the matrix, Lasch *et al.* [1] discussed a number of possibilities as reasons for ligand leakage, for instance, cleavage of polymer bonds and of anchoring and ligand bonds. All three types of cleavage have been confirmed by Johansson *et al.* [2] in the case of cross-linked Phenyl-Sepharoses and Phenyl-Superose.

Ligand leakage was most often studied from affinity supports based on agarose. A partial or complete release of ligands coupled to cyanogen bromide (CNBr)-activated matrices by solvolytic detachment was described in several studies [3–8].

To minimize the release of ligands, more stable matrices, *e.g.*, cross-linked agaroses [2,9] or cellulose beads [7], and various activation methods were used. Several studies [1,8–16] have shown that for ligands covalently attached by a more stable (*e.g.*, ether, secondary amine, urethane) bond the leakage was significantly decreased in comparison with ligands immobilized via an isourea linkage obtained with CNBr-activated supports.

After developing a novel technique to bind ligands via a urethane bridge [15,17] in high yield to supports containing hydroxyl groups, we examined in this study the stability of this linkage by monitoring the leakage of low-molecular-weight ligands ([^{14}C]glycine and [^{3}H]leucine) and of proteins (azocasein, M_r 22 000, and leucine aminopeptidase, M_r 300 000, immobilized by multi-point attachment) from cellulose beads (Divicell) and agarose supports (Sepharose).

0021-9673/92/$05.00

Naturally, single and manifold moorings of ligands lead to different leakage kinetics [6,18], which can be modelled theoretically by a leakage function derived earlier [19]. It has been shown [18] that in the case of proteins non-covalent binding by unusually strong adsorption has to be taken into account.

EXPERIMENTAL

Materials

Sepharose 4B, Sepharose CL-6B and CNBr-activated Sepharose 4B were purchased from Pharmacia (Uppsala, Sweden). Divicell (cellulose beads, particle size 80–200 μm) was obtained from Leipziger Arzneimittelwerk (Leipzig, Germany), 5-norbornene-2,3-dicarboximido carbonochloridate (Cl-CO-ONB) from the Institute of Drug Research (Berlin, Germany), carbonyldiimidazole (CDI) from Merck (Darmstadt, Germany) and [^{14}C]glycine and [^{3}H]leucine (specific activity 1.11 GBq/mmol and 2.38 TBq/mmol, respectively) from the Central Institute of Nuclear Research (Dresden, Germany). Azocasein was a gift from Dr. J. Langner (Institute of Biochemistry, Martin Luther University, Halle/Saale, Germany). Leucine aminopeptidase was prepared according to Hanson *et al.* [20]. All other reagents were of analytical-reagent grade.

Preparation of activated supports

Sepharose CL-6B and Divicell were activated with Cl-CO-ONB as described by Boeden *et al.* [17][a].

The activation of Sepharose 4B was carried out catalytically with Cl-CO-ONB in the presence of 4-dimethylaminopyridine within 20 min in dry acetone at room temperature [21].

Divicell epoxy was prepared by conversion of Divicell with epichlorohydrin as described recently [17].

CDI-activated cellulose beads were prepared by activation of Divicell with CDI according to Bethell *et al.* [22], but only one third of the CDI amount per millilitre of gel was used.

The activation level was determined for Cl-CO-ONB-activated supports to be 18–30 μmol/ml gel [15], for Divicell epoxy 30 μmol/ml gel [23] and for CDI-activated Divicell about 23 μmol/ml gel by UV spectrophotometric determination of the CDI concentration in solution at 260 nm prior to and after activation.

Immobilization of glycine

A mixture of non-labelled and ^{14}C-labelled glycine (specific activity 2.64 MBq/mmol) was coupled to the Cl-CO-ONB-activated supports at room temperature in 0.1 *M* borate buffer (pH 8.3) for 20 h, to CDI-activated cellulose beads in 1 *M* sodium carbonate buffer (pH 10) for 20 h, to Divicell epoxy in 0.1 *M* NaOH for 30 h (35°C) and to CNBr-activated Sepharose 4B in 0.1 *M* borate buffer (pH 8.3) for 2 h. The molar ratio between activated groups and added glycine was 1:1.5. The coupling yield related to the active groups was 40% (CDI-activated), 45% (epoxy-activated) and 60–80% (Cl-CO-ONB-activated). The coupling yield was calculated by the difference in the radioactivity of [^{14}C]glycine in coupling solutions before and after immobilization or by determination of the immobilized glycine after blocking with ethanolamine and washing (see below) according to the combustion method of Gács *et al.* [24], counting the [^{14}C]carbon dioxide formed (absorbed with methoxypropylamine). The found values for the two variants were in fair accordance.

The residual active groups were blocked by treatment with 1 *M* ethanolamine (pH 10) for 16 h at room temperature in all samples. The supernatant was then sucked off and the supports were washed three times with a five-fold volume of coupling buffer and finally with water on a sintered-glass funnel, followed by shaking of the gel with water for at least 2 h at room temperature until [^{14}C]glycine was no longer detected in the washings. The total amount of [^{14}C]glycine shed during the washing period with water was $\leq 0.1\%$ relative to the initial amount of glycine for all supports.

Immobilization of DL-*leucine*

A mixture of DL-leucine and ^{3}H-labelled leucine (specific activity 39.7 MBq/mmol) was coupled to Divicell ONB-carbonate with 19 μmol active groups/ml gel in 0.1 *M* borate buffer (pH 10.7) for 3 h at room temperature. The molar ratio between active groups and added leucine was 1:5 and the coupling yield about 50% relative to the active

[a] Cl-CO-ONB-activated Divicell = Divicell ONB-carbonate.

groups. After extensive washing of the gel with a twenty-fold volume of coupling buffer and finally with water the content of immobilized leucine was determined by the combustion method of Gács *et al.* [24] and measurement of the radioactivity of the water formed.

Immobilization of proteins

The coupling of proteins to Divicell ONB-carbonate with 30 μmol active groups/ml sedimented gel in 0.1 *M* borate buffer (pH 9.1) was done as described by Büttner *et al.* [15].

Azocasein was monitored spectrophotometrically at 366 nm [25]. Depending on the lot, the absorbance was $A_{0.5\%}$ = 10.7–12.0. The amount bound was estimated from the balance of azocasein added and that recovered in the filtrate and washings. The washings included the carrier inactivation with 0.2 *M* glycine buffer (pH 8.5) and two washings with 1 *M* NaCl and with borate buffer overnight. On average, 1.5 mg of azocasein per millilitre of sedimented gel were found, *i.e.*, the coupling yield was about 30%.

In order to trace the enzymatically active leucine aminopeptidase, it was determined by its catalytic activity and expressed in nkat/ml. Coupling and the washings were as with azocasein, but the buffer was 0.05 *M* Tris–HCl (pH 8.5). The substrate was 0.01 *M* L-leucine *p*-nitroanilide (LPNA). It was found that 48% of the added activity was bound, corresponding to 3.3 nkat per 5 ml settled cellulose beads.

Leakage of immobilized glycine from agarose and bead cellulose supports

A 1-g amount of suction-dried support with covalently bound glycine (*ca.* 1.5 ml of gel) was shaken with 3 ml of buffer containing 0.03% of sodium azide for 1000 h (see Table I and Fig. 2). At specified times, 25-μl aliquotes of the supernatant were withdrawn and the radioactivity of [^{14}C]glycine was measured by liquid scintillation counting (PW 4700 counter; Philips, Eindhoven, Netherlands).

To determine the on-column ligand leakage, some of the supports were tested in a continuously working column system (low-pressure conditions). Buffer (6 ml) was circulated through a column (5 cm × 1.0 cm I.D.) with 2 g of wet support (*ca.* 3 ml of gel) at a flow-rate of 3 ml/h for 100 h at room temperature.

Leakage of immobilized DL*-leucine from cellulose beads*

The release of leucine immobilized to Divicell ONB-carbonate (coupled amount 9.7 μmol/ml gel) was investigated during storage of 1 ml of sedimented gel in 3 ml of buffer containing 0.04% of sodium azide for 270 days at room temperature (with occasional shaking). Samples of 80 μl of the supernatant were taken and assayed for radioactivity at specified times.

At the end of the leakage experiments the radioactivity of the supports was checked by the combustion method [24].

Leakage of immobilized proteins

The cellulose–support conjugates, *e.g.*, 25 ml of gel suspension (corresponding to 5 ml settled gel), were shaken in 0.1 *M* borate buffer (pH 9.1) containing 0.02% of sodium azide at room temperature for up to 10 days.

The percentage leakages were calculated from the time course of the absorbance in the supernatant: $A(t) - A(0) = A_{corr}$; $C_x\,(t)/C_s = A_x/A_s$ [x denotes the unknown, s a standard solution (500 mg/ml) and *C* concentration]. It follows that $(m/V)/(500/100) = A_{corr}/A_{0.5\%}$, where *m* denotes the milligrams of azocasein per actual total sample volume and *V* the actual sample volume. Hence,

$$m = (A_{corr}/A_{0.5\%}) \cdot 500(V/100) \quad (1)$$

where $V/100$ adjusts the volumes of standard and sample and

$$\text{leakage (\%)} = (m \times 100)/B \quad (2)$$

where *B* denotes the amount of protein bound (mg).

The leakage of leucine aminopeptidase was followed by the enzymatic activity that was liberated into the supernatant as a percentage of the activity bound, *i.e.*, *B* in eqn. 2 was replaced with the bound activity in nanokatals and *m* by the total activity in the actual volume[a].

[a] Using in all calculations the actual volumes means that they were corrected for withdrawn volumes.

RESULTS AND DISCUSSION

Stability of immobilized amino acids

The use of cellulose beads, their activation, the immobilization of ligands and application to the chromatographic purification of proteins have been described recently [15,17]. Supports based on cellulose beads are a suitable chromatographic material because of their higher mechanical, thermal and chemical stability compared with agarose supports [17]. For investigations of ligand leakage we chose activation with 5-norbornene-2,3-dicarboximido carbonochloridate (Cl-CO-ONB), which leads to a urethane (carbamate) linkage between the ligand and matrix after coupling. The stability of these conjugates was compared with that of supports with covalently bound ligands via an isourea (coupling to CNBr-activated Sepharose 4B) and an ether and a secondary amine linkage, respectively (coupling to epichlorohydrin-activated cellulose beads). The three different coupling structures result in different leakage products, as represented schematically in Fig. 1 for the corresponding glycine conjugates.

The glycine leakage, including the portion resulting from the cleavage of glycosidic bonds of the matrix, was determined at various pH values at room temperature by calculation of the amount of the released ligand from the [^{14}C]glycine content of the cleavage products in the supernatants. The results of solvolytic detachment of immobilized glycine are summarized in Table I. The comparison of times after which 1% leakage has occurred shows that the stability of all conjugates increases with decreasing pH. It is noteworthy that the leakage from conjugates prepared with non-cross-linked Sepharose types increases steeply with increasing pH. At pH 4 the support on the basis of CNBr-activated Sepharose 4B is twenty times more stable than at pH 10. However, the stability of conjugates derived from Sepharose CL-6B and Divicell gels is only 1.2–1.3 times higher.

These findings are in accordance with results obtained by Johansson *et al.* [2] and Hearn *et al.* [12], who found a higher stability of agarose supports in water and weakly acidic media (*ca.* pH 4) than at basic pH values using cross-linked Phenyl-Sepharoses or -Superose (ether linkage) and [^{14}C]glycine immobilized onto CDI-activated Sepharose CL-6B (urethane linkage), respectively.

As expected, the highest leakage was found for the support based on CNBr-activated Sepharose 4B and the lowest for the Divicell epoxy derivative. The stability of the Sepharose CL-6B conjugate is considerably higher than that of Sepharose 4B conjugates, by a factor of 9 at pH 10, but only 1.6 times higher at pH 4. Divicell conjugates are extremely stable. It is obvious that the stability of coupled gels, which contain glycine immobilized to Cl-CO-ONB-activated supports, depends strongly on the matrix and increases in the order Sepharose 4B $<<$ Sepharose CL-6B $<$ Divicell. This means that the leakage caused by cleavage of glycosidic bonds is enormously decreased by cross-linking the agarose matrix. A similar result was obtained by Johansson *et al.* [2] for Phenyl-Sepharoses. The high stability of Divicell (a non-cross-linked support) can be explained by the existence of crystalline structures in the cellulose matrix [26].

At pH 10, the release of glycine bound to Divicell ONB-carbonate is diminished by a factor of 10 and 100 compared with that found for Cl-CO-ONB- and CNBr-activated Sepharose 4B, respectively. At pH 8.3 and 4 these differences in stability are smaller. Especially for the CNBr-activated gel this is due to the higher stability of the isourea linkage at lower pH. Glycine bound to Sepharose CL-6B by the urethane linkage is detached more slowly (ca. 25 times

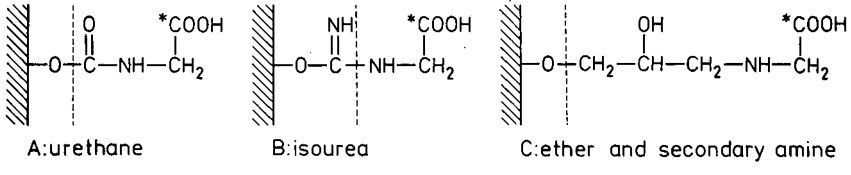

Fig. 1. Expected cleavage of the anchoring bonds. The dashed lines indicate the bonds split preferentially. Radioactive atoms are labelled with asterisks. Leakage products are (A) glycine and carbon dioxide, (B) glycine or N-carbamoylglycine, depending on the pH [3] and (C) N-(2,3-dihydroxypropyl)glycine.

TABLE I

LEAKAGE OF IMMOBILIZED GLYCINE FROM BEAD CELLULOSE AND AGAROSE SUPPORTS

After coupling of glycine (tracer [^{14}C]glycine) to activated supports the gels were treated with appropriate buffers and shaken gently at room temperature (see Experimental). For released glycine the detection limit was about 15 nmol/ml gel; error = ±4.4%.

Activated support	Immobilized glycine (μmol/ml gel)	Time for leakage of 1% glycine (h)[a]		
		pH 10.0[b]	pH 8.3[c]	pH 4.0[d]
CNBr-activated Sepharose 4B	17.0 ± 0.2	10	40	220
Cl-CO-ONB-activated Sepharose 4B	20.4 ± 0.3	90	250	630
Cl-CO-ONB-activated Sepharose CL-6B	10.2 ± 0.1	820	1050	1070
Divicell ONB-carbonate	24.1 ± 0.4	970	1350	1300
Divicell epoxy	13.5 ± 0.2	1400	1500	1600

[a] Release of glycine was determined up to 1000 h; values for >1000 h were estimated by graphical analysis.
[b] 1 *M* sodium carbonate.
[c] 0.1 *M* sodium tetraborate.
[d] 0.1 *M* sodium acetate.

at pH 8.3) than that from the corresponding support on the basis of CNBr-activated Sepharose 4B. A similar proportion was reported by Hearn *et al.* [12] for the release of ligands covalently attached to CNBr- and CDI-activated agarose.

The great differences in stability of the tested supports are also obvious from the time-dependent detachment of immobilized glycine which is shown in Fig. 2. A linear dependence was found for all supports. The rate of ligand leakage of glycine bound to CDI-activated bead cellulose is identical with that found for glycine immobilized to Divicell ONB-carbonate. When glycine is bound to Sepharose CL-6B via the urethane linkage (immobilization to Cl-CO-ONB-activated gel), the rate of solvolytic detachment is of the same order of magnitude as that determined by Hearn *et al.* [12] for [^{14}C]glycine immobilized to CDI-activated Sepharose CL-6B, *e.g.*, at pH 10 *ca.* 1.2 and 2% of glycine, respectively, were released during 1000 h of hydrolysis.

Provided that the rate of leaking does not change for a longer period, a total detachment of the immobilized glycine should be attained after 1000 h or about 1 year at pH 10 for supports derived from CNBr- and Cl-CO-ONB-activated Sepharose 4B, respectively. For the two bead cellulose supports 100% release of bound glycine could be expected after 11 and 16 years, respectively.

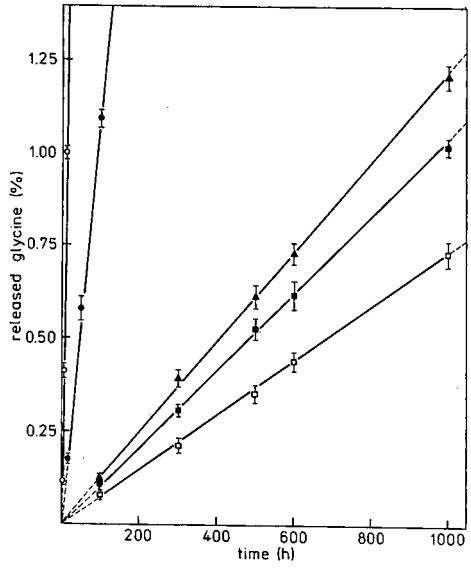

Fig. 2. Release of immobilized glycine (tracer [^{14}C]glycine) with time. The conjugates, as in Table I, were shaken in 1 *M* sodium carbonate (pH 10) containing 0.03% of sodium azide at room temperature. The percentage of released glycine was calculated from the radioactivity measurements in the supernatants related to the total amount of immobilized glycine via the specific radioactivity. Supports used: ○ = CNBr-activated Sepharose 4B; ● = Cl-CO-ONB-activated Sepharose 4B; ▲ = Cl-CO-ONB-activated Sepharose CL-6B; ■ = Divicell ONB-carbonate; □ = Divicell epoxy.

The results found for glycine leakage by circulation of the buffer solution through a gel column of the conjugates based on CNBr- and Cl-CO-ONB-activated Sepharose 4B and Divicell ONB-carbonate (data not shown) for a period of 100 h at pH 10 and room temperature were similar to those obtained from the batch experiments presented.

The leucine leakage was determined from the content of [^{3}H]leucine in the supernatants after incubation of the gels with an appropriate buffer at room temperature. The results are shown in Table II and again indicate that a maximum release of immobilized ligand occurs at basic pH. The amount of leucine detached was 7.0% after storage of the coupled gel for 270 days at pH 10.5. No substantial differences were found between pH 7.5 and 2.0. In either instance the leakage rate is approximately half of that at pH 10.5. A leaking of 1% of the immobilized leucine was obtained after 820 h (pH 10.5), 1800 h (pH 7.5) and 1440 h (pH 2.0). These values are comparable to those mentioned above for released glycine immobilized to Divicell ONB-carbonate.

It was estimated from the results at pH 2.0 that the leucine leakage (cleaving of the urethane linkage) was so small that only about half of the immobilized ligand would be detached after 11 years, assuming linear kinetics. In comparison with this, Johansson *et al.* [2] reported a half-life of 15 years at pH 2.0 for Phenyl-Sepharose CL-4B (cleavage of the ether linkage).

Leakage of immobilized proteins

The release of azocasein, shown in Fig. 3, is nonlinear: fast leakage within 5 days is followed by stability. The same result is obtained with the immobilized enzyme (Fig. 4). In all experiments with fixed proteins the total release did not exceed 10%. Although shaking of the gel is different from chromatographic flow, we obtained similar results when we used a low-pressure chromatographic flow instead of shaking.

As postulated earlier [18], there are at least three populations of immobilized proteins: one released by solvolytic cleavage of anchoring bonds and/or attack of present nucleophiles, a second which is extremely strongly adsorbed by multiple, chelate-like interactions and a third which is stable (leakage-resistant). The present results corroborate this classification. Despite prolonged extensive washings prior to the experiment until the tests for immobilized ligands in the filtrate were negative, about 8% of the fixed proteins were liberated under "operational conditions" within several days and then no further leakage, detectable by the analytical methods used, occurred.

These results are qualitatively in accordance with previous leakage experiments using leucine aminopeptidase immobilized to Sepharose 6B [6] and azocasein covalently bound onto Eupergit C [11].

Naturally, the strongly adsorbed protein can be removed more rapidly by means of more drastic and thorough washings, *e.g.*, as described by Ngo

TABLE II

LEAKAGE OF IMMOBILIZED LEUCINE FROM CELLULOSE BEADS

After coupling of DL-leucine (tracer [^{3}H]leucine) to Divicell ONB-carbonate, the supports were stored in buffer at room temperature (see Experimental). For released leucine the detection limit was 1 nmol/ml gel; error = ±6.2%.

Buffer	pH	Period of storage (days)	Leucine leakage	
			μmol/ml gel	%
0.1 *M* Sodium tetraborate	10.5	120	0.369	3.8
0.1 *M* Sodium tetraborate	10.5	270	0.678	7.0
0.01 *M* Sodium phosphate[a]	7.5	120	0.155	1.6
0.01 *M* Sodium phosphate[a]	7.5	270	0.339	3.5
0.1 *M* Glycine–HCl	2.0	120	0.194	2.0
0.1 *M* Glycine–HCl	2.0	270	0.330	3.4

[a] Containing 0.15 *M* NaCl.

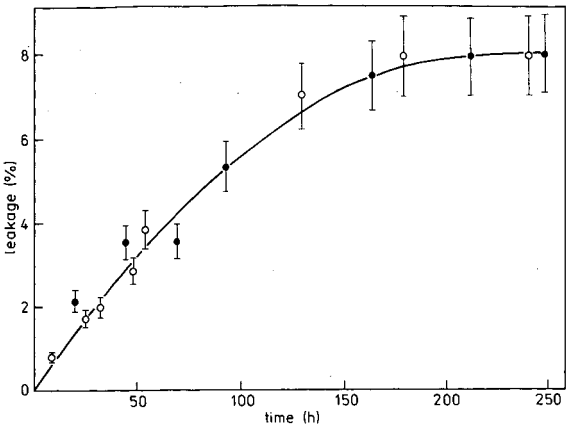

Fig. 3. Leakage of azocasein from cellulose beads. The conjugates, (●) 1.4 mg protein/ml settled gel and (○) 1.5 mg protein/ml, were shaken at room temperature in borate buffer (pH 9.1) and the liberated protein was determined in the filtered supernatant photometrically.

[16] for the complete washing out of non-covalently bound protein from supports after the coupling procedure. However, the applied washing solutions containing 1.5 *M* potassium thiocyanate, 8 *M* urea and 10% sodium dodecyl sulphate are not suitable for most proteins owing to impairment or abolition of their biological activity.

The much more sensitive method of counting the release of radioactively labelled compounds reveals an essentially slower solvolytic liberation of an immobilized low-molecular-weight ligand (single-point attachment) than of macromolecular ligands such as proteins (multi-point attachment) during the first 200 h. We interpret this finding as circumstantial evidence that the initial leakage of immobilized azocasein and leucine aminopeptidase is due to unusually strongly adsorbed protein molecules and not to cleavage of the urethane anchoring bond.

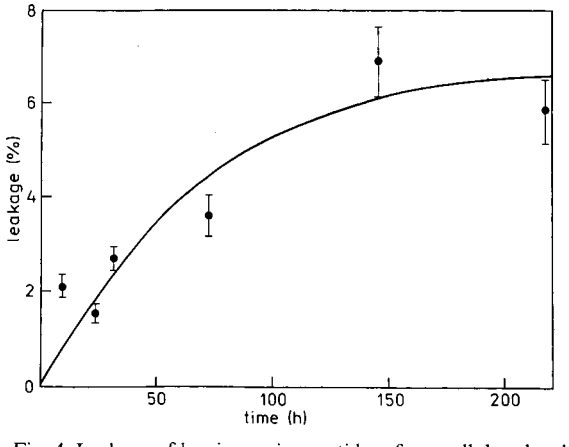

Fig. 4. Leakage of leucine aminopeptidase from cellulose beads. The conjugate, 0.67 nkat/ml settled gel, was shaken as the samples in Fig. 3.

CONCLUSIONS

Cellulose beads (Divicell) represent a more stable matrix than Sepharose 4B and Sepharose CL-6B. The stability of the urethane linkage between the matrix and the monovalently immobilized ligand is substantially higher than the isourea bond and comparable to that of an ether or secondary amine linkage. After the immobilization of proteins, a small part of the attached protein is non-covalently bound to the matrix and leaks very slowly. The results show that the proteins polyvalently bound to cellulose beads via the urethane linkage are extremely stable, and the leakage can be neglected.

ACKNOWLEDGEMENT

This work was supported by the Fonds der Chemischen Industrie, Germany (to J.L.).

REFERENCES

1 J. Lasch, R. Koelsch and R. Kühnau, in Yu. A. Ovchinnikov (Editor), *Proceedings of the 16th FEBS Congress, Moscow, 1984*, VNU Science Press, Utrecht, 1985, Part C, pp. 243–249.
2 B.-O. Johansson, U. Hellberg and O. Wennberg, *J. Chromatogr.*, 403 (1987) 85.
3 G. I. Tesser, H.-U. Fisch and R. Schwyzer, *Helv. Chim. Acta*, 57 (1974) 1718.
4 M. Wilchek, T. Oka and Y. J. Topper, *Proc. Natl. Acad. Sci. U.S.A.*, 72 (1975) 1055.
5 J. Schnapp and Y. Shalitin, *Biochem. Biophys. Res. Commun.*, 70 (1976) 8.
6 J. Lasch and R. Koelsch, *Eur. J. Biochem.*, 82 (1978) 181.
7 L. Peng, G. J. Calton and J. W. Burnett, *J. Biotechnol.*, 5 (1987) 255.
8 A. Lihme, C. Schafer-Nielsen, K. P. Larsen, K. G. Müller and T. C. Bøg-Hansen, *J. Chromatogr.*, 376 (1986) 299.
9 P. Füglistaller, *J. Immunol. Methods*, 124 (1989) 171.
10 R. Koelsch, J. Lasch, K. Bláha and J. Turková, *Enzyme Microb. Technol.*, 6 (1984) 31.
11 J. Lasch and F. Janowski, *Enzyme Microb. Technol.*, 10 (1988) 312.

12 M. T. W. Hearn, E. L. Harris, G. S. Bethell, W. S. Hancock and J. A. Ayers, *J. Chromatogr.*, 218 (1981) 509.
13 J. Drobník, J. Labský, H. Kudlvasrová, V. Saudek and F. Švec, *Biotechnol. Bioeng.*, 24 (1982) 487.
14 M. Wilchek and T. Miron, *Biochem. Int.*, 4 (1982) 629.
15 W. Büttner, M. Becker, Ch. Rupprich, H.-F. Boeden, P. Henklein, F. Loth and H. Dautzenberg, *Biotechnol. Bioeng.*, 33 (1989) 26.
16 T. T. Ngo, *Makromol. Chem., Macromol. Symp.*, 17 (1988) 229.
17 H.-F. Boeden, K. Pommerening, M. Becker, Ch. Rupprich, M. Holtzhauer, F. Loth, R. Müller and D. Bertram, *J. Chromatogr.*, 552 (1991) 389.
18 J. Lasch, R. Koelsch, S. Weigel, K. Bláha and J. Turková, in T. C. Gribnau, J. Visser and R. J. F. Nivard (Editors), *Affinity Chromatography and Related Techniques*, Elsevier, Amsterdam, 1982, pp. 245–254.
19 J. Lasch, *Experientia*, 31 (1975) 1125.
20 H. Hanson, D. Glaesser and H. Kirschke, *Hoppe Seyler's Z. Physiol. Chem.*, 340 (1965) 107.
21 H.-F. Boeden, W. Büttner, Ch. Rupprich, D. Büttner, S. Heinrich, M. Becker, M. Holtzhauer, *Makromol. Chem.*, in press.
22 G. S. Bethell, J. A. Ayers, W. S. Hancock and M. T. W. Hearn, *J. Biol. Chem.*, 254 (1979) 2572.
23 L. Sundberg and J. Porath, *J. Chromatogr.*, 90 (1974) 87.
24 I. Gács, Z. Vargay, E. Dobis, S. Dombi, K. Payer and L. Ötvös, *J. Radioanal. Chem.*, 68 (1982) 93.
25 J. Langner, A. Wakil, M. Zimmermann, S. Ansorge, P. Bohley, H. Kirschke and B. Wiederanders, *Acta Biol. Med. Ger.*, 31 (1973) 1.
26 R. D. Kremer and D. Tabb, *Int. Lab.*, July/August (1989) 40.

Journal of Chromatography, 589 (1992) 101–108
Elsevier Science Publishers B.V., Amsterdam

CHROM. 23 718

Activation of matrices by 4,6-diphenylthieno[3,4-*d*]-1,3-dioxol-2-one-5,5-dioxide

High-performance liquid affinity chromatographic separations

Max Hill* and Bernard Arrio

URA 1116 du CNRS, Bioénergétique Membranaire, Bât. 432, Université de Paris-Sud, Centre d'Orsay, 91405 Orsay Cedex (France)

(First received April 9th, 1991; revised manuscript received August 26th, 1991)

ABSTRACT

High-performance liquid affinity chromatography requires activated matrices with specific properties. Standard matrices were modified and activated and then their characteristics were compared. A new activating method based on the use of 4,6-diphenylthieno[3,4-*d*]-1,3-dioxol-2-one-5,5-dioxide was developed. The coupling of ligands with these new supports was very fast. The hydrolysis/aminolysis ratio was higher than with N-hydroxysuccinimide-activated matrices.

INTRODUCTION

High-performance liquid affinity chromatography (HPLAC) is a recent field of affinity chromatography which combines the high selectivity of immobilized ligands with the reproducibility, sensitivity and speed of high-performance liquid chromatography. Various aspects of HPLAC have been surveyed [1–6]. From the data, it appears that the choice of activated matrices is still limited. Two factors are determining: the matrix and the activation.

An ideal matrix must be hydrophilic, macroporous, uncharged and mechanically, biochemically and chemically stable; the suitability for ligand attachment is also an important criterion. Two categories of supports are commonly used: inorganic and polymeric.

Porous silica is the most frequently used inorganic support because of its high porosity, particle size and mechanical stability. Unfortunately, this support is degraded at pH 8.5 and sometimes irreversible adsorption or denaturation of biomolecules occurs. Polymeric materials are generally constituted of polysaccharide, polyacrylamide or polystyrene backbones. These polymers are stable in the pH range 1–14 and have an acceptable hydrophilicity. However, their particle size is often too large and their mechanical stability is insufficient, especially above 2500 p.s.i. We consider that synthetic polymer matrices have a great future.

A considerable variety of activating methods have been described [7]. An ideal activated group must have a fast coupling time, a high coupling capacity of ligands, a physiological coupling pH, easy regeneration of the matrix without charged groups, stable attachment with a ligand, no activity lost during storage and spectral characteristics giving the possibility of measuring hydrolysis of the activated group and/or the coupling with a ligand.

Activation of hydroxylated matrices represents an attractive method because hydrolysis of the activated groups regenerates the original hydroxyl

0021-9673/92/$05.00

groups. In the various procedures for activation of hydroxyl groups, the most suitable reagents are 1,1'-carbodiimidazole [8–12] and particularly chloroformates [13–16] and tresyl chloride [17–20].

After a survey of the literature, we selected two epoxy-activated acrylic polymers, Eupergit C30N and HEMA-AFC BIO EH. These matrices were modified and then reactivated. First, we developed a new activation technique using 4,6-diphenylthieno[3,4-d]-1,3-dioxol-2-one-5,5-dioxide (TDO) esters. This technique produced matrices which bound proteins successfully and provided an original and efficient approach of HPLAC. TDO-activated matrices may be useful for the coupling of unstable protein ligands where short times are essential. In particular, they could be useful with pH-sensitive ligands and proteins.

In order to improve the efficiency of the new activation method, we compared the TDO-activated matrices with N-hydroxysuccinimide (NHS)-activated matrices.

EXPERIMENTAL

Materials

Eupergit C 30N was a gift from Röhm Pharma (Weiterstadt, Darmstadt, Germany) and HEMA-AFC BIO EH from Alltech (Deefield, IL, USA). N,N'-Disuccinimidyl carbonate (DSC) was obtained from Aldrich (Strasbourg, France) and 2-mercaptoethanol, triethylamine, pyridine, 4-dimethylaminopyridine, 4-nitrophenyl chloroformate and TDO from Merck (Darmstadt, Germany).

Concanavalin A, type V, horseradish peroxidase, types II, VI and crude, methyl α-D-glucopyranoside, horse heart cytochrome *c* type III, *p*-nitrophenyl *p'*-guanidinobenzoate and soybean trypsin inhibitor (STI) were obtained from Sigma (St. Louis, MO, USA). Trypsin was purchased from Worthington Biochemical (Freehold, NJ, USA).

Modification of Eupergit C 30N and HEMA-AFC BIO EH

The matrices, (2 g) were suspended in 25 ml of 0.2 *M* pyrophosphate buffer (pH 8.5)–1 *M* 2-mercaptoethanol and stirred at 20°C for 12 h. The modified matrices were successively washed on a sintered funnel with water and acetonitrile and finally dried under vacuum.

Activation with DSC

The experimental details were essentially those described previously by Wilchek and Miron [21], but we used acetonitrile instead of acetone to dissolve DSC; 1.2 mmol of DSC per gram of modified Eupergit C 30N were used. NHS-activated ester was determined by a quantitative spectrophotometric assay [22].

Activation with TDO

TDO (115 mg, 0.35 mmol) and modified Eupergit C 30N or modified HEMA-AFC BIO (500 mg) in dry dichloromethane (10 ml) were stirred at 20°C, then pyridine (28 mg, 0.35 mmol) was added dropwise. The mixture was tirred at 20°C for 1 h and sonicated twice for 3 min. After filtration on a sintered funnel, the activated matrix was successively washed with acetonitrile (20 ml), cold water (10 ml), cold saturated $NaHCO_3$ solution (25 ml), cold 20% citric acid solution (40 ml), cold water (40 ml) and acetonitrile (20 ml).

The matrix was dried under reduced pressure, then stored at −10°C. TDO-activated ester was determined spectrophotometrically at 405 nm by hydrolysis with 0.1 *M* NaOH and compared with TDO samples.

Cytochrome c coupling

Method A: bath procedure. A 1.2-ml volume of coupling buffer (0.2 *M* sodium phosphate, pH 7.4) containing cytochrome *c* (5 mg/ml) was added to 40 mg of NHS- or TDO-activated matrices. Coupling proceeded for 15–30 min at 20°C with stirring. The matrices were thoroughly washed with coupling buffer and 1 *M* sodium chloride solution.

Bound cytochrome *c* was determined spectrophotometrically at 550 nm after sodium dithionite reduction. Modified (but non-activated) Eupergit C 30N and HEMA-AFC BIO were compared under the same conditions to check ligand coupling.

Cytochrome *c* coupling on initial epoxy-activated Eupergit C 30N (epoxides >600 μmol/g) and HEMA-AFC BIO EH (epoxides >1400 μmol/g) was performed under the experimental conditions recommended by Röhm Pharma and Alltech, but coupling proceeded at pH 7.4 for 72 h and at pH 10 for 48 h, respectively, instead of 15 min under our conditions.

Method B: column procedure. A 2.5-ml volume of

coupling buffer (0.2 *M* sodium phosphate, pH 7.4) containing cytochrome *c* (2 mg/ml) was recirculated (0.6 ml/min) at 20°C through a Dupont guard column packed with 20 mg of NHS- or TDO-activated Eupergit C 30N. The column was connected with a circulation cuvette under magnetic stirring. As sodium dithionite reduced TDO-activated Eupergit C 30N, bound cytochrome *c* was determined directly by absorbance measurement at 530 nm (oxidized cytochrome *c*).

Hydrolysis of activated matrices

We used method B to study the rate of hydrolysis of NHS- and TDO-activated Eupergit C 30N in 0.2 *M* sodium phosphate buffer (pH 7.4) at 20°C.

Concanavalin A coupling

Concanavalin A (Con A) was coupled by method A. A 500-mg amount of NHS-, TDO- or epoxy-activated Eupergit C30 N was stirred at 20°C for 12 h (96 h for epoxy-activated Eupergit C 30N) with 3 ml of 0.2 *M* phosphate buffer–1 m*M* $MnCl_2$–1 m*M* $CaCl_2$ (pH 7.4) containing Con A (15 mg/ml). After washing with the coupling buffer and then 1 *M* NaCl, the activated groups in excess were quenched by means of 0.1 *M* ethanolamine in 0.2 *M* pyrophosphate buffer (pH 8.5). The matrices were slurry packed into glass columns (200 × 3 mm I.D. or 150 × 6 mm I.D.).

STI coupling

STI was coupled to modified and the TDO-activated matrices according to the procedure described above. The coupling was performed in 0.2 *M* phosphate buffer (pH 7.4) for 2 h.

Amino acid analysis

The hydrolyses were carried out at 105°C for 24 h. The analyses were performed with a Biotronik LC 2000 analyser equipped with a Dionex DC6A resin column (Durrum Chemical) and a Spectra-glo spectrofluorimeter (Gilson). Post-column detection was carried out by measuring the fluorescence intensity of isoindole derivatives obtained by the action of *o*-phthalaldehyde in the presence of 2-mercaptoethanol. The results were calculated with a Spectra-Physics SP4100 integrator.

Chromatographic procedure

Chromatography was carried out with a Gilson autoanalytic gradient system. The column effluents were monitored with a Beckman 165 variable-wavelength detector.

RESULTS AND DISCUSSION

The polymers Eupergit C 30N and HEMA-AFC BIO EH were selected to test their suitability for HPLAC, since these matrices have already been used for ligand attachment [23,24]. However, the coupling time of ligands to epoxy groups is a slow process; this characteristic is not favourable for a fast chromatographic technique. Moreover, the reaction requires high pH. The coupling capacity is low and charged groups are introduced after coupling [1,5,6,25]. Further, the estimated optimum length of a spacer is *ca.* 10 Å[1,26], and the Eupergit C 30N spacer (6 Å) is slightly short.

To overcome these disadvantages, we modified the spacers and the activated groups of Eupergit C 30N and HEMA-AFC BIO EH. Mercaptoethanol was used to lengthen the spacer (Fig. 1). The reaction was virtually quantitative and did not introduce charges. Moreover, hydrophilicity was preserved and the new diol was not a 1,2-diol. According to the literature [14] this last structure seems to possess a lower yield of activation.

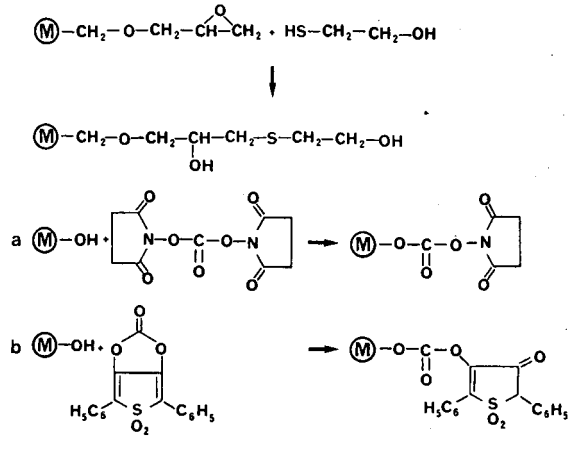

Fig. 1. Modification and activation of Eupergit C 30N.

Activation with NHS

To prepare the NHS–Eupergit C 30N we used DSC instead of hydroxysuccinimide chloroformate, an unstable reagent (Fig. 1a). The procedure is essentially the same as that described by Wilchek and Miron [21], with some modifications. The amount of activated groups was between 200 and 245 μmol/g of dry matrix determined by spectrophotometric assay at 260 nm [22]. In some experiments we used 4-nitrophenyl chloroformate to activate the matrix; higher activities were obtained, but unfortunately the matrix was less stable.

Activation with TDO

A new approach to activate the matrix was based on the use of TDO (Fig. 1b). This reagent is very efficient in the synthesis of amides and peptides [27,28]. TDO-activated matrices have not previously been used for affinity chromatography. Activation proceeded in one step and in less than 2 h. The amount of activated groups was between 240 and 250 μmol/g of dry Eupergit C 30N, determined by spectrophotometric assay at 405 nm. With HEMA-AFC BIO EH a smaller number of activated groups was observed (95 μmol/g).

Preliminary results showed that primary hydroxylated functions were preferentially activated. The dry TDO-activated matrices were yellow (orange at basic pH or in the presence of amines). The matrices, when subjected to hydrolysis or aminolysis, regenerated white powders and the released sulphone could be detected at 405 nm at alkaline pH.

The variations of the TDO absorption spectrum at different pH values are presented in Fig. 2; these spectra show two isosbestic points, at 312 and 381 nm. These colour changes are particularly advantageous to follow the evolution of an aminolysis (Fig. 3).

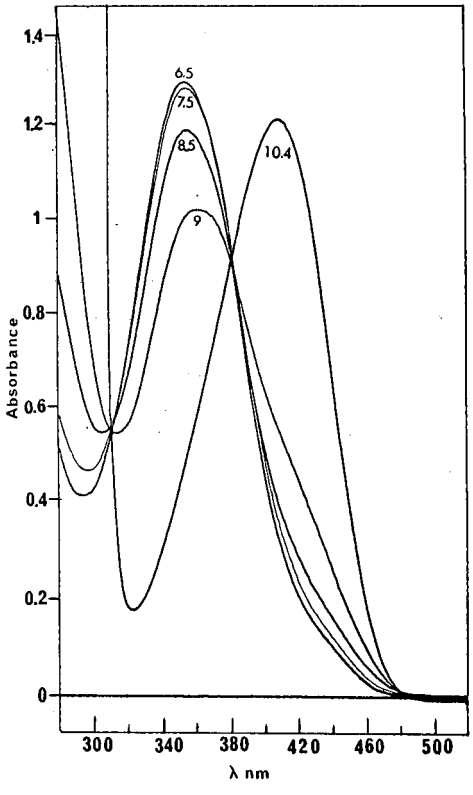

Fig. 2. TDO absorption spectrum at various pH values (6.5–10.4): 2 m*M* TDO, 0.2 *M* phosphate buffer and 0.1 *M* NaOH (pH 10.4, 20°C).

Comparison of the NHS and TDO-activated Eupergit C 30N

We compared hydrolysis and aminolysis of NHS– and TDO–Eupergit C 30N (Fig. 4). To study these reactions we used a flow technique; the solutions were recirculated through small columns containing the activated matrices. The rates of hydrolysis were measured in 0.1 *M* sodium phosphate (pH 7.4) at 260 nm for NHS and at 405 nm for TDO.

NHS–Eupergit C 30N had a half-time of about 29 min and TDO-Eupergit C 30N a half-time of about 20 min. The kinetics were very different and we observed that part of the material (15%) was rapidly released (NHS 0.5 min and TDO 1 min). This release might represent some particularly unstable carbonates.

To measure aminolysis, we followed the coupling of cytochrome *c* (2 mg/ml in 0.1 *M* sodium phosphate, pH 7.4); this ligand absorbs at 530 nm with-

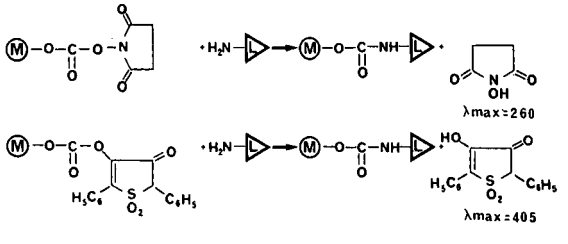

Fig. 3. Aminolysis of NHS– and TDO–Eupergit C 30N.

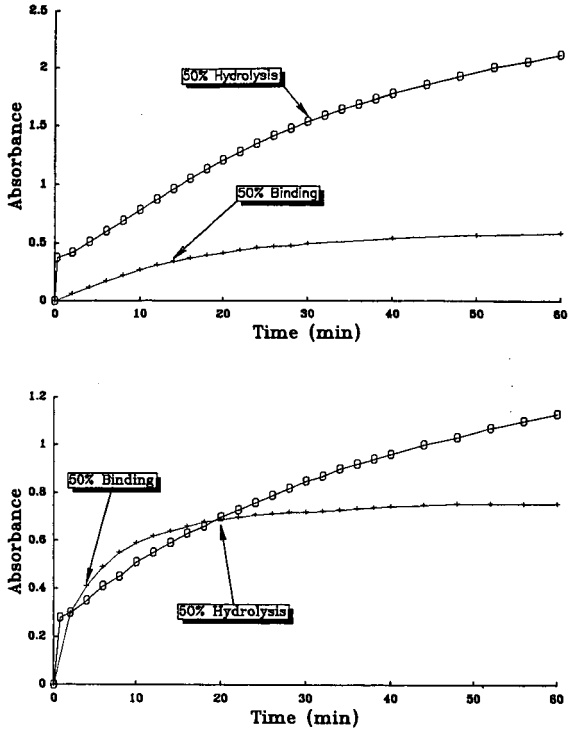

Fig. 4. Comparison of the hydrolysis ○, (measured at 260 nm for NHS and 405 nm for TDO) and cytochrome *c* binding +, for (top) NHS- and (bottom) TDO–Eupergit C 30N. For conditions, see Experimental.

out interference with NHS or TDO absorption. NHS–Eupergit C 30N coupled cytochrome *c* with a half-time of 13 min and TDO–Eupergit C 30N with a half-time of 3 min. It was also interesting to compare the hydrolysis/aminolysis ratios, which were 2.2 for the NHS matrix and 6.6 for the TDO matrix.

Hence the TDO matrices are particularly well adapted for the coupling of proteins.

Comparison of the coupling efficiency of the TDO, NHS and epoxy matrices

We also coupled cytochrome *c* (5 mg/ml) using method A at pH 7.4 for 15 min. With NHS – Eupergit C 30N (activity 245 μmol/g), 84 mg/g, *i.e.*, 6.8 μmol/g of cytochrome *c*, were bound. With TDO–Eupergit C 30N (activity 240 μmol/g), the binding of cytochrome *c* was higher at 140 mg/g, *i.e.*, 11.3 μmol/g.

These results showed the great efficiency of the TDO-activated matrices and their usefulness in coupling unstable ligands. TDO activation and coupling of ligands were lower with the HEMA-AFC BIO EH matrix (see Tables I and II).

When cytochrome *c* was coupled to epoxy–Eupergit C 30N (previous conditions but for 72 h), poor immobilization was found, 11 mg/g, *i.e.*, 0.89 μmol/g. With epoxy–HEMA-AFC BIO EH (pH 10, 48 h) only 2 mg/g, *i.e.*, 0.16 μmol/g, were bound. These observations were in agreement with the literature data concerning the epoxides [1,5,6,25].

In another experiment, the epoxy groups of the original Eupergit C 30N were hydrolysed into 1,2-diols, activated with TDO, then cytochrome *c* was coupled in the usual way. Activation was only 52 μmol/g and cytochrome *c* coupling 39 mg/g. This decrease in yields seems to be a general phenomenon observed with hydroxylated matrices having 1,2-diols [14,29]. The formation of a cyclic carbonate derivative has been invoked to explain this reactivity difference. All the coupling results are summarized in Table I.

TDO activation was also used successfully to prepare activated matrices from several diol silica matrices and some polymeric supports; this will be reported elsewhere.

TABLE I

COMPARISON OF THE ACTIVATED MATRICES AND COUPLING OF CYTOCHROME *c*

Dried activated matrix	Active groups (mmol/g matrix)	Bound cytochrome *c* (mg/g matrix)	Coupling time (pH 7.4, 20°C)
Epoxy–Eupergit C 30N	>600	11	72 h
Modified + NHS–Eupergit C 30N	245	84	15 min
Modified + TDO–Eupergit C 30N	240	140	15 min
Hydrolysed + TDO–Eupergit C 30N	52	39	30 min
Epoxy–HEMA-AFC BIO EH	>1400	2	48 h (pH 10)
Modified + TDO–HEMA-AFC BIO EH	95	36	30 min

TABLE II

COMPARISON OF THE COUPLING OF STI AND TRYPSIN CAPACITY ON MODIFIED MATRICES

Dried activated matrix	Active groups (μmol/g matrix)	Bound STI (mg/g matrix)	Coupling time (h)	Trypsin capacity (mg/g matrix)
Modified + TDO–Eupergit C 30N	246	57.2	2	38.2
Modified + TDO–HEMA-AFC BIO EH	95	13	2	10.6

Stability of TDO-activated matrices

No loss of activity was observed with a dry powder sample of activated TDO–Eupergit C 30N stored at −10°C for 6 months; these precautions were excessive.

Affinity chromatography

Illustrative of the use of TDO-activated matrices are the results obtained with the well known affinity chromatographic models, namely the purifications of peroxidase using a Con A-bound matrix and trypsin using an STI-bound matrix.

Affinity chromatography on concanavalin A–Eupergit C 30N

TDO coupling of ligands via their free amino acid groups yielded N-alkyl carbamates (Fig. 1b); it is well known that these linkages are stable [8–16].

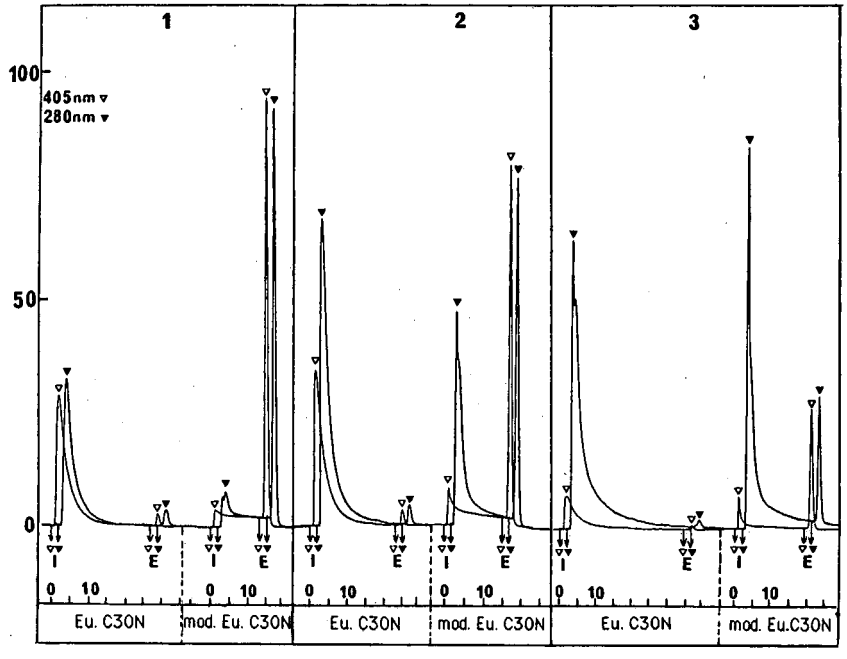

Fig. 5. Peroxidase purifications on Con A–Eupergit C 30N and Con A–modified Eupergit C 30N. (1) Peroxidase type VI; (2) peroxidase type II; (3) peroxidase crude. I = sample injection; E = peroxidase elution. Columns: 250 mm × 3 mm I.D. Conditions: at I, 250 μl of 2 mg/ml peroxidase were injected; mobile phase, 0.05 *M* sodium acetate–0.5 *M* NaCl–1 m*M* $CaCl_2$–1 m*M* $MnCl_2$ (pH 5.1); flow-rate, 0.5 ml/min; at E, 25 m*M* methyl α-D-glucopyranoside in the same mobile phase; flow-rate 1 ml/min. The detector response was calibrated in order to obtain the same amplitude at (▽) 405 and (▼) 280 nm. The 100% response corresponded to absorbances of 0.25 and 0.80 at 280 and 405 nm, respectively, using type VI peroxidase. To clarify the diagram, the records at 280 and 405 nm are arbitrarily shifted.

To demonstrate the efficiency of activated TDO matrices and illustrate their suitability for HPLAC, we purified horseradish peroxidase on a column containing immobilized Con A. Con A was coupled by method A to activated TDO–, NHS– and epoxy–Eupergit C 30N (see Experimental), then matrices with immobilized ligands were packed into columns. Con A–Eupergit C 30N columns were used to purify rapidly horseradish peroxidase. Immobilized Con A and purified peroxidase were not determined.

Horseradish peroxidase absorbs at 405 nm, a convenient property for discriminating peroxidase and contaminant proteins. The column effluent was monitored at 280 nm to obtain a measure of the total protein content and at 405 nm to detect the peroxidase. Three commercial grades of peroxidase were subjected to purifications (Fig. 5). Peroxidase samples were injected at a flow-rate of 0.5 ml/min; at higher flow-rates a small part of peroxidase was not immobilized, owing to the large particle size of Eupergit C 30N (30–80 μm) and its porosity (0.1–2.5 μm). On the other hand, the counter ligand methyl α-D-glucoside can be injected at 1 ml/min.

Fig. 5 clearly shows the low binding of peroxidase on a Con A–Eupergit column prepared from epoxy–Eupergit C 30N. Fig. 5. also illustrates the efficiency of the affinity column prepared from TDO–Eupergit.

The specificity of Con A–modified Eupergit C 30N for peroxidase is illustrated in Fig. 5 (from 1 to 3). As the amount of impurities increased, the ratio of the peaks at 280 and 405 nm corresponding to the eluted peroxidase remained constant. Hence the Con A–Eupergit C 30N and Con A–modified Eupergit C 30N did not undergo non-specific binding. Similar chromatograms were obsserved with NHS–Eupergit C 30N.

Affinity chromatography on STI–HEMA-AFC BIO EH and STI–Eupergit C 30N

STI (15 mg/ml) was coupled by method A to modified and TDO-activated matrices (see Experimental and Tables I and II). Then the matrices with immobilized ligand were packed into columns. Protein contents were determined by amino acid analysis.

In a typical procedure (Fig. 6), a sample of commercial trypsin (1 mg in 200 μl) was loaded onto an

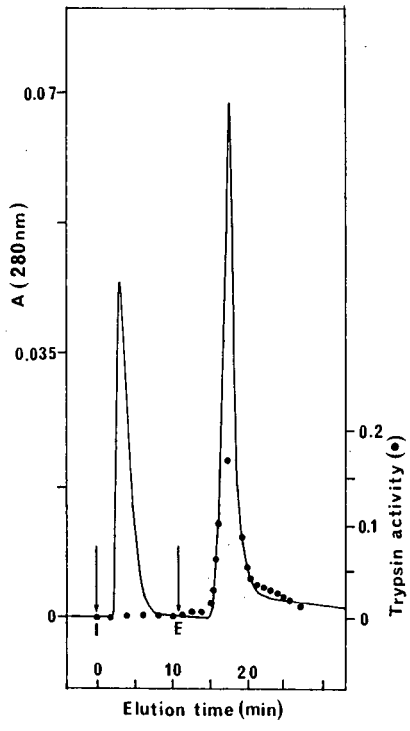

Fig. 6. Chromatography of bovine trypsin on an STI-modified HEMA-AFC BIO EH 1000 column (20 × 3 mm I.D.) previously equilibrated with 0.05 *M* Tris–HCl buffer (pH 7.5)–0.5 *M* NaCl–0.02 *M* $CaCl_2$. At I, 200 μl of 5 mg/ml trypsin were injected (flow-rate 1 ml/min). At E, active trypsin desorption was performed with 12 m*M* HCl–0.5 *M* NaCl (flow-rate, 1 ml/min). The trypsin activity of eluted fractions (900 μl each) was measured by NPGB hydrolysis.

STI–HEMA-AFC BIO EH column (200 × 3 mm I.D.). Desorption of the bound active trypsin was carried out with 12 m*M* HCl containing 500 m*M* NaCl. The protein content was determined by measuring the absorbance at 280 nm. Active trypsin was evaluated by *p*-nitrophenyl *p'*-guanidinobenzoate (NPGB) hydrolysis [30]. This method titrates the active sites and therefore the molarity of active trypsin. Two peaks were obtained from STI affinity chromatography of trypsin (Fig. 6): the first (unbound fraction) had no trypsin activity and the second (bound fraction) contained 100% of the trypsin activity. The recovery of enzyme activity was 93% of the loaded trypsin.

To assess the adsorption capacity of STI-bound matrices, trypsin solutions were pumped through 33

× 6 mm I.D. columns for 30 min in a dynamic process. As summarized in Table II, the STI-bound Eupergit C 30N showed a higher capacity toward trypsin. On the other hand, the yield was better with STI-bound HEMA-AFC BIO EH (74%) than with STI-bound Eupergit C 30N (60%).

Controls measurements with deactivated matrices were performed to check non-specific interactions between matrices and ligands and proteins to be purified. Whatever our HPLAC conditions, non-specific binding was not observed in the control experiments.

CONCLUSIONS

A new coupling procedure for HPLAC on acrylic polymers was developed based on TDO matrices. The properties of the TDO matrices fitted the criteria required for HPLAC, *i.e.*, fast coupling in the physiological pH range and high capacity of protein binding and stability. No additional charges were generated by aminolysis or hydrolysis. The TDO absorbance at 405 nm of the activated groups was particularly useful for monitoring the matrix hydrolysis and the ligand binding. Moreover, the observed aminolysis/hydrolysis ratio showed the usefulness of the TDO method compared with NHS activation.

Epoxy-activated matrices required pH or temperature conditions that are incompatible with sensitive ligands. The TDO activation process could be extended to any hydroxylated matrix and consequently to the matrices used for size-exclusion chromatography without preliminary derivatization reactions.

ACKNOWLEDGEMENT

The authors are deeply grateful to Dr. G. Auger for amino acid analyses.

REFERENCES

1 P.-O. Larsson, M. Glad, L. Hansson, M.-O. Mansson, S. Ohlson and K. Mosbach, *Adv. Chromatogr.*, 2 (1983) 41.
2 D. F. Hollis, S. Ralston, E. Suen, N. Cooke and R. G. L. Shorr, *J. Liq. Chromatogr.*, 10 (1987) 2349.
3 G. Fassima and I. M. Chaiken, *Adv. Chromatogr.*, 275 (1987) 247.
4 T. M. Phillips, *Adv. Chromatogr.*, 29 (1989) 133.
5 P.-O. Larsson, *Methods Enzymol.*, 104 (1984) 212.
6 K. Ernst-Cabrera and M. Wilchek, *Makromol. Chem. Macromol. Symp.*, 19 (1988) 145.
7 W. H. Scouten, *Methods Enzymol.*, 135 (1987) 30.
8 G. S. Bethell, J. S. Ayers, M. T. W. Hearn and W. S. Hancock, *J. Chromatogr.*, 219 (1981) 361.
9 R. S. Chapman and J. G. Ratcliffe, *Clin. Chim. Acta*, 118 (1982) 129.
10 S. C. Crowley, K. C. Chan and R. R. Walters, *J. Chromatogr.*, 359 (1986) 359.
11 M. T. W. Hearn, *Methods Enzymol.*, 135 (1987) 102.
12 H. A. Jonas, J. D. Newman and L. Harrison, *Proc. Natl. Acad. Sci. U.S.A.*, 83 (1986) 4124.
13 P. Cuatrecasas and I. Parikh, *Biochemistry*, 11 (1972) 2291.
14 K. Ernst-Cabrera and M. Wilchek, *Anal Biochem.*, 159 (1986) 267.
15 M. Wilchek, T. Miron and J. Kohn, *Methods Enzymol.*, 104 (1984) 3.
16 T. Miron and M. Wilchek, *Methods Enzymol.*, 135 (1987) 84.
17 P. Wikström and P.-O. Larsson, *J. Chromatogr.*, 388 (1987) 123.
18 G. Fassina, H. G. Swaisgood and I. M. Chaiken, *J. Chromatogr.*, 376 (1986) 87.
19 K. Nilsson and K. Mosbach, *Methods Enzymol.*, 135 (1987) 65.
20 K. Nakamura, K. Toyoda and Y. Kato, *J. Chromatogr.*, 478 (1989) 159.
21 M. Wilchek and T. Miron, *Appl. Biochem. Biotechnol.*, 11 (1985) 191.
22 T. Miron and M. Wilchek, *Anal. Biochem.*, 126 (1982) 433.
23 B. Solomon, Z. Hollander, R. Koppel and E. Katchalski-Katzir, *Methods Enzymol.*, 135 (1987) 160.
24 G. Fleminger, T. Wolf and B. Solomon, *J. Chromatogr.*, 510 (1990) 311.
25 I. Matsumoto, Y. Ito and N. Seno, *J. Chromatogr.*, 239 (1982) 747.
26 C. R. Lowe, M. J. Harvey, D. B. Craven and P. D. G. Dean, *Biochem. J.*, 133 (1973) 499.
27 O. Hollitzer, A. Seewald and W. Steglich, *Angew. Chem., Int. Ed. Engl.*, 15 (1976) 444.
28 R. Kirstgen, R. C. Sheppard and W. Steglich, *J. Chem. Soc., Chem. Commun.*, (1987) 1870.
29 R. R. Walters, *J. Chromatogr.*, 249 (1982) 19.
30 T. Chase, Jr. and E. Shaw, *Biochem. Biophys. Res. Commun.*, 29 (1967) 508.

Journal of Chromatography, 589 (1992) 109–119
Elsevier Science Publishers B.V., Amsterdam

CHROM. 23 641

Determination of chloropropanols in protein hydrolysates

C. A. van Bergen, P. D. Collier*, D. D. O. Cromie, R. A. Lucas, H. D. Preston and D. J. Sissons

Unilever Research Laboratory, Colworth House, Sharnbrook, Bedford MK44 1LQ (UK)

(First received January 10th, 1991; revised manuscript received July 18th, 1991)

ABSTRACT

Protein hydrolysates, widely used as seasonings and savoury flavours, have been reported to contain traces of chloropropanols. Methods of analysis have now been developed for identification and determination of a full range of chloropropanols in protein hydrolysates and composite savoury food products. Based on capillary gas chromatography of heptafluorobutyrate derivatives with electron-capture and mass spectrometric detection, the methods show that the main chloropropanols found in traditionally produced hydrolysates are (in order of abundance) 3-chloro-1,2-propanediol, 2-chloro-1,3-propanediol, 1,3-dichloro-2-propanol and 2,3-dichloro-1-propanol. The limits of detection are 50–100 $\mu g\ kg^{-1}$ for the diols and 10 $\mu g\ kg^{-1}$ for the dichloropropanols.

INTRODUCTION

Protein hydrolysates are widely used as seasonings and ingredients in processed savoury food products. They are commonly produced by hydrochloric acid hydrolysis of proteinaceous by-products from edible oil or starch extraction, such as soy bean and rape seed meals and maize gluten. Studies by Velisek and co-workers [1–6] have demonstrated the presence in protein hydrolysates of several chloropropanols and their fatty acid esters, and their formation in model hydrolysis systems from lipids (both synthetic and residual lipids extracted from raw materials used in hydrolysate manufacture). The main chloropropanol detected by Velisek and co-workers in protein hydrolysates was 1,3-dichloro-2-propanol (1,3DCP), together with smaller amounts of 2,3-dichloro-1-propanol (2,3DCP) and 3-chloro-1-propanol [4,6]. Model system studies with lipids [3] and glycerol [2] strongly suggest that 3-chloro-1,2-propanediol (3MCPD) and 2-chloro-1,3-propanediol (2MCPD) may also be expected in commercial protein hydrolysates, but to date no methods for their determination or data on their levels in protein hydrolysates have been published.

We now report methods of analysis suitable for the confirmed determination of a range of chloropropanols in protein hydrolysates and derived food products. Based on capillary gas chromatography of heptafluorobutyrate derivatives with electron-capture (GC–ECD) and mass spectrometric detection (GC–MS), the methods permit the determination of 3MCPD, 2MCPD, 1,3DCP, 2,3DCP and three isomeric monochloropropanols.

EXPERIMENTAL

Reagents

All reagents were of analytical-reagent grade unless otherwise stated. Sodium chloride, sodium hydroxide and anhydrous sodium sulphate were obtained from BDH. Diethyl ether and ethyl acetate (HPLC grade) were supplied by Fisons and hexane (glass-distilled) by Rathburns. Extrelut 20 and Extrelut 3 columns and refill material were obtained from Merck, glycidol (2,3-epoxy-1-propanol) from Sigma and heptafluorobutyrylimidazole (HFBI) from Pierce.

Standards

1-Chloro-2-propanol, 2-chloro-1-propanol and *p*-dichlorobenzene (PDCB) internal standard were

0021-9673/92/$05.00

obtained from Aldrich. 3-Chloro-1-propanol, 1,3-dichloro-2-propanol (1,3DCP) and 2,3-dichloro-1-propanol (2,3DCP) were supplied by Pfalz and Bauer. 3-Chloro-1,2-propanediol (3MCPD) was obtained from Fluka. A small sample of NMR-pure 2-chloro-1,3-propanediol was provided by Dr. F. Ruf (Maizena, Heilbronn, Germany).

Calibration solutions

A stock mixed standard solution containing 1 g l^{-1} of each chloropropanol in diethyl ether or ethyl acetate as appropriate (see *Sample preparation*) was prepared fresh for each batch of samples to be analysed. Calibration solutions covering the range 0.02–100 mg l^{-1} were prepared by serial dilution of the stock solution with diethyl ether or ethyl acetate as appropriate. A working strength (50 mg l^{-1}) solution of PDCB was obtained by dilution of a stock solution with hexane. Stock PDCB solutions were prepared monthly (0.1 g of PDCB in 100 ml of hexane). All stock and working strength solutions were kept refrigerated (0–5°C).

Sample preparation

Liquid protein hydrolysate (20 g) or solid hydrolysate (8 g dissolved to 20 g with 5 *M* sodium chloride solution) was applied to an Extrelut 20 column and allowed to equilibrate for 15 min (note: viscous samples may be mixed with Extrelut refill material before it is packed into a column). Chloropropanols were recovered from Extrelut columns by one of the following methods.

For analysis of all the chloropropanols (mono- and diols) a two-stage extraction separating the less abundant monools from the more abundant diols and other interfering compounds proved necessary. The Extrelut 20 column was first eluted with hexane–diethyl ether (90:10, v/v) to collect 50 ml (extract 1) containing the monools, followed by diethyl ether to collect 250 ml (extract 2) containing the chloropropanediols.

For analysis only of the chloropropanediols, the Extrelut column was eluted with diethyl ether only to collect 250 ml (extract 3). An alternative, faster procedure for analysis of chloropropanediols consisted of adding 3 g of hydrolysate liquor to a small (2 g, 1 cm diameter) Extrelut 3 column, followed by equilibration, then elution with ethyl acetate to collect 25 ml (extract 4).

Derivatization

Extract 1 (5 ml), or extract 2, 3 or 4 (1 ml), or the calibration solution (1 ml), was pipetted into a 25-ml volumetric flask. PDCB working solution (1 ml) was added and the solution made up to 25 ml with hexane. HFBI (200 μl) was added and the solution was mixed and allowed to stand at ambient temperature (20°C) for 15 min with intermittent shaking.

The mixture was then transferred to a screw-capped vial containing distilled water (2 ml), shaken (1 min), the separated organic layer washed twice more and a 10-ml aliquot filtered through a 4-cm column of anhydrous sodium sulphate (4 g) before analysis by GLC–ECD. Dried derivatized solutions were found to be stable for up to 3 days under refrigeration. When necessary, limits of determination were improved by taking a larger aliquot of the appropriate Extrelut extract for derivatization. Ether extracts 2 and 3 must (when aliquots greater than 2 ml are taken) be blown dry under a gentle stream of nitrogen before derivatization, to overcome sporadic ether-based interference problems.

Analysis by GC–ECD

Heptafluorobutyrate esters of the chloropropanols were separated and determined by capillary GC–ECD using a Perkin-Elmer Model 8320, Varian Model 3400 or Philips PU 4550 gas chromatograph fitted with a splitless injection port and a 25 m × 0.2 mm I.D. fused-silica column of immobilized OV-1 (0.33 μm) (Hewlett-Packard, part no. 19091Z-102). Optimum operating conditions were as follows: injector temperature, 280°C (vent opened after 0.6 min); injection volume, 3 μl maximum; carrier gas, helium, 12 p.s.i.g.; temperature programme, 50°C held for 2 min, then increased to 85°C at 1°C min^{-1} and to 250°C at 20°C min^{-1}, held at 250°C for 20 min; detector temperature, 350°C (Perkin-Elmer Model 8320). Detector responses to derivatized chloropropanols and the PDCB internal standard vary with temperature in an instrument-dependent fashion. The detector should be operated within a temperature range over which the response is least affected by temperature. Retention time data are presented in Table I. Chloropropanol levels were calculated from the height of the appropriate peak relative to that of the PDCB internal standard.

Confirmation by GC–MS

Identities of both derivatized and underivatized chloropropanols were confirmed by GC–MS using a VG70 HSE double-focusing mass spectrometer linked to a Hewlett-Packard Model 5890A gas chromatograph and operating in the electron impact (EI) mode at a beam energy of 70 eV, an emission of 100 μA and a source temperature of 200°C.

Underivatized Extrelut extracts were separated on a 15-m DB Wax fused-silica capillary column (J & W Scientific) under the following conditions: injector temperature, 220°C (splitless mode); carrier gas, helium, flow-rate, 1 ml min^{-1}; temperature programme, 65°C, held for 1 min, then increased at 15°C min^{-1} to 200°C. Retention times were as follows [min (′) s (″)]: 1-chloro-2-propanol, 1′49″; 2-chloro-1-propanol, 2′06″; 3-chloro-1-propanol, 3′10″; 1,3DCP, 4′19″; 2,3DCP, 4′43″; 3MCPD, 5′53″; 2MCPD, 6′14″. Quantitative analysis was carried out by selected-ion recording (SIR) at a resolution of 1 in 5000, monitoring characteristic ions at *m/z* 79 and 81 (1-chloro-2-propanol and 1,3DCP), 62 and 64 (2-chloro-1-propanol, 2MCPD and 2,3DCP), 58 and 76 (3-chloro-1-propanol) and 61, 79 and 81 (3MCPD).

HFBI-derivatized extracts were separated on a 25-m BP1 fused-silica capillary column (SGE) programmed from 50 to 85°C at 1°C min^{-1} and to 260°C at 30°C min^{-1} with a helium carrier gas flow-rate of 1.5 ml min^{-1}. Retention times were as follows: 2-chloro-1-propanol, 4′50″; 1-chloro-2-propanol, 5′00″; 3-chloro-1-propanol, 7′45″; 1,3DCP, 13′25″; 2,3DCP, 14′24″; 3MCPD, 20′30″; 2MCPD, 21′10″.

Quantitative analysis was carried out by monitoring characteristic ions at *m/z* 241 (1-chloro-2-propanol), 228 (2-chloro-1-propanol), 254 (3-chloro-1-propanol), 275 and 277 (1,3DCP), 253 (2,3DCP), 453, 289 and 291 (3MCPD) and 289 and 253 (2MCPD).

Hydrolysis of glycidol

Glycidol (1 g) was heated with 5 *M* hydrochloric acid (10 ml) in a sealed vial at 105°C for 16 h. The cooled mixture was neutralized with sodium hydroxide solution and cleaned up on an Extrelut 20 column using diethyl ether. The ether extract (containing a mixture of the isomeric chloropropanediols) was examined by the GC–ECD and GC–MS procedures described above.

Recovery and cross-over tests

Duplicate (20 g) solutions of 5 *M* sodium chloride containing 0.05, 0.10 and 100 mg kg^{-1} each of 1,3DCP, 2,3DCP and 3MCDP were analysed by the two-stage Extrelut clean-up procedure followed by HFBI derivatization and GC–ECD to establish the recoveries in each extract and through the method as a whole.

Aliquots (20 g) of a maize gluten liquid hydrolysate were spiked with 0.5–10 mg kg^{-1} of 3MCPD and 2MCPD and analysed by the two-stage Extrelut clean-up procedure followed by HFBI derivatization and GC–ECD. The original liquid hydrolysate was analysed (ten times) in two independent laboratories.

RESULTS AND DISCUSSION

Chromatography of HFBI derivatives

The separation of HFBI derivatives of commercially available chloropropanol standards under optimum conditions is shown in Fig. 1A. 2MCPD is not commercially available; accordingly, a mixture of 3MCPD and 2MCPD was obtained by hydrochloric acid treatment of glycidol; the separation of the HFBI-derivatized mixture is shown in Fig. 1B. Confirmation of the retention time of 2MCPD was finally obtained using a sample of pure 2MCPD kindly provided by Dr. F. Ruf (Maizena) (see Fig. 1C). The products of hydrolysis of glycidol were unambiguously identified as 3MCPD and 2MCPD by GC–MS comparison with authentic standards before and after HFBI derivatization. Retention time data demonstrating column stability are presented in Table I.

Calibration data confirmed the excellent linearity of the detector response to all the chloropropanols examined over the concentration range 0.01–1.0 mg l^{-1}. 1,3DCP and 2,3DCP gave almost identical responses, as did 3MCPD and 2MCPD. HFBI derivatization proved to be complete under the conditions used over the dichloropropanol concentration range 0.01–100 mg l^{-1}, and with 3MCPD up to at least 500 mg l^{-1}.

Sample preparation

Two-stage Extrelut clean-up. Preliminary examination of a number of commercially available protein hydrolysates using the three Extrelut clean-up methods described indicated that the chloropropa-

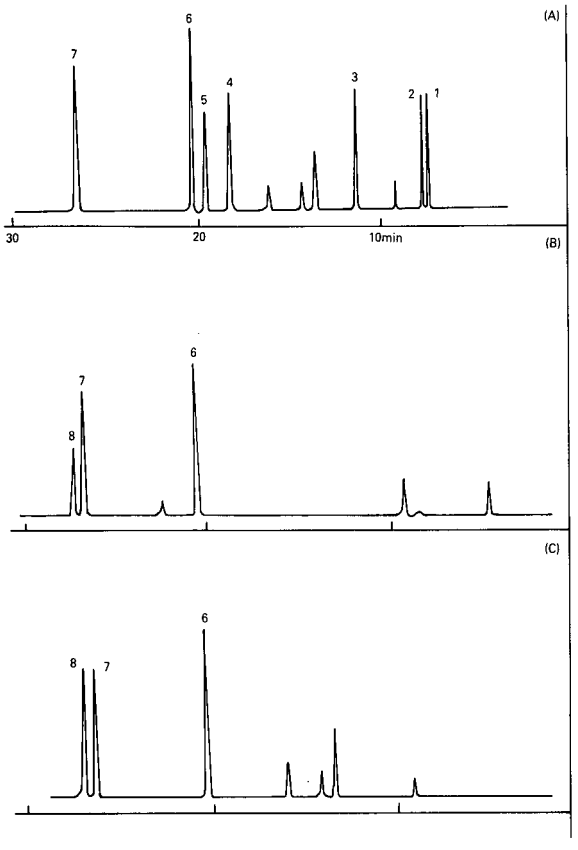

Fig. 1. Separation of (A) chloropropanol standards as HFB derivatives, (B) glycidol reaction products as HFB derivatives and (C) chloropropane diol standards as HFB derivatives. Column: 25 m × 0.2 mm I.D. OV-1- Peaks: 1 = 2-chloro-1-propanol; 2 = 1-chloro-2-propanol; 3 = 3-chloro-1-propanol; 4 = 1,3 DCP; 5 = 2,3DCP; 6 = PDCB (internal standard); 7 = 3MCPD; 8 = 2MCPD.

nediols (3MCPD and 2MCPD) are invariably much more abundant than the chloropropane monools and that extract 3 (diethyl ether) and extract 4 (ethyl acetate) contain species whose HFBI derivatives interfere with those of the chloropropane monools, and confirmed that hexane–diethyl ether extraction gives very poor recoveries of 3MCPD and 2MCPD. In view of these findings, attention was focused on two-stage extraction with hexane–diethyl ether followed by diethyl ether as a flexible and selective procedure for the analysis of both chloropropane monools and diols.

Recoveries of chloropropanols in extract 1 [(hexane–diethyl ether (90:10)] and extract 2 (diethyl ether) obtained from standard chloropropanol solutions in 5 *M* sodium chloride ranged from 90 to 106% monools in extract 1 and from 98 to 115% diols in extract 2, thus confirming that two-stage extraction is an efficient method for separating chloropropane monools from diols prior to their separate derivatization and analysis by GLC. The variable and sometimes high recoveries (100–218%) observed for 1-chloro-2-propanol in extract 1 are thought to arise from sporadic reagent-based interferences, which make this method unsuitable for analysis of low levels of 1-chloro-2-propanol unless mass spectrometric detection is employed.

Analysis of HFBI-derivatized extracts 1 and 2 obtained from commercial protein hydrolysates produced by traditional processes prior to 1986 indicate that the four main chloropropanols found in traditional hydrolysates are (in order of abundance) 3MCPD, 2MCPD, 1,3-DCP and 2,3-DCP (Table

TABLE I

RETENTION TIMES OF CHLOROPROPANOL HFBI DERIVATIVES

Chloropropanol	Retention time (min)			Retention time relative to PDCB		
	8.11.86	21.10.88	12.5.87	8.11.86	21.10.88	12.5.87
2-Chloro-1-propanol	8.20	8.16		0.39	0.40	
1-Chloro-2-propanol	8.45	8.41		0.41	0.41	
3-Chloro-1-propanol	11.80	11.77		0.57	0.57	
1,3-DCP	18.55	18.45		0.89	0.90	
2,3-DCP	19.65	19.60		0.95	0.96	
PDCB	20.77	20.50	21.40			
3MCPD	26.55	26.59	27.80	1.28	1.30	1.30
2MCPD			28.40			1.33

TABLE II

REPLICATION OF TWO-STAGE EXTRELUT EXTRACTION AND HFBI DERIVATIZATION PROCEDURE FOR PROTEIN HYDROLYSATES

Sample	Chloropropanol level found (mg kg^{-1})			
	1,3-DCP	2,3-DCP	3MCPD	2MCPD
1	3.9	0.44	239	43
	4.05	0.45	241	48
	4.07	0.45	273	42
	4.1	0.46	276	49
Mean:	4.03	0.45	257	45.5
2	0.19	0.02	20.8	3.1
	0.18	0.02	20.6	3.3
	0.22	0.02	16.8	3.0
Mean:	0.20	0.02	19.4	3.1
3	0.07	<0.01	238	31.9
	0.07	<0.01	244	32.3
	nd[a]	nd	215	27.7
	nd	nd	221	29.6
	nd	nd	226	30.3
	nd	nd	241	34.0
Mean:	0.07	<0.01	231	31.0
4	<0.01	<0.01	574	88.0
	<0.01	<0.01	564	86.4
	<0.01	<0.01	520	87.6
	<0.01	<0.01	534	86.4
	<0.01	<0.01	565	87.8
	<0.01	<0.01	575	86.2
	<0.01	<0.01	535	87.5
	<0.01	<0.01	525	86.1
Mean:	<0.01	<0.01	549	87.0

[a] nd = Not determined.

II). Indications of slight cross-over of chloropropanediols into eluate 1, and recoveries of the main chloropropanols from the two-stage extraction procedure were checked by analysis of a series of spiked hydrolysates. The typical results presented in Table III confirm that cross-over of the diols into extract 1 is less than 2% of the total diols recovered: excellent recoveries (93–120%) over a wide range of levels (0.05–100 mg/kg for the chloropropane monools and 0.5–350 mg kg^{-1} for the chloropropanediols) were obtained.

The results of replication studies are summarized in Tables II and IV and the results of an inter-laboratory multi-level spiking study on 3MCPD and 2MCPD are presented in Table V.

On the basis of all these data, the two-stage Extrelut extraction procedure coupled with HFBI derivatization and capillary GLC–ECD is clearly an accurate and sensitive method for the determination of dichloropropanols and monochloropropanediols in protein hydrolysates. Its limits of detection are 10 $\mu g\ kg^{-1}$ for 1,3-DCP and 2,3-DCP and 50–100 $\mu g\ kg^{-1}$ for 3MCPD and 2MCPD.

The method has been used to elucidate the mechanisms of formation of the chloropropanols [7]. It has been routinely and successfully used since 1986 to guide the development and monitor the performance of new processes designed to minimize the levels of chloropropanols in hydrolysates. In this period, chloropropanol levels in hydrolysates produced in Europe have substantially diminished.

The dichloropropanols have been virtually eliminated: 1,3-DCP levels are now below 50 $\mu g\ kg^{-1}$, in most hydrolysates below 20 $\mu g\ kg^{-1}$, and in many instances 1,3-DCP is no longer detectable (less than 10 $\mu g\ kg^{-1}$). 3MCPD levels have been reduced from up to 700 mg kg^{-1} to 10–20 mg kg^{-1}, and hydrolysates containing less than 2 mg kg^{-1} are now beginning to appear. 2MCPD levels have been reduced from up to 150 mg kg^{-1} to less than 20 mg kg^{-1} and hydrolysates containing less than 10 mg kg^{-1} are beginning to appear. The method has proved satisfactory for the analysis of these hydrolysates provided that precautions are taken to check for and eliminate sporadic reagent and solvent-based interferences which can occasionally interfere with the determination of low levels (less than 2 mg

TABLE III

LEVELS OF 3MCPD AND 2MCPD IN EXTRELUT EXTRACTS 1 AND 2 (E_1 AND E_2) FROM PROTEIN HYDROLYSATES

Results in mg kg^{-1} on original sample.

Sample	3MCPD		2MCPD	
	E_1	E_2	E_1	E_2
1	0.67	516	0.11	69.8
2	0.61	577	0.09	86.0
3	1.52	215	0.19	27.7
4	1.66	240	0.20	34.0
5	<0.05	1.7	<0.05	1.93

TABLE IV

INTER-LABORATORY REPLICATION STUDY: ANALYSIS OF HYDROLYSATE FOR 3MCPD AND 2MCPD BY TWO-STAGE EXTRELUT EXTRACTION AND HFBI DERIVATIZATION

	3MCPD found (mg kg^{-1})		2MCPD found (mg kg^{-1})	
	Lab. 1	Lab. 2	Lab. 1	Lab. 2
	1.36	1.22	1.11	1.14
	1.28	1.22	1.03	1.20
	1.15	0.95	0.92	1.06
	1.36	1.04	1.10	1.14
	1.38	0.98	1.13	1.12
	1.06	1.20	0.84	1.14
	1.16	1.13	0.93	1.06
	1.22	1.16	1.01	1.18
	0.96	1.09	0.74	1.20
	0.95	1.09	0.65	1.13
Mean:	1.19	1.11	0.95	1.14
95% confidence limits:	±0.109	±0.065	±0.110	±0.034
Standard deviation:	0.1526	0.0913	0.1542	0.047
Repeatability:	0.427	0.256	0.432	0.131

kg^{-1}) of 2MCPD. In these circumstances, drying of the washed derivatized extract 2 is essential.

Attempts to apply the method to composite food products (*e.g.*, sauces and soups) and flavours containing protein hydrolysates have been less successful. Chromatograms are frequently complex; matrix-derived peaks sometimes interfere with the comparatively small chloropropanol peaks derived from the low levels of hydrolysates normally present in such products, and lead to falsely high results or false positives. The GC–MS methods described under Experimental are essential for the reliable determination of chloropropanols in composite food products and flavours.

Single-stage Extrelut clean-up. The two-stage Extrelut extraction procedure is time consuming. In view of the diminishing need to monitor hydrolysates for 1,3DCP, the suitability of simpler and faster diethyl ether and ethyl acetate single-stage extraction procedures for the analysis of chloropropanediols as their HFBI derivatives was investigated.

These simpler procedures were found to give results in good agreement with those of two-stage extraction over the diol range 2–500 mg kg^{-1}. Replication studies of two-stage extraction and one-stage ethyl acetate extraction (Table VI) confirm that over the diol range 1–50 mg kg^{-1} these two methods give closely similar results with similar precision.

The results of an inter-laboratory replication test of the ethyl acetate extraction procedure (Table VII) indicate that it is suitable for the determination of 3MCPD in hydrolysates at levels below 1 mg kg^{-1}. It appears, however, that interference problems may limit its accurate application to 2MCPD determination to levels above 1 mg kg^{-1}, and that its use at lower 2MCPD levels should be approached with caution unless GC–MS facilities are available. Nevertheless, the ethyl acetate–HFBI–GC–ECD method is a rapid, precise and sensitive method for chloropropanediol analysis. Used in conjunction with screening methods based on other derivatives (*e.g.*, phenylboronates [8]), it could provide confirmed diol results without resort to GC–MS procedures.

GC–MS confirmation procedures

The identities and levels of chloropropanols found by GC–ECD of HFBI-derivatized Extrelut extracts were confirmed by GC–MS of both unde-

TABLE V

INTER-LABORATORY SPIKING STUDY: ANALYSIS OF HYDROLYSATE FOR 3MCPD AND 2MCPD BY TWO-STAGE EXTRELUT EXTRACTION AND HFBI DERIVATIZATION

Laboratory	3MCPD level (mg kg^{-1})			Recovery (%)
	Spiked	Found	Difference	
1	0	1.23		
	1.97	3.48	1.51	109
	4.96	5.97	1.01	96
	9.69	10.99	1.30	101
		Mean:	1.27	102
2	0	1.1		
	0.5	1.54	1.04	96
	0.5	1.59	1.09	99
	1.0	2.15	1.15	102
	1.0	2.23	1.23	106
	2.0	3.06	1.06	98
	2.0	3.28	1.28	106
		Mean:	1.14	101
	2MCPD level (mg kg^{-1})			
	Spiked	Found	Difference	
2	0	1.14		
	0.5	1.48	0.98	90
	0.5	1.53	1.03	93
	1.0	2.12	1.12	99
	1.0	2.18	1.18	102
	2.0	2.96	0.96	94
	2.0	3.15	1.15	100
		Mean:	1.07	96

Least mean squares correlation of MCPD found *vs.* MCPD spiked gave the following results:

Laboratory	Base level MCPD (mg kg^{-1})				Recovery (slope)	
	3MCPD		2MCPD		3 MCPD	2MCPD
	I[a]	II[a]	I[a]	II[a]		
1	1.23	1.29			0.992	
2	1.11	1.14	1.14	1.09	1.02	0.99

[a] I = Directly measured; II = calculated intercept of least mean squares plot.

rivatized and HFBI-derivatized standards and extracts 1–4.

Underivatized extracts and standards. The EI mass spectra of the underivatized chloropropanols can be readily characterized in terms of molecular structure and, in conjunction with GC retention times, provide unambiguous identification down to the low ng μl^{-1} level. Table VIII lists the major diagnostic and base ions present in these spectra: as expected, no molecular ions were observed. The

TABLE VI

REPLICATION OF 3MCPD AND 2MCPD ANALYSIS BY (A) TWO-STAGE AND (B) ONE-STAGE (ETHYL ACETATE) EXTRELUT ELUTION

Sample	3MCPD level (mg kg^{-1})		2MCPD level (mg kg^{-1})	
	A	B	A	B
1	49.9	53.1	1.3	1.8
	51.1	53.2	1.3	1.7
	51.0	53.9	1.3	1.6
	51.0	54.2	1.5	1.6
	50.0	53.9	1.3	1.7
Mean:	50.6	53.7	1.3	1.7
95% confidence limits:	±0.66	±0.54	±0.10	±0.09
Standard deviation:	0.533	0.432	0.08	0.07
2	10.9	11.3	1.0	1.0
	11.2	11.2	1.0	1.0
	11.2	11.8	0.9	1.1
	11.5	11.1	1.0	0.9
	11.3	12.7	1.1	1.2
Mean:	11.2	11.6	1.0	1.0
95% confidence limits:	±0.24	±0.73	±0.07	±0.12
Standard deviation:	0.194	0.591	0.06	0.10

TABLE VII

INTER-LABORATORY REPLICATION STUDY: ANALYSIS OF HYDROLYSATES FOR 3MCPD AND 2MCPD BY ETHYL ACETATE EXTRELUT EXTRACTION AND HFBI DERIVATIZATION

Sample	3MCPD level (mg kg^{-1})		2MCPD level (mg kg^{-1})	
	Lab. 1	Lab. 2	Lab. 1	Lab. 2
1	0.58	0.72	<0.5[a]	nd[b]
	0.57	0.68	<0.5[a]	nd
	0.68	0.72	<0.5[a]	nd
	0.58	0.72	<0.5[a]	nd
	0.51	0.72	<0.5[a]	nd
Mean:	0.58	0.71	<0.5[a]	nd
95% confidence limits:	±0.068	±0.02		
Standard deviation:	0.055	0.016		
2	10.9	10.4	<0.5[a]	nd
	9.7	10.6	<0.5[a]	nd
	9.0	10.6	<0.5[a]	nd
	9.7	10.6	<0.5[a]	nd
	9.5	10.3	<0.5[a]	nd
Mean:	9.76	10.5	<0.05[a]	nd
95% confidence limits:	±0.776	±0.156		
Standard deviation:	0.625	0.126		

[a] Interference with 2MCPD peak prevented accurate measurement.
[b] nd = Not determined.

TABLE VIII

CHARACTERISTIC IONS IN EI MASS SPECTRA OF CHLOROPROPANOLS

Chloropropanol	Molar mass	Ion (*m/z*) resulting from loss of					Base ion (*m/z*)
		H_2O	CH_2OH	HCl	CH_2Cl	CH_3	
3-Chloro-1-propanol	94	76/78		58			58 ($M^+ - HCl$)
2-Chloro-1-propanol	94		62/64	58			31 (CH_2OH^+)
1-Chloro-2-propanol	94				45	79/81	45 ($M^+ - CH_2Cl$)
1,3-DCP	128				79/81		79/81 ($M^+ - CH_2Cl$)
2,3-DCP	128			92/94			62/64 ($M^+ - CHOH - HCl$)
3MCPD	110		79/81		61		44 ($M^+ - CH_2Cl - OH$)
2MCPD	110	92/94					62/64 ($M^+ - CHOH - H_2O$)

spectra of the 3- and 2-chloropropane diols (Fig. 2) illustrate the value of mass spectrometry in distinguishing between isomeric structures and of Cl^{35}/Cl^{37} isotope ratios in determining fragmentation pathways.

HFBI-derivatized extracts and standards. EI mass spectra of the HFBI derivatives of the chloropropanols are dominated by ions derived from charge retention on the heptafluorobutyryl moiety, *e.g.*, *m/z* 69 (CF_3) 100 (C_2F_4), 119 (C_2F_5), 169 (C_3F_7) and 197 (C_3F_7 CO). Diagnostically significant ions are in general much less intense but, as shown in Table IX, permit differentiation between the various isomers. Although superficially more alike than those derived from underivatized materials, the HFBI derivative spectra contain characteristic fragments that permit unequivocal assignment of structure (Fig. 3).

Quantification. Quantitative analysis was performed by selected ion recording in which the characteristic ions were monitored at a resolution of 1 in 5000. Peaks detected at the appropriate retention time were quantified with reference to external standards interspersed with the experimental extracts: peak area responses of relevant ions were compared with those obtained from the appropriate standard chloropropanol, with particular emphasis being placed on the relative intensities of chlorine isotope ions. The responses of standards were found to be linear over the range 0.04–3 ng injected onto the

TABLE IX

CHARACTERISTIC IONS IN THE EI MASS SPECTRA OF THE HFBI DERIVATIVES OF CHLOROPROPANOLS

Chloropropanol HFBI derivative	Molar mass	Ion (*m/z*) resulting from loss of					Other structurally significant ions (*m/z*)
		$C_3F_7CO_2$	HCl	$C_3F_7CO_2$ + HCl	CH_2Cl	$C_3F_7CO_2$ + CH_2Cl	
3-Chloro-1-propanol	290	77/79[a]	254				
2-Chloro-1-propanol	290	77/79[a]					228 ($M^+ - CH_2 = CHCl$)
1-Chloro-2-propanol	290	77/89			241[a]		275/77 ($M^+ - CH_3$)
1,3-DCP	324	111		75/77[a]	275/77		
2,3-DCP	324	111		75/77[a]		62/66	253 ($M^+ - Cl - HCl$)
3MCPD	502	289		253	453	240	75/77[a]
2MCPD	502	289		253			($M^+ - C_3F_7COOH - C_3F_7COO$)

[a] Base ion (excluding HFB fragments).

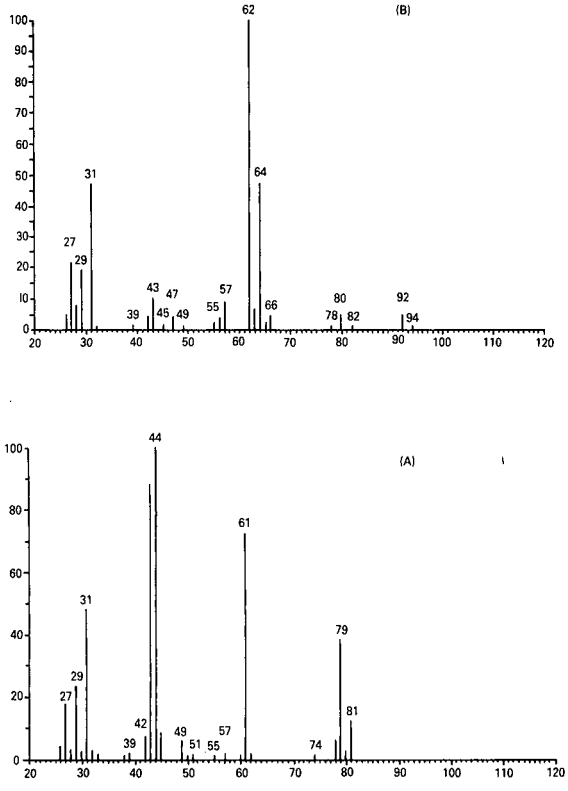

Fig. 2. Mass spectra of chloropropane diols: (A) 3MCPD; (B) 2MCPD.

GC column, and more concentrated extracts were diluted to within this range for quantitative analysis. Underivatized extracts gave the better sensitivity, owing to both shorter retention times and significantly greater intensities of the ions monitored. For straightforward protein hydrolysates, results obtained by the GC–MS and HFBI–GC–ECD methods were in reasonable agreement, with GC–MS detection limits of 10–20 $\mu g\ kg^{-1}$ for chloropropane monools and 20–80 $\mu g\ kg^{-1}$ for the diols. For more complex products (*e.g.* sauces, soup mixes, composite flavours, stock cubes), the GC–MS method often failed to confirm the presence of chloropropanols detected (often at substantial levels) by the HFBI–GC–ECD method, thus confirming the need to use the GC–MS method for the analysis of composite food products and flavours. Detection limits for the analysis of such complex products

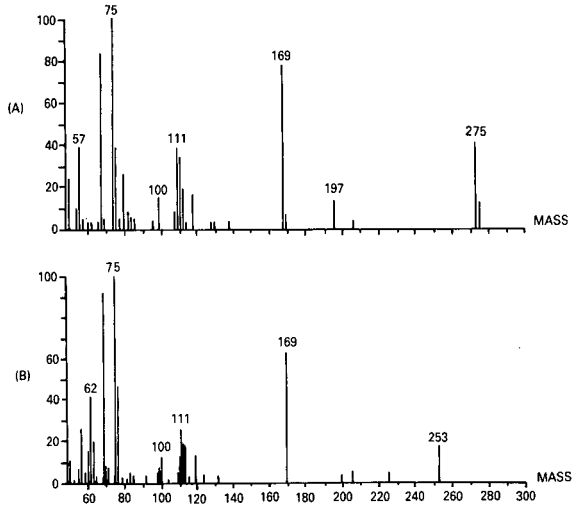

Fig. 3. Mass spectra of dichloropropanol HFB derivatives: (A) 1,3DCP; (B) 2,3DCP.

ranged from 30 to 40 $\mu g\ kg^{-1}$ for the chloropropane monools and from 100 to 300 $\mu g\ kg^{-1}$ for the diols.

CONCLUSIONS

Analysis of protein hydrolysates for a complete range of chloropropanols can be carried out with good recoveries, precision and sensitivity (limits of detection 10–100 $\mu g\ kg^{-1}$) by two-stage solid-phase extraction on diatomaceous earth (Extrelut columns) followed by HFBI derivatization and capillary GC–ECD. Analysis of protein hydrolysates for chloropropanediols (the principal chloropropanols found) can be more conveniently carried out by small-scale single-stage solid-phase extraction using ethyl acetate. Whilst giving results of comparable precision and sensitivity for 3MCPD (limit of detection 50–100 $\mu g\ kg^{-1}$), the method is less sensitive for 2 MCPD and may not be suitable for hydrolysates containing less than 1 $mg\ kg^{-1}$ 2MCPD unless used with MS detection.

Unambigous confirmation of results obtained by these methods can be obtained with similar sensitivities by capillary GC–MS of underivatized solid-phase extracts.

Analysis of composite food products and flavours for chloropropanols by the HFBI–GC–ECD

procedure gives false positives and high results: the GC–MS procedure is essential for the reliable analysis of such products.

ACKNOWLEDGEMENTS

We are indebted Dr. F. Ruf of Maizena for the gift of a pure sample of 2MCPD. We gratefully acknowledge the skilled technical assistance of G. Bookholt, J. Duke, H. C. Hadaway, W. L. Koelewijn, Mrs. H. Lall, H. G. Norbart and M. R. Tinkler.

REFERENCES

1 J. Velisek, J. Davidek, J. Hajslova, V. Kubelka, G. Janicek and B. Mankova, *Z. Lebensm.-Unters.-Forsch.*, 167 (1978) 241–244.
2 J. Velisek, J. Davidek, V. Kubelka, J. Bartosova, A. Tuckova, J. Hajalova and G. Hanicek, *Lebensm. Wiss. Technol.*, 12 (1979) 234–236.
3 J. Davidek, J. Velisek, V. Kubelka, G. Janicek and Z. Simicova, *Z. Lebensm.-Unters.-Forsch.*, 171 (1980) 14–17.
4 J. Velisek, J. Davidek, V. Kubelka, G. Janicek, Z. Svobodova and Z. Simikova, *J. Agric. Food Chem.*, 28 (1980) 1142–1144.
5 J. Velisek, J. Davidek, Z. Svobodova and Z. Simicova, *Sci. Pap. Prague Inst. Chem. Technol.* E53 (1982) 55–65.
6 J. Velisek and J. Davidek, *Sb. UTIZ, Potravin. Vedy*, 3 No. 1 (1985) 11–18.
7 P. D. Collier, D. D. O. Cromie and A. P. Davies, *J. Am. Oil Chem. Soc.*, 68, No. 10 (1991) in press.
8 W. J. Plantinga, W. G. van Toorn and G. H. D. van der Stegen, *J. Chromatogr.*, 555 (1991) 311.

Journal of Chromatography, 589 (1992) 121–126
Elsevier Science Publishers B.V., Amsterdam

CHROM. 23 730

Purification and determination of glutamine synthetase by high-performance immunoaffinity chromatography

J. Alhama, J. López-Barea, F. Toribio* and J. M. Roldán

Departamento de Bioquímica y Biología Molecular, Facultad de Veterinaria, Avda. Medina Azahara, Universidad de Córdoba, 14071 Córdoba (Spain)

(First received June 28th, 1991; revised manuscript received September 6th, 1991)

ABSTRACT

High-performance immunoaffinity chromatography (HPIAC) with anti-glutamine synthetase polyclonal antibodies bound to epoxy-activated silica was used to purify and determine this enzyme from the cyanobacterium *Synechocystis*. A single-step HPIAC procedure with cell-free extracts yielded electrophoretically homogeneous glutamine synthetase. In the determination of glutamine synthetase by HPIAC a linear response in the range 10–60 μg of enzyme was observed. Recoveries of 70% of the loaded enzymatic activity and 100% of protein were obtained. The determination of glutamine synthetase protein by HPIAC was compared with that obtained by rocket immunoelectrophoresis. The chromatographic method is proposed as a possible alternative to other immunochemical quantitative techniques, particularly when non-limiting amounts of samples are available.

INTRODUCTION

Affinity chromatography is a well known procedure for the purification of biomolecules and its principles and applications have been reviewed in detail [1,2]. The biospecificity of conventional affinity chromatography (low pressure) has been successfully combined with the fast operation, resolution and sensitive detection of high-performance liquid chromatographic (HPLC) systems [3]. Higher selectivity and specifity can be achieved by using antibodies or antigens as immobilized ligands, which adds the advantages of immunochemical reactions to the separation process. The resulting technique is known as high-performance immunoaffinity chromatography (HPIAC) [4].

Epoxy-activated silica has been widely used as a support in high-performance affinity chromatography (HPAC) owing to its porosity and mechanical rigidity, allowing work at the pressures and flow-rates usual in HPLC. The oxirane groups present in epoxysilica react with nucleophiles such as amino [5], hydroxyl [6], thiol[7] and carboxy [8] in the pH range 3–7.5 to form stable covalent bonds. In general, the coupling to epoxysilica of ligands with such functionalities can be easily carried out, rendering this support advantageous for many applications. Thus, we have recently used this support to immobilize a pyridine nucleotide analogue for one-step purification of $NADP^+$-dependent dehydrogenases from different cell-free extracts [9]. This affinity matrix is also suitable for immobilization of antigens or antibodies for analytical and preparative separations, which permit rapid isolation and high recovery of biologically active molecules.

In this work, HPIAC with linked polyclonal antibodies was used for the determination of glutamine synthetase (GS), an enzyme that catalyses the incorporation of ammonia into amino acids in a wide variety of organisms. In bacteria and cyanobacteria, GS has a molecular weight of 600 000 dalton with twelve identical 50 000-dalton subunits [10,11], while the eukaryotic enzyme has eight subunits of 45 000–48 000 dalton [12,13]. GS has been purified from many organisms by conventional affinity chromatography [13–15] but, as far as we know, no data exist on the use of HPLC or HPIAC for the purification of this enzyme. Based on the results re-

0021-9673/92/$05.00

ported here, we propose HPIAC for the one-step purification of GS, and as an excellent alternative to other non-chromatographic immunoquantitative procedures.

EXPERIMENTAL

Chemicals

Salts for the mobile phases and acetonitrile were purchased from Merck (Darmstadt, Germany). Tris, phenylmethylsulphonyl fluoride (PMSF), EDTA and 3-(N-morpholino)propanesulphonic acid (MOPS) were obtained from Sigma (St. Louis, MO, USA). Purified glutamine synthetase was a gift from Drs. Candau and Florencio (Universidad de Sevilla). Freund's adjuvants were from Difco Labs. All other chemicals used were of the highest purity available.

Equipment

HPIAC was performed using a Beckman liquid chromatographic system equipped with two Model 110B pumps, an Altex 210A injection valve with a 2.0-ml loop, a Model 163 variable-wavelength UV detector and a Model 406 analogue interface module. Integration of chromatograms was performed in a AT-compatible computer with the Beckman System Gold software. An Ultraffinity-TM prepacked epoxy-activated silica analytical column (5 cm × 0.45 cm I.D.) from Beckman was used for coupling anti-GS antibodies. High-purity water was obtained using a Milli-Q system (Millipore).

Cell culture

Synechocystis sp. PCC 6803 cells were grown at 37°C as described previously [16]. The medium was supplemented with 20 m*M* $NaNO_3$ as a nitrogen source. Cells growing at mid-log phase were harvested by centrifugation at 19 000 *g* for 25 min. The cells were washed with 50 m*M* MOPS buffer (pH 7) containing 1 m*M* EDTA and 1 m*M* PMSF (5 ml buffer/g wet cells) and centrifuged at 19 000 *g* for 10 min. Both processes were repeated three times. The pellet was then resuspended with buffer as described above and sonicated for 6 × 30 s at 1-min intervals. Cellular debris was removed by centrifugation at 39 000 *g* for 20 min. The cell-free extract contained 2.6 U GS/mg protein.

Enzyme activity and purification

The transferase activity of GS was determined as described previously [17]. One unit of activity is the amount of enzyme that catalyses the formation of 1 μmol of γ-glutamylhydroxamate per minute. The enzyme from *Synechocystis* was purified by ion-exchange and affinity chromatography on 2′,5′-ADP-Sepharose [15]. The elution from the affinity column was carried out by a pulse of ADP. Protein concentration was determined by the bicinchoninic acid assay [18] using bovine serum albumin as a standard.

Immunization and purification of antibodies

Purified GS was subjected to disc gel electrophoresis and its activity was localized on the gels. Gel sections containing GS were pooled, disrupted and emulsified in 4 ml of a mixture containing equal volumes of phosphate-buffered saline (PBS) and Freund's complete adjuvant and injected subcutaneously into a non-immunized rabbit. Bleeding and further booster injections were performed as reported previously [19]. After centrifugation and inactivation of complement, the immunoglobulin G (IgG)-enriched fraction was purified by chromatography on protein A-Sepharose according to Campbell and Remmler [20].

Electrophoresis

Sodium dodecyl sulphate–polyacrylamide gel electrophoresis (SDS–PAGE) was performed in slab gels according to Laemmli [21]. Acrylamide concentrations were 10% and 4% (w/v) for running and stacking gels, respectively. Rocket immunoelectrophoresis was carried out as described by Weeke [22], in agarose plates containing, per millilitre of gel, 21 μg of protein A-purified IgG-rich fraction from anti-GS serum. Samples of crude extracts (9 μl) were run overnight at 10°C and 10 V/cm. Proteins were stained with Coomasie Blue R250.

Coupling of antibodies to the epoxysilica column

The IgG fractions eluted from the protein A-Sepharose column were pooled and dialysed overnight against 0.5 *M* potassium phosphate buffer (pH 7) (coupling buffer). For the coupling, a solution containing 9.34 mg of protein in 12 ml was

used. The Ultraffinity-EP column was connected to an HPLC pump primed with coupling buffer. The column flow rate was maintained at 1 ml/min until liquid eluted from the column end, then it was changed to 0.2 ml/min and recycled for 36 h at 35°C. Subsequently the column was extensively washed with coupling buffer to remove unbound antibodies. Removal of ionically bound ligand was carried out, under identical conditions, by washing the column with 1 *M* KCl for 1 h at 1 ml/min and then with 20 m*M* KCl to eliminate hydrophobically bound antibodies. The remaining unreacted oxirane groups on the silica support were deactivated by pumping 0.5 *M* glycerol in 1 *M* potassium phosphate buffer (pH 4.5) at 0.2 ml/min for 8 h at 35°C. After washing with equilibrating buffer [50 m*M* MOPS (pH 7.0)–1 m*M* EDTA], the column was ready for use. When not in use, the column was stored at 4°C.

Chromatographic procedure

The silica anti-GS column was equilibrated with a loading buffer containing 50 m*M* MOPS, 250 m*M* KCl and 1 m*M* EDTA (pH 7). Samples (2 ml) were injected at a flow rate of 1 ml/min. After extensive washing with loading buffer, a pulse of 1 *M* KCl in loading buffer (2.0 ml) was applied to elute non-specifically retained compounds. Elution of GS was performed at 0.5 ml/min with a 2-ml pulse of loading buffer supplemented with 10% of acetonitrile and 2.5 *M* $MgCl_2$. GS transferase activity was measured in the 0.5-ml fractions collected. The influence of eluents on the baseline at 280 nm was corrected. The samples were filtered through 0.20-μm membrane hydrophilic filters before injection into the immunoaffinity column. The mobile phases were degassed under vacuum for 30 min in an ultrasonic bath and filtered before use. All chromatographic procedures were performed at room temperature.

RESULTS AND DISCUSSION

The high affinity and specificity of the antigen–antibody interactions turn HPIAC into an efficient analytical technique. The main aim of this work was to use HPIAC for the determination of GS in complex protein mixtures. Polyclonal antibodies used for coupling to epoxy-activated silica were obtained by protein A-Sepharose chromatography of

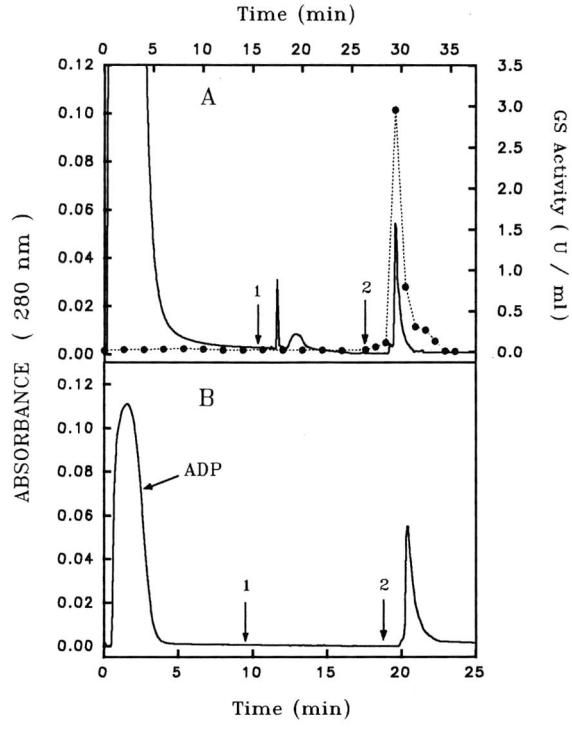

Fig. 1. HPIAC elution pattern of *Synechocystis* glutamine synthetase in (A) cell-free extracts and (B) conventionally purified preparations. (A) A *Synechocystis* crude extract sample (2 ml) containing 2.4 mg of total protein was chromatographied as described under Experimental. (B) A sample (2 ml) of *Synechocystis* glutamine synthetase purified by conventional chromatography, containing 50 μg of protein, was processed as described under Experimental. Solid lines, absorbance at 280 nm; ●, GS transferase activity. Times for different pulses are indicated with arrows: (1) 1 *M* KCl; (2) 10% acetonitrile in 2.5 *M* $MgCl_2$.

an anti-GS serum. Monospecifity of the purified antiserum, when challenged with crude extracts of *Synechocystis*, was demonstrated by immunoelectrophoretic procedures (not shown).

The effects of different factors such as ionic strength, type of buffer and pH on the binding of GS from *Synechocystis* to the anti-GS column were studied. Complete binding of up to 60 μg of GS was achieved using 50 m*M* MOPS buffer containing 250 m*M* KCl and 1 m*M* EDTA. Consequently, this solution was selected as the equilibrating buffer in the subsequent chromatography. On the other hand, different GSs antigenically related to the enzyme from *Synechocystis* were not effectively bound by the antibodies coupled to the column. Thus, the en-

zyme from the cyanobacterium *Synechococcus*, which presented high degree of cross-reactivity with our anti-GS IgGs in double immunodiffusion tests, was less than 20% retained by the HPIAC column under our experimental conditions. Negligible binding to the immunoaffinity column was also observed when injecting crude extracts of other cyanobacteria (*Calothrix*) or a photosynthetic bacteria (*Rhodobacter*). This restricted binding capacity corroborates the high specificity of immunochemical interaction. Thus, GSII isoenzyme from *Rhizobium* does not cross-react with polyclonal anti-GSI antibodies, illustrating differential recognition of isoenzymes from the same organism [23].

In most instances, values lower than 10^{-8} are typical for dissociation constants of immuno complexes in free solution [24]. However, the disruption of immobilized complexes can be achieved using different conditions, such as low-pH buffers, high salt concentrations (chaotropics), organic solvents or mixtures (organics plus salts). Proteins have to be treated gently in order to avoid denaturation; therefore, the elution conditions are specific for each case, depending on the particular affinity of antibodies towards the antigen to be purified. A wide range of conditions have been used to elute GS from the HPIAC polyclonal IgG column. Thus, acidic buffers such as acetic acid (pH 2.7) or glycine–HCl (pH 2.2) and organics such as 50% ethylene glycol or 10–30% acetonitrile were not effective for the disruption of the antigen-immobilized antibody complex, while $MgCl_2$ (2.5–3 *M*) showed a partial efficiency for enzyme elution. However, the GS retained in the column was completely eluted with 10% acetonitrile in 2.5 *M* $MgCl_2$, and this eluent was routinely used in the HPIAC experiments.

Fig. 1A shows the elution profile of protein and GS activity after chromatography of a *Synechocystis* crude extract. Traces of unspecifically adsorbed proteins were washed out with a 2-ml pulse of 1 *M* KCl. Elution of GS protein and activity was performed with a 2-ml pulse of 10% acetonitrile–2.5 *M* $MgCl_2$. The chromatographic behaviour of purified *Synechocystis* glutamine synthetase is shown in Fig. 1B: a well defined peak was again observed after the pulse of elution buffer, whereas no protein was detected, in this instance, after washing whith 1 *M* KCl. As the enzyme had been purified by affinity chromatography (2′,5′-ADP-Sepharose) and eluted by ADP, unretained ADP yielded a peak, a marker of the dead volume of the HPLC tubing.

Specificity of the bound antibodies was further corroborated by SDS-PAGE of samples obtained by concentrating the GS activity-containing fractions eluted from the HPIAC column (Fig. 2). Thus, one densely stained band was obtained after electrophoresis of GS purified by HPIAC of *Synechocystis* crude extracts (lane E). The same band was observed with purified GS, either before (lane B) or after (lane C) HPIAC processing. Comparison of lanes D, E and F confirms the power of the HPIAC for one-step purification of *Synechocystis* glutamine synthetase, although this was not the main aim of this work. By comparing with the molecular weight markers, an approximate value of 55 000 dalton can be inferred for the *Synechocystis* GS subunit, which is close to that previously reported [25] for the enzyme monomers of 52 000 dalton.

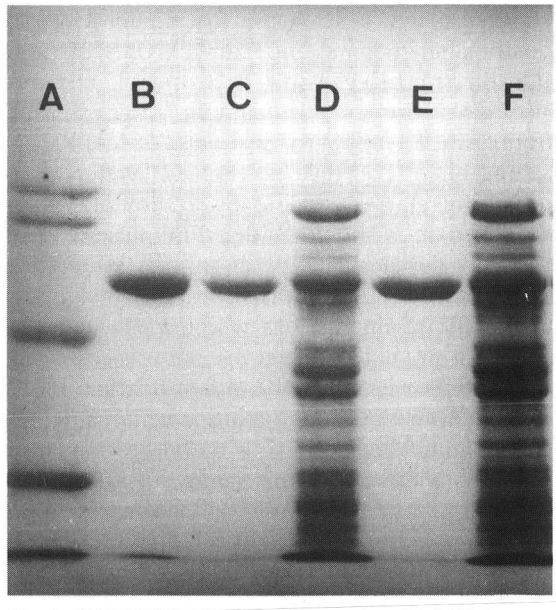

Fig. 2. SDS-PAGE of crude extracts and purified GS from *Synechocystis*. Conditions as indicated under Experimental. (A) 35 μg of a standard mixture containing the markers carbonic anhydrase (30 000), ovoalbumin (45 000), bovine serum albumin (67 000) and ovotransferrin (78 000 dalton); (B) 25 μg of GS purified by conventional affinity chromatography; (C) 15 μg of purified GS further processed by HPIAC; (D) and (F) *Synechocystis* crude extracts (108 and 162 μg of protein, respectively); (E) 22 μg of GS, purified by one-step HPIAC from *Synechochystis* crude extract.

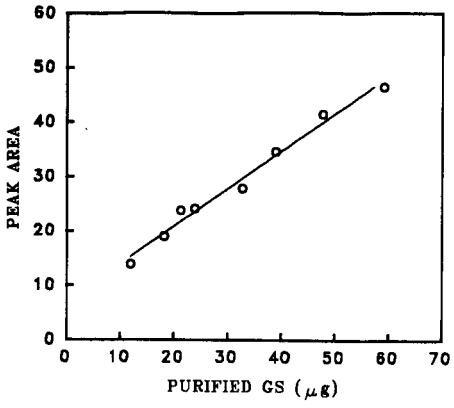

Fig. 3. HPIAC calibration graph for purified glutamine synthetase. Samples (2 ml) containing different amounts of purified GS were chromatographed according to the procedure described under Experimental. GS elution peak areas are expressed in arbitrary units.

An average of 70% of GS activity was recovered in the HPIAC process. This value does not take into account the slight inhibition promoted by the eluent on GS transferase activity. Futher, a linear relationship was obtained when the peak areas at 280 nm of eluted GS were plotted against the amounts of purified protein injected on to the column (Fig. 3). Linearity was also observed on injecting different dilutions of *Synechocystis* crude extracts (not shown), indicating a complete mass recovery of GS protein from the column under the elution conditions used [26,27]. This result opens up the possibility of determining GS in complex protein mixtures by using Fig. 3 as a standard.

Glutamine synthetase in *Synechocystis* cell-free extracts was determined by comparing rocket immunoelectrophoresis with HPIAC. Table I shows the results obtained. The amount of GS protein was determined by rocket immunoelectrophoresis in each cell-free extract sample by comparison with a standard of purified GS subjected to an identical process. A linear regression analysis of the data gave a correlation coefficient of 0.998. Additionally, HPIAC determination of GS protein in crude extracts was performed by measuring the specific peak area at 280 nm and comparing it with the calibration graph shown in Fig. 3. A correlation coefficient of 0.994 was calculated from the linear least-squares analysis of the data and a linear range (10–60 μg of GS) was found. The results obtained by both methods (averages 21.5 ± 0.5 and 24.1 ± 0.4 μg GS/mg total protein) allows HPIAC determination to be proposed as an alternative to non-chromatographic immunochemical quantitative methods. Rocket immunoelectrophoresis and the more sensitive enzyme-linked immunosorbent assay (ELISA) are able to detect minute amounts of antigens, starting from small amounts of protein mixtures, and allow several samples to be run at a time. However, both procedures consist of a series of steps which, in many cases, could result in a time-consuming overall process. Although the HPIAC determination described here requires larger amounts of samples (see Table I), further optimization of the HPIAC technique might shorten the time required, making it advantageous for the rapid, direct determination of antigens, particularly when non-limiting amounts

TABLE I

DETERMINATION OF GLUTAMINE SYNTHETASE IN CRUDE EXTRACTS FROM *SYNECHOCYSTIS*

Rocket immunoelectrophoresis				HPIAC			
Protein (μg)[a]	*h* (cm)	GS (μg)[a]	GS (μg)[b]	Protein (mg)[c]	Peak area[d]	GS (μg)[c]	GS (μg)[b]
4.88	1.7	0.11	24.00	1.20	24.11	25.33	21.25
6.97	2.3	0.17	24.31	1.55	30.04	33.74	21.71
8.13	2.6	0.20	24.39	2.17	38.04	45.10	20.80
9.76	3.1	0.24	24.50	2.35	42.50	52.01	22.13
12.20	3.6	0.28	23.51	2.53	44.70	54.55	21.57

[a] In 9 μl of crude extract.
[b] Per mg total protein.
[c] In 2 ml of crude extract.
[d] Expressed in arbitrary units.

of samples are available or in antigen-rich mixtures. On the other hand, immunoaffinity chromatography has been often used as a prepurification step, followed by determination by other HPLC techniques [28–30]. Additionally, the direct HPAC determination of proteins has been reported [27].

Non-specific binding to affinity chromatographic systems has been prevented by adding detergents such as Tween 20 to mobile phases [31] or by using a precolumn with linked non-immune γ-globulins [32]. In our case, accumulation of non-specifically adsorbed proteins was avoided by routine regeneration of the column with 30% acetonitrile after two or three runs. The column capacity appeared to remain constant after 50 runs.

Although the current trend in HPIAC is to use monoclonal antibodies, the results obtained with the polyclonal anti-GS system seem to be as reliable as those previously reported with monoclonals for other proteins [33]. Moreover, the production of this last type of antibodies is laborious and expensive and in many instances drastic elution conditions are needed [33,34]. The choice of monoclonal or polyclonal antibodies for a given HPIAC system could depend on a balance of the cost of producing the necessary amount of the ligand to be immobilized and the half-life of the column. In conclusion, we propose the use of HPIAC for the determination of different macromolecules in cell-free extracts, particularly when non-limiting amounts of samples are available.

ACKNOWLEDGEMENTS

This work was supported by the Comision Asesora de Investigación Científica y Técnica (Spain), Grant No. GR85-0014, and the Junta de Andalucía, No. GR-30016. The technical assistance of Dr. Antonio López-Ruiz and Margarita Escuder is gratefully acknowledged. We are indebted to Dr. Jesús Díez for critical reading of the manuscript and fruitful discussions.

REFERENCES

1 P. D. G. Dean, W. S. Johnson and F. A. Middle, in D. Rickwood and B. D. Hames (Editors), *Affinity Chromatography: a Practical Approach*, IRL Press, Lancaster, 1985, p. 1.
2 P. Mohr and K. Pommerening, *Affinity Chromatography: Practical and Theoretical Aspects*, Marcel Dekker, New York, 1985, p. 1.
3 S. Ohlson, L. Hansson, P. O. Larsson and K. Mosbach, *FEBS Lett.*, 93 (1978) 5.
4 T. M. Philips, *Adv. Chromatogr.*, 29 (1989) 133.
5 M. Landt, S. C. Boltz and L. G. Butler, *Biochemistry*, 17 (1978) 915.
6 P. Vretblad, *Biochim. Biophys. Acta*, 434 (1976) 169.
7 P. C. Simon and D. C. Van der Jagt, *Anal. Biochem.*, 82 (1977) 334.
8 J. Turkova, K. Blaha, M. Malanikova, D. Vancurova, F. Svec and J. Kalal, *Biochim. Biophys. Acta*, 524 (1978) 162.
9 J. Alhama, J. López-Barea and F. Toribio, *J. Chromatogr.*, 586 (1991) 51.
10 E. R. Stadtman and A. Ginsburg, in P. D. Boyer (Editor), *The Enzymes*, Vol. X, Academic Press, New York, 3rd ed., 1974, p. 755.
11 M. J. A. M. Sampaio, P. Rowell and W. D. P. Stewart, *J. Gen. Microbiol.*, 111 (1979) 181.
12 B. J. Miflin, P. J. Lea and R. M. Wallsgrove, in J. Mora and R. Palacios (Editors), *Glutamine: Metabolism, Enzymology and Regulation*, Academic Press, New York, 1980, p. 213.
13 G. Tholey, S. Bloch, M. Ledig, P. Mandel and F. Wedler, *Neurochem. Res.*, 12 (1987) 1041.
14 S. Weining and D. J. D. Nicholas, *Biochem. Int.*, 14 (1987) 337.
15 F. J. Florencio and J. L. Ramos, *Biochim. Biophys. Acta*, 838 (1987) 39.
16 M. Herdman, S. F. Delaney and N. G. Carr, *J. Gen. Microbiol.*, 79 (1973) 233.
17 B. M. Shapiro and E. R. Stadtman, *Methods Enzymol.*, 17a (1970) 910.
18 P. K. Smith, R. I. Krohn, G. T. Hermanson, A. K. Mallia, F. M. Gartner, M. D. Provenzano, E. K. Fujimoto, N. M. Goeke, B. J. Olson and D. C. Klenk, *Anal. Biochem.*, 150 (1985) 76.
19 A. López-Ruiz, J. M. Roldán, J. P. Verbelen and J. Diez, *Plant Physiol.*, 78 (1985) 614.
20 W. H. Campbell and J. L. Remmler, *Plant Physiol.*, 80 (1986) 435.
21 U. K. Laemmli, *Nature (London)*, 227 (1970) 680.
22 B. Weeke, in N. H. Axelsen, J. Kroll and B. Weeke (Editors), *Quantitative Immunoelectrophoresis*, (*Scand. J. Immunol.*, Vol. 2, Suppl. 1), Universitetsforlaget, Oslo, 1973, p. 37.
23 M. Rossi, R. Defez, M. Chivrazzi, A. Lamberti, A. Fuggi and M. Iaccarino, *J. Gen. Microbiol.*, 135 (1989) 629.
24 M. W. Steward and J. Steensgaard, *Antibody Affinity: Thermodynamic Aspects and Biological Significance*, CRC Press, Boca Raton, FL. 1983, p. 1.
25 A. Mérida, L. Leurentop, P. Candau and F. J. Florencio, *J. Bacteriol.*, 172 (1990) 4732.
26 A. L. Khurana, E. T. Butts and C. T. Ho, *J. Liq. Chromatogr.*, 12 (1989) 3019.
27 H. W. Jarret, *J. Chromatogr.*, 363 (1986) 456.
28 T. Hayashi, S. Sakamoto, I. Wada and H. Yoshida, *Chromatographia*, 27 (1989) 574.
29 L. S. Van Ginkel, H. Van Blitterswijk, P. W. Zoontjes, D. Van den Bosch and R. W. Stephany, *J. Chromatogr.*, 445 (1988) 385.
30 E. J. Trione, B. B. Krygier, J. M. Kathrein, G. M. Banowetz and L. A. Sayavedra-Soto, *Physiol. Plant.*, 70 (1987) 467.
31 T. Moreaux, M. T. Leidecker and C. Meyer, *Eur. J. Biochem.*, 179 (1989) 617.
32 R. J. Fido, *Plant Sci.*, 50 (1987) 111.
33 R. Sportman and G. S. Wilson, *Anal. Chem.*, 52 (1980) 2013.
34 N. E. Thompson, D. B. Aronson and R. R. Burgess, *J. Biol. Chem.*, 265 (1990) 7069.

Journal of Chromatography, 589 (1992) 127–134
Elsevier Science Publishers B.V., Amsterdam

CHROM. 23 710

Affinity partitioning of erythrocytic phosphofructokinase in aqueous two-phase systems containing poly(ethylene glycol)-bound Cibacron Blue

Influence of pH, ionic strength and substrates/effectors

M. Cristina Tejedor*, Cristina Delgado☆, Milagrosa Grupeli and Jose Luque

Departamento de Bioquimica y Biologia Molecular, Universidad de Alcala, 28871 Alcala de Henares (Madrid) (Spain)

(First received March 28th, 1991; revised manuscript received July 1st, 1991)

ABSTRACT

Phosphofructokinase (PFK) from rat eythrocyte haemolysates has a high affinity for Cibacron Blue F3G-A covalently bound to poly(ethylene glycol) (PEG–Cb) and thus the enzyme can be extracted into the top phase of poly(ethylene glycol)–dextran aqueous two-phase systems containing PEG–Cb. The pH, ionic strength and presence of substrates/effectors affect to different extents the affinity of the enzyme for PEG–Cb and the number of PEG–Cb molecules attached per molecule of PFK (the latter probably reflecting, at saturation, the influence on the aggregation state of the enzyme) and thus influence the yield of enzyme recovered in the top phase. Increasing the pH from 6 to 7 and then to 8 leads to a higher yield of PFK in the top phase. A change in pH from 6 to 7 and 8 results in an increased number of PEG–Cb molecules attached per molecule of enzyme while the affinity of PFK for PEG–Cb shows a minimum at pH 7. The ionic strength in the range 0.017–0.164 has less influence on the partitioning of PFK. The presence of substrates or effectors of the enzyme in general reduces the recovery of PFK in the top phase. Fructose 6-phosphate increases the number of PEG–Cb molecules attached but greatly reduces the affinity of PFK for PEG–Cb. In contrast, AMP slightly reduces the number of PEG–Cb molecules attached and the affinity of PFK for PEG–Cb. ATP and ATP–Mg^{2+} compete with PEG–Cb for the same binding sites in PFK. The best extraction of the enzyme is achieved at pH 8 and ionic strength 0.045: more than 95% of the enzyme is recovered in the top phase with a specific activity ten times higher.

INTRODUCTION

Affinity partitioning refers to extraction processes where one or several ligands selectively influence the partition of solutes (*e.g.* proteins) within aqueous two-phase systems of poly(ethylene glycol) (PEG) and dextran [1–3]. In principle, the ligand is immobilized to one of the polymers and thus restricted to one of the phases of the biphasic system. This methodology, which combines the simplicity and sensitivity of partitioning in aqueous two-phase systems with the specificity of affinity methods, has been extensively applied with two different purposes: first, to isolate a selected protein from crude extracts (yeast, animal cells, etc.) [4–6], and second, to recognize and characterize ligand–macromolecule interactions [7,8].

Triazine dyes covalently linked to PEG have been the ligands most extensively used in affinity partitioning and enzymes, especially among the groups of kinases and dehydrogenases, the target proteins [9–13]. The partition coefficient of the PEG–ligand is usually extremely high and therefore a great change in the partitioning of the protein is expected

☆ Present address: Molecular Cell Pathology Laboratory, Royal Free Hospital School of Medicine, Rowland Hill Street, London NW3 2PF, UK.

0021-9673/92/$05.00

on attachment of only one or two molecules of the ligand [14]. A number of parameters have a pronounced effect on the partitioning of proteins in the affinity biphasic systems. In general, the partition coefficient (K) of the protein approaches a saturation value with increasing concentration of polymer-bound ligand; an increase in the polymer concentration of the system gives rise to more extreme K for the polymer-bound ligand and therefore larger increases in K value for the target protein; a lower pH value enhances the binding of PEG–triazine dyes to most proteins, thus reducing the specificity [15,16]. Other parameters such as salt and salt concentration, temperature, molecular weight of the polymers, free ligands and bulk proteins have different effects on different proteins [9,15,16].

The molecular mechanism of affinity partitioning is, however, not completely understood. The current theory developed by Flanagan and Barondes [17] predicts a linear relationship between the increment in log K of the protein produced by the affinity ligand (Δ log K) and the number of PEG–ligand molecules attached per molecule of protein. However, in most instances the total number of binding sites obtained by other methods are higher than the values resulting from partition experiments and, therefore, the attempts to correlate the Δ log K_{max} (under saturating conditions) with the number of actual binding sites failed [7,8,12].

In an attempt to optimize the extraction of phosphofructokinase (E.C. 2.7.1.11) (PFK) from rat erythrocyte haemolysates by affinity partitioning, the influence of several experimental conditions, including pH, ionic strength and presence of substrates/effectors of the enzyme, were studied. PEG covalently bound to Cibacron Blue F3G-A (PEG–Cb) was used because of the strong affinity shown by PFK towards this triazine dye ligand. The enzyme source was a PFK-enriched fraction obtained by selective precipitation with PEG [18]. We have previously shown that the extraction of PFK from rat erythrocytes by using affinity partitioning with PEG–Cb is greatly enhanced when a PFK-enriched fraction is used instead of the whole haemolysate [13]. The effects of the experimental conditions on the partitioning of PFK were analysed in the light of the current theory, in order to obtain an insight into the mechanism of the affinity partitioning.

EXPERIMENTAL

Chemicals

Polyethylene glycol (PEG-6000, MW 6000–7500) and Cibacron Blue F3G-A were purchased from Serva (Heidelberg, Germany), dextran T-500 (MW 500 000) from Pharmacia (Uppsala, Sweden), nucleotides (sodium salts of ATP and AMP), dithioerythritol, glucose 6-phosphate, fructose 6-phosphate (F6P) and coupling enzymes from Boehringer (Mannheim, Germany), EDTA (disodium salt) from Sigma (St. Louis, MO, USA) and Tris, 2-mercaptoethanol and all other chemicals (analytical-reagent grade) from Merck (Darmstadt, Germany).

Preparation of haemolysate

Anaesthetized male Wistar rats weighing 180–200 g were decapitated and whole blood was collected in heparinized tubes and centrifuged (400 *g*, 10 min). Red cells were washed three times with 0.15 *M* sodium chloride solution and freed from leucocytes and platelets by removing the top layer of cells after centrifugation. Subsequently, the red cells were lysed by mixing with an equal volume of a hypotonic solution consisting of 2.7 m*M* EDTA and 0.7 m*M* 2-mercaptoethanol (pH 7.3). The mixture was frozen and thawed twice and finally centrifuged (15 000 *g*, 30 min) to remove stroma and non-solubilized haemoglobin. All these steps were carried out at 4°C.

Preparation of phosphofructokinase-enriched fraction

A PFK-enriched fraction was obtained from the erythrocyte haemolysate by precipitation with PEG according to Tejedor *et al.* [18]. In brief, one volume of haemolysate (total protein about 20 mg/ml) was mixed with one volume of a solution of 12% (w/w) PEG in 96 m*M* potassium phosphate buffer (pH 6) containing 1 m*M* EDTA and 10 m*M* 2-mercaptoethanol. The mixture of PEG and haemolysate was kept in an ice-bath for 30 min and then centrifuged (5000 *g*, 10 min). The supernatant was discarded and the pellet containing 80% of the original PFK with a specific activity eight times higher was dissolved in 1 volume of 25 m*M* sodium phosphate buffer (pH 7) containing 0.5 m*M* EDTA and 5 m*M* 2-mercaptoethanol. This PFK extract was used immediately.

Preparation of biphasic systems

All the biphasic systems used in this study consisted of 5% PEG and 7.5% dextran and had a volume ratio of top to bottom phases close to unity. Portions of 1 g were made up in graduated tubes by weighing 0.1 g of PFK extract, appropriate amounts of distilled water, 40% (w/w) PEG, 20% (w/w) dextran (standardized by polarimetry) and stock phosphate buffer to produce the pH and ionic strength required (see legends to the figures). The substrates/effectors were introduced into the system by replacing the distilled water with appropriate stock solutions to provide the desired concentration (see legends to the figures).

All the components were mixed well by 30–40 inversions and then the systems were left to settle at 4°C until complete separation of the phases was achieved. Aliquots from top and bottom phases were then analysed for protein concentration and enzymatic activity.

The affinity systems were prepared as above but using a 40% (w/w) stock solution of PEG in which increasing amounts of PEG had been replaced with PEG–Cb. The biphasic systems thus obtained had 5% total PEG (PEG + PEG–Cb) but increasing proportions of PEG–Cb from 0.05 to 0.5% (% PEG–Cb in the system). The substituted polymer (PEG–Cb) was prepared as described by Delgado *et al.* [13].

The partition coefficient, K, is defined as the ratio between the enzyme activities in the top and bottom phases of the systems. The percentage of PFK in the top phase of the system was calculated from the partition coefficient and volume ratio values as described by Johansson [16]. The concentrations of polymers in the systems are always expressed as w/w.

Enzyme and total protein assays

PFK activity was measured by the linear decrease in NADH absorbance (340 nm) in a test mixture containing 100 mM Tris–HCl (pH 7.1), 0.3 mM EDTA, 3 mM magnesium chloride, 90 mM potassium chloride, 0.15 mM NADH, 1.5 mM dithioerythritol, 1 mM phosphate, 3 mM F6P, 9 mM glucose 6-phosphate, 1.5 mM ATP, 0.1 U/ml aldolase (E.C. 4.1.2.13), 6 U/ml triosephosphate isomerase (E.C. 5.3.1.1) and 0.5 U/ml glycerol-3-phosphate dehydrogenase (E.C. 1.1.1.8). The total protein concentration was measured by the Coomassie Brilliant Blue assay [19].

RESULTS

The partitioning of rat erythrocytic PFK in an aqueous two-phase system consisting of 5% PEG, 7.5% dextran and increasing concentrations of PEG–Cb was studied under different conditions of pH, ionic strength and effectors of the enzyme (Fig. 1). PFK has affinity for the PEG–Cb under all the conditions studied, as shown by the increased partition coefficient (expressed on a logarithmic scale) in the presence of this polymer compared with the control system (not containing PEG–Cb). In all instances, the partition coefficient increases progressively with increasing concentration of PEG–Cb in the biphasic system finally to reach a plateau (Fig. 1).

The influence of the pH in the range 6–8 is shown in Fig. 1A. In the control system the partition coefficient in PFK has values of 0.1, 0.07 and 0.05 ($\log K = -1.00, -1.15$ and -1.30) for pH values of 6, 7 and 8, respectively. In the affinity systems, increases in the pH from 6 to 7 and 8 lead to increases in the partition coefficient at all concentrations of PEG–Cb (Fig. 1A).

The influence of the ionic strength was studied in the range 0.017–0.3 (Fig. 1B). In the control system the partition coefficient varies from 0.03 ($\log K = -1.52$) to 0.15 ($\log K = -0.82$). In the affinity systems, similar partitioning behaviours are found for PFK in the ionic strength range 0.017–0.082 (Fig. 1B). An increase in the ionic strength to 0.164 leads to lower values for the partition coefficient at concentrations of PEG–Cb up to 0.3% whereas above this concentration the partition coefficients are similar to those obtained in the ionic strength range 0.017–0.082 (Fig. 1B). A further increase in the ionic strength to 0.3 leads to lower partition coefficients at all concentrations of PEG–Cb (Fig. 1B).

The influence of a constant concentration of some substrates and effectors of PFK on its partitioning behaviour is shown in Fig. 1C. The partition coefficient of PFK is reduced by the presence of any of the substrates or effectors in the affinity systems. AMP has only a slight influence on the saturation curve followed by F6P (Fig. 1C). In the

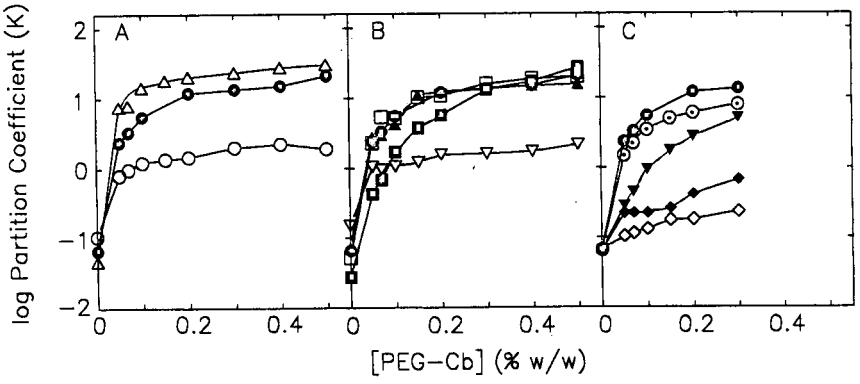

Fig. 1. Influence of increasing concentrations of PEG–Cb on the partitioning of erythrocytic PFK in a biphasic system consisting of 5% total PEG (PEG + PEG–Cb) and 7.5% dextran under the following experimental conditions: (A) (○) pH 6, (●) pH 7 and (△) pH 8 at a constant ionic strength of 0.045; (B) ionic strength (▲) 0.017, (●) 0.045, (□) 0.082, (■) 0.164 and (▽) 0.3 at pH 7; (C) (●) control, (⊙) 1 m*M* AMP, (▼) 1 m*M* F6P, (◆) 1 m*M* ATP and (◇) ATP–Mg^{2+} (1 m*M* ATP, 2.5 m*M* Mg^{2+}) at pH 7 and ionic strength 0.045. All the systems contain 0.25 m*M* EDTA, 2.5 m*M* 2-mercaptoethanol and sodium phosphate buffer as follows: to obtain a constant ionic strength of 0.045, 40.17 m*M*, 25 m*M* and 15.08 m*M* for pH 6, 7 and 8, respectively; to obtain a constant pH of 7, 9.1 m*M*, 46 m*M*, 92 m*M* and 169 m*M* for ionic strength 0.017, 0.045, 0.082, 0.164 and 0.3, respectively.

presence of ATP the saturation curve consists of two components (Fig. 1C). ATP–Mg^{2+} produces the greatest reduction in the PFK partition coefficient (Fig. 1C).

The maximum extraction of PFK in the top phase of the affinity biphasic systems takes place at pH 8 and ionic strength 0.045. The partition coefficient varies from 20 (log K = 1.3) in the biphasic system containing 0.2% PEG–Cb to 31 (log K = 1.5) in the system containing 0.5% PEG–Cb. These partition coefficients correspond to 95.24% and 96.88% of PFK extracted in the top phase, respectively. The higher the concentration of PEG–Cb the more viscous and hence more difficult to handle is the biphasic system, hence the extraction of PFK using the system containing 0.2% PEG–Cb might have advantages, especially when scaling up the system. The partition coefficient of the total proteins is of about 0.1, which leads to a purification factor of about 10 for PFK in the top phase.

The affinity partitioning effect promoted by PEG–Cb is quantitatively analysed in double-reciprocal plots of the increment in log K (Δ log K) (defined as the difference between log K in the presence and the absence of the ligand) *versus* the concentration of PEG–Cb (Fig. 2) in order to calculate the values for $[PEG–Cb]_{0.5}$ and Δ log K_{max}. The former corresponds to the concentration of PEG–Cb at which half of the available sites in the enzyme are occupied by the ligand, *i.e.* it measures the affinity. The latter measures the maximum change in the partition coefficient promoted by the ligand. The number of binding sites for the ligand is then calculated by the ratio between Δ log K_{max} and log K for the free ligand [7,16]. Log K for free PEG–Cb in the systems used in this study was in the range 0.3–0.6 with a mean value of 0.47. The number of binding sites thus obtained is given in Table I.

An increase in pH from 6 to 8 leads to a dramatic increase in Δ log K_{max} and hence the number of binding sites. The affinity of PFK for PEG–Cb has a minimum at pH 7 (shown by the increase in $[PEG–Cb]_{0.5}$) (Table I). Ionic strength in the range 0.017–0.164 has only a slight influence on Δ log K_{max} whereas the affinity of PFK for PEG–Cb decreases on increasing the ionic strength. This is especially marked when the ionic strength increases from 0.082 to 0.164 (Table I). When the ionic strength is further increased to 0.3, the double-reciprocal plot deviates considerably from a linear relationship (Fig. 2B) and therefore Δ log K_{max} and $[PEG–Cb]_{0.5}$ could not be calculated.

The presence of effectors or substrates of PFK influences the affinity and Δ log K_{max} to different extents (the control is at pH 7, ionic strength 0.045). F6P reduces drastically the affinity of PFK for PEG–Cb whereas Δ log K_{max} shows a maximum (Table I). In contrast, AMP produces only a slight

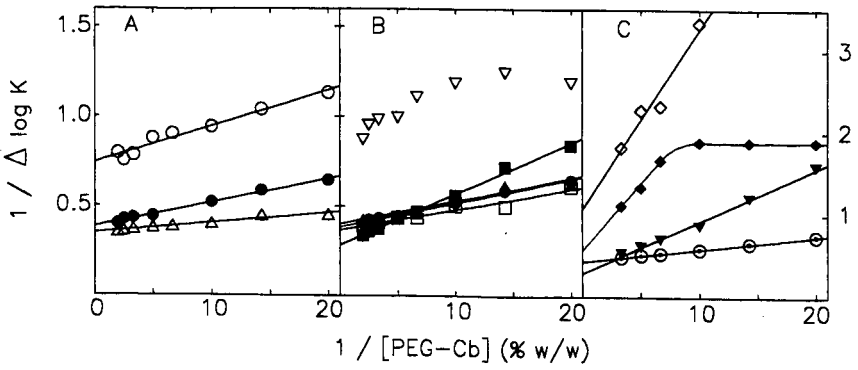

Fig. 2. Double-reciprocal plots of Δ log K (difference between log K in the presence and absence of PEG–Cb) *versus* concentration of PEG–Cb.

decrease in the affinity of PFK for PEG–Cb and has little influence on Δ log K_{max} (Table I).

In the presence of ATP two slopes are observed (Fig. 2C). One corresponds to a binding site which is not saturable by PEG–Cb ($[PEG–Cb]_{0.5}$ is infinite) and which accounts for 25% of the binding sites available (the total is the sum of binding sites for the two slopes). The other, accounting for 75% of the available binding sites, shows the largest reduction in the affinity of PFK for PEG–Cb under all the conditions tested (Table I). In the presence of ATP–Mg^{2+} both the affinity and Δ log K_{max} are considerably reduced (Table I).

In order to obtain an insight into the nature of the binding sites for PEG–Cb in erythrocytic PFK, affinity partitioning was studied at a single concentration of PEG–Cb (0.3%) and increasing concentrations of F6P or ATP (Fig. 3A). F6P produces a slight reduction in the log K which plateaus at a concentration of 1.5 mM. This behaviour of PFK could be expected in the presence of a non-competitor. However, increasing concentrations of ATP lead to a steady reduction in log K to approach the value for log K in the absence of PEG–Cb.

To analyse further the affinity partitioning effect, a plot of Δ^* log K (absolute value) *versus* the con-

TABLE I

AFFINITY PARTITIONING PARAMETERS FOR ERYTHROCYTIC PFK IN 5% PEG, 7.5% DEXTRAN TWO-PHASE SYSTEM CONTAINING PEG–Cb.

Maximum increment of the partitioning coefficient and relative binding affinity of PEG–Cb for erythrocytic PFK were calculated by linear regression of the double-reciprocal plots. The number of PEG–Cb binding sites was calculated from the simplified Flanagan and Barondes equation [17].

Experimental conditions	Δ log K_{max}	$[PEG–Cb]_{0.5}$ (%, w/w)	No binding sites
pH 6	1.3	0.025	2.8
pH 7	2.5	0.035	5.3
pH 8	2.8	0.015	6.0
Ionic strength 0.017	2.4	0.030	5.1
Ionic strength 0.045	2.5	0.035	5.3
Ionic strength 0.082	2.6	0.045	5.5
Ionic strength 0.164	3.0	0.100	6.4
1 mM F6P	3.3	0.200	7.0
1 mM AMP	2.3	0.050	4.9
1 mM ATP (1st slope)	0.5	–	1.1
1 mM ATP (2nd slope)	1.9	0.300	4.1
ATP–Mg^{2+}	0.9	0.200	1.9

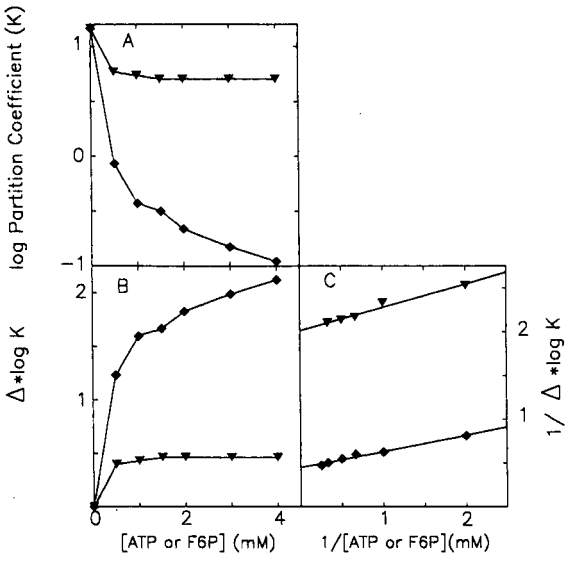

Fig. 3. (A) Influence of increasing concentrations of (▼) F6P and (◆) ATP on the partitioning of erythrocytic PFK in a biphasic system consisting of 5% total PEG (PEG + PEG–Cb), 7.5% dextran and 0.3% PEG–Cb at pH 7 and ionic strength 0.045. (B) Variation of Δ^* log K (difference between log K in the presence and absence of ATP or F6P) as a function of the concentration of F6P or ATP. (C) Double-reciprocal plots of the data in (B).

centration of F6P or ATP was constructed (Fig. 3B). Δ^* log K refers to the difference between log K in the presence and the absence of effector, both situations in the presence of 0.3% PEG–Cb. A double-reciprocal plot (Fig. 3C) provides the values for $[\text{effector}]_{0.5}$ and Δ^* log K_{max} · Δ^* log K_{max} represents the maximum reduction that can be produced by the substrate in the affinity partitioning promoted by 0.3% PEG–Cb (with this concentration of PEG–Cb, pH 7 and ionic strength 0.045, Δ log K was near 2.5). In the presence of F6P, Δ^* log K_{max} is equal to 0.5 and $[\text{F6P}]_{0.5}$ is infinite. These results taken together reflect that F6P cannot prevent the binding of PEG–Cb to PFK. In the presence of ATP, $[\text{ATP}]_{0.5}$ is 0.53 mM and Δ^* log K_{max} is equal to 2.5.

DISCUSSION

Rat erythrocytic PFK shows a high affinity for the triazine dye Cibacron Blue, similar to that already reported for yeast PFK. This behaviour allows the use of affinity partitioning in PEG–dextran two-phase systems with PEG–Cb as affinity ligand for a partial but significant purification of this enzyme from haemolysates with a yield of about 95%. Affinity partitioning has proved to be useful for the purification of several enzymes from yeast, animal tissues and plants [1–6]. In most instances single extraction steps are used as the partition coefficient of the protein of interest is many times higher than that of the bulk proteins [4,6]. A common feature for all the examples is the high yield in the selected protein achieved at the end of the process, which provides a great advantage over other more classical methods. In addition, combination of affinity partitioning with counter-current distribution (multiple extraction steps) has led to the fractionation of complex mixtures into several of their components [10].

Under all conditions studied, the partition coefficient of PFK plateaus *versus* the concentration of PEG–Cb. Two main conclusions are drawn from this behaviour: (a) there is a maximum amount of enzyme that can be extracted into the top phase of the biphasic system under any of the conditions studied and (b) under the conditions where the plateau is reached below the highest value (obtained at pH 8), the maximum value reached for the partition coefficient does not represent saturation of the extraction capacity of the biphasic system.

The affinity partitioning effect depends on two critical factors: the affinity of the enzyme for PEG–Cb and the number of PEG–Cb molecules attached per molecule of enzyme. Ideally, to achieve maximum extraction of the target protein, experimental conditions have to be selected to provide maximum values for both of them. With erythrocytic PFK the best extraction conditions are pH 8 and ionic strength 0.045, where a high affinity of PEG–Cb for PFK is observed together with a high value of Δ log K_{max}.

The decreased binding of PEG–Cb to erythrocytic PFK at low pH seems to be a peculiar feature of this enzyme. It is well documented that with triazine dyes, a lower pH value enhances the binding to most enzymes [14]. This behaviour in turn leads to a reduction in the specificity of the extraction. Other exceptions to this effect of pH include some serum proteins [20].

The changes in the affinity of PFK for PEG–Cb probably reflect conformational changes of the

binding site and/or surroundings promoted by the different experimental conditions. Δ log K_{max} is related to the number of binding sites for PEG–Cb per molecule of protein. Hence an increase in Δ log K_{max} will be found on association of PFK subunits to form larger oligomers, whereas a decrease in Δ log K_{max} will take place on dissociation of the subunits. Analysis of the data in Table I in this light indicates the following: a decrease in pH from 7 to 6 produces dissociation of erythrocytic PFK whereas an increase in pH to 8 leads to association to larger oligomers. Such effects of pH on erythrocytic PFK have been reported previously [21]. Ionic strength in the range 0.017–0.164 has little effect on the PFK self-association equilibrium. AMP has no influence on the self-association equilibrium and F6P produces aggregation of the enzyme. The effect of ATP on the self-association equilibrium of PFK cannot be studied using PEG–Cb as the affinity ligand, as it binds to the same sites as ATP and therefore the enzyme cannot be saturated with ATP for it to produce an effect.

The results obtained in the presence of F6P support the concept that maximum extraction of the enzyme in the top phase should be obtained when the enzyme is more aggregated. This would be the case if no negative effect on the affinity of PFK for PEG–Cb were to be produced (this makes the concentration of PEG–Cb required to achieve Δ log K_{max} impracticable). The reduction in affinity produced by F6P has also been found in studies with yeast PFK [7,22]. That behaviour was interpreted in two different ways: (a) the binding of F6P causes steric hindrance of the complex formation with the dye or (b) the substrate lowers the affinity to the dye by shifting the allosteric equilibrium towards the R-state [22]. The difference in Δ log K_{max} for the control system and the system with F6P indicates that F6P does not compete with PEG-Cb for the same binding sites in PFK.

The presence of two components in the saturation curve with ATP might represent displacement of the ATP by increasing concentrations of PEG–Cb from two binding sites in the enzyme with different affinities for ATP. The complete displacement of PEG–Cb by ATP (Δ log K_{max} and Δ^* log K_{max} have the same absolute value) strongly supports competition of ATP and PEG–Cb for the same binding sites and, as a result, ATP can be used to strip off the PFK efficiently from the PEG–Cb-containing phase. The magnitude of the competition might also indicate that all the ATP available sites in PFK are occupied by PEG–Cb. If some of the ATP binding sites were unoccupied by PEG–Cb, then the reduction in the partition coefficient would have consisted of two phases: in the first phase (lag phase), the ATP binds to the free available sites and no effect (or little) is seen in the affinity partitioning effect promoted by PEG–Cb; in the second phase, ATP and PEG–Cb bind to the same sites in PFK, resulting in a considerable reduction in the affinity partitioning as the concentration of ATP is increased.

In conclusion, affinity partitioning is a powerful technique for the rapid isolation of proteins from crude extracts. Advantage can be taken of experimental conditions known to promote aggregation of the protein provided that the affinity of the protein for the ligand is not reduced.

ACKNOWLEDGEMENTS

This work was supported by grants from the Comision Interministerial de Ciencia y Tecnologia, Spain. We thank Professor G. Kopperschläger for suggestions and critical discussion of the manuscript.

REFERENCES

1 P. Å. Albertsson, *Partition of Cell Particles and Macromolecules*, Wiley, New York, 3rd ed., 1986.
2 H. Walter, D. E. Brooks and D. Fisher (Editors), *Partitioning in Aqueous Two-Phase Systems, Theory, Methods, Uses and Applications to Biotechnology*, Academic Press, New York, 1985.
3 D. Fisher and I. A. Sutherland (Editors), *Separations Using Aqueous Phase Systems —Applications in Cell Biology and Biotechnology*, Plenum Press, New York, 1989.
4 G. Kopperschläger and G. Johansson, *Anal. Biochem.*, 124 (1982) 117–124.
5 G. Johansson and M. Joelsson, *Enzyme Microb. Technol.*, 7 (1985) 629–634.
6 H. Hustedt, K. H. Kroner, V. Menge and M. R. Kula, *Trends Biotechnol.*, 3 (1985) 139–144.
7 G. Johansson, G. Kopperschläger and P. Å. Albertsson, *Eur. J. Biochem.*, 131 (1983) 589–594.
8 G. Kopperschläger and G. Johansson, *Biomed. Biochim. Acta*, 44 (1985) 1047–1055.
9 K. H. Kroner, A. Cordes, A. Schelper, M. Morr, A. F. Buckman and M. R. Kula, in T. C. J. Gribnau, J. Visser and R. J. F. Nivard (Editors), *Affinity Chromatography and Related Techniques*, Elsevier, Amsterdam, 1982, pp. 491–501.

10 G. Johansson, M. Andersson and H. E. Akerlund, *J. Chromatogr.*, 298 (1984) 483–493.
11 G. Johansson and M. Andersson, *J. Chromatogr.*, 291 (1984) 175–183.
12 G. Kopperschläger and G. Birkenmeier, *J. Chromatogr.*, 376 (1986) 141–148.
13 C. Delgado, M. C. Tejedor and J. Luque, *J. Chromatogr.*, 498 (1990) 159–168.
14 G. Johansson, in D. Fisher and I. A. Sutherland (Editors), *Separations Using Aqueous Phase Systems. Applications in Cell Biology and Biotechnology*, Plenum Press, New York, 1989, pp. 7–14.
15 G. Johansson and M. Andersson, *J. Chromatogr.*, 303 (1984) 39–51.
16 G. Johansson, *Methods Enzymol.*, 104 (1984) 356–364.
17 S. D. Flanagan and S. H. Barondes, *J. Biol. Chem.*, 250 (1975) 1484–1489.
18 M. C. Tejedor, C. Delgado, A. Rubio and J. Luque, *Biosci. Rep.*, 6 (1986) 395–401.
19 M. M. Bradford, *Anal. Biochem.*, 72 (1976) 248–254.
20 G. Birkenmeier, G. Kopperschläger and G. Johansson, *Biomed. Chromatogr.*, 1 (1986) 64–77.
21 S. Vora, *Isozymes Curr. Top. Biol. Med. Res.*, 6 (1982) 119–167.
22 G. Kopperschläger, J. Kirchberger and T. Kriegel, in D. Fisher and I. A. Sutherland (Editors), *Separation Using Aqueous Phase Systems —Applications in Cell Biology and Biotechnology*, Plenum Press, New York, 1989, pp. 41–42.

Journal of Chromatography, 589 (1992) 135–140
Elsevier Science Publishers B.V., Amsterdam

CHROM. 23 711

Determination of profiles of non-collagenous proteins from rat bones by sodium dodecyl sulfate high-performance liquid chromatography

M. E. Kunkel*, A. Seo and R. L. Thomas

Department of Food Science, 223 Poole Agricultural Center, Clemson University, Clemson, SC 29634-0371 (USA)

(Received June 28th, 1991)

ABSTRACT

Sodium dodecyl sulfate–high-performance liquid chromatographic (SDS-HPLC) techniques for screening profiles of bone non-collagenous proteins (NCP) are described and compared with sodium dodecyl sulfate–polyacrylamide gel electrophoresis (SDS-PAGE) techniques. NCPs were obtained from long bones of neonatal and mature rats by sequential extraction with 4 *M* guanidine hydrochloride (GdnHCl) and 0.25 *M* EDTA followed by desalting. Desalted extracts were subjected to SDS-PAGE and SDS-HPLC. The results of the two analyses were comparable. There were differences in NCP profiles between mature rats and pups and between the GdnHCl and EDTA extracts. The methods described can be used for qualitative comparison of treatments and as a basis for further study.

INTRODUCTION

The analysis of individual non-collagenous proteins (NCPs) from hard tissues has traditionally been accomplished by harsh extraction steps followed by multiple liquid chromatographic, precipitation and concentration procedures [1,2]. Among the methods that have been developed to characterize the molecular weights of all the NCPs from rat compact bone are gel filtration chromatography followed by sodium dodecyl sulfate–polyacrylamide gel electrophoresis (SDS-PAGE) [3], fractional precipitations and ion-exchange chromatography followed by SDS-PAGE [3], calcium-induced precipitation followed by high-performance liquid chromatography (HPLC) [4] and two-dimentional gel electrophoresis with electroblotting [5]. The development of a rapid method that allows the comparison of NCPs *in toto* would be a useful screening tool for studies of the effects of nutritional stresses and disease states on the NCP composition of bone. When differences are identified by these comparisons, further studies on those specific NCPs can be undertaken.

EXPERIMENTAL

Materials

Bones were obtained from crl:COBS Sprague–Dawley descended rats (Charles Rivers Labs., Research Triangle Park, NC, USA). Reagents used for extractions were of either analytical-reagent or electrophoresis grade and were obtained from Fisher (Norcross, GA, USA)) or Sigma (St. Louis, MO, USA). Spectra Por 3 dialysis tubing (molecular weight cut-off 3500) was purchased from Spectrum Medical Industries (Los Angeles, CA, USA). Sephadex G-25-150 and PD-10 columns were obtained from Pharmacia (Uppsala, Sweden). All reagents and equipment used for electrophoresis and silver staining and the low-molecular-weight standards were supplied by Bio-Rad Labs. (Richmond, CA, USA). The HPLC equipment was obtained from Waters (Milford, MA, USA) and all reagents used for HPLC were of HPLC grade.

Sample preparation and NCP extraction

Femurs and tibias were removed from newborn rat pups and their dams and cleaned of soft tissues

0021-9673/92/$05.00

and marrow. The midshafts were isolated and placed in a cold solution of 4 *M* guanidie hydrochloride (GdnHCl) with a "cocktail" of protease inhibitors [2]. The solution containing the bones from the pups was placed on a rotary shaker at 4°C for 96 h. The bones from the dams were removed from he GdnHCl solution, lyophilized, crushed to increase the surface area and subjected to the same extraction procedure as the bones from the pups.

After 96 h, the GdnHCl solution was decanted and the bones were covered with 0.25 *M* EDTA–protease inhibitors solution [2] and placed on a rotary shaker at 4°C for 72 h.

The GdnHCl extracts were placed in Spectra Por 3 dialysis tubing and dialyzed extensively against water at 4°C. Following dialysis, the extracts were lyophilized, suspended in 500 μl of 20 m*M* Tris (pH 8.0), applied to a 20 cm × 2.5 cm I.D. column of Sephadex G-25-150 and eluted with 20 m*M* Tris (pH 8.0). All the eluate which contained material that absorbed at 280 nm was pooled and lyophilized.

The EDTA extracts were lyophilized without dialysis and desalted using PD-10 columns following the manufacturer's instructions with 20 m*M* Tris (pH 8.0) as the eluent.

SDS-PAGE

SDS-PAGE was conducted using gels that were 0.75 mm thick with 12% polyacrylamide (separating) and 4% polyacrylamide (stacking). A discontinuous Tris–glycine buffer system [6] was used with a Bio-Rad Labs. Mini-Protean II electrophoresis cell.

Desalted, lyophilized extracts were suspended in 500–1000 μl of 20 m*M* Tris (pH 8.0) and analyzed for protein content by the Bio-Rad Labs. protein assay method. SDS-PAGE dissociation buffer was mixed with the sample (1:1, v/v) and the mixture was boiled for 5 min. Approximately 1.5 μg of protein were placed in each well of the gel. One well of each gel contained 5 μl of low-molecular-weight standard (Bio-Rad Labs.) that had been diluted 1:100 (v/v) with sample buffer.

Electrophoresis was run at constant voltage of 200 for 45–60 min. Bands were then detected with silver stain following manufacturer's instructions (Bio-Rad Labs.).

The migration distances of each standard protein and the migration distance of the tracking dye was measured and R_F values were calculated. R_F values were also calculated for the unknown proteins and the relative molecular weights (M_r) of the unknowns were calculated from the R_F valves of the standards.

HPLC

HPLC analyses of extracts were performed using a Waters Model 440, HPLC absorbance detector Model 712 WISP autoinjector, Model 501 pump and Model 740 data module. The detector was set to monitor absorbance at 280 nm, the range was set to 0.02, the integrator attenuation was set to 32 and the chart speed was set to 10.

HPLC analyses were conducted by a modification of the method of Takagi [7]. The modifications made were to use two TSK G3000 SW columns (30 cm × 7.5 mm I.D.) and 0.1 *M* phosphate elution buffer (pH 6.0) containing 0.1 *M* sodium nitrate and 0.1% SDS at a flow-rate of 0.3 ml/min.

The same sample suspension as described for SDS-PAGE was mixed with an equal volume of 10% SDS–mercaptoethanol (3:1, v/v) and boiled for 5 min. A volume of the suspension calculated to contain 5–10 μg of protein was injected into the HPLC system. The M_r values of the NCPs were calculated from a plot of retention time *vs.* log M_r of low-molecular-weight standards which has been treated in the same manner. Fig. 1 shows an elution pattern for the low-molecular-weight standards used and a plot of log M_r of the standards *vs.* retention time.

Partially, purified NCP samples (a gift from Dr. C. W. Prince) were prepared as described above and injected into the HPLC system.

RESULTS

Fig. 2 shows a typical SDS-PAGE pattern for GdnHCl extracts from newborn pups and their dams. In the GdnHCl extract from the pups, there were discrete bands with M_r *ca.* 100 000, 60 000, 50 000, and 15 000. In the GdnHCl extract from the dams, the major discrete band was at M_r 15 000. In GdnHCl extracts from both the dams and the pups, there were many minor bands with M_r between 100 000 and 15 000.

Fig. 3 is a typical SDS-PAGE pattern for EDTA

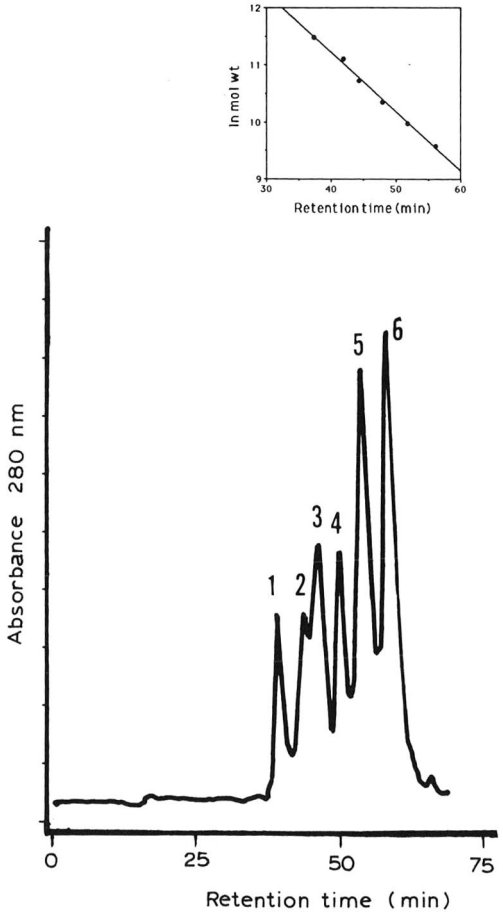

Fig. 1. SDS-HPLC of low-molecular-weight standards obtained with two TSK-G3000 columns in tandem. Standards used were the low-molecular-weight standards obtained from Bio-Rad Labs. Molecular weights of (1) 97 400, (2) 66 200, (3) 45 000, (4) 31 000, (5) 21 500 and (6) 14 400. Inset: plot of log M_r of the standards *vs.* retention time; $y = 15.358 - 0.1036x$.

extracts from newborn rat pups and their dams. In the EDTA extract from the pups, the major discrete bands had M_r 60 000, 20 000 and 10 000. The relative lightness of the bands in the EDTA extract reflects the lack of protein in the EDTA extract from newborn rat pups. In the EDTA extract from the dams, the major discrete bands had M_r 60 000, 45 000 and 15 000. As with the GdnHCl extracts, there were many minor bands with M_r between 100 000 and 15 000.

With 12% gels, no protein remained in the stack-

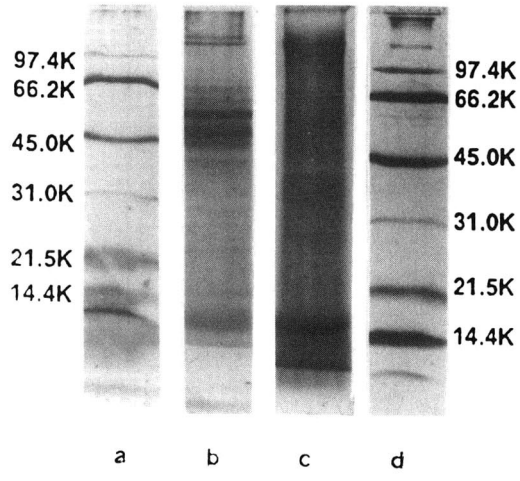

Fig. 2. SDS-PAGE profiles of GdnHCl extracts from tibias and femurs of newborn rat pups and their dams: 12% polyacrylamide gels were run with discontinuous Tris–glycine buffer systems and bands were detected with silver staining. Lanes: a = low-molecular-weight standards (Bio-Rad Labs.); b = GdnHCl extract from newborn rat pups; c = GdnHCl extract from dams; d = low-molecular-weight standards (Bio-Rad Labs.). K = kilodalton.

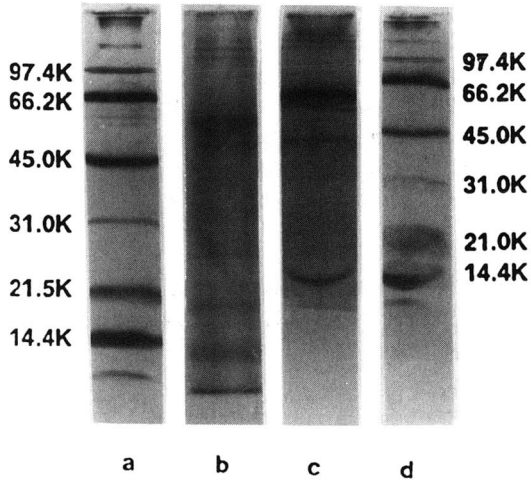

Fig. 3. SDS-PAGE profiles of EDTA extracts from tibias and femurs of newborn rat pups and their dams: 12% polyacrylamide gels were run with discontinuous Tris–glycine buffer systems and bands were detected with silver staining. Lanes: a = low-molecular-weight standards (Bio-Rad Labs.); b = EDTA extract from newborn rat pups; c = EDTA extract from dams; d = low-molecular-weight standards (Bio-Rad Labs.).

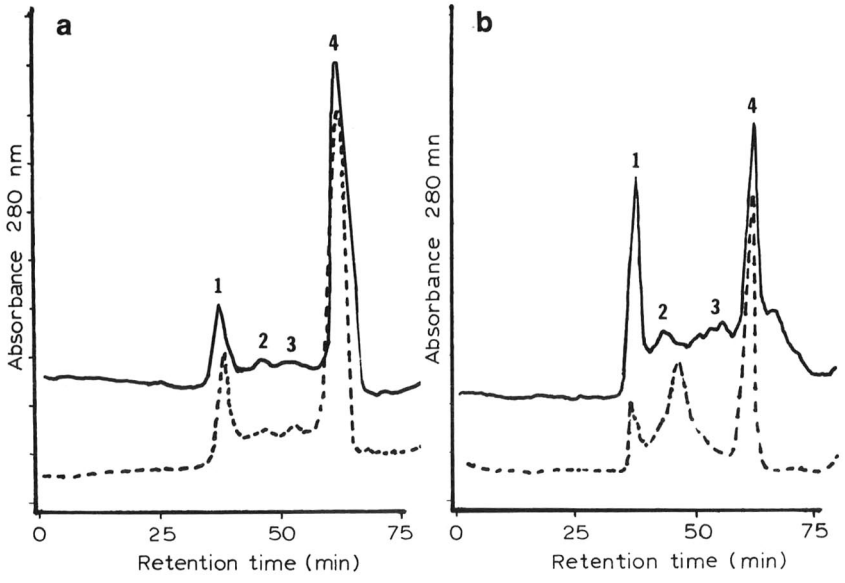

Fig. 4. SDS-PAGE profiles of (a) GdnHCl and (b) EDTA extracts from femurs and tibias of newborn rat pups (dashed lines) and their dams (solid lines). HPLC was performed using two 30-cm TSK 3000 columns in tandem, absorbance was monitored at 280 nm and the flow-rate was 0.3 ml/min. Between 5 and 10 μg of protein were injected. Peaks (M_r): 1 = 115 000; 2 = 55 000; 3 = 30 000; 4 = 12 000.

ing gels and the minimal staining at the dye front suggested that little proteolytic degradation had occurred.

Fig. 4 shows examples of SDS-HPLC profiles of GdnHCl and EDTA extracts from newborn pups and their dams. The percentage of the total peak area and M_r represented by each of the major peaks are given in Table I. From both extracts, there were major peaks with retention times of 35 and 57 min (peaks 1 and 4, respectively). There was also a set of poorly resolved peaks with retention times between 43 min (peak 2) and 50 min (peak 3). For GdnHCl extracts from the bones of mature rats, peak 1 represented 13.4% of the total peak area and peak 4 was 69.5% of the total peak area (Table I). For EDTA extracts from the bones of mature rats, peak 1 represented 13.2% of the peak area and peak 4 49.5% of the total peak area (Table I). For GdnHCl extracts from the bones of the pups, peak 1 was 18.1% and peak 4 was 57.4% of the total peak area.

TABLE I

PERCENTAGE OF TOTAL PEAK AREA AND APPARENT MOLECULAR WEIGHT (M_r) REPRESENTED BY EACH PEAK FROM SDS-HPLC OF GdnHCl AND EDTA EXTRACTS OF BONES OF NEWBORN RAT PUPS AND THEIR DAMS

n = 4 or 5.

Peak	M_r	GdnHCl extract		EDTA extract	
		Pups	Dams	Pups	Dams
1	115 000	18.1 ± 5.8	13.4 ± 3.2	27.5 ± 5.2	13.2 ± 3.3
2	55 000	–	6.4 ± 3.2	26.4 ± 5.2	32.6 ± 3.3
3	30 000	22.1 ± 5.8	8.2 ± 3.2	–	–
4	12 000	57.4 ± 5.8	69.5 ± 3.2	43.5 ± 5.2	49.5 ± 3.3
5	5000	0.2 ± 5.8	1.0 ± 3.6	–	0.5 ± 3.3

From the EDTA extract from the bones of the pups, peak 1 was 27.5% and peak 4 was 43.5% of the total peak area (Table I). Peak 2 was absent in the GdnHCl extract from the bones of the pups and was 26.4% of the total peak area in the EDTA extract from the bones of the pups. Peak 3 was 22.1% of the total peak area in the GdnHCl extract from the bones of the pups and was absent in the EDTA extract.

In some of the samples from both the GdnHCl and the EDTA extracts, a small peak with a retention time of 67 min (peak 5) was evident. This peak had M_r between 2000 and 4000 and might represent proteolytic degradation products. That this peak averaged less than 1% of the total peak area suggested that little degradation of the samples had occurred.

The SDS-HPLC method was also used on partially purified NCP samples. The partially purified sample that contained largely osteonectin had the major peak at 45 min which corresponded to peak 2. The partially purified sample that contained largely proteoglycans had its major peak at the same retention time as peak 1 (35 min).

DISCUSSION

The advantages of the method described in this paper include (1) a relatively short extraction time of about 1 week, which may explain the lack of obvious degradation, (2) the use of generally accepted GdnHCl and EDTA extraction procedures to separate NCPs associated with the non-mineralized phase and the mineralized phase of bone and (3) the use of 5–10 μg of protein for SDS-HPLC and 1.5 μg of protein for SDS-PAGE. These amounts of protein can be obtained from five neonatal rats and three mature rats.

There were clear differences in NCP profiles between GdnHCl and EDTA extracts in mature rats; there differences were not as apparent in neonatal rats, which may reflect the relative lack of mineralization in pups [8]. In the GdnHCl extract from the dams, the major bands detected by SDS-HPLC had M_r *ca.* 100 000 and 15 000, whereas with the pups there were discrete bands with M_r *ca.* 100 000, 60 000, 50 000 and 15 000 (Fig. 2). The SDS-PAGE of the EDTA extracts (Fig. 3) was simpler than that of the GdnHCl extract (Fig. 2). The greater simplicity of the gels of EDTA extracts is in agreement with data of Termine *et al.* [1]. The major components of the EDTA extract of fetal calf bones have been reported to have M_r values of 61 000–63 000, 31 000 and 22 000–26 000 [1], whereas those of rat compact bone have been reported to be above 50 000 [3]. The major bands detected by SDS-PAGE of the EDTA extracts from the newborn rat pups in this study had M_r *ca.* 60 000, 20 000, and 10 000.

The profiles of the NCPs obtained using SDS-HPLC corresponded closely with those from SDS-PAGE. In all samples there was a peak with M_r *ca.* 115 000 in both PAGE and HPLC; this protein, termed peak 1, can be tentatively identified as proteoglycans. In most of the samples, the proteins in the M_r range 30 000–60 000 were poorly resolved in both PAGE and HPLC. Nevertheless, it is possible to note differences in the relative amounts of peak 2 (M_r = 55 000), which can be tentatively identified as largely osteonectin, and peak 3 (M_r = 34 000) between the GdnHCl and EDTA extracts (Fig. 4). These differences were especially pronounced in the extracts from the dams. Peak 4 (M_r = 12 000) is a major band in both HPLC and PAGE and presumably represents the γ-carboxy glutamic acid proteins. Although the M_r of peak 2 is closer to that of α-2HS glycoprotein than that of osteonectin, the retention time of peak 2 was the same as that of a partially purified NCP preparation that contained largely osteonectin. That the gla proteins represented a larger percentage of the total NCPs in the bones of the dams than in the bones of the pups was expected [9] and is in agreement with the results of Kuboki *et al.* [4].

When these samples were applied to a single TSK-G3000 HPLC column in the absence of SDS, one or two peaks were obtained (data not shown). The addition of SDS partially resolved those peaks and lengthening the column further increased the resolution. It is possible that resolution could be further increased by further lengthening the column and/or monitoring absorbance at 230 or 210 nm in addition to 280 nm.

The use of methods such as that described in this paper to obtain NCP profiles does not allow the identification or quantification of specific NCPs, but does allow qualitative comparison of treatments and can indicate possible NCPs for further study.

ACKNOWLEDGEMENTS

The authors gratefully acknowledge the gift of partially purified NCPs from Dr. C. W. Prince, the assistance of Su-Jeng Lin in sample preparation and the support of the South Carolina Agricultural Experiment Station.

REFERENCES

1 J. D. Termine, A. B. Belcourt, K. M. Conn and H. K. Kleinman, *J. Biol. Chem.*, 256 (1981) 10403–10408.
2 W. T. Butler, M. Bhown, M. T. Dimuzio and A. Linde, *Coll. Res.*, 1 (1981) 187–199.
3 A. Linde, M. Jontell, T. Lundgren, B. Nilson and U. Swanberg, *J. Biol. Chem.*, 258 (1983) 1698–1705.
4 Y. Kuboki, H. Takita, T. Komori, M. Mizuno, E. Furu-uchi and K. Taniguchi, *Calcif. Tissue Int.*, 44 (1989) 269–277.
5 P. D. Delmas, R. P. Tracy, B. L. Riggs and K. G. Mann, *Calcif. Tissue Int.*, 36 (1984) 308–316.
6 U. K. Laemmli, *Nature (London)*, 227 (1970) 680–685.
7 T. Takagi, *J. Chromatogr.*, 219 (1981) 123–127.
8 A. Franzen, D. Heinegard, S. R. Lund and S. Olsson, *J. Bone Joint Surg.*, 64 (1982) 558–565.
9 P. V. Hauschka and F. J. Demuth, *J. Biol. Chem.*, 258 (1983) 176–182.

Journal of Chromatography, 589 (1992) 141–149
Elsevier Science Publishers B.V., Amsterdam

CHROM. 23 678

Determination of aflatoxin M1 using a dialysis-based immunoaffinity sample pretreatment system coupled on-line to liquid chromatography

Reusable immunoaffinity columns

A. Farjam, N. C. van de Merbel, A. A. Nieman, H. Lingeman and U. A. Th. Brinkman*

Department of Analytical Chemistry, Free University, De Boelelaan 1083, 1081 HV Amsterdam (Netherlands)

(First received February 20th, 1991; revised manuscript received August 9th, 1991)

ABSTRACT

A liquid chromatographic column-switching system containing a dialysis unit and an anti-aflatoxin immunoaffinity precolumn (immuno precolumn) is described for the automated determination of aflatoxin M1 in milk samples. Both a flat membrane dialysis unit working according to the flowing donor–flowing acceptor principle and a laboratory made hollow-fibre dialysis unit working according to the stagnant donor–flowing acceptor principle were evaluated. The hollow-fibre unit is superior with respect to repeatability (3% relative standard deviation) and detection limit (10 ng/l for aflatoxin M1 in milk), in spite of the fact that the overall recovery is only 6%. Interfering compounds, which would destroy the activity of the immuno precolumn, are efficiently removed from the system by the dialysis step; a single immuno precolumn can then be used for over 70 milk analyses. No decrease in the performance of either the immuno precolumn or the hollow-fibre dialysis unit is observed.

INTRODUCTION

Because of the complex sample matrix and the low detection limits (10–50 ng/l) required, the liquid chromatographic (LC) determination of aflatoxin M1 in milk and milk products usually needs an extensive sample clean-up [1,2]. Recently, immunoaffinity columns containing immobilized antibodies directed against aflatoxins have become commercially available. With these immuno columns, the whole sample pretreatment procedure is reduced to a one-step solid-phase extraction [3–6]. Owing to the selective antibody–antigen interaction, the aflatoxins immunosorbent packed into a stainless-steel precolumn can be incorporated into an automated column-switching system, allowing fully automated sample pretreatment and analysis [5,6]. Unfortunately, when analysing milk samples, these immuno precolumns cannot be reused. In contrast to aqueous standards, with milk samples a continuous decrease in the capacity is observed. Proteolytic enzymes present in milk probably cause the degradation of the immobilized antibodies. This assumption seems likely because, with an anti-oestrogen immuno precolumn, a decrease in immuno precolumn capacity was observed if protease-containing serum samples were analysed [7]. Heating of the milk samples was not extensively studied because this is a laborious off-line procedure and because during the initial experiments coprecipitation of the aflatoxins with the fatty material occurred.

As an immunoaffinity precolumn is relatively expensive, its reuse would significantly reduce the cost of analysis. With this aim in mind, on-line removal

0021-9673/92/$05.00

of the interfering milk components by means of dialysis, prior to immunoaffinity sample pretreatment, was studied in this work with a flat membrane dialyser and a hollow-fibre dialyser.

EXPERIMENTAL

Chemicals

Aflatoxin B2 was a gift from RIKILT (Wageningen, Netherlands) and aflatoxin M1 from the National Institute of Public Health and Environmental Protection (Bilthoven, Netherlands). Aflatoxins M2, P1 and Q1 were obtained from Sigma (St. Louis, MO, USA). LC-grade acetonitrile and methanol were purchased from Baker (Deventer, Netherlands). LC-grade water was prepared from demineralized water using a Milli-Q water purification system (Millipore, Bedford, MA, USA) with subsequent filtration through a 500 mm × 10 mm I.D. LC column filled with 40-μm Baker C_{18} bonded phase. All other chemicals were of analytical-reagent grade.

The LC eluents were degassed under vacuum in an ultrasonic bath. Plastic precolumns containing the immobilized monoclonal anti-aflatoxin antibodies were obtained as a gift from Koopman & Koek (Rijswijk, Netherlands). Unfortunately, it is not known exactly against which aflatoxins the antibodies were raised, and no information about the cross-reactivity is known. The precolumns were opened and the immunosorbent was removed and repacked in the stainless-steel precolumns as described previously [8]. When not in use, the immuno precolumns were stored in methanol–water (70:30, v/v).

Apparatus

An Amicon (Danvers, IL, USA) dialyser with a 15 000-dalton molecular-weight cut-off cellulose acetate membrane, with a 1.3-cm^2 accessible membrane area and with acceptor and donor channel lengths of 65 cm each and acceptor and donor volumes of 0.8 ml each, was used as the flat membrane dialysis unit.

The hollow-fibre membrane dialysis unit was constructed from 15 000-dalton molecular-weight cut-off cellulose acetate-based dialysis fibre which were cut from an Organon (Turnhout, Belgium) Nephross Allegro HF artificial kidney. Each fibre had an I.D. of 200 μm and a membrane thickness of 6.5 μm, and 105 fibers were glued into two fittings with Bindulin (Fürth, Germany) silicone glue. The average fibre length accessible for dialysis was about 10 cm. For use, the dialysis unit was inserted into a 25- or 30-ml sample vial which was equipped with a magnetic stirrer. When not in use, the unit was stored in a solution containing 0.02% sodium azide in LC-grade water.

The set-up of the LC system used for flat membrane dialysis with immunoaffinity preconcentration is shown schematically in Fig. 1. It consisted of two Gilson (Villiers-le-Bel, France) Model 302 pumps [one for the separation column (pump 4) and one for the water dilution step (pump 3)], two

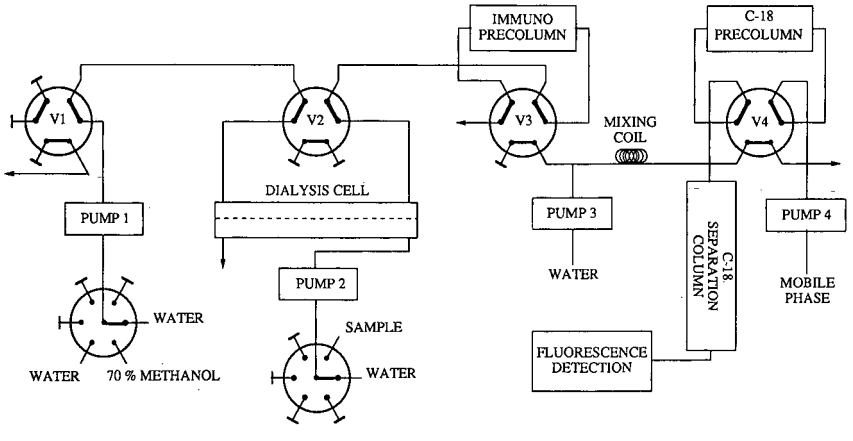

Fig. 1. Set-up of the total analytical system used for on-line dialysis/immuno preconcentration with the flat membrane dialysis unit.

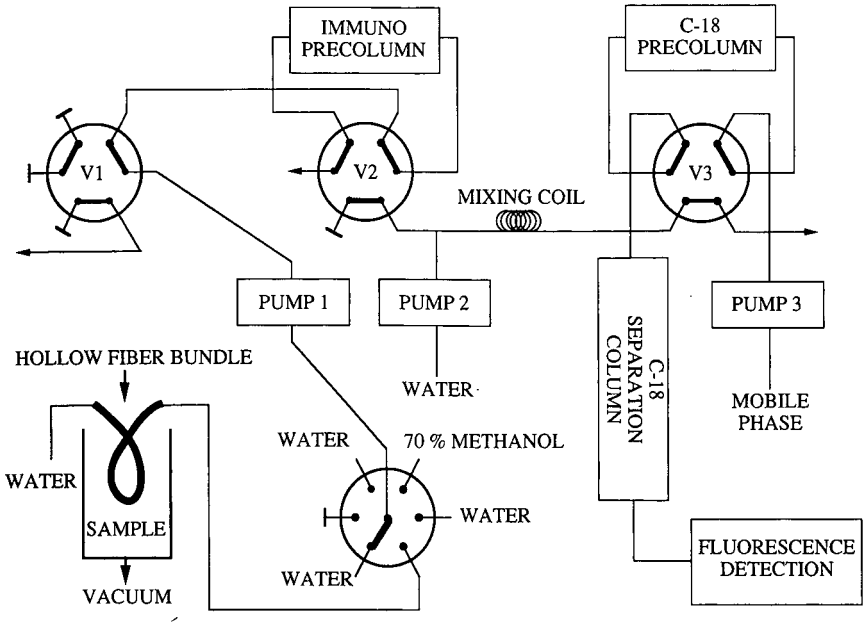

Fig. 2. Set-up of the total analytical system used for on-line dialysis/immuno preconcentration with the hollow-fibre membrane dialysis unit.

Applied Biosystems (Ramsey, NJ, USA) Spectroflow 400 pumps (pumps 1 and 2), a Spark (Emmen, Netherlands) Prospect 1.0 programmer containing the valve-switching units and the solvent-selection valves, a Perkin-Elmer (Beaconsfield, UK) LS-4 fluorescence detector (λ_{ex} = 364 nm, λ_{em} = 434 nm for aflatoxin M1; λ_{ex} = 365 nm, λ_{em} = 440 nm for all other aflatoxins) and a Kipp & Zonen (Delft, Netherlands) BD 40 recorder. The separation column was a laboratory-packed 100 mm × 3.0 mm I.D. or 200 mm × 3.0 mm I.D. glass column with 5-μm LiChrosorb RP-18 (Merck, Darmstadt, Germany), protected with a 10 mm × 2.0 mm I.D. guard column packed with the same material. The 20 mm × 3.0 mm I.D. stainless-steel C_{18} precolumn was packed with 40-μm Baker C_{18} bonded particles. The mixing coil was a stainless-steel LC capillary with an I.D. of 1.1 mm and an internal volume of 1 ml. Pumps 1 and 2 and all switching valves were computer controlled.

The set-up of the LC system used for hollow-fibre dialysis with immunoaffinity preconcentration is shown schematically in Fig. 2. It consisted of essentially the same components as the flat membrane dialysis system. The sample vial of the hollow-fibre unit was connected to an additional valve and a vacuum supply, controlled by the computer, such that the contents of the vial could be removed automatically.

Separation was performed at ambient temperature using acetonitrile–methanol–water (16:24:60 or 20:5:75, v/v/v) as the mobile phase. The flow-rate was 0.5 ml/min. The immuno precolumns were laboratory-made 10 mm × 10 mm I.D. stainless-steel columns equipped with 5-mm stainless-steel screens and PTFE rings as the column inlet and outlet.

Analytical procedures

Hollow-fibre dialysis/immuno preconcentration was performed with the set-up in Fig. 2. The time schedule of the analytical procedure is given in Table I. After placing a sample in the sample vial and preconditioning the immuno precolumn with 10 ml of water using pump 1, dialysis was started. During this process, water (as the acceptor phase) was sucked through the hollow-fibre bundle with pump 1 and subsequently pumped over the immuno precolumn for preconcentration of the analytes. Then the immuno precolumn was flushed with 5 ml of water (pump 1) to displace the remaining sample and to remove non-specifically bound impurities. Simultaneously, the C_{18} precolumn was precondi-

TABLE I

SCHEDULE OF THE ON-LINE ANALYTICAL PROCEDURE USING THE SET-UP ACCORDING TO FIG. 1

Step	Event	Valve positions[a]		
		Valve 1	Valve 2	Valve 3
1	Flushing immuno precolumn with water (20 min, 5.2 ml)	A	A	A
2	Flushing capillaries with sample	B	A	A
3	Flushing immuno precolumn with sample (4 min, 10.4 ml)	A	A	A
4	Flushing capillaries with water	B	A	A
5	Flushing immuno precolumn with water via pump 1 (2 min, 5.2 ml) and simultaneously flushing C_{18} precolumn with water via pump 2 (1 min, 4.7 ml)	A	A	B
6	Flushing capillaries with methanol–water (70:30, v/v)	B	A	B
7	Analyte desorption from immuno precolumn with methanol–water (70:30, v/v) (2 min, 0.52 ml) with subsequent dilution with water (2 min, 9.4 ml) and analyte reconcentration of the C_{18} precolumn	A	B	B
8	Desorbing C_{18} precolumn by switching on-line with separation column and flushing immuno precolumn with additional methanol–water (70:30, v/v) (0.25 min, 0.65 ml)	A	B	A
9	Flushing capillaries with water	B	A	A

[a] Position A corresponds with the valve positions shown in Fig. 1.

tioned with 5 ml of water via pump 2. Subsequently, the immuno precolumn and the C_{18} precolumn were switched in series and the immuno precolumn was desorbed with methanol–water (70:30, v/v) in the backflush mode using pump 1. The methanol–water eluate was diluted with water to a methanol content of 4% by pump 2 in order to allow preconcentration of the aflatoxins on the C_{18} precolumn. After transfer of the analytes to this precolumn, the actual separation was started by switching the C_{18} precolumn on-line with the separation column, using pump 3 for the eluent. The immuno precolumn was flushed with an additional 0.65 ml of methanol–water (70:30, v/v). Next the hollow-fibre bundle was purged with water via pump 1. At the same time the sample was removed from the vial by vacuum action and the vial and the outside of the hollow-fibre bundle were manually purged with about 100 ml of water. Finally, the sample vial was filled with the next sample, or with a sodium azide solution, if no further analysis had to be performed.

For hollow-fibre dialysis/C_{18} preconcentration the set-up according to Fig. 2 was modified such that the immuno precolumn was omitted, while V1 was directly connected to V3, that is, the acceptor stream was directly preconcentrated on the C_{18} precolumn.

For flat membrane dialysis/immuno preconcentration, the set-up according to Fig. 1 was used. The analytical procedure was the same as with hollow-fibre dialysis with immuno preconcentration, except that in place of a stagnant donor a flowing donor was used. Before analysis the capillary connecting pump 2 and the dialysis cell was disconnected from the donor inlet, purged until it was completely filled with sample and connected to the donor inlet again. This was done in order to reduce mixing effects.

For flat membrane dialysis/C_{18} preconcentration, the set-up according to Fig. 1 was modified such that the immuno precolumn was omitted, while V2 was directly connected to V4, that is, the acceptor stream was directly preconcentrated on the C_{18} precolumn.

The analytical procedures for direct preconcentration of samples on the C_{18} precolumn or on the immuno precolumn, without dialysis, have been described elsewhere [5,6].

Samples

Milk samples were freshly bought each morning, stored at 4°C and used during the same day. The samples were brought to room temperature on a water-bath 30 min before analysis; subsequently they were spiked and analysed without further pretreatment. For spiked milk samples the recovery was corrected by subtracting the amount of aflatoxin M1 found in the blank. The amount of analyte determined was calculated by peak-area comparison with a standard loop injection. As expected, blank values for aflatoxin M1 in milk were found to be 10–30 ng/ml. The identity of the aflatoxin M1 peak in the blank was confirmed by comparison of the retention time and the excitation and emission maxima with those for an aqueous standard.

The dialysis efficiency was determined as the ratio of the peak area found with dialysis to that found by direct preconcentration of the same sample, using a volume equal to the acceptor volume in the dialysis experiment (for explanation, see below).

RESULTS AND DISCUSSION

The 10 mm × 10 mm I.D. immuno precolumn allowed the preconcentration of aflatoxin M1 from aqueous standard solutions up to a volume of 30 ml with a constant recovery of about 70% (see also ref. 5). If larger volumes were preconcentrated, the recovery decreased owing to breakthrough. This implies that, for an accurate and precise performance of the final analytical procedure, the acceptor volume from the dialysis unit, which has to be preconcentrated on the immuno precolumn, should not exceed 30 ml. Consequently, the detection limit of the method will depend only on the analyte concentration which can be achieved in the acceptor phase. The ratio between the analyte concentration in this phase and the original analyte concentration in the sample (termed the dialysis efficiency in this paper) will therefore characterize the performance of the dialysis process most appropriately. If the donor and acceptor volumes are equal, the dialysis efficiency can be, at best, 0.5. However, if the donor volume is much larger than the acceptor volume, in theory a dialysis efficiency of 1.0 can be obtained. One main aim in the following experiments was to optimize the on-line dialysis processes with respect to the dialysis efficiency.

Owing to the limited availability and high cost of aflatoxin M1, the initial characterization of the dialysis units was performed with aflatoxin B2. Although the chemical structure of aflatoxin M1 is related more to aflatoxin B1 than to aflatoxin B2, the latter was used because of its higher intrinsic fluorescence sensitivity and the fact that aflatoxin B1 is toxic. Because of the much shorter analysis time, initial optimization and evaluation of on-line dialysis were performed with subsequent preconcentration on a C_{18} precolumn.

Flat membrane dialyser

Amongst the various donor–acceptor dialysis configurations (stagnant–stagnant, stagnant–flowing, flowing–stagnant and flowing–flowing), the last alternative was selected, because the expected donor and acceptor volumes far exceeded the volumes of the donor and acceptor chamber (0.8 ml each) of the unit.

Influence of dialysis time on recovery. A standard solution containing 80 ng/l of aflatoxin B2 was analysed with flat membrane dialysis and C_{18} preconcentration. The donor and acceptor flow-rates were kept constant in all experiments at 0.5 and 0.52 ml/min, respectively, using the counter-current mode. According to theory, the recovery should be constant, irrespective of the duration ot the dialysis process. This was found to be true for dialysis times of at least 10 min. As a 10-min dialysis time gave a yield of 80–90% of that obtained under steady-state conditions, this time was chosen to characterize the dialysis unit in the subsequent experiments.

Influence of donor flow-rate on dialysis efficiency. With a constant dialysis time of 10 min and a constant acceptor flow-rate of 0.52 ml/min, *i.e.*, with an acceptor volume of 5.2 ml, experiments were performed using a donor flow-rate of 0.5, 1.0 or 2.0 ml/min, *i.e.*, with donor volumes of 5.0, 10 and 20 ml, respectively. Over this range a virtual constant dialysis efficiency of 0.1 ± 0.005 was found. One can therefore expect that a further increase in the donor flow will not significantly improve the efficiency.

Influence of acceptor flow-rate on dialysis efficiency. With the same dialysis time of 10 min and a constant donor flow-rate of 0.5 ml/min (total donor volume 5 ml), the acceptor flow-rate was varied as 0.26, 0.52 and 1.3 ml/min (volumes of 2.6–13 ml).

Under these conditions, the dialysis efficiency decreased (0.11, 0.09 and 0.05, respectively). Although a further decrease in the acceptor flow-rate will certainly improve the efficiency further, such an approach is highly impractical because of the long dialysis times required for what is intended to be an on-line method.

On-line combination of dialysis and immuno preconcentration. On the basis of the above, as a compromise, a donor flow-rate of 0.65 ml/min and an acceptor flow-rate of 0.52 ml/min were chosen to combine dialysis and immunoaffinity preconcentration on-line. Of course, different flow-rates would also have been suitable; the present values were selected because of the available pump settings.

As a compromise between a short analysis time and low detection limits, a dialysis time of 20 min, corresponding to donor and acceptor volumes of 13 and of 10.6 ml, respectively, was chosen. Eleven milk samples spiked with 0–500 ng of aflatoxin M1 were analysed. The trend of a decreasing recovery with an increase in the number of analyses, clearly observed in a previous study in which no dialysis step was included in the procedure [6], was not found with the present system (*cf.*, Fig. 3). This indicates that constituents of the milk sample that adversely affect the activity of the immuno precolumn have indeed been removed. A drawback of the system is the poor reproducibility for aflatoxin M1 in spiked milk [60–100 ng/l; relative standard deviation (R.S.D.) = 12% (n = 9), possibly caused by air bubbles formed in the donor stream from time to time.

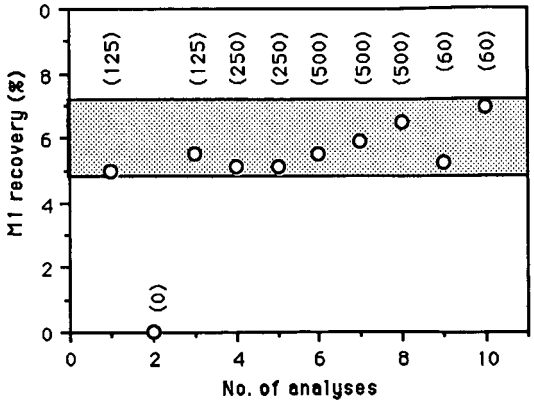

Fig. 3. Recovery as a function of number of analyses performed with the flat membrane dialysis/immunoaffinity preconcentration system. Crude milk samples were spiked with the indicated amounts of aflatoxin M1 and dialysed for 20 min, with donor and acceptor volumes of 13 and 10.6 ml, respectively.

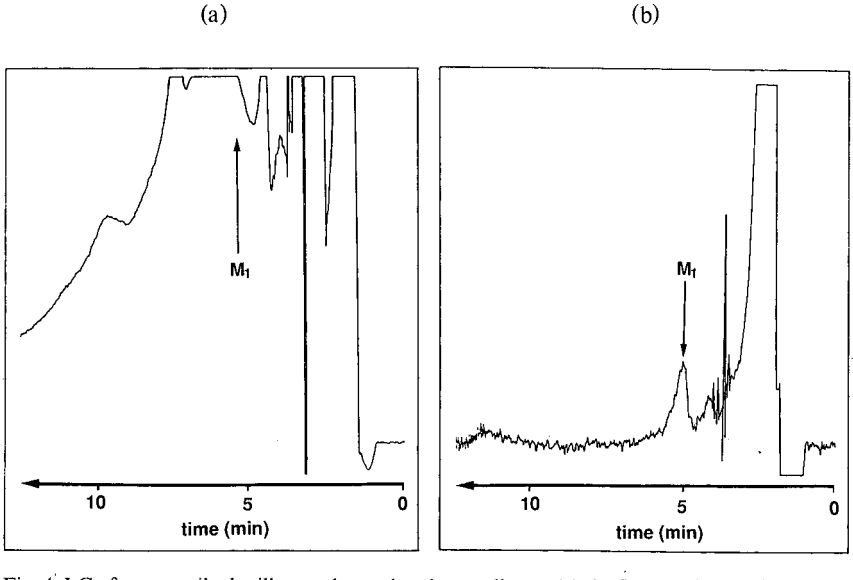

Fig. 4. LC of a non-spiked milk sample, analysed according to (a) the flat membrane dialysis/C_{18} preconcentration procedure or (b) the hollow-fibre dialysis/immunoaffinity preconcentration procedure. Donor and acceptor volumes: (a) 6.5 and 5.3 ml, respectively; (b) 26 and 21.5 ml, respectively, with the fluorescence detector set to a five times higher sensitivity.

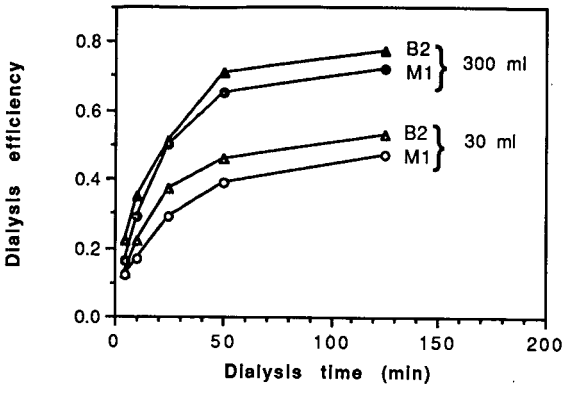

Fig. 5. Dialysis efficiency as a function of dialysis time. Acceptor volume, 25 ml. The dialysis time was varied between 5 and 125 min by adjusting the acceptor flow-rate. Plots were recorded for donor volumes of either 30 or 300 ml, containing either 30 ng/l of aflatoxin M1 or 4 ng/l of aflatoxin B2. The analyses were run according to the hollow-fibre dialysis/C_{18} preconcentration procedure. Dialysis efficiencies calculated as described under Experimental.

As was to be expected, combining dialysis with immunoaffinity sample pretreatment did not increase the selectivity of the system and similar chromatograms were obtained with and without dialysis. The high selectivity of the immunoaffinity step can be seen by comparing the chromatograms of the dialysis/immunoaffinity preconcentration and the dialysis/C_{18} preconcentration system (Fig. 4). In the latter instance, after dialysis, the sample was preconcentrated directly on a C_{18} precolumn. In both instances non-spiked crude milk samples were analysed. The aflatoxin M1 concentration in the sample was 25 ng/l. One should note the differences in sample volume and detector sensitivity with the two methods in Fig. 4. The bad peak shape for aflatoxin M1 in Fig. 4 can be explained by the poor performance of the analytical column.

Hollow-fibre dialysis unit

In order to improve the reproducibility and also the dialysis efficiency of the system, another dialysis unit was designed. The surface area of the dialysis membrane and its thickness are significant parameters which determine the speed of the dialysis process. Improvement of either parameter with the flat membrane dialyser is technically difficult. We therefore evaluated the use of hollow-fibre membranes, which are very stable and easy to handle, although they have a membrane thickness of only between 5 and 10 μm.

The construction and design of the hollow-fibre membrane dialyser are described under Experimental. The overall membrane area available for dialysis was calculated to be 60–70 cm^2, which is about 50 times larger than that with the flat membrane dialyser. Because of the hollow-fibre bundle design, stagnant donor-flowing acceptor dialysis, with the inner fibre volume flushed by the acceptor phase and the bundle inserted in the sample solution, seemed most appropriate for analysis.

Dialysis efficiency. The efficiency of the hollow-fibre dialysis unit was determined using the hollow-fibre dialysis/C_{18} preconcentration system (see Experimental). In Fig. 5 the dialysis efficiency is displayed as a function of the dialysis time. In all experiments the acceptor volume was held constant at 25 ml. The dialysis time was varied between 5 and 125 min by adjusting the acceptor flow-rate. All four plots show a steep initial rise, a plateau being reached for dialysis times of over about 50 min. This means that, for an on-line analytical system, dialysis times between 10 and 500 min are a good compromise between short analysis time and high recovery.

Fig. 5 also demonstrates that the dialysis efficiency depends on the sample volume (stagnant donor volume) used. Using, *e.g.*, a 300-ml instead of 30-ml donor volume, gives a dialysis efficiency of 0.65 instead of 0.39 for aflatoxin M1 and of 0.71 instead of 0.46 for aflatoxin B2 (dialysis time 50 min). Actually, with an infinitely large donor volume, the dialysis efficiency will reach a plateau value of 1.0.

It should be obvious that, with a larger donor volume, a higher concentration gradient between the donor and acceptor phases and hence a higher transfer rate of analytes can be achieved, that is, the amount of analytes transferred will be higher. Consequently, although the recovery will decrease, the detection limit will improve, as the absolute amount of analyte which is extracted from the increased sample volume will be larger.

Finally, from Fig. 5 one can read that a 30-ml donor volume dialysed for 20 min with a total acceptor volume of 25 ml will give a dialysis efficiency for both aflatoxins tested of about 0.3. This is three times better than with the flat membrane dialysis unit.

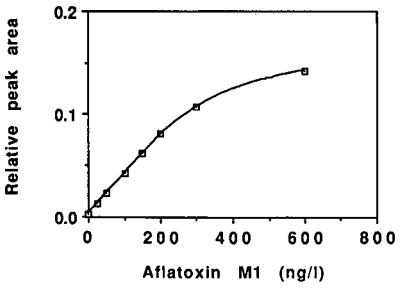

Fig. 6. Calibration graph recorded with milk samples spiked with aflatoxin M1. Crude untreated milk samples were analysed according to the hollow-fibre dialysis/immunoaffinity preconcentration procedure. Donor and acceptor volumes, 25 ml each.

On-line hollow-fibre dialysis/immuno preconcentration: analytical data

A donor volume of 25 ml was adopted, as a vial of this size was available which was suitable for magnetic stirring and had a proper fitting at the bottom, which could be used for automated removal of sample solutions via a vacuum supply.

Standard samples. A calibration graph was constructed using aqueous standard samples containing 10–300 ng of aflatoxin M1 (dialysis time 20 min; acceptor volume 25 ml). The graph was linear in this range (r = 0.9993; n = 6). The recovery found was 20% for aqueous samples.

Spiked milk samples. As with the aqueous solutions, spiked milk samples were analysed without any prior sample pretreatment. The calibration graph (Fig. 6) for aflatoxin M1 was linear (r = 0.9998; n = 6) up to 200 ng/l of analyte. The recovery with milk samples was, however, distinctly lower (6%; R.S.D. = 3%, n = 5) than with spiked water samples (20%). The lower recovery is probably due to analyte–protein interactions which occur in milk samples. Although this recovery is low, it is not a problem during the analysis of real samples because relatively large sample volumes can be processed with a repeatability of *ca.* 3%. Under the conditions used (25-ml samples), the detection limit for aflatoxin M1 in milk was 10 ng/l (signal-to-noise ratio = 3:1). Increasing the sample volume to 300 ml will improve the detection limit by almost a factor of two (*cf.*, Fig. 5). Another method to improve the detection limit, without increasing the analysis time, is to use a hollow-fibre bundle which contains more fibres. Actually, a bundle containing four times more fibres can still be placed in the present

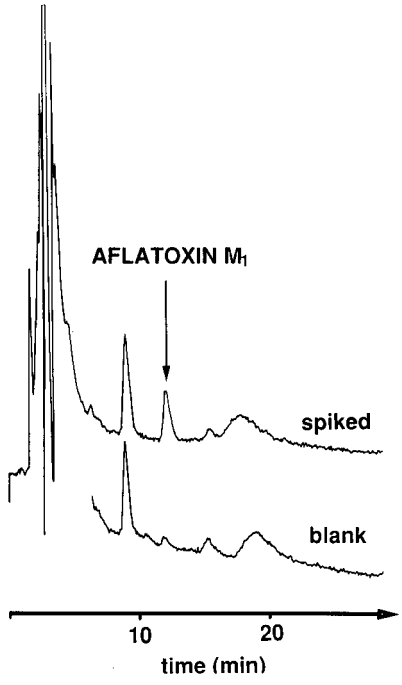

Fig. 7. LC of a crude milk sample spiked with 50 ng/l of aflatoxin M1, and the corresponding blank. Hollow-fibre dialysis/immunoaffinity preconcentration was performed with donor and acceptor volumes of 25 ml each. Mobile phase, acetonitrile–methanol–water (20:5:75, v/v/v). For further details, see Experimental.

25-ml sample vial without affecting the stirring efficiency of the sample.

Chromatograms of a crude milk sample spiked with 50 ng/l of aflatoxin M1 and of the corresponding blank are shown in Fig. 7. The hollow-fibre dialysis/immunoaffinity preconcentration was performed with donor and acceptor volumes each of 25 ml. The aflatoxin M1 level found in the blank sample corresponded to the detection limit of the method of 10 ng/l. With the initial mobile phase of acetonitrile–methanol–water (16:24:60, v/v/v) an interfering peak coincided with the aflatoxin M1 peak. When acetonitrile–methanol–water (20:5:75, v/v/v), was used the two peaks could be separated efficiently, as is evident from Fig. 7. Detailed study showed that the peak at a retention time of 9 min is not due to aflatoxin B1, B2, G1, G2, M2, P1 or Q1, but is probably caused by the silicone glue used in the dialysis unit. The peak with the same retention time as aflatoxin M1 in the blank is probably due to an interferent dissolved from the dialysis membrane by milk constituents.

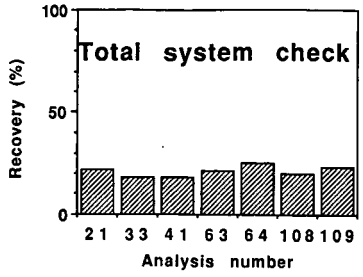

Fig. 8. Recovery as a function of the number of analyses performed with the same anti-aflatoxin immuno precolumn according to the hollow-fibre dialysis/immunoaffinity preconcentration procedure. Each data point corresponds to the analysis of a standard solution containing 300 ng/l of aflatoxin M1. For further explanation, see text.

The initial aim of installing a dialysis unit was to increase the lifetime of the immuno precolumn. As already indicated by the good reproducibility of the recoveries obtained with spiked milk samples, the immuno precolumn indeed showed good stability. For further confirmation, the performance of the immuno precolumn was checked regularly by analysing a standard solution containing 300 ng/l of aflatoxin M1 using the hollow-fibre dialysis/immunoaffinity preconcentration procedure. As this analyte amount was close to the total capacity of the immuno precolumn (*cf.*, Fig. 6), deactivation of the immuno precolumn should certainly lead to a decrease in recovery. Fig. 8 shows the recoveries found with the control experiments. No significant decrease in the capacity was observed during 109 runs performed with the same immuno precolumn. About 70% of all runs were used to analyse crude milk samples, and the remaining 30% for constructing calibration graphs and performing the control experiments. In other words, at least 70 milk analyses can be performed with a single immuno precolumn. Also, the hollow-fibre unit did not noticeably deteriorate owing to, *e.g.*, fouling or clogging of the membrane, during the stated number of analyses. This is a useful advantage of the present method over that of Tuinstra *et al.* [9], who had to use defatted milk in their on-line dialysis/C_{18} preconcentration system.

CONCLUSIONS

A flat membrane dialysis unit (flowing donor–flowing acceptor dialysis) and laboratory-made hollow-fibre dialysis unit (stagnant donor–flowing acceptor dialysis) were both coupled on-line to an immunoaffinity sample pretreatment LC system. With both systems overall recoveries of 6% were achieved for aflatoxin M1 in milk (dialysis time 220 min). Because the sample volume was about double with the hollow-fibre system, the detection limit was correspondingly lower. In addition, with milk samples the hollow-fibre system showed a better reproducibility of 3% R.S.D. compared with 12% for the flat membrane system. Both systems allowed the repeated analysis of milk samples without exchanging the immuno precolumn. With the hollow-fibre system, over 70 milk samples were analysed without observing any decrease in performance. The capacity of the immuno precolumn and the dialysis efficiency of the hollow-fibre unit remained constant during these runs, and no fouling or blocking of the dialysis membrane was observed.

The results demonstrate the applicability of the hollow-fibre system for the trace-level determination of aflatoxin M1 (detection limit 10 ng/l) in untreated milk. For unattended analysis, full automation of the system can be achieved by using an inexpensive peristaltic pump to flush the hollow-fibre dialysis unit.

ACKNOWLEDGEMENT

This work was supported by the Dutch Foundation for Technical Science, Grant No. 46.0616.

REFERENCES

1 M. J. Shepherd, M. Holmes and J. Gilbert, *J. Chromatogr.*, 354 (1986) 305–312.
2 N. Takeda, *J. Chromatogr.*, 288 (1984) 484–488.
3 D. N. Mortimer, J. Gilbert and M. J. Shepherd, *J. Chromatogr.*, 407 (1987) 393–398.
4 M. Sharman, A. L. Patey and J. Gilbert, *J. Chromatogr.*, 474 (1989) 457–461.
5 A. Farjam, N. C. van de Merbel, H. Lingeman, R. W. Frei and U. A. Th. Brinkman, *Int. J. Environ. Anal. Chem.*, in press.
6 A. Farjam, R. de Vries, H. Lingeman and U. A. Th. Brinkman, *Int. J. Environ. Anal. Chem.*, 44 (1991) 175–184.
7 A. Farjam, A. E. Brugman, H. Lingeman and U. A. Th. Brinkman, *Analyst (London)*, 116 (1991) 891–896.
8 A. Farjam, G. J. De Jong, R. W. Frei, U. A. Th. Brinkman, W. Haasnoot, A. R. M. Hamers, R. Schilt and F. A. Huf, *J. Chromatogr.*, 452 (1988) 419–433.
9 L. G. M. Th. Tuinstra, P. G. M. Kienhuis, W. A. Traag, M. M. L. Aerts and W. M. J. Beek, *J. High Resolut. Chromatogr.*, 12 (1989) 709–713.

Journal of Chromatography, 589 (1992) 151–158
Elsevier Science Publishers B.V., Amsterdam

CHROM. 23 664

Optimization of an ion-exchange high-performance liquid chromatographic method for the determination of carboxylic acids, sugars, glycerol and ethanol in wines

M. Calull, E. López, R. M. Marcé, J. C. Olucha and F. Borrull*

Departament de Química, Universitat de Barcelona, Pça. Imperial Tarraco 1, 43005 Tarragona (Spain)

(First received April 24th, 1991; revised manuscript received June 18th, 1991)

ABSTRACT

Optimization of ion-exchange high-performance liquid chromatography with refractive index detection of major carboxylic acids, sugars, glycerol and ethanol in wines was carried out by using a super-modified simplex method and a modelling response surface method. A modification of the CRF criterion (chromatographic response function) for selectivity optimization was used, including different weighting factors for each pair of peaks (VCP criterion; variable coefficient parameters).

INTRODUCTION

The traditional method for the determination of carboxylic acids involves individual enzymatic analysis, but is time consuming and tedious. To overcome these drawbacks, high-performance liquid chromatography (HPLC) has recently been applied to the determination of organic acids in wines.

Several HPLC methods are in current use including reversed-phase chromatography [1–12] and ion-exchange chromatography with either strong cation- or weak anion-exchange resins [13–18]. Two principal methods are based on the first technique, the direct method, with detection at 210 nm [2,3,9, 11] or refractive index detection [1,10], and the derivatization method, using different reagents such as phenacyl [5,6,12], *p*-nitrophenyl [4] or *p*-nitrobenzyl [7] bromide with detection at 254 nm.

When ion chromatography is used, separation is usually carried out with a polymeric cation exchanger in the hydrogen form, where the primary mechanism for the separation of acids is ion exclusion at the pH used. Detection is carried out with a UV detector [13,14,17] in order to eliminate the interference from sugar, or with an IR detector [13,17,18], which can only be applied to dry wines.

When ion-exclusion HPLC with IR detection is applied to a dry wine, the method determines major carboxylic acids, most sugars (glucose and fructose), glycerol and ethanol, all of them important enological parameters, very rapidly. For the simultaneous determination of major carboxylic acids, sugars, glycerol and ethanol in wines, different mobile phases (dilute acids), column temperatures and flow-rates have been used by several workers [13,14, 16–18]. The aim of this study was to optimize the chromatographic conditions for the determination of these compounds.

Two main approaches have been described for the optimization process, sequential and simultaneous techniques [19]. Both have been used in HPLC optimization and their advantages and drawbacks have been described [20–21]. The super-modified sequential simplex method [23,24] and the simultaneous modelling of the response surface method [20,21] were used to optimize the chromatographic parameters, pH and flow-rate of the mobile phase and column temperature.

A computer program allows us to select the

0021-9673/92/$05.00

model, compute the coefficients from the experimental data and, after validation of the selected equation, indicate the experimental conditions corresponding to the best response, and to display the response surface calculated. The parameter space chosen to model the response surface was the same as that used for the simplex method.

To carry out the optimization method, it is necessary to define the criterion to be maximized [21,22]. First, the *CRF* criterion (chromatographic response function) was used, but the characteristics of this analysis forced us to modify this criterion and introduce a new criterion, *VCP* (variable coefficient parameters), with weighting factors for each pair of peaks in the resolution term and the number of peaks appearing in the chromatogram.

EXPERIMENTAL

Equipment

A Shimadzu Model LC-9A pump and a Shimadzu RID-6A detector were used. The chromatographic separation was carried out with an ION-300 (300 × 7.8 mm I.D.) column containing a polymeric cation exchanger in the hydrogen form, with an Ion Guard GC-801 column (Interaction).

Reagents and standards

Standard solutions of the major carboxylic acids found in wine (tartaric, lactic, malic, acetic, citric and succinic acids) (Aldrich), glucose, fructose, glycerol and ethanol (all of analytical-reagent grade; Merck) were prepared in water to provide a concentration of 250 ppm, except for the ethanol, which was prepared at 500 ppm.

The mobile phase was prepared with sulphuric acid (Merck) at different concentrations. All solutions were prepared with ultra-pure water obtained with a Milli-Q purification system (Millipore). All standards and solvents were filtered with 0.45-μm membrane.

RESULTS AND DISCUSSION

To carry out the optimization process it was necessary to define the variables to be optimized and their parameter spaces. The temperature of the column, the concentration of the sulphuric acid in the mobile phase and the flow-rate were chosen. The parameter spaces were determined from bibliographic data and the instrumental limitations.

The range of temperatures chosen was between 30°C (10°C higher than room temperature) and 80°C (maximum temperature recommended for the column used). The recommended eluent for the column was sulphuric acid diluted to between 0.01 and 0.05 *N*. Other strong acids, such as perchloric and nitric acid, can be used, but halide-containing acids, such as hydrochloric acid, are not recommended owing to their corrosive effect on stainless steel. The recommended eluent flow-rate for the ION-300 column is 0.1–0.6 ml/min. Higher flow-rates are not possible because of the increase in the pressure of the column, and for the ION-300 150 atm must not be exceeded.

When the parameter space had been defined, the super-modified simplex method and the modelling surface response method were used to determine the optimum conditions.

Simplex method

The sequential super-modified simplex method [23,24] was used. This version offers some advantages over the modified simplex method [25]. It has the ability to change its size and orient itself to fit a response surface by second-order and Gaussian estimation of the position of an optimum vertex from the previously obtained response. The criterion used to stop the simplex optimization was the coefficient of variation (COV), the relative standard deviation of the response, in the simplex expressed as a percentage of the mean response.

Before applying the method, it was necessary to determine the criterion to be maximized. In the present work the *CRF* criterion was selected [20], and the expression used was:

$$CRF = a \sum_{i=1}^{n} (R_{i+1,i}) + b(t_m - t_l)$$

where a and b are the weighting factors, R_i the resolution value between two adjacent peaks, t_m is the maximum desired analysis time and t_l the retention time of the last peak.

If the same importance is given to two terms, the weighting factors have to be $a = b = 1$. In this instance the simplex method goes to conditions with a low COV value (0.58%) after 22 experiments, but under these conditions a poor resolution was obtain-

ed for a pair of peaks. Under these conditions, only one peak appears for malic acid and fructose whereas good resolution between the remainder of the peaks can be observed. In this criterion the resolution values between peaks 5–6, 8–9 and 9–10 were not taken into account in the optimization process because peak pairs with a resolution higher than 3 for all the experimental conditions have not been considered. When very different values of the resolution are obtained in the chromatogram, it is necessary not to consider the best resolved peaks in order to increase the importance of the resolution values corresponding to the less resolved peaks in the global criterion.

In order to increase the importance of the resolution term compared with the analysis time term, some different weighting factor values were studied and finally of $a = 1$ and $b = 0.3$ were considered in the CRF criterion. Under the optimum conditions, the resolution between fructose and malic acid improves at the expense of analysis time, but good resolution is not yet obtained.

Ten peaks appear in the optimization analysis, three of which have poor resolution (glucose, malic acid and fructose), depending on the experimental conditions; sometimes the worst resolution was between glucose and malic acid and sometimes it was between malic acid and fructose and the ethanol peak with a high retention time and very separated from the remainder of the peaks. In this instance, greater importance was given to increasing the resolution between these two badly resolved peaks than was given to other peaks.

To increase the importance of the resolution term between the different peaks, a new coefficient was introduced in the CRF expression, similar to that used by Glajch *et al.* [26] in the COF criterion.

$$\mathrm{COF} = \sum_{i=1}^{n} a_i \ln(R_i/R_{i,\mathrm{d}}) + b(t_\mathrm{m} - t_1)$$

where R_i is the resolution for the ith pair of peaks, $R_{i,\mathrm{d}}$ is the desired resolution for the ith pair and a_i is a weighting parameter for each pair of peaks.

The weighting factor c_i was included such that the separation between each pair of peaks could be made larger or smaller. On the other hand, another term for the number of peaks (n) is introduced to force the appearance of the maximum number of peaks in the chromatogram.

The global criterion VCP including the previous mentioned modification is expressed as:

$$VCP = a \sum_{i=1}^{n} c_i R_{i+1,i} + b(t_\mathrm{m} - t_1) + n$$

This criterion implies the identification of each peak in the chromatogram and the absence of crossovers.

This criterion was used to develop the simplex method with values of the weighting factors of $a = 1$ and $b = 0.6$ (to increase the importance of the resolution term compared with the time term); coefficient values of $c_i = 3$ for the pairs of peaks 2–3, 3–4 and 4–5, $c_i = 1$ for the pairs of peaks 1–2, 6–7 and 7–8 and $c_i = 0$ for the pairs of peaks 5–6, 8–9 and 9–10 were chosen for this experiment. The maximum analysis time was established as 25 min.

Under these conditions the simplex method was developed and after eighteen experiments (Table I) (COV 1.2%) the optimum conditions were obtained in experiment number 15 as follows: concentration of the sulphuric acid in the mobile phase 0.01 N, temperature of the column 71°C and flow-rate 0.572 ml/min.

In Fig. 1 the simplex movements can be observed. The initial simplex is shown as a dotted line, and the lines describe the different movements (the contractions are not shown). The different experimental points quickly lead to a low value of the concentration of the sulphuric acid in the mobile phase, and then the different movements lead to a high value of the variables y and z, temperature and flow-rate, respectively.

The chromatogram obtained under these conditions is shown in Fig. 2, where the best resolution between the peaks of the glucose, malic acid and fructose can be observed with an analysis time of less than 25 min.

Modelling response surface method

This simultaneous method allows the optimization of different experimental parameters knowing the influence of each parameter on the response. The parameter space chosen to model the response surface was the same as that used for the simplex method. The experimental design shown in Fig. 3 was selected in this study in order to obtain a correct modelling of the response surface.

A third-order linear model with interaction was

TABLE I

EXPERIMENTAL POINTS WHEN THE SIMPLEX METHOD IS DEVELOPED USING THE *VCP* CRITERION

Vertex No.	Variable			Response (*VCP*)	COV (%)
	H_2SO_4 concentration (*N*)	Temperature (°C)	Flow-rate (ml/min)		
1	0.010	30	0.300	1.93	
2	0.048	42	0.371	9.97	
3	0.019	77	0.371	16.04	
4	0.019	42	0.583	11.31	
5	0.038	65	0.512	12.98	
6	0.031	56	0.459	12.13	17.21
7	0.014	71	0.547	21.42	28.78
8	0.026	80	0.424	19.98	
9	0.024	75	0.463	16.55	21.77
10	0.011	80	0.415	21.21	
11	0.017	77	0.439	20.97	12.71
12	0.016	77	0.507	21.23	3.15
13	0.017	77	0.473	21.10	
14	0.010	74	0.523	22.00	1.78
15	0.010	71	0.572	22.02	
16	0.010	68	0.600	21.85	
17	0.014	70	0.600	21.34	
18	0.014	72	0.558	21.23	1.20

selected as the equation to relate the response R to the flow-rate and pH of the mobile phase and to the temperature of the column parameters:

$$VCP = axyz + bx^2 + cy^2 + dz^2 + exy^2 + fxz^2 + gyz^2 + hx + iy + jz + k$$

where $a, b, c, \ldots, j$ are the coefficients to be evaluated, x is the concentration of the sulphuric acid, y is the temperature of the column and z is the flow-rate of the mobile phase.

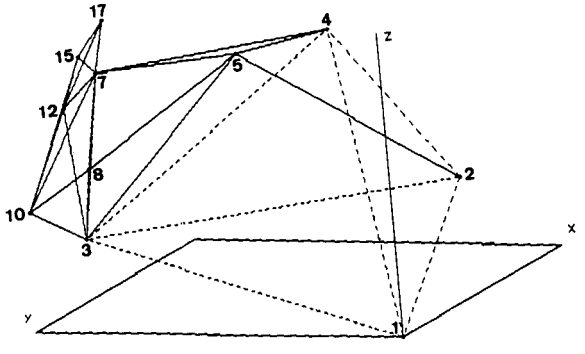

Fig. 1. Movements of the simplex method when the *VCP* criterion is used.

After the experiments, the values of the different coefficients were as follows: $a = -4.21$, $b = -1831.66$, $c = -0.01$, $d = 224.20$, $e = \cdot.70$, $f = 201.38$, $g = -0.10$, $h = 76.02$, $i = 1.21$, $j = -183.55$ and $k = 11.62$. These parameters were calculated by a simplex method and the value to be minimized is the sum of the residual square between the calculated values and the theoretical values, $\Sigma(R_{calc} - R_{theo})^2$. The results were obtained with a $\Sigma(R_{calc} - R_{theo})^2 = 19.55$, an acceptable value for this method with the number of experiments carried out. The different values obtained are given in Table II.

To obtain a graphic representation of the response of the variables to be optimized, it was necessary to fix one variable and to represent the response of the other two. In Fig. 4 the representation of the response of the temperature and concentration of the sulphuric acid on the mobile phase at a constant flow-rate of 0.6 ml/min can be seen. Fig. 4 shows that the temperature is a more impor-

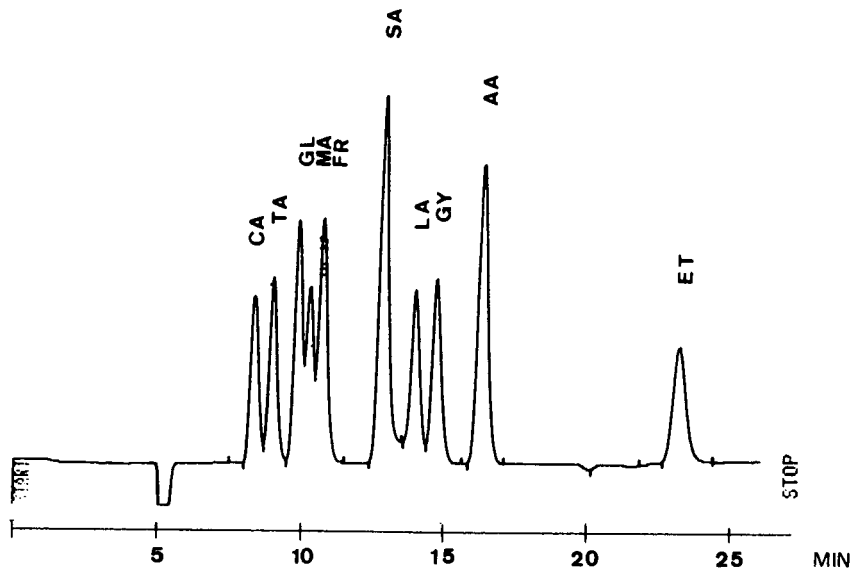

Fig. 2. Chromatogram of a standard solution under the optimum conditions chosen with the simplex method when the *VCP* criterion is used. Temperature, 71°C; flow-rate, 0.572 ml/min; concentration of sulphuric acid in the mobile phase, 0.01 *N*. CA = citric acid; TA = tartaric acid; GL = glucose; MA = malic acid; FR = fructose; SA = succinic acid; LA = lactic acid; GY = glycerol; AA = acetic acid; ET = ethanol.

tant variable than the concentration of sulphuric acid in the mobile phase, and the maximum response was obtained at a low concentration (with a low importantce of this variable in this region) and a high value of the temperature, near 70°C.

Fig. 5 shows the variation of the response surface in front of the temperature and the flow-rate at a concentration constant of 0.026 *N*. In this instance, a major importance of the variable temperature compared with the variable flow-rate is observed. The

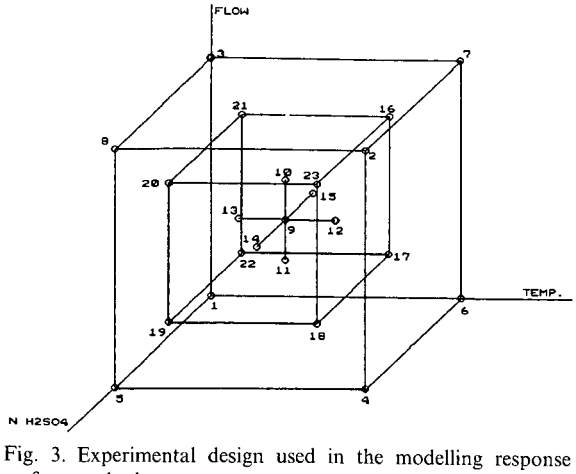

Fig. 3. Experimental design used in the modelling response surface method.

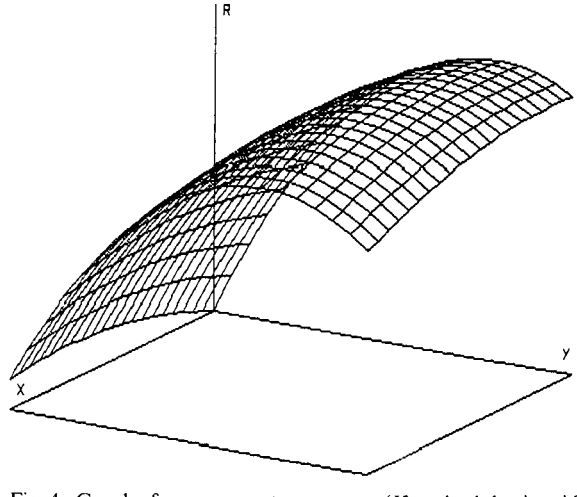

Fig. 4. Graph of response *vs.* temperature (*Y*) and sulphuric acid concentration (*X*) in the mobile phase at a flow-rate of 0.572 ml/min.

TABLE II

EXPERIMENTAL POINTS USED WITH THE MODELLING RESPONSE SURFACE METHOD

Expt. No.	Variable			R_{theo}	R_{calc}	$R_{calc} - R_{theo}$
	H_2SO_4 concentration (N)	Temperature (°C)	Flow-rate (ml/min)			
1	0.010	30	0.300	5.15	5.87	−0.72
2	0.050	80	0.600	21.18	19.92	1.26
3	0.010	30	0.600	11.37	10.64	0.73
4	0.050	80	0.300	17.96	18.93	−0.97
5	0.050	30	0.300	7.57	6.26	1.31
6	0.010	80	0.300	19.56	19.65	−0.09
7	0.010	80	0.600	20.86	22.65	−1.40
8	0.050	30	0.600	10.69	11.94	−1.24
9	0.030	55	0.450	15.47	15.25	0.23
10	0.030	55	0.525	16.45	17.39	−0.94
11	0.030	55	0.375	14.04	15.63	−1.60
12	0.030	68	0.450	16.17	16.85	−0.38
13	0.030	42	0.450	11.65	11.09	0.56
14	0.040	55	0.450	9.68	10.06	−0.38
15	0.020	55	0.450	17.96	18.74	−0.77
16	0.018	70	0.540	20.78	19.57	1.20
17	0.018	70	0.360	12.98	13.01	−0.02
18	0.042	70	0.360	18.30	17.45	0.85
19	0.042	40	0.360	13.15	12.72	0.44
20	0.042	40	0.540	19.23	17.88	1.35
21	0.018	40	0.540	9.42	10.21	−0.79
22	0.018	40	0.360	16.18	15.15	1.03
23	0.042	70	0.540	15.42	14.98	0.44
				$\Sigma(R_{calc} - R_{theo})^2 =$		19.55

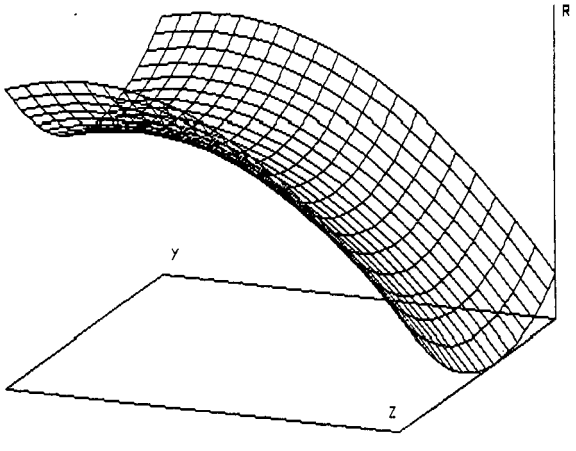

Fig. 5. Graph of response vs. temperature (Y) and flow-rate (Z) at a sulphuric acid concentration of 0.026 N.

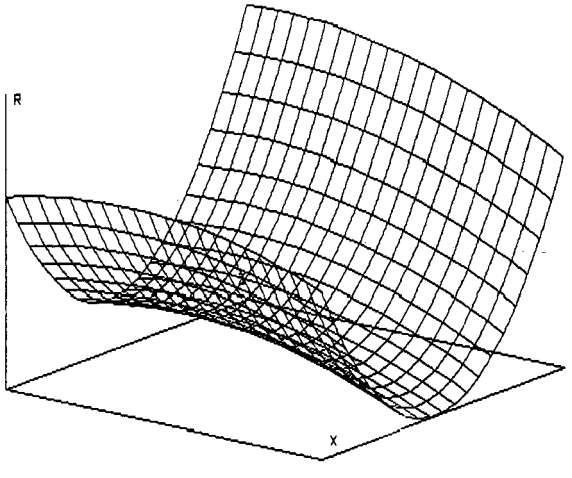

Fig. 6. Graph of the response vs. flow-rate (Z) and sulphuric acid concentration in the mobile phase (X) at a temperature of 74°C.

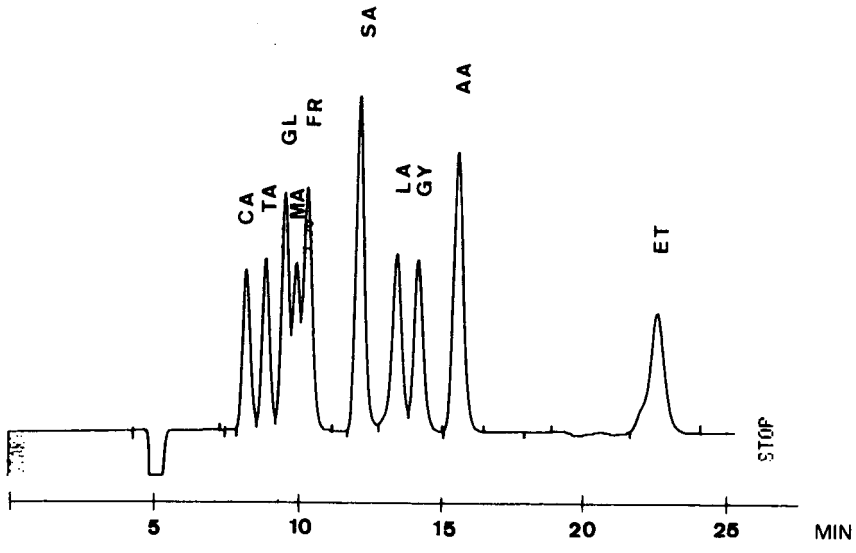

Fig. 7. Chromatogram of a standard solution under the optimum conditions. Temperature, 74°C; flow-rate, 0.6 ml/min; sulphuric acid concentration in the mobile phase, 0.026 *N*. Abbreviations as in Fig. 2.

best results were obtained at high temperature and extreme values of the parameter space for the flow-rate.

In Fig. 6, the influence of the flow-rate and concentration of sulphuric acid at constant temperature on the response can be observed. Similar results were obtained to those in the Fig. 5, the best results at a low or a high flow-rate and a small influence of the concentration of the sulphuric acid parameter, better at low concentrations. Although good results

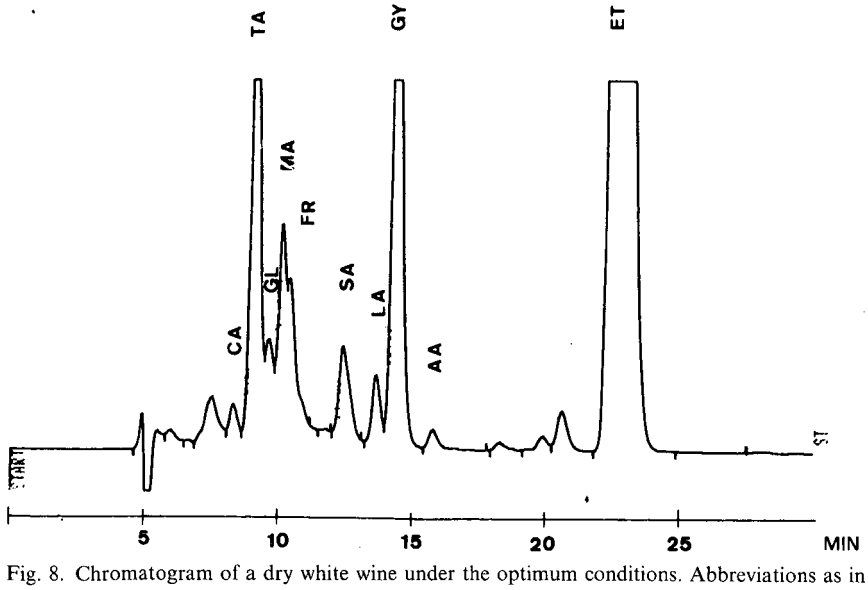

Fig. 8. Chromatogram of a dry white wine under the optimum conditions. Abbreviations as in Fig. 2.

are obtained at low and high values of flow-rate, the best response corresponds to high values of the flow-rate, as in the Fig. 5.

The optimum values of the parameters were a temperature near 70°C, a high flow-rate and a low concentration of sulphuric acid in the mobile phase. The optimum conditions considered were temperature 74°C, flow-rate 0.600 ml/min and concentration of sulphuric acid 0.026 *N*. The chromatogram obtained with these conditions is shown in Fig. 7. The results obtained with the simplex method and the modelling response surface method were similar and no important differences can be observed between the two chromatograms despite the different sulphuric acid concentrations, mainly owing to the small influence of this parameter.

The above chromatographic conditions were applied to determine these compounds in a white wine and the results obtained are shown in Fig. 8.

CONCLUSIONS

The simplex method and the modelling response surface method were used to optimize the different variables in an ion-exchange process. A modification of the *CRF* criterion was used as the parameter to be maximized in the separation of the carboxylic acids, sugars, glycerol and ethanol in wine samples.

The *VCP* criterion can be applied when highly different resolution values are found between the various peak pairs in the chromatographic separation. This criterion increases the importance of the badly resolved peaks in resolution terms.

REFERENCES

1 M. C. Polo, F. Barahona and I. Cáceres, *Connais. Vigne Vin*, 3 (1986) 175.
2 D. Tusseau and C. Benoit, *J. Chromatogr.*, 395 (1987) 323.
3 D. Blanco, M. J. Moran, M. D. Gutiérrez and A. Sanz, *Chromatographia*, 24 (1987) 347.
4 E. Grushka, H. D. Durts and J. Kikta, *J. Chromatogr.*, 112 (1975) 673
5 E. Mentasti, M. C. Gennaro, C. Sarzanini, C. Barochi and M. Savigliano, *J. Chromatogr.*, 322 (1985) 177.
6 F. Caccamo, G. Carfagnini, A. Di Corcia and R. Samperi, *J. Chromatogr.*, 362 (1986) 47.
7 W. Steiner, E. Muller, D. Frohlich and R. Battaglia, *Mitt. Geb. Lebensmittelunters Hyg.*, 75 (1984) 37.
8 P. Symonds, *Ann. Nutr. Aliment.*, 32 (1978) 957.
9 R. Schwarzenbach, *J. Chromatogr.*, 251 (1982) 339.
10 C. Droz and H. Tanner, *Schweiz. Z. Obst- Weinbau*, 118 (1982) 434.
11 R. M. Marcé, M. Calull, R. M. Manchobas, F. Borrull and F. X. Rius, *Chromatographia*, 29 (1990) 54.
12 R. M. Marcé, M. Calull, F. Borrull and F. X. Rius, *Am. J. Enol. Vitic.*, 41 (1990) 289.
13 R. F. Frayne, *Am. J. Enol. Vitic.*, 37 (1986) 281.
14 A. Schneider, V. Gerbi and M. Redoglia, *Am. J. Enol. Vitic.*, 38 (1987) 151.
15 J. Haginaka, J. Wakai, H. Yadua and T. Nomura, *J. Chromatogr.*, 447 (1988) 373.
16 J. P. Goiffon, A. Blanchere and C. Reminiac, *Analusis*, 13 (1985) 218.
17 P. Pfeiffer und F. Radler, *Z. Lebens.-Unters.-Forsch.*, 181 (1985) 24.
18 J. D. McCord, E. Trousdale and D. D. Y. Ryu, *Am. J. Enol. Vitic.*, 35 (1984) 28.
19 D. L. Massart, B. G. M. Vandeginste, S. N. Deming, Y. Michotte and L. Kaufman, *Chemometrics: a Textbook*, Elsevier, Amsterdam, 1988.
20 J. C. Berridge, *Techniques for the Automated Optimization of HPLC Separations*, Wiley, Chichester, 1985.
21 P. J. Schoenmakers, *Optimization of Chromatographic Selectivity. A Guide to Method Development*, Elsevier, Amsterdam, 1986.
22 L. R. Snyder, J. L. Glajch and J. J. Kirkland, *Practical HPLC Method Development*, Wiley, New York, 1988.
23 E. Morgan, K. W. Burton and G. Nickless, *Chemometr. Intell. Lab. Syst.*, 7 (1990) 209.
24 E. Morgan, K. W. Burton and G. Nickless, *Chemometr. Intell. Lab. Syst.*, 8 (1990) 97.
25 J. A. Nelder and R. Mead, *Comput. J.*, 3 (1965) 308.
26 J. L. Glajch, J. J. Kirkland, K. M. Squire and J. M. Minor, *J. Chromatogr.*, 199 (1980) 57.

Journal of Chromatography, 589 (1992) 159–164
Elsevier Science Publishers B.V., Amsterdam

CHROM. 23 699

High-performance liquid chromatographic determination of pilocarpine hydrochloride and its degradation products using a β-cyclodextrin column

Kent D. Sternitzke, Tony Y. Fan and Danny L. Dunn*

Analytical Chemistry, Alcon Laboratories, Inc., 6201 South Freeway, Fort Worth, TX 76134-2099 (USA)

(First received April 4th, 1991; revised manuscript received August 21st, 1991)

ABSTRACT

A high-performance liquid chromatographic (HPLC) method for the determination of pilocarpine, isopilocarpine, pilocarpic acid and isopilocarpic acid was developed. A β-cyclodextrin column achieved the separation in less than 10 min. Baseline resolution of all four compounds permitted the determination of each degradation product in the presence of pilocarpine. The calibration graphs for each compound were linear, and pilocarpine degradation products could be determined without a correction for the ultraviolet detector response using a pilocarpine standard. A comparison of β-cyclodextrin separation with the USP HPLC method demonstrated similar results for pilocarpine contents in several commercial ophthalmic formulations.

INTRODUCTION

Pilocarpine hydrochloride is a miotic (cholinergic) used to control intraocular pressure [1]. Because of its widespread use for the treatment of glaucoma, much effort has been made to develop methods to determine this drug and its degradation products.

The degradation routes of pilocarpine are shown in Fig. 1. Pilocarpine (**I**) can undergo degradation by either epimerization to isopilocarpine (**II**) or hydrolysis to pilocarpic acid (**III**) [2]. Isopilocarpine can degrade further to isopilocarpic acid (**IV**). Competition between the degradation routes is dependent on both pH and temperature [3–7]. Because all three degradation products show decreased cholinergic activity, it is desirable to determine pilocarpine in the presence of the degradation products in ophthalmic formulations. Determination of the degradation products is also often desirable to acquire information concerning product stability and demonstrate material balance.

A variety of methods have been applied to the determination of pilocarpine in ophthalmic solutions, including ^{13}C NMR [6,7], spectrophotometry and polarimetry [8,9] and gas chromatography [10]. However, high-performance liquid chromatography [HPLC] has proved to be the most sensitive and selective technique for the accurate determination of pilocarpine and small amounts of degradation products [11–20].

Many studies have dealt with the HPLC of pilocarpine, utilizing a wide selection of stationary and mobile phases. Several methods involved octadecylsilane (C_{18}) columns with aqueous mobile phase systems [11–15]. Although some separation was attained, baseline resolution was usually not achieved, and some of the methods suffered from a high back-pressure, short column lifetime, long run times and irreproducibility. Silica columns with an aqueous phosphate buffer–methanol mobile phase have achieved some resolution of the carpines, but not sufficient to determine small amounts of isopilocarpine [16]. The use of a phenyl column resolved the carpines [17,18], but the resolution and column lifetimes were observed to be inconsistent in our

0021-9673/92/$05.00

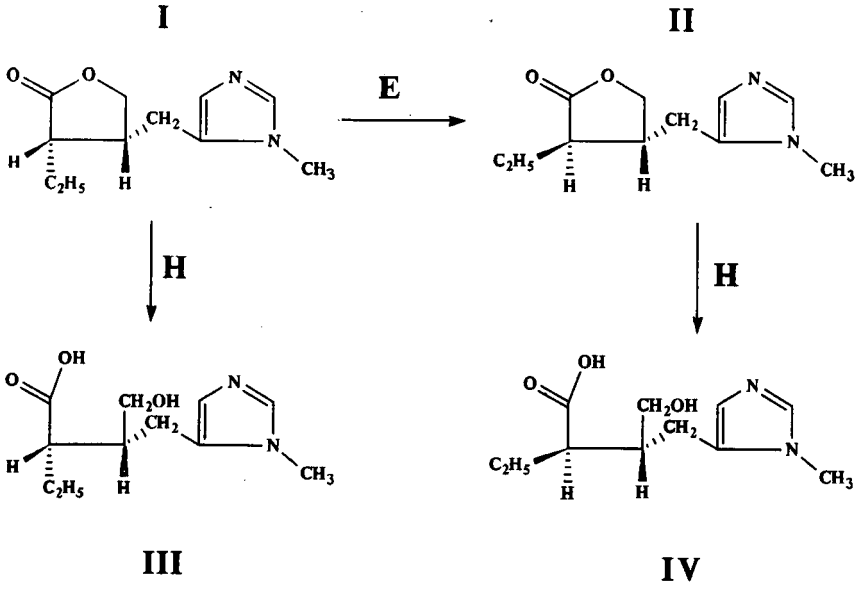

Fig. 1. Degradation reactions of pilocarpine. **I**, pilocarpine; **II**, isopilocarpine; **III**, pilocarpic acid; **IV**, isopilocarpic acid. Reactions: epimerization; H = hydrolysis.

laboratory. A recently published analysis on a cyano column gave an excellent separation, but required a mobile phase pH of 2.5 [19].

The present USP method for pilocarpine ophthalmic solution is a normal-phase system, utilizing a silica column and a mobile phase consisting of ammonia in isopropyl alcohol and hexane [20]. Although baseline resolution of the carpines is attained and column lifetimes are long, determination of the carpic acids is impossible owing to their complete retention on the HPLC column. It would be desirable to have a method that combines high resolution, determination of carpic acids and good column lifetime.

In this paper we present an improved HPLC method for the analysis of ophthalmic formulations containing pilocarpine and each of its degradation products using a β-cyclodextrin column. Baseline resolution of all four compounds is achieved in less than 10 min. Calibration graphs are given for each compound. Pilocarpine and its degradation products were determined in several commercial ophthalmic formulations and the results compared with those of the USP method.

EXPERIMENTAL

Reagents

Sodium sulfate, ammonium sulfate, pilocarpine hydrochloride and isopilocarpine nitrate were obtained from Aldrich (Milwaukee, WI, USA), phosphoric acid from J. T. Baker (Phillipsburg, NJ, USA) and HPLC-grade triethylamine from Fisher Scientific (Pittsburgh, PA, USA). Isopilocarpine hydrochloride, acquired from Inland Alkaloid (Tipton, IN, USA) was found to be a mixture of pilocarpine hydrochloride and isopilocarpine hydrochloride (42:58), and this mixture was used for evaluating chromatographic resolution. All chemicals except triethylamine were of analytical reagent grade and used as received.

Pilocarpic acid and isopilocarpic acid were prepared by dissolving the Inland Alkaloid mixture in 1 *M* sodium hydroxide solution at room temperature in a manner similar to that of Repta and Higuchi [21]. In alkaline solution, hydrolysis opens the γ-lactone ring of the carpines [16,22]. Conversion of the carpines (**I** and **II**) to the carpic acids (**III** and **IV**) was rapid (less than 1 min) and complete, as no

carpine peaks were observed in subsequent chromatograms.

Chromatography

Separations were performed isocratically on a 25 × 0.46 cm I.D. β-cyclodextrin (5 μm) column (Cyclobond I; Rainin, Woburn, MA, USA). Occasionally new β-cyclodextrin columns received from Rainin would not give baseline resolution of pilocarpine and isopilocarpine and could not be used for analytical work. The mobile phase was prepared by dissolving 40 g of ammonium sulfate and 20 ml of triethylamine in 1000 ml of water; the pH was adjusted to 4.0 by the addition of phosphoric acid. The flow-rate of a Waters (Milford, MA, USA) Model 510 HPLC pump was set at 1.0 ml/min, resulting in a back-pressure of 100 bar. AWaters WISP 710B autosampler was used to make 10-μl injections. Output from a Waters Model 486 variable-wavelength ultraviolet detector, set at 214 nm, was connected to a Waters Model 746 electronic integrator for recording data.

All dilutions to prepare samples and standards for injection were made with mobile phase. Because of its acidic pH and high ionic strength, the mobile phase was capable of dispersing a variety of ophthalmic vehicles. For instance, an ophthalmic gel could be dissolved in mobile phase without the use of additional reagents to disperse the gel matrix, thus saving a step in sample preparation. Final concentrations of pilocarpine were about 0.04 mg/ml, as this gave a reasonable signal-to-background ratio without overloading the column. At this concentration, several injections of pilocarpine were needed to equilibrate the column prior to quantitative analysis.

RESULTS AND DISCUSSION

Preliminary development

Although some separation occurred on α- and γ-cyclodextrin columns, the resolutions were not comparable to those observed on a β-cyclodextrin column for any of the mobile phases tested. Only β-cyclodextrin columns achieved baseline separation of the carpines. For instance, with the mobile phase described under Experimental, the resolution of pilocarpine and isopilocarpine was found to be 0.59, 2.25 and 0.26 on α-, β- and γ-cyclodextrin columns, respectively.

Mobile phase optimization with the β-cyclodextrin columns included adjustment of pH, ionic strength and column modifier concentration. Minimum use of organic mobile phase modifiers, such as methanol or acetonitrile, was necessary to increase retention with a concomitant increase in the separation of pilocarpine and isopilocarpine. However, tailing was severe, as is common for amine compounds in reversed-phase HPLC systems with a high aqueous content. High concentrations of triethylamine column modifier decreased tailing, but the tailing remained too excessive for baseline resolution of the carpines until the mobile phase ionic strength was increased by the addition of sodium or ammonium sulfate. The resulting decrease in tailing was accompanied by a comparatively small increase in retention time. Therefore, it was possible to attain greater resolutions with higher salt concentrations.

Chromatographic resolution

Fig. 2 presents a chromatogram of pilocarpine and its three degradation products, with the ionic strength mobile phase used for the remainder of the work presented here. The peaks in this chromatogram exhibit good symmetry, as measured by calculation of tailing factors according to the US Phar-

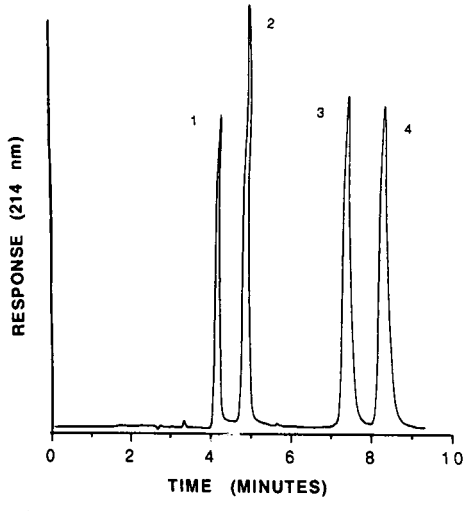

Fig. 2. Chromatogram demonstrating the separation of pilocarpine and its degradation products on β-cyclodextrin. Peaks: 1 = pilocarpic acid; 2 = isopilocarpic acid; 3 = pilocarpine; 4 = isopilocarpine.

macopeia [23]. Tailing was calculated as 1.40 for pilocarpine, 1.14 for isopilocarpine and less than 1.10 for both of the carpic acids.

Chromatographic resolution is critical in pilocarpine analysis because there is usually a small amount of degradation products in the presence of a much larger amount of pilocarpine. The resolution between pilocarpine and isopilocarpine calculated according to the US Pharmacopeia [23] was 2.25, whereas that between pilocarpic acid and isopilocarpic acid was 2.53. This is superior to any previously reported HPLC method and is sufficient to determine each species without interference.

Dynamic range

A five-point calibration graph generated for pilocarpine exhibited linear behaviour over the range 25–150% of 0.04 mg/ml, the final dilution concentration used for samples. For the calibration line, R^2 = 0.9992 and y-intercept = 0.34% of the maximum response. Hence the use of a single-point is justified. A set of ten standard replicates near 0.04 mg/ml had a relative standard deviation of 0.62%. This level of precision is sufficient to justify 0.04 mg/ml as a suitable concentration for a standard.

Stability samples of pilocarpine ophthalmic solution usually contain isopilocarpine at concentrations less than 10% of the labeled pilocarpine. In order to test the accuracy of this method for determining the isopilocarpine content of such samples, solutions were prepared with pilocarpine present at 0.04 mg/ml and isopilocarpine present at 2%, 6% and 10% of this concentration. The resulting calibration line for isopilocarpine had R^2 = 0.9998 and y-intercept = 0.15% of the maximum response. The chromatographic peak for pilocarpine does not appear to interfere with that of isopilocarpine.

Pilocarpic acid and isopilocarpic acid elute several minutes before pilocarpine and are baseline resolved from each ohter. Calibration graphs were prepared for each acid at concentrations of 1%, 3% and 5% of the 0.04 mg/ml concentration used for pilocarpine. These concentrations are typical for partially degraded ophthalmic solutions. A three-point calibration line for pilocarpic acid had R^2 = 0.9975 and y-intercept = 3.1% of the maximum response and for isopilocarpic acid R^2 = 0.9997 and y-intercept = 2.1% of the maximum response. This degree of linearity at low concentrations suggests that the acids do not interfere with each other

TABLE I

CHROMATOGRAPHIC ANALYSIS OF COMMERCIAL PILOCARPINE OPHTHALMIC FORMULATIONS: COMPARISON OF ANALYSIS ON A β-CYCLODEXTRIN COLUMN AND THE USP METHOD

Sample[a]	% of label claim				
	Pilocarpic acid[b]	Isopilocarpic acid[b]	Pilocarpine[b]	Isopilocarpine[b]	Pilocarpine[c]
Ophthalmic gel	5.7	–	105	1.5	106
Ophthalmic solutions:					
Manufacturer 1					
Lot 1	1.7	–	101	0.9	102
Lot 2	1.7	–	102	0.9	103
Lot 3	0.8	–	102	0.6	101
Manufacturer 2	2.2	–	96	0.3	96
Manufacturer 3	4.4	0.2	99	0.8	96
Manufacturer 4	5.4	–	101	–	98
Manufacturer 5	–[d]	–	95	–	94

[a] 10-μl injections, two injections each of two independently prepared replicates per lot. Results are stated in % of label claim for pilocarpine.

[b] HPLC analysis on a β-cyclodextrin column.

[c] USP HPLC analysis: silica gel colum; mobile phase, n-hexane–2% ammonia hydroxide in isopropyl alcohol (70:30). HPLC analysis of gel preceded by digestion in lead acetate.

[d] Interference from epinephrine prevented the determination of pilocarpic acid.

and are not interfered with by pilocarpine. A small amount of interference was caused by unidentified peaks eluting near to the solvent front in some of the ophthalmic formulations tested.

Analysis of ophthalmic gels and solutions

The method was compared with the USP method in the analysis of five commercially available pilocarpine ophthalmic solutions and a pilocarpine ophthalmic gel. The ophthalmic solutions selected were 2% in pilocarpine hydrochloride or nitrate in aqueous vehicles. The gel, Pilopine HS Gel (Alcon Labs., Fort Worth, TX, USA), contains 4% pilocarpine hydrochloride in a Carbomer 940 (BF Goodrich, Cleveland, OH, USA) vehicle. As stated previously, direct dilution with mobile phase was sufficient to prepare either formulation for HPLC analysis.

The samples were diluted with mobile phase to obtain a concentration of about 0.04 mg/ml pilocarpine and analyzed by the HPLC method reported here. These samples had previously been analyzed by the USP HPLC method with analysis of the gel preceded by digestion in lead acetate. The results are presented in Table I. The two methods are comparable for pilocarpine determination, but the present method also permits the determination of all three degradation products. Pilocarpine standards can be used to determine all four analytes, and a correction for the ultraviolet response at 214 nm was found to be unnecessary as the ratio of the molar absorptivities ($\varepsilon^{214}_{\text{carpic acid}}/\varepsilon^{214}_{\text{carpine}}$) was measured as unity.

Detection limits

Detection limits were calculated for each species. For the carpic acids, the signal-to-noise ratio was 3 when the concentrations were *ca.* 0.2% of a 0.04 mg/ml pilocarpine injection. The detection limit for isopilocarpine was dictated by the degree of separation from pilocarpine. The isopilocarpine signal became an indistinguishable shoulder on the pilocarpine peak when the isopilocarpine concentration was about 0.3% that of pilocarpine. These detection limits demonstrate satisfactory levels of sensitivity for most analyses.

CONCLUSIONS

The HPLC method presented here is an improvement on existing methods for the determination of pilocarpine hydrochloride in ophthalmic formulations. The determination of pilocarpine in aged ophthalmic samples gave results comparable to those obtained by the current USP HPLC method. However, separation on a β-cyclodextrin column is superior because complete determination of degradation products is also possible. Isopilocarpine, pilocarpic acid and isopilocarpic acid all gave well resolved peaks and a linear response in the presence of a 100-fold larger concentration of pilocarpine. The β-cyclodextrin HPLC method appears to be accurate and sensitive enough for the routine determination of pilocarpine and its degradation products in ophthalmic samples.

Complete separations are obtained in less than 10 min on a β-cyclodextrin column, compared with *ca.* 15 min on a phenyl column [17], 16 min on a cyano column [19], 18 min on a C_{18} column [12] and 7 min with the USP method on a 10-cm silica column (16 min on a 25-cm column [20]). The slight increase in time for analysis on a β-cyclodextrin column over the USP method is compensated for by the ability to determine the carpic acids.

A possible disadvantage of this method is the high salt concentration in the mobile phase, requiring thorough rinsing of the HPLC system after use to avoid damage to pump seals. The β-cyclodextrin HPLC column used here was found to have a lifetime of several months or more than 1000 injections with no precolumn. This lifetime is longer than that of the phenyl columns used for pilocarpine determination, but shorter than that of the silica columns used in the USP method. It was found that the use of ammonium sulfate in place of sodium sulfate increased the column lifetime with no effect on retention times and resolution, possibly owing to the less aggressive impurities in ammonium salts [24].

ACKNOWLEDGEMENT

The authors thank Elise Alexander, Supervisor of QA Product Chemistry for Alcon Labs., for arranging the analysis of pilocarpine ophthalmic samples by the USP method.

REFERENCES

1 *Physicians Desk Reference for Ophthalmology*, Medical Economics, Oradell, NJ, 1990.
2 P. H. Chung, T. F. Chin and J. L. Lach, *J. Pharm. Sci.*, 59 (1970) 1300.
3 R. A. Anderson and J. B. Cowle, *Br. J. Opthalmol.*, 52 (1968) 607.
4 H. Bundgaard, E. Falch, C. Larsen, G. L. Mosher and T. Mikkelson, *J. Pharm. Sci.*, 75 (1986) 775.
5 H. Bundgaard, E. Falch, C. Larsen and T. J. Mikkelson, *J. Pharm. Sci.*, 75 (1986) 36.
6 M. A. Nunes and E. B. Hanssen, *J. Pharm. Sci.*, 63 (1974) 716.
7 G. A. Neville, F. B. Hasan and I. C. P. Smith, *Can. J. Chem.*, 54 (1976) 2094.
8 J. B. Murray, *Proc. Soc. Anal. Chem.*, 7 (1970) 107.
9 B. S. Scott, D. L. Dunn and E. D. Dorsey, *J. Pharm. Sci.*, 70 (1981) 1046.
10 W. F. Bayne, L. C. Chu and F. T. Tao, *J. Pharm. Sci.*, 65 (1976) 1724.
11 S. K. W. Khalil, *J. Pharm. Sci.*, 66 (1977) 1625.
12 J. J. O'Donnell, R. Sandman and M. V. Drake, *J. Pharm. Sci.*, 69 (1980) 1096.
13 A. Noordam, L. Maat and H. C. Beyerman, *J. Pharm. Sci.*, 70 (1981) 96.
14 D. L. Dunn and R. E. Thompson, *J. Chromatogr.*, 264 (1983) 264.
15 R. W. Wood and J. R. Robinson, *Int. J. Pharma.*, 20 (1984) 285.
16 H. Bundgaard and S. H. Hansen, *Int. J. Pharma.*, 10 (1982) 281.
17 J. M. Kennedy and P. E. McNamara, *J. Chromatogr.*, 212 (1981) 331.
18 J. L. Van Ackeren, R. M. Venable and I. W. Wainer, *J. Assoc. Off. Anal. Chem.*, 67 (1984) 924.
19 A. Gomez-Gomar, M. Gonzalez-Aubert and J. Costa-Segarra, *J. Pharm. Biomed. Anal.*, 7 (1989) 1729.
20 D. L. Dunn, B. S. Scott and E. D. Dorsey, *J. Pharm. Sci.*, 70 (1981) 446.
21 A. Repta and T. Higuchi, *J. Pharm. Sci.*, 60 (1971) 1465.
22 H. Bundgaard, E. Falch, C. Larsen and T. J. Mikkelson, *J. Pharm. Sci.*, 75 (1986) 36.
23 *United States Pharmacopeia*, United States Pharmacopeial Convention, Rockville, MD, 22nd Revision, 1989.
24 *Cyclobond HPLC Column Operating Instructions*, Advanced Separation Technologies, Whippany, NJ, 1989.

Journal of Chromatography, 589 (1992) 165–170
Elsevier Science Publishers B.V., Amsterdam

CHROM. 23 707

Separation of soy lecithin using gel permeation chromatography

Richard E. Shansky* and Robert E. Kane

Analytical Sciences Department, Research and Development Center, Boehringer Ingelheim Pharmaceuticals, Inc., 175 Briar Ridge Road, Ridgefield, CT 06877 (USA)

(Received June 25th, 1991)

ABSTRACT

Gel permeation chromatography was applied to develop a broad relative molecular mass profile of soy lecithin. A non-aqueous mobile phase and an organic polymer-based stationary phase were found to be necessary in order to achieve interpretable chromatographic elution. Calibration of the column was performed using polystyrene standards. A broad peak was observed at a relative molecular mass of *ca.* 8000 in the two soy lecithin lots studied. This peak disappeared at sufficiently low concentrations of soy lecithin injected. The results suggested that this peak was due to the formation of reverse micelles or non-covalent aggregates of the phospholipid components and not to polymeric or protein-like high relative molecular mass component(s). No other high molecular mass (> 2000) components were detected under the conditions used.

INTRODUCTION

Lecithin derived from soy beans is a complex mixture of phosphatides (chiefly phosphatidylcholine, -ethanolamine and -inositol) and other substances such as triglycerides, fatty acids and carbohydrates [1]. It has many industrial applications including use as an emulsifier and stabilizer in foods. Soy lecithin is also widely used in pharmaceutical manufacturing as a suspending agent for aerosol-delivered drugs. The establishment of procedures that adequately characterize soy lecithin for industrial uses is therefore of obvious importance. Various chromatographic methodologies have been reported and can provide information such as phospholipid ratios [2]. In this work, it was of interest to develop a test which would detect other possible lower level components such as those of higher relative molecular mass (greater than 1000). Described here is a procedure based on gel permeation chromatography (GPC) which provides information regarding the relative molecular mass distribution of soy lecithin components. In the course of the development of this GPC methodology, an anomalous chromatographic behavior was observed at high sample concentrations. As will be shown, the data suggest the source of this anomaly is the formation of reverse micelles or aggregates of the phospholipid components of soy lecithin. Injection of low concentrations (1 mg/ml or less) of soy lecithin was found to be critical in order to produce a true relative molecular mass profile.

EXPERIMENTAL

Materials

Two lots of aerosol-grade soy lecithin (designated A and B) were obtained from a commercial source. A polydivinylbenzene GPC column and polystyrene relative molecular mass markers were purchased from Alltech (Deerfield, IL, USA). L-α-Phosphatidylcholine and L-α-phosphatidylinositol were purchased from Sigma (St. Louis, MO, USA). Tetrahydrofuran was obtained from EM Science (Gibbstown, NJ, USA).

0021-9673/92/$05.00

Chromatographic conditions

A Hewlett-Packard HP 1090L automated high-performance liquid chromatographic (HPLC) system was used. Data were collected on a Hewlett-Packard HP1000 Lab Automation System utilizing a Model 18652A A/D converter. Chromatograms were reprocessed and plotted using the SigmaPlot program (version 3.1) from Jandel Scientific (Corte Madera, CA, USA). The mobile phase was tetrahydrofuran (THF) pumped at a flow-rate of 0.5 ml/min. The injection volume was 10 μl and the UV detection wavelength was 254 nm. All samples and standards were dissolved in THF for injection. Chromatography was performed at room temperature.

The column was a 250 mm × 10 mm I.D. Alltech GPC column packed with a proprietary stationary phase, described by the manufacturer as polydivinylbenzene. The particles were nominally of 5 μm diameter with pores of nominally 1000 Å.

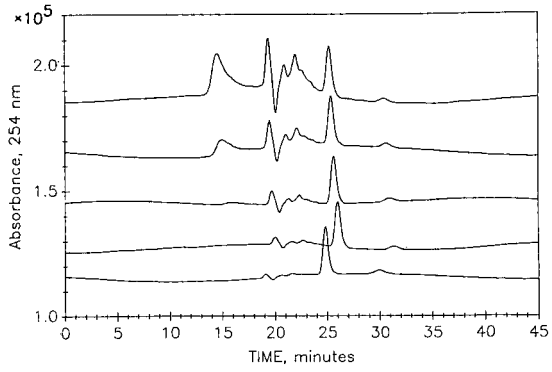

Fig. 1. GPC elution profiles of lot A. From bottom to top, sample concentration was 0.5, 1.0, 2.0, 4.0 and 8.0 mg/ml. Mobile phase, THF; flow-rate, 0.5 ml/min; injection volume, 10 μl; detection, UV at 254 nm. Chromatography was performed at room temperature. The column was a 250 mm × 10 mm I.D. Alltech GPC as described under Experimental. In this and other figures containing overlays, chromatograms are artificially offset from each other for clarity; therefore, the signal axis represents only relative (not absolute) values for each chromatogram.

RESULTS

Initial studies (data not shown) utilized a silica-based, zirconium-treated DuPont GF250 column designed for aqueous gel filtration HPLC and a mobile phase of hexane–isopropanol–acetate buffer (pH 4.2) (8:8:1). This system was found to be unsuitable, possibly owing to polar and/or ionic interactions with the negative charge of the stationary phase packing [3]. The major components of soy lecithin (phospholipids, fatty acids, etc.) were retained beyond the permeation volume of the column. Hence there was no assurance that macromolecular components were not also being retained. Under these conditions, assignment of relative molecular masses based on calibration standards could not be done with confidence.

A non-adsorptive sizing separation mechanism was desired. The major components of soy lecithin are of relatively low relative molecular mass (<1000) and would be expected to elute (poorly resolved) near the permeation volume. Any larger components (*e.g.*, proteins) could then be assigned relative molecular masses in conjunction with appropriate calibration standards. To achieve this, a column packed with a rigid organic-based gel was used.

Figs. 1 and 2 show the GPC elution profile of soy lecithin lots A and B, respectively, at several different concentrations (for clarity, the overlaid chromatograms were artificially offset; this did not affect the data or their interpretation). Qualitatively similar profiles were observed for these two soy lecithin lots because their compositions should be similar. The peak at *ca.* 25 min was not related to the sample as it remained constant in size as a function of soy lecithin concentration and also appeared in blank injections of THF alone (not shown).

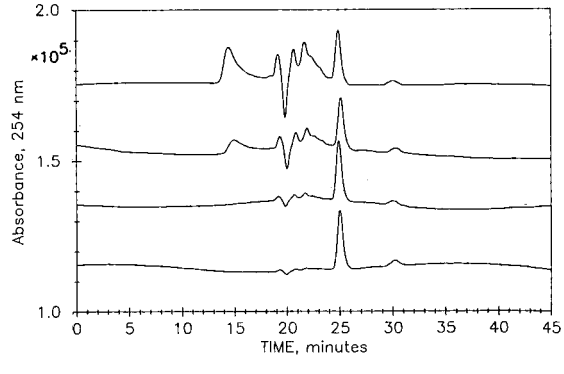

Fig. 2. GPC elution profiles of lot B. From bottom to top, sample concentration was 0.5, 1.0, 4.0 and 8.0 mg/ml. Other conditions as in Fig. 1.

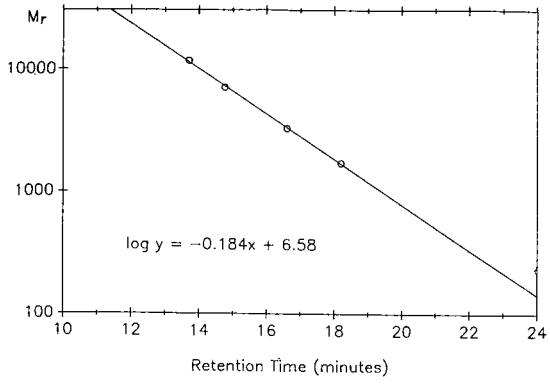

Fig 3. Relative molecular mass calibration plot based on elution of polystyrene relative molecular mass markers. Chromatographic conditions as in Fig. 1.

Four polystyrene standards of known average relative molecular mass (M_r) were injected under identical conditions. Using the resulting retention times, an M_r calibration plot for this column was constructed and is shown in Fig. 3. Linear regression yielded an equation that was used to calculate a polystyrene-equivalent M_r for each peak in the soy lecithin profiles generated using 8 mg/ml injections. This is shown in Table I.

Table I indicates that the series of overlapping peaks between 19 and 23 min in Figs. 1 and 2 have M_r in the range 300–1100. A calculation of the formula weight of the most common C_{16}–C_{18} phospholipids yields a range from 660 to 860. The corresponding fatty acids have a formula weight of 250–290. Injection of authentic phosphatidylinositol and phosphatidylcholine standards produced peaks of

TABLE I

POLYSTYRENE-EQUIVALENT RELATIVE MOLECULAR MASSES OF SOY LECITHIN GPC PEAKS

Lot A		Lot B	
Retention time (min)	M_r	Retention time (min)	M_r
14.43	8400	14.52	8060
19.15	1100	19.37	1030
20.68	590	20.89	540
21.70	390	21.94	350
22.23	310		
24.89	100	25.19	90

TABLE II

RELATIVE MOLECULAR MASS OF BROAD PEAK AS A FUNCTION OF SOY LECITHIN CONCENTRATION

Lot A		Lot B	
Concentration (mg/ml)	M_r	Concentration (mg/ml)	M_r
2	7100	2	5000
4	6550	4	6720
8	8400	8	8060
15	10 480	15	7530
167	10 100	197	10 300

M_r 490 and 230, respectively. Therefore, it is very likely that the series of overlapping peaks between 19 and 23 min correspond to the major phospholipid and/or fatty acid components of soy lecithin.

As mentioned earlier, the peak at *ca.* 25 min was found in a blank injection of THF alone. Table I indicates that this peak has M_r 90–100. As THF itself has a formula weight of 72, this peak most likely represents the elution of THF (or contaminant of THF) at the permeation volume of the column.

For the purpose of this work, there was a need to characterize components over a broad M_r range to ensure the consistency of the soy lecithin as a raw material for pharmaceutical purposes. In this regard, it was of interest to focus on the broad peak eluting at 14–15 min, which has an apparent M_r of 8000–9000. The magnitude of this peak is directly proportional to the injected soy lecithin concentration, strongly suggesting that it is related to the component(s) of the sample. The retention time and therefore the apparent relative molecular mass were also found to vary as a function of injected soy lecithin concentration, as shown in Table II.

Because of the broadness of the peak, assignments of the retention times vary. This results in some variability in relative molecular mass assignment. For both lots, however, there appears to be a distinct shift to higher M_r at high concentrations as a result of shorter retention times. It is unlikely that this shift in M_r was due to any chemical changes (*e.g.*, polymerization) in the soy lecithin under the chromatographic conditions employed. Indeed, harsh treatments are necessary to modify soy lecithin chemically [4]. Further, such a high M_r compo-

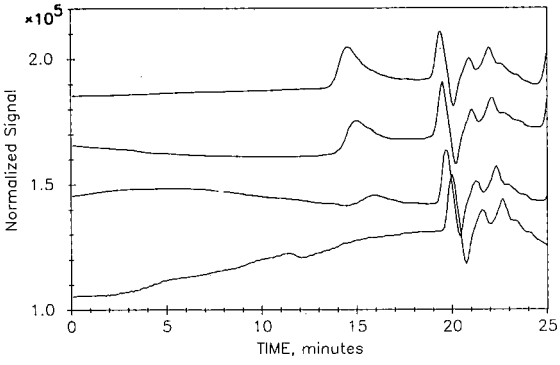

Fig. 4. Normalized elution profile of lot A. The signal (ordinate) values in each chromatogram from Fig. 1 were multiplied by a factor which compensates for the difference in injected sample concentration. From bottom to top, sample concentration was 1.0, 2.0, 4.0 and 8.0 mg/ml. Other conditions as in Fig. 1.

nent is not known to be present in the proportions indicated by the profile (five runs ranging from 2 to 15 mg/ml showed an average relative abundance of 28% according to peak integration). Therefore, the presence of this band would appear to be some type of artifact arising from the separation of the components of soy lecithin in this system.

A more detailed examination of the profile as a function of sample concentration was done. Figs. 4 and 5 are derived from the data shown in Figs. 1 and 2 with two changes: (1) the high-M_r region has been expanded by truncation of the elution time axis at 25 min; and (2) the absorbance values have been normalized to sample concentration. Under ideal conditions, concentration-normalized chromatograms should be essentially superimposable. As shown in Figs. 4 and 5, the broad peak at 14–15 min diminishes in size as the sample concentration is reduced whereas the phospholipid peaks at 19–23 min remain essentially unchanged. At the lowest concentration employed, the broad peak has completely disappeared and no other high-M_r (>2000) components are detectable.

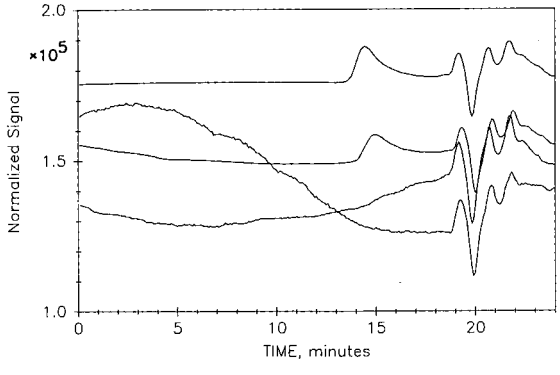

Fig. 5. Normalized elution profile of lot B. The signal (ordinate) values in each chromatogram in Fig. 2 were multiplied by a factor which compensates for the difference in injected sample concentration. From bottom to top, sample concentration was 0.5, 1.0, 4.0 and 8.0 mg/ml. Other conditions as in Fig. 1.

DISCUSSION

An increase in sample concentration generally results in an increase, rather than a decrease, in retention volume in GPC [5]. This effect has been studied for polystyrene [6,7] and becomes more pronounced as the relative molecular mass of the polystyrene increases, apparently owing to a decrease in the effective dimensions of the polymer [5]. The high viscosity of concentrated solutions can also cause tailing of solute bands due to viscous streaming effects [5]. For both large and small solutes, high sample loads can induce changes in the distribution coefficient as the solute proceeds through the column [8]. However, this change is also in the direction of increased retention volume as a function of sample concentration. From this discussion, it would appear that the most commonly reported sample overload artifacts in GPC do not yield reductions in retention volume. This suggests that a different effect may be operating in this work.

A possible explanation for the presence of a component of high relative molecular mass in soy lecithin is that the broad peak represents phospholipid aggregates. A high soy lecithin concentration would tend to favor their formation. These aggregates are not completely broken up by dilution through the chromatographic system until a sufficiently low concentration of soy lecithin is used. Although the exact nature of these aggregates was not determined, the formation of high-M_r aggregate species [9] and/or micelles [10] of phospholipids in organic solvents has been documented. In a different chromatographic system, a concentration-dependent aggregation of one particular protein has been demonstrated [11].

The concept that micelles can elute intact through a gel permeation column has long been rec-

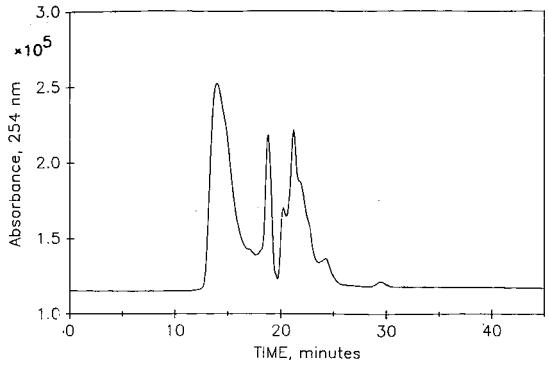

Fig. 6. GPC elution profile of lot B. Sample concentration, 167 mg/ml. Other conditions as in Fig. 1.

ognized and led to a theoretical elaboration by Coll [12]. Inclusion of the surfactant under study in the mobile phase at a concentration just above its critical micelle concentration (CMC) can be employed to suppress equilibrium-induced dissociation of micelles [13]. However, this has been shown more recently not to be necessary if the surfactant is injected at a concentration far above its CMC [14,15]. In this instance, the hydrodynamic volume of micelles may be adequately determined [15]. Of relevance to the work presented here, reversed micelles and other molecular aggregates have been observed in, and can be studied by, size-exclusion chromatography with organic solvents [16–18].

Given the probable identification of the broad peak at 14–15 min as phospholipid aggregate(s), it is of interest to examine the remainder of the high-

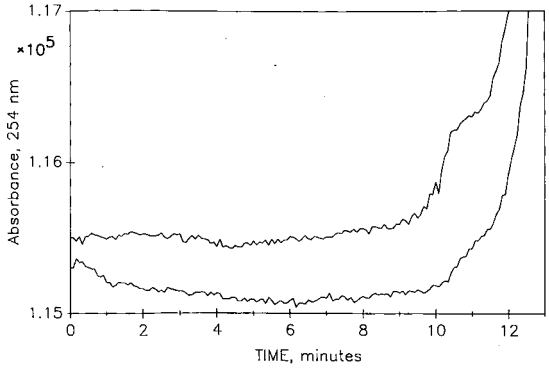

Fig. 7. High-sensitivity comparison of two soy lecithin lots in the region corresponding to $M_r > 15\,000$. Upper trace, lot A; lower trace, lot B. Other conditions as in Fig. 1.

M_r region of the GPC elution profile for the presence of other species. Fig. 6 shows the profile obtained for lot B at the highest concentration tested, 167 mg/ml. No additional peaks appear in this chromatogram relative to those at lower concentration (Figs. 1 and 2). In Fig. 7, a high sensitivity/high sample concentration comparison is made between lots A and B for the portion of the chromatograms corresponding to $M_r > 15\,000$. No additional peaks are observed in either sample (the rising baseline at 10–12 min corresponds to the front of the aggregate-like peak).

The results presented here could be further confirmed using static light-scattering experiments or with an on-line low-angle laser light-scattering (LALLS) detector [19]. Indeed, light scattering has been applied to the study of lecithin micelles in apolar solvents, a system designed to mimic the delivery of therapeutic aerosols from pressurized metered dose inhalers (MDIs) [10]. Using GPC and LALLS separately or in combination, it might be possible to study in more detail aggregate or micelle formation with specified solvents. Experiments along these lines are in progress.

ACKNOWLEDGEMENTS

We thank Dr. Daniel McNamara for helpful discussions and the management of Boehringer Ingleheim Pharmaceuticals, R&D, for their support during this project.

REFERENCES

1 *Food Chemicals Codex*, National Academy Press, Washington, DC, 3rd. ed., 1981, p. 166–167.
2 A. Nasner and L. Kraus, in J. N. Hawthorne and D. Lekim (Editors), *Soya Lecithin Dietetic Applications: Proceedings of the Second International Colloquium on Soya Lecithin, Brighton, April 3, 1982*, Semmelweis-Verlag, Hoya, 1983, pp. 26–34.
3 R. M. Sheeley, W. J. Hurst, D. M. Sheeley and R. A. Martin, *J. Liq. Chromatogr.*, 10 (1987) 3173.
4 M. Ghyczy, in B. F. Szuhaj (Editor), *Lecithins: Sources, Manufacture and Uses*, American Oil Chemists' Society, Champaign, IL, 1989, Ch. 8.
5 W. W. Yau, J. J. Kirkland and D. D. Bly, *Modern Size Exclusion Chromatography: Practice of Gel Permeation and Gel Filtration Chromatography*, Wiley, New York, 1979, pp. 241–246.
6 S. Mori, *J. Appl. Polym. Sci.*, 21 (1977) 1921.
7 J. Janca, *J. Chromatogr.*, 134 (1977) 263.
8 J. J. Kirkland and P. E. Antle, *J. Chromatogr.*, 15 (1977) 137.

9 M. Schneider, in B. F. Szuhaj (Editor), *Lecithins: Sources, Manufacture and Uses*, American Oil Chemists' Society, Champaign, IL, 1989, pp. 117 and 123.
10 R. M. Evans, D. Attwood, S. M. Chatham and S. J. Farr, *J. Pharm. Pharmacol.*, 42 (1990) 601.
11 N. Grinberg, R. Blanco, D. M. Yarmush and B. L. Karger *Anal. Chem.*, 61 (1989) 514.
12 H. Coll, *Sep. Sci.*, 6 (1971) 207.
13 P. Schmidt and H. Sucker, *Fresenius' Z. Anal. Chem.*, 250 (1970) 384.
14 H. H. Teo, M. G. Styring, S. G. Yeates, C. Price and C. Booth, *J. Colloid Interface Sci.*, 114 (1986) 416.
15 M. G. Styring, H. H. Teo, C. Price and C. Booth, *J. Chromatogr.*, 388 (1987) 421.
16 J. H. Lyngaae-Joergensen, *Makromol. Chem.*, 167 (1973) 311.
17 P. L. Dubin, in T. Provder (Editor), *Size Exclusion Chromatography (GPC) (ACS Symposium Series*, Vol. 138), American Chemical Society, Washington, DC, 1980, pp. 225–238.
18 P. Spacek and M. Kubin, *J. Appl. Polym. Sci.*, 30 (1985) 143.
19 H. H. Stuting I. S. Krull, R. Mhatre, S. C. Krzysko and H. G. Barth, LC · GC, 7 (1989) 402.

Journal of Chromatography, 589 (1992) 171–176
Elsevier Science Publishers B.V., Amsterdam

CHROM. 23 735

Optimization of an isocratic high-performance liquid chromatographic separation of carotenoids

Neal E. Craft* and Stephen A. Wise

Organic Analytical Research Division, Chemical Science and Technology Laboratory, National Institute of Standards and Technology, Gaithersburg, MD 20899 (USA)

Joseph H. Soares, Jr.

Nutritional Sciences Department, University of Maryland, College Park, MD 20742 (USA)

(First received June 28th, 1991; revised manuscript received September 10th, 1991)

ABSTRACT

Using a polymeric C_{18} high-performance liquid chromatographic (HPLC) column, which demonstrated excellent separation selectivity toward carotenoid compounds in an earlier column evaluation, the effects of mobile phase modifier, modifier concentration, and column temperature were investigated. A seven-component carotenoid mixture was used to monitor changes in separation selectivity in response to variations in HPLC conditions. Both acetonitrile and tetrahydrofuran (THF) improved the resolution of echinenone and α-carotene; THF was selected for use as a modifier due to its solvating properties. At concentrations greater than 6% THF, the resolution of lutein and zeaxanthin deteriorated significantly. Temperature was varied from 15 to 35°C in 5°C increments. Resolution of lutein/zeaxanthin and β-cartone/lycopene were better at lower temperatures while echinenone/α-carotene separation improved as temperature increased. An acceptable separation of all seven carotenoids was achieved at 20°C using 5% THF as a mobile phase modifier. Method applicability is demonstrated for serum and food carotenoids.

INTRODUCTION

During the past decade carotenoid pigments have become highly publicized compounds due to their potential roles in cancer prevention [1–4], as antioxidants [5], and in the reduction of atherogenesis [6]. As a result, several publications have reported high-performance liquid chromatographic (HPLC) methods for the determination of carotenoids [7–12], but no publications have reported the influence of individual HPLC parameters on the separation of multiple carotenoids. Few laboratories have the time or the resources to evaluate a large sample of HPLC columns during analytical method development. Therefore, most "new" methods of separation are only slight adjustments in mobile phase composition. Recently, Epler *et al.* [13] evaluated 65 HPLC columns under standardized conditions with respect to carotenoid separation and recovery. In this study they observed, as others have reported [11,12] that polymeric C_{18} phases exhibited excellent selectivity for structurally similar carotenoids, whereas monomeric C_{18} phases, which represent the majority of the commercial C_{18} columns available, exhibited less selectivity for structurally similar carotenoids. Extensive investigations of the stationary phase characteristics responsible for differences in selectivity between monomeric and polymeric C_{18} phases for the separation of polycyclic aromatic hydrocarbon isomers have been reported by Sander and Wise [14]. Many of these same stationary phase characteristics influence the separation of carotenoids.

This report describes the optimization of an isocratic carotenoid HPLC separation using one HPLC column that exhibited very good separation

of the carotenoid mixture during the column evaluation study. The influence of multiple solvent modifiers and temperature on the separation of a carotenoid mixture was examined.

EXPERIMENTAL

Reagents

An ethanolic solution containing between 0.2 and 1.0 μg/ml of lutein [(3*R*,3′*R*,6′*R*)-β,ε-carotene-3,3′-diol, Kemin Industries, Des Moines, IA, USA], zeaxanthin[(3*R*,3′*R*)-β,β-carotene-3,3′-diol],β-cryptoxanthin [(3*R*)-β,β-caroten-3-ol, Atomergic Chemetals, Farmingdale, NY, USA], echinenone (β,β-caroten-4-one) (Hoffmann-La Roche, Nutley, NJ, USA), lycopene (ψ,ψ-carotene, extracted from tomato paste), α-carotene [(6′*R*)-β,ε-carotene], and β-carotene (β,β-carotene, Sigma, St. Louis, MO, USA) was prepared to monitor column separation selectivity. The following solvents were used in the mobile phase mixtures: acetone, acetonitrile, chloroform, diethyl ether, ethyl acetate, hexane, methanol, methylene chloride, tetrahydrofuran (THF) containing butylated hydroxytoluene (BHT) and toluene. All solvents were HPLC grade or equivalent and were used without further treatment.

HPLC

The HPLC system consisted of: a dual piston, quaternary low-pressure gradient solvent delivery system equipped with helium sparging and column temperature control; a high sensitivity, programmable, rapid scanning, UV–visible detector fitted with both deuterium and tungsten lamps and an 8-μl flow cell; and manual and automatic injection valves. Carotenoids were monitored at 445 nm and a computer-controlled data system was used to process data permitting review and manipulation of peak integration. The HPLC column contained 300 Å pore diameter, 5 μm particle size, silica polymerically modified with C_{18} (Vydac 201TP, 25 × 4.6 cm I.D. Separations Group, Hesperia, CA, USA). Other columns with similar chemistries could be substituted with minor modifications in mobile phase composition [13]. A 0.2 μm inline filter was placed between the pump and injection valve to trap particles resulting from piston seal wear. All stainless steel frits between the injection valve and the detector were replaced with biocompatible ceramic frits to minimize carotenoid precipitation and degradation [13,15]. A guard column containing 5-μm C_{18} material similar to the analytical column was directly attached to the analytical column inlet to remove particulate material and protect the column.

A methanol-based mobile phase was modified with 5 to 10% of the solvents listed under *Reagents* to determine the influence of each solvent on the separation of the carotenoid test mixture. After the modifier yielding the best selectivity was selected (THF), incremental portions were added to methanol to achieve the best separation of all seven carotenoids as determined by the shortest analysis time without compromising the resolution of all carotenoid peaks.

Column temperature was varied in 5°C increments between 15 and 35°C to investigate the influence of temperature on the separation of the carotenoid mixture. Temperature was regulated by the thermostatically controlled column oven on the HPLC system. The 15°C column temperature was achieved by placing a beaker of dry ice at the forced air inlet to reduce the chamber temperature to below ambient.

Carotenoid recovery

"Total recovery" was determined by flow injection analysis (FIA). To perform the FIA, the HPLC column was replaced by a 2000 mm × 0.8 mm I.D. PTFE tubing and the individual carotenoid solutions were introduced using a manual injector fitted with a 20-μl loop and recording the peak area at 445 nm. This process was repeated five times for each carotenoid. Then the HPLC column was replaced and each individual carotenoid solution was injected onto the column and "peak area" was recorded. Recovery of carotenoids from the HPLC column was determined by dividing the mean "peak area" by mean "total recovery" of the five injections of each carotenoid solution.

RESULTS AND DISCUSSION

The carotenoids included in the test mixture span a wide polarity range and represent β,β; β,ε; ψ,ψ; monoketo; monohydroxy; and dihydroxy carotenoids. These compounds account for approximately 90% of carotenoids in human blood and the

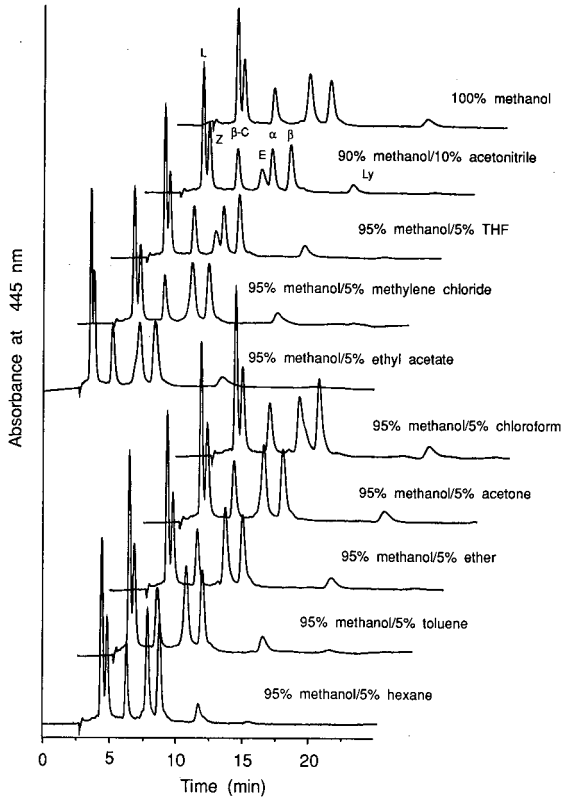

Fig. 1. The effect of nine solvent modifiers on the separation of seven carotenoids. Chromatographic conditions: Vydac 201TP C_{18}, 5 μm, 250 × 4.6 mm I.D. column; mobile phase as listed, 1.0 ml/min; UV–VIS at 445 nm; column temperature 25°C. Peaks: L = lutein; Z = zeaxanthin; β-C = β-cryptoxanthin; E = echinenone; α = α-carotene; β = β-carotene; Ly = lycopene.

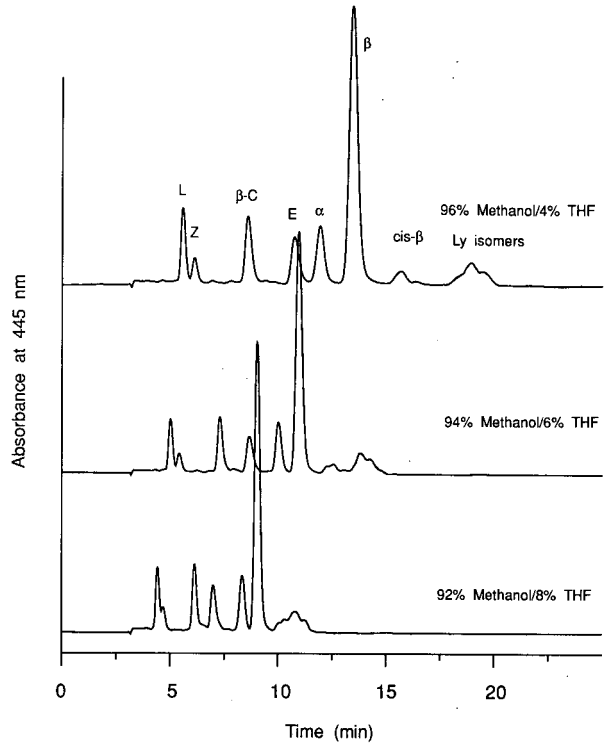

Fig. 2. The effect of three concentrations of THF on the separation of seven carotenoids. Chromatographic conditions as in Fig. 1. Peaks: *cis*-β = β-carotene *cis* isomers; Ly isomers = lycopene isomers; other peaks as in Fig. 1.

three major carotenoids in the US diet [7,16]. Therefore, an HPLC separation developed using this mix should find wide applicability to both food and serum carotenoid analyses.

A wide pore (300 Å), polymerically bonded C_{18} column with "biocompatible" frits was incorporated based on results of a previous column evaluation study in which polymerically modified C_{18} columns demonstrated greater resolution of the carotenoids in the ethanolic mixture [13]. Also for duplicate HPLC columns with different frit materials, recovery was improved in columns fitted with "biocompatible" materials (titanium and Hastelloy C) rather than stainless steel [13,15]. In the same study, total carotenoid recovery was found to be higher for nearly all columns when using methanol-based mobile phases rather than acetonitrile-based mobile phases. In the case of the polymeric C_{18} columns, the use of methanol actually resulted in improved carotenoid resolution. For this reason, our initial optimization began with a methanol-based mobile phase.

The influence of the mobile phase modifiers on the separation of the seven carotenoids in the test mix is illustrated in Fig. 1. With this particular column and 100% methanol as the mobile phase, echinenone coelutes with α-carotene, and lycopene is too far removed from β-carotene, substantially increasing analysis time. The only two modifiers that facilitated the separation of echinenone and α-carotene were acetonitrile and THF. Both solvents also selectively reduced the retention time of lycopene. The solubility of both the xantholphylls and carotenes is greater in THF than acetonitrile [17]. Therefore to improve carotenoid solubility, THF was selected as the modifier; although the resolution of the

lutein/zeaxanthin pair and echinenone/α-carotene pair was slightly decreased.

Mobile phases of methods previously developed using a similar C_{18} column have been modified with chloroform, THF, and a mixture of acetonitrile–THF [11,12,18]. Each of these reports illustrated the superior selectivity of the polymeric C_{18} column toward carotenoid compounds and especially geometric isomers, however, none of these reports addressed the separation of the carotenoid pairs discussed above.

The effect of varying the proportion of THF from 4 to 8% on the separation of the carotenoid mixture is illustrated in Fig. 2. As the THF concentration increases, resolution decreases between the pairs lutein/zeaxanthin and β-carotene/lycopene. At a column temperature of 25°C, 3 to 5% THF results in good separation of all the carotenoids in the mixture.

Previously, our laboratory has reported that column temperature alters column selectivity, specifically with respect to solute shape recognition [19,20]. Using 5% THF in methanol, column temperature was varied between 15 and 35°C to determine if the separation of structurally similar carotenoids could be improved (Fig. 3). At 15°C echinenone and lycopene are more strongly retained with respect to β-carotene ($\alpha_{E/\beta}$ 0.80 *vs* 0.67, and $\alpha_{1y/\beta}$ = 1.60 *vs.* 1.24, respectively, at 15 and 35°C). As a result, at 15°C, echinenone and α-carotene are not baseline resolved and lycopene elutes distant from the other carotenoids. Beginning at 25°C and

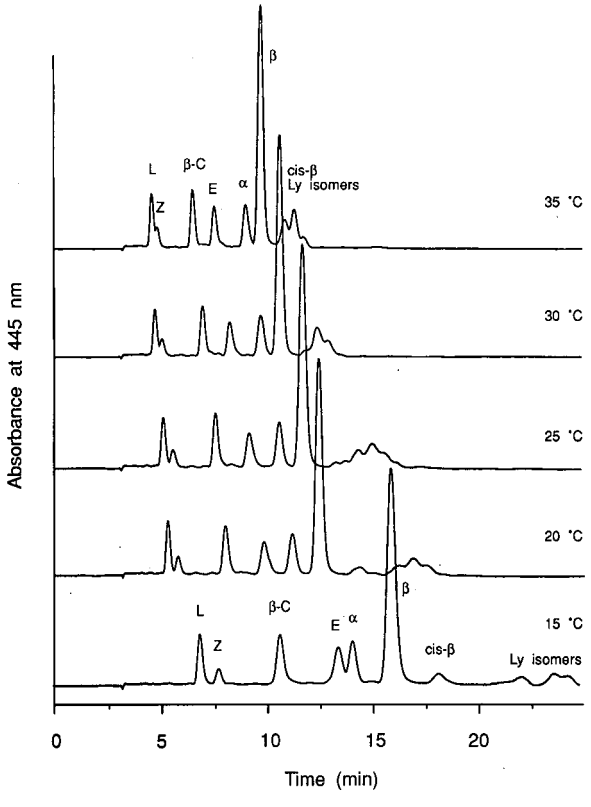

Fig. 3. The effect of five column temperatures on the separation of seven carotenoids. Chromatographic conditions: Vydac 201TP C_{18} column; 5% THF in methanol; 1.0 ml/min; UV/VIS at 445 nm; column temperature as listed. Peak identifications as in Fig. 2.

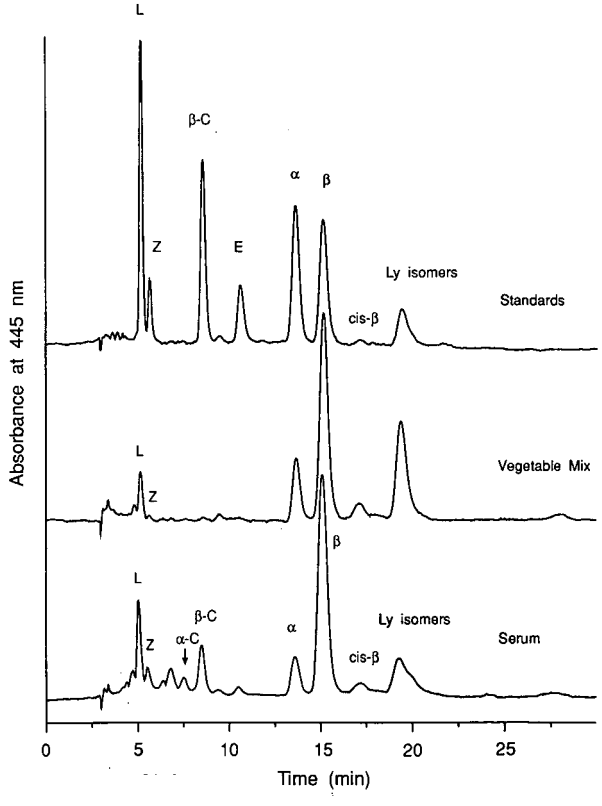

Fig. 4. The separation of serum and mixed diet carotenoids using the optimized HPLC method. Chromatographic conditions: Vydac 201TP C_{18} column; 5% THF in methanol; 1.0 ml/min; UV/VIS at 445 nm. Peaks: L = lutein; Z = zeaxanthin; α-C = α-cryptoxanthin; β-C = β-crytoxanthin; α = α-carotene; β = β-carotene; *cis*-β = β-carotene; *cis*-β = β-carotene *cis* isomers; Ly isomers = lycopene isomers.

above, resolution decreases between the lutein/zeaxanthin pair and β-carotene/lycopene pair. A column temperature of 20°C was selected, because all carotenoids in the mixture are well resolved from each other, a baseline separation exists between the *trans* isomer of β-carotene and its geometric isomers, and there is partial resolution of the geometric isomers of lycopene. Lesellier *et al.* [21] recently described the separation of *trans/cis*-α- and β-carotenes and observed that temperature was a significant factor in optimizing the separation of these isomers. Using a narrow pore (80 Å) polymeric C_{18} column, they identified 21–22°C as the optimum temperature for the separation of *trans*-α- and β-carotene from their *cis* isomers. However, using the narrow pore column they were unable to resolve the *cis* isomers from each other. Previously, we have demonstrated the separation of individual geometric isomers of β-carotene using a wide pore polymeric C_{18} columns [22].

In our recent column evaluation study [13], we found that total carotenoid recovery from the HPLC column was influenced by the column packing, mobile phase, and frit material. The percent recovery and standard deviation of individual carotenoids measured by FIA using the optimized HPLC system described above are: lutein, 96 ± 6%; zeaxanthin, 107 ± 9%; β-cryptoxanthin, 94 ± 5%; echinenone, 92 ± 6%; α-carotene, 95 ± 3%; β-carotene, 96 ± 3%; and lycopene, 108 ± 6%. Recovery of each carotenoid was greater than 92% and total carotenoid recovery was 98 ± 6%. This demonstrates that the system not only resolves these major carotenoids but also elutes them quantitatively from the LC column.

The applicability of the method is demonstrated in Fig. 4 in which the separations of serum carotenoids and dietary carotenoids are illustrated. Most isocratic reversed-phase HPLC methods fail to resolve lutein and zeaxanthin when the capacity factor (k') for the hydrocarbon carotenoids is kept below 10 [7–9]. Previously, polymeric C_{18} phases have been reported to exhibit superior ability to recognize subtle differences in molecular structure [20,22,23]. In this application, the lutein/zeaxanthin pair, geometric isomers of β-carotene (*trans*/9-*cis*/13-*cis*), and geometric isomers of lycopene (*trans*/13-*cis*) are separated within 20 min. Although superior to monomeric C_{18} phases in many ways, polymeric C_{18} columns are not without problems. The total carbon load is lower in wide-pore polymeric phases (due to the lower surface areas of wide pore silicas) which results in weaker retention of the carotenoids and limits the amount and type of modifier used in the mobile phase. The large pore diameter and thick surface coating slows mass transfer resulting in slightly broader peaks. Lastly, column reproducibility from various production lots tends to be more variable than for monomeric C_{18} phases [13]. Because of these difficulties, duplication of the results illustrated in this manuscript with a different polymeric C_{18} column may require slight modifications in the mobile phase composition, but similar separations should be attainable.

In summary, the isocratic separation of carotenoids was optimized using a polymeric C_{18} column. Stainless steel frits were replaced with "biocompatible" frits to minimize oxidative degradation of the analytes and a methanol-based mobile phase was used to improve selectivity and recovery. Nine solvent modifiers were investigated to determine their effect on separation selectivity and THF was found to be the most beneficial modifier. Various combinations of THF composition and column temperature were assessed to achieve the best overall separation. The recovery of individual carotenoids and a mixture of seven carotenoids from the HPLC column was nearly 100%.

ACKNOWLEDGEMENTS

The authors gratefully acknowledge the helpful discussions with Lane C. Sander regarding stationary phase chemistry and the assistance of Katherine S. Epler with the initial column evaluations. The authors are grateful to Chris Nelson of Kemin Industries and Hemmige Bhagavan of Hoffmann-La Roche for their generous contributions of carotenoids.

This work is taken in part from a dissertation submitted by N.E.C. to the Graduate School of the University of Maryland in partial fulfillment of the requirements for the Ph.D. degree in Nutritional Sciences.

Certain commercial equipment, instruments, or materials are identified in this paper to specify adequately the experimental procedure. Such identification does not imply recommendation of endorse-

ment by the National Institute of Standards and Technology, nor does it imply that the materials or equipment identified are neccesarily the best available for the purpose.

REFERENCES

1 M. S. Menkes, G. W. Comstock, J. P. Vuilleumeir, K. J. Helsing, A. R. Rider and R. Brookmeyer, *N. Engl. J. Med.*, 20 (1986) 1250.
2 G. A. Colditz, L. G. Branch, R. J. Lipnick, W. C. Willett, B. Rosner, B. M. Posner and C. H. Hennekens, *Am. J. Clin. Nutr.*, 41 (1985) 32.
3 W. C. Willett, B. F. Polk, B. A. Underwood, M. J. Stampfer, S. Pressel, B. Rosner, J. O. Taylor, K. Schneider and C. G. Hames, *N. Engl. J. Med.*, 310 (1984) 430.
4 R. Peto, R. Doll, J. D. Buckley and M. B. Sporn, *Nature (London)*, 290 (1981) 201.
5 G. W. Burton and K. U. Ingold, *Science (Washington, D.C.)*, 224 (1984) 569.
6 J. M. Gaziano, J. E. Manson, P. M. Ridker, J. E. Buring and C. H. Hennekens, *Circulation*, 82 (1990) 796.
7 J. G. Bieri, E. D. Brown and J. C. Smith, *J. Liq. Chromatogr.*, 8 (1985) 473.
8 C. S. Yang and M.-J. Lee, *J. Nutr. Growth Cancer*, 4 (1987) 19.
9 A. L. Sowell, D. L. Huff, E. W. Gunter and W. J. Driskell, *J. Chromatogr.*, 431 (1988) 424.
10 D. A. Kalman, G. E. Goodman, G. S. Omenn, G. Bellamy and B. Rollins, *J. Natl. Cancer Inst.*, 79 (1987) 975.
11 R. J. Bushway, *J. Liq. Chromatogr.*, 8 (1985) 1527.
12 F. W. Quackenbush, *J. Liq. Chromatogr.*, 10 (1987) 643.
13 K. S. Epler, L. C. Sander, S. A. Wise, R. G. Ziegler and N. E. Craft, *J. Chromatogr.*, 595 (1992) in press.
14 L. C. Sander and S. A. Wise, *LC · GC*, 8 (1990) 378.
15 D. W. Nierenberg and D. C. Lester, *J. Nutr. Growth Cancer*, 3 (1986) 215.
16 N. E. Craft, S. A. Wise, and J. H. Soares, Jr., *J. Agric. Food Chem.*, submitted for publication.
17 N. E. Craft and J. H. Soares, Jr., *J. Agric. Food Chem.*, in press.
18 F. W. Quackenbush and R. L. Smallidge, *J. Assoc. Off. Anal. Chem.*, 69 (1986) 767.
19 L. C. Sander and N. E. Craft, *Anal. Chem.*, 62 (1990) 1545.
20 L. C. Sander and S. A. Wise, *Anal. Chem.*, 61 (1989) 1749.
21 E. Lesellier, C. Marty, C. Berset and A. Tchapla, *J. High Resolut. Chromatogr. Chromatogr. Commun.*, 12 (1989) 447.
22 N. E. Craft, L. C. Sander and H. F. Pierson, *J. Micronutr. Anal.*, 8 (1991) 209.
23 L. C. Sander and S. A. Wise, *Anal. Chem.*, 56 (1984) 504.

Journal of Chromatography, 589 (1991) 177–183
Elsevier Science Publishers B.V., Amsterdam

CHROM. 23 721

Determination of aromatic sulfonic acids in aqueous environmental samples by anion-exchange chromatography coupled to particle beam mass spectrometry and UV spectrophotometry

In Suk Kim, Fassil I. Sasinos, Dharmendra K. Rishi, Robert D. Stephens and Mark A. Brown*,☆

Hazardous Materials Laboratory, California Department of Health Services, 2151 Berkeley Way, Berkeley, CA 94704 (USA)

(First received April 23rd, 1991; revised manuscript received September 3rd, 1991)

ABSTRACT

Aromatic sulfonic acids are determined in water using anion-exchange liquid chromatography. Quantification is by UV absorption spectrophotometry (quantification limits 2–80 ng on-column) and confirmation by particle beam electron impact ionization mass spectrometry. Separations with several anion-exchange columns using acetonitrile and ammonium acetate or sodium hydroxide (requiring a membrane suppressor for desalting) mobile phases are represented. Average recoveries are 82% for six monosulfonic acids (spiked at 0.1, 1.0 and 100 ppm) and 95% for two disulfonic acids (spiked at 1.0 and 100 ppm) (S.D. 12%, UV quantification). Mass spectra (2.0 μg on-column) show molecular and major diagnostic fragment ions corresponding to losses of SO_2, HSO_2, SO_3 and HSO_3.

INTRODUCTION

Interest in the application of anion-exchange liquid chromatography (LC) for the direct separation of organic anions has grown with the appreciation of the importance of this class of compounds in agricultural, pharmaceutical and environmental chemistry. Recently more than 95% of the organic materials in aqueous samples from the Stringfellow hazardous waste site were shown to be a series of chlorinated aromatic mono- and disulfonic acid waste products from DDT manufacture [1–3]. Anion-exchange LC coupled with negative chemical ionization (NCI) particle beam mass spectrometry (MS) were used for determination of molecular weights of these previously uncharacterized compounds. Electron impact (EI, positive ion) ionization MS and UV spectrophotometry were also used to obtain essential fragmentation and structural information [3,4]. One compound in this series, 4-chlorobenzenesulfonic acid (PCBSA), has been identified as a major component of the total dissolved organic carbon at more than one hazardous waste site [1,2,5]. The polarity, non-volatility and thermal lability of these compounds had led them to be previously overlooked by gas chromatography (GC)-based methods. Similarly, the dissolved organic materials contained in other aqueous samples such as Casmalia groundwater monitoring well and Santa Clara drinking water have been shown to be optimally resolved by anion-exchange chromatography [6].

Several other studies have shown MS detection coupled with anion exchange to be a powerful combination [7–10]. Ion spray atmospheric pressure ionization MS has been applied to organic anions

☆ Present address: Office of Technology Assessment, O+E, 600 Pennsylvania Avenue S.E., Washington, DC 20003, USA.

0021-9673/92/$05.00

including alkyl and aromatic sulfonic acids, and collisionally activited dissociation (CAD) MS–MS experiments were used to generate sufficient characteristic fragment ions [10] or of CAD MS–MS experiments to generate fragmentation for analyte confirmation. Non-volatile tetraalkylammonium salts in the chromatographic mobile phase were made compatible with the LC–MS interface by the use of a membrane suppressor that exchanged the alkylammonium cations with the volatile hydronium ions prior to introduction into the mass spectrometer [7]. Anion-exchange chromatography of carbohydrates with thermospray (TSP) MS detection using non-volatile buffers and a membrane suppressor for desalting has also been reported [8]. Anion-exchange LC has been succesfully coupled with TSP-MS for the analysis of phenols and their corresponding glucuronides and sulfate conjugates. In that study, tandem CAD MS–MS was used to generate a much greater amount of fragmentation and structural information than was possible with TSP-MS alone [9]. The relatively soft chemical ionization available with TSP tends to generate very simple mass spectra with only molecular or solvent adduct ions. Additional structural information requires modifications such as the use of special solvents to generate sufficient diagnostic and structural information for analyte confirmation and identification.

Applications of LC–MS to the analysis of non-volatile biological molecules such as peptides, amino acids, nucleotides, steroids, lipids, phospholipids, fatty acids, carbohydrates and drugs and their metabolites have recently been reviewed [6,11]. Cation-exchange chromatography with fluorescence detection also has been reported as a sensitive method for the determination of propranolol, a β-adrenoceptor blocker, and its glucuronide and sulfate glucuronide metabolites in plasma and urine [12].

Particle beam MS for LC detection has been shown to be a broad-range technique for the determination of a variety of non-volatile compounds in environmental samples [2,6,13]. It has advantages over other LC–MS interfacing systems in that a single system can provide positive and negative chemical ionization with a variety of reagent gases to maximize molecular weight information, and provides conventional EI mass spectra with diagnostic fragment ions that are especially useful for analyte confirmation without the necessity for CAD MS–MS experiments. This paper described a general method for the determination of aromatic sulfonic acids in aqueous media. It uses a variety of anion-exchange LC systems with UV and particle beam MS detection.

EXPERIMENTAL

Analytical standards

Nine commercially available (Aldrich, Milwaukee, WI, USA) aromatic mono- and disulfonic acids as either the sodium salt or free acid (whichever was the purest) were used as model compounds (listed in Table I, plus 2-naphthalenesulfonic acid).

Anion-exchange chromatography

Anion-exchange chromatographic columns were obtained from Dionex (Sunnyvale, CA, USA) (OmniPac Model PAX-100 and -500, 25 cm × 2 mm I.D., polymer based) and Scientific Glass Engineering (SGE) (Ringwood, Australia) (SAX Model 250GL, 25 cm × 2 mm, silica based). Flow-rates were always 0.25 ml/min for both isocratic and gradient conditions. The following chromatographic gradient conditions were used: with the PAX-100 column with a mobile phase consisting of water–acetonitrile–ammonium acetate (250 m*M*, pH 6.0), 0 min, 88:10:2; 5 min, 70:10:20; and 10 min, 34:43:23; with the PAX-500 column were with a mobile phase consisting of water–acetonitrile–sodium hydroxide (200 m*M*), 0 min, 90:10:0; and 18 min, 0:40:60, with a membrane separator; and with the SAX column with a mobile phase consisting of water–acetonitrile–ammonium acetate (100 m*M*, pH 6.0), 0 min, 85:0:15; 10 min, 83:2:15; and 30 min, 55:30:15. For gradient elutions with the SAX column a constant aqueous ammonium acetate and variable acetonitrile mobile phase composition was used. The organic polymer-based OmniPac columns can be used with a much wider variety of mobile phases including both aqueous sodium hydroxide or ammonium acetate and acetonitrile gradients for greater chromatographic flexibility. The Dionex micromembrane suppressor, which must be used with non-volatile eluants such as sodium hydroxide, converts non-volatile sodium salts into the corresponding hydrogen form before introduction into the particle beam MS interface, *e.g.*, $NaOH \rightarrow H_2O$.

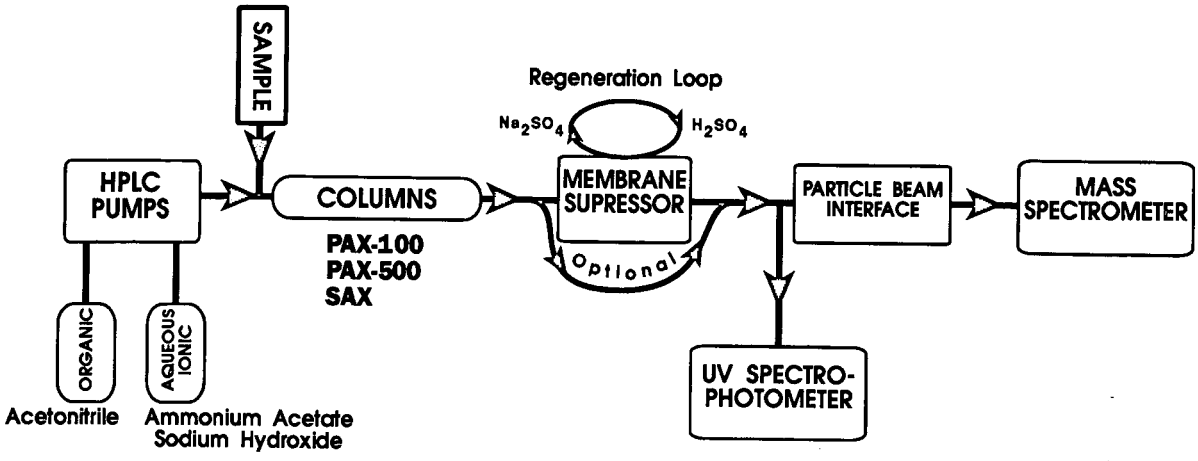

Fig. 1. Configuration of the anion-exchange LC system, the membrane suppressor (if used) and the particle beam mass spectrometer used.

Liquid chromatography with particle beam mass spectrometry and UV absorption spectrometry.

Fig. 1 shows the coupling of the anion-exchange liquid chromatographic system, the membrane suppressor (if used) and the particle beam mass spectrometer used in this study. The LC pumps for both UV and MS detection were a Dionex GPM-2 gradient pump (low flow-rate model) for aqueous sodium hydroxide mobile phase, or a Hewlett-Packard 1050 LC or Shimadzu LC-600 (Shimadzu Scientific Instruments, Columbia, MD, USA) equipped with a SIL-6B autoinjector for volatile mobile phases with pHs between 5 and 7.

The mass spectrometer was a Hewlett-Packard (Palo Alto, CA, USA) Model 5988A equipped with a Hewlett-Packard particle beam LC interface. The ionization modes were EI and negative- and positive-ion chemical ionization (NCI and PCI) with isobutane as a reagent gas. The MS conditions were essentially those specified by the manufacturer: source temperature, 250°C; electron energy, 70 eV (EI) or 200 eV (NCI and PCI); scan time, 2 s; source pressure, *ca.* $2 \cdot 10^{-5}$ Torr (EI) or $2 \cdot 10^{-4}$ Torr (isobutane NCL and PCI); and helium pressure for the particle beam interface, 50 P.S.I. Typically 3–6 mass spectral scans from a single peak were averaged and an equal number of scans from the previous chromatographic minimum (as a background) was averaged and subtracted.

The UV detectors were a Dionex UV–VIS fixed-wavelength detector (254 nm) and Model 4270 integrator or a Hewlett-Packard Model 1040 diode-array detector and a Model 79994A Chem Station for data acquisition. Quantification with UV absorption was at 230 nm with peak-area integration.

Spike and recovery of aromatic sulfonic acids in water

The volumes of water used for spiking experiments were determined by the sulfonic acid level required in the final concentrate to meet required quantification limits (Table II). The spiked water samples were lyophilized (Freezemobile 12 SL; Vir-Tis, Gardiner, NY, USA) over 1–72 h, treated with dry methanol (up to 10% of the original volume of the aqueous sample depending on the amount of residue after lyophilization) and the mixture was sonicated with a Branson Model 2200 sonicator (Branson Ultrasonics, Danbury, CT, USA) for 20 min at room temperature (being careful to exclude water vapor) and acetone added (6 times the methanol volume) to precipitate inorganic salts such as sodium sulfate and carbonate. After 1 h the mixture was filtered (Whatman No. 1 paper). Acetone (30 ml) was used for washing the container and the filter-paper and the combined filtrate was evaporated under reduced pressure with a rotary evaporator. This precipitation step may be repeated for samples containing large amounts of inorganic salts. The final residue was dissolved in a known volume of methanol (0.25–20 ml) for injection. The replicates referred to in Table I were complete and included individual replicate sample preparation.

Total organic carbon determination for aqueous samples

The total organic carbon in aqueous samples was measured both before and after lyophilization (and reconstitution with distilled water) with a Dohrman DC 180 total organic carbon analyzer (Rosemount Analytical Division, Santa Clara, CA, USA). It was measured initially for the whole aqueous Casmalia groundwater sample and then for a lyophilized sample reconstituted to its original volume in distilled water.

RESULTS AND DISCUSSION

Anion-exchange chromatograms of the monosulfonic acid standards with particle beam MS detection (full scan, EI) are shown in Figs. 2 and 3. Fig. 2 also shows the EI mass spectra for the six monosulfonic acids corresponding to the peaks of the chromatogram shown. Fragmentation of these aromatic sulfonic acids under EI conditions involves the loss of SO_2, HSO_2, SO_3 or HSO_3. The presence of these fragment ions in the EI spectra are invaluable for confirmation without requiring the use of more complicated MS–MS experiments. With selected ion monitoring the molecular ion and fragments corresponding to loss of SO_2, HSO_2, SO_3 and HSO_3 under these conditions, the limits of detection are less than 250 ng.

In each instance the identity of the peak is unabiguously confirmed from a molecular and corresponding diagnostic fragmentation ions. A carryover or "memory" effect can be seen in some spectra. For example, the spectrum of 4-hydroxybenzenesulfonic acid (Fig. 2) shows in addition to the M^+, $[M-SO_2H]^+$ and $[M-SO_3H]^+$ ions a much smaller cluster at m/z 192 and 194 that probably come from the earlier eluting 4-chlorobenzenesulfonic acid. Possible the low volatility of these compounds makes them remain in or near the MS ion source.

These anion-exchange chromatograms with EI

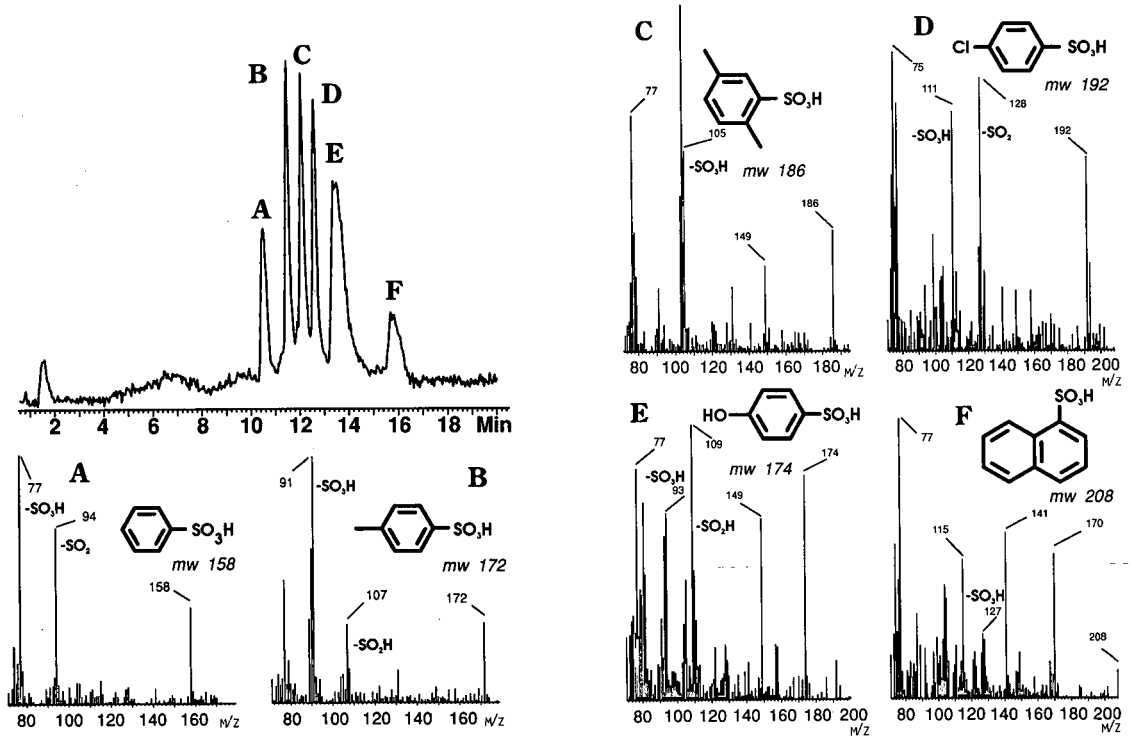

Fig. 2. Anion-exchange chromatogram (PAX-100 column with aqueous ammonium acetate–acetonitrile gradient) of six monosulfonic acid standards (2.0 μg each) with particle beam MS detection (full scan, EI) and (below) corresponding mass spectra obtained from this chromatogram. Chromatographic gradient conditions with a mobile phase consisting of water–acetonitrile–ammonium acetate (250 mM, pH 6.0): 0 min, 88:10:2, 5 min, 70:10:20; 10 min, 34:43:23.

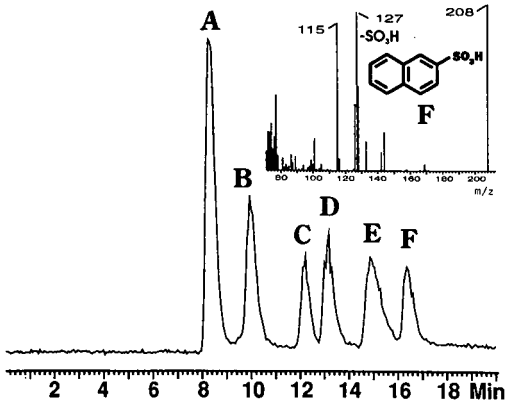

Fig. 3. Anion-exchange chromatogram (PAX-500 column with aqueous sodium hydroxide–acetonitrile gradient and micromembrane suppressor) of six monosulfonic acid standards (0.4 μg each) with particle beam MS detection (full scan, EI) and corresponding mass spectrum of 2-naphthalenesulfonic acid (mol.wt. 208; peak F) obtained from this chromatogram. Chromatographic gradient conditions with a mobile phase consisting of water–acetonitrile–sodium hydroxide (200 m*M*): 0 min, 90:10:0; 18 min, 0:40:60.

particle beam MS detection were produced with the OmniPac PAX-100 (with ammonium acetate, no suppressor, Fig. 2) and PAX-500 (with sodium hydroxide and the micromembrane suppressor, Fig. 3) columns. Because of the pressure limitations of currently available membrane suppressor desalting systems, the particle beam LC interface is ideally

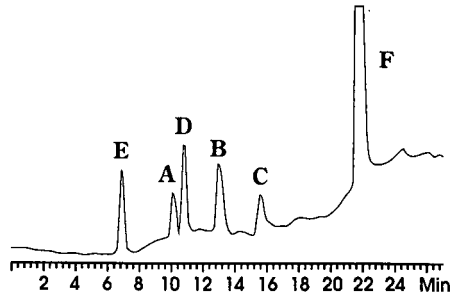

Fig. 4. Anion-exchange chromatograms (SAX column with constant aqueous ammonium acetate–gradient acetonitrile) of six monosulfonic acid standards (20 ng each) with UV detection (230 nm). Chromatographic gradient conditions with a mobile phase consisting of water–acetonitrile–ammonium acetate (100 m*M*, pH 6.0): 0 min, 85:0:15; 10 min, 83:2:15, 30 min, 55:30:15.

matched because of its inherently low back-pressure. Fig. 4 shows the same six standards as used in Fig. 2 (20 ng each), chromatographed on the SAX column using ammonium acetate and UV detection. The relative elution order of the six monosulfonic acids changes considerably between the PAX columns and the SAX column.

EI ionization gives approximately equal responses with six aromatic sulfonic acids (Figs. 2 and 3). NCI only gives a good response and spectral quality for 4-chlorobenzenesulfonic acid (base ion *m/z* 156, [M − HCl] [2]. PCI gives a poor response for all the standards used in this study.

TABLE I

SPIKE AND RECOVERY RESULTS FOR SIX MONO- AND TWO DISULFONIC ACID STANDARDS SPIKED INTO TAP WATER (TW) AND DISTILLED WATER (DW)

A = benzenesulfonic acid; B = 4-toluenesulfonic acid; C = xylenesulfonic acid; D = 4-chlorobenzenesulfonic acid; E = 4-hydroxybenzenesulfonic acid; F = 1-naphthalenesulfonic acid; G = 2,6-naphthalenesulfonic acid; H = 1,5-naphthalenesulfonic acid.

Spike (ppm)	Matrix	Volume (ml)	Recovery ± S.D.[a] (%)							
			A	B	C	D	E	F	G	H
0.01	DW	300	NT[b]	94 ± 7.1	85 ± 10	78 ± 5.3	NT	83 ± 5.0	NT	NT
0.01	TW	300	NT	73 ± 9.4	75 ± 10	78 ± 8.0	NT	78 ± 9.4	NT	NT
1.00	DW	10	NT	81 ± 5.2	92 ± 7.6	85 ± 4.4	NT	87 ± 4.6	96 ± 3.2	142 ± 8.8[c]
1.00	TW	10	NT	75 ± 9.8	88 ± 12	74 ± 7.0	NT	79 ± 11	62 ± 4.9	96 ± 2.6
100.0	DW	5	76 ± 6.5	90 ± 3.9	82 ± 5.3	91 ± 6.6	71 ± 5.3	90 ± 6.3	77 ± 6.1	94 ± 8.8
100.0	TW	5	78 ± 3.3	82 ± 6.1	83 ± 10	89 ± 4.6	65 ± 6.9	87 ± 4.9	75 ± 11.7	116 ± 3.6

[a] Standard deviation calculated from 6–12 replicate sample extracts.
[b] NT = specific analyte not tested at this concentration.
[c] Recovery of 1,5-naphthalenesulfonic acid was consistantly high in distilled water even with freshly prepared standards, suggesting that a positive interference may be present in this blank.

Recoveries of aromatic sulfonic acid standards added into tap water and distilled, deionized water are shown in Table I. With UV detection, the quantification limits range from 2 to 80 ng injected on-column (Table II). Quantification limits for the disulfonic acids are greater than those for the monosulfonic acids. The disulfonic acids were not used in the chromatographic experiments reported here, but were included in the Table I spike and recovery experiments to demonstrate that this recovery method can be generalized to disulfonic in addition to monosulfonic acids in aqueous samples.

Application to environmental samples

The total organic carbon (TOC) concentration in the Casmalia groundwater monitoring well sample was 7400 ± 270 ppm (± standard deviation, $n=3$). After lyophilization of this sample and reconstitution with distilled water to the original volume, the TOC became 1500 ± 32 ppm. Hence in the Casmalia sample 21% of the TOC is non-volatile and is retained after the lyophilization process. This compares with more than 95% of the TOC in Stringfellow waste site samples being non-volatile [2]. Fig. 5 shows an anion-exchange chromatogram (SAX column) of the Casmalia groundwater monitoring well sample both before (top) and after (bottom) lyophilization with UV detection (265 nm). The early-eluting peaks appear to be selectively lost during the lyophilization process.

Fig. 6a shows the corresponding anion-exchange chromatogram of the Casmalia lyophilizate with EI particle beam detection. The chromatographic conditions were slightly modified compared with Fig. 5. The presence of toluenesulfonic acid in this sample is qualitatively indicated by comparison of the extracted ion profile (Fig. 6a) with the full EI mass spectra of this compound (Fig. 2). The major ions of the toluenesulfonic acid standard, M^+, $[M-HSO_2]^+$ and $[M-HSO_3]^+$, all coincide in Fig. 6a. Spiking the sample with 10 μg of authentic standard shows co-elution with the unknown peak (Fig. 6b). A 10-μg sample of the toluenesulfonic acid alone shows a slightly shorter retention time (38.4 *versus* 37.0 min) under these conditions (Fig. 6c). We have observed that retention times with anion-exchange chromatography are at least as sensitive to both sample loading and the presence of other analytes as is typically seen for reversed-phase chromatography. The identification of toluenesulfonic acid is purily qualitative in this experiment. This is

TABLE II

CORRELATION COEFFICIENTS (R) AND QUANTIFICATION LIMITS FOR FIVE-POINT CALIBRATION WITH SIX MONO- AND TWO DIAROMATIC SULFONIC ACIDS WITH ANION-EXCHANGE LC (SGE SAX COLUMN WITH CONSTANT AQUEOUS AMMONIUM ACETATE–GRADIENT ACETONITRILE MOBILE PHASE) AND UV DETECTION (230 nm)

The calibration concentration range is 1–2000 ng injected.

Compound	R	Quantitation Limit (ng injected)[a]
A	0.999	12
B	0.999	12
C	0.999	12
D	0.998	5
E	0.999	13
F	0.995	2
G	0.998	30
H	0.990	80

[a] Quantitation limit is the concentration of the linear five-point calibration line corresponding to the lower 95% prediction limit abscissa intercept, *i.e.*, the minimum concentration at which the predicted peak area includes zero at the 95% prediction confidence limit, or the lowest calibration concentration, whichever is the larger number.

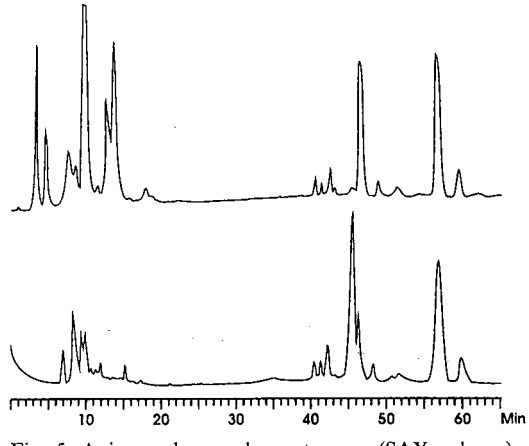

Fig. 5. Anion-exchange chromatogram (SAX column) of the Casmalia groundwater monitoring well sample both before (top) and after (bottom) lyophilization with UV detection (265 nm). The early-eluting peaks are selectively lost during the lyophilization process.

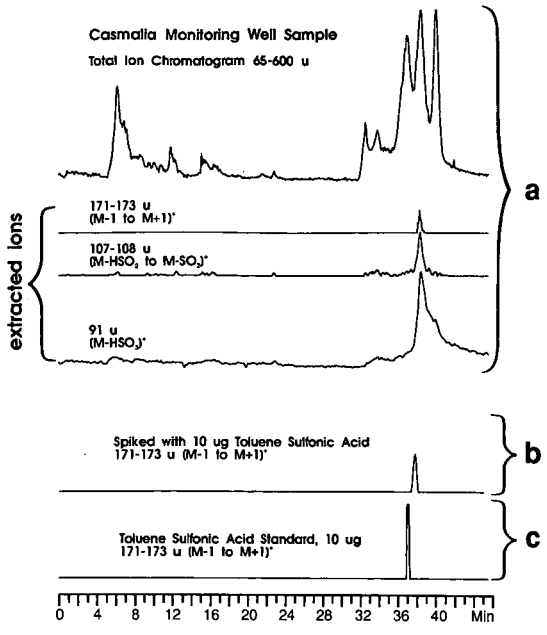

Fig. 6. (a) Anion-exchange chromatogram (chromatographic conditions slightly different to those in Fig. 5) of the Casmalia lyophilizate with EI particle beam MS detection showing both full scan (top), and extracted ion chromatograms (u = atomic mass units) (M^+, $[M-HSO_2]^+$ and $[M-HSO_3]^+$) (vertical scale $\times 10$) of the major ions of toluenesulfonic acid standard. (b) Same conditions but with the sample spiked with 10 μg of toluenesulfonic acid. (c) Same conditions but with only a 10-μg sample of the toluenesulfonic acid.

because quantification, relying on UV absorption, is effectively blocked by the large amounts of interfering material present in this real sample.

Aromatic sulfonic acids have been shown to occur as organic pollutants in aqueous samples at several hazardous waste sites. These materials are not well determined by conventional GC-based methods. The application of anion-exchange LC–particle beam MS will help to increase our understanding of this non-volatile and water-soluble organic fraction of environmental aqueous samples.

ACKNOWLEDGEMENTS

M. A. B. gratefully acknowledges EPA EMSL, Las Vegas, for their partial financial support, and thanks Rosanne Slingsby, John Stillian, Karen Cambell and Robert Joyce of Dionex for providing materials used for this project and John Hsu of this laboratory for technical assistance.

REFERENCES

1 M. A. Brown, I. S. Kim, R. Roehl, F. I. Sasinos and R. D. Stephens, *Chemosphere*, 19 (1989) 1921.
2 M. A. Brown, I. S. Kim, F. I. Sasinos and R. D. Stephens, *Environ. Sci. Technol.*, 24 (1990) 1832.
3 M. A. Brown, I. S. Kim, J. S. Hsu, F. I. Sasinos and R. D. Stephens, in *Proceedings of the United States Environmental Protection Agency Symposium on Waste Testing and Quality Assurance, Washington, DC, July 1990*, Vol. II, US Environmental Protection Agency, 1990, p. 8.
4 Science Applications International Corp. (SAIC), La Jolla, CA, *Stringfellow Remedial Investigation, 1987, Draft Final Report, Sections 1, 2 and 3*, submitted to the California Department of Health Services, Toxic Substances Control Division, Sacramento, CA.
5 R. D. Stephens, N. B. Ball, T. S. Fisher, R. Roehl and W. M. Draper, in *Proceedings of the United States Environmental Protection Agency Symposium of Waste Testing and Quality Assurance, Washington, DC, July 1987*, Vol. 1, US Environmental Protection Agency, 1987, p. 15.
6 M. A. Brown, I. S. Kim, F. I. Sasinos and R. D. Stephens, in M. A. Brown (Editor) *Liquid Chromatography/Mass Spectrometry: Application in Agricultural, Pharmaceutical and Environmental Chemistry* (ACS Symposium Books Series, No. 420), American Chemical Society, Washington, DC,1990, Ch. 13, p. 198.
7 J. J. Conboy, J. D. Henion, M. W. Martin and J. A. Zweigenbaum, *Anal. Chem.*, 62 (1990) 800.
8 R. C. Simpson, C. C. Fenselau, M. R. Hardy, R. R. Townsend, Y. C. Lee and R. J. Cotter, *Anal. Chem.*, 62 (1990) 248.
9 W. M. Draper, F. R. Brown, R. Bethem and M. J. Miille, in M. A. Brown (Editor) *Liquid Chromatography/Mass Spectrometry: Application in Agricultural, Pharmaceutical and Environmental Chemistry* (ACS Symposium Books Series, No. 420), American Chemical Society, Washington, DC,1990, Ch. 17, p. 253.
10 R. J. Vreeken, U. A. Th. Brinkman and G. J. de Jong, *Biomed. Environ. Mass Spectrom.*, 19 (1990) 481
11 K. B. Tomer and C. E. Parker, *J. Chromatogr.*, 492 (1989) 189.
12 V. G. Belolipetskaja, V. K. Piotrovskii, V. I. Metelitsa and S. A. Pavlinov, *J. Chromatogr.*, 491 (1989) 507.
13 T. D. Behymer, T. A. Bellar and W. L. Budde, *Anal. Chem.*, 62 (1990) 1686.

Journal of Chromatography, 589 (1992) 185–195
Elsevier Science Publishers B.V., Amsterdam

CHROM. 23 660

Measurement of stability constants for complexes of divalent cations with tartaric acid by ion chromatography

Fred Hung-Jye Lin

Department of Chemical Engineering, National Cheng Kung University, Tainen, 70101 (Taiwan)

Csaba Horváth*

Department of Chemical Engineering, Yale University, New Haven, CT 06520 (USA)

(First received February 26th, 1991; revised manuscript received July 30th, 1991)

ABSTRACT

Single-column ion chromatography was used with ethylenediammonium tartrate in the eluent for the rapid separation of divalent metal ions and for the measurement of the complexation constants of divalent metal ions with tartrate. A theoretical framework was developed for the interpretation of the effect of pH, tartaric acid and ethylenediamine concentrations on the retention factors. Equilibrium constants for the ion-exchange process were evaluated and the concomitant enthalpy and entropy changes calculated.

INTRODUCTION

Since liquid chromatography began to evolve as an analytical and instrumental technique in the 1960s, high-performance liquid chromatography (HPLC) has become a widely employed method for the analysis and purification of non-volatile substances. It has also found limited use in the measurement of physico-chemical data.

Ion chromatography, introduced by Small *et al.* [1] in 1975, represents an extension of HPLC to the analysis of inorganic ions by employing a conductivity detector and a dual column system. In 1980 Fritz *et al.* [2] developed a single-column method for ion chromatography which allows for both a decrease and increase with indirect and direct detection, respectively. As a result, ion chromatography has become a convenient method for determining the level of ionic species in many industrial processes and for monitoring of air and water pollutants in the environment. Now a variety of detectors are available and ion chromatography is used also in other fields such as biochemistry, pharmacy and forensic science. The fundamentals and applications of ion chromatography have been reviewed in recent books [3–5].

Eluents with complexing agents [6] have often been employed in ion chromatography to enhance selectivity for metal ions. The use of a complexing agent in the eluent also improves the sharpness of separation and broadens the scope of cation chromatography with a conductivity detector. The presence of the complexing agent, however, frequently makes the detection of metal ions difficult. Elchuk and Cassidy [7] circumvented this problem in the chromatographic analysis of lanthanides with α-hydroxyisobutyric acid by using postcolumn derivatization and spectrophotometric detection.

Often, however, postcolumn derivatization engenders excess band broadening. For this reason, Sevenich and Fritz [8–10] used ethylenediamine together with α-hydroxyisobutyrate in the eluent to carry out the analysis without postcolumn derivatization.

Ion chromatography is now well suited to separate ions and conductivity detectors have been

0021-9673/92/$05.00

greatly improved in recent years [11] to provide sensitive and "universal" detection of ions in solution. However, only a few theoretical studies have been conducted to establish the effect of complexation on changing the conditions during cation elution. Although Sevenich and Fritz [8] showed that the retention factors decrease with increasing pH, different trends have also frequently been observed.

The aim of this work was to develop a theoretical model for the retention of divalent cations which form complexes with tartrate ligand. The experimentally observed effects of temperature, pH, tartaric acid and ethylenediamine concentrations on the retention and separation of cations is then examined within the theoretical framework.

EXPERIMENTAL

Instrument

A Model HLC-601 fully automated high-speed ion chromatograph (Shimadzu, Tokyo, Japan) was used. The microcomputer-controlled single-plunger pump with a Bourdon tube pulsation damper of 5-ml volume was used to generate eluent flow in the range 0.1–9.9 ml/min at a maximum pressure of 70 kg/cm^2. The motor-driven sample injection valve was equipped with a 100-μl sample loop.

The column was thermostated with a precision of ± 0.1°C in the temperature range 30–60°C by an oven with hot-air circulation. Prior to entering the injection valve and the column, the eluent first passed through a heat-exchanger coil which was also located in the oven.

The 1.4-μl conductivity cell of the detector was equipped with a.c. five-pole ring electrodes and its cell constant was 10 cm^{-1}. The highest detector sensitivity was $2 \cdot 10^{-2}$ μS/cm. The detector cell was maintained at a temperature 3°C higher than that of the column by a 50-μl heating coil, made of $^1/_{16}$-in. 316 stainless-steel tubing (100 cm × 0.25 mm I.D.) in order to maintain a stable baseline.

Column

A 50 mm × 4.6 mm I.D. TSK-Gel IC-Cation column (Tosoh, Tokyo, Japan) was packed with 10-μm sulphonated polystyrene-type cation-exchange resin particles, having a capacity of 46 μequiv./g.

Materials

Fresh deionized, distilled water prepared with a Mega-Pure System, Model MP-12A (Corning Glass, New York, USA) was used. Analytical-reagent grade $CaCl_2$, $CdCl_2$, $Zn(NO_3)_2$, $Co(NO_3)_2$, $Ni(NO_3)_2$, $Mn(NO_3)_2$, tartaric acid, ethylenediamine (EDA), sodium hydroxide and nitric acid were supplied by Shimakyu Chemical (Osaka, Japan).

Isocratic elution was carried out with solutions containing 0.2, 1.0, 2.0, 3.0, 4.0 and 5.0 m*M* tartaric acid and 0.2, 0.4, 0.8, 1.2 m*M* ethylenediamine. The eluent pH was adjusted by using sodium hydroxide or nitric acid. All eluents were filtered through a 0.5-μm filter before use.

Methods

In all experiments, 100-μl samples were injected without precolumn derivatization. The flow-rate was 0.8 ml/min and experiments were carried out at 30, 40, 50 and 60°C. The detector settings were in ranges of 200, 500 and 1000 and the gain was 100 or 200. The recorder full-scale was set to 1 V. The column was periodically washed with 0.1% nitric acid in order to remove polyvalent ions from the resin. The samples were prepared by dissolving the chloride or nitrate of the metals in the eluent to obtain a concentration of 0.05 m*M*. The pH of the eluent was measured with a Model AT-200 potentiometric automatic titrator (Kyoto Electronics, Tokyo, Japan) at each temperature with temperature compensation and was adjusted to the predetermined value by using 1 *M* nitric acid or 1 *M* sodium hydroxide solution. Chromatographic experiments started with setting of the oven temperature and pumping the eluent through the system. After the oven temperature had reached the desired value, the detector range was adjusted so that the signal output was about 50% of the 1 V full-scale at the background conductivity.

The mobile phase volume in the heat exchanger and in the connecting tubing was measured carefully together with the extra-column volume associated with the injector and detector and were taken into account in the calculation of the void volume of the column. The flow-rate was measured each time before injection by using 0.5 m*M* potassium chloride solution as inert eluite and the reproducibility was found to be within 0.1%.

THEORY

In ion chromatography, separations occur owing to differences in the retention of an eluite by oppositely charged binding sites of the stationary phase. In the process described here, the sample cations interact with the sulphonic acid groups of the ion-exchange resin, and compete with the eluting cations for the exchange sites. When a pulse of sample cations is injected onto the column equilibrated with eluting cations, the sample cations are retained by the exchange sites at the chromatographic surface with concomitant expulsion of eluting cations. This pulse of eluting cations moves down the column unretained, whereas sample cations are gradually eluted in a process characterized by their competition with the eluting cations for the ion-exchange sites of the stationary phase.

Equilibrium considerations

The three cation-exchange processes underlying the separation are given by the following three equilibria:

$$M^{2+} + \overline{ER_2} \rightleftharpoons \overline{MR_2} + E^{2+} \quad (1a)$$

$$M^{2+} + 2\,\overline{HR} \rightleftharpoons \overline{MR_2} + 2\,H^{+} \quad (1b)$$

and

$$2\,H^{+} + \overline{ER_2} \rightleftharpoons 2\,\overline{HR} + E^{2+} \quad (1c)$$

where M^{2+}, H^{+} and E^{2+} are the divalent metal cations, hydrogen ion and fully protonated ethylenediamine in the mobile phase, respectively. $\overline{MR_2}$, $\overline{HR}$ and $\overline{ER_2}$ indicate that the species are bound to the stationary phase. The subscript 2 on R indicates that two exchange sites bind a cationic species. The pertinent equilibrium constants are given by

$$K_m^e = [\overline{MR_2}][E^{2+}]/[M^{2+}][\overline{ER_2}] \quad (2a)$$

$$K_m^h = [\overline{MR_2}][H^{+}]^2/[M^{2+}][\overline{HR}]^2 \quad (2b)$$

and

$$K_h^e = [\overline{HR}]^2[E^{2+}]/[H^{+}]^2[\overline{ER_2}] \quad (2c)$$

Let f represent the fraction of the exchange sites in the stationary phase which are occupied by hydrogen ions. At low sample concentrations, *i.e.*, under conditions of linear chromatography, the fraction of the exchange sites which are occupied by ethylenediamine cations can be approximated by $1 - f$. Then the equilibrium constants K_h^e and K_m^e can be calculated by the following relationships:

$$K_h^e = 2f^2C[E^{2+}]/(1 - f)[H^{+}]^2 \quad (3)$$

and

$$K_m^e = 2[\overline{MR_2}][E^{2+}]/[M^{2+}]C(1 - f) \quad (4)$$

where C is the resin capacity.

The fraction of the protonated exchange sites f can be evaluated when K_h^e is known:

$$f = \frac{-[H^{+}]^2K_h^e + \sqrt{[H^{+}]^4K_h^{e2} + 8C[E^{2+}][H^{+}]^2K_h^e}}{4C[E^{2+}]} \quad (5)$$

For any equilibrium reaction the enthalpy change, ΔH^0, is a constant at a given temperature and can be calculated from the well known Van 't Hoff equation:

$$\Delta H^0 = -\mathrm{d}(R \ln K)/\mathrm{d}(1/T) \quad (6)$$

where K is the equilibrium constant, R is the gas constant and T is the absolute temperature. The entropy change at any temperature, ΔS^0, can be calculated from

$$\Delta S^0 = \Delta H^0/T + R \ln K \quad (7)$$

Retention factor

The magnitude of retention is most conveniently expressed by the dimensionless retention factor, k', which can be evaluated directly from the chromatogram. In linear chromatography:

$$k' = (t_r - t_0)/t_0 = \phi K_{Chrom} \quad (8)$$

where t_r is the retention time of the eluite, t_0 is the mobile phase hold-up time, ϕ is the phase ratio and K_{Chrom} is the chromatographic equilibrium constant. K_{Chrom} represents the distribution of the eluite beween the two phases, and can be calculated by

$$K_{Chrom} = (1 - f)CK_m^e\alpha_m/2[E^{2+}] \quad (9)$$

where α_m is given by

$$\alpha_m = [M^{2+}]/[M]_t \quad (10)$$

i.e., it is the fraction of the total metal in mobile phase which exists as the free metal ion.

The phase ratio, ϕ, of the column is calculated as

$$\phi = \frac{W}{V_m\rho_r} = \frac{(1 - \varepsilon_e)(1 - \varepsilon_i)}{\varepsilon_e + (1 - \varepsilon_e)\varepsilon_i} \quad (11)$$

and

$$V_m = V_0[\varepsilon_e + (1 - \varepsilon_e)\varepsilon_i] \quad (12)$$

where V_0 is the empty column volume, V_m is the space occupied by the mobile phase, W is the weight of ion-exchange resin present in the column and ε_i, ε_e and ρ_r are the intraparticular porosity, interparticular porosity and the true density of ion-exchange resin, respectively.

Combining eqns. 8, 9 and 11 we obtain for the retention factor the following expression:

$$k' = \frac{W(1-f)CK_m^e\alpha_m}{V_m\rho_r \cdot 2[E^{2+}]} \quad (13)$$

In the pH range of interest, ethylenediamine is fully protonated. The value of α_m can be calculated from the two acid ionization constants of tartaric acid, K_1 and K_2, to obtain the fractions of the total tartrate, A^{2-}, and acid tartrate, HA^-, at the pH of the mobile phase, *i.e.*, β_a and β_{ha}, by using the following relationships:

$$\beta_a = \frac{[A^{2-}]}{[A]_t} = \frac{1}{\left(1 + \frac{[H^+]^2}{K_1K_2} + \frac{[H^+]}{K_2}\right)} \quad (14)$$

and

$$\beta_{ha} = \frac{[HA^-]}{[A]_t} = \frac{1}{\left(1 + \frac{[H^+]}{K_1} + \frac{K_2}{[H^+]}\right)} \quad (15)$$

so that α_m is evaluated as

$$\alpha_m = \frac{[M^{2+}]}{[M]_t} = \frac{1}{1 + K_{ma}^a[A^{2-}] + K_{mha}^{ha}[HA^-]} \quad (16)$$

Measurements by ion chromatography can be used to evaluate the stability constant of the complex, K_{ma}^a, formed from the metal ion and the tartrate ligand A^{2-} and given by

$$K_{ma}^a = [MA]/[M^{2+}][A^{2-}] \quad (17)$$

Combining eqns. 13 and 16, we obtain

$$\frac{1}{k'} = \frac{2[E^{2+}](1 + K_{ma}^a[A^{2-}] + K_{mha}^{ha}[HA^-])}{\phi(1-f)CK_m^e} \quad (18)$$

Eqn. 18 also contains the stability constant of the complex, K_{mha}^{ha}, formed between the metal ion and the acid tartrate ligand HA^-, and is given by:

$$K_{mha}^{ha} = [MHA^+]/[M^{2+}][HA^-] \quad (19)$$

However, the magnitude of the product $K_{mha}^{ha}[HA^-]$ in eqn. 18 is usually much smaller than that of the other terms in the denominator, and it can therefore be neglected. Further, $[A^{2-}] = \beta_a[A]_t$, so that we can express the reciprocal of retention factor as

$$\frac{1}{k'} = \frac{2[E^{2+}](1 + K_{ma}^a\beta_a[A]_t)}{\phi(1-f)CK_m^e} \quad (20)$$

According to eqn. 20, a plot of $1/k'$ against $[A]_t$ yields a straight line and the formation constant K_{ma}^a can be obtained as the ratio of its slope and intercept.

The resolution of two eluites also depends on the separation factor, α_{21}, which is defined for any two components as

$$\alpha_{21} = k'_2/k'_1 \quad (21)$$

where k'_1 and k'_2 are the retention factors for components 1 and 2, respectively.

RESULTS AND DISCUSSION

According to eqn. 14, the signal from the conductivity detector is proportional to the eluite concentration and to the difference between the limiting equivalent conductances of the eluting and eluite cations. The addition of a complexing agent to the eluent will not disturb this rule but may decrease the degree of ionization of the eluite and lower the detector signal.

Fig. 1A shows the retention factor at various tartrate concentrations. According to eqn. 20, a plot of $1/k'$ against $[A]_t$ yields a straight line and this is shown in Fig. 2. Perfect straight lines were obtained. From such plots the formation constant K_{ma}^a can be obtained as the ratio of the slope and intercept. The adjusted retention times t'_r from the data of Sevenich and Fritz [8] with 2.0 mM tartrate in the eluent at room temperature are also plotted in Fig. 2 for comparison. The adjusted retention time is defined as the difference between the retention time of the eluite peak and the mobile phase hold-up time. From Fig. 2, it can be seen that the slope obtained by Sevenich and Fritz is different from that obtained here. The divergence of the slopes is attributed to the use of different EDA concentrations, which affects the magnitude of f, and to the difference in temperature, which affects the magnitude of K_{ma}^a and K_m^e according to eqn. 20.

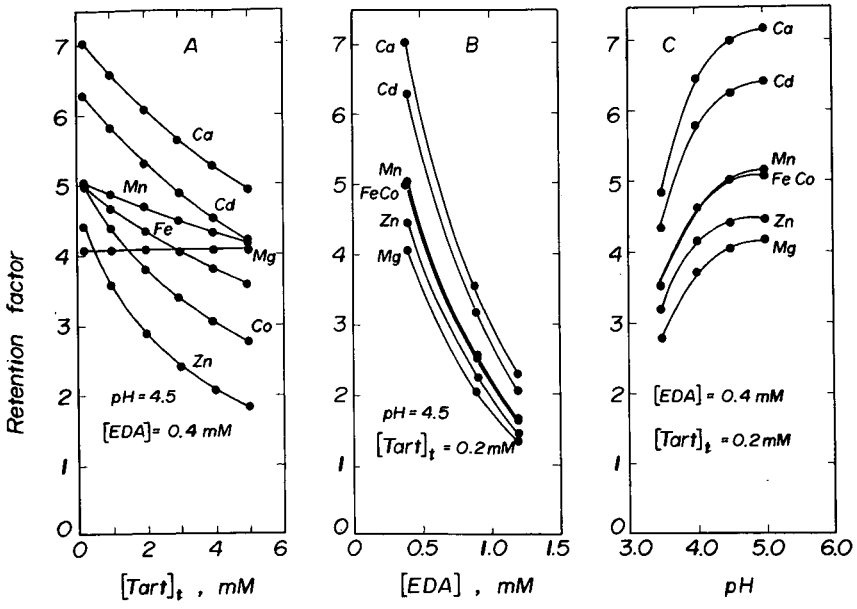

Fig. 1. Effect of the mobile phase composition on the retention factor of divalent metal ions in single-column ion chromatography with tartrate and ethylenediamine in the eluent at 30°C. (A) Fixed ethylenediamine concentration and changing tartrate concentration at pH 4.5; (B) fixed tartrate concentration and changing ethylenediamine concentration at pH 4.5; (C) fixed tartrate and ethylenediamine concentrations and changing pH.

The dependence of the logarithmic formation constants K^{a}_{ma} calculated from Fig. 2 on the reciprocal of absolute temperature are shown by the Van 't Hoff's plots in Fig. 3. The phase ratio, ϕ, was calculated to be 0.43, the ion-exchange capacity of the resin was 0.04 mequiv. cm^{-3} of true resin volume and β_a at pH 4.5 was calculated as 0.568 from eqn. 14. The two acid ionization constants of tartaric acid at near zero ionic strength used in our experiments were $K_1 = 9.1 \cdot 10^{-4}$ and $K_2 = 4.3 \cdot$

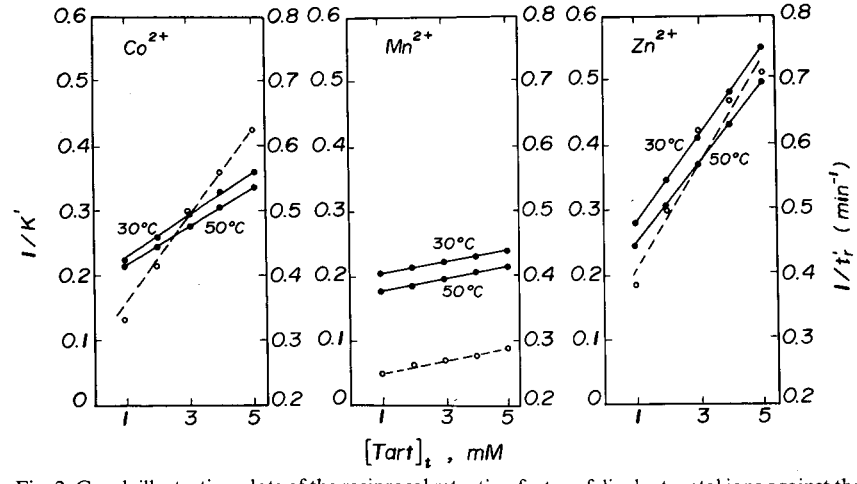

Fig. 2. Graph illustrating plots of the reciprocal retention factor of divalent metal ions against the concentration of tartrate in the mobile phase at pH 4.5. The concentration of ethylenediamine was 0.4 mM and measurements were made at 30 and 50°C (●). The data of Sevenich and Fritz [8] with 2.0 mM EDA in the eluent at room temperature are also plotted for comparison (○). The reciprocal of adjusted retention time is shown on the right-hand ordinate.

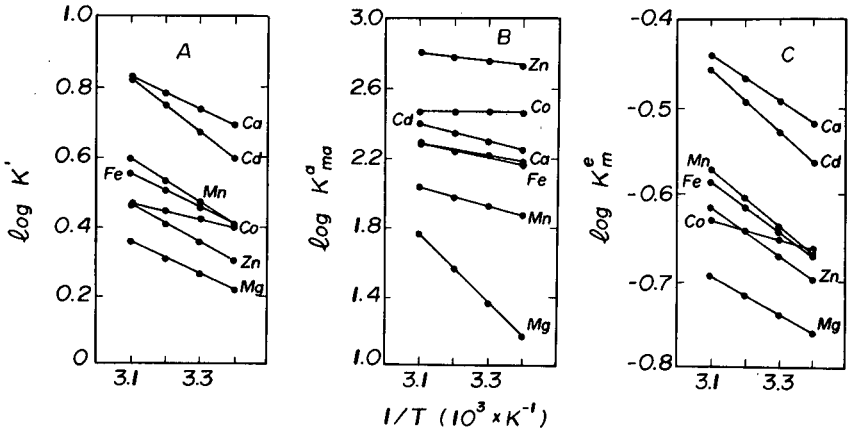

Fig. 3. Van 't Hoff plots of equilibrium data obtained with divalent metal ions. (A) Retention factor measured with 0.4 mM ethylenediamine and 0.2 mM tartaric acid in the mobile phase at pH 4.5; (B) stability constant for complexation with tartrate in aqueous solution of 1–13 millimolal ionic strength; (C) ion-exchange equilibrium constant with ethylenediammonium ion towards ion.

10^{-5} molal [12]. The f values calculated for various ethylenediamine concentrations and pH values are listed in Table I.

The retention factors of divalent metals measured by using 0.2 mM tartrate and 0.4 mM ethylenediamine at various pH values are shown in Fig. 1C. It can be seen that the retention factors increase with pH, a result which apparently contradicts the conclusions put forward by Sevenich and Fritz from their experimental observations [8]. The origin of this discrepancy has been examined as follows.

For any given ion chromatographic column the ion-exchange capacity and the phase ratio are constants and can be determined *a priori*. From eqns. 5 and 20, it can be seen that if the concentrations of ethylenediamine, $[E^{2+}]$, and tartaric acid, $[A]_t$, were constant and the oven temperature was the same, k' is a function of pH with K^e_h, K^e_m and $K^a_{ma}\beta_a$ as parameters. As $K^a_{ma}\beta_a$ has been calculated previously by using the data from Fig. 2, the pertinent K^e_h and K^e_m values can be obtained by minimizing the sum of squares of the deviations between the calculated and measured retention factors at more than two pH values. From the data in Fig. 1C, it was found that $K^e_h = 66$ gives the best fit of the retention factor data obtained at low pH where precipitation of hydroxides is circumvented and the chelation with ethylenediamine can be neglected. As K^e_h is not very sensitive to temperature under the conditions of the experiment, it can be assumed to be constant in the temperature range 30–60°C.

The enthalpy and entropy changes for the complexation of metal ions with tartrate calculated from Fig. 3B by using eqns. 6 and 7 are listed in Table II. The complexation processes is endothermic for all ions except cobalt and the entropy change is positive in all instances. The positive entropy change may be attributed to the water molecules that are displaced from the coordination sphere of metal ions.

A comparison of stability constants for the complexes of divalent metal ions with tartrate measured in this work with those from the literature which

TABLE I

EFFECT OF ETHYLENEDIAMINE CONCENTRATION AND pH ON THE FRACTION OF PROTONATED SITES, f, IN THE STATIONARY PHASE

The f values were calculated from eqn. 5 by using 0.04 mequiv. cm^{-3} and 66 for the ion-exchange capacity of the resin and for the ion-exchange equilibrium constant, K^e_h, respectively.

$[E^{2+}]$ (mM)	Fraction of protonated sites, f, at pH			
	3.5	4.0	4.5	5.0
0.2	0.45	0.17	0.058	0.019
0.4	0.34	0.12	0.041	0.013
0.8	0.26	0.090	0.030	0.009
2.0	0.17	0.058	0.019	0.006

TABLE II

ENTHALPY AND ENTROPY CHANGES AT 25°C

ΔH^0_{ma} is associated with complex formation of divalent ion with tartrate, ΔH^0_{ex} is for the ion-exchange process of metal ions with ethylenediammonium ion on the exchange sites and ΔH^0_k is the retention enthalpy. The corresponding entropy changes are ΔS^0_{ma} and ΔS^0_{ex}.

Metal ion	Enthalpy change (kJ/g · mol)			Entropy change (J/g · mol · K)	
	ΔH^0_{ma}	ΔH^0_{ex}	ΔH^0_k	ΔS^0_{ma}	ΔS^0_{ex}
Zn^{2+}	2.5 ± 0.4	5.3 ± 0.4	5.4 ± 0.4	60.9 ± 0.2	5 ± 1
Mg^{2+}	38 ± 2	4.4 ± 0.3	4.4 ± 0.3	152 ± 2	0 ± 1
Ca^{2+}	3.0 ± 0.4	4.8 ± 0.4	4.8 ± 0.4	52 ± 1	6 ± 1
Cd^{2+}	8.0 ± 0.7	7.0 ± 0.4	7.0 ± 0.4	71 ± 1	12 ± 1
Co^{2+}	−0.9 ± 0.3	2.0 ± 0.3	2.1 ± 0.3	44 ± 1	−6 ± 1
Mn^{2+}	8.6 ± 0.6	6.1 ± 0.4	6.2 ± 0.4	65 ± 1	7 ± 1
Fe^{2+}	7.0 ± 0.6	5.2 ± 0.3	5.2 ± 0.3	65 ± 1	4 ± 1

were measured under various conditions by using other methods are listed in Table III. As can be seen, the stability constant measured by ion chromatography are in good agreement with those measured by other methods.

On the basis of these results, we can explain why at a fixed ethylenediamine concentration but a low tartaric acid concentration, *i.e.*, 0.2 millimolal, the retention time increases with pH as shown in Fig. 1C. When the tartrate concentration is low, the retention of metal ions is influenced predominantly by the pushing effect of the ethylenediammonium ion, which occupies a large fraction of exchange sites. In contrast, at higher tartrate concentrations, *e.g.*, 2 millimolal, the retention of metal ions is predominantly affected by the pulling effect of tartrate ion. Consequently, their retention decreases with increasing pH owing to the greater complexing capacity of tartrate at higher pH [8].

At sufficiently high ethylenediamine concentrations, the value of the protonated fraction f is negligible. Therefore, according to eqn. 18, the retention factor should be inversely proportional to ethylenediamine concentration at constant tartrate concentration, temperature and pH. In order to examine the validity of eqn. 18, the data illustrated in Fig. 1B for the dependence of k' on the concentration of ethylenediamine were replotted in Fig. 4, which shows double logarithmic plots of the retention factor against ethylenediamine concentration for various divalent metal ions. The negative slopes were all close to unity and thus lend support to the validity of eqn. 18. This shows, in fact, that a divalent metal can bind with two sulphonic acid groups on the ion-exchange column used. Further, the straight lines in Fig. 4 are parallel so that the separation factor for any two metals, $\log \alpha_{21} = \log k'_2 - \log k'_1$, is constant at varying ethylenediamine concentration. This means that ethylenediamine

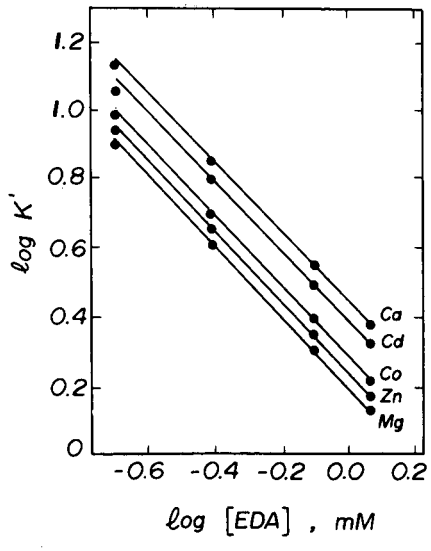

Fig. 4. Graph illustrating plots of the logarithmic retention factors for various divalent metal ions against the logarithmic ethylenediamine concentration in the eluent containing 0.2 m*M* tartaric acid at pH 4.5 and 30°C.

TABLE III

COMPARISON OF STABILITY CONSTANTS FOR COMPLEXES OF DIVALENT METAL IONS WITH TARTRATE MEASURED BY ION CHROMATOGRAPHY (IC) IN THIS WORK WITH THOSE REPORTED IN THE LITERATURE AND MEASURED EITHER BY DISTRIBUTION BETWEEN TWO PHASES (P) OR BY THE GLASS ELECTRODE (GE) OR BY ION-EXCHANGE (IE)

In the present work the range of ionic strength was 1–13 millimolal.

Ions	Temperature (°C)	Log K^a_{ma}	Reference[a]	Method[a]	Ionic strength[a]
Zn^{2+}	30	2.75 ± 0.03	–	IC	–
	40	2.76 ± 0.03	–	IC	–
	20	2.69 ± 0.08	13	P	a
	25	3.31 ± 0.08	14	P	b
Mg^{2+}	30	1.18 ± 0.01	–	IC	–
	40	1.39 ± 0.02	–	IC	–
	37	1.91	15	GE	c
Ca^{2+}	30	2.20 ± 0.01	–	IC	–
	40	2.22 ± 0.01	–	IC	–
	37	2.17	16	GE	d
Cd^{2+}	30	2.27 ± 0.01	–	IC	–
	40	2.31 ± 0.01	–	IC	–
	20	3.71 ± 0.03	13	P	a
	30	1.1 ± 0.2	17	P	f
Co^{2+}	30	2.48 ± 0.02	–	IC	–
	40	2.47 ± 0.02	–	IC	–
	20	2.8 ± 0.1	13	P	b
	25	3.08 ± 0.02	18	GE	a
	25	3.02 ± 0.02	19	IE	g
	25	2.50 ± 0.01	20	P	b
Mn^{2+}	30	1.89 ± 0.04	–	IC	–
	40	1.94 ± 0.04	–	IC	–
	20	2.92 ± 0.05	13	P	a
	32	1.44	21	GE	h
Fe^{2+}	30	2.17 ± 0.01	–	IC	–
	40	2.21 ± 0.01	–	IC	–
	20	2.24	22	IE	h

[a] (a) Constant ionic strength of 0.1 millimolal by addition of $KClO_4$; (b) constants corrected to zero ionic strength; (c) 0.2 *M* $NaClO_4$; (d) 0.090 *M* $NaClO_4$; (e) 0.1 *M* $NaClO_4$; (f) constant ionic strength of 1 molal by addition of $NaClO_4$; (g) ionic strength between 0 and 0.155 molal; (h) constant ionic strength of 0.1 molal by addition of $NaClO_4$.

does not affect the selectivity of the chromatographic system to metal ions.

From Fig. 1C it is also evident that the separation factor for any two metals does not vary much with changing pH. On the other hand, the poor resolution of Mn(II), Fe(II) and Co(II) at 0.2 m*M* tartrate concentration can be improved by increasing the tartrate level as shown in Fig. 1A. In contrast, the selectivity of chromatographic separation for Mg(II), Mn(II) and Cd(II) ions is improved by lowering the tartrate level.

As shown by the Van 't Hoff plots in Fig. 3A, the capacity factor increases with increase in temperature. The retention enthalpies calculated from the slope of the Van 't Hoff's plots are listed in Table II.

The ion-exchange equilibrium constant K^c_m of metal ions with ethylenediamine is shown to increase with temperature in Fig. 3C. This reaction is accompanied by a small enthalpy change and a positive entropy change, as is shown in Table II, for all metals except cobalt. From Table II it is seen that the retention enthalpies are essentially the same as the enthalpy changes of the ion-exchange equilibria between the corresponding metal and ethylenedi-

amine ions, but are significantly different from those of the tartrate complexation reaction. This observation further supports the notion that at sufficiently low tartrate concentrations, the retention of metals is governed by the pushing effect of ethylenediammonium ion rather than by the pulling effect of the tartrate.

The preferred concentration range for ethylenediamine and/or tartaric acid in the eluent is from 0.1 to 10 millimolal. At lower concentrations the buffering capacity of the eluent is too low to give a stable and well controlled chromatographic system. On the other hand, if the concentration is too high, the concomitantly high background noise adversely affects the sensitivity of analysis.

It was found that with large samples the retention also depends on the eluite concentration, and this manifestation of non-linear chromatography will be investigated in another study. In this study the eluite concentrations were all kept low enough to ensure that the elution is linear. With 100-μl samples the concentration of the eluites did not exceed 0.05 mM. Under such conditions the signal-to-noise ratio is about 20:1 and the accuracy of the stability constant measurement by ion chromatography is expected to be commensurate.

Fig. 5 shows the chromatogram of magnesium and calcium ions obtained with 0.2 mM tartaric acid and 0.4 mM EDA in the eluent at pH 4.5 and 30°C. The background conductivity is 156 μS/cm. The plate number is about 1700 for each peaks. The eluite concentration decreases in the chromatographic process and the magnitude of dilution, given by the ratio of the eluite concentrations in the sample and in the eluent peak, can be calculated as the ratio of the peak width at half-height to the injection volume for triangular peaks. Thus, from Fig. 5, the peak concentrations are calculated to be 0.02 and 0.013 millimolal for magnesium and calcium, respectively.

The sensitivity of the eluite in ion chromatographic analysis may be defined as the measured conductivity change per unit change in the eluite concentration in the sample. From Fig. 5, the chromatographic sensitivities are 24 and 7.4 S cm^2/equiv. for magnesium and calcium, respectively. It is believed that the difference in the chromatographic sensitivities is due to the effect of dilution, the ionization fraction of the eluites and the difference in the limiting equivalent conductivities of the eluent and the eluite cations. Although there are two major eluent cations, the hydrogen ion is buffered by the tartaric acid and only the ethylenediammonium ion is replaced by the eluite cation at the peak in order to maintain electroneutrality. From the limiting equivalent conductivity of magnesium and calcium ions at 25°C, *i.e.*, 53.0 and 59.5 S cm^2/equiv. [23], respectively, and Fig. 5 the limiting equivalent conductivity of the diprotonated EDA at 25°C is calculated to be 79 S cm^2/equiv. The fractions of ionization of magnesium and calcium ions are calculated from the respective stability constants in Table III and eqn. 16 to be 1.0 and 0.98, respectively.

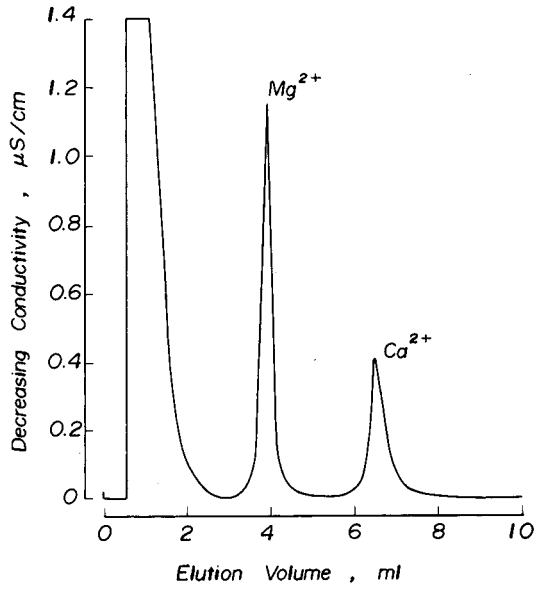

Fig. 5. Indirect detection of magnesium and calcium ions. Column, 4.6 × 50 mm I.D. 10-μm cation exchanger with capacity of 46 μequiv./g; eluent, 0.2 mM tartaric acid–0.4 mM EDA (pH 4.5); temperature, 30°C; flow-rate, 0.8 ml/min; pressure, 16 kg/cm^2; sample, 100 μl of solution 0.05 millimolal for both ions.

The limiting equivalent conductivity of ethylenediammonium ion is larger than those of the eluite ions so that negative eluite peaks are obtained. The limiting equivalent conductivities of lead and some rare earth metal ions are *ca.* 70 S cm^2/equiv. [23], which is too close to that of EDA to give sufficient chromatographic sensitivity for quantitative analysis by the chromatographic system employed in this study.

In order to study the effect of eigenpeaks on the retention of the eluite, the sample was diluted from 10 to 0.05 millimolal with either distilled water or by the eluent. In either instance, the retention of the eluites did not show observable changes, whereas there was a large change in the peak which appears in the void.

CONCLUSIONS

Single-column ion chromatography using a TSK high-performance ion-exchange column with ethylenediammonium tartrate in the eluent was used for the rapid separation of common divalent cations. With the conductivity detector not only were trace amounts of the sample components determined but also the complexation reaction and ion-exchange process could be studied at the same time.

A theoretical model was developed to describe quantitatively the effect of pH, tartaric acid and ethylenediamine concentration on the retention factor of divalent cations in single-column ion chromatography. The equilibrium constant for the ion-exchange process was calculated from chromatographic retention data and the enthalpy and entropy change for the chromatographic process was also obtained.

Further, a method has been presented for the evaluation of the complexation constant between tartrate ligand and divalent metal ions by ion chromatography from their capacity factors measured at various tartaric acid concentrations.

The elution conditions, including temperature, pH, tartaric acid and ethylenediamine concentration, were found to influence the retention of divalent cations in different ways. The retention factor increases with both the temperature and the tartaric acid concentration, but decreases with increasing EDA concentration. The retention factor increases with pH at low tartaric acid concentration, but decreases with pH when the tartaric acid concentration is relatively high.

It is likely that the use of another driving ion, such as lithium, would have been more appropriate than ethylenediamine if we had used a postcolumn reactor with a fluorescence detector instead of the conductivity detector to detect the metal complex. Such a system and the optimization of sensitivity and separation efficiency is under investigation.

ACKNOWLEDGEMENT

Financial support of this work was provided by the National Science Council of the Republic of China through grant NSC 78-0402-E-006-18.

SYMBOLS

A	tartaric acid
A^{2-}	free tartrate ion
C	ion-exchange resin capacity (mequiv. cm^{-3})
E^{2+}	fully protonated ethylenediamine
$\overline{ER_2}$	adsorbed ethylenediammonium ion
f	fraction of the exchange sites in the stationary phase occupied by hydrogen ions
H^+	hydrogen ion
HA^-	free acid tartrate ion
$\overline{HR}$	adsorbed hydrogen ion
k'	retention factor
K_1, K_2	acid ionization constants of tartaric acid (molal)
K_{Chrom}	chromatographic equilibrium constant
K_h^e	equilibrium constant for the exchange of hydrogen ion with the adsorbed ethylenediammonium ion
K_m^e	equilibtium constant for the exchange of metal ion with the adsorbed ethylenediammonium ion
K_m^h	equilibrium constant for the exchange of metal ion with the adsorbed hydrogen ion
K_{ma}^a	stability constant of the complex formed between the metal ion and the tartrate ligand ($molal^{-1}$)
K_{mha}^{ha}	stability constant of the complex formed between the metal ion and the acid tartrate ligand ($molal^{-1}$)
M^{2+}	divalent cation
$\overline{MR_2}$	adsorbed divalent cation
R	gas constant ($kJ/g \cdot mol \cdot K$)
$\overline{R}$	exchange site of the stationary phase
t_0	mobile phase hold-up time (min)
t_r	retention time of the eluite (min)
V_m	space occupied by the mobile phase in the column (cm^3)
V_0	empty column volume (cm^3)
W	weight of ion-exchange resin present in the column (g)

Greek symbols

α_{21}	separation factor defined in eqn. 21
α_m	fraction of the total metal present as free metal ion in the mobile phase
β_a	$[A^{2-}]/[A]_t$
β_{ha}	$[HA^-]/[A]_t$
ϕ	phase ratio of the column
ΔH^0	standard enthalpy change for an equilibrium reaction (kJ/g · mol)
ΔH_k^0	retention enthalpy (kJ/g · mol)
ΔS^0	standard entropy change for an equilibrium process (J/g · mol · K)
ε_i	intraparticular porosity
ε_e	interparticular porosity
ρ_r	true density of ion-exchange resin (g/cm^3)

Subscripts

ex	associated with the ion-exchange process of metal ions with ethylenediammonium ion on the exchange sites
i	inert ions not adsorbed to the exchange sites
m	metal ion
ma	associated with complex formation of divalent ion with tartrate
t	total concentration

Other

[ ]	concentration of the species specified within (molal)

REFERENCES

1 H. Small, T. S. Stevens and W. D. Bauman, *Anal. Chem.*, 47 (1975) 1801.
2 J. S. Fritz, D. T. Gjerde and R. M. Becker, *Anal. Chem.*, 52 (1980) 1519.
3 J. G. Tarter, *Ion Chromatography*, Marcel Dekker, New York, 1987.
4 P. R. Haddad and P. E. Jackson, *Ion Chromatography —Principles and Applications*, Elsevier, Amsterdam, 1990.
5 D. T. Gjerde and J. S. Fritz, *Ion Chromatography*, Hüthig, Mamaroneck, NY, 2nd ed., 1987.
6 J. Inczédy, *Analytical Applications of Complex Equilibria*, Wiley, New York, 1976, p. 273.
7 S. Elchuk and R. M. Cassidy, *Anal. Chem.*, 51 (1979) 1434.
8 G. J. Sevenich and J. S. Fritz, *Anal. Chem.*, 55 (1983) 12.
9 G. J. Sevenich and J. S. Fritz, *J. Chromatogr.*, 347 (1985) 147.
10 G. J. Sevenich and J. S. Fritz, *J. Chromatogr.*, 371 (1986) 361.
11 H. Small and T. E. Miller, *Anal. Chem.*, 54 (1982) 462.
12 J. S. Fritz and G. H. Schenk, Jr., *Quantitative Analytical Chemistry*, Allyn and Bacon, Boston, 3rd ed., 1974.
13 J. Stary, *Anal. Chim. Acta*, 28 (1963) 132.
14 D. L. G. Rowlands and C. B. Monk, *Trans. Faraday Soc.*, 62 (1966) 945.
15 N. Tripathy, K. K. Tripathy and R. K. Patnaik, *J. Indian Chem. Soc.*, 44 (1967) 329.
16 N. Tripathy and R. K. Patnaik, *J. Indian Chem. Soc.*, 42 (1965) 712.
17 H. E. Hellwege and G. K. Schweitzer, *J. Inorg. Nucl. Chem.*, 27 (1965) 99.
18 C. B. Monk, *J. Chem. Soc.*, (1965) 2456.
19 R. G. Seys and C. B. Monk, *J. Chem. Soc.*, (1965) 2452.
20 P. G. Manning and C. B. Monk, *Trans. Faraday Soc.*, 57 (1961) 1996.
21 K. K. Tripathy and R. K. Patnaik, *J. Indian Chem. Soc.*, 44 (1967) 511.
22 C. F. Timberlake, *J. Chem. Soc.*, (1964) 1229.
23 R. A. Robinson and R. H. Stokes, *Electrolyte Solutions*, Butterworth, Stoneham, MA, 1959, p. 463.

Journal of Chromatography, 589 (1992) 197–199
Elsevier Science Publishers B.V., Amsterdam

CHROM. 23 688

Carbonate eluents in ion chromatography

Fractions of resin capacity linked to anions present in the eluent

Ü. Haldna

Institute of Chemistry, Estonian Academy of Sciences, Akadeemia tee 15, 200108 Tallinn (Estonia)

(First received February 27th, 1991; revised manuscript received July 19th, 1991)

ABSTRACT

The eluting ions OH^-, HCO_3^- and CO_3^{2-} in carbonate eluents are absorbed on the resin in the separation column. In an equilibrium state, the concentrations of these ions on the resin depend on the composition of the carbonate eluent used. A method for determining the concentrations of the OH^-, HCO_3^- and CO_3^{2-} absorbed on the stationary phase is suggested and an example of its application to HIKS-1 resin is presented.

INTRODUCTION

Since its introduction in 1975 [1], ion chromatography (IC) has become the dominant analytical method for determining a number of anions. Often these analyses are performed with conductimetric detection. To obtain the lowest detection limits possible for the sample anions studied, suppressed IC is applied. This technique requires that the eluent used should have a sufficient eluting efficiency in the separation column, and in the suppressor it should be easily convertible into a weak acid solution with a very low conductivity. Carbonate eluents, aqueous solutions of sodium carbonate and sodium hydrogencarbonate, which have been widely used in IC since its introduction [2], meet these requirements fairly well. The composition of carbonate eluents, *viz.*, the concentrations of Na_2CO_3 and $NaHCO_3$, may be varied over a wide range depending on the sample to be analysed and the capacity of the separation column used. The Na_2CO_3 and $NaHCO_3$ solutions elute the sample anions by a cooperative effect of the three species present in these eluents (OH^-, HCO_3^- and CO_3^{2-}).

A study [3] of ion-exchange equilibria between the carbonate eluents and anion-exchange resins in the separation column did no yield quantitative results. In order to obtain a deeper insight into the ion-exchange processes taking place in the separation column, it seemed to be useful to determine the percentages of the total capacity of the separation column bonded to each of the eluting anions (OH^-, HCO_3^-, CO_3^{2-}). It should be noted that the fraction of the column capacity occupied by the sample anions is usually negligibly small. Hence we can write

$$\bar{C}_{OH^-} + \bar{C}_{HCO_3^-} + 2\bar{C}_{CO_3^{2-}} = Q \quad (1)$$

where Q is the capacity of the ion-exchange resin in the separation column (mmol/cm^3) and the $\bar{C}$ terms are the concentrations of the respective ions sorbed on the resin (mmol/cm^3). The quantities to be calculated are $F_{OH^-} = \bar{C}_{OH^-}Q^{-1}$, $F_{HCO_3^-} = \bar{C}_{HCO_3^-}Q^{-1}$ and $F_{CO_3^{2-}} = \bar{C}_{CO_3^{2-}}Q^{-1}$.

0021-9673/92/$05.00

METHOD

Neglecting the activity coefficients, the $\bar{C}$ terms in eqn. 1 are given by

$$\bar{C}_A = (K_A^B)^{-1/y} D^{x/y} C_A \quad (2)$$

where K_A^B and $D_B = \bar{C}_B/C_B$ are the ion-exchange constant and partition coefficient, respectively, C_A and C_B are the concentrations in the solution (in the eluent), A is an anion in the eluent (A = OH^-, HCO_3^- and CO_3^{2-}) with charge x and B is an anion in the sample with charge y. In principle, the values of F_{OH^-}, $F_{HCO_3^-}$ and $F_{CO_3^{2-}}$ should not depend on the sample being analysed, *i.e.*, on the choice of B, but rather on the eluent composition used. Nevertheless, it is impossible to avoid the use of ions B in the calculations because otherwise the respective K_A^B and D_B values would not be available. It is obvious that we have to calculate three kinds of quantities: K_A^B, D_B and C_A. The concentrations in the liquid phase (C_{OH^-}, $C_{HCO_3^-}$ and $C_{CO_3^{2-}}$) were obtained according to ref. 4.

The partition coefficient [5]

$$D_B = \bar{C}_B/C_B = (t_B - t_0)L/v \quad (3)$$

is related to the retention times t_B (for the ion under study) and t_0 (for the non-sorbed component); L is the column length and v is the linear velocity of eluent in the column. In this work, we used the retention times t_B for four anions (Cl^-, NO_3^-, HPO_4^{2-} and SO_4^{2-}), each measured with 25 different carbonate eluents, employing a separation column packed with HIKS-1 ion-exchange resin [6].

Calculation of the ion-exchange constants K_A^B is the most tedious and complicated. The method suggested in ref. 4, which applies the linear regression approach, minimizes the sum of squares along the Q/D_B axes. After some experimentation we found it not to be applicable to large data sets because it often yields negative equilibrium constant values. Therefore, we present an alternative method for calculating the K_A^B values based on a non-linear regression algorithm [7]. This method minimizes the sum

$$Y = \sum (t_{B,calc.} - t_{B,exp.})^2 \quad (4)$$

using some estimates for K_A^B. The latter are then varied to obtain the lowest possible value of Y [7]. It is important to point out that in the algorithm applied [7], the signs of the parameters adjusted (K_A^B) are given by the researcher. For calculation of t_B values using currently available K_A^B values, we first need the partition coefficient (D_B) available as a root of the quadratic equation

$$aD_B^2 + bD_B + c = 0 \quad (5)$$

where

$$a = 2(K_{CO_3^{2-}}^B)^{-1} C_{CO_3^{2-}}$$

$$b = (K_{OH^-}^B)^{-1} C_{OH^-} + (K_{HCO_3^-}^B)^{-1} C_{HCO_3^-}$$

$$c = -Q$$

Eqn. 5 was derived for the case $y = 1$ (Cl^- and NO_3^-); if $y = 2$ (HPO_4^{2-} and SO_4^{2-}), we have to use

$$aD_B + bD_B^{0,5} + c = 0 \quad (6)$$

where

$$a = 2(K_{CO_3^{2-}}^B)^{-0,5} C_{CO_3^{2-}}$$

$$b = (K_{OH^-}^B)^{-0,5} C_{OH^-} + (K_{HCO_3^-}^B)^{-0,5} C_{HCO_3^-}$$

$$c = -Q$$

The D_B values obtained by eqn. 5 (or eqn. 6) allow us to calculate

$$t_{B,calc.} = vD_B/L + t_0 \quad (7)$$

which is needed for Y (eqn. 4). Using the non-derivative iterative procedure [7] and the $t_{B,exp.}$ values taken from ref. 6, we calculated the K_A^B values presented in Table I. These K_A^B values are statistically significant if A = CO_3^{2-} and HCO_3^- (except for sulphate ions if A = HCO_3^-) and crude estimates only if A = OH^-. This indicates that the column capacity fraction accounting for OH^- ions (F_{OH^-}) is low, which results in uncertain $K_{OH^-}^B$ estimates, *i.e.*, the iterated $K_{OH^-}^B$ values depend considerably on the choice of the respective zero estimates. The constants given in Table I and partition coefficients [5] D_B (eqn. 3) calculated from the t_B values [6] were used to obtain the fractions of the capacity of the HIKS-1 resin linked to the OH^-, HCO_3^- and CO_3^{2-} ions present in the carbonate eluent used:

$$F_{OH^-} = (K_{OH^-}^B)^{-1} D_B C_{OH^-} Q^{-1} \quad (8)$$

$$F_{HCO_3^-} = (K_{HCO_3^-}^B)^{-1} D_B C_{HCO_3^-} Q^{-1} \quad (9)$$

$$F_{CO_3^{2-}} = 2(K_{CO_3^{2-}}^B)^{-1} D_B^2 C_{CO_3^{2-}} Q^{-1} \quad (10)$$

Eqns. 8–10 are appropriate for Cl^- and NO_3^-

TABLE I

ION-EXCHANGE CONSTANTS[a] CALCULATED BY THE NON-LINEAR REGRESSION METHOD

B	$K^B_{OH^-} = \frac{\bar{C}_B C_{OH^-}}{C_B \bar{C}_{OH^-}}$	$K^B_{OH^-} = \frac{\bar{C}_B C^2_{OH^-}}{C_B \bar{C}^2_{OH^-}}$	$K^B_{HCO_3^-} = \frac{\bar{C}_B C_{HCO_3^-}}{C_B \bar{C}_{HCO_3^-}}$	$K^B_{HCO_3^-} = \frac{\bar{C}_B C^2_{HCO_3^-}}{C_B \bar{C}^2_{HCO_3^-}}$	$K^B_{CO_3^{2-}} = \frac{\bar{C}^2_B C_{CO_3^{2-}}}{C^2_B \bar{C}_{CO_3^{2-}}}$	$K^B_{CO_3^{2-}} = \frac{\bar{C}^2_B C^2_{CO_3^{2-}}}{C^2_B \bar{C}^2_{CO_3^{2-}}}$
Cl^-	1.370[b]		2.23 ± 0.73		0.430 ± 0.009	
NO_3^-	0.747[b]		2.11 ± 0.12		3.890 ± 0.100	
HPO_4^{2-}		⩾10.0[b]		1.04 ± 0.06		2.15 ± 0.04
SO_4^{2-}		0.58[b]		96.0[b]		6.19 ± 0.32

[a] The presented root-mean-square errors were calculated using twelve values of K^B_A obtained with different zero estimates.
[b] Statistically insignificant at a confidence level $P = 0.95$.

($y = 1$). For HPO_4^{2-} and SO_4^{2-} ($y = 2$), we used

$$F_{OH^-} = (K^B_{OH^-})^{-0,5} D_B^{0,5} C_{OH^-} Q^{-1} \quad (11)$$

$$F_{HCO_3^-} = (K^B_{HPO_4^{2-}})^{-0,5} D_B^{0,5} C_{HCO_3^-} Q^{-1} \quad (12)$$

$$F_{CO_3^{2-}} = 2(K^B_{CO_3^{2-}})^{-0,5} D_B C_{CO_3^{2-}} Q^{-1} \quad (13)$$

RESULTS AND DISCUSSION

The mean values of F_{OH^-}, $F_{HCO_3^-}$ and $F_{CO_3^{2-}}$ for all four ions considered (B) are presented in Table II. The probable errors of the calculated F_{OH^-}, $F_{HCO_3^-}$ and $F_{CO_3^{2-}}$ values (with 24 degrees of freedom) may be calculated as follows: (i) for F_{OH^-} and $F_{HCO_3^-}$, 0.5–1.0 times the value given in Table II; (ii) for $F_{CO_3^{2-}}$, 0.06–0.2 times the value given in Table II. The data presented in Table II allow three conclusions to be drawn: (1) the fraction $F_{CO_3^{2-}}$ is always the largest, decreasing with increasing sum of concentrations C; (2) the second large fraction is, as a rule, $F_{HCO_3^-}$, increasing with increasing sum C; as expected when $C_{NaHCO_3} = 0$, $F_{HCO_3^-} < F_{OH^-}$; (3) the fraction F_{OH^-} is the lowest, increasing with decreasing C_{NaHCO_3}; in other words, as expected, F_{OH^-} is larger for eluents with higher pH.

TABLE II

FRACTION OF THE CAPACITY OF THE HIKS-1 RESIN BONDED TO OH^- (F_{OH^-}), HCO_3^- ($F_{HCO_3^-}$) AND CO_3^{2-} ($F_{CO_3^{2-}}$) IONS

$C_{NaHCO_3}/C_{Na_2CO_3}$	Fraction	$C = C_{NaHCO_3} + C_{Na_2CO_3}$ (mM)				
		2	4	6	8	12
3.00	F_{OH^-} (%)	1.5	1.2	0.9	0.8	0.6
	$F_{HCO_3^-}$ (%)	18.8	24.7	28.0	30.8	35.8
	$F_{CO_3^{2-}}$ (%)	79.7	74.1	71.1	68.4	63.6
1.00	F_{OH^-} (%)	2.8	2.4	2.1	1.9	1.7
	$F_{HCO_3^-}$ (%)	10.3	13.9	16.9	19.0	23.5
	$F_{CO_3^{2-}}$ (%)	86.9	83.7	81.0	79.1	74.8
0.50	F_{OH^-} (%)	4.4	3.7	3.3	3.1	3.0
	$F_{HCO_3^-}$ (%)	7.8	9.6	11.1	12.5	16.1
	$F_{CO_3^{2-}}$ (%)	87.8	86.6	85.6	84.5	80.9
0.33	F_{OH^-} (%)	5.2	4.6	4.2	3.9	3.9
	$F_{HCO_3^-}$ (%)	6.6	7.9	8.8	9.9	12.6
	$F_{CO_3^{2-}}$ (%)	88.2	87.5	87.0	86.2	83.5
0.00	F_{OH^-} (%)	7.8	8.0	7.8	8.3	9.7
	$F_{HCO_3^-}$ (%)	3.9	4.1	4.1	4.2	4.9
	$F_{CO_3^{2-}}$ (%)	88.3	87.9	88.1	87.5	85.4

These conclusions apply to the HIKS-1 resin, for which ion-exchange occurs on $-CH_2N^+(CH_3)_3$ groups. It is to be expected that the behaviour of F_{OH^-}, $F_{HCO_3^-}$ and $F_{CO_3^{2-}}$ for other resins with the same functional group will be similar to that for HIKS-1.

The computer programs used were written in Fortran-4 and are available on request.

REFERENCES

1 H. Small, T. S. Stevens and W. C. Bauman, *Anal Chem.*, 47 (1975) 1801.
2 F. C. Smith and R. C. Chang, *The Practice of Ion Chromatography*, Wiley, New York, Chichester, Brisbane, Toronto, 1983.
3 O. A. Shpigun, O. N. Obrezkov and R. N. Rubinstein, *Acta Comm. Univ. Tartuensis*, 743 (1986) 185.
4 Ü. Haldna, *Zh. Fiz. Khim.*, 65 (1991) 181.
5 M. M. Senyavin, E. V. Venetsianov and A. M. Dolgonosov, *Zh. Anal. Khim.*, 42 (1987) 82.
6 Ü. Haldna, I. Jakovleva, R. Palvadre and R. Juga, *Proc. Estonian Acad. Sci.*, 39 (1990) 44.
7 Ü. Haldna and R. Juga, *Proc. Estonian Acad. Sci.*, 39 (1990) 137.

Journal of Chromatography, 589 (1992) 201–207
Elsevier Science Publishers B.V., Amsterdam

CHROM. 23 723

Mixed potential response at metallic electrodes in potentiometric detection for ion chromatography

Peter W. Alexander

Department of Analytical Chemistry, University of New South Wales, P.O. Box 1, Kensington, NSW 2033 (Australia)

Bronisław K. Głód

Institute of Physical Chemistry of the Polish Academy of Sciences, Kasprzaka 44/52, 01-224 Warsaw (Poland)

Paul R. Haddad*

Department of Analytical Chemistry, University of New South Wales, P.O. Box 1, Kensington, NSW 2033 (Australia)

(First received July 6th, 1991; revised manuscript received August 15th, 1991)

ABSTRACT

The response characteristics of metallic copper and silver–silver chloride electrodes in a single potentiometric detector were evaluated in an ion chromatographic system. A cell design was used in which the position of the electrodes can be moved easily. Response to inorganic anions was found to be possible with either the copper or the silver–silver chloride electrode acting as the indicator electrode in the same cell where a change in function is achieved by simple movement of the electrodes in the cell. Either negative or positive peaks may be observed in direct or indirect detection modes depending on the choice of mobile phase composition and on the electrode positions in the detector. Optimum separations and the best potentiometric response were achieved with 1 m*M* sodium perchlorate as the eluent. The response to chloride and bromide is shown to be more sensitive at the silver electrode and to nitrate, nitrite, iodide, thiosulphate and thiocyanate at the copper electrode. The best detection limit was found to be 10 pmol for bromide at the silver–silver chloride electrode.

INTRODUCTION

The development of potentiometric detectors for ion chromatography (IC) has been reported previously with various types of indicator electrodes [1–6], but the sensitivity and working ranges were limited. The studies reported here were made with an improved cell design and resulted in better sensitivity for some anions and a wider detector dynamic range. This study was also concerned with the control of the selectivity of the electrodes used in a cell design in which the position of each electrode can be altered easily.

In conventional potentiometric cells, the indicator (or sensor) electrode and the reference electrode are separated by a salt bridge. Cell designs used for chromatographic detection have been reported using a variety of sensor electrodes and usually with a reference electrode of either saturated calomel or silver–silver chloride (Ag/AgCl). The latter has also been used as an indicator electrode for IC detection by several research groups [3], and the electrode potential has been measured with respect to another Ag/AgCl ectrode separated from the mobile phase by a salt bridge, such as an agar-agar. The metallic copper indicator electrode has also been used in several configurations, such as tubular and wire designs, for flow-injection analysis and liquid chromatography [1,2,7–9]. In these earlier studies, the electrode potential was measured relative to a reference

0021-9673/92/$05.00

electrode separated by a salt bridge from the flowing stream.

The electrodes used in this study were metallic copper and Ag/AgCl electrodes but without any salt bridge between them. It is shown that the response of the cell depends on the positioning of the electrodes in the flow path. Detector selectivity can therefore be controlled for response to various anions. For comparison, the response of a UV detector placed in series with the potentiometric detector was also examined.

EXPERIMENTAL

Instrumentation

The electrodes used were metallic wires made from copper and silver metal (both 0.5 mm in diameter). The latter was coated with silver chloride according to the electrolytic method described elsewhere [10]. The wire electrodes were placed in a Perspex cell of dimensions 4 × 3 × 1 cm, as shown in Fig. 1, with a 1-mm flow-through channel. It was possible to change the position of the silver electrode from point A to B. The cell is similar to a design reported previously [2], with Omnifit connectors (supplied by Activon, Sydney, Australia) and rubber septa. The copper electrode was connected to the positive input of an Activon pH/mV-meter and the silver electrode to the negative input connection. The potential difference between the electrodes was then measured.

The potentiometric cell was mounted at the outlet of an ion-exchange chromatographic column (Waters IC-PAK A, 50 mm × 4.6 mm I.D., 30 μequiv./ml). This low-capacity ion-exchange column gave us the possibility of using a low buffer concentration. A Waters (Milford, MA, USA) liquid chromatographic system was used with a pump (Type 510), injection valve (Type U6K) and UV detector (Type 484) connected in series with the potentiometric cell. The UV detector was set at 210 nm (direct detection) or 280 nm (indirect detection) and the UV data were recorded on an ABB SE 120 two-pen strip-chart recorder (Goerz Metrawatt, Vienna, Austria) together with the potentiometric response from the mV-meter.

Reagents and solutions

All reagents were of analytical-reagent grade and were dissolved in water purified on a Milli-Q water purification system (Millipore, Bedford, MA, USA). Mobile phases were degassed using an ultrasonic bath and filtered through a 0.45-μm membrane filter prior to use. A range of mobile phases was used, with the best results being obtained with 1 m*M* sodium perchlorate or 0.4 m*M* potassium hydrogenphthalate adjusted to pH 7.0 with sodium hydroxide. Stock solutions of solute anions were prepared as 10 m*M* solutions in Milli-Q water and diluted to the required concentrations when necessary.

Procedures

The anion sample solutions were injected into the chromatographic system with 10- and 100-μl syringes (Hamilton, Reno, NV, USA) through the injection port. Volumes injected were varied from 0.2 to 100 μl and the signal output of each detector was monitored continuously on the chart recorder. The potentiometric cell was used in two configurations, as shown in Fig. 1, where the Ag/AgCl electrode was placed in either position A or B before recording chromatographic data. The chromatograms could then be compared to determine the effect of the change in the position of the electrodes.

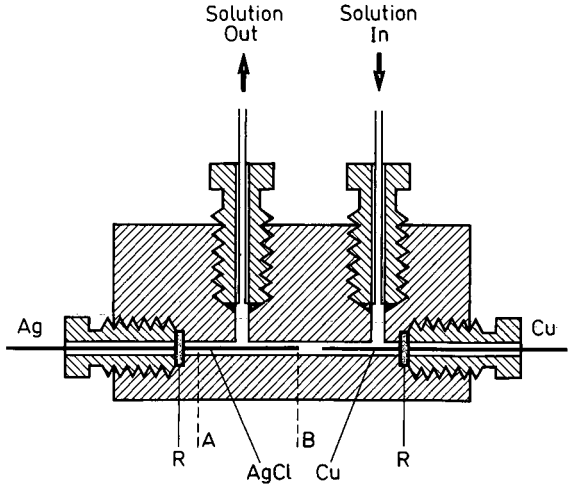

Fig. 1. Schematic diagram of the flow cell used for potentiometric detection, constructed of Perspex and showing the two electrodes used. A and B refer to the two positions used for the Ag/AgCl electrode when recording chromatograms and R represents the rubber septa.

RESULTS AND DISCUSSION

Response mechanisms

The main aim of this work was to determine the optimum conditions for the most sensitive potentiometric response while still maintaining the optimum chromatographic separation of the common inorganic anions tested. Chromatographic peaks could be observed as either positive or negative changes in the measured potential of the electrochemical cell shown in Fig. 1. The direction of the change in potential depended on the mobile phase composition and on the configuration of the two electrodes, which could be positioned in two ways: (A) where the Ag electrode was effectively out of the liquid stream and (B) where it was in the stream, close to the copper electrode.

These factors were found to control the detector response characteristics according to the following mechanisms: (1) direct detection of halide ions at the Ag/AgCl electrode due to an increase in halide concentration at the electrode surface, resulting in decreased silver ion concentration; this causes a decrease in the silver electrode potential and therefore a *positive peak* (as the detector signal is given by the potential of the copper electrode minus that of the Ag/AgCl electrode); (2) direct detection of copper complexing anions at the copper electrode, as a result of the decreasing Cu^{2+} and Cu^{+} concentration due to anion complexation, giving a decrease in the potential of the copper electrode and hence a *negative peak*; and (3) indirect detection (*i.e*, vacancy detection) at the copper electrode caused by an increase in Cu^{2+} concentration where the injected anion was less strongly complexing than the buffer, producing a *positive peak*.

The above mechanisms can be described according to the following equations for the measured detector voltages:

$$E_B = E^{Cu}{}_B - E^{Ag}{}_B$$

$$E_S = E^{Cu}{}_S - E^{Ag}{}_S$$

where E_B is the baseline buffer potential and E_S is the potential due to the buffer plus eluted sample at the peak maximum. The peak height, E_p, is therefore given by:

$$E_p = E_S - E_B = (E^{Cu}{}_S - E^{Cu}{}_B) - (E^{Ag}{}_S - E^{Ag}{}_B)$$

In previous studies reported with the copper electrode [2], the term in the second set of parentheses was zero because a salt bridge was used to separate the silver electrode as a reference electrode from the mobile phase. In this study, the silver electrode is no longer a true reference electrode.

The individual electrode potentials in the above equation are given by the Nernst equation as described previously [2] and are dependent on the free metal ion concentrations at the electrode surfaces. These potentials will depend on the extent of complex formation at the surfaces due to the presence of complexing or precipitating agents in both the buffer and sample solutions, as discussed in numerous previous publications and reviewed by Haddad and Jackson [1]. The slope of the calibration graph for each anion is therefore dependent on the relative

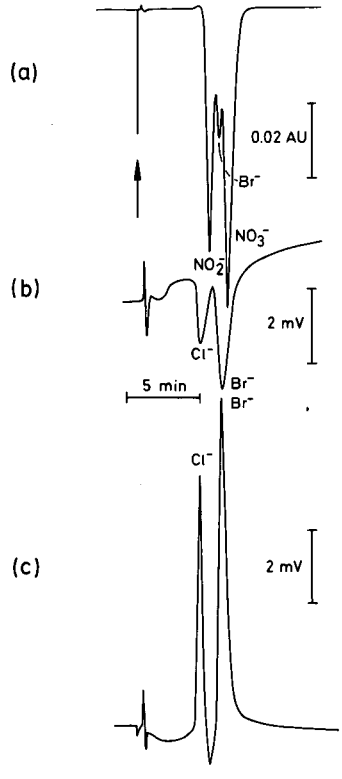

Fig. 2. Chromatograms recorded using 1.0 m*M* perchlorate as eluent with the following detectors: (a) the UV detector at 210 nm; (b) the copper electrode as the sensor with the Ag/AgCl electrode in position A in Fig. 1; and (c) using the silver electrode as the sensor in position B in Fig. 1. Flow-rate of the eluent, 1 ml/min; injection volume, 20 μl.

stability constants or solubility products for the formation of the complexes or precipitates at the silver and copper electrodes. The slope is also dependent on the buffer concentration used. The above mechanism is confirmed by the chromatographic results shown in Figs. 2–4, as discussed below.

Chromatograms observed with potentiometric detection

In chromatography, the best conditions from the standpoint of chromatographic separation are often different from those required for optimum detector sensitivity. Optimum conditions for the potentiometric IC method should be characterized by complete separation of components and detection limits comparable to, or better than, those given by a UV detector, with retention times no longer than about 20 min.

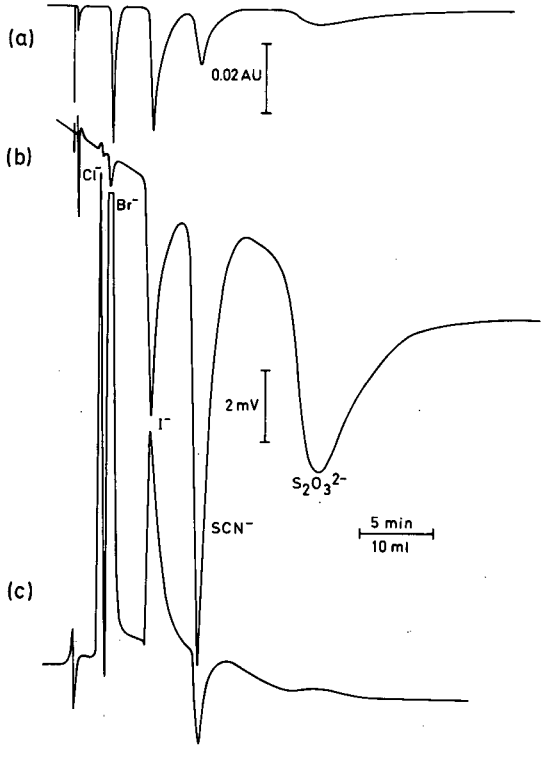

Fig. 3. Chromatograms recorded using 1.0 *M* perchlorate as eluent with the following detectors: (a) the UV detector at 210 nm; (b) the copper electrode as the sensor with the Ag/AgCl electrode in position A in Fig. 1; and (c) the silver electrode as the sensor in position B in Fig. 1. Flow-rate of 0.5 ml/min.

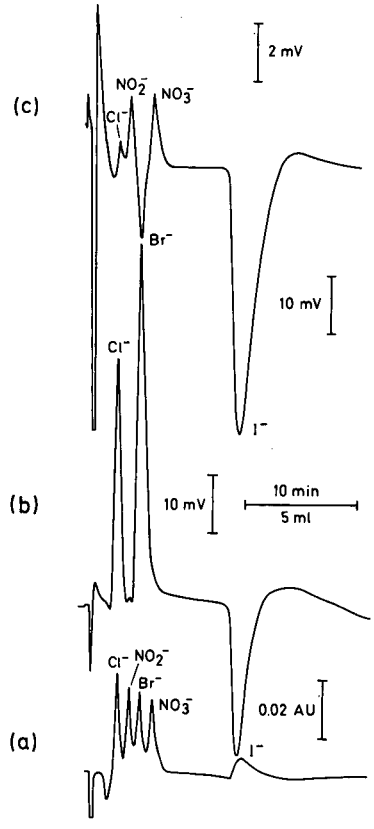

Fig. 4. Chromatograms recorded using 0.4 m*M* phthalate as eluent with (a) the UV detector at 280 nm, (b) the silver electrode as the sensor in position B in Fig. 1 and (c) the copper electrode as the sensor with the Ag/AgCl electrode in position A in Fig. 1. Flow-rate, 0.5 ml/min.

The response of the Ag/AgCl electrode was found to be critical with respect to its position in the flow path of the eluent stream and the position of the copper electrode. The silver electrode could be moved between positions A and B in Fig. 1 without dismantling the cell. When the electrodes were situated close together (position B in Fig. 1), the response of the potentiometric detector was controlled by the response at both electrodes, but mainly by the potential changes occurring at the Ag/AgCl electrode. However, when the electrodes were in position A, the potential was controlled almost solely by changes occurring at the copper electrode. These conclusions can be deduced from the chromatographic data shown in Figs. 2–4. Movement of

the Ag/AgCl electrode into intermediate positions between A and B had little effect on the peaks observed until the electrode had been moved completely out of the main stream into position A. The working end of the electrode was not moved through the septum and it was therefore possible to move the electrode many times without affecting the AgCl surface layer. For this reason, reproducibility of the repsonse was not affected.

For optimum peak separation [1], it is known that a high buffer concentration, a high buffer pH and a high anion-exchange selectivity coefficient for the buffer anion cause a decrease in retention time. However, from the point of view of optimizing the potentiometric detection response at metallic electrodes, the above conditions are not ideal. Low buffer concentrations and buffer components known to have small complexation constants with the metal ions from each electrode are required for the best detection limit in the direct detection mode. It is also known [1,2] that a sensitive direct response at a copper metal electrode requires strong complexation of copper ions by solute anions.

To achieve these optimum conditions, different mobile phases were examined, including phosphate, phthalate, carbonate, sulphate, perchlorate, naphthalenemonosulphonate, naphthalenedisulphonate and camphorsulphonic acid. Various pH values and flow-rates were also used. In all instances, it was found that the optimum conditions for the chromatographic separation were not the same as those for sensitive detection of inorganic anions. It was then necessary to compromise in order to select conditions suitable for the separation and detection of various anion mixtures. An example of such a compromise is presented in Fig. 2, which shows the chromatogram obtained for chloride, nitrite, bromide and nitrate using 1 m*M* perchlorate as the mobile phase with the electrodes in different positions, (a) is the UV (210 nm) response, (b) is the copper and (c) is the silver electrode potentiometric detector response. It was found that the potentiometric detector was more sensitive than the UV detector for chloride and bromide when the silver electrode detector was used as the sensor electrode (position B in Fig. 1), and positive peaks were observed for chloride and bromide. Negative peaks and significant peak tailing evident in Fig. 2b on the copper electrode were due to the copper acting as the sensor electrode. Under these conditions nitrate and nitrite could not be detected on the silver or the copper electrode. This may be of some advantage when serious peak overlap occurs, as with the UV detector.

Fig. 3 shows another example of a separation with the same mobile phase (1 m*M* perchlorate) but with a different mixture of anions (chloride, bromide, iodide, thiocyanate and thiosulphate). Again, chloride and bromide were the most sensitive at the Ag–AgCl electrode, showing positive peaks. However, thiocyanate and thiosulphate were most sensitive at the copper electrode and gave negative peaks. At times, a mixed potential response arising from both electrodes was observed. For example, thiocyanate gave a small negative peak (Fig. 3c) which was the sum of a large, negative peak on the copper electrode and a smaller, positive peak on the silver electrode. On the other hand, iodide gave a negative peak on the Cu electrode and a positive peak on the silver. The iodide peak observed in Fig. 3c was therefore of mixed potential origin due to the difference between the silver and copper electrode potentials.

As mentioned above, experiments were also performed with other mobile phases. With phthalate buffer as the mobile phase, as shown in Fig. 4, the separation and detection of chloride, nitrite, bromide, nitrate and iodide was found to be possible. The detection of iodide was most sensitive with the copper electrode (Fig. 4c). The silver electrode detector (Fig. 4b) appeared to be sensitive only to the halides. On the copper electrode it was possible to detect all analysed components but with lower sensitivity than for the halides. Chloride, nitrate and nitrite gave positive peaks on the copper electrode due to the indirect response. Bromide and iodide gave negative peaks due to the direct electrode response. These results confirmed the mechanisms discussed above whereby the mode of detection depends on the ratio of buffer and sample concentrations and their compexation constants with copper ions. UV detection at 280 nm (Fig. 4a) was found to give indirect detection under the conditions used in this study.

Different selectivities and baseline drifts were observed for the three types of detectors. For example, chloride gave a large peak only on the silver electrode detector and thiosulphate only on the copper

electrode, and hence there is an opportunity to control the selectivity. With respect to baseline stability, from Fig. 3 it may be observed that the copper electrode detector is characterized by a higher drift than the silver electrode. Further, some anions, especially iodide, caused a long response time and a drifting baseline potential after the injection of a high concentration (10 m*M*).

Calibration

Figs. 5 and 6 show calibration graphs for the two different electrode configurations determined from the chromatograms in 1 m*M* perchlorate. The plots are shown in a semilogarithmic format in order to display the wide concentration range studied. These plots indicate the curvature expected [1–3] for potentiometric detectors and show the working concentration ranges for each anion on the silver and copper electrodes. In Fig. 5, when the electrodes were situated close together, as discussed previously, the calibration response was different from that

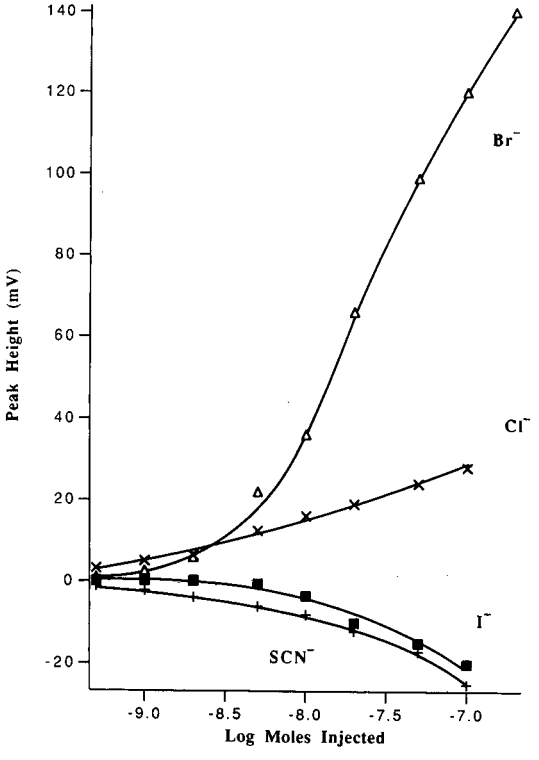

Fig. 5. Calibration graphs for each anion determined with the Ag/AgCl electrode as the sensor in position B in Fig. 1.

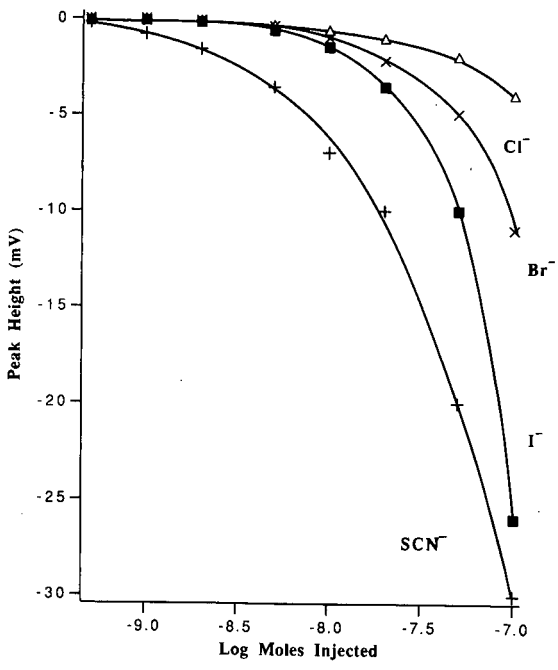

Fig. 6. Calibration graphs for each anion determined with the copper electrode as the sensor with the Ag/AgCl electrode in position A in Fig. 1.

shown in Fig. 6, when the Ag/AgCl electrode was out of the main solution stream.

The detection limits for each anion with the two different cell configurations are shown in Table I, together with retention times in the eluent used. Again, it is clear from Figs. 5 and 6 and Table I that chloride and bromide are best detected with the silver electrode and iodide and thiocyanate at the copper electrode. The detection limits compare favour-

TABLE I

RETENTION TIMES AND POTENTIOMETRIC DETECTION LIMITS[a] AT THE SENSOR ELECTRODES FOR 1.0 m*M* PERCHLORATE AS ELUENT

Anion	Retention time (min)	D_L^{Ag} (mol)	D_L^{Cu} (mol)
Cl^-	1.9	$1 \cdot 10^{-11}$	$2 \cdot 10^{-9}$
Br^-	2.7	$1 \cdot 10^{-11}$	$2 \cdot 10^{-9}$
I^-	5.6	$1 \cdot 10^{-9}$	$5 \cdot 10^{-10}$
SCN^-	9.0	$2 \cdot 10^{-10}$	$2 \cdot 10^{-11}$

[a] D_L^{Cu} is the detection limit using copper as the sensor electrode and D_L^{Ag} that using silver as the sensor electrode.

ably with those reported previously for potentiometric detectors [3]. The UV detector was far less sensitive than the potentiometric detectors under the conditions used in this study.

CONCLUSIONS

The results show clearly that there is an advantage in varying the flow-cell design in order to achieve the desired selectivity of electrode response. The function of each electrode can be changed according to its position in the cell used, and the sensor electrode can be chosen by use of the appropriate configuration. It was shown that the UV detector and both potentiometric detectors are characterized by different selectivities.

The value of this work to the practising chromatographer is that the cell configuration can be chosen according to the requirements for a particular application, for example in the analysis of sea water where there is a high concentration of chloride. However, the calibration graphs must be constructed for the particular configuration chosen for the analytical application of interest.

Detection limits are of the order of 10 pmol injected for the anions detected, and are in some instances lower than with UV detection. The silver electrode sensor is characterized by a smaller drift and faster response time than the copper electrode. The potentiometric detector developed in this study therefore offers improvements over other detection methods in terms of sensitivity, selectivity, cost effectiveness, simplified construction and ease of maintenance.

REFERENCES

1 P. R. Haddad and P. E. Jackson, *Ion-Chromatography: Principles and Applications*, Elsevier, Amsterdam, 1990, pp 323–343.
2 P.W. Alexander, M. Trojanowicz and P. R. Haddad, *Anal. Lett.*, 17 (1984) 309.
3 J. E. Lockridge, N. E. Fortier, G. Schmuckler and J. S. Fritz, *Anal. Chim. Acta*, 192 (1987) 41.
4 E. C. V. Butler and R. M. Gershey, *Anal. Chim. Acta*, 164 (1984) 153.
5 M. P. Keuken, J. Slanina, P. A. C. Jongejan and F. P. Bakker, *J. Chromatogr.*, 439 (1988) 13.
6 F. A. Schultz and D. E. Mathis, *Anal. Chem.*, 46 (1974) 2253.
7 P. W. Alexander and C. Maitra, *Anal. Chem.*, 53 (1981) 1590.
8 P. W. Alexander, P. R. Haddad and M. Trojanowicz, *Anal. Chem.*, 56 (1984) 2417.
9 P. R. Haddad, P. W. Alexander and M. Trojanowicz, *J. Chromatogr.*, 324 (1985) 319.
10 R. G. Bates, *Determination of pH, Theory and Practice*, Wiley, New York, 2nd ed., 1973, p. 330.

Journal of Chromatography, 589 (1992) 209–214
Elsevier Science Publishers B.V., Amsterdam

CHROM. 23 755

Potentiometric detection of carboxylic acids and inorganic anions in ion-exclusion chromatography using camphorsulphonic acid as eluent

Bronisław K. Głód☆, Paul R. Haddad* and Peter W. Alexander

Department of Analytical Chemistry, University of New South Wales, P.O. Box 1, Kensington N.S.W. 2033 (Australia)

(First received July 6th, 1991; revised manuscript received September 7th, 1991)

ABSTRACT

The use of potentiometric detection in ion-exclusion chromatography of carboxylic acids (oxalic, citric, tartaric, malic, lactic, succinic and acetic acid) is reported. A comparison of the performance characteristics of potentiometric detection with those obtained by UV absorbance is given. A treatment of the electrode response characteristics, based on ionic equilibria in the bulk solution, is presented in order to determine the mechanism of response at the indicator electrode. The results show that the response is Nernstian and arises as a result of the effect of solute species on the concentration of Cu(II) generated at the electrode surface. Experimental data for inorganic anions and aliphatic acids show close agreement with the theoretical response. The selectivity of the potentiometric detector is illustrated by reference to the analysis of white wine.

INTRODUCTION

Potentiometry has frequently been applied to selective detection in flow-injection analysis through the use of membrane electrodes. More recent investigations [1–3] have shown that metallic wire electrodes can also be successfully utilized as the indicator electrode for potentiometric detection in liquid chromatography. Metallic copper indicator electrodes have been particularly successful in this regard and can give sensitive and quite universal potentiometric response even when copper ions are not present in the mobile phase.

In previous papers we have utilized the metallic copper wire electrode as a potentiometric detector in various chromatographic systems and for the analysis of many different classes of compounds [1–3], including carboxylic acids. These reports have shown that detection of carboxylic acids is possible after separation using anion-exchange and ion-exclusion columns. The mobile phase components used in these studies (phthalate, phosphate or citrate buffers) are characterised by relatively high complexation with the copper ions. In some cases (*e.g.* ref. 1) this leads to the observation of indirect detection wherein the sensing electrode monitors the decrease in the concentration of the mobile phase buffer which accompanies the elution of a solute. Detection limits using phosphoric acid mobile phases were in the range 0.2 nmol (for oxalic acid by ion-exchange chromatography [1]) to 200 nmol (for acetic acid by ion-exclusion chromatography [3]).

The present study shows the advantages of separation and potentiometric detection of carboxylic acids in ion-exclusion chromatography using camphorsulphonic acid as the mobile phase buffer. Direct potentiometric response to some inorganic anions (*e.g.* chloride and phosphate) is also noted. A theoretical treatment of the electrode response characteristics based on ionic equilibria in the bulk solution is presented in order to determine the mechanism of response at the indicator electrode.

☆ Permanent address: Institute of Physical Chemistry, Polish Academy of Sciences, Kasprzaka 44/52, 01-224 Warsaw, Poland.

0021-9673/92/$05.00

The results show that the response is Nernstian and arises due to the effect of eluted solutes on the Cu(II) concentration generated spontaneously at the electrode surface.

THEORY

The potential of a metallic copper electrode is based on the Cu^{2+}/Cu^0 redox couple existing at the electrode surface. When such an electrode is equilibrated with a mobile phase containing a copper-complexing ligand, or when a copper-complexing solute contacts the electrode, the potential is dependent on the mass transport of the ligand or solute to the electrode surface and hence on flow-rate. However, the theoretical electrode response can be derived more easily in terms of the Nernst equation with the assumption that the electrode potential is determined by the bulk concentrations of complexing species and that mass transport effects need not be considered. Therefore, in the following theoretical treatment the approximation is made that at a constant flow-rate the electrode potential is dependent on Nernstian response to the bulk ligand concentrations. We begin by assuming 1:1 stoichiometry for the copper–ligand complex and by neglecting complexation of Cu^+ (carboxylic acids show weak complexation of Cu^+ in comparison to Cu^{2+}). Moreover, the detector cell design eliminates reactions with the silver/silver chloride reference electrode.

In the presence of a complexing agent, B^{n-}, in a buffered mobile phase and in a neutral medium, the potential of the metallic copper electrode may be described by the Nernst equation:

$$E_1 = E^0_{Cu^{2+}/Cu^0} + \frac{RT}{2F}\ln[Cu^{2+}]_B \tag{1}$$

where R is the universal gas constant, T is the temperature and F is the Faraday constant. The subscript B denotes that the indicated concentration exists in the presence of the mobile phase buffer. When a copper-complexing solute ligand, L^{m-}, passes the electrode, the electrode potential will alter, producing a peak. The potential at the peak maximum is given by:

$$E_2 = E^0_{Cu^{2+}/Cu^0} + \frac{RT}{2F}\ln[Cu^{2+}]_L \tag{2}$$

where the subscript L denotes that the indicated concentration exists in the presence of both the solute ligand and the buffer (that is, during elution of the ligand). The complexation reaction between B^{n-} and Cu^{2+}, and the associated formation constant, are given below:

$$Cu^{2+} + B^{n-} \leftrightharpoons CuB^{(2-n)+} \tag{3}$$

$$K_B = \frac{[CuB^{(2-n)+}]_B}{[Cu^{2+}]_B[B^{n-}]_B} \tag{4}$$

At the peak maximum, the following equilibrium exists:

$$Cu^{2+} + L^{m-} \leftrightharpoons CuL^{(2-m)+} \tag{5}$$

and the following two constants must be considered:

$$K_B = \frac{[CuB^{(2-n)+}]_L}{[Cu^{2+}]_L[B^{n-}]_L} \tag{6}$$

$$K_L = \frac{[CuL^{(2-m)+}]_L}{[Cu^{2+}]_L[L^{m-}]_L} \tag{7}$$

The mass balance equation for copper ions at the electrode surface can be written as:

$$[Cu^{2+}]_B + [CuB^{(2-n)+}]_B = [Cu^{2+}]_L + [CuB^{(2-n)+}]_L + [CuL^{(2-m)+}]_L \tag{8}$$

By writing mass balance equations for B and L and combining these with eqns. 1, 2, 4 and 6–8, we can obtain the following expression for the change in electrode potential (ΔE) occurring at the peak maximum:

$$\Delta E = E_2 - E_1 = \frac{RT}{2F}\ln\left[\frac{1 + K_B c_B}{1 + K_B c_B + K_L c_L}\right] \tag{9}$$

where c_B and c_L are the total (analytical) concentrations of B and L (both free and complexed), respectively. Eqn. 9 may be rewritten as:

$$\Delta E = -29\log\left[1 + \left(\frac{K_L c_L}{1 + K_B c_B}\right)\right] \tag{10}$$

Taking into account dilution effects occurring on the chromatographic column, eqn. 10 becomes:

$$\Delta E = -29\log\left[1 + \left(\frac{c_i V_i K_L N^{0.5}}{(2\pi)^{0.5} V_R (1 + K_B c_B)}\right)\right] \tag{11}$$

where c_i and V_i are the injected concentration and volume of solute, V_R is the retention volume and N is the number of theoretical plates for the column. Eqn. 11 shows that the peak height is inversely proportional to the buffer concentration and to its copper complexation constant. This indicates that a low detection limit can be expected for low buffer concentrations. On the other hand, use of dilute buffers is likely to cause some experimental difficulties, such as elevated noise level during potential measurement on a high resistance cell and unstable pH. For practical analyses, the optimum chromatographic conditions are therefore likely to sacrifice some sensitivity in return for stable chromatography.

EXPERIMENTAL

Instrumentation and reagents

A Waters (Milford, MA, USA) Model 510 HPLC pump, Model U6K universal injector and a Model 484 tunable absorbance detector (operated at a wavelength of 210 nm) were used. The electrochemical cell used for potentiometric detection has been described previously [4] and consisted of a metallic copper indicator electrode and a Ag/AgCl reference electrode housed in a Perspex flow-through cell. The reference electrode was prepared using the electrolytic method described elsewhere [5]. The potential difference between the electrodes was monitored with an Activon (Sydney, Australia) Model 101 pH/millivolt meter. Separations were performed on a Bio-Rad (Richmond, VA, USA) Aminex ion-exclusion HPX-87H organic acid analysis column (300 × 7.8 mm I.D., hydrogen form 8% cross-linked cation exchanger, 9 μm particle diameter). Chromatograms were recorded on an ABB Goerz Metrawatt (Vienna, Austria) SE 120 recorder. The flow-rate used in all experiments was 1 ml/min.

All reagents were of analytical reagent grade and were used without further purification. Camphorsulphonic acid was obtained from Sigma (St. Louis, MO, USA). The mobile phase was prepared from triply distilled water passed through a Millipore (Bedford, MA, USA) Milli-Q water purification system and was filtered through a Millipore 0.45-μm membrane filter and degassed in an ultrasonic bath prior to use.

Procedures

Chromatograms were recorded using 1 m*M* camphorsulphonic acid as mobile phase. The column was equilibrated for at least 30 min prior to use and was operated at ambient temperature. Stock solutions of solute acids were prepared as 10 m*M* solutions in Milli-Q water and diluted to the required concentrations before use. Solute solutions (20 μl) were injected into the chromatographic system with a 100-μl syringe (Hamilton, Reno, NV, USA) and the potentiometric and UV signals were

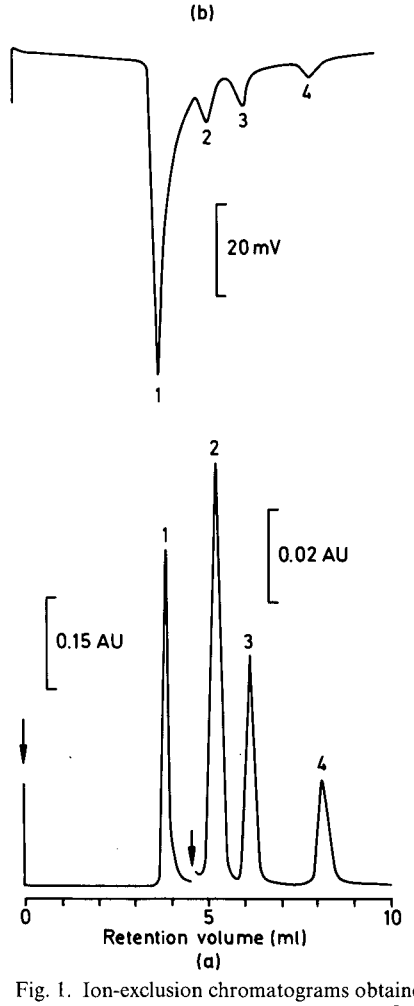

Fig. 1. Ion-exclusion chromatograms obtained with (a) UV and (b) potentiometric detectors. Sample: 10^{-7} mol of: 1 = oxalic, 2 = tartaric, 3 = malic and 4 = succinic cids. Column: Bio-Rad Aminex HPX 87-H 300 × 7.8 mm I.D. Mobile phase: 1 m*M* camphorsulphonic acid.

monitored continuously on the chart recorder. The wine sample was filtered and injected without further treatment.

RESULTS AND DISCUSSION

Conditions of ion-exclusion separation

This study aimed to identify the optimal chromatographic conditions from the potentiometric detection viewpoint as well as that of the chromatographic separation itself. From eqn. 11, maximum sensitivity is expected when a low concentration of a weakly copper-complexing buffer is used. Such dilute buffers are suited to ion-exclusion chromatography, in which even pure water can be used as a mobile phase [6,7]. However, it is conventional to use a dilute acid (*e.g.* 0.1–1 m*M*) as eluent in order to ensure that the peak shape is symmetrical and that the retention time is independent of solute concentration. In our experiments, phosphoric acid, phthalic acid, benzoic acid, naphthalenesulphonic acid and camphorsulphonic acid were employed as eluent buffers. Best results were obtained with camphorsulphonic acid, which is characterised by very weak complexation of copper ions and by a high dissociation constant, thereby giving a solution of high conductance. Ion-exclusion chromatograms obtained using 1 m*M* camphorsulphonic acid with potentiometric and UV detection are shown in Figs. 1 and 2 for a range of carboxylic acids (citric, tartaric, acetic, malic, lactic, oxalic and succinic) and inorganic anions (chloride and phosphate).

Detection limits

Detection limits obtained with the potentiometric detector are presented in Table I, together with those for UV detection. It is interesting to note that for oxalic acid and chloride, a better detection limit was obtained using the potentiometric detector than was achievable by UV detection. Furthermore, the potentiomeric detection limit for oxalic acid was 10 times lower than that reported previously [1–3] when alternative eluents were employed. For other species, the UV detector was the more sensitive.

Calibration plots

Calibration curves for the potentiometric detector are presented in Fig. 3. The largest potentiometric response is observed for oxalic acid and occurs

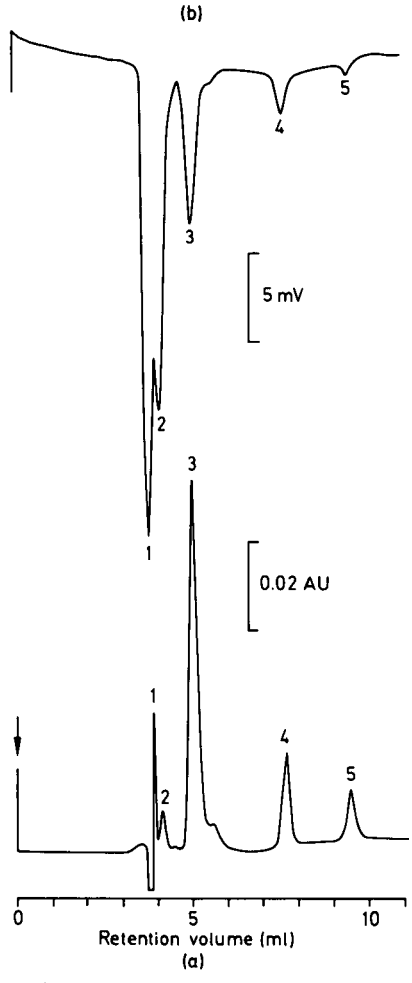

Fig. 2. Ion-exclusion chromatograms obtained with (a) UV and (b) potentiometric detectors. Sample: 10^{-7} mol of: 1 = chloride, 2 = phosphate, 3 = citric acid, 4 = lactic acid and 5 = acetic acid. Other conditions as for Fig. 1.

because the stereochemistry of this species is favourable for copper complexation. Calibration plots are non-linear over the concentration range studied, in comparison to the UV calibration plots (not shown) which exhibited linearity over a small range of low concentrations.

Eqn. 11 can be rearranged to permit calculation of K_L, the complexation constant between the solute and Cu(II). Values of K_L (expressed as the average obtained for a series of solute injections up to $5 \cdot 10^{-8}$ mol) are presented in Table I. A clear inverse correlation exists between the detection limit and the

TABLE I

RETENTION VOLUMES (V_R), DETECTION LIMITS FOR UV (D_L^{UV}) AND POTENTIOMETRIC DETECTORS (D_L^{Pot}), AND COMPLEXATION CONSTANTS (K_L) CALCULATED FROM EQN. 11.

Solute (acid)	V_R (ml)	D_L^{UV} (nmol)	D_L^{Pot} (nmol)	K_L
Oxalic acid	3.85	0.05	0.02	$1.2 \cdot 10^5$
KCl	3.90	0.50	0.2	$9.3 \cdot 10^3$
Na_3PO_4	4.05	0.17	20	$1.7 \cdot 10^2$
Citric acid	4.95	0.03	0.2	$1.6 \cdot 10^4$
Tartaric acid	5.50	0.03	0.3	$1.5 \cdot 10^4$
Malic acid	6.05	0.06	0.4	$1.4 \cdot 10^4$
Lactic acid	7.70	0.09	10	$3.9 \cdot 10^2$
Succinic acid	8.15	0.14	10	$3.4 \cdot 10^2$
Acetic acid	9.45	0.27	50	$7.6 \cdot 10^1$

magnitude of the complexation constant. Fig. 4 shows the theoretical calibration curves for the potentiomeric detector, calculated from eqn. 11 using the complexation constants presented in Table I. Experimental calibration data are also shown and it can be seen that good agreement between theoretical and experimental data exists. Whilst it is recognised that the complexation constants used for this calculation are not from independent measurements, it is noteworthy that it was possible to correctly predict the shapes of the calibration curves.

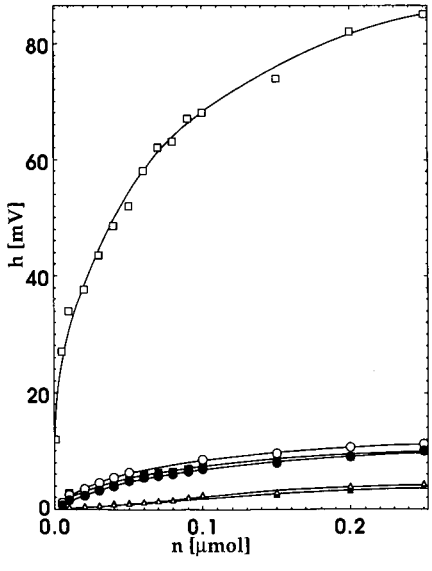

Fig. 3. Calibration curves obtained for potentiometric detection. Solutes: □ = oxalic acid; ○ = tartaric acid; ■ = malic acid; ● = succinic acid; △ = citric acid; ▲ = lactic acid. Other conditions as in Fig. 1. h = Peak height, n = amount of injected sample.

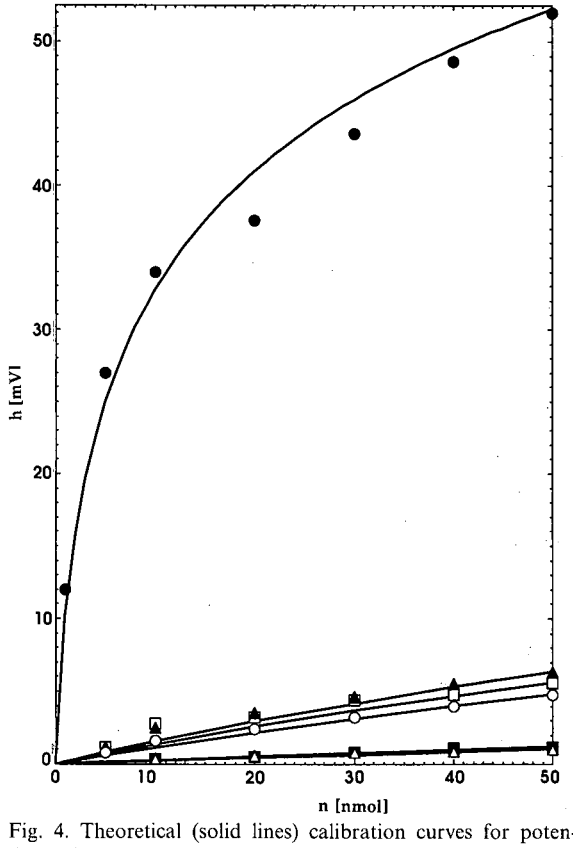

Fig. 4. Theoretical (solid lines) calibration curves for potentiometric detection, calculated from eqn. 11. Experimental values (taken from Fig. 3) are shown as points. Solutes: ● = oxalic acid; ▲ = tartaric acid; □ = malic acid; ○ = succinic acid; ■ = citric acid; △ = lactic acid.

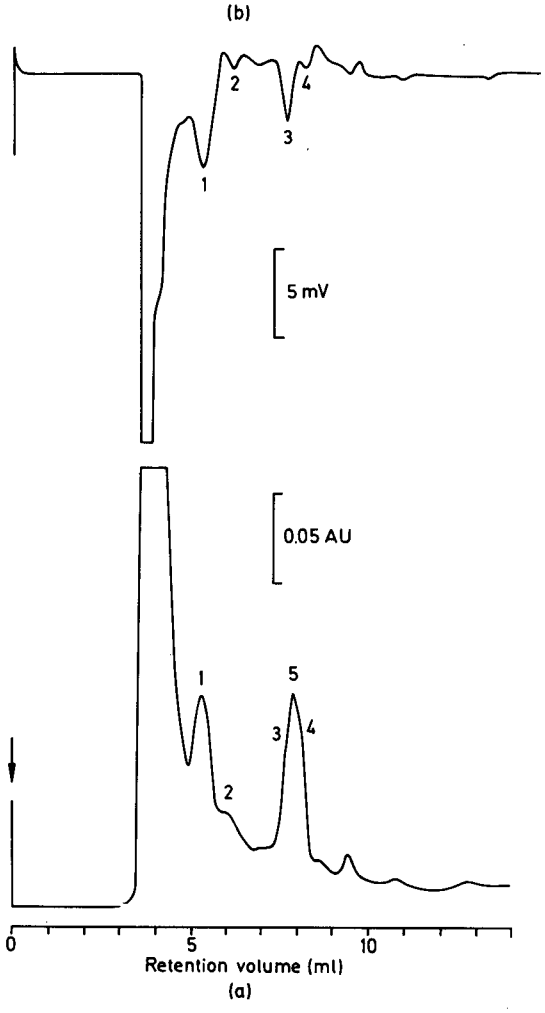

Fig. 5. Ion-exclusion chromatogram of white wine. Injection volume: 10 μl. Peak: 1 = tartaric acid, 2 = malic acid and fructose, 3 = lactic acid, 4 = succinic acid and 5 = unknown. Other conditions as in Fig. 1.

Agreement between theory and experiment decreased when larger amounts of solute were injected, suggesting that the simple theoretical model used is valid only for small solute concentrations.

Selectivity

Potentiometric detectors generally show high selectivity which favours their use in flow-injection analysis rather than as chromatographic detectors. However, the metallic copper electrode shows response to a wide range of solutes including amines, amino acids, oxidants, reductants, *etc.*, as well as to the carboxylic acids and inorganic anions studied here. The selectivity of this detector therefore falls between the extremes of conventional potentiometric devices (high selectivity) and universal (low selectivity) detectors, such as UV. This intermediate selectivity means that the copper electrode detector can be employed for general purpose use, but may also exhibit advantageous selectivity in certain applications.

One example of this is the analysis of wine using the chromatographic conditions described in this paper, as shown in Fig. 5. With UV detection (Fig. 5a), peaks for lactic acid and succinic acid are obscured by an unidentifieed component, and malic acid is co-eluted with fructose. In contrast, the insensitivity of the potentiometric detector to both fructose and the unidentified interferent permits the determination of each of these carboxylic acids (Fig. 5b).

CONCLUSIONS

The results show that improved detection limits for the potentiometric detector can be achieved by correct choice of the mobile phase buffer, giving a sensitivity rivalling the UV detector and detection selectivity which differs from that attainable with UV detection. The theoretical description of detector response enabled us to predict the direction of the response and the shape of the calibration curves.

REFERENCES

1 P. W. Alexander, P. R. Haddd and M. Trojanowicz, *Chromatographia*, 20 (1985) 179.
2 P. R. Haddad, P. W. Alexander and M. Trojanowicz, *J. Chromatogr.*, 315 (1984) 261.
3 P. R. Haddad, P. W. Alexander, M. Y. Croft and D. F. Hilton, *Chromatographia*, 24 (1987) 487.
4 P. W. Alexander, M. Trojanowicz and P. R. Haddad, *Anal. Lett.*, 17 (1984) 309.
5 R. G. Bates, *Determination of pH, Theory and Practice*, Wiley, New York, 2nd ed., 1973, p. 330.
6 B. K. Głód, A. K. Piasecki and J. Stafiej, *J. Chromatogr.*, 457 (1988) 43.
7 P. R. Haddad and P. E. Jackson, *Ion Chromtography: Principles and Applications* (*Journal of Chromatography Library*, Vol. 46), Elsevier, Amsterdam, 1990, pp. 202–212.

Journal of Chromatography, 589 (1992) 215–222
Elsevier Science Publishers B.V., Amsterdam

CHROM. 23 686

Accuracy of computer-simulated gas chromatographic separations based on a linear elution strength model

M. C. Roman

Department of Chemistry, University of Rhode Island, Kingston, RI 02881 (USA)

R. W. Siergiej*,☆

Rohm and Haas Company, Spring House, PA 19477 (USA)

(First received March 5th, 1991; revised manuscript received August 13th, 1991)

ABSTRACT

Computer simulation using commercially available software (DryLab GC) for temperature-programmed gas chromatography was investigated for accuracy of predicted retention and resolution. The simulations, based on a linear elution strength model, were evaluated for a variety of samples, temperature programming rates and stationary phases. Reliable simulations were obtained for both linear and segmented temperatures programs. Predicted retention times were accurate to within ±4% and the resolution of adjacent bands was generally accurate to within ± 12%.

INTRODUCTION

Temperature programming is widely used in the development of gas chromatographic (GC) separations and is especially useful for the analysis of mixtures covering a wide range of volatilities. Increasing the column temperature has a predominant effect of reducing retention, but the selectivity of a column can also be affected [1–6]. The influence of temperature on selectivity can be exploited in the development of GC separations; however, optimizing the selectivity by varying the temperature program can be difficult, especially for complex mixtures. Changing a programming rate to improve the resolution of a given solute pair may reduce the separation of other solute pairs. The choice of temperature programming rate is often achieved through trial and error, but the difficulty of applying this approach to optimization increases as the number of peaks present in a chromatogram increases.

A number of approaches to the systematic optimization of temperature in GC have been described [7–17], including the use of computer simulation [18–20]. Although the utility of systematic approaches has been clearly documented, the widespread use of computer-assisted optimization techniques has not occurred. Software designed for the optimization of temperature-programmed GC separations has not been readily available, and many chromatographers lack the expertise needed to develop computer programs to perform the required calculations. Software (DryLab GC) for GC simulations based on a linear elution strength (LES) model has recently been described by Bautz *et al.* [21]. Data from two experimental runs carried out at different linear temperature programming rates are used as input for the LES model. Computer simulations can then be predicted for other linear temperature programming rates, isothermal runs or multi-segment temperature programs. Accuracy of

☆ Present address: Medical Products Division, W. L. Gore & Associates, Inc., 1500 North Fourth Street, P.O. Box 800, Flagstaff, AZ 86002, USA.

0021-9673/92/$05.00

computer simulations was reported for the separation of a mixture of phenols on a non-polar column.

In this study we investigated the accuracy of computer simulations using DryLab GC for a variety of experimental conditions. The effect of column polarity on the accuracy of predicted retention times and resolution was studied. We also investigated the accuracy of separations optimized with the use of computer-simulated relative resolution maps and multiple-ramp temperature programs.

EXPERIMENTAL

Equipment

The gas chromatograph was an HP5890 equipped with a split–splitless injector port, flame ionization detector and an HP7673A automatic sampler (Hewlett-Packard, Avondale, PA, USA). Data collection was accomplished with a Model 6000 Laboratory Data System (PE/Nelson Analytical, Palo Alto, CA, USA). Fused-silica capillary columns used in this study included DB-1 (30 m × 0.32 mm I.D.), DB-1 (15 m × 0.25 mm I.D.) and DB-1701 (15 m × 0.32 mm I.D.) (J & W Scientific, Folsom, CA, USA) and Supelcowax (15 m × 0.25 mm I.D.) (Supelco, Bellefonte, PA, USA). The film thickness for each column was 0.25 μm. Hydrogen was used as the carrier gas for all separations. Sample injections were made in the split mode using injection volume of 1 μl with a splitting ratio of 100:1.

Software

Simulations were calculated using the computer program DryLab GC (LC Resources, Lafayette, CA, USA) run on an IBM 3270-PC (XT) computer equipped with a math coprocessor.

Samples

Aliphatic hydrocarbon standards ranging from C_{10} to C_{26} were obtained from Sadtler Research Labs. (Philadelphia, PA, USA). The hydrocarbon mixture contained *ca.* 0.5 mg/ml of each hydrocarbon in hexane. A "pesticide test mix" containing α-BHC, β-BHC, aldrin, *o,p'*-DDD, *p,p'*-DDD, *p,p'*-DDE, *o,p'*-DDT, *p,p'*-DDT, dieldrin, endrin, heptachlor, heptachlor epoxide and lindane was purchased from Supelco. The concentration of each pesticide ranged from 0.025 to 0.26 mg/ml in isooctane. Salicylaldehyde, N-methylaniline, decanol, methyl decanoate and 1-bromodecane were obtained from Aldrich (Milwaukee, WI, USA). These solutes were dissolved in acetone at concentrations of *ca.* 0.5 mg/ml.

RESULTS AND DISCUSSION

The accuracy of predicted retention times was evaluated for the separation of a homologous series of straight-chain aliphatic hydrocarbons on a non-polar (DB-1) column. Experimental data were collected at three linear temperature programming rates (10, 20 and 30°C/min from 35 to 300°C). Predicted retention times for each programming rate were calculated using experimental data from the remaining two runs as input for the DryLab GC program (*e.g.*, data from the 10 and 20°C/min runs were used as input to predict retention times for 30°C/min).

Experimental and predicted retention times for C_{10}–C_{26} *n*-alkanes are compared in Table I. The average error of calculated retention times is less than ±3% for each of the three programming rates. This degree of accuracy should be acceptable for most GC method development purposes. Predicted retention times for the 20°C/min programming rate are the most accurate. These retention times were calculated by interpolation of the 10 and 30°C/min data and are consistently greater than the experimental retention times. Larger errors are observed when simulations are made by extrapolation of experimental data. Predicted retention times for the 10 and 30°C/min programming rates were obtained by extrapolation and have slightly larger average errors than the 20°C/min data. The magnitude of the retention time error depends not only on whether the calculations involve interpolation or extrapolation but also on the degree of difference between the experimental retention times and predicted retention. A plot of relative error *versus* experimental retention time for the 20°C/min run is shown in Fig. 1A. The errors are systematic and correlate with the experimental retention time. Similar correlations are observed for the 10 and 30°C/min predictions.

The usual aim of chromatographic method development is to obtain acceptable resolution in a minimum amount of time. Although the accurate prediction of retention time is desirable, it is also neces-

TABLE I

COMPARISON OF EXPERIMENTAL AND CALCULATED RETENTION TIMES FOR *n*-ALKANE MIXTURE ON A 30-m DB-1 COLUMN

n-Alkane	Retention time (min)					
	10°C/min[a]		20°C/min[a]		30°C/min[a]	
	Expt.	Calc.	Expt.	Calc.	Expt.	Calc.
C_{10}	3.17	3.07	2.32	2.34	1.91	1.88
C_{11}	4.54	4.40	3.08	3.11	2.44	2.40
C_{12}	5.95	5.73	3.83	3.86	2.95	2.90
C_{13}	7.34	7.12	4.55	4.59	3.45	3.40
C_{14}	8.67	8.45	5.24	5.27	3.91	3.86
C_{15}	9.93	9.69	5.89	5.93	4.36	4.30
C_{16}	11.13	10.84	6.50	6.54	4.77	4.72
C_{17}	12.27	11.99	7.09	7.13	5.17	5.12
C_{18}	13.36	13.08	7.65	7.69	5.55	5.49
C_{19}	14.40	14.09	8.18	8.22	5.91	5.85
C_{20}	15.39	15.08	8.69	8.74	6.26	6.19
C_{21}	16.34	15.98	9.17	9.23	6.59	6.52
C_{22}	17.25	16.91	9.64	9.70	6.91	6.84
C_{23}	18.12	17.78	10.09	10.14	7.12	7.14
C_{24}	18.96	18.62	10.52	10.57	7.50	7.43
C_{25}	19.77	19.40	10.93	10.98	7.78	7.71
C_{26}	20.54	20.17	11.33	11.38	8.05	7.98
Av. error (%)[b]	−2.39 ± 0.56		0.64 ± 0.16		−1.19 ± 0.28	

[a] Temperature programming rate.

[b] Errors in retention time are calculated as the average error divided by the average retention time × 100. Uncertainties are reported as ± 1 standard deviation.

sary to obtain accurate predictions of resolution as a function of separation conditions. The retention time difference (Δt_r) of adjacent bands is proportional to resolution and can be used to judge the accuracy of computer simulations [21]. Predicted and experimental retention time differences for adjacent bands were calculated for the hydrocarbon data and the average errors are summarized in Table II. Predicted retention time differences are generally accurate to within 5%. As a result of the correlation between the percentage error in predicted retention time and the experimental retention time, adjacent peaks in a computer simulation will have retention time errors of similar magnitude. In the calculation of Δt_r of adjacent peaks the retention time errors will tend to be offset, resulting in predicted resolutions that are relatively unaffected by the magnitude of retention time errors. In contrast to retention time errors, predicted resolution errors should therefore be independent of retention time in any given computer simulation. This is confirmed by the 20°C/min data shown in Fig. 1B, in which the error of retention time differences exhibits no correlation with retention time.

To be generally useful as an aid for GC method development, the LES model should be capable of providing accurate simulations for separations obtained with both polar and non-polar stationary phases. The effect of stationary phase polarity on the accuracy of computer simulations was investigated using a test mixture of randomly selected compounds spanning a wide range of polarity: salicylaldehyde, N-methylaniline, decanol, methyl decanoate, 1-bromodecane and hexadecane). This mixture was separated using columns of low polarity (DB-1), intermediate polarity (DB-1701) and high polarity (Supelcowax). Linear temperature programming rates of 2 and 25°C/min from 35 to

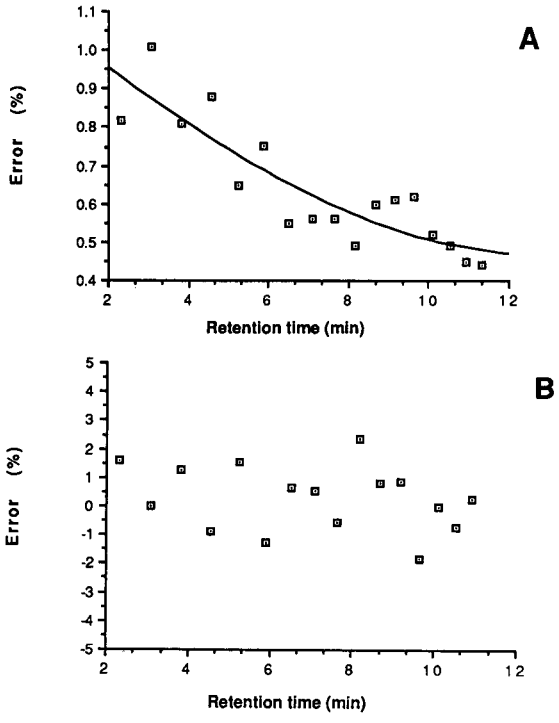

Fig. 1. Comparison of percentage error *vs.* retention time for *n*-alkanes separated on a 30-m DB-1 column with a programming rate of 20°C/min from 35 to 300°C. (A) Predicted retention times and (B) predicted retention time difference of adjacent bands.

TABLE II

SUMMARY OF ERRORS IN PREDICTED RETENTION TIME DIFFERENCES FOR *n*-ALKANE MIXTURE

Heating rate (°C/min)	Av. error, Δt_r(%)[a]
10	−1.5 ± 2.4
20	0.29 ± 1.1
30	−0.64 ± 1.2

[a] Errors in Δt_r are calculated as the average retention time difference of adjacent bands divided by the average difference in retention times for all adjacent bands × 100.

275°C were used to generate input data. Simulated and experimental runs were then carried out at intermediate rates of 12 or 13.5°C/min. Relative errors for predicted retention times and retention time differences are presented in Table III. The retention time errors for the non-polar column are slightly larger than those for either the polar or intermediate-polarity columns, but for all three columns the errors are less than 4%. The difference between the polar and intermediate-polarity columns is not significant. Owing to the relatively large variability in the errors of predicted retention time differences, no significant differences are observed between the three columns. The predicted retention time differences are accurate to within ±12% for all three

TABLE III

COMPARISON OF EXPERIMENTAL AND CALCULATED RETENTION TIMES FOR TEST MIXTURE ON COLUMNS OF DIFFERENT POLARITY

Compound	Retention time (min)					
	DB-1[a]		DB-1701[b]		Supelcowax[c]	
	Expt.	Calc.	Expt.	Calc.	Expt.	Calc.
Salicylaldehyde	5.27	5.46	4.78	4.88	1.91	1.88
N-Methylaniline	5.57	5.77	5.28	5.40	2.44	2.40
Decanol	8.16	8.44	7.38	7.49	9.69	9.88
Methyl decanoate	8.74	9.01	7.51	7.63	8.19	8.35
1-Bromodecane	9.04	9.34	7.63	7.76	8.00	8.18
Hexadecane	11.65	11.99	9.70	9.87	8.22	8.38
Av. error, t_r (%)[c]	3.33 ± 0.26		1.82 ± 0.30		2.15 ± 0.22	
Av. error, Δt_r (%)[c]	0.26 ± 3.87		4.30 ± 3.74		−2.96 ± 7.97	

[a] Programming rate 13.5°C/min, 14-m column.
[b] Programming rate 12.0°C/min.
[c] See footnote to Tables I and II.

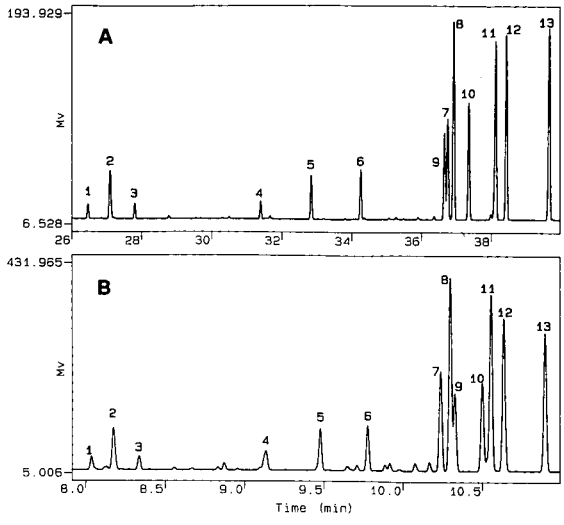

Fig. 2. Comparison of chromatograms for pesticide sample demonstrating the change in relative retention with programming rate. Conditions: 30-m DB-1 column programmed at (A) 5°C/min and (B) 25°C/min from 35 to 330°C. Peaks 1 = α-BHC; 2 = β-BHC; 3 = lindance; 4 = heptachlor; 5 = aldrin; 6 = heptachlor epoxide; 7 = *p,p'*-DDE; 8 = *o,p'*-DDD; 9 = dieldrin; 10 = endrin; 11 = *p,p'*-DDD; 12 = *o,p'*-DDT; 13 = *p,p'*.DDT.

columns. These results suggest that column polarity does not significantly affect the accuracy of simulations based on the LES model.

Computer simulation is very useful for optimizing separations in which the relative retentions of peaks change at different temperature programming rates. A practical feature of this computer program is the ability to calculate and plot relative resolution maps (similar to window diagrams [19]). The utility of relative resolution maps is demonstrated for the separation of thirteen pesticides. Input data for computer simulations were obtained at temperature programming rates of 5 and 25°C/min from 35 to 330°C. A comparison of the two chromatograms (Fig. 2) shows that the relative retention of peaks 7–11 changes significantly. A relative resolution map for the pesticide mixture (Fig. 3) displays the predicted resolution between the worst-resolved pair of peaks over a broad range of temperature programming rates. Three significant maxima are present at programming rates of 3.9, 9.2 and 31°C/min. (Accurate programming rates for these resolution maxima were obtained using tabulated values of predicted resolution *vs.* programming rate.) The highest achievable resolution predicted by the relative resolution map occurs at a rate of 3.9°C/min. The minimum resolution at this rate is predicted to be 1.8, which would indicate baseline resolution of all components. Computer-simulated and experimental chromatograms at 3.9°C/min are shown in Figure 4. Excellent agreement is observed between the predicted and experimental values. Baseline resolution was achieved, but the separation required nearly 50 min for completion.

An advantage of using relative resolution maps is that they allow the chromatographer to select con-

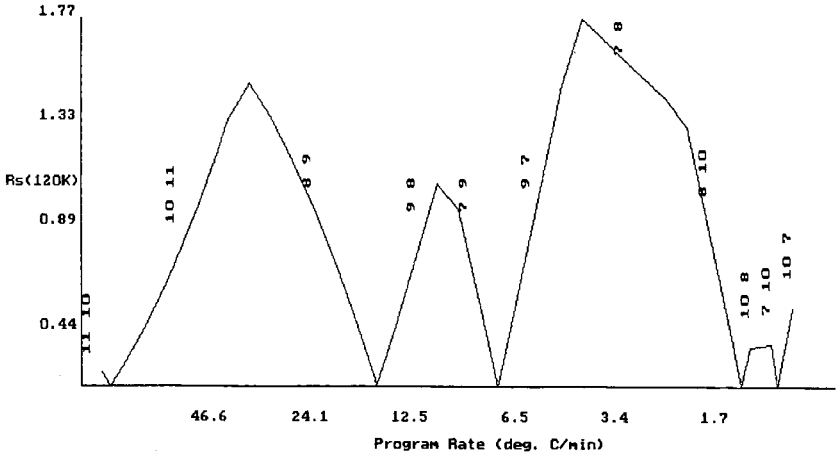

Fig. 3. Relative resolution (R_s) map for pesticide sample. Separation conditions as in Fig. 2. 120 K is the calculated number of theoretical plates (120 000).

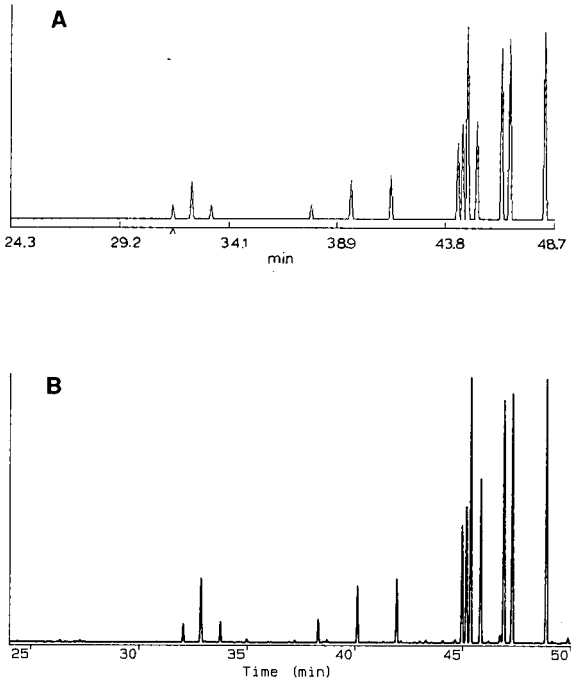

Fig. 4. Comparison of predicted *vs.* experimental chromatograms for pesticide mixture with a programming rate of 3.9°C/min. Other conditions as in Fig. 2. (A) Computer simulation; (B) experimental separation.

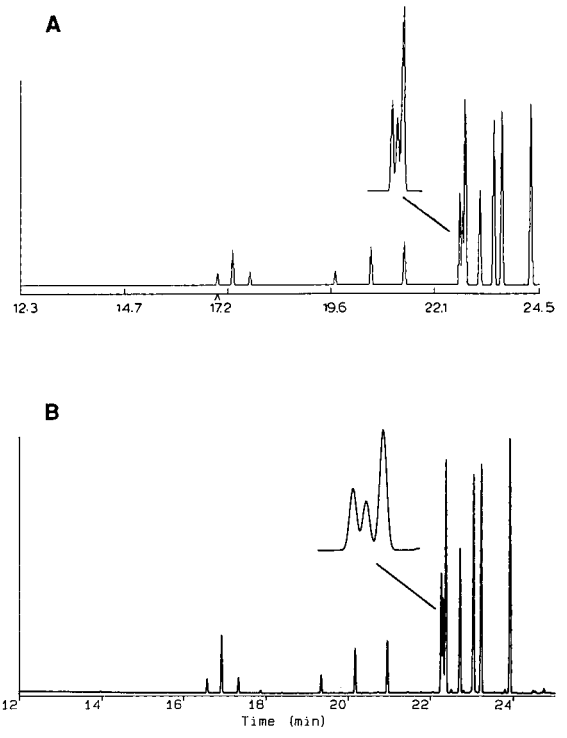

Fig. 5. Comparison of predicted *vs.* experimental chromatograms for pesticide sample with a programming rate of 9.2°C/min. Other conditions as in Fig. 2. (A) Computer simulation; (B) experimental separation.

ditions that, although not providing maximum resolution, allow other factors such as speed and sensitivity to be taken into consideration. If less than baseline resolution is acceptable, two other maxima in the relative resolution map predict that adequate separation can be achieved in much less time. Temperature programming rates in the range 8–10°C/min are commonly used for GC method development. The resolution maximum at 9.2°C/min falls in this range, but it is a local optimum and is predicted to provide neither the best resolution nor the fastest separation time. A chromatographer who explores a limited range of temperature programming rates during method development could mistakenly conclude that this local optimum gives the "best" separation.

A comparison of computer-simulated and experimental chromatograms at 9.2°C/min is shown in Fig. 5. Although baseline resolution of all peaks has not been achieved (as predicted), the separation time has been reduced to 24 min. A further reduction in separation time is predicted by the resolution maximum corresponding to a programming rate of 31°C/min. Computer-simulated and experimental chromatograms at this rate are compared in Fig. 6. The experimental and predicted retention times show excellent agreement. The observed resolution for the two critical band pairs is slightly less than predicted because the computer simulation does not take into asccount the effect of temperature on column efficiency. At the expense of resolution, the separation time and sensitivity have been substantially improved over the 3.9°C/min run. The separation time has been reduced to less than 10 min (five-fold decrease) and the sensitivity increased by a factor of 3.

The accuracy of computer simulations of multiple-ramp temperature programs was also investigated. Manual optimization of multiple-ramp programs can be extremely tedious and time consum-

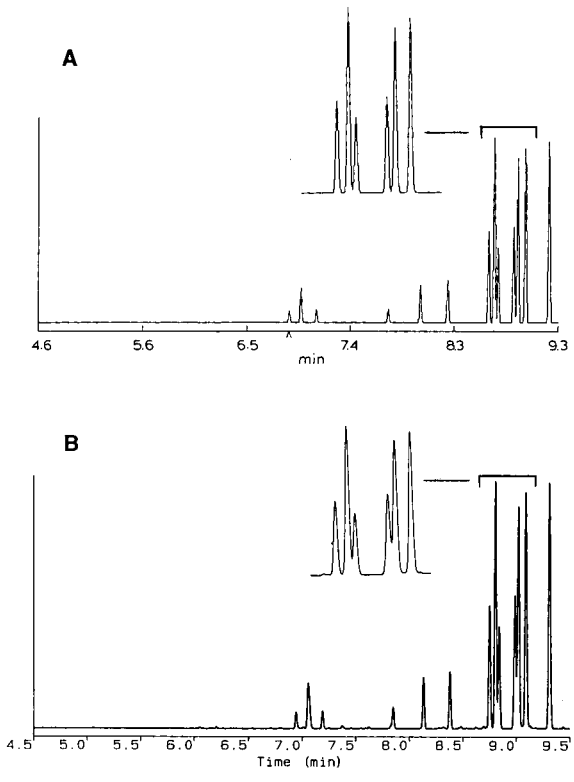

Fig. 6. Comparison of predicted *vs.* experimental chromatograms for pesticide sample with a programming rate of 31°C/min. Other conditions as in Fig. 2. (A) Computer simulation; (B) experimental separation.

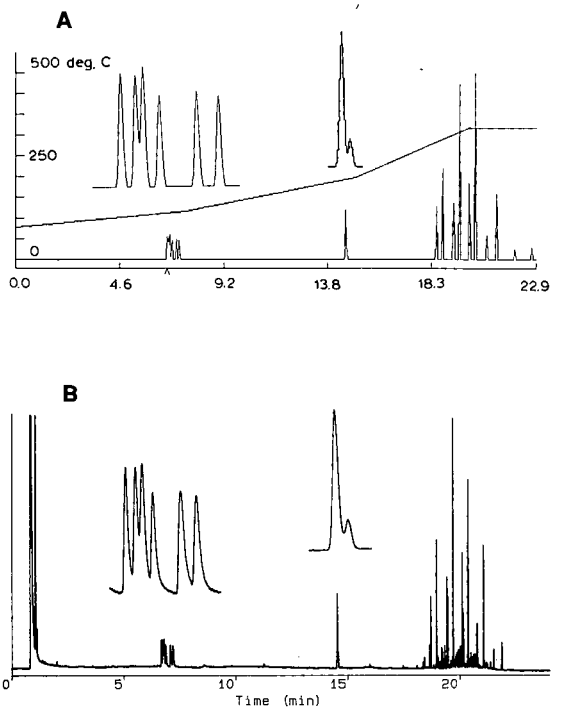

Fig. 7. Comparison of predicted *vs.* experimental chromatograms for an unknown sample using a four-segment temperature programme. Conditions: DB-1701 column programmed at 80, 120, 200 and 320°C at 0, 7.5, 15 and 20 min, with a final isothermal segment at 320°C for 4 min. (A) Computer simulation; (B) experimental separation.

ing, but using computer simulation a large number of multiple-ramp programs can be quickly evaluated. The chromatographic analysis of a sample containing a mixture of unknown components was optimized in preparation for analysis by mass spectrometry. This example illustrates that the identity of chromatographic peaks need not be known for optimization provided that corresponding peaks in the two chromatograms used for input data can be matched. Experimental and simulated chromatograms for a four-segment temperature program are shown in Fig. 7. Programming rates of 5, 11 and 24°C/min were used in succession, followed by a final isothermal segment. Retention times were accurately predicted to within ± 1% and the predicted resolutions of adjacent bands (measured as retention time differences) were accurate to within ± 9%.

CONCLUSIONS

Computer simulations based on a linear elution strength model were found to be reliable for the optimization of GC temperature programs. Retention times and retention time differences were accurately predicted for separations involving a variety of samples and column types. Predicted retention times were accurate to within ± 4% and resolution was generally accurate to within ± 12%.

REFERENCES

1 R. A. Hively and R. E. Hinton, *J. Gas Chromatogr.*, 6 (1968) 203.
2 W. J. Jennings, *Gas Chromatography with Glass Capillary Columns*, Academic Press, New York, 1980, p. 121.
3 K. Grob and G. Grob, *Chromatographia*, 19 (1983) 481.

4 A. Aerts, J. Rijks, A. Bembard and L. Blomberg, *J. High Resolut. Chromatogr. Chromatogr. Commun.*, 9 (1986) 49.
5 R. R. Freeman and W. J. Jennings, *J. High Resolut. Chromatogr. Chromatogr. Commun.*, 10 (1987) 231.
6 Y. Guan, J. Kiraly and J. A. Rijks, *J. Chromatogr.*, 472 (1989) 129.
7 C. A. Streuli, W. H. Muller and M. Orloff, *J. Chromatogr.*, 101 (1974) 17.
8 S. L. Morgan and S. N. Deming, *J. Chromatogr.*, 112 (1975) 267.
9 S. L. Morgan and S. N. Deming, *Sep. Purif. Methods*, 5 (1976) 333.
10 J. Holderith, T. Toth and A. Varadi, *J. Chromatogr.*, 119 (1976) 215.
11 R. J. Laub and J. H. Purnell, *J. Chromatogr.*, 161 (1978) 49.
12 W. A. Spencer and L. B. Rogers, *Anal. Chem.*, 52 (1980) 950.
13 H.-J. Stan and B. Steinbach, *J. Chromatogr.*, 290 (1984) 311.
14 V. Bartu, S. Wicar, G.-J. Scherpenzeel and P. A. Leclercq, *J. Chromatogr.*, 370 (1986) 219.
15 V. Bartu, S. Wicar, G.-J. Scherpenzeel and P. A. Leclercq, *J. Chromatogr.*, 370 (1986) 235.
16 P. Lu, B. Lin, X. Chu, C. Luo, G. Lai and H. Li, *J. High Resolut. Chromatogr. Chromatogr. Commun.*, 9 (1986) 702.
17 E. E. Akporhonor, S. L. Vent and D. R. Taylor, *J. Chromatogr.*, 405 (1987) 67.
18 E. M. Sibley, C. Eon and B. L. Karger, *J. Chromatogr. Sci.*, 11 (1973) 309.
19 E. V. Dose, *Anal. Chem.*, 59 (1987) 2414.
20 E. V. Dose, *Anal. Chem.*, 59 (1987) 2420.
21 D. E. Bautz, J. W. Dolan, W. D. Raddatz and L. R. Snyder, *Anal. Chem.*, 62 (1990) 1560.

Journal of Chromatography, 589 (1992) 223–230
Elsevier Science Publishers B.V., Amsterdam

CHROM. 23 732

Prediction of the elution profiles of high-concentration bands in gas chromatography

Jeffry Roles and Georges Guiochon*

**Department of Chemistry, University of Tennessee, Knoxville, TN 37996-1501, and Division of Analytical Chemistry, Oak Ridge National Laboratory, Oak Ridge, TN 37831-6120 (USA)*

(Received July 10th, 1991)

ABSTRACT

The prediction of band profiles in non-linear gas chromatography requires the use of a mass balance equation for the carrier gas and for the components of the feed. An additional equation is required to account for the non-linearity of the pressure profile and the compressibility of the gas phase. Thus, the sorption effect, which is insignificant in liquid chromatography, becomes of major importance in gas chromatography. Originating from the difference between the partial molar volumes of the retained components in the mobile and the stationary phases, this effect combines with the isotherm effect to control the elution profile of high-concentration bands. The influence of the various parameters which determine the relative intensity of the sorption and the isotherm effects is discussed and illustrated.

INTRODUCTION

The profiles of elution bands in gas chromatography has been abundantly discussed, especially in the 1960s and 1970s [1–11]. The work done prior to 1977 has been reviewed by Conder and Young [12]. Because of the gas-phase compressibility, however, the problem of the accurate prediction of band profiles is much more complex in gas than in liquid chromatography. There is not even a closed-form solution available for the ideal model, in which the column efficiency is assumed to be infinite [13], whereas such a solution has been derived for liquid chromatography [13–15].

The sorption effect, which is negligible in liquid chromatography because the partial molar volumes of the solute in the stationary and mobile phases are nearly equal, is very significant in gas chromatography. It was identified very early [2], shortly after the discovery of gas chromatography itself [1]. Whether under steady-state conditions with a stream of pure carrier gas, or during the migration of a high-concentration band, the pressure profile along a column is monotonously decreasing. The pressure profile is in fact little changed by the passage of the band [12]. As the partial pressure of the component studied is high within the band, the local partial pressure of the carrier gas is lower within the band than in the part of the column where it is pure. However, the mass flow-rate of the carrier gas is constant, so the local velocity increases within the band [16]. This causes the high concentrations in the band to move faster than the lower concentrations. This is the classical mechanism of the formation of a discontinuity in the absence of axial dispersion (*i.e.*, when the ideal model is valid) [5]. In practice, a shock layer is formed instead [17,18].

Because of the gas-phase compressibility, a mass balance equation must be used for the carrier gas and for each component of the sample. Thus, the simplest problem, the calculation of the profile of a high concentration band for a pure component, involves two coupled partial differential equations [5,6,10]. This explains the need to resort to numerical solutions. The numerical analysis of the problem has been discussed previously by Rouchon *et al.* [10], using the method suggested by Godunov [11] for equation systems of the type found in chromatog-

0021-9673/92/$05.00

raphy. This method provides an extremely fast algorithm. Except for the influence of the column efficiency, early results demonstrated excellent agreement between the experimental band profiles and those calculated from the isotherm measured with an independent method [19]. A proper procedure to account for the influence of the column efficiency has been demonstrated [20]. It is entirely applicable to the calculations of band profiles in gas chromatography.

The aim of this work was to compare the elution band profiles obtained experimentally and those calculated from an independent determination of the equilibrium isotherm and the column efficiency, and to study the dependence of the intensity of the sorption effect on the column pressure drop and on the carrier gas flow-rate. This latter study is essentially based on the results of numerical calculations made using the equilibrium-diffusive model of chromatography validated by the agreement between experimental and calculated profiles.

THEORY

Basic assumptions

The model of chromatography used in this work is adapted to the practical problem with which we are dealing. We study the surface heterogeneity of powders of various materials, such as ceramics (*e.g.*, alumina), liquid chromatographic stationary phases, pigments and fillers. A porous-layer open-tubular column is prepared and we determine the adsorption isotherms of selected probe compounds [21–24]. The column efficiency is high and its pressure drop low [22]. In gas–solid chromatography, the initial curvature of the equilibrium isotherms is usually strong, so the range of partial pressures to be investigated is small [23], rarely exceeding a few millibars. This justifies the simplifying assumptions made to a general model of chromatography.

We assume that the carrier gas and the probe vapor have an ideal behavior. The correction for non-ideal behavior, using the first virial coefficients [12], is negligible [23]. We assume that the column is radially homogeneous and that the integrated Poiseuille law is valid, so we can treat the problem as unidimensional. The porous layer cannot be radially homogeneous, but the column is narrow and has only one gas channel, so radial heterogeneity of the layer thickness merely contributes to increase the height equivalent to a theoretical plate. It is important, however, that the layer thickness be homogeneous along the column length and that there is no local accumulation of particles creating a zone of low permeability. Because of the high carrier gas compressibility, this would invalidate the pressure profile model and the James and Martin coefficient would give a wrong correction for that effect [23].

We assume also that the carrier gas is not adsorbed by the stationary phase, which is true with helium on the materials investigated, and that the local pressure remains constant during the migration of a band, *i.e.*, the pressure profile is steady. This, again, is a more than reasonable assumption within the range of partial pressures investigated. The volume occupied by the sample is negligible compared with the column volume (the volume occupied by a typical 10-μg sample of diethyl ether is equivalent to that of 15 mm of the open-tubular column used). The perturbations to the flow profile resulting either from the sorption effect or from the change in viscosity due to the presence of a vapor which is much less viscous than the carrier gas are negligible because the probe vapor concentration exceeds 0.1% only over a very short part of the column, at its inlet [23]. Similarly, the effect of the heat of adsorption is negligible, because the amount of probe component adsorbed is very small and the heat generated locally by adsorption is small compared with the latent heat of the adsorbent.

The combination of these assumptions leads to a simplified equilibrium-diffusive model. This model is based on the use of two differential mass balance equations, one for the probe vapor and one for the carrier gas [10]. The adsorption isotherm and the column efficiency have to be determined by independent measurements. As shown previously by Rouchon *et al.* [19], good agreement should be expected between the experimental and calculated profiles.

Mass balance equations

Consider the flux, F_i (in moles per unit cross-sectional area) of the probe component into a differential section of the column of length, dz. Suppose that the adsorption–desorption kinetics are infinitely fast. As the column is an open tube, the column non-ideal band broadening is due essentially

to axial diffusion in the mobile phase and to the parabolic flow profile in the tube [25]. The flux F_i of the probe into the incremental volume is then given by

$$F_i = Cudt - D \cdot \frac{\partial C}{\partial z} \cdot dt \quad (1)$$

where C is the local concentration at the point z, u is the linear mobile phase velocity at this point and D is the apparent dispersion coefficient of the solute, which is assumed to be constant, independent of the concentration. Assuming that the mobile phase is an ideal gas, and denoting by p the partial pressure of the component considered (P will be the local pressure, hence $X = p/P$ will be the mole fraction of the component), we may rewrite eqn. 1 as

$$F_i = \frac{1}{RT}\left(pudt - D \cdot \frac{\partial p}{\partial z} \cdot dt\right) \quad (2)$$

Because the mobile phase is an ideal gas, it expands during its migration along the column and neither the partial pressure of the component nor the carrier gas velocity remains constant. They must be incremented and the flux out of the column section, F_o, is given by:

$$F_o = \frac{1}{RT}\left[\left(p + \frac{\partial p}{\partial z} \cdot dz\right)\left(u + \frac{\partial u}{\partial z} \cdot dz\right)dt - D \cdot \frac{\partial}{\partial z}\left(p + \frac{\partial p}{\partial z} \cdot dz\right)dt\right] \quad (3)$$

Expanding eqn. 3 and neglecting the term in $(dz)^2$ gives:

$$F_o = \frac{1}{RT}\left(pu + u \cdot \frac{\partial p}{\partial z} \cdot dz + p \cdot \frac{\partial u}{\partial z} \cdot dz - D \cdot \frac{\partial p}{\partial z} - D \cdot \frac{\partial^2 p}{\partial z^2} \cdot dz\right)dt \quad (4)$$

Combining eqns. 2 and 4 gives the next flux entering the slice of column:

$$\Delta F = \frac{1}{RT}\left(-u \cdot \frac{\partial p}{\partial z} - p \cdot \frac{\partial u}{\partial z} + D \cdot \frac{\partial^2 p}{\partial z^2}\right)dz\, dt \quad (5)$$

The net amount of material (in moles) entering the slice during the time dt is

$$dn = \left(\frac{V_g}{RT} \cdot \frac{\partial p}{\partial t} + m_g \cdot \frac{\partial q}{\partial t}\right)dz\, dt \quad (6)$$

where V_g is the volume available to the gas phase per unit column length, m_g is the mass of stationary phase contained in the unit length of column and q is the stationary phase concentration of the component in equilibrium with the partial pressure p. Hence the net flux per unit of column cross-sectional area is

$$\Delta F = \frac{1}{RT}\left(\frac{\partial p}{\partial t} + \frac{m_g RT}{V_g} \cdot \frac{\partial q}{\partial t}\right)dz\, dt \quad (7)$$

Combining eqns. 5 and 7 gives

$$u \cdot \frac{\partial p}{\partial z} + p \cdot \frac{\partial u}{\partial z} + \frac{\partial p}{\partial t} + \frac{m_g RT}{V_g} \cdot \frac{\partial q}{\partial t} = D \cdot \frac{\partial^2 p}{\partial z^2} \quad (8)$$

Eqn. 8 is the mass balance of the component in a gas chromatographic column. This equation can be rearranged into

$$\frac{\partial}{\partial z}(pu) + \frac{\partial}{\partial t}\left(p + \frac{m_g RT}{V_g} \cdot q\right) = D \cdot \frac{\partial^2 p}{\partial z^2} \quad (9)$$

It is convenient to replace in eqn. 9 the partial pressure, p, of the component by XP, X being its mole fraction and P the local pressure of the mobile phase (see below). The product uP is proportional to the mobile phase mass flow-rate, $\dot{F}$. Hence the solute mass balance equation becomes

$$\frac{\partial}{\partial z}(\dot{F}X) + \frac{\partial}{\partial t}\left(PX + \frac{m_g RT}{V_g} \cdot q\right) = D \cdot \frac{\partial^2 PX}{\partial z^2} \quad (10)$$

A similar mass balance equation must be written for the carrier gas, as its local density varies with the pressure along the column. As for the single-component problem the mole fraction of the carrier gas is the complement of the solute mole fraction, the mass balance for the carrier gas is written as

$$\frac{\partial}{\partial z}(\dot{F}) + \frac{\partial}{\partial t}\left(PX + \frac{m_g RT}{V_g} \cdot q\right) = 0 \quad (11)$$

Eqns. 10 and 11 contain four functions, the mole fraction of the component, X, its concentration in the stationary phase, q, the total flow-rate, $\dot{F} = Pu$, and the local pressure of the mobile phase, P. Hence we need two more equations. Obviously, as we are using the equilibrium-diffusive model, the first equation will be the equilibrium isotherm relating the concentrations of the component in the two phases at equilibrium:

$$q = f(XP) = pX \quad (12)$$

The second equation relates the local pressure to the column parameters and to the abscissa. It could be the differential Darcy or Poiseuille law:

$$u = -\frac{1}{\Phi\eta} \cdot \frac{\partial P}{\partial z} \tag{13}$$

where $1/\Phi$ is the column permeability and η the mobile phase viscosity. Difficulties arise in the determination of the mobile phase viscosity as a function of the local composition. As the permeability of an open-tubular column is high, the pressure profile under steady-state conditions is very flat. Local changes in the mobile phase viscosity and velocity cannot affect it greatly. Further, in gas–solid chromatography, the samples are usually small and the probe partial pressure is low. Integration of eqn. 13 when the column is swept with pure carrier gas, with no sample, under steady-state conditions, gives

$$P(z) = P_o \sqrt{\left(\frac{P_i}{P_o}\right)^2 - \frac{z}{L}\left[\left(\frac{P_i}{P_o}\right)^2 - 1\right]} \tag{14}$$

where $P(z)$ is the local pressure of the mobile phase, P_i and P_o the inlet and outlet pressures and L the column length. Eqn. 14 gives the pressure profile along the column. In the following, we shall assume as a first approximation that the local pressure does not change during the elution of a high concentration band. The pressure profile also remains constant and is given by eqn. 14. As we assume the validity of the integrated Darcy law, the local pressure does not deviate from that pressure given by eqn. 14. However, the local velocity is perturbed by the passing of the band (sorption effect).

The system of eqns. 10–12 and 14 constitutes the system of partial differential equations representing the equilibrium-diffusive model in gas chromatography in the case of a single component and of relatively fast kinetics of mass transfer. This model takes into account all the major effects encountered in non-linear gas chromatography, and especially the isotherm effect, the sorption effect and the effect of a finite column efficiency.

Discussion of the model

A simpler form of this model has been derived, discussed and used by several groups, especially by Aris and Amundson [5], Conder and Purnell [4] and Guiochon and co-workers [6–8]. The problem was studied within the framework of the ideal model. In this model, the column efficiency is assumed to be infinite, the axial dispersion is assumed to be negligible and the second-order term in the right-hand side of eqns. 10 and 11 disappears. Numerical solutions of this model were calculated with difficulty in the case of a linear isotherm by Guiochon and Jacob [6]. The accuracy of these solutions was poor. Rouchon *et al.* [10] derived much more accurate numerical solutions, using the Godunov algorithm [11], a first-order finite differences approach. Rouchon *et al.* [10] suggested that the effect of the finite column efficiency could be simulated by carefully choosing the space and time increments used in the integration. The errors that are produced by the first-order finite difference approximation propagate through the calculation and result in calculated band profiles which resemble the experimental band profiles eluted from columns with finite efficiency. The numerical diffusion caused by these errors can be used to simulate correctly the effect of the axial dispersion [20,26].

This procedure was implemented in the calculation method described by Guiochon *et al.* [20] and applied to the calculation of band profiles in liquid chromatography. In this case, two simplifying assumptions may be made. First, the flow velocity may be assumed to be constant along the whole column, as the mobile phase is not compressible. Second, for the same reason and also as the partial molar volumes of the solute in both the stationary and the mobile phases are very close, the mass balance equation for the mobile phase is unnecessary. The semi-ideal model [20] is a rapid procedure designed for the numerical calculation of solutions of eqn. 10 with no dispersion term (ideal model). However, by choosing the space and time increments carefully, one can actually obtain an accurate numerical solution of the second-order partial differential eqn. 10, with a finite dispersion coefficient. The dispersion coefficient, D, in eqn. 10 is related to the column height equivalent to a theoretical plate, H, by $D = Hu/2$ [3]. If the space and time increments, δz and δt, of the integration are chosen so that $\delta z = H$ and $\delta t = 2H(1 + k'_0)/u$ (k'_0 is the retention factor of the component at infinite dilution), the band profile obtained is an accurate solution of eqn. 10 [20,26].

Following the previous work of Guiochon and

co-workers [20,27–29], it was simple to modify the algorithm used for liquid chromatography to calculate numerical solutions of the system of partial differential equations of gas chromatography (eqns. 10–14), taking into account the band broadening contribution due to axial dispersion, the isotherm and the sorption effects, and the column pressure drop. The finite difference equation are given by

$$(uPX)_i^{n+1} = (uPX)_i^n - \frac{\delta z}{\delta t}\left\{P^n X_i^n + \frac{m_g RT}{V_g} \cdot q(P^n X_i^n) - \left[P^n X_{i-1}^n + \frac{m_g RT}{V_g} \cdot q(P^n X_{i-1}^n)\right]\right\} \quad (15)$$

and

$$(uP)_i^{n+1} = (uP)_i^n - \frac{\delta z}{\delta t} \cdot \frac{m_g RT}{V_g}\left[q(P^n X_i^n) - q(P^n X_{i-1}^n)\right] \quad (16)$$

where the local pressure, P, is given by

$$P^n = P_o \sqrt{\left(\frac{P_i}{P_o}\right)^2 - \frac{n\delta z}{L}\left[\left(\frac{P_i}{P_o}\right)^2 - 1\right]} \quad (17)$$

The combination of eqns. 15–17 in a computer program, together with the proper choice of initial and boundary conditions and an isotherm equation, permit the rapid calculation of elution band profiles. In order to insure that the effect of axial diffusion is accurately simulated, one must set the ratio $\delta z/\delta t$ equal to $u_z/2$, where u_z is the average velocity $\bar{u}/(1 + k')$ corresponding to the most retained portion of the solute and δz is equal to the column HETP [20,26–28].

Initial and boundary conditions

The initial condition used in elution is an empty column. The concentration of the component is zero everywhere in the column which is filled with pure carrier gas:

$$p(z,t = 0) = 0 \quad (18)$$

The boundary condition is the concentration (or partial pressure profile) of the component at column inlet, on injection of the feed sample. This profile is digitized, *i.e.*, it is a series of rectangles of constant width, δt. It was desired to simulate the injection of a narrow rectangular plug of vapor, having the minimum physically realistic width possible. Two constraints must be considered. First, the height $p_{INJ,j}$ (where j is the time increment rank) of the rectangle injected cannot exceed the vapor pressure of the component, p^0. Second, the width of the plug, t_p, cannot be less than δt. If the area, A, required for the injected sample is greater than $p^0\delta t$, then t_p is determined by filling each successive time increment until all the area is used up. If A is less than $p^0\delta t$, then $t_0 = \delta t$ and the height of the injection profile is $A/\delta t$.

The boundary conditions are given in Table I.

TABLE I

BOUNDARY CONDITIONS USED IN THE NUMERICAL INTEGRATION OF THE NON-EQUILIBRIUM MODEL

t_p, Width of the rectangular injection plug; p_i, partial pressure of the solute in the injection plug; P_i, inlet pressure of the carrier gas; P_o, outlet pressure of the carrier gas; δt, time increment in the numerical calculation; X_j^k, mole fraction of the component in the column, at time $j\delta t$, at the position $k\delta z$; u_j^k, carrier gas velocity at time $j\delta t$, at the position $k\delta z$; P^n, carrier gas pressure at position $n\delta z$.

Time interval	u_j^n	X_j^n
$j = 0$	$u_j^n = \frac{P_o u_o}{P^n}$	$X_0^n = 0$
$0 < j \leqslant \frac{t_p}{\delta t}$	$u_j^0 = \frac{P_o u_o}{P_i}\frac{p_i + P_i}{P_i}$	$X_j^0 = \frac{p_i}{P_i}$
$\frac{t_p}{\delta t} < j$	$u_j^0 = \frac{P_o u_o}{P_i}$	$X_j^0 = 0$

RESULTS AND DISCUSSION

The accuracy of the algorithm of Rouchon *et al.* [10] was demonstrated by comparing calculated profiles and experimental profiles exhibiting an important sorption effect [19]. The ability of the modified form of this algorithm to take into account the column axial dispersion was tested as follows. Band profiles were calculated using column efficiencies ranging from 500 to 8000 theoretical plates. The plate number, N, for the simulated band profile was then calculated by

$$N = t_R^2/\sigma_t^2 \quad (19)$$

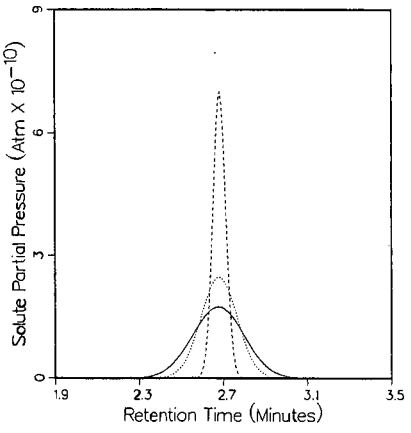

Fig. 1. Calculated elution profiles for different column efficiencies. Experimental conditions: linear isotherm with a slope of 0.02 mol/g · atm; column length, 1500 cm; column I.D., 0.53 mm; column temperature, 60°C; column pressure drop, 0.34 atm; outlet pressure, atmospheric; gas hold-up time, 22.7 s; mass of stationary phase, 44 mg; sample size, 50 pg; column efficiency, solid line 500 plates, dotted line 1000 plates, dashed line 8000 plates.

where t_R is the peak retention time (measured as the first normalized moment) and σ_t^2 is the peak variance (measured as the normalized, centered second moment, in time units). Peak areas corresponding to infinite dilution and a linear isotherm were used in the program. In each instance, the agreement between the plate number which was simulated and the plate number which was calculated from the band profile is excellent (within 1%). Three of these simulated band profiles are shown in Fig. 1.

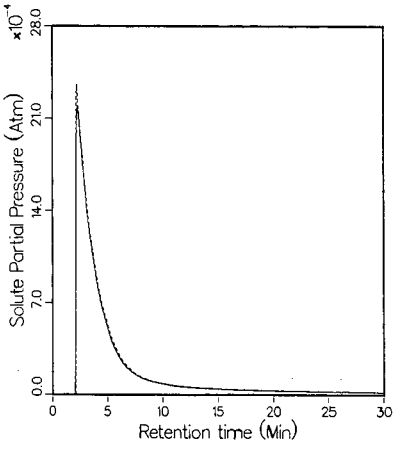

Fig. 2. Comparison between experimental (solid line) and calculated (dashed line) elution profiles. Experimental conditions as in Fig. 1, except non-linear isotherm of 1-chlorobutane on α-alumina at 40°C; sample size, 4.1 μg. Difference parameters between the experimental and the calculated profiles [23]: $t_{RMS} = 0.79\%$, $\Delta = 1.2 \times 10^{-4}$.

In Fig. 2, we compare an experimental profile recorded for a sample of 1-chlorobutane on an open-tubular column coated with a thin layer of particles of alumina for liquid chromatography (Universal Scientific, Atlanta, GA, USA) and the profile calculated with the procedure discussed above, using the adsorption isotherm obtained by ECP. The agreement between these two profiles is excellent. Their only difference is in the top of the band, which is sharper for the calculated profile. Similar agreements have been reported with data acquired on porous-layer open-tubular columns coated with α-alumina for ceramic [23] and on conventional columns packed with graphitized carbon black [19]. Because the isotherm was obtained with a pulse technique, the agreement reported with carbon black demonstrated that, in gas chromatography as in liquid chromatography, the relationship between the elution band profile and the thermodynamics of the phase equilibrium involved in the retention is well understood. In the present case, however, the isotherm is derived by the ECP method, from the experimental profile in Fig. 2. As the ECP method is based on the solution of the ideal model, the agreement between the two profiles merely shows that our calculation procedure is correct and accounts properly for the influence of the column efficiency and the gas compressibility.

There are two major differences between the propagation of high concentration bands in gas and in liquid chromatography. First, there is no sorption effect in liquid chromatography or, rather, it is negligible. Second, equilibrium isotherms in gas–solid chromatography tend to be concave upwards much more often than in liquid chromatography. As a consequence, the sorption and the isotherm effects have opposite directions and it is possible to find experimental conditions under which they compensate each other. We present here a study of the combination between the sorption and the isotherm effects.

Figs. 3–5 show series of calculated band profiles which are derived from a single isotherm, different for each figure. The average flow velocity is assumed to be constant, but the column inlet pressure (and

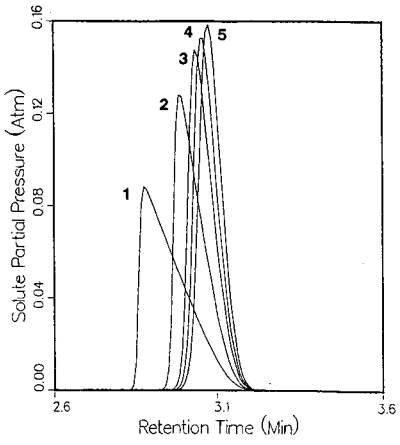

Fig. 3. Influence of the average pressure of the carrier gas on the overloaded elution profiles in gas chromatography. Profiles calculated for columns with different permeability operated at the same average velocity. Linear isotherm. Experimental conditions as in Fig. 1, except gas hold-up time, 23.6 s; sample size, 9.2 μg; column efficiency, 8000 plates. Inlet pressure: 1 = 1.5; 2 = 7.5; 3 = 15; 4 = 22.5; 5 = 37.5 atm.

hence also the average column pressure) is increased. This corresponds to a comparison between columns having decreasing permeabilities, but operated at the same average velocity.

In Fig. 3, a linear isotherm is used. The source of the band asymmetry is uniquely in the sorption effect. Because, under the influence of the sorption effect, the velocity associated with a concentration increases with increasing concentration, this effect tends to give a steep band front and a diffuse rear part of the profile, very much like what is observed with a Langmuir isotherm. The intensity of the sorption effect at constant sample size decreases with increasing average column pressure. We see that the band, which is strongly asymmetric for a low inlet pressure (*e.g.*, an open-tubular column), becomes nearly symmetrical for a low-permeability column, requiring a very high inlet pressure to achieve the same retention times.

The use of a convex upward isotherm, such as a Langmuir isotherm, would merely reinforce the sorption effect and the results (not shown) are not very illustrative. In Figs. 4 and 5, on the other hand, we have used a concave upward isotherm belonging to type III of the BET isotherm classification. We have taken for this isotherm the equation

$$q = \frac{ap}{1 - p/p^0} \tag{20}$$

which is similar to the Langmuir equation, but uses a negative constant in the denominator. This equation is empirical, but convenient for illustrative purposes.

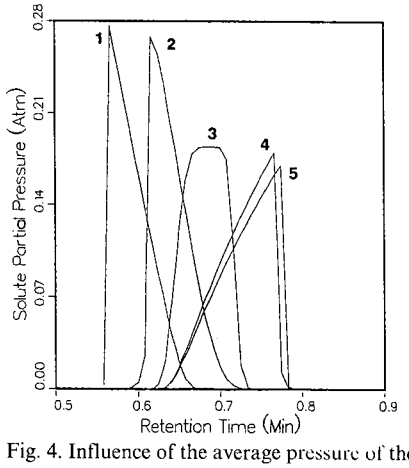

Fig. 4. Influence of the average pressure of the carrier gas on the overloaded elution profiles in gas chromatography. Profiles calculated for columns with different permeability operated at the same average velocity. Non-linear isotherm. Experimental conditions as in Fig. 1, except non-linear isotherm (eqn. 20, with a = 0.002 mol/g · atm, p^0 = 0.9 atm); gas hold-up time, 23.6 s; sample size, 9.2 μg; column efficiency, 8000 plates. Inlet pressure: 1 = 1.01; 2 = 2.0; 3 = 3.0; 4 = 7.5; 5 = 15.5 atm.

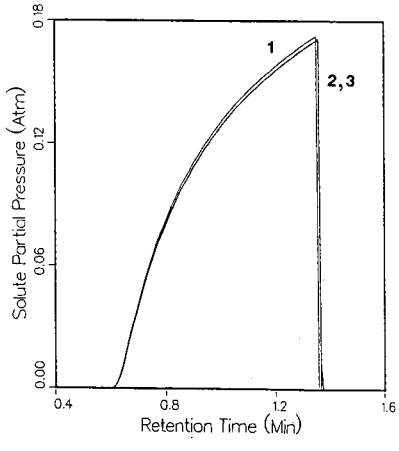

Fig. 5. Influence of the average pressure of the carrier gas on the overloaded elution profiles in gas chromatography. Profiles calculated for columns with different permeability operated at the same average velocity. Non-linear isotherm. Experimental conditions as in Fig. 4, except p^0 = 0.3 atm. Inlet pressure: 1 = 1.5; 2 = 3.0; 3 = 5.0 atm.

The amount adsorbed at equilibrium becomes infinite for $p = p^0$, which corresponds to capillary condensation near the vapor pressure. In Fig. 4, the experimental conditions correspond to a moderate curvature of the isotherm. At high values of the column inlet pressure (*i.e.*, for low-permeability columns), the isotherm effect dominates and the band has a diffuse front profile and a steep rear shock layer. In contrast, at low values of the column average pressure (*i.e.*, for high-permeability columns), the isotherm effect is more than compensated by a strong sorption effect which offsets its influence on the band profile. The band profile is Langmuirian at low values of the column average pressure. There is an intermediate value of the average column pressure where the influences of the two effects balance and a shock layer appears on either side of the band [7,8].

When the initial curvature of the isotherm is strong, the isotherm effect is already dominant at low values of the column average pressure and, thus, remains so when the average pressure increases. This phenomenon is illustrated in Fig. 5, where a change in the column permeability at constant flow velocity has almost no effect on the band profile.

These results demonstrate that the same model which permits accurate predictions of band profiles in liquid chromatography also gives excellent results in gas chromatography. The approximations made to a general equilibrium-diffusive model of chromatography are different because of the widely different physico-chemical properties of the mobile phase, but the model remains equally applicable. As a consequence, excellent results should be expected from its application to other forms of chromatography, and notably to supercritical fluid chromatography. The main question to investigate in this field is the degree of importance of the sorption effect. It is certainly less important than in gas chromatography, as suggested by the results shown in Figs. 3 and 4, but may not be entirely negligible as it is in liquid chromatography.

ACKNOWLEDGEMENTS

This work was supported in part by Grant DE-FG05-88ER13859 of the US Department of Energy, Office of Basic Energy Research, and by the cooperative agreement between the University of Tennessee and the Oak Ridge National Laboratory. We acknowledge the support of our computational effort by the University of Tennessee Computing Center.

REFERENCES

1 A. T. James and A. J. P. Martin, *Biochem. J.*, 50 (1952) 679.
2 C. H. Bosanquet and G. O. Morgan, in D. H. Desty (Editor), *Vapour Phase Chromatography*, Butterworths, London, 1957, p. 35.
3 P. C. Haarhoff and H. J. van der Linde, *Anal. Chem.*, 38 (1966) 573.
4 J. R. Conder and J. H. Purnell, *Trans. Faraday Soc.*, 64 (1968) 3100.
5 R. Aris and N. R. Amundson, *Mathematical Methods in Chemical Engineering*, Prentice Hall, Englewood Cliffs, NJ, 1973.
6 G. Guiochon and L. Jacob, *Chromatogr. Rev.*, 14 (1971) 77.
7 P. Valentin and G. Guiochon, *Sep. Sci.*, 10 (1975) 245.
8 P. Valentin and G. Guiochon, *Sep. Sci.*, 10 (1975) 289.
9 J. R. Conder, *Chromatographia*, 7 (1974) 387.
10 P. Rouchon, M. Schonauer, P. Valentin and G. Guiochon, *Sep. Sci.*, 22 (1987) 1793.
11 S. K. Godunov, *Math. Sb.*, 47 (1959) 271.
12 J. R. Conder and C. L. Young, *Physicochemical Measurements by Gas Chromatography*, Wiley, New York, 1979, Ch. 2.
13 J. N. Wilson, *J. Am. Chem. Soc.*, 62 (1940) 1583.
14 E. Glueckauf, *J. Chem. Soc.*, (1947) 1302.
15 S. Golshan-Shirazi and G. Guiochon, *J. Phys. Chem.*, 94 (1990) 495.
16 A. B. Littlewood, *Gas Chromatography*, Academic Press, New York, 2nd ed., 1970.
17 H.-K. Rhee and N. R. Amundson, *Chem. Eng. Sci.*, 27 (1974) 2049.
18 B. C. Lin, S. Golshan-Shirazi, Z. Ma and G. Guiochon, *Anal. Chem.*, 60 (1988) 2647.
19 P. Rouchon, M. Schonauer, P. Valentin, C. Vidal-Madjar and G. Guiochon, *J. Phys. Chem.*, 89 (1985) 2076.
20 G. Guiochon, S. Golshan-Shirazi and A. Jaulmes, *Anal. Chem.*, 60 (1988) 1856.
21 J. Roles and G. Guiochon, *J. Phys. Chem.*, 95 (1991) 4098.
22 J. Roles and G. Guiochon, *J. Chromatogr.*, 591 (1992) 225.
23 J. Roles and G. Guiochon, *J. Chromatogr.*, 591 (1992) 237.
24 J. Roles and G. Guiochon, *J. Chromatogr.*, 591 (1992) 259.
25 M. J. E. Golay, in D. H. Desty (Editor), *Gas Chromatography*, Butterworths, London, 1958, p. 35.
26 B. C. Lin, Z. Ma and G. Guiochon, *J. Chromatogr.*, 484 (1989) 83.
27 S. Golshan-Shirazi and G. Guiochon, *J. Chromatogr.*, 506 (1990) 495.
28 B. C. Lin, S. Golshan-Shirazi, Z. Ma and G. Guiochon, *J. Chromatogr.*, 500 (1990) 185.
29 M. Czok and G. Guiochon, *Anal. Chem.*, 62 (1990) 189.

Journal of Chromatography, 589 (1992) 231–239
Elsevier Science Publishers B.V., Amsterdam

CHROM. 23 719

Prediction of retention indexes

IV. Chain branching in alkylbenzene isomers with C_{10-13} alkyl chains identified in a scintillator solvent

C. T. Peng* and R. L. Hua

Department of Pharmaceutical Chemistry, School of Pharmacy, University of California, San Francisco, CA 94143-0446 (USA)

D. Maltby

Mass Spectrometry Research Laboratory and Department of Pharmaceutical Chemistry, School of Pharmacy, University of California, San Francisco, CA 94143 (USA)

(First received June 18th, 1991; revised manuscript received September 2nd, 1991)

ABSTRACT

Twenty solvent components in a commercial scintillator were identified by chromatography on polar and non-polar columns and by gas chromatography–mass spectrometry (GC–MS) as isomeric 1-(alkyl)$_m$(alkyl)$_n$benzenes with formulae $C_{16}H_{26}$, $C_{17}H_{28}$, $C_{18}H_{30}$ and $C_{19}H_{32}$. These isomers occur in four clusters of chromatographic peaks representing *ca.* 6, 44, 34 and 16% of the total solvent mass. The retention indexes of the isomers are influenced by the lengths of the alkyl chains in the molecule, and their polarity and polarizability can affect the column difference, which is the difference between retention indexes on polar and non-polar columns. 1-Methylalkylbenzenes have higher retention indexes and larger column differences than the evenly distributed isomers, such as 1-butylhexyl-, 1-pentylhexyl, 1-pentylheptyl- and 1-pentyloctylbenzene. The results demonstrate the effect of structural symmetry on the retention indexes of the isomers. This study shows that the ability to relate GC data and column differences to structures can facilitate the interpretation of GC–MS data in the structure identification of isomers.

INTRODUCTION

The retention index (I) of a compound can be predicted from its chemical structure using a quantitative structure–retention index relationship (SRIR) [1,2]. This relationship can also be applied to tentatively identify structures from the retention indexes of unknown chromatographic peaks. According to the SRIR, compounds differing from each other by one carbon atom generally differ in their retention indexes by about 100, but this rule has not been extended to predict the I values of isomers containing a constant number of carbon atoms and branched alkyl chains.

Recently, "improved" liquid scintillation cocktails have been introduced by manufacturers to minimize the environmental impact of hydrocarbon solvents. A scan by gas chromatography–mass spectrometry (GC–MS) of the "improved" cocktails was reported to fail to identify the components [3]. Apparently additional analytical data are needed. We found the use of SRIR, I and column differences to be useful in facilitating structural identification and this paper reports our findings.

0021-9673/92/$05.00

EXPERIMENTAL

The liquid scintillator Opti-Fluor was obtained from Packard Instruments (Downers Grove, USA, IL). 1-Phenylalkanes, *n*-alkanes and tributyl phosphate were purchased from Aldrich (Milwaukee, WI, USA).

GC analysis

Dilute solutions of the liquid scintillators in *n*-hexane were analysed on Hewlett-Packard Model 5890 and 5880A gas chromatographs, equipped with thermal conductivity detectors, using non-polar and polar fused-silica capillary columns (30 m × 0.53 mm I.D., film thickness 1.0 μm for DB-Wax and 1.5 μm for DB-1) from J&W Scientific (Folsom, CA, USA). The injector was set at 250°C and the detector at 300°C. The temperature was linearly programmed during the run. The oven temperature was initially at 40°C for 4 min and then increased at 8°C/min to 280°C for the DB-1 and to 200°C for the DB-Wax column. The maximum oven temperature was maintained for 20 min before the run was terminated. A mixture of *n*-alkanes from *n*-hexane to *n*-tricontacosane (c_6–C_{32}) was used as markers for *I* calculation. *I* was calculated by the equation of Van den Dool and Kratz [4] as reported previously [1,2].

GC–MS analysis

For GC–MS analysis the gas chromatograms were obtained on fused-silica capillary columns (30 m x 0.32 mm I.D.) coated with DB-1 and DB-Wax stationary phases. The temperature program was from 150 to 270°C at 4°C/min for DB-1 from 90 to 230°C at the same rate for DB-wax. Concentration was measured by the total ionization current. These chromatograms are of slightly higher resolution because narrower bore columns were used.

MS was performed on a V670-SE instrument (VG Analytical, Manchester, UK). The instrument was operated in the electron impact (EI) mode. The source temperature was 270°C, the interface temperatures were 280°C, the filament current was 200 μA and the electron energy was 70 eV. The data were acquired by scanning from 30 to 500 dalton at 0.7 s per decade. A V6 Opus Data System was used for data acquisition and processing.

RESULTS AND DISCUSSION

GC analysis

Sample of Opti-Fluor were chromatographed on DB-1 and DB-Wax fused-silica capillary columns. A single-component analyte can be identified by *I* and column difference (ΔI), the latter being defined as the difference between the *I* values on polar and non-polar columns, and its magnitude reflects the polarity and polarizability of the analyte. Opti-Fluor gave about twenty chromatographic peaks in four clusters, in addition to other peaks. The four peak clusters spanned a region of 368 *I* units from 1526 to 1894 on the non-polar column and a region of 414 *I* units from 1729 to 2143 on the polar column. Their apparent column differences ranged from 200 to 250. On the non-polar column the first cluster contained four closely eluted peaks, and each of the three succeeding clusters contained five closely eluted peaks. These four clusters represent *ca.* 6, 44, 34 and 16% of the total solvent mass. Different fractions of the vacuum distillate of the liquid scintillator showed almost identical peak patterns. The residue in the distillation flask also showed a similar pattern of chromatographic peaks plus a single large peak with an *I* value of 2216 on DB-1 and a column difference of 361, indicating possibly a hydroxylic compound, but no effort was made to identify it further. The toluene extract of the scintillator yielded a peak pattern similar to that of the original liquid scintillator.

Chromatograms of Opti-Fluor on DB-1 and DB-Wax columns obtained by GC—MS analysis are shown in Fig. 1. The presentation of these chromatograms is superior to those from an integrator. All the *I* calculations and column differences were based on chromatograms obtained with the 0.53 mm I.D. column.

A list of aromatic hydrocarbons, their retention indexes on DB-Wax and DB-1 columns and their column differences are given in Table I. The presence of a branched alkyl chain in the aromatic hydrocarbons lowers the column differences. Column differences for the solvent components from Opti-Fluor are estimated to be about 200–250, which is considerably lower than the column differences given for 1-phenylalkanes and other aromatic hydrocarbons. These low column differences, similar to those for isopropylbenzene and *m*-diisopropylben-

zene, suggest that the solvent components may be branched-chain alkylbenzenes.

GC–MS analysis and fragmentation patterns

The identity of the solvent components was determined by GC–MS. Table II lists the alkylbenzenes and their mass fragments from the GC–MS analysis. The four clusters of alkylbenzenes have the general formulae $C_{16}H_{26}$, $C_{17}H_{28}$, $C_{18}H_{30}$ and $C_{19}H_{32}$. The mass fragmentation data are given in terms of mass peaks (m/z) and their relative abundances in Table II.

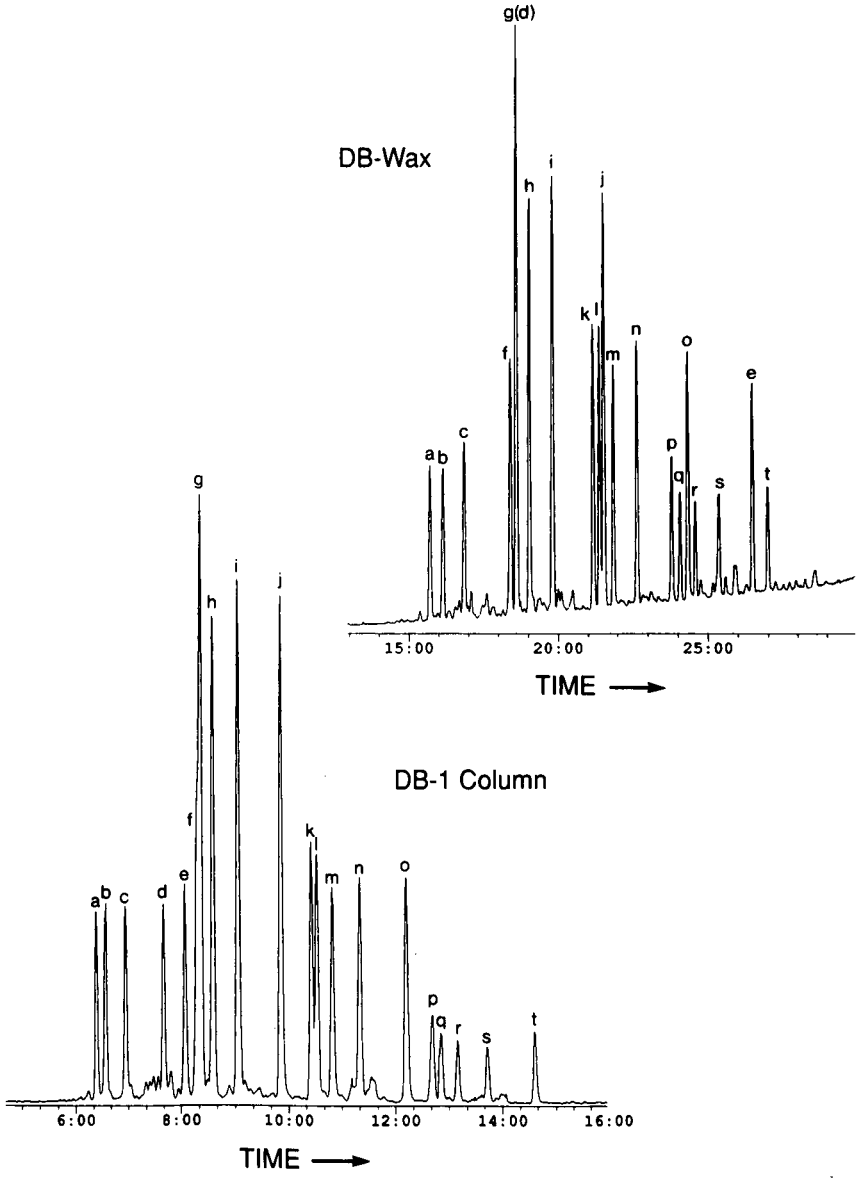

Fig. 1. Chromatograms of solvent components of Opti-Fluor on DB-1 and DB-Wax columns. The peaks on the DB-1 column are identified in Tables II and III. Peaks a–d represent $C_{16}H_{26}$ isomers, f–j $C_{27}H_{28}$ isomers, k–o $C_{18}H_{30}$ isomers and p–t $C_{19}H_{32}$ isomers. On the CB-Wax column, all the peaks follow the same elution pattern as on DB-1, with the exception of peaks d, j, o and t, which have shifted to higher retention indices. Peak d is completely overlapped by peak g on the polar column. Peak e is tributyl phosphate and has a large column difference of 470. Time in min.

TABLE I

RETENTION INDEXES ON POLAR AND NON-POLAR COLUMNS AND COLUMN DIFFERENCES OF SOME ARENES AND 1-PHENYLALKANES

Compound	Formula	Retention index (I_{obs})		Column difference (ΔI)
		DB-Wax	DB-1	
Arenes				
Isopropylbenzene	C_9H_{12}	1166	913	253
Cyclopropylbenzene	C_9H_{10}	1297	1010	387
p-Methylisopropylbenzene	$C_{10}H_{14}$	1283	1020	263
Diethylbenzene	$C_{10}H_{14}$	1305	1041	264
m-Diisopropylbenzene	$C_{12}H_{18}$	1360	1144	216
Cyclohexylbenzene	$C_{12}H_{16}$	1716	1312	404
α-Methylnaphthalene	$C_{11}H_1$	1896	1296	600
β-Methylnaphthalene	$C_{11}H_{12}$	1932	1284	648
1-Phenylbutyronitrile	$C_{11}H_{12}N$	2129	1304	825
Tributyl phosphate	$C_{12}H_{27}O_4P$	2075	1622	453
n-Alkylbenzenes and 1-phenylalkanes[a]				
Benzene	C_6H_6	947	654	293
Toluene	C_7H_9	1051	754	287
Ethylbenzene	C_8H_{10}	1129	858	271
n-Propylbenzene	C_9H_{12}	1206	945	261
n-Butylbenzene	$C_{10}H_{14}$	1306	1047	259
1-Phenylhexane	$C_{12}H_{18}$	1515	1254	261
1-Phenylheptane	$C_{13}H_{20}$	1611	1348	264
1-Phenyloctane	$C_{14}H_{22}$	1715	1456	259
1-Phenylnonane	$C_{15}H_{24}$	1821	1560	261
1-Phenyldecane	$C_{16}H_{26}$	1928	1664	264
1-Phenyldodecane	$C_{18}H_{30}$	2141	1870	271
1-Phenyltridecane	$C_{19}H_{32}$	2275	1978	297

[a] Linear regression equations for 1-phenylalkanes:
On DB-1: $I = (101.38 \pm 0.57)Z + (41.22 \pm 7.32)$ ($n = 12$, $R^2 = 0.9997$, $p = 0.0001$);
On DB-Wax: $I = (100.74 \pm 1.39)Z + (318.91 \pm 18.00)$ ($n = 12$, $R^2 = 0.9997$, $p = 0.0001$).

The general structure is represented as 1-(alkyl)$_m$(alkyl)$_n$benzene, where $n > m$ and both refer to the number of carbon atoms in the alkyl groups. The value of $m + n$ is 10 for $C_{16}H_{26}$, 11 for $C_{17}H_{28}$, 12 for $C_{18}H_{30}$ and 13 for $C_{19}H_{32}$. In the mass spectra, the mass peaks are those of the molecular ions, phenyl(alkyl)$_{n-1}$, phenyl(alkyl)$_{m+1}$, phenylethyl (m/z 105) and phenylmethyl (m/z 91, 92) ions. In the fragmentation of 1-methyl(alkyl)$_{m+n-1}$ benzenes, the phenylethyl ion is the dominant mass peak but in the fragmentation of all other alkylbenzenes the phenylmethyl ion is dominant. Fragmentation occurs at the marked bonds adjacent to the tertiary carbon atom in the molecule, as shown in Fig. 2.

Chain branching and isomers

The isomers differ in the number of CH_2 groups in the two alkyl chains of 1-(alkyl)$_m$(alkyl)$_n$benzenes. The value of m may vary from 1 to $n - 1$ while the value of $m + n$ remains constant. Shifting the CH_2 group from the alkyl chain to the short alkyl chain will make the molecule more symmetrical, and the more symmetrical isomer has a lower I value.

Table III lists the I values of 1-(alkyl)$_m$(alkyl)$_n$ benzenes on DB-1 and DB-Wax columns. The chromatographic peaks, shown in Fig. 1, are labeled alphabetically and identified in Table II accordingly to the alphabetical letters listed in the first

TABLE II

MASS FRAGMENTATION DATA FOR 1-(ALKYL)$_m$(ALKYL)$_n$BENZENES

Peak	Compound	Formula	Mol.wt.	Mass fragments (relative abundance, %)[a]
a	1-Butylhexylbenzene	$C_{16}H_{26}$	218	91(100), 105(27), 147(50), 161(41), 218(27)
b	1-Propylheptylbenzene	$C_{16}H_{26}$	218	91(100), 105(18), 133(53), 175(32), 218(26)
c	1-Ethyloctylbenzene	$C_{16}H_{26}$	218	91(100), 104(23), 119(100), 189(39), 21(32)
d	1-Methylnonylbenzene	$C_{16}H_{26}$	218	91(38), 105(100), 218(26)
	1-Decylbenzene[b]	$C_{16}H_{26}$	218	91(100), 92(98), 105(20), 133(12), 218(66)
e	Triethyl phosphate	$C_{12}H_{27}O_4P$	266	99(100), 155(44), 211(32)
f	1-Pentylhexylbenzene	$C_{17}H_{28}$	232	91(100), 105(23), 119(10), 161(66), 232(18)
g	1-Butylheptylbenzene	$C_{17}H_{28}$	232	91(100), 105(82), 147(30), 175(26), 218(12), 232(20)
h	1-Propyloctylbenzene	$C_{17}H_{28}$	232	91(100), 105(14), 133(76), 189(43), 232(35)
i	1-Ethylnonylbenzene	$C_{17}H_{28}$	232	91(88), 105(20), 119(100), 203(55), 232(35)
j	1-Methyldecylbenzene	$C_{17}H_{28}$	232	91(28), 105(100), 106(30), 232(40)
k	1-Pentylheptylbenzene	$C_{18}H_{30}$	246	91(100), 105(19), 161(32), 175(27), 246(20)
l	1-Butyloctylbenzene	$C_{18}H_{30}$	246	91(100), 105(16), 147(30), 189(16), 246(10)
m	1-Propylnonylbenzene	$C_{18}H_{30}$	246	91(100), 105(26), 133(100), 203(53), 246(37)
n	1-Ethyldecylbenzene	$C_{19}H_{30}$	246	91(100), 119(67), 217(30), 246(22)
o	1-Methylundecylbenzene	$C_{18}H_{30}$	246	91(29), 105(100), 106(33), 246(37)
	1-Phenyldodecane[b]	$C_{18}H_{30}$	246	91(92), 92(100), 105(13), 133(11), 246(45)
p	1-Pentyloctylbenzene	$C_{19}H_{32}$	260	91(100), 105(16), 161)26), 189(21), 260(16)
q	1-Butylnonylbenzene	$C_{19}H_{32}$	260	91(100), 147(36), 203(22), 260(15)
r	1-Propyldecylbenzene	$C_{19}H_{32}$	260	91(100), 105(15), 133(41), 217(23), 260(16)
s	1-Ethylundecylbenzene	$C_{19}H_{32}$	260	91(100), 105(12), 119(61), 231(21), 260(12)
t	1-Methyldodecylbenzene	$C_{19}H_{32}$	260	105(100), 106(15), 260(15)
	1-Phenyltridecane	$C_{19}H_{32}$	260	91(78), 92(100), 105(11), 133(8), 260(41)

[a] Mass fragments of alkyl groups that are split off are listed as follows: ethyl = 29; propyl = 43; butyl = 57; pentyl = 71; hexyl = 85, heptyl = 99; octyl = 113; nonyl = 127; decyl = 141; undecyl = 165.

[b] 1-Phenylalkanes were not present in the solvent components of the liquid scintillator but were introduced for comparison.

column. On the DB-1 column the chromatograph peaks a–d belong to $C_{16}H_{26}$ isomers, f–j to $C_{17}H_{28}$ isomers, k–o to $C_{18}H_{30}$ isomers and p–t to $C_{19}H_{32}$ isomers. On the DB-Wax column, all the peaks follow the same elution pattern as shown on DB-1, with the exception of 1-methyl(nonyl, decyl, undecyl and dodecyl)benzenes which are represented by peaks d, j, o and t, respectively. These 1-methyl isomers are more polarizable and show larger column differences than the evenly branched or more symmetrical isomers. Plotting the I values of these isomers against the number of carbon atoms in the short alkyl group yields a family of curves, as shown in Fig. 3. The straight-chain 1-phenylalkanes are not found in the scintillator but were added during analysis for comparison. These graphs show that 1-phenylalkanes and 1-methylalkylbenzenes have considerably higher I values than the branched-chain isomers. The large differences between the I values of these isomers were not expected.

Chain branching and the A and GRF values

The I values of a homologous series, such as 1-phenylalkanes, may be calculated by the following linear regression equation:

$$I = AZ + (\mathrm{GRF})_z \qquad (1)$$

where A is the regression coefficient representing the I increment for atom addition, $(\mathrm{GRF})_z$ the intercept representing the group retention factors of substituents and functional groups and Z the number of atoms in the molecule. Both A and GRF can be predetermined. The basis for using this equation for I calculation is given in ref. 2.

Table IV shows that the isomers of $C_{16}H_{26}$,

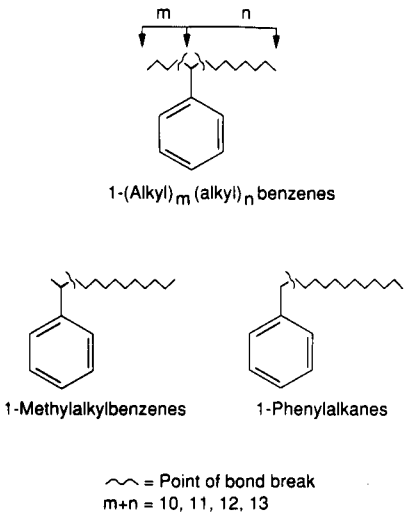

Fig. 2. Structures of the alkylbenzenes and the points of bond breakage. The m and n in 1-(alkyl)$_m$(alkyl)$_n$benzenes represent the carbon numbers in the alkyl chain with $n > m$ and $m + n = 10$ for $C_{16}H_{26}$ isomers, 11 for $C_{17}H_{28}$ isomers, 12 for $C_{18}H_{30}$ isomers and 13 for $C_{19}H_{32}$ isomers. The isomers are formed by shifting the methylene groups from the long to the short chain. Bond breakage occurs at the tertiary carbon atom for all isomers, including 1-phenylalkanes and 1-methylalkylbenzenes.

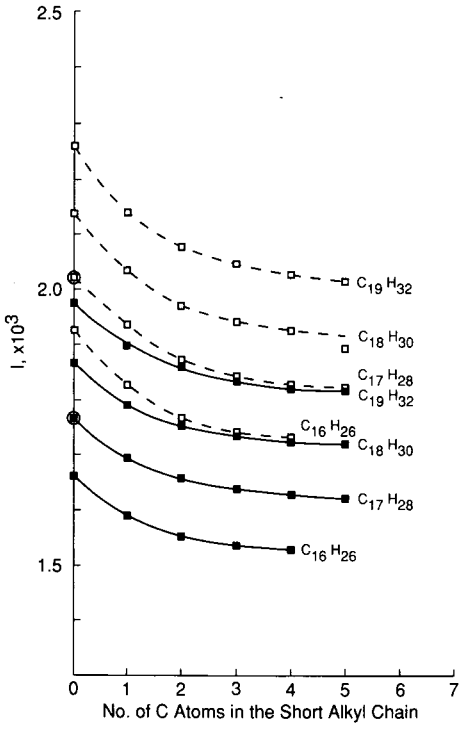

Fig. 3. Plots of retention indices of the solvent components on (solid lines) DB-1 and (dashed lines) DB-Wax columns against the number of carbon atoms in the short chain in the molecule. 1-Phenylalkanes are included for comparison. The I values of 1-phenylundecane ($C_{17}H_{28}$) on polar and non-polar columns are extrapolated from the regression equation in Table I.

$C_{17}H_{28}$, $C_{18}H_{30}$ and $C_{19}H_{32}$ can be selected to form seven homologous series. Plotting the I values against increasing number of carbon atoms in the second alkyl chain in the molecule yields straight lines, as shown in Fig. 4. Four series are formed with methyl, ethyl, propyl and butyl as the short alkyl chain. The A values for these series on DB-1 were found to be 102, 101, 100 and 98 and the GRF values were -39, -59, -59 and -45, respectively. The remaining three series are formed with decyl, nonyl and octyl as the long alkyl chain. The A values for these three series are 71, 78 and 87 and their GRF values are $+491$, $+339$ and $+159$, respectively. The observed A values (A_{obs}), listed in Table IV, are in agreement with the A values from linear regression equations. According to eqn. 1, the GRF and A values are mutually compensatory. It is therefore difficult to relate the unusually high GRF values to some apparent structure characteristics in the alkylbenzene molecule. However, these changes may be interpreted as disturbances that the addition of a methylene group to the short alkyl chain may have on the chromatographic properties of the molecule, such as electron density distribution. The A and GRF values will regress to normal values when a sufficient number of CH_2 groups are added to the short alkyl chain to yield a more symmetrical molecule. It should be pointed out that the number of data values for these homologous series is small, and a single incorrect data value can seriously distort the regression analysis. The regression analysis was performed with SAS/STAT statistical analysis procedures on a Model 486 personal computer. Data given for each homologous series include (i) the number of data point (n), (ii) standard errors of the regression coefficient and the intercept (SE), (iii) the coefficient of determination (R^2) and (iv) the probability of obtaining a greater F statistic than that observed if the hypothesis is true, i.e., the significance probability (p). The meaning of these terms is given in ref. 5.

TABLE III

RETENTION INDEXES OF 1-(ALKYL)$_m$(ALKYL)$_n$BENZENES ON NON-POLAR AND POLAR CAPILLARY COLUMNS

Peak	Compound	Formula	Retention index				Column difference (ΔI)
			DB-1		DB-Wax		
			I_{obs}	I_p	I_{obs}	I_p	
a	1-Butylhexylbenzene	$C_{16}H_{26}$	1526	1519	1729	1720	203
b	1-Propylheptylbenzene	$C_{16}H_{26}$	1534	1529	1743	1740	209
c	1-Ethyloctylbenzene	$C_{16}H_{26}$	1553	1549	1767	1770	214
d	1-Methylnonylbenzene	$C_{16}H_{26}$	1588	1584	1833	1830	245
	1-Phenyldecane	$C_{16}H_{26}$	1664	1654	1928	1950	264
e	Tributyl phosphate	$C_{12}H_{27}O_4P$	1622		2092		470
f	1-Pentylhexylbenzene	$C_{17}H_{28}$	1620	1614	1820	1810	200
g	1-Butylheptylbenzene	$C_{17}H_{28}$	1626	1619	1828	1820	202
h	1-Propyloctylbenzene	$C_{17}H_{28}$	1636	1629	1843	1840	207
i	1-Ethylnonylbenzene	$C_{17}H_{28}$	1656	1649	1873	1870	217
j	1-Methyldecylbenzene	$C_{17}H_{28}$	1692	1684	1933	1930	241
k	1-Pentylheptylbenzene	$C_{18}H_{30}$	1719	1714	1918	1910	199
l	1-Butyloctylbenzene	$C_{18}H_{30}$	1723	1719	1928	1920	205
m	1-Propylnonylbenzene	$C_{18}H_{30}$	1735	1729	1943	1940	208
n	1-Ethyldecylbenzene	$C_{18}H_{30}$	1755	1749	1972	1970	217
o	1-Methylundecylbenzene	$C_{18}H_{30}$	1791	1784	2036	2030	245
	1-Phenyldodecane	$C_{18}H_{30}$	1870	1854	2140	2150	270
p	1-Pentyloctylbenzene	$C_{19}H_{32}$	1814	1814	2015	2010	201
q	1-Butylnonylbenzene	$C_{19}H_{32}$	1821	1819	2026	2020	205
r	1-Propyldecylbenzene	$C_{19}H_{32}$	1833	1829	2046	2040	213
s	1-Ethylundecylbenzene	$C_{19}H_{32}$	1856	1849	2079	2070	223
t	1-Methyldodecylbenzene	$C_{19}H_{32}$	1894	1884	2143	2130	249
	1-Phenyltridecane	$C_{19}H_{32}$	1978	1954	2275	2250	297

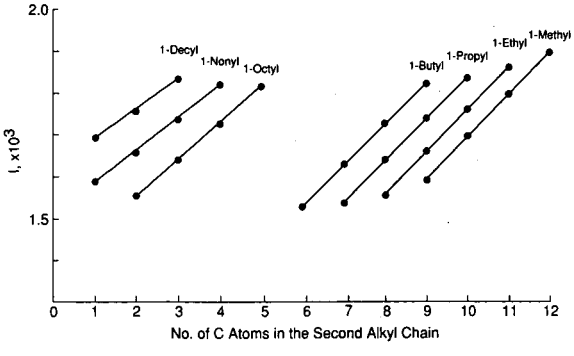

Fig. 4. Linear plots of the retention indices of homologues *vs.* the number of carbon atoms in the alkyl chain in 1-(alkyl)$_m$ (alkyl)$_n$ benzenes. The homologues are formed by allowing one alkyl chain in the molecule to be fixed in length while increasing the number of carbon atoms in the other alkyl chain. Linear plots for homologues with fixed long alkyl chains and fixed short alkyl chains have different slopes.

Chain branching and predicted retention indexes

The I values of the phenylalkanes can also be predicted on the assumption that $A = 100$, by the following equation [1,2]:

$$I_p = 100Z + \sum m_i - \sum n_i \quad (2)$$

where I_p is the predicted I, Z is the number of carbon atoms in the phenylalkane, m_i is the group retention factor (GRF) for the phenyl ring and n_i is the GRF for the tertiary carbon or methyl branching; the subscript "i" refers to the ith functional group or substitution. The term $100Z$ is known as the base value. The GRF for the phenyl ring is +54 on DB-1 and +350 on DB-Wax. The GRF for the tertiary carbon connected to a methyl group and a phenyl ring is about −70 on DB-1 and about −120 on DB-Wax columns. Addition of a CH_2 unit to the

TABLE IV

RETENTION INDICES OF BRANCH-CHAIN 1-(ALKYL)$_m$(ALKYL)$_n$BENZENES

Compound	Formula	Retention index[a]				Linear regression equation[b]	
		DB-1		DB-wax		On DB-1	On DB-Wax
		I_p	A_{obs}	I_p	A_{obs}		
Homologues with fixed short chain							
1-Methylnonylbenzene	$C_{16}H_{26}$	1588	104	1833	100	$(101.70 \pm 0.66)Z - (38.5 \pm 11.50)$	$(103.30 \pm 1.11)Z + (178.50 \pm 19.45)$
1-Methyldecylbenzene	$C_{17}H_{28}$	1692	99	1933	103	($n=4$, $R^2=0.9999$, $p=0.0001$)	($n=4$, $R^2=0.9998$, $p=0.0001$)
1-Methylundecylbenzene	$C_{18}H_{30}$	1791	103	2036	107		
1-Methyldodecylbenzene	$C_{19}H_{32}$	1894		2143			
1-Ethyloctylbenzene	$C_{16}H_{26}$	1553	103	1767	106	$(1000.80 \pm 0.53)Z - (59.00 \pm 9.28)$	$(103.50 \pm 1.07)Z + (111.50 \pm 18.80)$
1-Ethylnonylbenzene	$C_{17}H_{28}$	1656	99	1873	99	($n=4$, $R^2=0.9999$, $p=0.0001$)	($n=4$, $R^2=0.9998$, $p=0.0001$)
1-Ethyldecylbenzene	$C_{18}H_{30}$	1755	101	1972	107		
1-Ethylundecylbenzene	$C_{19}H_{32}$	1856		2079			
1-Propylheptylbenzene	$C_{16}H_{26}$	1534	102	1743	100	$(99.6 \pm 0.65)Z - (58.50 \pm 1.36)$	$(100.90 \pm 0.52)Z + (128.00 \pm 9.11)$
1-Propyloctylbenzene	$C_{17}H_{28}$	1636	99	1843	100	($n=4$, $R^2=0.9999$, $p=0.0001$)	($n=4$, $R^2=1.0000$, $p=0.0001$)
1-Propylnonylbenzene	$C_{18}H_{30}$	1735	98	1943	103		
1-Propyldecylbenzene	$C_{19}H_{32}$	1833		2046			
1-Butylhexylbenzene	$C_{16}H_{26}$	1526	100	1729	99	$(98.20 \pm 0.42)Z - (44.50 \pm 7.44)$	$(99.10 \pm 0.26)Z + (143.50 \pm 4.64)$
1-Butylheptylbenzene	$C_{17}H_{28}$	1626	97	1828	100	($n=4$, $R^2=1.0000$, $p=0.0001$)	($n=4$, $R^2=1.0000$, $p=0.0001$)
1-Butyloctylbenzene	$C_{18}H_{30}$	1723	98	1928	98		
1-Butylnonylbenzene	$C_{19}H_{32}$	1821		2026			
Homologues with fixed long chain							
1-Ethyloctylbenzene	$C_{26}H_{26}$	1553	83	1767	76	$(87.00 \pm 1.26)Z - (159.00 \pm 22.18)$	$(82.90 \pm 1.81)Z + (437.50 \pm 31.71)$
1-Propyloctylbenzene	$C_{17}H_{28}$	1636	87	1843	85	($n=4$, $R^2=0.9996$, $p=0.0001$)	($n=4$, $R^2=0.9990$, $p=0.0005$)
1-Butyloctylbenzene	$C_{18}H_{30}$	1723	91	1928	87		
1-Pentyloctylbenzene	$C_{19}H_{32}$	1814		2015			
1-Methylnonylbenzene	$C_{16}H_{26}$	1588	68	1833	40	$(77.80 \pm 2.86)Z - (338.50 \pm 50.15)$	$(64.90 \pm 6.90)Z + (783.00 \pm 121.07)$
1-Ethylnonylbenzene	$C_{17}H_{28}$	1656	79	1873	70	($n=4$, $R^2=0.9973$, $p=0.0013$)	($n=4$, $R^2=0.9779$, $p=0.0111$)
1-Propylnonylbenzene	$C_{18}H_{30}$	1735	86	1943	83		
1-Butylnonylbenzene	$C_{19}H_{32}$	1821		2026			
1-Decylbenzene	$C_{16}H_{26}$	1665					
1-Methyldecylbenzene	$C_{17}H_{28}$	1692	63	1933	39	$(70.50 \pm 4.33)Z - (491.00 \pm 78.02)$	$(56.50 \pm 10.10)Z + (966.67 \pm 182.05)$
1-Ethyldecylbenzene	$C_{18}H_{30}$	1755	78	1972	74	($n=3$, $R^2=0.9962$, $p=0.0391$)	($n=3$, $R^2=0.9690$, $p=0.1127$)
1-Propyldecylbenzene	$C_{19}H_{32}$	1833		2046			

[a] I_p = observed retention index; A_{obs} = observed A value, obtained from the difference between I values of two homologues differing by one methylene group.

[b] The linear regression equations are given in the form $(A \pm \text{S.E.})Z + (GRF \pm \text{S.E.})$, where A is the regression coefficient, GRF the intercept, and S.E. the standard error. For the meaning of other terms, see text.

methyl to form an ethyl group further lowers I by -35 on DB-1 and by -60 on DB-Wax. Shifting the CH_2 group from the long to the short alkyl group will also lower I. The predicted I values (I_p) of the isomers of 1-(alkyl)$_m$(alkyl)$_n$benzenes are listed in Table III. Their calculation is based on the use of the following GRF values: for the DB-1 column, base value $100Z$, phenyl ring $+54$, methyl -70, ethyl -35, propyl -20, butyl -10 and pentyl -5, and for the DB-Wax column, base value $100Z$, phenyl ring $+350$, methyl -120, ethyl -60, propyl -30, butyl -20 and pentyl -10. The negative GRF values for the higher alkyl groups are cumulative from the methyl group onwards and only increments are given above. The error between the predicted and the observed I values is less than 3%.

CONCLUSIONS

In a homologous series, the I value of the molecule increases by *ca.* 100 units for each increase in the number of carbon atoms [1,2]. In an isomeric series the number of carbon atoms remains constant but the I values vary according to structural symmetry. For example, in the isomeric series represented by $C_{19}H_{32}$, the straight-chain 1-phenyltridecane has the highest I. Shifting a methylene group to position 1 in the alkane chain to create 1-methyldodecylbenzene lowers the I by 70. The abrupt decrease in I is attributed to the presence of a tertiary carbon atom resulting from chain branching. In 1-ethylundecylbenzene, I is further lowered by 35. A small decrease in I appears to accompany each shift of the methylene group until the two chains are approximately equal in length, and the molecule appears to be more symmetrical. The bonds at the tertiary carbon are weakened and can break to yield the observed mass fragments in GC–MS analysis.

The column difference (ΔI) reflects the polarity and polarization of the molecule [2]. 1-Phenyltridecane has the largest column difference, 1-methyldodecylbenzene the next largest and 1-hexylheptylbenzene the least. A small column difference implies that the molecule appraoches aliphatic hydrocarbons in chromatographic behavior.

The ability to predict I values and to derive information on structure from the I values and the column differences has facilitated our interpretation of the data from GC–MS in the effort to identify the isomers of 1-(alkyl)$_m$(alkyl)$_n$(benzenes).

ACKNOWLEDGEMENTS

This publication was made possible by grant number CA33537 from the National Cancer Institute. We acknowledge the Mass Spectrometry Facility, University of California San Francisco, supported by NIH Division of Research Resources grants RR01614 and RR04112. We thank Z. C. Yang and S. Q. Liu for assistance with the analyses.

REFERENCES

1 C. T. Peng, S. F. Ding, R. L. Hua and Z. C. Yang, *J. Chromatogr.*, 436 (1988) 137.
2 C. T. Peng, Z. C. Yang and S. F. Ding, *J. Chromatogr.*, 586 (1991) 85.
3 J. McCormick, *Trans. Am. Nucl. Soc.*, 61 (1990) 10.
4 H. van den Dool and P. D. Kratz, *J. Chromatogr.*, 11 (1963) 463.
5 *SAS/STAT User's Guide, Release 6.03 Edition*, SAS Institute, Cary, NC, 1988, pp. 854–857.

Journal of Chromatography, 589 (1992) 241–248
Elsevier Science Publishers B.V., Amsterdam

CHROM. 23 731

Flame infrared emission detection of hydrogen

Mokhtar Mofidi, M. Keith Hudson* and Kathy Underhill

Department of Electronics and Instrumentation, University of Arkansas at Little Rock, 2801 S. University, Little Rock, AR 72204 (USA)

(First received June 26th, 1991; revised manuscript received September 10th, 1991)

ABSTRACT

The feasibility of using flame infrared emission (FIRE) for the detection of organic hydrogen was demonstrated. A FIRE radiometer was modified to monitor the 2.7-μm water vapor band emission and was used as a gas chromatographic detector. The system provided good quantification of hydrogen at moderate sensitivity. Detection limits for pentane were found to be 0.05 μl or 31 μg using the hydrogen/air flame. Maximum signal was monitored using a 1:1 stoichiometric flame at a height-in-flame of 3.7 mm, very similar to carbon mode FIRE studies. While no direct interferences were found, the presence of chlorine in the analyte compound did show a quenching effect. The hydrogen mode can be combined with carbon mode FIRE and with other detection methods, such as flame ionization detection, to give a detection system of great versatility, both in gas chromatography and various process monitoring applications.

INTRODUCTION

The fact that organic compounds, made up of carbon and hydrogen, combust to form carbon dioxide and water vapor has been known for many years. That this combustion reaction is efficient for the conversion of organic reactants to these products is attested to by the fact that combustion and incineration are major methods of destruction for hazardous organic materials. Analytically, carbon dioxide and water vapor have been used as analytes in determinations of carbon and hydrogen by gravimetric procedures and in IR absorption analysis in process monitoring [1].

The infrared emissions from flames were originally studied in detail by Plyler [2] who noted bands at 2.7 and 4.3 μm for a bunsen flame. The 4.3-μm band was assigned to carbon dioxide while the 2.7-μm band was assigned to both water vapor, from a fundamental vibration, and to the overtone of the carbon dioxide emission band. This and other early studies were carried out to model the emissions from jet aircraft engines, mainly to enable the construction of IR missile guidance systems. While it was noted that these emissions were at least semi-quantitative, no interest was shown in IR emission for analytical work for some time.

Recently, the feasibility of using IR emission from a flame for analysis was shown, using the 4.4-μm carbon dioxide emission band [3]. A special IR radiometer was constructed and used to determine organic compounds as a function of carbon dioxide emission as the compounds were burned in a hydrogen/air flame. This method was applied to monitoring the chromatographic effluent from both liquid and gas chromatography [3,4], with good results. While other recent work has dealt with the determination of carbonate and chlorine from aqueous solutions by flame infrared emission (FIRE) [5,6], no work has been attempted using the 2.7-μm band. This paper investigated the utility of using this band for the quantitation of hydrogen from organic compounds.

EXPERIMENTAL

Instrumentation

A Varian Aerograph Model 705 gas chromatograph (Varian, Palo Alto, CA, USA) was used in this study. A small opening was made in the side of

0021-9673/92/$05.00

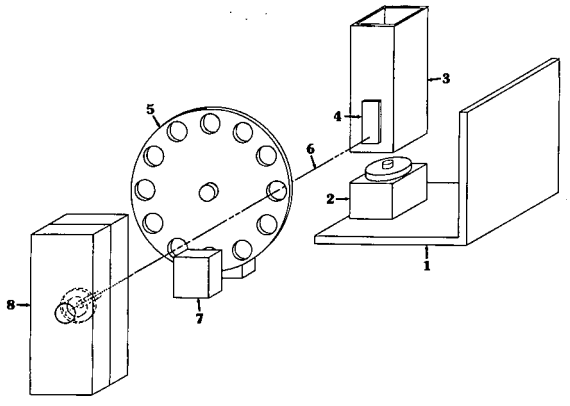

Fig. 1. Isometric close-up of FIRE system. 1 = Mount; 2 = burner; 3 = chimney; 4 = salt window; 5 = chopper; 6 = optical path; 7 = reference sensors; 8 = PbSe detector/filter/aperture assembly.

the oven to allow a stainless steel capillary tube of 1.5 mm I.D. to pass from the column end into a special hydrogen–air burner [4]. The FIRE detector used in this study was a modified version of that employed by Hudson *et al.* [7] as used in combination with a flame ionization detector (FID). The FIRE radiometer used a 630-Hz optical chopper, 2.4 mm I.D. aperture for field of view limiting, and a PbSe IR sensor as described previously. Modifications for hydrogen detection included: the use of a bandpass filter centered at 2.7 μm (Oriel Corp, Stratford, CT, USA), with a bandwidth of 0.1 μm full-width at half-height, mounted directly in front of the PbSe IR sensor; the addition of a height controller with adjustments in 1-mm increments for precise height in flame studies; substitution of a chimney painted flat black and mounted over the burner to reduce air drafts caused by the chopper blade and minimize background noise; and the use of a salt window mounted on the chimney to pass IR emissions, but further block air drafts. Fig. 1 shows a diagram of the radiometer.

A modified preamplifier circuit with a LF411 low offset low-drift field effect transistor (FET) input operational amplifier with adjustable gain control, and a reference circuit using a LM311 high-performance voltage comparator were designed and used. This circuit is shown in Fig. 2. The amplified PbSe signal was processed by an Ithaca Model 3981 (Ithaca, NY, USA) PC lock-in-amplifier (LIA) system, which was installed in a Zenith 12 MHZ IBM-AT compatible computer (Zenith Data Systems, St. Joseph, Michigan, USA). Software was written to control the LIA, display data, and allow digital storage and retrieval of data [8,9]. A hand-held solid-state laser (Emerging Technologies, Little Rock, AR, USA) was used to optically align the burner and PbSe IR sensor, allowing a precise determination of optical path for positioning and height-in-flame measurements.

Hydrogen, used as flame fuel, was obtained locally, as were the helium and nitrogen carrier gases. Air used as flame oxidant was compressed, filtered, and dried in house. Oxygen was used as the oxidant in some studies, and was obtained locally. Gas flows were monitored and controlled using flow meters with built-in metering valves (Cole-Parmer, Chica-

TABLE I

SIGNAL/MOL HYDROGEN

Compound	Signal/mol H	
	Air oxidant	Oxygen oxidant
Pentane	11.87	–
Hexane	11.58	5.127
Heptane	11.03	4.659
Octane	11.12	4.272
Nonane	11.19	–
Cyclohexane	11.77	5.810
Methylcyclohexane	10.93	4.327
3-Methylpentane	11.62	–
tert.-Butanol	10.24	3.967
Methanol	7.84	4.098
Ethanol	9.02	4.844
1-Propanol	10.71	4.935
2-Propanol	10.69	4.821
Carbon tetrachloride	0.00[a]	0.000[a]
Chloroform	0.00[a]	0.000[a]
Dichloromethane	N/A[a]	N/A[a]
Tetrachloroethane	N/A[a]	N/A[a]
Benzene	25.16[a]	5.149
Toluene	23.18[a]	2.143
2-Butanone	11.85	5.573
Butylacetate	11.42	1.172
Mean	11.60	4.30
S.D. $(n-1)$	1.12	1.24

[a] These compounds not included in mean and standard deviation calculation (see text). N/A: Some signal for large injections, negligible relative to other listed compounds (see text).

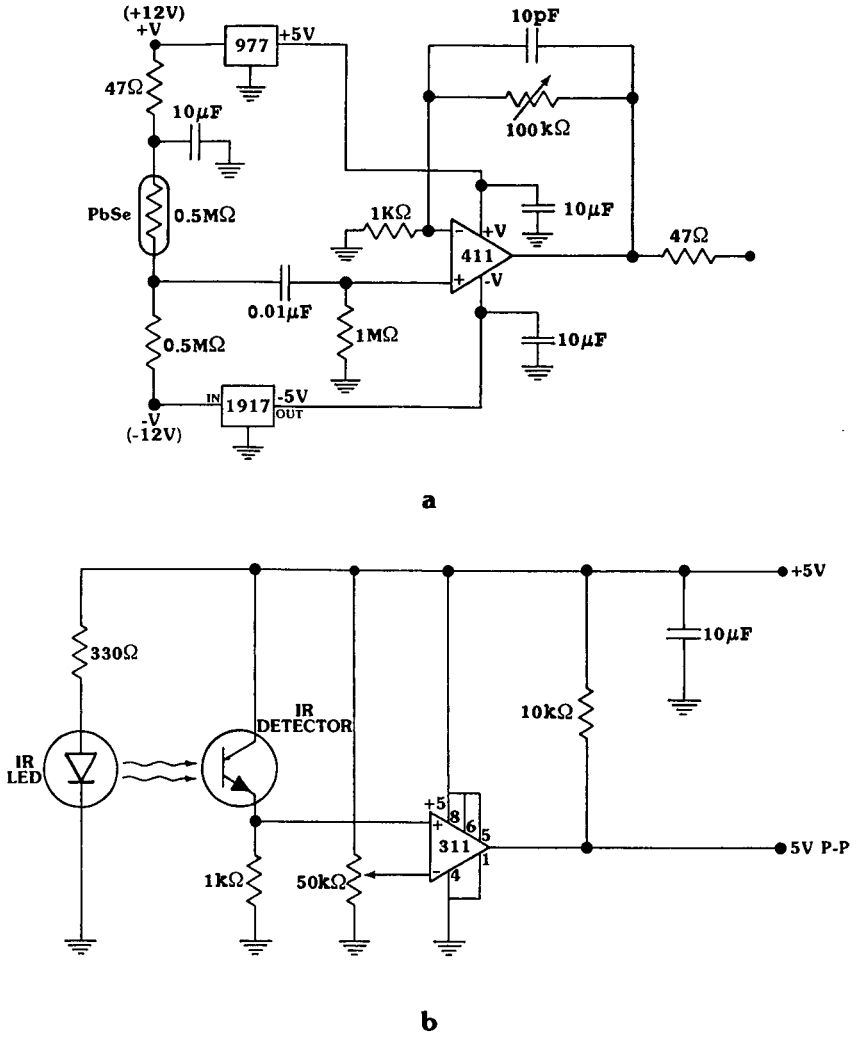

Fig. 2. (a) Preamplifier circuit; (b) reference circuit.

go, IL, USA). The column used was a 2-m 10% OV-101 on Chromosorb W HP packed in stainless steel (1/4 in.) (Supelco, Bellefonte, PA, USA).

Reagents

A variety of liquid organic compounds, totaling 21, were tested. These are shown in Table I. All compounds were reagent grade or the best possible grade.

Procedure

Injections of each individual liquid compound were made to measure the detector's response per mol of hydrogen using a Hamilton syringe Model 801 (Hamilton, Reno, NV, USA). For each compound injected during response studies, the injection inlet and column temperature were held higher than the boiling point of the specific compound being tested to ensure complete vaporization of the sample and passage through the column with little interaction. Detection limits were determined by using pentane and hexane in a 1:50 ratio. The column temperature was held above the boiling point of pentane and below that of hexane to allow effective separation while minimizing column effects on the pentane.

Burner flow-rates were typically 116 ml/min hydrogen and 330 ml/min air. Carrier flow was 43 ml/min for both helium and nitrogen. Sample injections were typically 1 μl. Other flow-rates and injection volumes were used, as indicated in the discussion.

RESULTS AND DISCUSSION

To study the fire for hydrogen, several parameters were considered which necessitated changes in the FIRE radiometer as previously used for carbon quantification [4,7]. The water vapor band, centered at 2.7 μm, required an obvious change in the bandpass of the IR filter used. The 2.72 $\pm$ 0.05 μm filter was the most suitable for this purpose which was readily available from optical suppliers. The narrow bandwidth limited the amount of blackbody radiation incident on the PbSe detector while allowing passage of most of the water band. Also, its transmittance (T) of 70% gave a good optical throughput at the detector. Flame drafts interfere with the stability of the hydrogen/air flame and cause a dramatic increase in observed noise. The burner chimney was designed to completely eliminate the effect of outside influences on the flame. The chimney's salt plate window effectively allowed the IR radiation to pass through the system while blocking the chopper induced air drafts. The chimney also served to form the essentially isothermal background on which the flame was viewed, further enhancing stability. The addition of the height controller to the burner base, along with the laser alignment unit, allowed much greater precision for the height in flame measurements. The modified preamplifier and reference circuits were used to decrease noise in those circuits and to allow variable gain in the preamplifier.

The use of a PC based lock-in-amplifier gave the operator greater control over the FIRE detection system. The software allowed the operator to set all lock-in parameters and to acquire, process, and store data to disk. Data could be retrieved for further processing and analysis.

Initial studies of the water and carbon dioxide bands indicated several important differences. First, the use of a hydrogen/air flame causes a 2.7-μm water vapor band background. Interestingly, hydrogen was chosen as the fuel in early FIRE work because there was no significant background at the 4.3-μm carbon dioxide band. Unfortunately, there is no analogous fuel for hydrogen studies at 2.7 μm. In order to quantify hydrogen, the background would have to be constant enough to differentiate the small differences in signal between the flame and flame plus sample. Secondly, most references indicate that the 2.7-μm band is due to both water and an overtone of carbon dioxide [2,3]. If this were true, a suitable calibration factor would have to be determined to achieve useful results from this band. A third difference is the emission intensity difference of water vapor compared to that of carbon dioxide. Obviously, two hydrogen atoms are required to form one water molecule, whereas carbon dioxide requires only one carbon atom, but how this difference effects sensitivity was not apparent.

Origins and characteristics of the 2.7-μm emission band

If the 2.7-μm emission band actually was a combination band of water vapor and carbon dioxide, data interpretation would be a great deal more complicated and minimally require a subtraction procedure based on the intensity of the carbon dioxide band at 4.3 μm. Since this was deemed of primary importance to the overal feasibility of any method we would base on 2.7-μm emission, this effect was investigated first. Carbon compounds that do not contain hydrogen were injected to quantify the effect of the carbon dioxide overtone at 2.7-μm without the presence of compound-produced water vapor. Injections of carbon monoxide, carbon dioxide, and carbon tetrachloride were made, up to 0.5 ml for the gas and 10 μl for the liquid samples. We had expected some small to moderate contribution from the carbon dioxide overtone at the 2.7-μm band region since this was indicated in the literature [2,3]. No signal was monitored at 2.7 μm for any size injections of these compounds. It there is a contribution from a carbon dioxide overtone at this wavelength, it is negligible under the conditions employed in this study. This observation allowed all resulting 2.7-μm data to be treated using calibration curves at least squares fits, greatly simplifying data analysis.

The emission intensity of the water molecule at 2.7 μm compared to that for the carbon dioxide molecule at 4.3 μm is experimentally considerably

lower. This intensity difference is the product of several factors: the response of the PbSe detector at the two wavelengths, the number of moles of hydrogen *versus* the number of moles of carbon contained in the sample compound, the bandpass and $\%T$ of the filters employed, and the actual IR emissivity difference between the two combustion products. The detectivity or response factor, D^*, at 25°C of the PbSe detector at 2.7 μm is $6 \cdot 10^8$ cm $\cdot$ $Hz^{1/2}/W$. At 4.4 μm, the detectivity is $3.2 \cdot 10^8$ cm $\cdot$ $Hz^{1/2}/W$. A 70%T filter having a 0.1-μm bandpass centered at 2.72 μm was used for hydrogen. This filter exhibits less throughput when compared to the 87 %T, 0.6-μm bandpass filter as used previously with carbon. However, the hydrogen mode was operated in a source noise limited condition, as was the previous carbon mode unit. Comparisons of the relative change in signal monitored indicate that there is less IR emission for each water molecule than for carbon dioxide molecules. However, this could not be accurately quantified with this experimental setup.

The large signal seen for the hydrogen flame at 2.7 μm is certainly the limiting factor in the FIRE detection of hydrogen. While significant work was expended to achieve a smaller flame size to reduce background, the original burner configuration [4] was found to be optimum in regard to flame geometry and signal output. The actual limiting noise from the flame is not the larger DC component of the background signal, but the relatively small AC component superimposed on top of it.

Detection limits for the hydrogen detector were studied by using repetitive injections of a pentane in hexane mixture, as used in the previous carbon mode study [7]. In this case, noise was measured from digitally stored chromatograms by taking the standard deviation over an area of 30 or more seconds run time where no injections were made. Peak heights for a series of repetitive injections near the noise level were compared to arrive at an average injection size which resulted in a signal equal to two times the average peak to peak noise figure. The signal-to-noise ratio = 2 was chosen on the basis of its use in the literature and to allow ease of comparison to other methods. A detection limit for pentane of 0.05 μl, corresponding to 31 μg, was found. This level is over an order of magnitude larger than that seen for carbon mode signals, which were 0.002 μl and 1.5 μg pentane. This difference seems due to the higher source noise limit imposed by the hydrogen flame background at 2.7 μm.

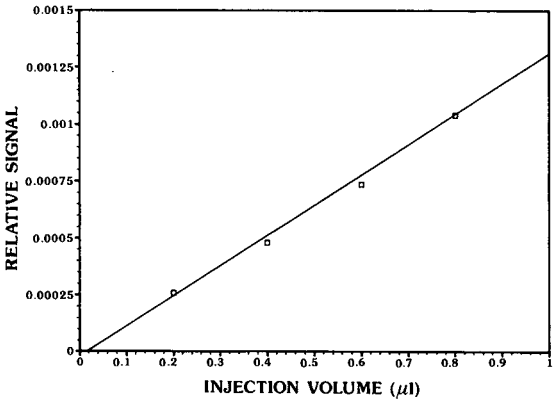

Fig. 3. Relative signal for hexane *vs.* injection volume.

Linear range was studied for injections of several different compounds. Fig. 3 shows the results of successively decreasing injections of hexane, indicating a linear relationship. The same solutions used for detection limit studies demonstrated a similar linear relationship at lower injection volumes for pentane. The linear range for hydrogen detection is similar to that for carbon mode operation, limited on the low end by the water vapor flame background noise. High end limits were found to be the same as for the carbon mode, limited by GC column overload. This indicates a linear range of slightly over three orders of magnitude.

Quantification of moles hydrogen

Carbon-mode FIRE detection has been shown to give a similar signal with regard to moles of carbon introduced into the flame, regardless of the functionality of the compound [7]. A study was conducted of the hydrogen mode unit to ascertain the functionality effects seen at 2.7 μm. Repetitive injections, normally 1 μl, of several sample compounds were made and the results were tabulated. The raw data were converted to give relative signal per mole hydrogen by using the injected volume, the density of the compound, compound formula weight, and the number of moles of hydrogen contained in the compound. Table I lists the compound, the relative signal integrated area, and the relative signal per mole of hydrogen calculated for each. An overall average signal of 12.43, with a standard deviation of

4.55, was obtained. This level of quantification does not compare favorably with the previously studied carbon mode average of 2.35 with a standard deviation of 0.19 [7].

Closer inspection of the data in Table I does reveal some trends. The chlorinated compounds show either no signal or such a small signal that areas could not be accurately determined. While no signal was expected for hydrogenless carbon tetrachloride, all other halocarbons tested contained hydrogen. Note also that the aromatics indicated a much larger signal than expected. The only other group showing a difference in signals was the lighter alcohols, with a slightly suppressed signal. If the aromatic and chlorinated functionalities are removed from the response calculations, an average of 11.60 value with a standard deviation of 1.12 results. This figure is significantly better and similar to that obtained for carbon-mode operation.

Several factors may enter into this difference seen in response for various functional groups. Looking first at the aromatics, it can be noted that initial carbon mode studies revealed similar data [3,8]. This was attributed to the tendency of aromatics to combust to carbon particles, which result in a significant blackbody emission. While this effect was apparently minimized in later carbon work, which used a similar radiometer and burner as this study, some blackbody emission may still be involved. The blackbody curve has greater intensity at 2.7 than at 4,4 μm, and still may be the mechanism giving rise to the greater observed signal levels. This hypothesis is supported by data collected using a hydrogen/oxygen flame on the burner. Data for the aromatics show a sharp decrease in emission, roughly in line with other compounds. The higher flame temperatures associated with oxygen operation should have resulted in less carbon particle formation.

The effect giving less signal for the halocarbons and alcohols may be found by considering the reactions for the combustion of all elements present in the tested compounds. Choosing dichloromethane and methanol as examples:

$$CH_2Cl_2 \rightarrow CO_2 + H_2O + 2HCl$$

$$CH_3OH \rightarrow CO_2 + 2H_2O$$

Carbon combusts to carbon dioxide, hydrogen to water vapor, and chlorine to hydrogen chloride, when present. Note that the flame supplies hydrogen and oxygen to these reactions and combusts by the balanced equation:

$$2H_2 + O_2 \rightarrow 2H_2O$$

For carbon, the predominant path is to combine with oxygen and form, eventually, carbon dioxide. This has been shown to occur at near 100% efficiency [7]. Recent work has also been performed on combustion of chlorine, using a reducing flame, showing quantitative formation of hydrogen chloride which was then monitored by FIRE at 3.8 μm [6]. However, for hydrogen two pathways exist. The organic hydrogen may combine with oxygen to form a water vapor molecule, as usually expected for combustion, or may combine with a chlorine atom to form a hydrogen chloride molecule. The latter pathway, while obvious from the reactions, was not expected to be significant prior to the response experimental studies. However, if one examines the occurrences in the flame regions, it may be that the combination of organic hydrogen and chlorine is the preferred mechanism.

Initially, we assumed that the hydrogen and oxygen in the flame, from the fuel and air supplies, would be present in enough excess to assure that organic carbon would combust to carbon dioxide, organic hydrogen to water vapor, and organic chlorine to hydrogen chloride. On closer examination, it becomes clear that this is not necessarily the case. It is required for the breakage of bonds that sufficient thermal energy be imparted to the molecule. This requires that some amount of hydrogen and oxygen from the supply be combusted to generate sufficient heat prior to compound combustion. A significant amount of supply gas must be combusted before organic compound breakup, which would then occur higher in the flame. In this case, as organic carbon, organic hydrogen, and organic chlorine are converted, they begin to seek another atom with which to combine and form a stable combustion product. Organic carbon normally reacts to form carbon dioxide, and is removed from the reactant stream. Organic hydrogen has the two aforementioned pathways, however, the organic chlorine atom is spatially much closer than a hydrogen from the flame gas supply. It would appear that much of the organic hydrogen is taken up by chlorine, giving hydrogen chloride at the expense of water vapor

and the 2.7-μm emission band. A similar argument for alcohols is not as clear. While OH radical formation is known to occur in spectroscopic flames [10], little is known about any IR emission attributed to OH. Additionally, organic hydrogens may not recombine preferentially with OH from the same carbon chain. A lone hydrogen may have to scavenge a flame fuel OH to form a water molecule, which would be in lower concentration, and not emit until in a higher, cooler flame zone, if at all. In any case, a stable OH with no emission or emission at another wavelength would cause a decrease in water vapor band intensity at 2.7 μm. The higher temperature of the hydrogen/oxygen flame was expected to minimize this effect, and this is verified by the data in Table I. Oxygen operation had little or no effect on the signals monitored for halocarbons.

Several fuel to air ratios were used in an attempt to achieve a greater signal-to-noise ratio, lower detection limits, and better relative response. In studies of HCl emissions, Kubala *et al.* [6] used a hydrogen rich flame. However, for hydrogen quantification, the same flame stoichiometry was used as for previous carbon studies, that is, essentially 1:1. Results with hydrogen/oxygen operation were not generally as satisfactory as when air was used as the oxidant. This is thought to be primarily due to the burner design. Height-in-flame measurements were carried out concurrently with the fuel/air studies. For the 1:1 stoichiometric flame a maximum signal height of 3.7 mm above the burner head was found. This height is very similar to that previously reported for carbon mode FIRE work.

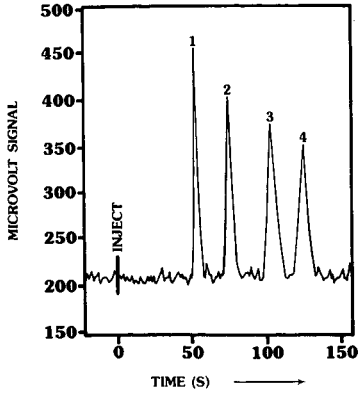

Fig. 4. Chromatogram for equal volume mixture injection (4 μl). Peaks: 1 = pentane; 2 = hexane; 3 = cyclohexane; 4 = heptane.

Fig. 4 shows a chromatogram obtained using the FIRE hydrogen mode detector. An injection of 4 μl of a equal volume mixture of pentane, hexane, heptane, and cyclohexane was made with an injector temperature of 150°C, a column temperature of 75°C, and a carrier flow-rate of 40 ml/min. The relative high noise associated with the 2.7-μm background is readily apparent in this chromatogram. However, the authors feel that this figure demonstrates the utility of selective detection of organic hydrogen and the performance of this FIRE detection mode.

CONCLUSIONS

FIRE detection can be used in a hydrogen mode to detect and quantify organic hydrogen. This mode does not result in as good a quantitation as the carbon mode, nor is it as sensitive. However, this study suggests that hydrogen mode FIRE can be combined into an instrument for multimode detection. Such a carbon/hydrogen detector would reveal significantly more information in a chromatogram than a single mode unit. Also, many of the problems associated with hydrogen and carbon FIRE modes may be overcome through the use of properly designed furnace based system, eliminating the flame background problem. The authors are currently working on such a multimode FIRE detector for carbon/hydrogen determination. Such an instrument, especially utilizing furnace-based combustion and excitation, should result in much greater utility in gas chromatographic and in many industrial process monitoring applications, as well as possibly providing a new device for measuring carbon/hydrogen ratios.

ACKNOWLEDGEMENTS

The authors would like to express their appreciation to Reagan Cole and Doug Wilson for their assistance with electronic circuits used in this study, to Armand Tomany for machining work, and to Mike Dugan for drafting figures. We would also like to thank Weiqun Zhang for assistance in data collection.

This work was partially supported by Southwest Missouri State University Faculty Research Grant number 15221-890-7 and Arkansas Science and

Technology Authority grant number 91-B-09. Portions of this work were presented at the 1991 National Association of Graduate and Professional Students Conference, Norman, OK, March 7–10, 1991 and at the 47th Southwest Regional American Chemical Society Meeting, San Antonio, TX, October 2–4, 1991 (Paper No. 56).

REFERENCES

1 H. H. Willard, L. L. Merritt, J. A. Dean and F. A. Settle, *Instrumental Methods of Analysis*, Wadsworth, Belmont, CA, 7th ed., 1988, p. 795.
2 E. K. Plyler, *J. Res. Nat. Bur. Stand.*, 40 (1948) 113.
3 M. K. Hudson and K. W. Busch, *Anal. Chem.*, 59 (1987) 2603.
4 M. K. Hudson and K. W. Busch, *Anal. Chem.*, 60 (1988) 2110.
5 S. W. Kubala, D. C. Tilotta, M. A. Busch and K. W. Busch, *Anal. Chem.*, 61 (1989) 1841–1846.
6 S. W. Kubala, D. C. Tilotta, M. A. Busch and K. W. Busch, *Anal. Chem.*, 61 (1989) 2785–2791.
7 M. K. Hudson, T. Fau, K. Underhill and S. Applequist, *J. Chromatogr.*, 513 (1990) 21–29.
8 M. K. Hudson, W. G. Hood and R. Henson, *Proc. Arkansas Acad. Sci.*, 44 (1990) 67–70.
9 M. K. Hudson and W. G. Hood, *Proc. Arkansas Acad. Sci.*, 45 (1991) in press.
10 W. Tsang and R. F. Hampson, *J. Phys. Chem. Ref. Data*, 15 (1986) 1087–1280.

Journal of Chromatography, 589 (1992) 249–256
Elsevier Science Publishers B.V., Amsterdam

CHROM. 23 728

Gas chromatographic separation of diastereomeric amino acid derivatives on chiral stationary phases

Application to the determination of enantiomeric composition in (*S*)-(+)-2-butanol

De-Ming Liu

Nanjing Institute of Geology and Palaeontology, Academia Sinica, Chi-Ming-Ssu, Nanjing 210008 (China)

(First received June 8th, 1990; revised manuscript received July 26th, 1991)

ABSTRACT

Diastereomeric derivatives of amino acid enantiomers were formed by the reaction of either their amino or carboxylic acid group with a chiral reagent. (*S*)-(+)-2-Butyltrifluoroacetyl and methyltrifluoroacetyl-(*S*)-(−)-prolyl derivatives of (*R,S*)-amino acids were resolved by gas chromatography on achiral and chiral stationary phases, respectively. The elution order of *sec.*-butyltrifluoroacetyl derivatives of (*R,S*)-leucine was established on Chirasil-Val. The combination of using (*S*)-(+)-butanol with a highly selective Chirasil-Val was used to determine the exact enantiomeric composition in the chiral alcohol. The mean value of the (*R*)-(−)-2-butanol obtained was 2.02%.

INTRODUCTION

Over the past 15 years, extensive developments have been made in the separation and analysis of amino acids by gas chromatography (GC). Undoubtedly, the most attractive application of GC in the amino acid field has been the resolution of amino acids into their optically active enantiomers. GC is the most effective and nowadays the most popular means of establishing the optical configuration or optical purity of chiral compounds, either singly or in mixtures [1–4]. Generally, GC resolution of amino acid enantiomers can be achieved by using either achiral or chiral stationary phase methods [5–9].

Resolution on an achiral phase requires the conversion of enantiomers into diastereomers with a suitable chiral reagent prior to GC analysis. (*S*)-(+)-2-Butanol and trifluoroacetyl (TFA)-(*S*)-(−)-prolyl chloride (S-TPC) have been the most popular chiral reagents in the above diastereomeric method [10–12]. One disadvantage of the method is that chiral reagents of highly optical purity are not always readily available, and optical impurity results in some determination errors in GC analyses.

With the introduction of chiral stationary phases, the direct GC resolution of amino acid enantiomers becomes possible. Since 1966, a variety of chiral phases with differing thermal stabilities have been developed [13–15]. The problem of optically impure reagents does not arise in the method which uses chiral phases. However, difficulties were encountered in separating low-volatility (*R,S*)-amino acids such as proline and aspartic acid applied in biogeochemical studies [16]. These two [*R,S*]-amino acids showed a low separation factors as TFA derivatives and were poorly resolved as heptafluorobutyryl (HFB)-alkyl derivatives [17,18]. In order to obtain high sensitivity, HFB-alkyl derivatives of amino acids are very useful when using electron-capture

0021-9673/92/$05.00

detection [19]. Hence the two methods are sometimes complementary; in other words, a certain pair of amino acids can be well resolved on an achiral stationary phase rather than on a chiral phase, and *vice versa*.

In order to overcome the difficulties of optical impurity in chiral reagents, the advantage of combining the use of a chiral reagent with a chiral phase has been demonstrated [20,21]. This procedure allows all stereomers to be completely separated and the errors due to the enantiomeric impurity of the chiral reagent can be eliminated [22].

In this work, the second chiral centre, necessary for the formation of diastereomeric derivatives, was introduced by two classes of derivatizations with chiral reagents. One was based on esterification with (*S*)-(+)-2-butanol and the other on acylation with S-TPC. These two classes of diastereomeric derivatives were then resolved on achiral and chiral phases, respectively. The (*S*)-(+)-2-butyl-TFA derivatives of (*R,S*)-leucine chromatographed on Chirasil-Val were then applied to the determination of enantiomeric composition in a chiral alcohol.

EXPERIMENTAL

Chemicals and reagents

Racemic and optically active amino acids were obtained from the Shanghai Institute of Biochemistry (Shanghai, China) and from L. Light (Colnbrook, UK). N-Trifluoroacetyl-(*S*)-(−)-prolyl chloride was synthesized as described previously [23]. Trifluoroacetic anhydride (TFAA) was purchased from BDH (Poole, UK), (*S*)-(+)-2-butanol from Fluka (Buchs, Switzerland) and *sec.*-butyl alcohol [(±)-2-butanol] from Tokyo Kasei Kogyo (Tokyo, Japan).

Methanol and dichloromethane (DCM) were dried and fractionated before use. Solutions of 1.25 *M* methanol, 3 *M sec.*-butyl alcohol and 3 *M* (*S*)-(+)-2-butanol in hydrochloric acid were prepared by bubbling dry hydrogen chloride gas into the respective alcohols until the required weights were obtained.

Apparatus and GC conditions

GC was carried out using the following instruments and achiral and chiral columns: (A) HP 5890A gas chromatograph (Hewlett-Packard, Palo Alto, CA, USA) and an HP-5 fused-silica column (25 m × 0.32 mm I.D.) (Hewlett-Packard); (B) the same instrument as in (A) but with a Chirasil-L-Val fused-silica column (25 m × 0.25 mm I.D.) (Chrompack, Middelburg, Netherlands); (C) GC-5A gas chromatograph (Shimadzu, Kyoto, Japan) and an OV-17 glass capillary column (30 m × 0.37 mm I.D.) (Shanghai Reagent Plant, Shanghai, China); (D) same instrument as in (C) but with a Chirasil-Val glass capillary column [24] (23 m × 0.25 mm I.D.) (Dalian Institute of Chemical Physics, Dalian, China). The instruments were equipped with a flame ionization detector and fitted with an HP 3396A and Shimadzu E-1A integrator, respectively. The injector and detector temperatures were 250°C and the splitting ratio was *ca.* 1:100. The temperature programmes were as follows: (A) 5 min at 80°C, then increased at 4°C/min to 185°C; (B) 95°C isothermal; (C) 3 min at 180°C, then increased at 2°C/min to 230°C; and (D) 105°C isothermal for (*S*)-(+)-2-butyl TFA derivatives and 150°C isothermal for methyl TFA-(*S*)-(−)-prolyl derivatives. The carrier gas was nitrogen, except (A) hydrogen.

Formation of derivatives

(S)-(+)- and (±)-2-butyl-TFA derivatives. A solution containing 50–500 nmol of each (*R,S*)-amino acid was added to a vial and evaporated to dryness at 40°C with a stream of dry nitrogen. Remaining traces of water were removed by re-evaporation with DCM and the amino acids were esterified by the addition of 200 μl of acidic 2-butanol, with vortex mixing and heating at 105°C for 1 h. After cooling, the solution was removed with nitrogen at 45°C and the last traces of 2-butanol were removed by re-evaporation with DCM. N-Trifluoroacetyl derivatives were prepared by dissolving the residue in 200 μl of DCM and 100 μl of TFAA with heating at 120°C for 20 min in an oil-bath. After cooling to room temperature, the solution was removed using a stream of nitrogen and the residue was dissolved in 100 μl of DCM.

Methyl-TFA-(S)-(−)-prolyl derivatives. A solution containing 35–70 μmol of each (*R,S*)-amino acid was dried at 50°C with dry nitrogen. The residue of the amino acid mixture was dissolved in 1 ml of acidic methanol and heated at 90°C, without capping, to synthesize the amino acid methyl esters. The methyl esters were then dissolved in 1 ml of

DCM and made to react with 1 ml of S-TPC together with 3–6 drops of triethylamine to synthesize the methyl-TFA-(*S*)-(−)-prolyl esters. With the addition of triethylamine, the pH of the mixture was checked to verify that it was basic (pH 10–12). This derivatization was carried out at room temperature for 1 h, and 1 ml of 6 *M* hydrochloric acid was added to terminate the reaction. The solution was then stirred and centrifuged to separate the aqueous and organic layers. The organic layer containing the diastereomeric amino acid esters was removed and dried by shaking with anhydrous magnesium sulphate. The magnesium sulphate was washed with 1.5 ml of DCM, filtered and then combined with the initial solution. The DCM was evaporated with a stream of dry nitrogen at room temperature and the residue was dissolved in 200 μl of DCM.

RESULTS AND DISCUSSION

Different kinds of derivatizing reagents used in derivatizations and the diastereomeric derivatives formed are listed in Table I. Four stereomers can be formed when an (*R,S*)-amino acid, having one chiral centre, reacts with an optically impure reagent. The stereomers are designated *RS*, *SR*, *RR* and *SS*, where the first letter indicates the configuration of the amino acid and the second the configuration of the chiral reagent. For example, when (*R,S*)-valine is reacted with optically impure S-TPC, four reaction products are obtained. Their interrelationships are shown in Fig. 1. The separation parameters of (*S*)-(+)-2-butyl-TFA esters and methyl-TFA-(*S*)-(−)-prolyl esters of (*R,S*)-amino acids, which were obtained on HP-5 and OV-17 stationary phases, re-

TABLE I

DIASTEREOMERIC AMINO ACID DERIVATIVES FOR GAS CHROMATOGRAPHY

Classification	No.	Esterifying reagent[a]	Acylating reagent	Derivative[b]
I	1	$CH_3CH_2\overset{*}{C}HCH_3 \cdot HCl$ (OH)	$(CF_3CO)_2O$	R-$\overset{*}{C}$H-COO$\overset{*}{C}$H$CH_3CH_2CH_3$ (NHCOCF$_3$)
		(*S*)-(+)-2-Butanol	TFAA	(*S*)-(+)-2-Butyl-TFA esters of (*R,S*)-amino acid
	2	$CH_3CH_2\overset{*}{C}H(OH)CH_3 \cdot HCl$	TFAA	R-$\overset{*}{C}$H-COO$\overset{*}{C}$H$(CH_3)CH_2CH_3$ (NHCOCF$_3$)
		(±)-2-Butanol		(±)-2-Butyl-TFA esters of (*R,S*)-amino acid
II	1	$CH_3OH \cdot HCl$	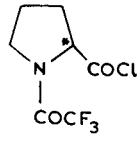	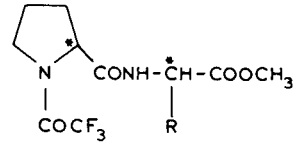
		Methanol	S-TPC	Methyl-TFA-(*S*)-(−)-prolyl esters of (*R,S*)-amino acid

[a] Asterisks denote chiral centres.
[b] R = Radicals of different complexities.

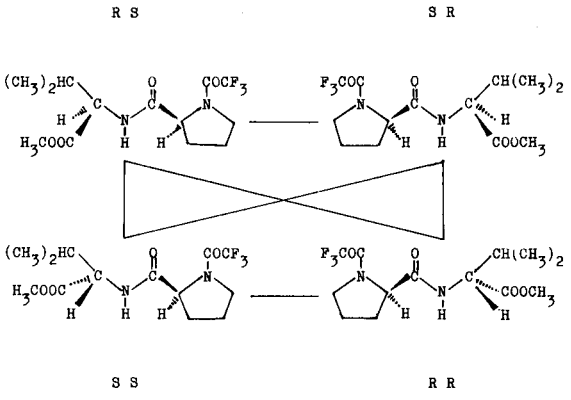

Fig. 1. Structures of methyl-TFA-(*R,S*)-prolyl derivatives of (*R,S*)-valine. Horizontal lines connect enantiomers; vertical and diagonal lines connect diastereomers.

spectively, are listed Table II. As *RS* and *SR*, and *RR* and *SS*, are enantiomers of each other, they cannot be resolved on achiral stationary phases. Therefore, separation parameters were based on the value of *RR* + *SS*/*RS* + *SR*. Figs. 2 and 3 show the GC resolution of these two classes of diastereomeric amino acid derivatives on the above stationary phases. It can be seen from the chromatograms that (*S*)-(+)-2-butyl-TFA esters and methyl-TFA-(*S*)-(−)-prolyl esters of (*RS*)-Pro and -Asp show a good resolution obtained by the diastereomeric method. The first peak of each enantiomeric pair of amino acids represents the *RS*/*SR* enantiomers on the chromatograms and the second the *RR*/*SS* enantiomers. They can only appear as diastereomeric pairs. This means that they co-elute with their enantiomers and add to the peak area. Hence an inherent error is present in GC analysis.

Fig. 4 illustrates the resolution of the conversion from three (*R,S*)-amino acids to the (*S*)-(+)-2-butyl-TFA derivatives by reaction with (*S*)-(+)-2-butanol. The two small peaks between two dominant peaks are due to the reaction of a small amount of (*R*)-(−)-butanol reagent. (*S*)-(+)-2-Butyl-TFA esters of glycine cannot be resolved on Chirasil-L-Val under the same isothermal conditions. Therefore, no small peak of the (*R*)-(−)-derivative [25] was observed on the chromatogram. When *sec.*-butyl alcohol, instead of (*S*)-(+)-2-butanol, reacted with a mixture of (*RS*)- and (*S*)-leucine (1:1, w/w), the resulting derivatives yielded four peaks [14] with relative areas of 1:1:3:3 on a Chirasil-Val column, as shown in Fig. 5. Each (*R*)- or (*S*)-leucine derivative can give a pair of peaks, which are approximately equal in area and appear close to each other. Similarly, four separate peaks were observed, as shown in Fig. 6, when methyl-TFA-(*S*)-(−)-prolyl esters

TABLE II

COMPARISON OF RETENTION TIMES (t_R) AND SEPARATION FACTORS (α) OF (*S*)-(+)-2-BUTYL-TFA (BTFA) DERIVATIVES AND METHYL-TFA-(*S*)-(−)-PROLYL (MTFP) DERIVATIVES OF (*R,S*)-AMINO ACIDS ON HP-5 AND OV-17 COLUMNS, RESPECTIVELY

Amino acid	Abbreviation	BTFA[a]		MTFP[b]	
		t_R (min)	α	t_R (min)	α
(*RS*)-Alanine	Ala	8.26 8.30	1.005	10.80 12.16	1.126
Glycine	Gly	8.87		13.14	
(*RS*)-Valine	Val	11.76 12.05	1.025	13.78 15.36	1.115
(*RS*)-Leucine	Leu	14.15 14.44	1.021	15.96 17.18	1.076
(*RS*)-Proline	Pro	19.49 19.87	1.020	22.72 24.96	1.099
(*RS*)-Aspartic acid	Asp	25.55 25.79	1.009	25.90 26.64	1.029

[a] Resolved on HP-5 column.
[b] Resolved on OV-17 column.

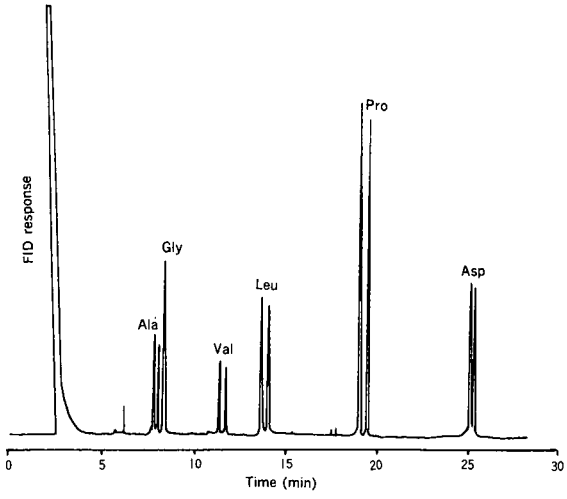

Fig. 2. GC resolution of (*S*)-(+)-2-butyl-TFA derivatives of (*R,S*)-amino acids on an HP-5 cross-linked column. Peaks: *RS*/*SR*, (*S*)-(+)-2-butyl-TFA esters of (*R*)-Ala, -Val, -Leu, -Pro and -Asp, and (*R*)-(−)-2-butyl-TFA esters of (*S*)-Ala, -Val, -Leu, -Pro and -Asp; *RR*/*SS*, (*R*)-(−)-2-butyl-TFA esters of (*R*)-Ala, -Val, -Leu, -Pro and -Asp, and (*S*)-(+)-2-butyl-TFA esters of (*S*)-Ala, -Val, -Leu, -Pro and -Asp; *R*/*S*, (*R*)-(−)-2-butyl-TFA ester and (*S*)-(+)-2-butyl-TFA ester of Gly.

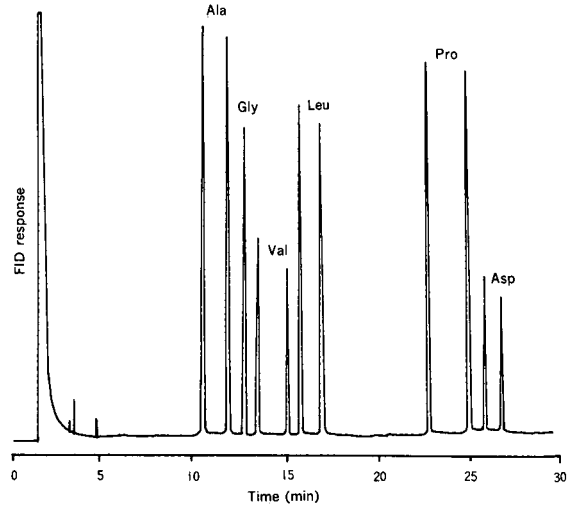

Fig. 3. GC resolution of methyl-TFA-(*S*)(−)-prolyl derivatives of (*R,S*)-amino acids on OV-17 support-coated open-tubular column. Peaks: *RS*/*SR*, methyl-TFA-(*S*)(−)-prolyl esters of (*R*)-Ala, -Val, -Leu, -Pro and -Asp, and methyl-TFA-(*R*)-(+)-prolyl esters of (*S*)-Ala, -Val, -Leu, -Pro and -Asp; *RR*/*SS*, methyl-TFA-(*R*)-(+)-prolyl esters of (*R*)-Ala, -Val, -Leu, -Pro and -Asp, and methyl-TFA-(*S*)-(−)-prolyl esters of (*S*)-Ala, -Val, -Leu, -Pro and -Asp; *R*/*S*, methyl-TFA-(*R*)-(+)-prolyl ester and methyl-TFA-(*S*)-(−)-prolyl ester of Gly.

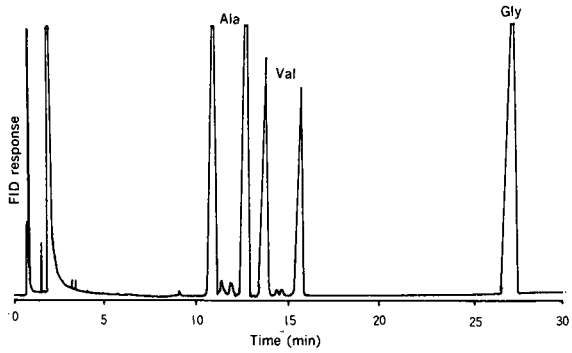

Fig. 4. GC resolution of (*S*)-(+)-2-butyl-TFA derivatives of (*R,S*)-amino acids on Chirasil-L-Val wall-coated open-tubular (WCOT) column. Peaks: *RS*, (*S*)-(+)-2-butyl-TFA esters of (*R*)-Ala and -Val; *RR*, (*R*)-(−)-2-butyl-TFA esters of (*R*)-Ala and -Val; *SR*, (*R*)-(−)-2-butyl-TFA esters of (*S*)-Ala and -Val; *SS*, (*S*)-(+)-2-butyl-TFA esters of (*S*)-Ala and -Val; *R* + *S*, (*R*)-(−)-2-butyl-TFA and (*S*)-(+)-2-butyl-TFA esters of Gly.

of (*R*)- and (*S*)-valine (1:2, w/w) were chromatographed on Chiralsil-Val. The behaviour of two classes of diastereomeric amino acid derivatives on chiral stationary phases is shown in Table III. (*R,S*)-Leucine shows the best resolution as (*S*)-(+)-2-butyl-TFA derivatives.

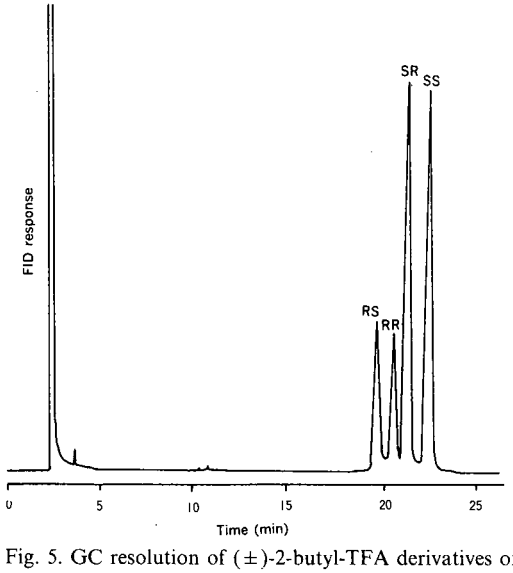

Fig. 5. GC resolution of (±)-2-butyl-TFA derivatives of (*RS*)- and (*S*)-leucine mixture on Chirasil-Val WCOT column. Peaks: *RS*, (*S*)-(+)-2-butyl-TFA ester of (*R*)-Leu; *RR*, (*R*)-(−)-2-butyl-TFA ester of (*R*)-Leu; *SR*, (*R*)-(−)-2-butyl-TFA ester of (*S*)-Leu; *SS*, (*S*)-(+)-2-butyl-TFA ester of (*S*)-Leu.

TABLE III

COMPARISON OF SEPARATION FACTORS (α) AND RESOLUTIONS (R) OF (*S*)-(+)-2-BUTYL-TFA DERIVATIVES AND METHYL-TFA-(*S*)-(−)-PROLYL DERIVATIVES OF (*R,S*)-AMINO ACIDS ON CHIRASIL-VAL COLUMNS

Amino acid	α		R		Resolving agent
	SR/RS	*SS/RR*	*SR/RS*	*SS/RR*	
(*RS*)-Alanine	1.068	1.131	1.727	1.596	(*S*)-(+)-2-butanol[a]
	1.074	1.078	1.810	2.430	S-TPC[b]
(*RS*)-Valine	1.059	1.025	3.556	2.542	(*S*)-(+)-2-butanol[a]
	1.115	1.045	1.020	2.180	S-TPC[b]
(*RS*)-Leucine	1.084	1.097	2.950	3.170	(±)-2-Butanol[b]

[a] Resolved on Chirasil-L-Val.
[b] Resolved on Chirasil-Val.

The use of two different types of diastereomeric derivatives, (*S*)-(+)- and (±)-2-butyl-TFA esters of (*R,S*)-amino acids, can readily identify the exact elution order of each stereomer, *i.e.*, the derivatives obtained by using (*S*)-(+)-2-butanol produce two dominant peaks during GC for a given racemic amino acid. It can be expected that the first and the last peaks are *RS* and *SS*, respectively, or *vice versa*. When (±)-2-butanol is used, the derivatives of (*R*)- and (*S*)- amino acids in the ratio 1:3 produce two pair of peaks with different heights. This result clearly demonstrates that the first of the four peaks is *RS* and the last is *SS*, the second *RR* and the third *SR*.

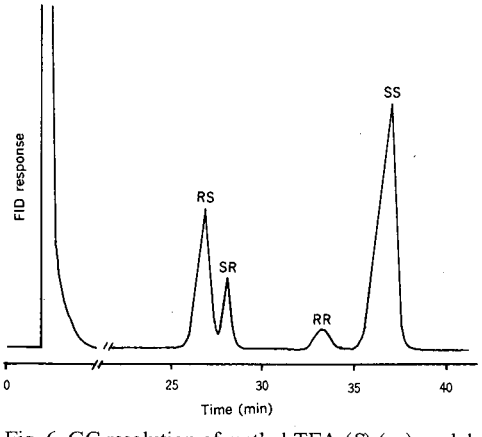

Fig. 6. GC resolution of methyl-TFA-(*S*)-(−)-prolyl derivatives of (*R,S*)-valine (1:2, w/w) on Chirasil-Val WCOT column. Peaks: *RS*, methyl-TFA-(*S*)-(−)-prolyl ester of (*R*)-Val; *SR*, methyl-TFA-(*R*)-(+)-prolyl ester of (*S*)-Val; *RR*, methyl-TFA-(*R*)-(+)-prolyl ester of (*R*)-Val; *SS*, methyl-TFA-(*S*)-(−)-prolyl ester of (*S*)-Val.

The chromatographic characteristics of the chiral stationary phase to resolve all stereomers can be utilized to determine the concentration of enantiomeric composition of (*S*)-(+)-2-butanol. Two 10 μmol/ml solutions were prepared, one containing (*RS*)-leucine and the other pure (*S*)-leucine. The two groups of leucine solutions were used to prepare a standard solution with a known *R/S* ratio. These solutions were derivatized and chromatographed as described above. The amount of each of the four isomers was determined by measuring the peak area. The percentage of (*R*)-(−)-butanol impurity was calculated from

$$\% = \frac{SR}{SR + SS} \cdot 100 \qquad (1)$$

and/or

$$\% = \frac{RR}{RR + RS} \cdot 100 \qquad (2)$$

where *SR*, *SS*, *RR* and *RS* are peak areas of the resulting isomers on the chromatogram. If a series of different enantiomeric ratios of amino acids are used, a suitable equation for calculation should be selected for the accuracy of measurement. When a low concentration of (*R*)-amino acid ($S \gg R$) is

TABLE IV

DETERMINATION OF THE PERCENTAGE OF (*R*)-(−)-2-BUTANOL IN COMMERCIAL (*S*)-(+)-2-BUTANOL USING THE CHIRASIL-VAL COLUMN

Leucine ratio[a] (*R*:*S*)	Peak area				(*R*)-(−)-2-Butanol (%)			
	RS	*RR*	*SR*	*SS*	Eqn. 1	Eqn. 2	Mean	SD
0:100	192	n.d.[b]	1508	71358	2.07	−		
15: 85	12364	152	1404	67447	2.04	n.c.[c]		
50: 50	9630	196	253	9919	2.49	2.00	2.02	0.38
	10021	170	274	10862	2.46	1.67		
	28933	423	684	28417	2.35	1.44		
	63263	957	1344	61562	2.14	1.49		

[a] Numbers in this column represent only the relative weights of (*RS*)-and (*S*)-leucine used; they do not represent true concentration ratios owing to the presence of enantiomeric impurities.
[b] Not detectable.
[c] Not calculable.

used, the peak area of *RR* is very small; likewise, when a low concentration of (*S*)-amino acid (*R* >> *S*) is used, the peak area of *SR* is also small. To avoid inaccuracy caused by the determination of small peak areas, the calculations involving these small peak areas should be omitted, *i.e.*, the former uses eqn. 1 and the latter eqn. 2. The results obtained from separate derivatizations are presented in Table IV. The mean value of the percentage of (*R*)-(−)-2-butanol and the standard deviation are 2.02% and 0.38% respectively.

CONCLUSION

The achiral and chiral phase methods can be combined as a new approach for separating all stereomers with a high enantioselectivity. This technique is suitable for the precise measurement of enantiomeric composition in chiral reagents and will be useful in eliminating errors when very different proportions of an enantiomeric mixture are analysed.

ACKNOWLEDGEMENTS

This work was supported by the Director Fund (No. 900402–3) of Nanjing Institute of Geology and Paleontology, Academia Sinica, and by the National Natural Science Foundation (No. 85040041) of China. I thank Ms. Wan-Gui Yao for her assistance and discussions.

REFERENCES

1 K. Ueda, S. L. Morgan, A. Fox, J. Gilbart, A. Sonesson, L. Larsson and G. Odham. *Anal. Chem.*, 61 (1989) 265.
2 H. Brückner and M. Hausch, in G. Lubec and G. Arosenthal (Editors), *Amino Acids: Chemistry, Biology and Medicine*, ESCOM Science, Leiden, 1990, p. 1172.
3 J. C. Dabrowiak and D. W. Cooke, *Anal. Chem.*, 43 (1971) 791.
4 W. A. Bonner, *J. Chromatogr. Sci.*, 10 (1972) 159.
5 A. Tunlid and G. Odham, *J. Microbiol. Methods*, 1 (1983) 63.
6 A. Tunlid and G. Odham, *Biomed. Mass Spectrom.*, 11 (1985) 428.
7 D.-M. Liu, X. Lan and J.-Q. Wang, *Acta Paleontol. Sin.*, 26 (1987) 353.
8 K. A. Kvenvolden, D. J. Blunt and H. E. Clifton, *Geochim. Cosmochim. Acta*, 43 (1979) 1505.
9 B. Nagy, M. H. Engel, J. E. Zumberge, H. Ogino and S. Y. Chang, *Nature (London)*, 289 (1981) 53.
10 K. Blau and G. S. King, *Handbook of Derivatives for Chromatography*, Heyden, London, 1977, p. 576.
11 D.-M. Liu and J.-Q. Wang, *Se Pu*, 5 (1987) 105.
12 M.-X. Zhao and J. L. Bada, *Nature (London)*, 339 (1989) 463.
13 W. A. König, *J. High Resolut. Chromatogr. Chromatogr. Commun.*, 5 (1982) 588.
14 W. A. König, *The Practice of Enantiomer Separation by Capillary Gas Chromatography*, Hüthig, Heidelberg, 1987, p. 72.
15 S. G. Allenmark, *Chromatographic Enantioseparation, Methods and Applications*, Ellis Horwood, Chichester, 1988, p. 224.
16 C. Lee, J. L. Bada and E. Peterson, *Nature (London)*, 259 (1976) 183.
17 T. Saeed, P. Sandre and M. Verzele, *J. Chromatogr.*, 186 (1979) 611.
18 I. Abe, K. Izumi, S. Kuramoto and S. Musha, *J. High Resolut. Chromatogr. Chromatogr. Commun.*, 4 (1981) 549.

19 D.-M. Liu, *J. High Resolut. Chromatogr.*, 12 (1989) 239.
20 W. Rahn and W. A. Konig, *Hoppe-Seyler's Z. Physiol. Chem.*, 357 (1976) 1223.
21 J. H. Liu and W. W. Ku, J. T. Tsay, M. P. Fitzgerald and S. Kim, *J. Forensic Sci.*, 27 (1982) 41.
22 J. H. Liu and W. W. Ku, *Anal. Chem.*, 53 (1981) 2180.
23 E. A. Hoopes, E. T. Peltzer and J. L. Bada, *J. Chromatogr. Sci.*, 16 (1978) 36.
24 G.-D. Lai, H.-C. Li, P.-C. Lu, G. J. Nicholson and E. Bayer, presented at the *5th National Symposium on Chromatography, Chengdou, China, October 7–13, 1985.*
25 H. Brückner and M. Langer, *J. Chromatogr.*, 542 (1991) 161.

Journal of Chromatography, 589 (1992) 257–263
Elsevier Science Publishers B.V., Amsterdam

CHROM. 23 685

Application and chiral recognition of heptakis (2,6-di-O-methyl-3-O-trifluoroacetyl)-β-cyclodextrin as a stationary phase for the gas chromatographic separation of enantiomers

Georgi Stoev

Institute of Organic Chemistry, Bulgarian Academy of Sciences, Sofia 1113 (Bulgaria)

(First received March 20th, 1991; revised manuscript received August 12th, 1991)

ABSTRACT

The separation of a large number of enantiomeric pairs of various classes (bornanes, aromatics, etc.) with heptakis(2,6-di-O-methyl-3-O-trifluoroacetyl)-β-cyclodextrin, used as a stationary phase in capillary gas chromatography, widens the scope of the application of the latter. The analysis of the selectivity of this phase with respect to individual substances and the separation achieved made it possible to draw some conclusions on the steric disposition of the enantiomers.

INTRODUCTION

An important breakthrough has been achieved recently in the gas chromatographic separation of enantiomers by using modified α,β-cycoldextrins (CDs) as chiral stationary phases in high-resolution capillary columns [1–4]. Schurig and Nowotny were the first to use open-tubular columns coated with a solution of heptakis(2,6-di-O-methyl-3-O-trifluoroacetyl)-β-cyclodextrin in OV-1701 for the gas chromatographic separation of volatiles belonging to different classes of compounds, such as γ-lactones, oxiranes, ketones and spiroketals. No derivatization procedures were necessary for most of the resolved chiral molecules.

Trifluoroacetylation of 2,6-O-alkyl-CDs is useful because CF_3COO groups are able to form additional hydrogen bonds and to induce dipole–dipole interactions between them and the enantiomers. Later, 2,6-dipentyl-3-O-trifluoroacetyl-CDs (α, and γ) were synthesized and coated on fused-silica capillary columns [5]. These phases were used for the separation of alcohols, polyols, amines and other compounds after derivatization with trifluoroacetyl anhydride.

This paper extends the scope of enantiomeric separations on heptakis(2,6-di-O-trifluoroacetyl)-β-CD to compounds of different types (bornanes, aromatics, etc.). Some assumptions are made concerning the mechanism of chiral recognition and the steric disposition of the investigated compounds in the cavity of the CD. The steric disposition of enantiomers in the cavity is assessed by the steric interaction between the latter and the enantiomers. The larger the difference between the energies of formation of the diastereomeric complexes, the higher is the selectivity α of the modified CD used as a stationary phase in gas chromatographic separations. Hence, on the basis of selectivity it is possible to make assumptions regarding the chiral recognition, to model the modification of CDs, to evaluate the extent of modification, etc. In some instances the steric disposition of the molecules in a CD can be exactly determined by molecular modelling [6,7], but this is an expensive and mostly inaccessible method. Therefore, we decided to use the data for

0021-9673/92/$05.00

the chromatographic separation of enantiomeric pairs and the steric direction with modified CDs, which also offer the opportunities for different intermolecular interactions. For this purpose we used compounds of different classes with CDs modified to various extents.

EXPERIMENTAL

Synthesis of heptakis(2,6-di-O-methyl-3-O-trifluoroacetyl)-β-CD

This compound was synthesized as described previously [8] and purified by column chromatography. The purity was controlled by thin-layer chromatography (TLC) (R_F = 0.30) with toluene–ethanol (90:10, v/v). Trifluoroacetylation was performed similarly to a reported procedure [1,9]. The extent of acetylation was controlled by TLC and IR spectrometry. A completely trifluoroacetylated phase (I) and a partially trifluoroacetylated phase (II) (*ca.* 75% by IR spectrometry) were prepared.

Preparation of glass capillary columns

Pyrex glass tubing (Schott Ruhrglass, Mainz, or Jenaglass, Jena, Germany) were drawn out to capillaries of 0.26 mm I.D. using a Shimadzu GDM1 drawing machine. Acid leaching, rinsing and deactivation were performed as described [10,11]. The columns were coated with a 0.3% solution of the modified β-CD I and II and OV-1701 (Macherey, Nagel & Co., Düren, Germany) (12:88) in dichloromethane.

The capillary columns were tested with a Grob test mixture to assess their efficiency and inertness.

Gas chromatography

A Pye Unicam Model 304 or a Perkin-Elmer Sigma 300 instrument with split injection and flame ionization detectors were used. Nitrogen served as the carrier gas. Data were registered with a Shimadzu CR-1B electronic integrator.

Solutes

Compounds of different classes (bornanes, aromatics, etc.) were analysed.

RESULTS AND DISCUSSION

Bornanes (bicyclo[2.2.1]heptanes)

The selectivity of phase I with respect to bornan-2-one (**1**) is satisfactory, α = 1.05 (Table I). Compound **1** was analysed also with phase II (con-

TABLE I

GAS-CHROMATOGRAPHIC DATA ON THE SEPARATION OF ENANTIOMERS ON HEPTAKIS(2,6-DI-O-METHYL-3-O-TRIFLUOROACETYL)-β-CD (PHASE I) IN OV-1701

The separation was carried out with a capillary column (25 m × 0.26 mm I.D.) with nitrogen as the carrier gas at a flow-rate of 25–35 cm/s.

No.	Substance		Temperature (°C)	Selectivity (α)	Resolution (*R*)
1	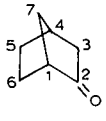		80	1.05	0.6
2	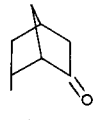	*endo*	80	–	–
3	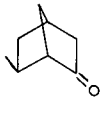	*exo*	80	1.19	3.9

TABLE I *(continued)*

No.	Substance		Temperature (°C)	Selectivity (α)	Resolution (R)
4	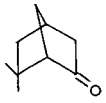		80	1.05	1.0
5	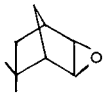	*exo*	100	1.11	2.2
6	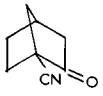		140	1.14	3.5
7			80	1.05	1.5
8	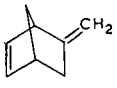		80	1.05	1.5
9	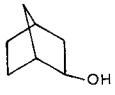		80	1.05	1.5
10	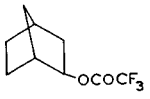		70	1.06	1.6
11	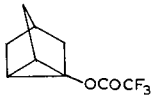		80	–	–
12	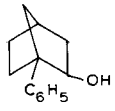		120	1.04	1.7
13	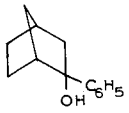		120	–	–
14	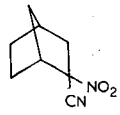		120	1.07	0.5
15	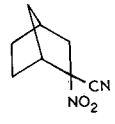		120	–	–

(Continued on p. 260)

TABLE I *(continued)*

No.	Substance	Temperature (°C)	Selectivity (α)	Resolution (R)
16	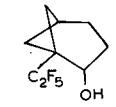	80	1.04	0.7
17	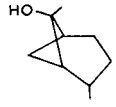	80	–	–
18	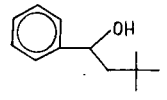	100	1.03	1.2
19	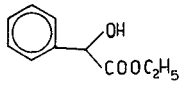	100	1.07	2.0
20	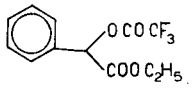	100	1.03	1.4
21	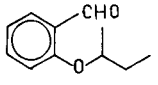	110	–	–
22	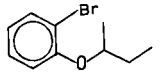	80	–	–
23	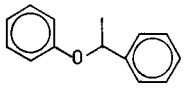	140	1.02	1.4
24	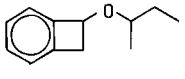	90	1.06	1.8

taining hydroxyl groups). It was found that phase II shows the same selectivity for **1**, but the separation of the enantiomers was $R = 0.6$, on account of tailing due to hydrogen bonds. The same selectivity of phases I and II with respect to **1** reveals that it is determined predominantly by the interaction between the hydrophobic parts of the bornane skeleton and the cavity of the CD, after the penetration of **1** into the latter.

The addition of one or two methyl groups at C-6 of bornan-2-one (compounds **2**–**4**) has a considerable impact on the separation. When the methyl group is in an *endo* position (**2**) the enantiomeric pair cannot be separated. This pair is less strongly retained than **3** (Fig. 1). In **3** the methyl group is in an *exo* position and with respect to this pair phase I exhibits considerable selectivity ($\alpha = 1.19$). It should be emphasized that no tailing is observed in

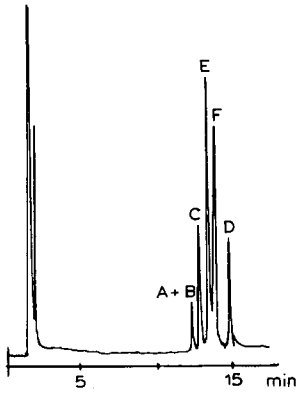

Fig. 1. Separation of racemic mixtures of **2** (A, B), **3** (C, D) and **4** (E, F) on a 25 m × 0.26 mm I.D. capillary column, coated with 0.2 μm of phase I. Oven temperature, 80°C; carrier gas, nitrogen; flow-rate, 30 cm/s.

the analysis of these compounds with phase II. Hence the inserted methyl group favours a disposition of **2** and **3** such that the carbonyl group cannot form hydrogen bonds with the hydroxyl groups at the C-2 of CD. As the methyl group cannot generate interaction forces with the cavity of CD other than dispersion forces, it is evident that in **2** the position of this group is such that the norbornane skeleton cannot fit to the hydrophobic internal surface of the CD cavity. With **3** the fitting is very close. This indicates that the methyl group in **2** prevents the bornane skeleton from fitting to the internal surface of the CD on the plane formed by the C-2, C-3, C-7 and C-5, C-6, C-7 atoms. When the methyl group is in an *exo* position it represents a prolongation of this plane, whereby it enhances the Van der Waals forces of attraction. These suppositions are corroborated by **4** containing *endo*-CH_3 and *exo*-CH_3 groups at C-6. With respect to **4**, phases I and II exhibit an intermediate selectivity between **2** and **3**.

The substitution of the keto group of **4** by an epoxy ring in an *exo* position (**5**) considerably raises the selectivity, from 1.05 to 1.11, despite the fact that the chromatographic procedure was carried out at a temperature 30°C higher than that for **3**. Moreover, when the chromatographic procedure is performed with phase II the tailing diminishes, *i.e.*, the oxygen atom of the epoxy ring in **5** is disposed in such a way in the cavity that it cannot form hydrogen bonds with 2-OH groups of CD. The high selectivity of **5** can be explained by the fact that the epoxy ring enlarges the contact surface area, *i.e.*, it is now with the C-2, O, C-3, C-7 and C-5, C-6, C-7 atoms.

On synthesizing **6** from **1** the selectivity of phases I and II considerably increases and at the same time the tailing is reduced.

The double bond between C-5 and C-6 in the bornan-2-one skeleton of **7** and 8 has no effect on the selectivity of the stationary phase, *i.e.*, the selectivity is again determined by the bornane skeleton and not by the C=O or $=CH_2$ groups. From the fact that the selectivity and separation rates with **7** and **8** are identical follows that their behaviours towards the stationary phase are similar. In contrast to **1**, where C=O is at C-2 and tailing occurs, in **7** C = O is at C-3 and no tailing is observed. For the series **1–5** the bornane skeleton fits to the internal surface of CD on the planes formed by C-2, C-3, C-7 and C-5, C-6, C-7. In this position the C=O group is at the orifice of the CD cavity and may form hydrogen bonds with the 2-OH group of the CD. With **7** C=O is at C-3 and no tailing is observed with phase II. This presupposes the same disposition of the bornane skeleton in the CD as in **1–5**, but the C=O group is inside the cavity and not at the orifice.

The replacement of the keto group in **1** by a hydroxyl group in **9** again has no effect on the selectivity of the phase, but the separation is poor owing to hydrogen bonding. To prevent tailing, which is induced by the hydrogen bonds between the stationary phase and the solutes, Amstrong and coworkers [12,13], who used a polar CD-derivative phase containing OH groups, acetylated solutes with trifluoroacetic anhydride. Li *et al.* [5] also acetylated solutes, although they separated them with perdi-O-methyl-3-O-trifluoroacetyl)-α-, -β- or -γ-CDs. Further, Schurig *et al.* [14] separated menthols, alcohols and diols by permethylated 2,3,6-β-CD, but not with 2,6-dimethyl-3-trifluoroacetyl-β-CD, perhaps because of the incomplete acetylation or hydrolysis of the latter.

Compound **11** can be seen as a derivative of **10** by linking the C-2 and C-5 atoms, whereby the bornane skeleton is altered and thus cannot fit to the internal surface of the cavity.

The addition of a benzene ring to the bornane skeleton offers a new opportunity for interaction

between the solute and the CD. It becomes possible for the bornane skeleton to fit in the cavity and the benzene ring to remain outside and *vice versa*. No supposition can be made regarding the disposition of **12** and **13** in the cavity.

On accumulation of negative electric charges on the CN and NO_2 groups on C-2 in the bornane skeleton (**14**), there is nevertheless a separation of the enantiomeric pairs (Fig. 2a, b). If the values of R and α for **14** are compared with those of **1** and **9**, it can be concluded that the CN group in an *endo* position at C-2 has no effect on selectivity, whereas NO_2 forms hydrogen bonds with 2-OH groups of phase II. No tailing was observed when I was used for chromatographic analysis. It can be stated that the hydrogen bonds are stronger than those of **1** and **9** as the tailing is stronger and, despite the higher selectivity, the separation is poorer. After rearrangement of the groups in **15** the phase does not exhibit any selectivity. From this it follows that the *endo*-CN group at C-2, through interaction with the CF_3CO groups, guides the bornane skeleton to adhere to the cavity of β-CD similarly to **6**.

Both phases I and II exhibit almost the same selectivity with respect to **16** (1-perfluoroethyl-2-hydroxybicyclo[1.1.3]heptane) as **1**, **4** and **9** (Fig. 2c). The unsatisfactory separation is due again to the hydrogen bonds. The phases, however, do not exhibit selectivity if the OH group is introduced at the bridge of the skeleton, compound **17** (7-methyl-2,7-dihydroxybicyclo[1.1.3]heptane). This indicates that the substitution at C-7 hinders the adherence of the skeleton to the cavity of the β-CD.

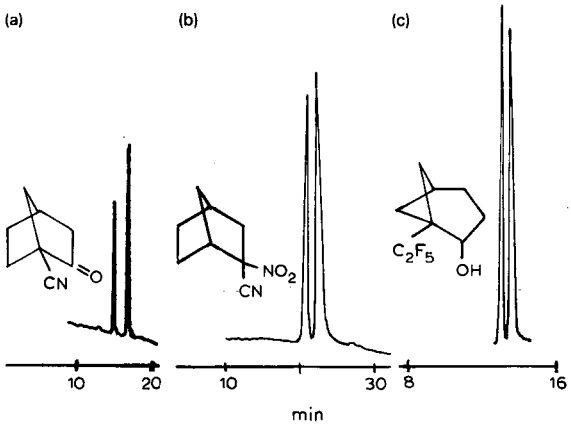

Fig. 2. Separation of enantiomers of some bornane derivatives on a 25 m × 0.26 mm I.D. capillary column coated with 0.15 μm of phase I at a linear velocity 30 cm/s of nitrogen.

Benzene derivatives

In these compounds one of the substituents at the chiral centre is a benzene ring and the other is a hydrogen atom. The two remaining valences of the chiral centre are linked with groups having various polarities and volumes.

The role of the volume of the substituent on the separation in the case of **18** is noteworthy. With **19** the separation is good because of the well expressed selectivity, $\alpha = 1.07$, *i.e.*, the C_2H_5COO group exhibits a considerable impact by interaction with the CF_3COO groups of the stationary phase. The acetylation of the hydroxyl group giving **20** reduces tailing but also decreases the selectivity as well. Hence, with these compounds the benzene ring has a marked effect on the selectivity in addition to the hydroxyl group.

The role of the substituent with respect to the selectivity of **21–24** is interesting. No separation of the enantiomers takes place with **21**. No separation occurs even if the electronegative bromine is substituted for the aldehyde group (**22**). However, if a benzene ring is substituted for the methyl group at the chiral centre of **21** (**23**) the enantiomeric pair can be separated.

Compound **24** has two chiral centres, but on account of the consideration on the effect of the substituents presented above, it was possible to separate an enantiomeric pair with a chiral centre at the four-membered ring. This pair was synthesized by stereoselective synthesis especially to confirm this prediction.

ACKNOWLEDGEMENTS

The author expresses his gratitude to Dr. Schied and Dr. Raskopf of the Faculty of Chemistry at the Ruhr University, Bochum, Germany, for presenting some of the compounds investigated and for their significant support in the performance of this investigation.

REFERENCES

1 H. P. Nowotny, D. Schmalzing, D. Wistuba and V. Schurig, *J. High Resolut. Chromatogr.*, 12 (1989) 383.
2 H. P. Nowotny, *Dissertation*, Universität Tübingen, 1989.
3 W. A. König, S. Lutz, G. Wenz and E. von der Bey, *J. High Resolut. Chromatogr. Chromatogr. Commun.*, 11 (1988) 506.
4 W. A. König, S. Lutz and G. Wenz, *Angew. Chem.*, 100 (1988) 989; *Angew. Chem., Int. Ed. Engl.*, 27 (1990) 979.
5 W. Y. Li, H. L. Jin and D. W. Armstrong, *J. Chromatogr.*, 509 (1990) 303.
6 H. Karfunkel, Ciba-Geigy, Basle, unpublished work.
7 A. M. Stalcup, S.-C. Chang, D. W. Armstrong and J. Pitha, *J. Chromatogr.*, 513 (1990) 181.
8 J. Boger, R. J. Corcoran and J. M. Lehn, *Helv. Chim. Acta*, 61 (1978) 2190.
9 F. Cramer, G. Mackensen and K. Seusse, *Chem. Ber.*, 102 (1969) 494.
10 V. Schurig and H. P. Nowotny, *J. Chromatogr.*, 441 (1988) 155.
11 K. Grob, *Making and Manipulating Capillary Columns for Gas Chromatography*, Hüthig, Heidelberg, 1986, p. 124.
12 D. Armstrong, W. Li, Ch. D. Chang and J. Pithe, *Anal. Chem.*, 62 (1990) 914.
13 D. Armstrong, W. Li and J. Pithe, *Anal. Chem.*, 62 (1990) 214.
14 V. Schurig, J. Buyten, J. Peene and Ph. Mussche, *J. High Resolut. Chromatogr.*, 13 (1990) 470.

Journal of Chromatography, 589 (1992) 265–270
Elsevier Science Publishers B.V., Amsterdam

CHROM. 23 706

Comparison of extraction methods for polychlorinated dibenzo-*p*-dioxins and dibenzofurans in fly ash using gas chromatography–mass spectrometry

Adrian Beard, Krishnat Naikwadi and Francis W. Karasek*

Department of Chemistry, University of Waterloo, Waterloo, Ontario N2L 3G1 (Canada)

(First received April 25th, 1991; revised manuscript received August 23rd, 1991)

ABSTRACT

Four method for the extraction of polychlorinated dibenzo-*p*-dioxins and dibenzofurans in municipal solid waste (MSW) incinerator fly ash samples were examined. A Soxhlet method was found to be the most efficient. However, the time required for extraction was more than 24 h. Ultrasonic extraction (UE) proved to be an inexpensive, efficient, reliable and rapid method. Studies of the effect of extraction time and temperature in UE showed that higher temperatures, longer times of extraction and increased number of repeated extractions with fresh solvent resulted in higher extraction efficiency.

INTRODUCTION

Polychlorinated dibenzo-*p*-dioxins (PCDDs) and dibenzofurans (PCDFs) are the major toxic chlorinated organic contaminants of fly ash, and are produced by the incineration of any kind of waste that provides the necessary precursors [1–5]. The formation of PCDDs and PCDFs from combustion is a universal phenomenon. They have been detected in the emissions from automobiles, domestic stoves, furnaces and especially in minicipal solid waste (MSW) incineration, where they first were detected in fly ash by Olie *et al.* [1]. Because of their extremely high toxicity [6,7] and uncertain genotoxic potential [8], their determination in environmental samples is of great interest. In particular, the determination of PCDDs and PCDFs in MSW incinerator fly ash is important, because thousands of tons of such fly ash are produced every day.

MSW incinerator fly ash is usually extracted using a Soxhlet method for the isolation of organic pollutants. Soxhlet extraction (SE) is very time consuming and needs large amounts of organic solvents (350 ml) such as toluene or benzene. Ultrasonic extraction (UE) has been demonstrated to be a viable method for the extraction of other non-volatile organics, *e.g.*, polycyclic aromatic hydrocarbons in fly ash [9,10]. Previous studies of the UE of fly ash employed solvent and sample amounts comparable to those in the Soxhlet method, resulting in unsatisfactory extraction efficiencies for PCDDs and PCDFs [11].

This paper describes four methods for the extraction of PCDDs and PCDFs from MSW incinerator fly ash. A typical SE requires 350 ml of solvent, at least 5 g of fly ash and 24 h of extraction time. The UE method studied here required 60 ml of solvent, 1.0 g of fly ash and 4.5 h for effective extraction. Advantages of the UE method over other methods of extraction are discussed.

EXPERIMENTAL

Samples and materials

The fly ash was from an MSW incinerator in the USA. The same batch of fly ash was used in all experiments. Prior to extraction the fly ash was sieved and the fraction containing smaller particles

0021-9673/92/$05.00

(< 150 μm) was used for extraction. Except for the SE, where 5.0 g were used, in all other methods 1.0 g of fly ash used.

Benzene and toluene were obtained from BDH (distilled-in-glass, suitable for chromatography and residue analysis). Quantification was done with a [^{13}C]PCDD standard mixture, which was synthesized in our laboratory [12] and contained the following concentrations (ng/μl) of each congener group: tetra(T)CDD (0.2), penta(P)CDD (1.0), hexa(H_6)CDD (3.0), hepta(H_7)CDD (4.0) and octa (O)CDD (1.8). The same standard was used for spiking the fly ash for recovery estimates. PCDFs were quantified externally using a standard containing a total of 9.7 ng/μl of PCDFs.

Procedures

Four methods of extraction were studied. Repeated extractions of fly ash samples from the same bulk of the stock fly ash were conducted separately for each method. All primary extracts obtained were concentrated to a volume of 1–2 ml using rotary evaporation and then further concentrated to *ca.* 50 μl in vials by a gentle stream of high-purity nitrogen. The exact volume of extract for each sample was determined using a high-performance liquid chromatographic syringe immediately after gas chromatographic–mass spectrometric (GC–MS) analysis. The general procedures used for all methods of extraction were as follows.

Soxhlet extraction (SE). Detailed procedures for Soxhlet extraction were reported previously [13]. Our extractions were conducted using 5 g o fly ash samples and different times and amounts of organic solvents (see Table II).

Acid digestion and Soxhlet extraction (ADSE). A 5-g amount of fly ash and 60 ml of 1 *M* hydrochloric acid were sonicated for 1.5 h at 45°C. The fly ash was filtered using a Buchner funnel and washed with 3 × 50 ml of deionized water (until the filtrate was neutral). The aqueous filtrate was extracted with 100, 50 and 50 ml of toluene in a separating funnel. The filter with the fly ash residue was placed in a glass thimble and extracted in a Soxhlet apparatus using 300 ml of toluene for a specific time. Both extracts (filtrate and Soxhlet) were combined before the concentration step.

Extraction by column elution (ECE). A 1.0-g amount of fly ash was packed into a glass column (20 cm × 0.8 cm I.D.) containing a glass-wool plug at the bottom. The column was eluted using 240 ml of benzene in three fractions of 80 ml which were collected and analysed separately. As the flow was driven only by gravity, each fraction took *ca.* 75 min to elute. The column was kept at 25°C during the elution. It is possible to heat the column to 100°C to increase the extraction efficiency [14].

Ultrasonic extraction (UE). A Branson Model 5200 ultrasonic bath (9.4 l, ultrasonic unit 200 W) was used. A water-filled supporting beaker containing capped test-tubes with fly ash and solvent was suspended from the lid of the bath. A maximum of six test-tubes were sonicated at once. Although the bath has a thermostat to set and control the temperature, it varied over a range of 3–4°C during the experiment. The temperature values given are the averages of several measurements of the water temperature in the beaker. Several experiments were conducted to study the effect of variation of the conditions of ultrasonication for the extraction of PCDDs and PCDFs from the fly ash samples.

Treatment of extracts. All sample extracts were first screened by GC with electron-capture detection (ECD) to assess the amount of chlorinated compounds present and whether the sample was suitable for GC–MS analysis. The instruments and conditions used are summarized in Table I. The detection limit of the applied methods is about 2 ppb[a] per congener group totalling 10 ppb of PCDDs. Several extractions were conducted using the above four methods. Although the SE method is used traditionally for the extraction and isolation of environmental contaminants from solid samples, the method is time consuming, requiring more than 24 h for satisfactory extraction. In addition, it requires large amounts of solvent (350 ml) and sample (usually more than 5 g). Hence there is a need for a simple, less expensive and reliable method for the extraction of environmental contaminants from solid samples such as MSW incinerator fly ash.

RESULTS AND DISCUSSION

The amounts of dioxins extracted using the four methods of extraction under various conditions are given in Table II. All the experiments reported were

[a] Throughout this article, the American billion (10^9) is meant.

TABLE I

INSTRUMENTS AND CONDITIONS FOR GC–MS

Gas chromatograph	Hewlett-Packard 5890
Mass-selective detector	Hewlett-Packard 5970
Workstation	Hewlett-Packard 59970
Column	DB-5, 30 m × 0.25 mm I.D.
Injection	On-column, volume 1 or 2 μl
Temperature programme	80°C for 1 min, 15°C/min to 230°C, then 3°C/min to 300°C, held for 10 min
Run time	45 min
Ionizing voltage	70 eV
Ions monitored	$[M-COCl]^+$, M^+, $[M+2]^+$, $[M+4]^+$, for each congener group of tetra- to octa-CDD and -CDF, and ^{13}C-labelled CDD.
Retention time windows	14.5, 18.5, 22.5, 26.5, 31.0, 35.0 min for tetra-, penta-, hexa-, hepta- and octa-CDD and -CDF, respectively.

repeated three times. The amounts of total PCDDs and PCDFs extracted varied within ±5% in the repeated experiments.

For the recovery study, fly ash was spiked with a ^{13}C-labelled dioxin mixture prior to extraction. The relative extraction efficiency of a particular method can be assessed based on the recovery of the added ^{13}C-labelled reference material. The amount of total dioxins extracted using the four different methods and the values corrected according to recoveries are shown in Fig. 1. In the SE method two solvents, benzene and toluene, were studied. Toluene was better than benzene with respect to efficiency of extraction of dioxins. Moreover, toluene is easier to handle than the highly carcinogenic benzene. From Fig. 1 it can be seen that the SE and the ADSE methods have similar extraction efficiencies for PCDDs. A minor difference in the efficiency for H_6CDD extraction was noticed, which was offset by smaller differences of opposite nature for other compounds. In the ADSE method acid digestion, filtration and extraction of the aqueous acidic layer are additional time-consuming steps compared to the straightforward SE of fly ash. The extraction efficiency does not differs significantly between the SE and ADSE methods. Hence Soxhlet extraction alone is satisfactory for the extraction of solid samples such as MSW incinerator fly ash.

The efficiency of the UE method for the extractionof PCDDs and PCDFs from fly ash was studied under different conditions with variations in extrac-

TABLE II

AMOUNTS OF DIOXINS EXTRACTED (CORRECTED FOR RECOVERIES USING INTERNAL STANDARD) FROM FLY ASH (ng/g) USING VARIOUS METHODS OF EXTRACTION UNDER VARIOUS CONDITIONS

Experiment No.	Method	Solvent	Time (h)	Temperature (°C)	TCDD	PCDD	H_6CDD	H_7CDD	OCDD	Sum
1	SE	Benzene	24	40–60	2	75	220	240	86	620
2	SE	Toluene	48	40–80	16	200	410	740	280	1650
3	ADSE	Toluene	48	40–80	9	210	550	640	300	1710
4	ECE	Toluene	3.75	25	7	42	150	180	85	460
5	UE	Benzene	1.5	30	7	57	150	160	62	440
6	UE	Toluene	1.5	42	7	120	300	350	180	960
7	UE	Toluene	1.5	68	6	52	370	470	260	1160
8	UE	Toluene	1	68	7	130	330	450	240	1160
9	UE	Toluene	3	68	7	130	360	450	250	1200
10	UE	Toluene	6	68	7	120	380	480	270	1260
11[a]	UE	Toluene	1.5	68	7	31	72	98	61	270
12[a]	UE	Toluene	1.5	68	2	8	22	28	20	80
13[b]	UE	Toluene	1.5	68	2	8	22	28	20	80
14[b]	UE	Toluene	1.5	68	2	10	21	28	22	83

[a] Second extraction of the fly ash from experiments 9 and 10; quantification based on external standard, amounts not corrected for recoveries.

[b] Third extraction of the fly ash from experiments 9 and 10; quantification based on external standard, amounts not corrected for recoveries.

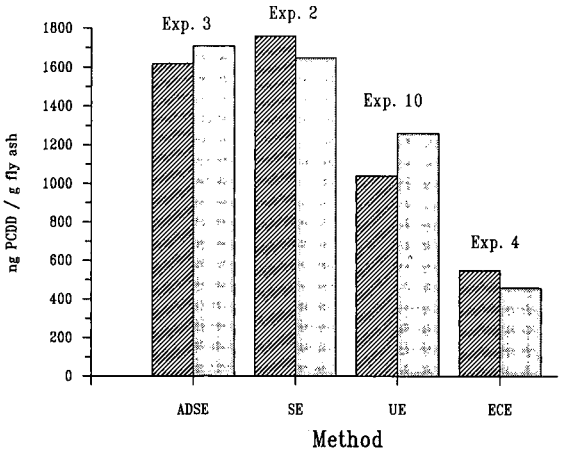

Fig. 1. Comparison of amounts of PCDDs extracted from MSW incinerator fly ash using different methods of extraction. See Table II for experiment numbers. Hatched boxes = quantified by external standard; dotted boxes = corrected for recovery of [^{13}C]PCDD.

tion time and temperature (Table II). It was observed that the extraction efficiency using the UE method was highest with higher temperatures and longer extraction times. Assigning the 24-h Soxhlet extraction a 100% extraction efficiency, about a 70% extraction efficiency was achieved within 1.5 h by UE at 68°C (experiment 7 in Table II). Re-extraction of the same fly ash twice and summation of the amounts of PCDDs and PCDFs, *i.e.*, the sum of experiments 9, 11 and 13 or of 10, 12 and 14, respectively, gave the amounts of total PCDDs and PCDFs extracted by UE, which were about the same as those of the SE method.

The temperature applied during extraction plays a very important role. The temperature during the SE method using benzene ranged from 40 to 55°C and using toluene from 45 to 80°C. In the UE method temperature can be controlled precisely. In this study the UE extraction was studied up to 68°C (which is the upper limit of the ultrasonicator) and the results are reported in Table II. Temperatures higher than 68°C in the UE method could have resulted in a higher extraction efficiency in a shorter time. The UE method also requires only 60 ml solvent and 1 g of fly ash sample compared with 350 ml of solvent and more than 5 g of fly ash needed in the SE method. The influence of temperature on extraction can also be seen from the amount of PCDDs extracted by SE at higher temperatures (45–80°C) and ECE at room temperature (25°C). Although the sample-to-solvent ratio (calculated) in the ECE is similar to that in the SE method, the extraction efficiency remains less than 50% for the ECE method. The efficiency of the ECE method can be improved by heating the column externally during the elution [14].

Fig. 2 shows the amounts of the individual tetra- to octachlorodioxins extracted from the fly ash. The pattern is a typical example of PCDDs detected in MSW incinerator fly ash, and was always the same, regardless of the total amount of dioxins extracted. The similarity of the pattern may be due to an even distribution of dioxins on and in the interior of the fly ash particles and specific solubilities of dioxin congeners in a particular solvent.

It was observed that in all the methods studied an increase in the temperature of the extraction resulted in a higher efficiency of the extraction of PCDDs from the fly ash. This might raise the question of whether PCDDs are formed from precursors by the catalytic activity of the fly ash at temperatures of about 50–80°C, which would lead to a seemingly enhanced extraction. To study this hypothesis, pre-extracted fly ash was spiked with pentachlorophenol (PCP). PCP has been shown to be an excellent and efficient precursor for the formation of PCDDs [15]. In order to distinguish between non-extracted native dioxins in the fly ash and those that were formed during the ultrasonic treatment at higher

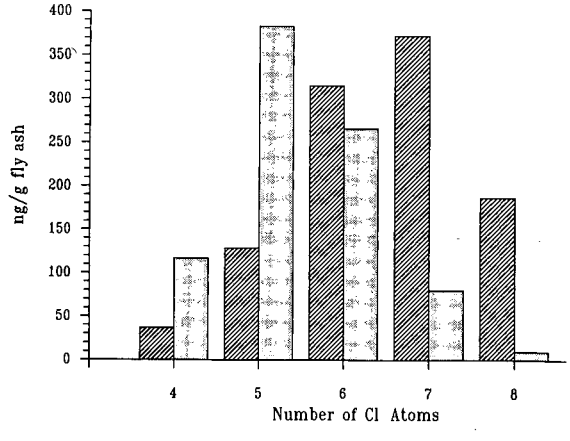

Fig. 2. Congener pattern for PCDDs and PCDFs extracted from MSW incinerator fly ash (experiment number 10 in Table II). Hatched boxes = dioxins; dotted boxes = furans.

temperatures, ^{13}C-labelled PCP used. ^{13}C-labelled dioxins were not detected in the extract of fly ash heated to 68°C during extraction. This leads to the conclusion that no dioxins are formed during ultrasonic treatment at a temperature of *ca.* 68°C for 3–6 h, at least not from chlorinated phenols, which are the most likely precursors for PCDDs at low temperatures. It has been reported that PCDD formation can occur above 150°C [15,16]. Hence it is less likely that the PCDDs and PCDFs are formed at 80°C during extraction, which was suggested recently [17].

Prolonging the ultrasonication time from 1.5 to 6 h, as shown in Fig. 3, had little effect on the amounts of PCDDs and PCDFs extracted. However, extracting the same sample (experiment 10) repeatedly with fresh solvent did yield larger amounts (Table II, experiments 11 and 12). From the overall comparison of the methods with respect to extraction efficiency, the methods ranked in the order acid digestion + Soxhlet = Soxhlet > sonication > column elution. Although acid digestion prior to Soxhlet extraction has been reported to be more effective [11], this was not found in our study. This shows that the efficiency of the method of extraction varies with different fly ash samples. The superiority of the Soxhlet extraction is due to the use of large amounts of solvent (*i.e.*, taking into account the total amount of solvent used and the cycle rate of "refreshing" the solvent). The temperature in the Soxhlet extractor reaches about 80°C if toluene is used, which seems to have a profound effect on the efficiency of extraction of PCDDs. The UE method can also recover a large portion of PCDDs and PCDFs from the fly ash. In the UE

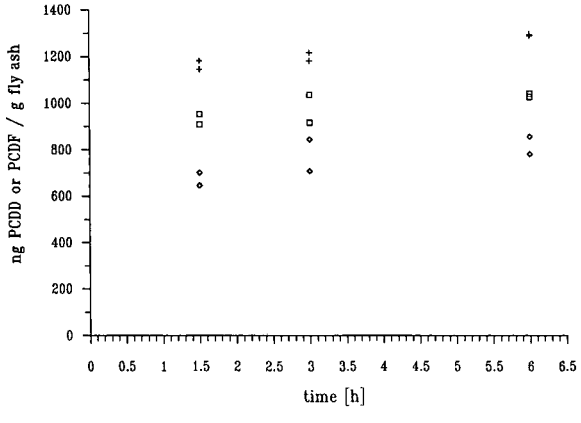

Fig. 3. Influence of sonication time on the amounts of PCDDs and PCDFs extracted. □ = PCDDs quantified by external standard; + = PCDDs corrected for recovery of [^{13}C]PCDD; ◇ = PCDF quantified by external standard.

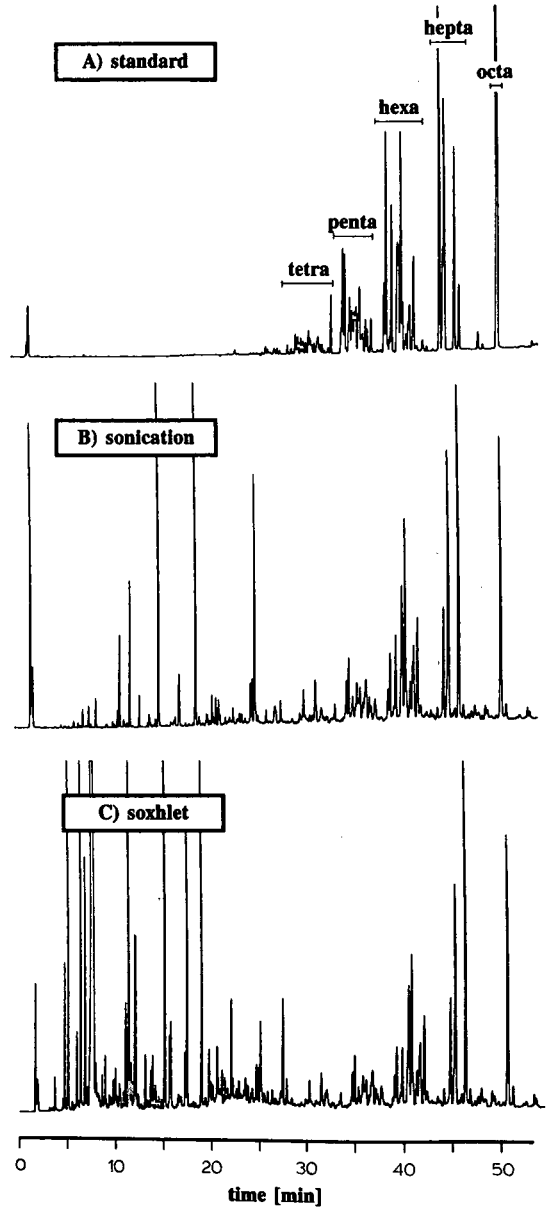

Fig. 4. GC–ECD showing PCDDs and PCDFs patterns in (A) standard containing labelled PCDDs (8.1 ng), native PCDDs (5.1 ng) and native PCDFs (14.2 ng); (B) sonication extract from experiment 10; and (C) Soxhlet extract from experiment 2.

method the solvent-to-sample ratio seems to be very important and renewal of the solvent once or twice during extraction increases the extraction efficiency considerably. In contrast to these methods, column elution only extracts the superficially adsorbed PCDDs and PCDFs on the fly ash, because even with large amounts of solvent, the amount extracted cannot be enhanced in experiment 6, where 98% of the PCDDs were extracted in the first 80 ml of benzene and the remaining 80-ml two fractions contained the rest. Temperature may have been a limiting factor because the elution was done at room temperature.

GC-ECD of fly ash extracts obtained by the SE and UE methods is shown in Fig. 4. In the retention time window of the PCDDs and PCDFs, there is no significant difference between two chromatograms resulting from sample extracts from the SE and UE methods. This shows that the UE method can be an excellent alternative to the time-consuming SE method. The peak patterns in the chromatograms are markedly different for the peaks eluting before a retention time of 20 min. Soxhlet extraction appears to be more efficient in extracting fast-eluting compounds, *i.e.*, compounds with higher volatility and lower molecular weight.

CONCLUSION

Ultrasonication is a fast, efficient and easy method for the extraction of PCDDs and PCDFs from MSW incinerator fly ash. It requires only 1 g of sample, 60 ml (3 × 20 ml) of toluene and an extraction time of 4.5 h (3 × 1.5 h), compared with more than 5 g of sample, 350 ml of toluene and more than 24 h in the Soxhlet extraction method. Hence the amounts of sample and solvent and the time required for the extraction of PCDDs and PCDFs by the SE method are about five times lower using the UE method. The UE method might also be applied to other matrices such as soil and sediments.

REFERENCES

1 K. Olie, P. L. Vermeulen and O. Hutzinger, *Chemosphere*, 8 (1977) 455.
2 W. B. Crummett and D. I. Townsend, *Chemosphere*, 13 (1984) 777.
3 C. L. Hail, R. B. Blair, J. S. Stanley, D. P. Redford and R. M. Lucas in G. Choudhary, L. H. Keit and C. Rappe (Editors), *Chlorinated Dioxins and Dibenzofurans in the Total Environment*, Butterworth, London 1983, p. 439.
4 A. Cavallaro, *Chemosphere*, 9 (1980) 611.
5 R. C. Lao, C. Chiu, R. S. Thomas, K. Li and J. Lockwood, *Chemosphere*, 12 (1983) 607.
6 J. A. Bradlaw and J. L. Caferline, *J. Assoc. Off. Anal. Chem.*, 62 (1976) 904.
7 A. Poland, E. Glover and A. S. Kende, *J. Chem. Biol.*, 251 (1976) 4926.
8 *Polychlorinated Dibenzo-p-dioxins and Dibenzofurans (Environmental Health Criteria*, 88), World Health Organization, Geneva, 1989.
9 W. H. Griest, B. A. Tomkins and J. R. Caffrey, *Anal. Chem.*, 60 (1988) 2169.
10 G. A. Junk and J. J. Richard, *Anal. Chem.*, 58 (1986) 962.
11 R. M. M. Kooke, J. W. A. Lustenhouwer, K. Olie and O. Hutzinger, *Anal. Chem.*, 53 (1981) 461.
12 K. P. Naikwadi and F. W. Karasek, *Int. J. Environ. Anal. Chem.*, 38 (1990) 329.
13 K. P. Naikwadi, F. W. Karasek and H. Hatano, *J. Chromatogr.*, 511 (1990) 281.
14 L. C. Dickson, D. Lenoir, O. Hutzinger, K. P. Naikwadi and F. W. Karasek, *Chemosphere*, 19 (1989) 1435.
15 F. W. Karasek and L. C. Dickson, *Science*, 237 (1987) 754.
16 K. P. Naikwadi and F. W. Karasek, in R. Clement and R. Kagel (Editors), *Emissions from Combustion Processes*, Lewis, Boca Raton, Ann Arbor, Boston 1990, 57.
17 N. Alexandrou and J. Pawliszyn, *Anal. Chem.*, 61 (1989) 2770.

Journal of Chromatography, 589 (1992) 271–279
Elsevier Science Publishers B.V., Amsterdam

CHROM. 23 646

Determination of sulfur components in light petroleum streams by high-resolution gas chromatography with chemiluminescence detection

Birbal Chawla* and Frank Di Sanzo

Mobil Research and Development Corporation, Paulsboro Research Laboratory, 600 Billingsport Road, Paulsboro, NJ 08066 (USA)

(First received May 30th, 1991; revised manuscript received July 25th, 1991)

ABSTRACT

A versatile high-resolution gas chromatographic system utilizing universal sulfur chemiluminescence detection (USCD) coupled with flame ionization detection (FID) was optimized for the determination of sulfur components in light petroleum process streams. The normalized area precision for individual species was *ca.* 1.5–6.0% (relative standard deviation) for the major components at a total 1.7 (w/w) of sulfur level. The system is capable of speciating sulfur components in petroleum process streams containing 0.01–3.13% (w/w) of sulfur. The linear relationship (r^2 = 0.998) between the USCD absolute sulfur response and the total sulfur content of several samples of petroleum process streams clearly indicated that, in addition to speciation, total sulfur can simultaneously be determined with reasonable accuracy.

INTRODUCTION

Sulfur compounds are one of the most important heteroatom constituents of petroleum and are often determined by gas chromatography (GC) using flame photometric detection (FPD). FPD was introduced in 1966 by Brody and Chaney [1] and it continues to have widespread use [2,3]. Other commercially available detectors for sulfur determination are the electrolytic conductivity (Hall) detector [2,4,5], atomic emission detector [2,6,7] and electron-capture detector [8].

Although FPD is widely used, it has several major drawbacks. FPD is based on the S_2^* chemiluminescence emission bands at 384 and 394 nm [3]. The electronically excited S_2^* species are formed by the sulfur atoms produced in a hydrogen-rich flame. The intensity (I) of this emission which is due to the molecular band, is of the form $I = [S]^n$. The exponent n is theoretically 2, but the response to sulfur ranges between first and second order, depending on the heteroatom environment [9]. The FPD response is also affected by co-eluting water or hydrocarbons, which can quench the chemiluminescence to a significant extent [10,11]. Although dual-flame photometric detectors have been developed to overcome some of these problems, they generally suffer from hydrocarbon interference at trace sulfur levels.

During the last decade, several attempts have been made [12–15] to develop a system for "universal" sulfur-selective chemiluminescence detection (USCD). Recently, such a detector has become commercially available. The USCD instrument is coupled directly to the flame housing of a flame ionization detection (FID) instrument. Benner and Stedman [16] demonstrated that the USCD responses to individual sulfur compounds were equal on a sulfur weight basis and hydrocarbon interferences were minimal. Further, there was no decrease in the detector response or any interferences from carbon dioxide and water vapor. It was also shown that USCD was very sensitive and provided detection limits that are at least 10–15 times lower than that of FPD.

This paper describes the optimization and oper-

0021-9673/92/$05.00

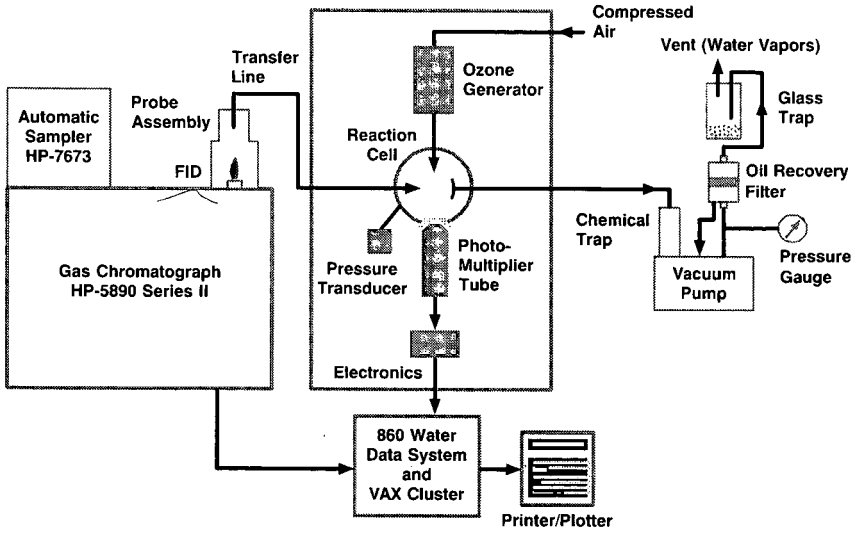

Fig. 1. Schematic diagram of the major components of a universal sulfur chemiluminescence detection system.

ational characteristics (linear response, sensitivity and stability) of a universal sulfur chemiluminescence detector coupled to a gas chromatograph. The identification of a series of sulfur components such as thiophene (TH), benzothiophene (BTH), dibenzothiophene (DBTH) and their alkyl-substituted homologs present in various light petroleum process streams (catalytically cracked gasolines, kerosenes and diesels) are also reported. The sulfur content of the samples investigated covers a wide range of 0.01–3.13% (w/w).

EXPERIMENTAL

A schematic diagram of the major components of the Model 350 universal sulfur-selective chemiluminescence detector (Sievers Research, Boulder, CO, USA) coupled to a gas chromatograph is shown in Fig. 1. A probe assembly was mounted on top of a flame ionization detector. The probe was preset high (*ca.* 5 mm) above the flame to avoid being damaged when inserted. The optimum position of the probe was determined by adjusting the Allen screw on top of the flame interface housing. At the optimum probe position, the FID background signal as monitored by a Hewlett-Packard Model 5890 GC digital display was *ca.* 250 ± 50 pA at a range of 2.

The combustion products formed in the flame were transferred under a reduced pressure of about 9 ± 2 Torr to the chemiluminescence reaction chamber. A high-capacity vacuum pump (Model E2M5; Edwards High Vacuum, West Sussex, UK) was used. To minimize oil loss, a large coalescing oil return/recovery filter (P/N 18/18-371H; Ditto, Mount Laurel, NJ, USA) was fitted to the pump exhaust outlet to trap vaporized oil. A pressure gauge was also installed between the oil return/recovery filter and the pump (see Fig. 1) to monitor potential plugging of the filter during its continuous use. The outlet of the oil filter was then atttached to a glass trap for collecting the outgoing water–oil emulsion and then finally to a vent line. During method development, no clogging of the oil return/recovery filter was observed over a period of 2–3 months. The pump was filled with Mobil 1 oil and remained in continuous use (24 h per day) for about 2–3 months without requiring an oil change or any replacement of the oil return/recovery filter. In order to remove unreacted ozone, nitrogen oxides and other potentially oil-destructive gases, a trap containing Hopcalite (Callery Chemical, Pittsburgh, PA, USA) and soda-lime (7:3, v/v) was placed between the reaction cell and the vacuum pump.

A Hewlett-Packard Model HP-5890 Series II gas chromatograph, equipped with a split/splitless in-

jection port, an automatic sampler (HP-7673) and a flame ionization detector was employed under the following operating conditions: column, DB-1 (60 m × 0.25 mm I.D.), 0.25-μm film thickness (J & W Scientific, Folsom, CA, USA); oven temperature, programmed from 35 to 100°C at 10°C/min and then to 225°C at 2°C/min, with a final hold for 20 min; injector, split/splitless, used in split mode at 275°C; injector insert, capillary liner (unpacked), HP P/N 18740-80190; injection volume 0.5–1.0 μl (neat sample); FID range, 2; carrier gas, helium; split vent, 100 ml/min; purge vent, 1.4 ml/min; column-outlet flow-rate, 2.0 ml/min (ambient temperature); linear velocity, 30 cm/s (methane at 35°C); air flow-rate, 375 ml/min (38 p.s.i.g.); hydrogen flow-rate, 180 ml/min (60 p.s.i.g.); column head pressure, 35 p.s.i.g.; run time, 95 min; USCD probe, ceramic, 105 mm × 1.3 mm O.D. × 0.5 mm I.D. (Sievers); probe conditioning: 3–4 h at air flow-rate 600 ml/min (50 p.s.i.g.), hydrogen flow-rate 230 ml/min (70 p.s.i.g.) and pump exhaust line pressure 0–1 p.s.i.g.; and USCD signal control, 0.06 s (integrated time for photon counts).

Proper positioning of the probe in the flame ionization detector is critical for long-term USCD stability. The probe is correctly positioned if the last 2–3 mm of the probe tip are glowing when the probe is rapidly but carefully removed from the FID tower assembly. The position of the probe is adjusted by using the two Allen screws on the probe assembly.

Data acquisition, processing, storage and retrieval were performed using a Waters Assoc. 860 Networking Computer System coupled with an in-house VAX cluster.

RESULTS AND DISCUSSION

Optimization of sulfur chemiluminescence detector

A dilute solution of dibenzothiophene ($1.28 \cdot 10^{-6}$ mol/ml) in *n*-heptane was used to optimize the air and hydrogen flow-rates (Figs. 2–5). The optimum conditions for USCD were air at 38 p.s.i.g. (375 ml/min) and hydrogen at 60 p.s.i.g. (180 ml/min) (Figs. 2 and 4). The maximum FID and USCD responses were attained at similar air flow-rates (Figs. 2 and 3). However, the FID response decreased linearly with increasing hydrogen flow-rate (Fig. 5) and, at the USCD-optimized hydrogen flow-rate the FID response was less than the FID response when operated under conventional conditions.

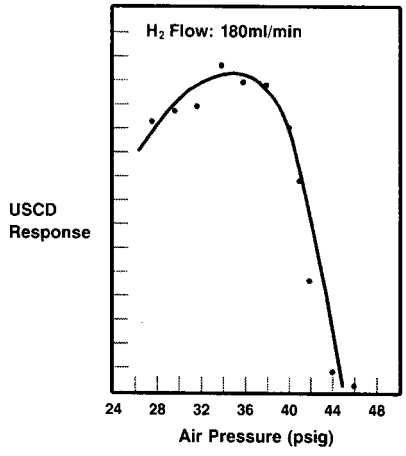

Fig. 2. USCD response *vs.* air pressure (hydrogen flow-rate 180 ml/min).

Optimization of GC separation

Three fused-silica capillary columns were investigated for the GC separation of light petroleum streams: (i) Petrocol DH (100 m × 0.25 mm I.D.), 0.50-μm film thickness (Supelco, Bellefonte, PA, USA); (ii) DB-1301 (30 m × 0.25 mm I.D.), 0.25-μm film thickness (J&W Scientific, Folsom,

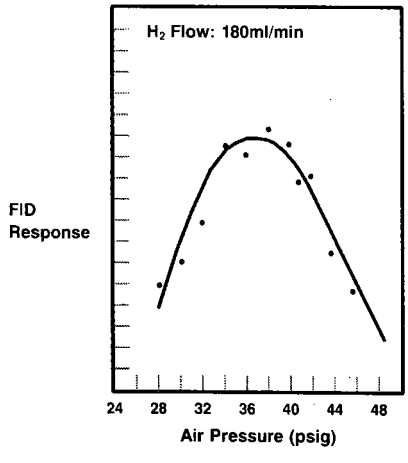

Fig. 3. FID response *vs.* air pressure (hydrogen flow-rate 180 ml/min).

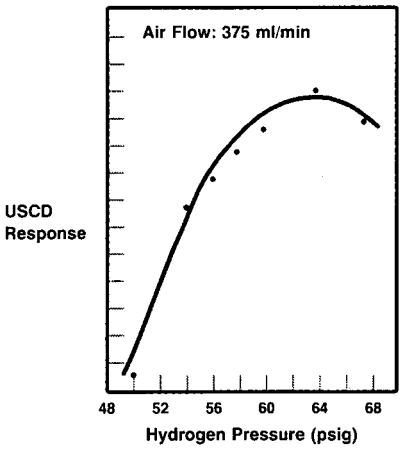

Fig. 4. USCD response *vs.* hydrogen pressure (air flow-rate 375 ml/min).

CA, USA); and (iii) DB-1 (60 m × 0.25 mm I.D.), 0.25 μm film thickness (J&W Scientific). Although the 100-m column gave satisfactory separations of sulfur species in gasoline and diesel range streams, it encountered two difficulties. First, the column bled excessively at the final column temperature of about 300°C. As the USCD probe was very sensitive to column bleeding, the 100-m column was found to be unsuitable for quantitative work. Second, the analysis time was relatively long (*ca.* 160 min). The 30-m (DB-1301) column did not yield satisfactory resolution of the sulfur species. The 60-m (DB-1) column gave acceptable resolution in the shortest analysis time.

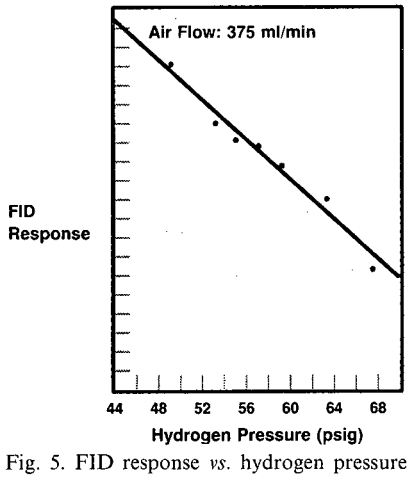

Fig. 5. FID response *vs.* hydrogen pressure (air flow-rate 375 ml/min).

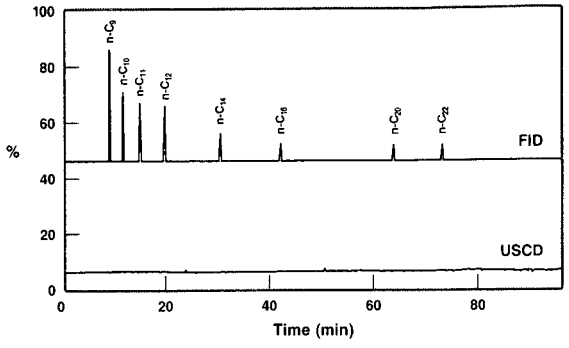

Fig. 6. FID and USCD chromatograms for a mixture of *n*-alkanes.

In order to obtain quantitative results from the GC separations, it was essential to minimize injection port sample discrimination. A mixture containing C_9–C_{22} *n*-alkanes was analyzed using FID (Fig. 6). It was found that extending the capillary column 6–7 mm rather than the 2–4 mm recommended by Hewlett-Packard from the end of the ferrule into the injection port splitter gave the best quantitative results. Excellent agreement was obtained between the actual % (w/w) and the experimentally observed % (w/w) for each of the *n*-alkanes present in the mixture (Table I).

TABLE I

MASS DISCRIMINATION OPTIMIZATION OF THE GC SYSTEM

n-Alkane	Retention time (min)	Concentration (%, w/w)			
		Actual	Experimental		
			FID (300°C)[a]	FID[b]	
				300°C	275°C
C_9	9.60	26.53	26.63	27.21	27.07
C_{10}	12.19	11.63	11.54	11.78	11.67
C_{11}	15.69	13.84	13.62	13.88	13.60
C_{12}	20.20	20.83	20.36	20.67	20.52
C_{14}	30.89	10.56	10.14	10.13	10.14
C_{16}	42.27	6.25	6.30	6.11	6.08
C_{20}	63.64	5.91	6.26	5.69	5.93
C_{22}	72.93	4.45	4.90	4.20	4.57

[a] GC–FID results obtained under normal FID hydrogen/air conditions at an injector temperature of 300°C.

[b] GC–FID results obtained under FID hydrogen/air conditions optimized for maximum USCD sulfur response at two injector temperatures.

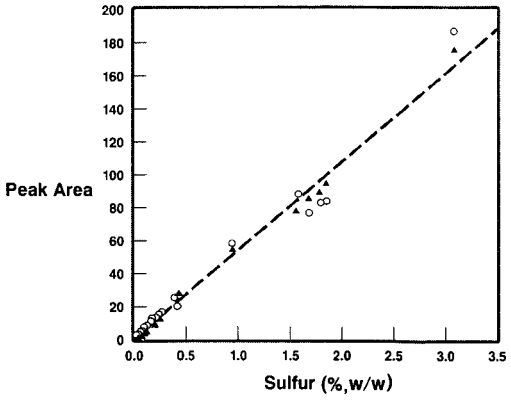

Fig. 7. USCD response at two injector temperatures. ○ = 300°C, area × 10^{-6} = 52.665 [S] + 0.4095, r^2 = 0.976. ▲ = 275°C, area × 10^{-6} = 52.808 [S] − 0.3855, r^2 = 0.993.

Effect of injector temperature on USCD linear response

The USCD has been shown to have a linear response [17,18] which is generally independent of the sample compound. In order to establish its linear response and its detection limits, 22 samples of light petroleum streams (gasoline, kerosene, diesel boiling point range) with various sulfur contents from 0.03 to 3.13% (w/w) were analyzed under the same chromatographic operating conditions. The USCD response for all these samples in terms of total area under the resulting peaks was plotted against the total sulfur content. These samples were analyzed at two different injector temperatures, 300 and 275°C. The linear fits for the data obtained at two temperatures are presented in Fig. 7. The USCD response increases linearly with increasing sulfur content. The linear fit was better when the injector temperature was 275°C ($r^2 = 0.993$ *versus* 0.976 at 300°C), perhaps because of improved injector splitter performance and/or decreased losses of the more reactive sulfur species (sulfides, thiols) present in some of the samples. It was decided to use 275°C as the injector temperature for subsequent work.

Identification of organosulfur compounds in petroleum process streams

A dilute solution (1.28 · 10^{-6} mol/ml) of dibenzothiphene in *n*-heptane was used to confirm the USCD selectivity (Fig. 8). Under USCD-optimized operating conditions, only DBTH was detected.

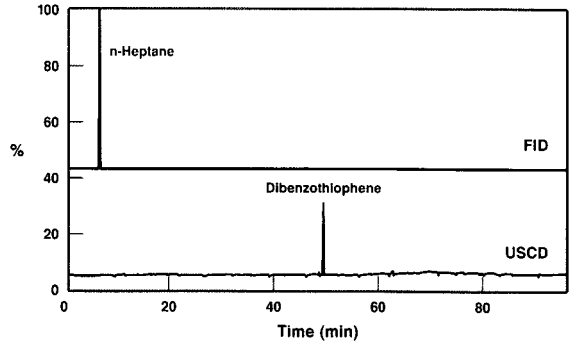

Fig. 8. FID and USCD responses for a dilute solution of dibenzothiophene.

The USCD/FID chromatograms for a diesel range petroleum stream and a catalytically derived FCC gasoline range stream are shown in Figs. 9 and 10, respectively. The sulfur-containing compounds were identified by comparision of their retention times with those of reference standards (Table II) and/or by GC–mass spectrometry (MS).

Precision

The short-term precision of the USCD response in terms of absolute total peak area was determined by making several independent injections of a light petroleum process stream. The precision of the USCD data was found to be better than 3%, indicating that the USCD has good short-term stability when properly optimized.

The precision of the normalized sulfur weight percentage of several selected thiophene groups was determined for a diesel range sample (Fig. 9, Table III). The USCD data showed that 70% of the thiophene groups had a precision of better than 3%. The precision of relatively smaller amounts of unsubstituted benzothiophene and dibenzothiophene was *ca.* 8% and that of a "sulfides and thiophenes" group, which was spread over a section of the initial 18 min of the chromatogram and was only *ca.* 0.5% (w/w) of the total sample, could be obtained with a precision as high as 24%.

Because of the long-term drift in the USCD absolute response, frequent calibrations are necessary. Although not investigated here, the use of an internal standard may resolve the drift in response provided that a reasonable wide "window" is available in the chromatogram. If only the normalized

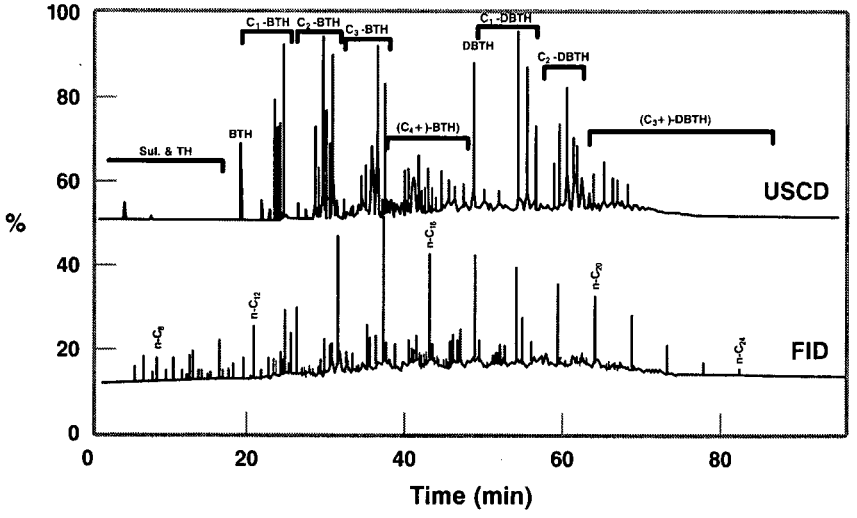

Fig. 9. Comparison of USCD and FID chromatograms obtained from a single injection of a light petroleum stream (1.73%, w/w, S).

area percentage response is required, then the long-term drift problem is not critical as long as the USCD instrument is properly installed and optimized.

Comparison between different probes

After 2 months of continuous use, the USCD response had decreased by a factor of approximately ten. A new probe was installed and conditioned as

TABLE II

RETENTION TIME DATA FOR SELECTED THIOPHENES

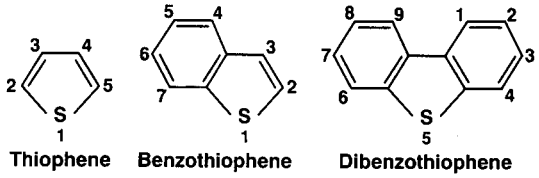

Compound	Retention time (min)	Compound	Retention time (min)
Thiophene	5.26	3,6-Dimethyl-	60.15
2-Methyl-	6.71	3-Ethyl-	60.18
3-Methyl-	6.81	3,7-Dimethyl-	60.91
2,5-Dimethyl-	8.56	2,8-Dimethyl-	60.94
Benzothiophene	18.43	3,8-Dimethyl-	60.98
3-Methyl-	24.08	1,4-Dimethyl-	61.17
Dibenzothiophene	48.25	1,6-Dimethyl-	61.25
4-Methyl-	53.71	1,8-Dimethyl-	61.40
3-Methyl-	54.77	1,3-Dimethyl-	61.82
2-Methyl-	54.74	3,4-Dimethyl-	61.95
1-Methyl-	55.89	1,9-Dimethyl-	62.04
4,6-Dimethyl-	59.01	2,4-Dimethyl-	62.07
2-Ethyl-	59.59	1,7-Dimethyl-	62.08
2,6-Dimethyl-	60.04	1,2- and 2,3-	62.79
1-Ethyl-	60.14	Dimethyl-	

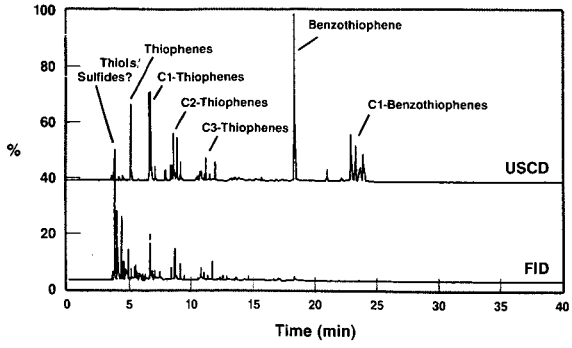

Fig. 10. Comparison of USCD and FID chromatograms obtained from a single injection of an FCC gasoline.

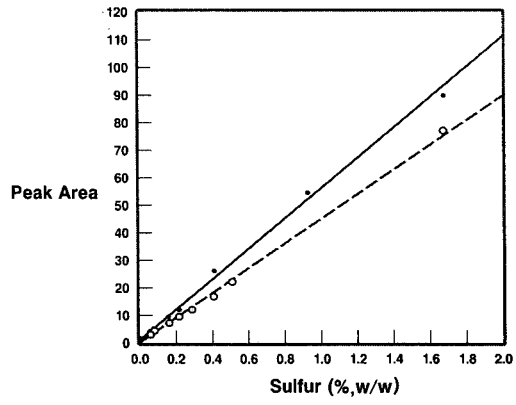

Fig. 11. USCD response with two different probes. ● = First probe, area × 10^{-6} = 55.362 [S] − 0.0304, r^2 = 0.997. ○ = Second probe, area × 10^{-6} = 46.075 [S] − 0.8645, r^2 = 0.998.

described above. Ten light petroleum stream samples were analyzed and the results were compared with those obtained with the old probe when new. The excellent linear fits obtained by plotting the USCD response against the sulfur content of the samples are shown in Fig. 11.

The precision of the data obtained using the two different probes remained approximately the same. However, the absolute USCD response obtained using the first probe immediately after conditioning

TABLE III

PRECISION OF THE USCD RESPONSE FOR SELECTED THIOPHENE GROUPS[a] PRESENT IN A LIGHT PETROLEUM STREAM (1.73%, w/w, S)

Injection No.	Contribution (wt.%)									
	Sul. and TH[b]	BTH	C_1-BTH	C_2-BTH	C_3-BTH	C_{4+}-BTH	DBTH	C_1-DBTH	C_2-DBTH	C_{3+}-DBTH
1	0.68	0.80	6.47	10.96	11.80	16.42	2.69	16.76	15.43	17.96
2	0.71	0.67	5.43	10.70	10.69	17.41	2.77	17.53	16.11	17.96
3	0.45	0.66	5.93	10.82	11.79	17.09	2.55	16.77	15.83	18.11
4	0.42	0.65	5.61	10.54	11.40	16.98	2.78	17.10	16.15	18.36
5	0.35	0.68	5.68	10.27	11.13	17.33	2.31	17.32	16.42	18.51
6	0.44	0.59	5.74	10.51	11.40	17.35	2.70	17.32	15.52	18.43
7	0.62	0.70	5.45	10.43	11.65	17.54	2.67	16.81	16.27	17.85
8	0.67	0.66	5.70	10.29	11.18	17.47	2.53	17.44	15.79	18.28
9	0.62	0.69	5.60	10.33	11.42	17.48	2.70	17.18	15.81	18.18
10	0.42	0.57	5.64	10.55	11.56	17.70	2.39	17.08	16.11	17.98
11	0.45	0.70	5.77	10.59	11.31	17.48	2.67	17.09	16.00	17.94
12	0.41	0.58	5.87	10.72	11.87	17.74	2.67	16.40	15.87	17.88
Mean	0.51	0.65	5.68	10.52	11.40	17.42	2.62	17.10	15.99	18.14
S.D.	0.12	0.05	0.15	0.18	0.33	0.25	0.15	0.33	0.26	0.23
R.S.D.[c] (%)	23.53	7.69	2.64	1.71	2.89	1.44	5.73	1.92	1.63	1.27

[a] See Fig. 9 for peak identifications.

[b] Sulphides and thiophenes grouping consisting of a number of sulfur compounds at low concentrations plus an unidentified peak which is probably due to H_2S.

[c] Relative standard deviation.

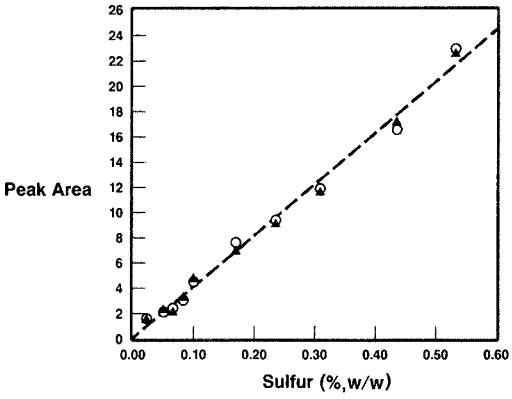

Fig. 12 Reproducibility of the USCD response with several light petroleum streams. ○ = Day 1, area × 10^{-6} = 41.478 [S] − 0.1070, R^2 = 0.999. ▲ = Day 2, area × 10^{-6} = 41.455 [S] − 0.0922, r^2 = 0.998.

was *ca.* 15–18% higher than that obtained using the new second probe. The difference in absolute responses with the two different probes was probably due to the different inner diameters of the probes and their position in the FID housing. The gaseous sample which is transferred from the flame ionization detector to the USCD reaction cell depends significantly on the probe inner diameter and the probe position in the flame ionization detector.

TABLE IV

COMPARISON OF USCD AND ELEMENTAL DETERMINATIONS OF TOTAL SULFUR IN LIGHT PETROLEUM STREAMS

USCD area × 10^6 ("unknown")	Sulfur (%, w/w)		Difference (%)
	Elemental	USCD data	
1.263	0.027	0.032	18.52
1.944	0.046	0.046	0.0
1.945	0.056	0.051	8.92
3.006	0.076	0.071	6.58
4.331	0.10	0.104	4.00
7.451	0.18	0.189	5.00
9.686	0.24	0.238	0.83
12.094	0.31	0.297	4.19
17.551	0.43	0.417	3.02
22.832	0.54	0.555	2.79

Determination of total sulfur by USCD

Ten samples of the light petroleum process streams with various sulfur contents from 0.027 to 0.54% (w/w) were used to evaluate whether the USCD can be used for determining the total sulfur content in addition to speciation. A new probe was installed and two sets of measurements were made on two different days. The USCD response (total peak area) data obtained from these two sets of measurements were plotted against total sulfur content (Elemental determinations). Two excellent and almost precisely overlapping linear relationships were observed between the USCD response and the sulfur content of the petroleum samples (Fig. 12).

The total sulfur contents of these ten samples were determined by treating the linear fit of day 1 as a calibration and using the total-peak-area data from day 2 as "unknown" samples. The results obtained are given in Table IV.

The excellent agreement between the USCD results and the elemental determinations of sulfur content (Table IV) strongly suggests that USCD could be used to determine total sulfur in the light streams within the accuracy indicated in Table IV.

ACKNOWLEDGEMENTS

We are grateful to R. A. Wolny for the GC–MS data and C. K. Lee, Mobil R&D, for providing the light petroleum stream samples and helpful discussions. We are grateful to Professor M. L. Lee of Brigham Young University for providing some of the sulfur standards.

REFERENCES

1 S. S. Brody and J. E. Chaney, *J. Gas Chromatogr.*, 4 (1966) 42.
2 M. Dressler, *Selective Gas Chromatographic Detectors*, Elsevier, Amsterdam, 1986, Ch. 7–9.
3 S. O. Farwell and C. J. Barinaga, *J. Chromatogr. Sci.*, 24 (1986) 483.
4 H. V. Drushel, *J. Chromatogr. Sci.*, 21 (1983) 375.
5 R. C. Hall, *J. Chromatogr. Sci.*, 12 (1974) 152.
6 P. C. Uden, Y. Young, T. Wang and Z. Cheng, *J. Chromatogr.*, 468 (1989) 319.
7 M. Zakaria M.-F. Gonnord and G. Guiochon, *J. Chromatogr.*, 271 (1983) 127.
8 J. E. Johnson and J. E. Lovelock, *Anal. Chem.*, 60 (1983) 812.
9 J. F. McGaughey and S. K. Gangwal, *Anal. Chem.*, 52 (1980) 2079.
10 C. D. Pearson and W. J. Hines, *Anal. Chem.*, 49 (1977) 123.

11 F. Berthou, Y. Dreano and P. Sandra, *J. High Resolut. Chromatogr. Chromatogr. Commun.*, 7 (1984) 679.
12 J. K. Nelson, R. H. Getty and J. W. Birks, *Anal. Chem.*, 55 (1985) 1767.
13 S. A. Nyarady, R. M. Barkley and R. E. Sievers, *Anal. Chem.*, 57 (1985) 2074.
14 J. S. Gaffney, D. J. Spandau, T. J. Kelly and R. Tanner, *J. Chromatogr.*, 347 (1985) 121.
15 A. A. Turnipseed and J. W. Birks in J. W. Birks (Editor), *Chemiluminescence and Photochemical Reaction Detection in Chromatography*, VCH, New York, 1989, Ch. 2, pp. 39–97.
16 R. L. Benner and D. H. Stedman, *Anal. Chem.*, 61 (1989) 1268.
17 R. L. Shearer, D. L. O'Neil, R. Rios and M. D. Baker, *J. Chromatogr. Sci.*, 28 (1990) 24.
18 R. S. Hutte, N. G. Johansen and M. F. Legier, *J. High Resolut. Chromatogr.*, 13 (1990) 421.

Journal of Chromatography, 589 (1992) 281–286
Elsevier Science Publishers B.V., Amsterdam

CHROM. 23 708

Use of oxidative degradation followed by capillary gas chromatography–mass spectrometry and multi-dimensional scaling analysis to fingerprint unresolved complex mixtures of hydrocarbons

A. T. Revill

Petroleum and Environmental Geochemistry Group, Department of Environmental Sciences, Polytechnic South West, Drake Circus, Plymouth, Devon PL4 8AA (UK)

M. R. Carr

Plymouth Marine Laboratory, West Hoe, Plymouth, Devon PL1 3DH (UK)

S. J. Rowland*

Petroleum and Environmental Geochemistry Group, Department of Environmental Sciences, Polytechnic South West, Drake Circus, Plymouth, Devon PL4 8AA (UK)

(First received June 25th, 1991; revised manuscript received August 27th, 1991)

ABSTRACT

Unresolved complex mixtures (UCMs) of hydrocarbons are a common feature of the gas chromatograms of bacterially degraded crude oils, some refined oils (*e.g.*, lube oils) and of oil-polluted sediment extracts. It is often difficult to identify the original source oil in polluted sediments by existing methods. A study was made of the use of chemical oxidation of ten UCMs to yield gas chromatographically resolvable compounds and analysis of the oxidation products by quantitative gas chromatography–mass spectrometry. The data were then used to calculate inter-sample Euclidean distances. These values were input into a multi-dimensional scaling program which allows similar samples to be clustered. This technique allows UCMs in a number of different sediments to be compared with their likely source oils.

INTRODUCTION

When crude oil is altered either by weathering processes in the environment, in oil reservoirs by bacteria or refining by man, the resulting residues often consist of chromatographically unresolved complex mixtures (UCMs) of hydrocarbons. The characterization of these UCMs is an important goal in oil pollution studies [1] and in oil–source rock and oil–oil correlation exercises in oil exploration geochemistry [2]. The distributions of the small amounts of resolved alkanes which survive weathering and bacterial degradation (usually called biomarkers [3–8]) are often used for these correlations, but these may not reflect accurately the identity of the original oils. Biomarkers rarely constitute more than 1% of the total hydrocarbons [9] and if mixtures of oils with different biomarker concentrations are present, their profiles may be misleading. Recent work has shown that oxidative degradation of UCMs yields some gas chromatographically resolvable products [10–12]. It has been suggested

0021-9673/92/$05.00

that these products (*e.g.*, acids, lactones and ketones) may be useful for "fingerprinting" UCMs [10]. Indeed, the oxidation products of UCMs isolated from sediments known to be contaminated with fresh Nigerian crude [13] and a tank oil [14] were successfully used to identify the source oils.

This paper describes modifications to the existing method for application to smaller amounts of UCMs (2 mg compared with 50 mg in the original study [10]), duplicate oxidations to test the reproducibility and quantification of the individual resolved oxidation products. The resulting data are analysed by cluster analysis and multi-dimensional scaling (MDS) in an attempt to improve upon the subjective comparisons made in the initial study. Application of the modified technique to a number of case studies is described.

EXPERIMENTAL

Samples

Samples (Table I) of Sullom Voe sediment (Garths Voe), Ninian crude oil, Mersey sediment (Dungeon's Lane) and Tia Juana Pesado crude oil were supplied by the Field Studies Council Research Centre (FSCRC), and a sample of the Esso *Bernicia* fuel oil was supplied by the Sullom Voe Oil Terminal.

Isolation and oxidation of UCMs

Oils and sediments were extracted and hydrocarbon fractions isolated by published methods [15]. Each hydrocarbon fraction was further separated by silver ion thin-layer chromatography to yield the "saturated aliphatic fraction", then desulphurized [16], and any resolved components were removed by urea clathration (and in some instances thiourea clathration [17]) to yield the UCMs.

Oxidation of the UCMs (*ca.* 2 or 50 mg) was carried out with chromium(VI) oxide–acetic acid [11] for 1 h at 70 ± 2°C (molar ratio of oxidant to substrate = 10:1). Oxidation of 2 mg samples was performed using microscale apparatus (Wheaton) with all reagents, where practical, scaled down in proportion to the original method. This was not possible with solvent volumes, and therefore all 2-mg oxidations were carried out in 1 cm^3 (*cf.*, 10 cm^3) of solvent.

Gas Chromatography (GC)

GC was carried out on a Carlo-Erba Mega series gas chromatograph fitted with a fused-silica capillary WCOT column (30 m × 0.32 mm I.D.) coated with DB-5 (0.1 μm film thickness) (J&W Scientific). On-column injection with temperature programming from 40 to 300°C at 5°C/min, followed by an isothermal period of 10 min, and hydrogen as the carrier gas at a flow-rate of 2 cm^3/min was employed.

Gas chromatography–mass spectrometry (GC–MS)

The GC conditions were as above except that helium was used as the carrier gas. A Kratos MS25 double-focusing mass spectrometer operating in the electron impact mode with source temperature 250°C, ionizing voltage 40 eV and filament emission current 400 μA was used.

Two internal standards (naphthalene-d_8 and perylene) were added to each sample at 5 μg mg^{-1} of oxidation products. Major oxidation products, *i.e.*, *n*-carboxylic acids, γ-methyl-γ-lactones and alkyl ketones, were identified by GC–MS as reported previously [10].

The peak heights and areas of each component were measured by integration using a Kratos DS90 data system with peak baselines adjusted manually. This integration data was then downloaded to a PC for further data processing.

Chromatogram comparison

The component peak heights in each mass chromatogram for each sample were compared with the corresponding mass chromatograms of all other samples. This was achieved using a purpose-written BASIC program which adjusted peak retention times by comparison with the internal standards and then compared peaks by retention time. A "window" of ± 5 s was set for a positive match. Any components found to be missing in a sample were given a height value of zero. All components were measured by comparison with the peak height of the internal standard (naphthalene-d_8, m/z 136, assuming a response factor of 1). Data were then transferred to an IBM mainframe computer for statistical analysis.

Statistical analysis

Euclidean distances were calculated using a pur-

pose-written program within the SAS statistical package, according to the following:

$$D_{jk} = \sum_{i=1}^{n} (x_{ij} - x_{ik})^2$$

where D_{jk} = distance between samples j and k, X_{ij} = peak i integral for sample j and X_{ik} = peak i integral for sample k.

Thus, each sample has a distance from all others in a multi-dimensional space [18], where, if N is the number of samples, there are $N-1$ dimensions. This analysis produces a distance matrix which is then analysed by cluster analysis [19] to identify groups of samples, followed by non-parametric MDS [20], which replaces distances with ranks. This projects the information onto two dimensions while maintaining the distances as closely as possible [21]. The resulting two-dimensional plot is only important in terms of the relative closeness of samples, the axes having no scales or units.

RESULTS AND DISCUSSION

Oxidation of the isolated UCMs produced good yields (total *ca.* 90%) of resolved (typically *ca.* 15%) and unresolved (typically *ca.* 85%) products, as found oreviously [10] (Table I). This was true whether smaller (*ca.* 2 mg) or larger (*ca.* 50 mg) UCM samples were oxidized. The components produced were typical of the method [10,11] and included resolved carboxylic acids, lactones and ketones (Fig. 1). Quantification, cluster analysis and MDS (see Experimental) produced the results shown diagramatically in Fig. 2 and 3. Although pattern recognition and various statistical methods (*e.g.*, principal components analysis, discriminant analysis, cluster analysis) have been widely reported for chromatographic data [22–26], the small number of samples (twelve) and relatively large number of variables (*ca.* 100 components) in this study required a different statistical approach to those commonly used. We therefore employed techniques developed for environmental analysis [21] (*e.g.*, the analysis of volatile organic compounds in water samples on a seasonal basis), where the statistical constraints are similar. Thus, a strategy of calculating the Euclidean distance between samples and the use of this information in a multi-dimensional scaling package was adopted. The method was then tested on a series of samples involving various degrees of hydrocarbon pollution in a number of sediments.

Samples 1–3: reproducibility study

Initial work [10] showed that the oxidation method produced reproducible yields and distributions of

TABLE I

GRAVIMETRIC DATA FOR ALL SAMPLES ANALYSED

Figures in italics are taken from ref. 10.

No.	Sample	Alkanes (%)	UCM[a] (%)	Total yield (%)	Oxidized[b] yield (%)
1,2	Silkolene 150 (2 mg)	78	86	94	–
3	Silkolene 150 (50 mg)	79	86	95	*71*
4	Amoco tank oil	*16*	*68*	*87*	–
5	Newgale beach oil	*16*	*21*	*75*	–
6	*Sivand* cargo	*55*	*76*	*83*	–
7	Humber sediment	*43*	*87*	*83*	–
8	Sullom Voe sediment	66	9	95	70
9	Ninian crude oil	52	31	89	55
10	*Bernicia* fuel oil	28	62	84	69
11	Tia Juana Pesado crude oil	22	85	87	71
12	Mersey sediment	55	80	95	40

[a] Urea non-adduct expressed as a proportion of total alkanes.

[b] Oxidized material is that not eluting with hexane from a silica gel chromatographic column.

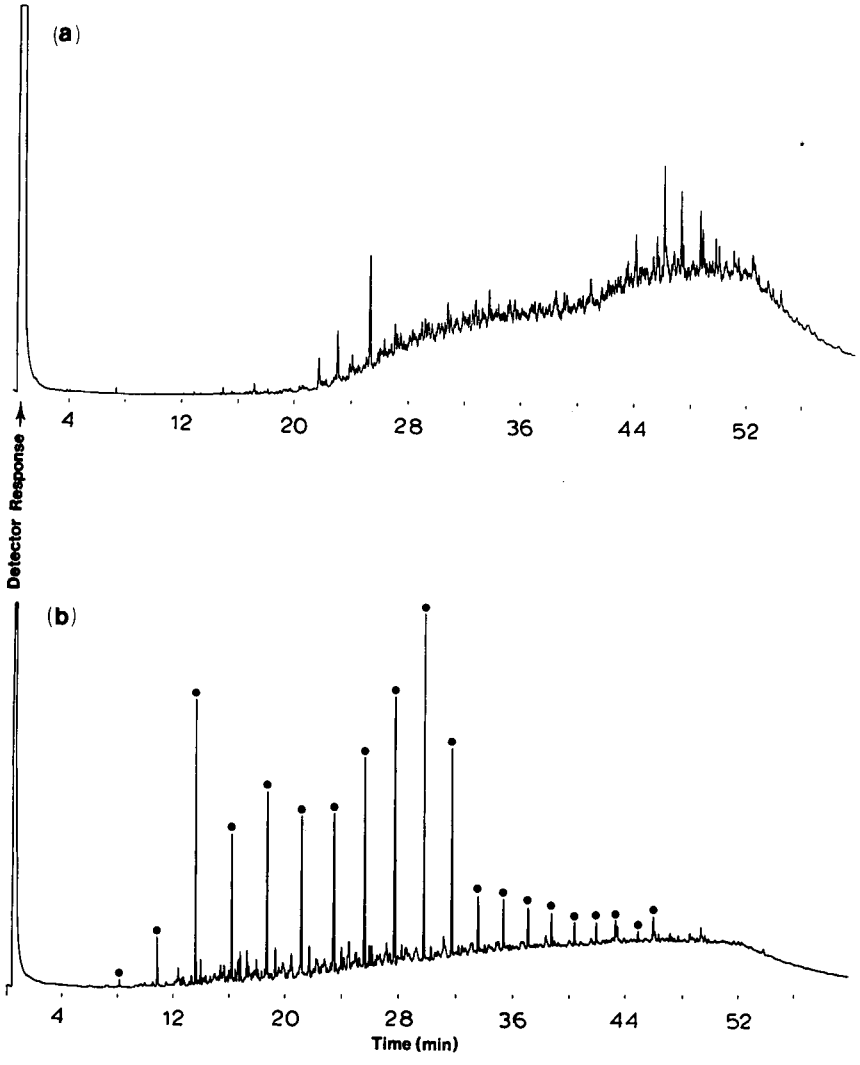

Fig. 1. Gas chromatograms of (a) fuel oil UCM and (b) total oxidation products. ● = *n*-Carboxylic acids.

products when 50-mg amounts of UCM isolated from grossly polluted sediments were oxidized. However, it was necessary to scale the method down for the present studies of long-term chronic hydrocarbon contamination as it was impracticable to isolate 50 mg of UCM from these sediments. About 2 mg was found to be the minimum practical working amount. To verify the oxidation method, 2- and 50-mg samples of lube oil (Silkolene 150) were oxidized (samples 1–3) and the results compared (Figs. 2 and 3). The two small-scale (2-mg) oxidations (samples 1 and 2) showed particularly good reproducibility and recovery (>90%), but they did not correlate well with the oxidation of the 50-mg sample (sample 3). This is not surprising. The oxidizing environments are very different owing to the different concentrations of oxidant involved (see Experimental). Initial results of the 2-mg duplicate analyses are encouraging, but further replication is obviously desirable, and will be carried out.

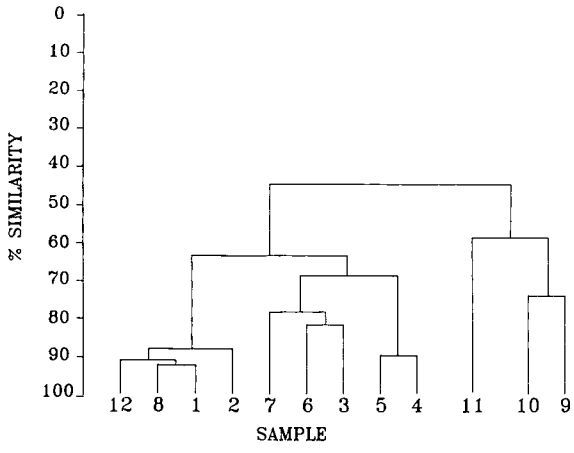

Fig. 2. Similarity dendrogram of all samples from cluster analysis. For sample identity, see Table I.

Sample 4–7: Amoco and Sivand oil spills

The initial UCM fingerprinting studies carried out by Gough and Rowland [10] involved two well documented, large oil spills. The qualitative results from these studies have been made quantitative and included in the present database for comparison. The results show a good correlation (*ca.* 90% similarity) between the Amoco tank oil and Milford Haven sediment as found previously [10]. The results for the *Sivand* oil (sample 6) and Humber sediment (sample 7) also show a good correlation (*ca.* 78% similar), although not as good as in the previous example. The latter result is also in agreement with previous work [13], and suggests that there have been other inputs of hydrocarbons to the Humber sediment in addition to the *Sivand* oil.

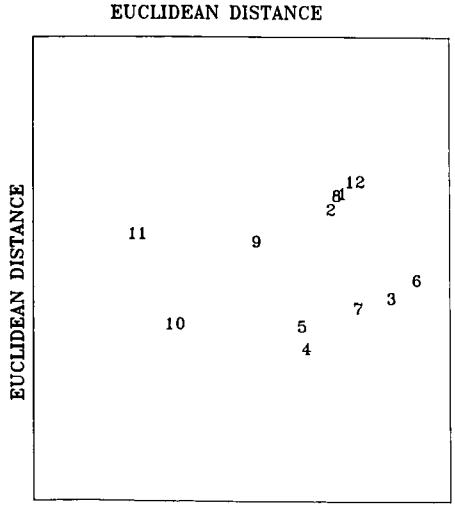

Fig. 3. All-samples plot of Euclidean distances from MDS analysis. For sample identity, see Table I.

Samples 8-10: Sullom Voe Oil Terminal

The Sullom Voe Oil Terminal (Shetland, UK) receives oil from the North Sea Ninian Field, which it then stabilizes and holds ready for transport. Despite the proximity of the oil terminal, numerous previous surveys of sublittoral sediments [27] in the area have shown that the concentrations of aliphatic hydrocarbons rarely exceed 100 μg/g dry sediment. However, in some sediments the GC profiles are mainly UCMs and interest has arisen as to their source. Several sources have previously been suggested, including a general background of chronic hydrocarbon accumulation, residues of Ninian crude oil possibly discharged with process waters, fuel oil spilled from the Esso *Bernicia* in 1978 [28] and a possible contribution from nearby peat deposits. Traditional biomarker techniques were not completely effective in fingerprinting these degraded oil residues, partly owing to difficulties caused by an input of biogenic triterpanes from nearby peat deposits [7,29]. The sterane distribution was more useful, but these compounds occur at lower concentrations in oils than the triterpanes and tend to be biodegraded more easily [30]. The results of UCM oxidation, GC–MS cluster and MDS analysis in this study showed that neither the Ninian (sample 9) nor the *Bernicia* (sample 10) oil UCMs were very similar ($\leqslant$50% similarity, Fig. 3) to the UCM in the sediments. Indeed, the clustering of the sediment, close to the Silkolene lube oil samples, suggests that a chronic accumulation from sources such as road runoff may be a more likely source [31]. The peat was found to contain no UCM, so this source can also be discounted.

Samples 11 and 12: Mersey oil spill

On August 19th, 1989, there was an accidental spillage of 150 tonnes of Tia Juana Pesado (TJP; Venezuela) heavy asphaltic crude oil from the Shell refinery at Stanlow, Elsmere Port, into the River Mersey estuary [32]. Early analyses using GC–MS to monitor biomarkers found no direct evidence for the presence of TJP crude oil in the Mersey sediments

[32]. This was mainly due to the high background concentration (*ca.* 200 ppm) of biomarker hydrocarbons from other sources. As it is heavily biodegraded, gas chromatograms of TJP oil exhibit a significant UCM of hydrocarbons and it was hoped that the UCM composition of the oil could be compared with that of the sediment by the oxidation method. Results of these analyses for the sediment (sample 11) and the TJP oil (sample 12) confirmed the biomarker results (< 50% similarity) that the spill of TJP has apparently had little impact on the overall sediment hydrocarbon loading (Figs. 2 and 3). TJP crude oil has a relatively low percentage of hydrocarbons (*ca.* 50%), of which 46% are aliphatic. This, combined with the already high background level of oil hydrocarbons in the sediments [32], suggests that the TJP is not a large contributor of UCM to the Mersey sediments.

CONCLUSIONS

The analysis of ten UCMs by oxidation, GC–MS and MDS has shown that the oxidation product profiles of these UCMs can be used to fingerprint different oils. The method is enhanced by the use of non-subjective multivariate statistical techniques and should prove useful in pollution studies and oil exploration as a means of characterizing and correlating degraded oils.

ACKNOWLEDGEMENTS

We thank Dr. M. Gough for access to samples and data, R. Srodzinski for help with the GC–MS and the Field Studies Council Research Centre (FSCRC) and Shetland Oil Terminal Environmental Advisory Group (SOTEAG) for samples and permission to publish data. The Natural Environment Research Council (NERC) is thanked for funding A.T.R. (Studentship GT4/88/AAPS/60) and BP for supporting the project.

REFERENCES

1 J. A. Butt (Editor-in-Chief), *Characterization of Spilled Oil Samples: Purpose, Sampling, Analysis and Interpretation*, Wiley, Chichester, on behalf of the Institute of Petroleum, London, 1986.
2 L. B. Magoon and G. E. Claypool (Editors), *Alaska North Slope Oil/Rock Correlation Study (AAPG Studies in Geology*, No. 20), The American Association of Petroleum Geologists, Tulsa, OK, 1985.
3 G. Pym, J. E. Ray, G. W. Smith and E. V. Whitehead, *Anal. Chem.*, 47 (1975) 1617.
4 W. K. Seifert and J. M. Moldowan, *Geochim. Cosmochim. Acta*, 42 (1978) 77.
5 W. K. Seifert, J. M. Moldowan and R. W. Jones, in *Proceedings of the 10th World Petroleum Congress, 1979*, Vol. 2, Heyden, London, 1980, p. 433.
6 R. P. Philp, *Geochim. Cosmochim. Acta*, 47 (1983) 267.
7 D. M. Jones, S. J. Rowland and A. G. Douglas, *Mar. Pollut. Bull.*, 17 (1986) 24.
8 K. E. Peters, J. M. Moldowan, A. R. Driscole and G. J. Demaison, *AAPG Bull.*, 73 (1989) 454.
9 J. Rullkotter, A. S. Mackenzie, D. H. Welte, D. Leythaeuser and M. Radke, *Org. Geochem.*, 6 (1984) 817.
10 M. A. Gough and S. J. Rowland, *Nature (London)*, 344 (1990) 648.
11 M. A. Gough and S. J. Rowland, *Energy Fuels*, in press.
12 S. D. Killops and M. A. H. A. Al-Juboori, *Org. Geochem.*, 15 (1990) 147.
13 D. M. Jones, S. J. Rowland, A. G. Douglas and S. Howells, *Int. J. Environ. Anal. Chem.*, 24 (1986) 227.
14 S. Howells, J. Patey, C. Turner and N. M. Dodd, *Oil Pollution Research Unit Report 27*, Field Studies Council, Angle, Dyfed, Wales, 1986.
15 A. G. Douglas, P. B. Hall, B. Bowler and P. F. V. Williams, *Proc. R. Soc. Edinburgh, Sect. B*, 80 (1981) 113.
16 M. Blumer, *Anal. Chem.*, 29 (1957) 1039.
17 M. T. J. Murphy, A. McCormick and G. Eglinton, *Science*, 157 (1967) 1040.
18 C. Chatfield and A. J. Collins, *Introduction to Multivariate Analysis*, Chapman and Hall, London, 1980.
19 B. Everitt, *Cluster Analysis*, Social Science Research Council, Heinemann, London, 1980.
20 J. B. Kruskal and M. Wish, *Multidimensional Scaling*, Sage, Beverly Hills, CA, 1984.
21 R. F. C. Mantoura, P. M. Gschwend, O. C. Zafiriou and K. R. Clarke, *Environ. Sci. Technol.*, 16 (1982) 38.
22 O. M. Kvalheim and N. Telnaes, *Anal. Chim. Acta*, 191 (1986) 97.
23 K. Urdal, N. B. Vogt, S. P. Sporstol, R. G. Lichtenthaler, H. Mostad, K. Kolset, S. Nordenson and K. Esbensen, *Mar. Pollut. Bull.*, 17 (1986) 366.
24 M. M. A. Ruyken and F. W. Pijpers, *Anal. Chim. Acta*, 194 (1987) 25.
25 A. Grant, *Mar. Pollut. Bull.*, 21 (1990) 297.
26 O. M. Kvalheim, *Chemometr. Intell. Lab. Syst.*, 2 (1987) 127.
27 N. M. Dodd and S. Howells, *Oil Pollution Research Unit Report to Shetland Oil Terminal Environmental Advisory Group*, Field Studies Council, Angle, Dyfed, Wales, 1985.
28 *Mar. Pollut. Bull.*, 10 (1979) 35.
29 M. M. Quirk, R. L. Patience, J. R. Maxwell and R. E. Wheatley, in J. Albaiges (Editor), *Analytical Techniques in Environmental Chemistry: Proceedings of International Congress, Barcelona, 1978*, Pergamon, Oxford, 1980, p. 23.
30 R. P. Philp and C. A. Lewis, *Annu. Rev. Earth Planet. Sci.*, 15 (1987) 363.
31 M. T. Bomboi and A. Hernandez, *Water Res.*, 25 (1991) 557.
32 N. J. Davies and G. A. Wolff, *Mar. Pollut. Bull.*, 21 (1990) 481.

Journal of Chromatography, 589 (1992) 287–294
Elsevier Science Publishers B.V., Amsterdam

CHROM. 23 696

Determination of chemical warfare agents, their hydrolysis products and related compounds in soil

Paul A. D'Agostino* and Lionel R. Provost

Defence Research Establishment Suffield, P.O. Box 4000, Medicine Hat T1A 8K6 (Canada)

(First received May 1st, 1991; revised manuscript received August 19th, 1991)

ABSTRACT

A procedure based on sequential hexane and dichloromethane extraction followed by trimethylsilyl derivatization and capillary column gas chromatographic–mass spectrometric (GC–MS) confirmation was developed for the verification of chemical warfare agents, their hydrolysis products and related compounds in soil. The chemical warfare agents sarin, soman and mustard and the simulant triethyl phosphate were added to four different soil types at the 50 and 5 μg/g levels and recovered with efficiencies varying from nearly 100% to about 5%. The recovery efficiencies were in the range 50–90% for most soil types contaminated with soman, mustard and triethyl phosphate. Sarin recovery was generally the lowest (5–30%). Hydrolysis products, due to degradation of the spiked chemical warfare agents during the course of the experiments, were detected and confirmed as trimethylsilyl derivatives. The developed sample handling and analysis procedure was applied to soil samples in support of range clearance operations. The chemical warfare agent tabun and sixteen related components and their hydrolysis products were identified during capillary column GC–MS analysis of soil extracts.

INTRODUCTION

The use of chemical weapons, although prohibited by the 1925 Geneva Protocol, has been reported recently in several armed conflicts, including the Iran–Iraq war [1]. Verification of the use of chemical warfare agents has often been difficult, in part owing to inadequate battlefield sampling and identification procedures. Soil has been used as a sampling medium for the verification of alleged use of chemical warfare agents and was used as a medium in a recent multi-national round robin exercise coordinated by the Finnish Research Project for Chemical Warfare Verification [2].

A number of methods have been reported for the detection of organophosphorus [3–7] and sulfur vesicant [8–11] chemical warfare agents in soil. Sample handling methods, usually based on solvent extraction, vary considerably and remain a problem for the detection of chemical warfare agents and their hydrolysis products in soil. Prior experience, using dichloromethane as an ultrasonic extraction solvent, was successful for the verification of the sulfur vesicant mustard in soil [9–11]. However, the same extraction method resulted in less satisfactory yields for soil contaminated with the organophosphorus chemical warfare agent sarin. Deficiencies in soil sample handling procedures, and a perceived role for these verification procedures in investigations of allegations of the use of chemical warfare agents, suggested the development of new or improved soil sample handling methods. For these reasons a study was initiated with the primary objective being the development of an efficient sample handling procedure that would allow capillary column gas chromatographic–mass spectrometric (GC–MS) confirmation of chemical warfare agents and their hydrolysis products in soil.

Four different soils, ranging from sand to sandy clay loam were spiked at the 50 and 5 μg/g levels with sarin (isopropyl methylphosphonofluoridate), soman (pinacolyl methylphosphonofluoridate), triethyl phosphate and mustard [bis(2-chloroethyl) sulfide], and extracted with a number of candidate

0021-9673/92/$05.00

solvents. Successive extraction of spiked soil with hexane and dichloromethane, followed by trimethylsilyl derivatization of the soil, appeared to be the most promising approach for the concentration of these chemical warfare agents and their hydrolysis products from soil. The developed method was successfully applied to a series of VX-spiked soil samples during a recent multi-national round-robin analytical exercise [2] and was utilized for the verification of chemical warfare agents and their hydrolysis products in soil contaminated with small amounts of tabun during range clearance operations at the Defence Research Establishment Suffield.

EXPERIMENTAL

Standards

Sarin, soman, mustard and triethyl phosphate were provided by the Organic Chemistry Laboratory, Defence Research Establishment Suffield. Distilled-in-glass solvents were purchased from BDH (Edmonton, Canada). The trimethylsilylation agent bis(trimethylsilyl)trifluoroacetamide (BSTFA) (containing 1% trimethylchlorosilane) and silylation-grade pyridine were purchased from Pierce (Rockford, IL, USA).

Soil Samples and Sample Handling

The four Defence Research Establishment Suffield Experimental Proving Grounds soils, used for spiking experiments, were dried for 3 days, sieved (2 mm) and characterized by the Alberta Environmental Centre (Mr. P. Yeung, Vegreville, Canada) using the Canadian Soil Classification standards.

Samples of 1 g of soil were weighed into 16 mm x 125 mm glass culture tubes, spiked with either 50 μl of a 1 mg/ml standard (spike level 50 μg/g) or 50 μl of a 0.1 mg/ml standard (spike level 5 μg/g) containing sarin, soman, triethyl phosphate and mustard in dichloromethane, and allowed to stand for 60 min at 4°C prior to solvent extraction. Spiked soil samples and blanks were extracted with 2 × 2 ml of hexane by ultrasonic vibration (10 min) and then centrifuged (10 min at 700 *g*). The soil was re-extracted using the above procedure with dichloromethane. Both the hexane and dichloromethane extracts were concentrated separately to 1 ml by nitrogen blowdown. Trimethylsilyl (TMS) derivatization was performed following solvent extraction of the soil samples by adding 100 μl of BSTFA, 100 μl of pyridine and 1 ml of dichloromethane to the soil and allowing it to stand at 60°C for 20 min. Derivatized soil samples were centrifuged for 15 min at 700 *g* and the supernatant was removed, concentrated to 300 μl by nitrogen blowdown and analysed within 24 h to minimize degradation. All soil sample extracts were stored in PTFE-lined screw-capped glass vials at 4°C prior to analysis.

Soil samples, taken in support of range clearance operations, were removed from a site suspected to have been contaminated by a leaking container intended for chemical decontamination. An undried portion of the soil sample was extracted with dichloromethane shortly after receipt and tabun was found to be the principal sample component, based on capillary column GC analysis using phosphorus-mode flame photometric detection. The remaining soil was stored at 4°C and subjected to the developed sample handling procedure about 90 days after initial sampling.

Instrumental

Capillary column GC was performed with a Hewlett Packard 5890 gas chromatograph equipped with an on-column injector of our own design [9] and a flame ionization detector. Data were acquired in triplicate at both spiking levels with percentage recoveries being calculated by external standard calibration. A 15 m × 0.32 mm I.D. DB-1701 J&W capillary column (film thickness 0.25 μm) was used for all GC analyses with the following temperature programs: initial temperature 40 or 50°C (held for 2 min), then increased at 10°C/min to 280°C (held for 0–5 min). Capillary column GC–MS analyses were performed with a Model 70/70E double-focusing mass spectrometer (VG Analytical, Wythenshawe, UK) interfaced to a Varian Model 3700 gas chromatograph. Electron impact MS operating conditions were as follows: emission, 0.1 mA; electron energy, 70 eV; source temperature, 200°C; and source pressure, 2×10^{-6} Torr. Full scanning MS data were acquired at a resolution of 1000 (10% valley definition) with an accelerating voltage of 6 kV over a mass range of 500–40 u.

RESULTS AND DISCUSSION

Four soil types, ranging from sand to sandy clay loam, were spiked at the 50 and 5 μg/g levels with sarin, soman, mustard and triethyl phosphate in a effort to develop a sample handling and analysis procedure that would allow verification of chemical warfare agents and their degradation products in soils. The spiking levels selected were well below typical battlefield contamination levels, which have been estimated to be *ca.* 100–1000 μg/g based on a contamination density of 1–10 g/m^2 (soil density *ca.* 1 g/cm^3 and a sampling depth of 1 cm). The 50 μg/g spiked soil samples were considered to be typical of soil contamination levels hours or days after an attack. The 5 μg/g spiked samples were considered reasonable for soil collected days after an attack or for samples that had undergone natural weathering.

A variety of solvents, including, hexane, dichloromethane, chloroform, acetone, methanol, acetonitrile and water, were investigated for the extraction of compounds of chemical defence interest, with the following scheme being selected on the basis of these preliminary investigations. Soil samples, either spiked or unspiked, were extracted sequentially with hexane and dichloromethane. The extracts were then concentrated and analysed by capillary column GC and GC–MS. The most likely degradation products, due to hydrolysis of sarin and soman would be isopropyl methylphosphonic acid and pinacolyl methylphosphonic acid, respectively, and methylphosphonic acid, whereas thiodiglycol would be expected following mustard hydrolysis [12]. These hydrolysis products, with the exception of thiodiglycol, cannot be determined by direct capillary column GC methods. Thiodiglycol may be determined directly at the nanogram level, converted back to mustard [13] or derivatized with pentafluorobenzoyl chloride [14]. The organophosphorus acids, formed after hydrolysis of sarin and soman, may be determined using GC sample introduction after methylation [15] or *tert.*-butyldimethylsilylation [16]. More recently, liquid chromatography–thermospray mass spectrometry has been used to identify organophosphorus acids [17], organophosphorus pesticides [18–20] and VX [21]. Thermospray MS offers the analyst the possibility of direct MS analysis but at the expense of sensitivity. Typical detection limits are two to three orders of magnitude above those routinely obtained by GC–MS analysis of the derivatives. For this reason, TMS derivatization of the remaining soil, following hexane and dichloromethane extraction, was selected as the final step for the concentration of chemical warfare agents and their degradation products.

Soil Spiking Experiments

Table I lists the recoveries of sarin, soman, mustard and triethyl phosphate from the four different soils. The principal hydrolysis products of sarin, soman and mustard were screened for as their TMS derivatives along with the spiked agents in all the TMS extracts. An estimate of hydrolysis product content was made by comparing the detector response of these products to that of the corresponding chemical warfare agent. Trace amounts of chemical warfare agents or hydrolysis products indicate confirmed mass spectrometric detection, but at levels below 1% of the initial agent spike level.

Sarin was generally difficult to extract efficiently from all the soil types. The recovery was usually highest in the dichloromethane extract, with total recoveries of 30–40% for the recovery of sarin from the loamy sand and sandy loam. The TMS derivative of isopropyl methylphosphonic acid was only detected in the loamy sand and sandy loam TMS extracts after spiking at the 50 μg/g level.

Soman was recovered fairly efficiently from all four soil types, with total recoveries typically in the 30–90% range. Most of the soman was found in the dichloromethane extracts of the soils. Soman and the TMS derivative of pinacolyl methylphosphonic acid were generally detected in the TMS extract, with the greatest recoveries being associated with the higher spike levels.

The soman simulant triethyl phosphate was recovered during the dichloromethane and TMS steps with good efficiency (50–90%) at both the 5 and 50 μg/g level in all soil types except for the sand. This soil appears to be a difficult medium as the recovery of all the spiked agents was generally lower than that obtained for the other three soil types. Hydrolysis of triethyl phosphate was considered unlikely under these experimental conditions and possible hydrolysis products were not screened for.

Mustard recovery was good with total recoveries in the 50–90% range for all soil types except the sandy clay loam. Mustard was generally recovered

TABLE I

EXTRACTION DATA FOR SARIN, SOMAN, TRIETHYL PHOSPHATE AND MUSTARD ADDED TO SOILS AT 50 AND 5 μg/g

Compound	Soil	Level (μg/g)	Recovery after each step (%)[a]			Total recovery (%)
			Hexane	CH_2Cl_2	TMS	
Sarin	Sand	50	ND	5±1	ND (1[b])	5
		5	ND	ND	ND	0
	Loamy sand	50	6.7±0.2	32.7±0.7	ND (trace[b])	39
		5	2.0±0.7	23±7	ND	25
	Sandy loam	50	1±0.3	31±5	ND (trace[b])	32
		5	ND	30±4	ND	30
	Sandy clay loam	50	ND	6.7±0.2	ND	7
		5	ND	Trace	ND	Trace
Soman	Sand	50	1.0±0.3	24±3	12.5±0.5 (8±3[b])	37
		5	ND	17±1	2±2	19
	Loamy sand	50	23.1±0.8	50.7±0.4	12.5±0.5 (10±2[b])	86
		5	3±1	58±5	Trace	61
	Sandy loam	50	4±1	56±8	8±2 (trace[b])	68
		5	Trace	67±7	Trace	67
	Sandy clay loam	50	ND	30±1	3.2±0.6	33
		5	ND	22±5	7.6±0.4	30
Triethyl phosphate	Sand	50	ND	4±1	32±6	36
		5	ND	ND	25±13	25
	Loamy sand	50	1.4±0.2	30±1	32±4	63
		5	ND	27±9	30±3	57
	Sandy loam	50	ND	25±6	40±10	65
		5	ND	28±5	51±7	79
	Sandy clay loam	50	ND	6±1	56±4	62
		5	ND	5.6±0.3	80±7	86
Mustard	Sand	50	39±6	5±1	ND (10.6±0.1[b])	44
		5	44±5	3.5±0.2	ND (17±5[b])	48
	Loamy sand	50	80±3	4.7±0.9	ND (5±2[b])	85
		5	75±4	5.1±0.5	ND	80
	Sandy loam	50	50±5	7±2	ND (3.1±0.6[b])	57
		5	74±3	5±1	ND	79
	Sandy clay loam	50	10.9±0.6	6.0±0.7	ND (7±2[b])	17
		5	14±2	ND	ND (27±10[b])	14

[a] Mean ± S.D. ($n=3$); ND = not detected; trace = <1%

[b] Detected as TMS derivative of hydrolysis product(s) (not included in total recovery).

in the hexane extract and the presence of the mustard hydrolysis product thiodiglycol was confirmed in most of the TMS extracts. Thiodiglycol recovery, although not included in the total mustard recovery estimates, was fairly high for the two soil types (sand and sandy clay loam) for which the mustard recovery was lower.

Figs. 1 and 2 illustrate typical capillary column gas chromatograms obtained for the 50 μg/g spike of the sandy clay loam and the loamy sand respectively. These chromatograms clearly illustrate the presence of the spiked agents and their hydrolysis products in each of the three sample extracts. All the spiked agents and the mustard hydrolysis product thiodiglycol were detected in the sandy clay loam extracts. These agents and the hydrolysis product related to soman, pinacolyl methylphosphonic acid, were observed in the loamy sand ex-

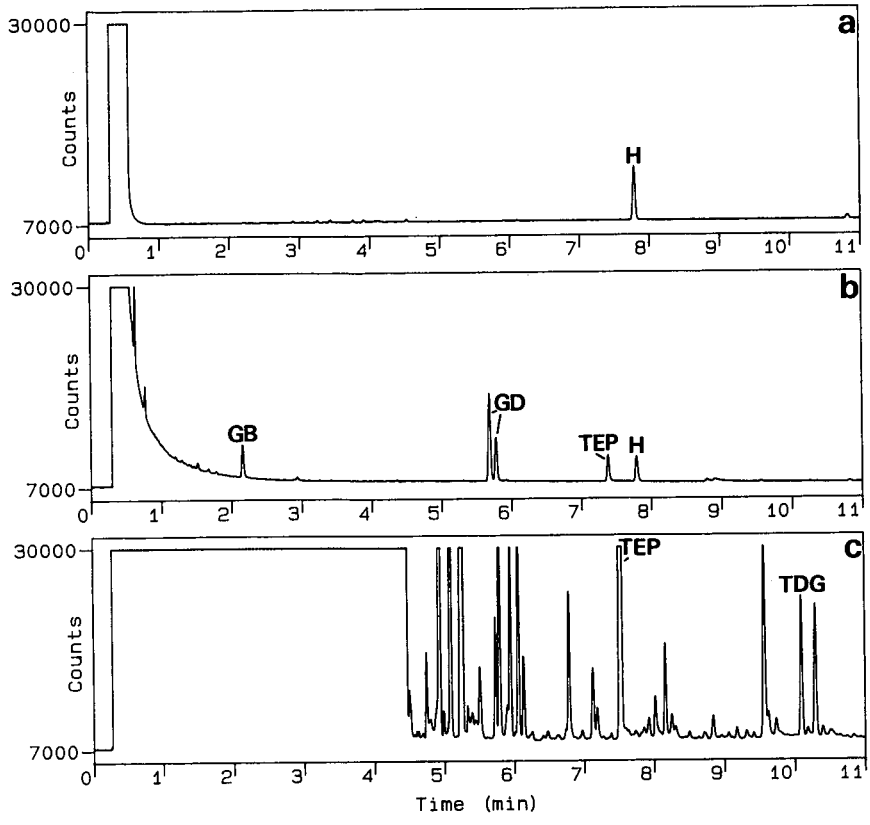

Fig. 1. Capillary column gas chromatograms of successive extraction of 50 μg/g of sarin (GB), soman (GD), triethyl phosphate (TEP) and mustard (H) added to sandy clay loam with (a) hexane, (b) dichloromethane and (c) TMS derivatizing agent. TDG = di-TMS derivatative of thiodiglycol. For conditions, see text.

tracts. Compounds were confirmed by capillary column GC–MS analysis.

Application

The developed procedure has been used for the detection of chemical warfare agents, their degradation products and related compounds in soil during range clearance operations. This sample contained tabun, a chemical warfare agent not used for method development, and sixteen compounds related to tabun. Most of the compounds, identified in the dichloromethane and TMS extracts (Fig. 3) and listed in Table II, have been previously characterized during analysis of munitions grade tabun [22]. Evidence of tabun hydrolysis was evident during GC–MS analysis of the TMS extract. Tabun, present at a trace level (Fig. 4a), and the TMS derivatives of three hydrolysis products, ethyl hydrogendimethylphosphoramidate (Fig. 4b), diethyl hydrogenphosphate (Fig. 4c) and ethyl dihydrogenphosphate (Fig. 4d) were identified on the basis of the acquired electron impact mass spectra (Table III). The first and third hydrolysis products were due to hydrolysis of the cyano and both the cyano and amine functional groups, respectively, of tabun, whereas the second product was probably due to hydrolysis of the amine function group of the principal impurity of munitions grade tabun, diethyl dimethylphosphoramidate [22].

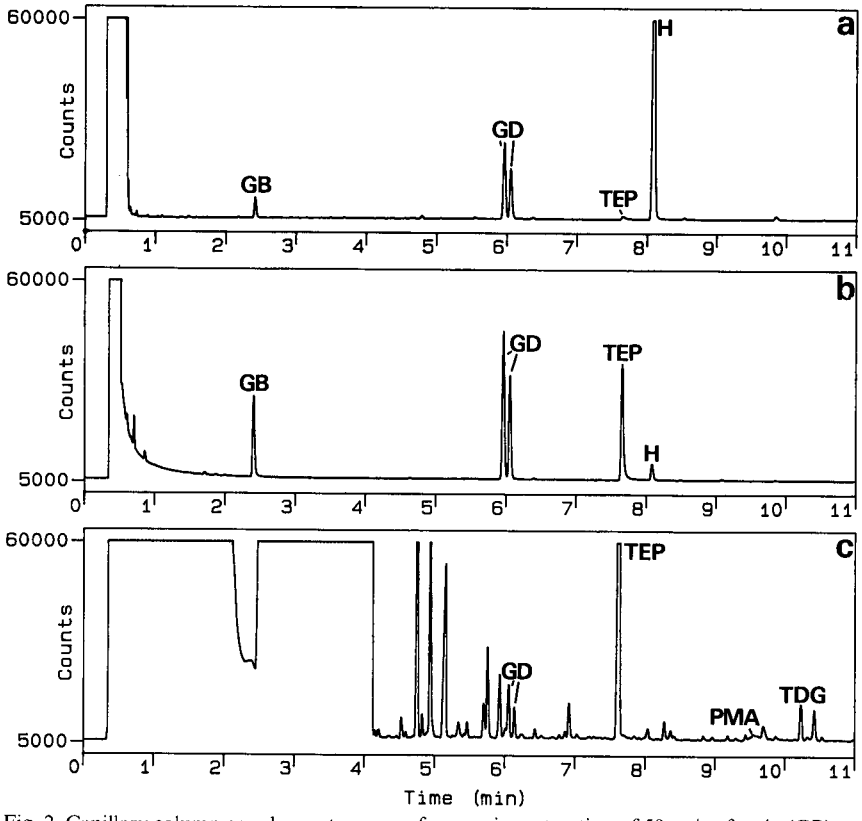

Fig. 2. Capillary column gas chromatograms of successive extraction of 50 μg/g of sarin (GB), soman (GD), triethyl phosphate (TEP) and mustard (H) added to loamy sand with (a) hexane, (b) dichloromethane and (c) TMS derivatizing agent. TDG = di-TMS derivative of thiodiglycol; PMA = TMS derivative of pinacolyl methylphosphonic acid. For conditions, see text.

TABLE II

COMPOUNDS IDENTIFIED IN RANGE CLEARANCE SOIL SAMPLES

Peak No.[a]	Mol. Wt.	Compound
1	181	Diethyl dimethylphosphoramidate
2	182	Triethyl phosphate
3	180	Ethyl tetramethylphosphorodiamidate
4	161	Tetramethylphosphorodiamidic cyanide
5	288	Bis(ethyl dimethylphosphoramidic) anhydride
6	289	Dimethyl phosphoric ethyl dimethylphosphoramidic anhydride
7	287	Ethyl dimethylphosphoramidic tetramethylphosphorodiamidic anhydride
8	219[b]	Unknown
9	395	Bis(ethyl dimethylamidophosphonyl) dimethylamidophosphonate
10	360[b]	Unknown
11	225[c]	TMS derivative of ethyl hydrogendimethylphosphoramidate
12	162	Ethyl dimethylphosphoroamidocyanidate (tabun)
13	226[c]	TMS derivative of diethyl hydrogenphosphate
14	270[c]	Di-TMS derivative of ethyl dihydrogenphosphate
15	—	Phthalate
16	386[b]	TMS derivative
17	330[b]	TMS derivative

[a] See the chromatograms in Fig. 3.
[b] Based on electron impact MS data.
[c] Identification based on interpretation of acquired MS data (Table III).

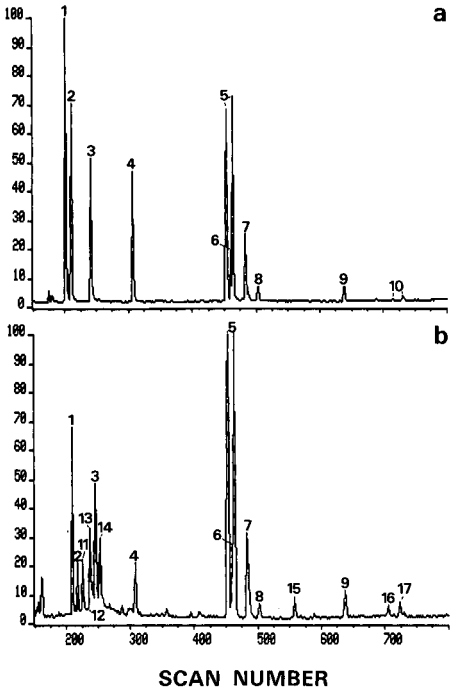

Fig. 3. Capillary column GC–total ion current (500–40 u) MS of range clearance soil sample after successive extraction with (a) dichloromethane and (b) TMS derivatizing agent. Tabun and sixteen related compounds were identified (see Table II). For conditions, see text; one MS scan = 1.8 s.

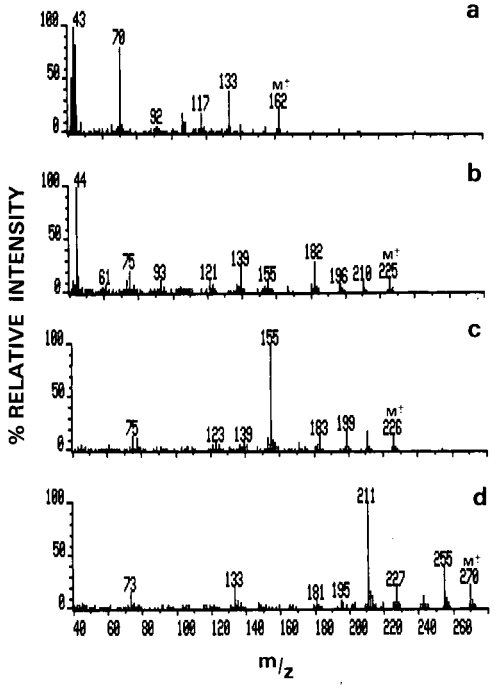

Fig. 4. Electron impact mass spectra of (a) tabun, (b) TMS derivative of ethyl hydrogendimethylphosphoramidate, (c) TMS derivative of diethyl hydrogenphosphate and (d) di-TMS derivative of ethyl dihydrogenphosphate acquired during analysis of range clearance soil sample (Fig. 3).

TABLE III

PRINCIPAL ELECTRON IMPACT IONS FOR HYDROLYSIS PRODUCTS OF TABUN (PEAK NUMBERS 11, 13 AND 14)

Peak 11 = TMS derivative of ethyl hydrogendimethylphosphoramidate $[(C_2H_5O)(O)P(OTMS)(N(CH_3)_2)]$; 13 = TMS derivative of diethyl hydrogenphosphate $[(C_2H_5O)_2(O)P(OTMS)]$; 14 = di-TMS derivative of ethyl dihydrogenphosphate $[(C_2H_5O)(O)P(OTMS)_2]$.

Possible ion structure	*m/z* (relative intensity, %)		
	Peak 11	Peak 13	Peak 14
M^+	225 (11)	226 (12)	270 (21)
$[M-CH_3]^+$	210 (8)	211 (17)	255 (38)
$[M-C_2H_3]^+$	198 (2)	199 (17)	243 (10)
$[M-OC_2H_3]^+$	182 (30)	183 (12)	227 (18)
$[N(CH_3)_2]^+$	44 (100)		
$[(OH)_2P(OC_2H_5)_2]^+$		155 (100)	
$(M-CH_3-OC_2H_4]^+$			211 (100)

CONCLUSIONS

A procedure based on sequential hexane and dichloromethane extraction followed by trimethylsilyl derivatization and capillary column GC–MS confirmation has been developed for the verification of chemical warfare agents, their hydrolysis products and related compounds in soil. The developed procedure was applied to soil samples in support of range clearance operations. Trace amounts of tabun and sixteen tabun related components and their hydrolysis products were identified in the range clearance samples. The ability of the developed procedure to identify the chemical warfare agent tabun, not evaluated during spiking, and its degradation products and related compounds in uncharacterized soil clearly illustrates its potential for the verification of chemical warfare agents, their

hydrolysis products and related compounds at trace levels in soil.

REFERENCES

1 *Report of the Mission Dispatched by the Secretary-General to Investigate Allegations of the Use of Chemical Weapons in the Conflict Between the Islamic Republic of Iran and Iraq*, S/20060, United Nations Security Council, New York, July 20th, 1988.
2 *International Interlaboratory Comparison (Round Robin) Test for the Verification of Chemical Disarmament. F.I. Testing of Existing Procedures*, Ministry of Foreign Affairs of Finland, Helsinki, 1990.
3 A. Verweij and H. L. Boter, *Pestic. Sci.*, 7 (1976) 355–362.
4 J. Kaaijk and C. Frijlink, *Pestic. Sci.*, 8 (1977) 510–514.
5 *Identification of Potential Organophosphorus Warfare Agents*, Ministry for Foreign Affairs of Finland, Helsinki, 1979.
6 *Identification of Degradation Products of Potential Organophosphorus Warfare Agents*, Ministry for Foreign Affairs of Finland, Helsinki, 1980.
7 *Trace Analysis of Chemical Warfare Agents*, Ministry for Foreign Affairs of Finland, Helsinki, 1981.
8 A. Heyndrickx, J. Cordonnier and A. De Bock, *Arch. Belg. Med. Soc. (Toxicol.)*, (1984) 102–109.
9 P. A. D'Agostino and L. R. Provost, *J. Chromatogr.*, 331 (1985) 47–54.
10 P. A. D'Agostino and L. R. Provost, *J. Chromatogr.*, 436 (1988) 399–411.
11 P. A. D'Agostino and L. R. Provost, *Biomed. Environ. Mass Spectrom.*, 15 (1988) 553–564.
12 R. Trapp, *The Detoxification and Natural Degradation of Chemical Warfare Agents*, Stockholm International Peace Research Institute, Taylor and Francis, London and Philadelphia, 1985.
13 E. R. J. Wils, A. G. Hulst and J. van Laar, *J. Anal. Toxicol.*, 12 (1988) 15–19.
14 R. M. Black and R. W Read, *J. Chromatogr.*, 449 (1988) 261–270.
15 J. Aa. Tørnes and B.A. Johnsen, *J. Chromatogr.*, 467 (1989) 129–138.
16 J. G. Purdon, J. G. Pagotto and R. K. Miller, *J. Chromatogr.*, 475 (1989) 261–272.
17 E. R. J. Wils and A. G. Hulst, *J. Chromatogr.*, 454 (1988) 261–272.
18 D. Barcelo, *Biomed. Environ. Mass Spectrom.*, 17 (1988) 363–369.
19 A. Farran, J. De Pablo and D. Barcelo, *J. Chromatogr.*, 455 (1988) 163–172.
20 L. D. Betowski and T. L. Jones, *Environ. Sci. Technol.*, 22 (1988) 1430–1434.
21 E. R. J. Wils and A. G. Hulst, *J. Chromatogr.*, 523 (1990) 151–161.
22 P. A. D'Agostino, L. R. Provost and K. M. Looye, *J. Chromatogr.*, 465 (1989) 261–283.

Journal of Chromatography, 589 (1992) 295–299
Elsevier Science Publishers B.V., Amsterdam

CHROM. 23 716

Analysis of benzyloxy-terminated poly(1,3,6-trioxocane)s by supercritical fluid chromatography

H. Pasch*,☆, H. Krüger and H. Much

Central Institute of Organic Chemistry, Division of Macromolecular Compounds, Rudower Chaussee 5, O-1199 Berlin (Germany)

U. Just

Federal Institute for Materials Research and Testing, Department 3, Organic Materials, Unter den Eichen 87, 1000 Berlin 45 (Germany)

(First received May 29th, 1991; revised manuscript received August 29th, 1991)

ABSTRACT

Benzyloxy-terminated poly(1,3,6-trioxocane)s are separated into oligomers by supercritical fluid chromatography. Depending on the chemical structure of the polytrioxocane, two to three peaks are obtained for each degree of polymerization, corresponding to different types of functionality. Up to a degree of polymerization of $n=7$ the α,ω-dihydroxy, α-hydroxy-ω-benzyloxy and α,ω-dibenzyloxy species are well separated.

INTRODUCTION

Macromers and telechelics are known to be oligomers with exactly one or two functional end-groups. Therefore, they are important intermediate products for further polymer reactions. An exact knowledge of the macromer and telechelic functionality is necessary for the application. The separation of functional polymers according to the type of functional groups is possible using liquid chromatography at the critical point of adsorption [1]. In this case a functionality-type distribution is obtained; the corresponding molar mass distribution of the fractions may also be obtained when size-exclusion separations of the fractions are carried out in a second dimension [2].

The use of a single liquid chromatographic method usually yields separations in which different distribution functions overlap (functionality, molar mass, chemical composition). The resolution of these methods is not sufficient to separate a polymer into its oligomers and the oligomers into components of different functionality.

Supercritical fluid chromatography (SFC) has become a popular tool to separate polymers into their oligomers [3–6]. Using highly efficient and selective capillary columns, unique separations may be achieved. However, so far only limited experimental data are available on simultaneous separation according to functionality and molar mass. Therefore, it is the aim of the present paper to study the potential of SFC in regard to this problem.

EXPERIMENTAL

The preparation of the poly(1,3,6-trioxocane) samples is described in ref. 7.

In brief, 1,3,6-trioxocane was cationically polymerized in the presence of benzyl alcohol (Table I, samples 1–3). Additionally, for sample 1 an extraction of the aqueous solution with diethyl ether was

☆ Present address: Deutsches Kunststoff-Institut, Schlossgartenstrasse 6, W-6100 Darmstadt, Germany.

0021-9673/92/$05.00

TABLE I
CHARACTERISTICS OF SAMPLES TESTED

Sample	$\bar{M}_n$[a]	Hydroxyl number	Hydroxyl group equivalent
1	550	135.0	1.33
2	1410	53.1	1.34
3	385	164.0	1.13
4	680	3.5	0.04
5	960	113.7	1.95

[a] $\bar{M}_n$ = Number-average molecular weight, as determined by vapour pressure osmometry (VPO).

carried out to remove the α,ω-dibenzyloxy oligomers.

For sample 4, 1,3,6-trioxocane was polymerized in the presence of dibenzyl formal. As a result the product consists mostly of α,ω-dibenzyloxy oligomers.

Sample 5 was synthesized according to a route described in ref. 8. The first set of experiments was carried out on a Carlo Erba SFC 3000 instrument with flame ionization detection (FID). The mobile phase was 100% carbon dioxide (Linde). Samples were injected through a pneumatically operated Valco injection valve in a timed-split mode. An SE-54 10 m × 100 μm I.D. capillary column (Carlo Erba) was used. The oven temperature was 120°C and the FID temperature was maintained at 330°C.

The second set of experiments was carried out on an SB Biphenyl-30 10 m × 50 μm I.D. capillary column (Lee Scientific) using Dionex SFC 600 D equipment. Oven temperatures of 100 and 130°C were maintained. Timed-split injection was carried out on a Valco injection valve.

All polymer samples were injected as 30% (w/w) solutions in methylene chloride.

RESULTS AND DISCUSSION

The cationic ring-opening polymerization of 1,3,6-trioxocane in the presence of benzyl alcohol results in the formation of components with different endgroups. In agreement with the active chain-end mechanism, α-hydroxy-ω-benzyloxy oligo (1,3,6-trioxocane)s (I) and cyclic oligomers (II) are formed along with α,ω-dihydroxy (III) and α,ω-dibenzyloxy oligo (1,3,6-trioxocane)s (IV) (Fig. 1) [7].

Accordingly two types of distribution functions are expected: molar mass distribution and functionality-type distribution. In a first set of experiments a number of samples (see Table I) were investigated on a methylsiloxane capillary column (SE-54) using Carlo Erba SFC 3000 equipment. A density program was applied consisting of an initial isobaric step, in which the sample solvent was eluted, and two linear ramp steps for the separation of the oligomers. After optimization of the ramp rates and the hold times, chromatograms were obtained, showing the expected oligomer distribution (see Fig. 2). For each degree of oligomerization two peaks, a smaller one and a bigger one, were obtained, indicating a second type of distribution. Obviously components of two different types of functionality were present in the samples. However, the expected three to four different types of functional components could not be separated.

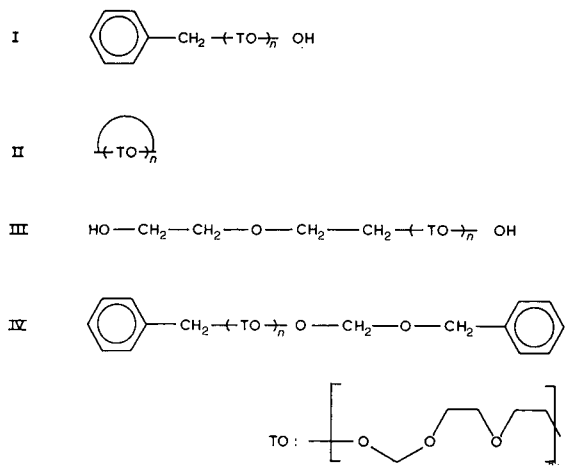

Fig. 1. Structures of compounds I–IV.

A higher resolution was expected when the polarity of the stationary phase was increased. In addition, a 50 μm I.D. instead of a 100 μm I.D. column was used.

The separation of a low-molecular-weight poly(1,3,6-trioxocane) on an SB Biphenyl-30 stationary phase is shown in Fig. 3. Again density programming was used but the hold steps were deleted. In program A (see Fig. 4), consisting of two ramp steps with rates of 0.03 and 0.02 g ml^{-1} min^{-1}, well resolved peaks were obtained in the first part of the chromatogram. In the second part of the chromatogram the peaks were very close to each other. Accordingly the first ramp rate was increased to 0.1 g ml^{-1} min^{-1} and the second ramp rate was de-

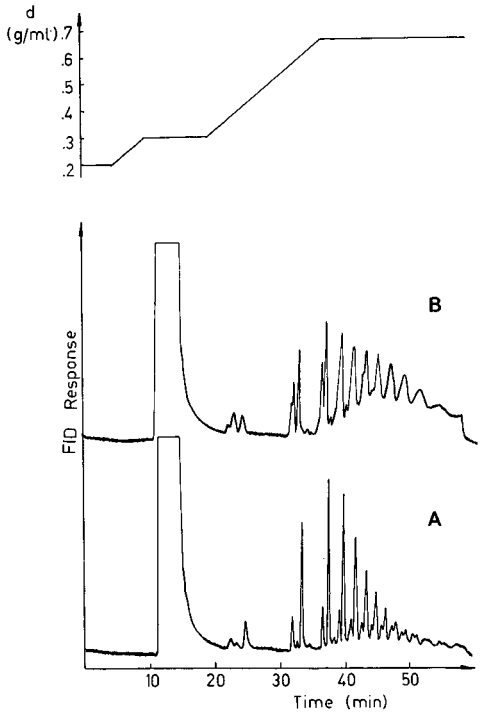

Fig. 2. SFC chromatograms of samples 1 (A) and 2 (B) on a methylsiloxane capillary column, density programming, oven temperature 120°C.

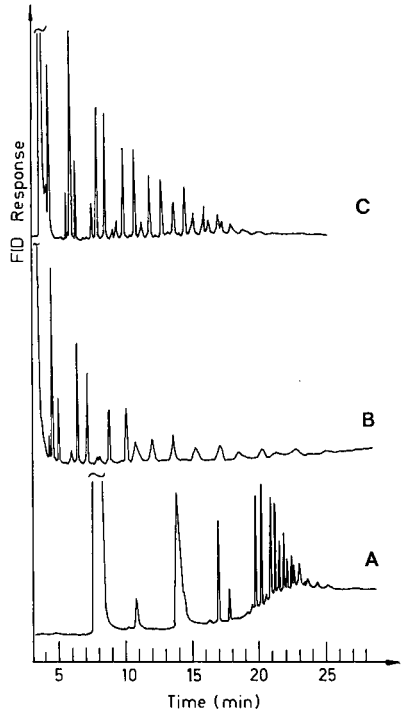

Fig. 3. SFC chromatograms of sample 3 on a SB-Biphenyl 30 capillary column with different density programmes, oven temperature 100°C.

creased to 0.01 g ml^{-1} cm^{-1}. In this case very broad peaks were obtained in the second part of the chromatogram. Optimum resolution was achieved using ramp rates of 0.06 and 0.02 g ml^{-1} min^{-1} (see Fig. 3C).

A further improvement was expected when the oven temperature was increased from 100 to 130°C. After adjusting the density programming to an optimum resolution, well resolved peaks were obtained (see Fig. 5). With respect to the previously discussed molar mass and functionality-type distributions, the number of peaks indicated that for each degree of polymerization more than two peaks were obtained. For sample 3 the hydroxyl group equivalent was determined to be 1.13, and it was assumed that all types of functionalities (I–IV) might be present.

In order to assign the peaks, samples which contain predominantly one type of functionality were investigated. As can be seen in Fig. 6A, sample 4 exhibits a normal oligomer distribution with minor peaks of other functionalities.

This sample was prepared in the presence of dibenzyl formal, which finally leads nearly exclusively to dibenzyl-functionalized oligomers. Accordingly the hydroxyl equivalent is very low. The following

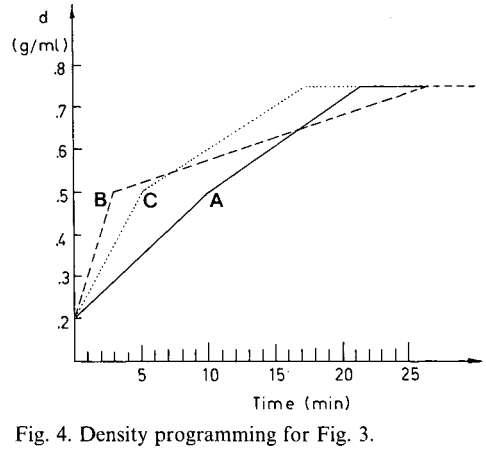

Fig. 4. Density programming for Fig. 3.

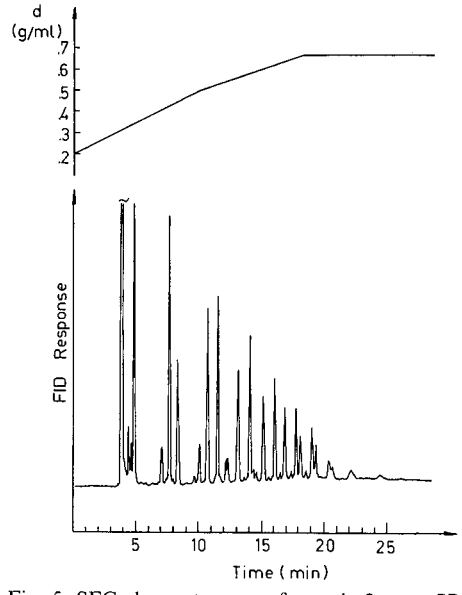

Fig. 5. SFC chromatogram of sample 3 on a SB-Biphenyl 30 capillary column, oven temperature 130°C.

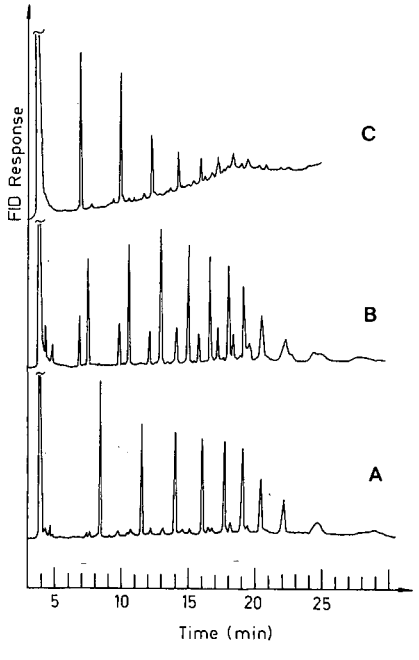

Fig. 6. SFC chromatograms of samples 4 (A), 1 (B) and 5 (C) on a SB-Biphenyl 30 capillary column. For density programme, see Fig. 5.

average structure could be assumed which corresponds to the functionality type IV.

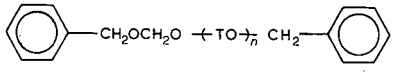

The polymerization of 1,3,6-trioxocane without dibenzyl formal was supposed to give an oligomer mixture containing exclusively α,ω-dihydroxy components (functionality type III). Fig. 6C shows a typical oligomer distribution, however, the efficiency of the separation was less than in Fig. 6A. The reason is thought to be higher polarity of the α,ω-dihydroxy oligomers, causing solubility problems with the mobile phase.

A polytrioxocane sample in which the α,ω-dibenzyl components were removed by extraction in water–diethyl ether is shown in Fig. 6B. Accordingly, this sample contains mainly α,ω-dihydroxy and α-hydroxy-ω-benzyloxy oligomers.

Based on the interpretation of the chromatograms in Fig. 6A–C, the peaks in Fig. 5 could be assigned. Within one degree of oligomerization the components of different functionality were eluted in the order III–I–IV. The lowest molar mass components of I and III ($n = 0$), *i.e.* benzyl alcohol and diethylene glycol, were eluted shortly after the sample solvent at 4–5 min. Therefore the peak at 7.12 min corresponds to III with $n = 1$, the peak at 7.73 min corresponds to I with $n = 1$ and the peak at 8.37 min corresponds to IV with $n = 0$. The assignment of the other peaks is summarized in Table II.

A number of minor peaks in Fig. 5 could not be assigned to either a certain degree of oligomerization or functionality type III, I or IV. Some of them may correspond to a cyclic oligomer series (functionality type II), however an unambiguous assignment was not possible. According to Krüger *et al.* [7] the amount of cyclic oligomers is of the order of 1% (w/w).

After assigning the oligomer peaks to the different functionalities, calibration curves of molar mass *versus* retention time could be obtained (see Fig. 7). In our case, for the three functionality types similar calibration curves were obtained, indicating that the separation occurred according to the size of the oligomer molecule. From the shape of the curves it

TABLE II

ASSIGNMENT OF THE OLIGOMER PEAKS IN THE SFC CHROMATOGRAM OF SAMPLE 3

n	III		I		IV	
	M^a (g/mol)	$t_R{}^b$ (min)	M (g/mol)	t_R (min)	M (g/mol)	t_R (min)
0	–	–	–	–	228	8.37
1	224	7.12	226	7.73	346	11.55
2	342	10.08	344	10.78	464	14.07
3	460	12.38	462	13.18	582	16.10
4	578	14.35	580	15.20	700	17.73
5	696	16.10	698	16.85	818	19.05
6	814	17.42	816	18.20	936	20.38
7	932	18.55	934	19.37	1054	22.12
8	1050	–	1052	20.62	1172	24.50

[a] M = Molar mass.
[b] t_R = Retention time.

could be assumed that increasing the oligomer chain length by one TO-unit resulted in an increase in the retention time by a constant increment.

CONCLUSIONS

Benzyloxy-terminated poly(1,3,6-trioxocane)s are distributed according to molar mass and end functionality. The first distribution can be described by size-exclusion chromatography, the second by high-performance liquid chromatography. Using SFC it is possible to characterize both distributions by one chromatographic technique. The molar mass as well as the functionality-type distribution could be described in detail, assigning the single peaks to a certain type of functionality and degree of polymerization. It has been shown that a biphenyl siloxane capillary column is most suited for this problem. The calculation of average molar masses and functionalities simultaneously from the intensity of the single peaks would be a very fast method for the determination of structural parameters. This problem will be dealt with in forthcoming investigations.

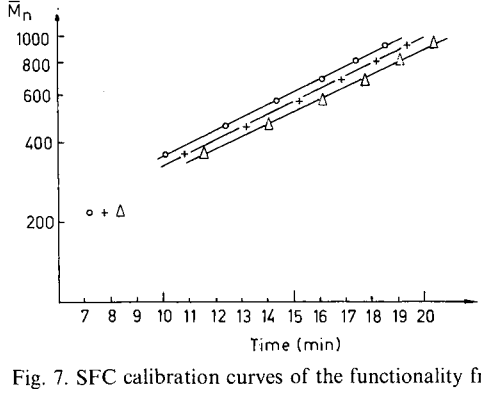

Fig. 7. SFC calibration curves of the functionality fractions III (○), I (+) and IV (△).

ACKNOWLEDGEMENT

The support in carrying out experiments on the Carlo Erba instrument by Mr. Frank Mellor of the Central Institute of Physical Chemistry is greatly appreciated.

REFERENCES

1 S. G. Entelis, V. V. Evreinov and A. V. Gorshkov, *Adv. Polym. Sci.*, 76 (1986) 129.
2 G. Schulz, H. Much, H. Krüger and C. Wehrstedt, *J. Liq. Chromatogr.*, 13 (1990) 1745.
3 C. M. White (Editor), *Modern Supercritical Fluid Chromatography*, Hüthig Verlag, Heidelberg, 1988, pp. 163–180.
4 F. P. Schmitz, H. Hilgers and E. Klesper, *J. Chromatogr.*, 267 (1983) 267.
5 S. Mori, T. Saito and M. Takeuchi, *J. Chromatogr.*, 478 (1989) 181.
6 F. P. Schmitz and E. Klesper, *J. Chromatogr.*, 388 (1987) 3.
7 H. Krüger, H. Much, G. Schulz and C. Wehrstedt, *Makromol. Chem.*, 191 (1990) 907.
8 H. Krüger, *Acta Polym.*, 37 (1986) 601.

Journal of Chromatography, 589 (1992) 301–306
Elsevier Science Publishers B.V., Amsterdam

CHROM. 23 681

Study of the retention behaviour of barbiturates by overpressured layer chromatography using silica gel bonded with tricaprylmethylammonium chloride

Katalin Kovács-Hadady

BIOGAL Pharmaceutical Co. Ltd., Pallagi 13, Debrecen (Hungary)

(First received June 10th, 1991; revised manuscript received August 9th, 1991)

ABSTRACT

The chromatographic behaviour of twelve barbituric acid derivatives was studied by overpressured layer chromatography using silica gel impregnated with tricaprylmethylammonium chloride (TCMA). The retention of the barbiturates decreased with increasing TCMA concentration on the layer. The R_F values increased with increasing methanol content of the eluent. The pH and the inorganic salt concentration in the eluent had no effect on the retention. Similar results were obtained earlier for different types of compounds, *e.g.*, amino- and nitrosalicylic acids, pyrimidine derivatives, penicillins, cephalosporins and tetracyclines. Several similarities have been observed between chromatographic processes performed either on silica gel layers or on a dynamically modified silica high-performance liquid chromatographic column with eluents containing an ion-pairing reagent. It has been shown that no ion pairing occurs on silica gel layers impregnated with TCMA. Hydrophobic interactions play an important role in the retention of the compounds. The retention is controlled by the TCMA adsorbed on the silica gel layer. The results of the best separations are given.

INTRODUCTION

The use of quaternary ammonium compounds in chromatographic practice is widespread. For ion-pairing chromatographic separations of acid-type compounds, cetrimide (cetyltrimethylammonium chloride or bromide) is frequently used. Several papers have been published by Hansen and co-workers [1–7] in which high-performance liquid chromatography (HPLC) on a dynamically modified silica column was used with eluents containing cetrimide. It was shown that cetrimide binds to the silanol groups of the silica gel; at the same time, a proton dissociates and the silica surface is hydrophobized. This process takes place during the preliminary equilibration or development.

Szepesi and co-workers [8,9] extended the model of the dynamically modified silica column to experiments involving overpressured layer chromatography (OPLC). In the OPLC technique developed by Tyihák and co-workers [10–12], the layer acts as a "spread-out" column. Instead of the equilibration usually performed in HPLC, preliminary impregnation seemed to be useful with thin layers. The retention of organic acids, studied under these conditions by Szepesi *et al.* [8], was highly dependent on the ion-pairing reagent concentration of the solution used for impregnation of the layers.

In an earlier study, we used tricaprylmethylammonium chloride (TCMA) for the separation of different amino- and nitrosalicylic acids [13]. TCMA is known to be an ion-pairing reagent and is used for the preparation of ion-selective membrane electrodes, *e.g.*, salicylate electrodes [14–17]. With eluents containing methanol and water but not TCMA, the retention of salicylic acid derivatives increased with increasing TCMA concentration of the impregnating solution. The pH had no effect on the retention in the range 2–12 [13]. We observed a similar retention behaviour for basic pyrimidine derivatives (minoxidil and its intermediates) [18], penicillins and cephalosporins [19] and tetracyclines

0021-9673/92/$05.00

(unpublished results), which have amphoteric characteristics.

Our findings suggest that no ion pairing occurs on silica gel layers impregnated with TCMA. The adsorption of TCMA on the silica gel (this may also be chemisorption) exhibits a Langmuir-type isotherm [18]. With increasing amount of adsorbed TCMA, the surface of the silica gel becomes hydrophobic. At 0.1–0.2 *M* TCMA concentration in the impregnating solution, the quaternary ammonium compound forms a monolayer on the silica surface and the retention is controlled by hydrophobic interactions.

In this work, the retention behaviour of twelve barbituric acid derivatives (Fig. 1) was studied under similar conditions to those in the earlier work [13,18,19].

EXPERIMENTAL

Chemicals and reagents

Silica gel layers (Art. 5554) were obtained from E. Merck (Darmstadt, Germany). The layers were developed with methanolic TCMA solution overnight in an unsaturated normal chamber. Three sides of the plates were impregnated with Impres (Laboratory Instruments, Budapest, Hungary) as pretreatment for OPLC development.

TCMA was purchased from Fluka (Buchs, Switzerland). All other chemicals were of analytical-reagent grade. Barbituric acid derivatives were of pharmacopoeial quality and were kindly provided by Alkaloida and Chinoin Pharmaceutical Works (Tiszavasvári and Budapest, Hungary, respectively). Portions of 1 μl of 5 mg ml^{-1} ethanolic solutions of barbiturates were applied.

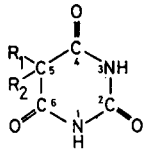

barbituric acid

derivatives	R_1	R_2
amobarbital	ethyl	isopenthyl
aprobarbital	allyl	isopropyl
barbital	ethyl	ethyl
butobarbital	ethyl	butyl
crotylbarbital	ethyl	crotyl
cyclobarbital	ethyl	cyclohexenyl
diallyl barbital	allyl	allyl
hexobarbital	cyclohexenyl	methyl , 3-methyl
pentobarbital	ethyl	1-methylbutyl
phenobarbital	ethyl	phenyl
proxibarbal	allyl	β-hydroxypropyl

Fig. 1. Structures of the studied barbituric acid derivatives.

Apparatus

A Chrompres^{25} OPLC instrument (Laboratory Instruments) was used for the development of the chromatograms at a membrane pressure of 20 bar and a flow-rate of 1 ml min^{-1}. The spots were detected under a UV lamp at 254 nm. For the determination of TCMA adsorbed on the layer, Fourier transform IR (FT-IR) spectrometry was used [19].

RESULTS AND DISCUSSION

Effects of TCMA concentration on retention

The effects of the TCMA concentration in the impregnating solution on the retentions of the barbiturates are shown in Fig. 2. The retentions increased with increasing TCMA concentration when eluents containing methanol and water were used. For pentobarbital, a significant increase in retention was observed at 0.01 *M* TCMA (Fig. 2A), whereas the retentions of the other compounds increased at 0.05 *M* or higher TCMA concentrations. The retention *vs.* TCMA concentration curves are very similar, and at 0.1–0.2 *M* TCMA concentrations only small differences exist in the retentions. In the studied TCMA concentration range, the smallest retention change was observed for proxibarbal (Fig. 2A).

These retention *vs.* TCMA concentration curves (Fig. 2) are very similar to those measured for barbiturates on a dynamically modified silica column with eluents containing cetrimide [20]. At a given cetrimide concentration, proxibarbal and barbital had the smallest and phenobarbital, pentobarbital and amobarbital the highest k' values. This similarity indicates that the retention mechanism is sim-

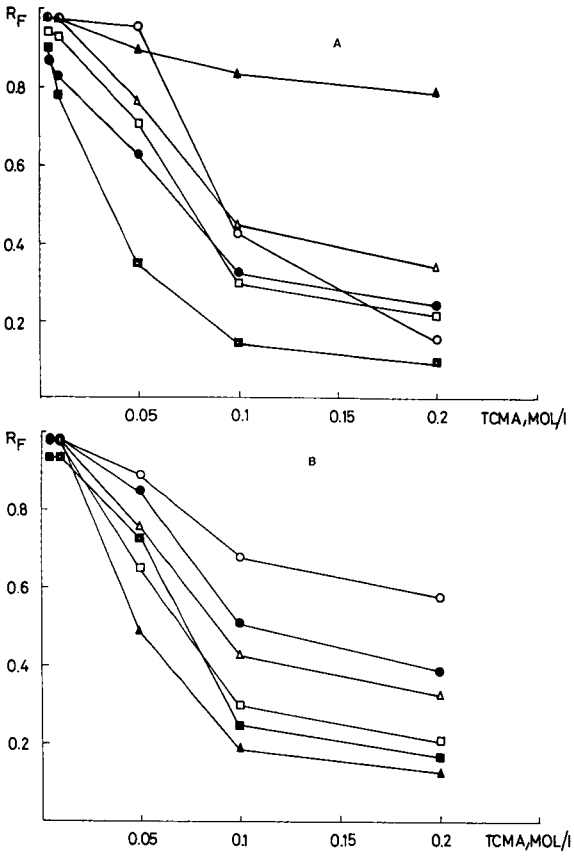

Fig. 2. Effect of TCMA concentration on retention. Eluent: methanol–water (30:70, v/v). (A) ○ = Barbituric acid; ● = hexobarbital; □ = cyclobarbital; ■ = pentobarbital; △ = crotylbarbital; ▲ = proxibarbal. (B) ○ = Barbital; ● = diallylbarbital; □ = butobarbital; ■ = phenobarbital; △ = aprobarbital; ▲ = amobarbital.

ilar on silica gel layers impregnated with TCMA and on a dynamically modified silica column with eluents containing cetrimide, in spite of the fact that there is a difference between the alkyl moieties of the quaternary ammonium compounds. Cetrimide contains three methyl groups and one cetyl group and TCMA contains three capryl groups and one methyl group.

We also used eluents containing cetrimide at pH 10, where all the barbituric acid derivatives are fully dissociated. The chromatograms were developed on silica gel layers impregnated with 0.1 *M* TCMA. There was no difference between the retentions measured in the presence or the absence of cetrimide; it is possible that stronger interactions occur between the compounds and TCMA adsorbed on the silica surface than with cetrimide in the eluent.

Effects of methanol content of the eluent

With increasing methanol content of the eluent (from 10 to 50%), the retentions of the barbituric acid derivatives decreased (Fig. 3). On layers impregnated with 0.05 *M* TCMA, the retentions of some derivatives (barbituric acid, barbital and diallylbarbital) did not decrease with increasing methanol content, and the others showed only small differences compared with the results obtained on layers impregnated with 0.1 or 0.2 *M* TCMA. This can be explained by the fact that at 0.05 *M* or lower impregnating solution concentration not all the silanol groups of the silica gel are completely covered by TCMA, and the barbitals interact both with the silanol groups and with the capryl groups.

The same tendency was observed for amino- and nitrosalicylic acids [13], pyrimidine derivatives [18], penicillins and cephalosporins [19] and tetracyclines (unpublished results). Gazdag *et al.* [21] studied the retention characteristics of different organic acids on a dynamically modified silica column with eluents containing cetrimide. The k' values decreased significantly at methanol concentrations higher than 40%. Their measurements in methanol–water showed that the adsorption of cetrimide on silica gel exhibited a maximum at about 50% methanol content. Gazdag *et al.* [21] suggested that the explanation for this is that cetrimide is adsorbed on the silica surface in two ways: by means of a silanophilic interaction and by ion exchange with the proton of the silanol group. The effect of the former process becomes stronger with increasing organic solvent content of the eluent, whereas that of the latter decreases.

On silica gel layers impregnated with TCMA, we could not perform direct experiments to study the correlation between the amount of adsorbed TCMA and the methanol content of the eluent. TCMA is an oily compound immiscible with water and methanol–water mixtures of low methanol content. Therefore, "indirect" investigations were made: the silica gel layers were impregnated with 0.1 *M* TCMA and the layers were then developed by means of OPLC, using eluents with different methanol contents (15–75%). The amount of adsorbed TCMA was measured by means of FT-IR spectrometry.

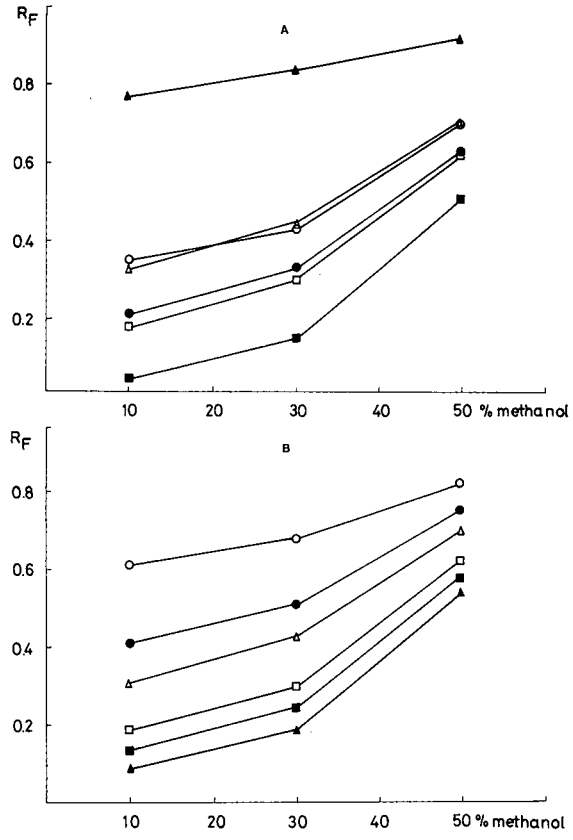

Fig. 3. Effect of methanol content of the eluent on retention. Silica gel impregnated with 0.1 *M* TCMA. Symbols in (A) and (B) as in Fig. 2.

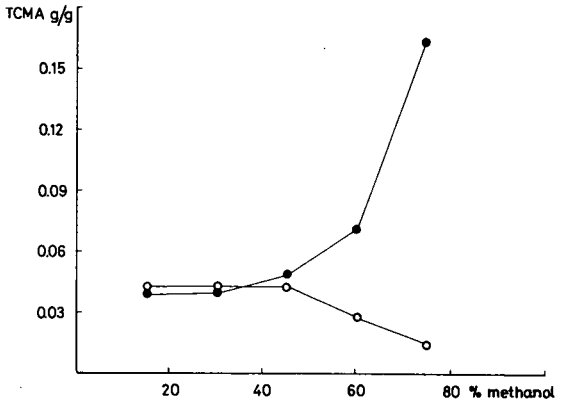

Fig. 4. Effect of methanol content of eluent on TCMA adsorbed on silica gel impregnated with 0.1 *M* TCMA. ○ = Near the start; ● = near the front.

In our opinion, this "indirect" method is better in OPLC or thin-layer chromatographic (TLC) developments, because it reflects the true situation existing during the chromatographic process. The results of the experiments can be seen in Fig. 4. With increasing methanol content of the eluent the amount of adsorbed TCMA, removed from near the start, decreases whereas that near to the front increases. With methanol–water mixtures of high methanol content, most of silanol groups became free again, and the hydrophobic interactions existing between the capryl groups and barbiturates diminished.

Effects of pH and inorganic salt concentration in the eluent on retention

The effect of the pH of the eluent on the retention of barbituric acid derivatives was investigated at pH 2 and 10, to study the chromatographic behaviour of undissociated species (for barbiturates, $pK_a \approx 3$–7) and dissociated species. It was found that the pH of the eluent had no effect on the retention; it makes no difference to the retention of the dissociated or undissociated form of a given compound. The same finding was obtained with amino- and nitrosalicylic acids [13], pyrimidine derivatives [18], penicillins and cephalosporins [19] and tetracyclines (unpublished results). During their experiments on reversed-phase (C_2-bonded) high-performance TLC layers impregnated with cetrimide and other quaternary ammonium compounds (tetrabutylammonium chloride, tetramethylammonium chloride), Tomkinson *et al.* [22] also observed that the solvent pH was not an important factor in the determination of the final retentions of dihydroxybenzoic acids.

It was found by Hansen and co-workers [2,4,7] that the selectivity of the chromatographic techniques based on a dynamically modified silica column was independent of the pH of the silica surface. In their opinion, the presence of cetrimide and buffer in the eluent can control the surface characteristics. Gazdag *et al.* [21] measured the adsorption of cetrimide on silica, and observed that cetrimide did not adsorb on the silica surface at low pH. Above pH 4, the extent of adsorption suddenly increased. This is in accordance with the dissociation

TABLE I

R_s VALUES OF BARBITURATES ON SILICA GEL LAYERS IMPREGNATED WITH 0.05 *M* TCMA

Eluent: methanol–water (30:70) containing 0.25 *M* sodium chloride. Abbreviations: bacid = barbituric acid; barb = barbital; diallyl = diallylbarbital; buto = butobarbital; pheno = phenobarbital; hexo = hexobarbital; cyclo = cyclobarbital; pento = pentobarbital; crotyl = crotylbarbital; apro = aprobarbital; amo = amobarbital; proxi = proxibarbal.

Compounds	R_s	Compounds	R_s	Compounds	R_s	Compounds	R_s	Compounds	R_s
bacid/barb	2.5	barb/pheno	10.9	diallyl/crotyl	1.2	pheno/cyclo	0.6	cyclo/apro	3.0
bacid/diallyl	5.1	barb/hexo	9.4	diallyl/apro	1.8	pheno/pento	2.3	cyclo/amo	2.6
bacid/buto	8.5	barb/cyclo	9.2	diallyl/amo	8.1	pheno/crotyl	4.5	cyclo/proxi	11.8
bacid/pheno	8.3	barb/pento	10.4	diallyl/proxi	8.6	pheno/apro	3.9	pento/crotyl	5.7
bacid/hexo	7.5	barb/crotyl	6.2	buto/pheno	0.3	pheno/amo	2.2	pento/apro	5.3
bacid/cyclo	7.5	barb/apro	6.8	buto/hexo	1.4	pheno/proxi	13.5	pento/amo	0.7
bacid/pento	8.4	barb/amo	13.5	buto/cyclo	0.3	hexo/cyclo	0.8	pento/proxi	12.5
bacid/crotyl	5.8	barb/proxi	4.7	buto/pento	2.7	hexo/pento	3.5	crotyl/apro	0.6
bacid/apro	6.1	diallyl/buto	5.9	buto/crotyl	4.6	hexo/apro	2.4	crotyl/amo	6.9
bacid/amo	9.7	diallyl/pheno	5.7	buto/apro	4.0	hexo/amo	3.9	crotyl/proxi	9.7
bacid/proxi	0.4	diallyl/hexo	4.2	buto/amo	2.7	hexo/proxi	12.3	apro/amo	6.3
barb/diallyl	4.9	diallyl/cyclo	4.6	buto/proxi	14.3	cyclo/pento	2.6	apro/proxi	10.2
barb/buto	11.6	diallyl/pento	6.6	pheno/hexo	1.6	cyclo/crotyl	3.5	amo/proxi	15.8

of the silanol groups. The anionic sites readily bind the cationic cetrimide, whereas at acidic pH the binding of proton is favourable.

Our findings with different types of compounds [13,18,19] suggest that the desorption of TCMA on silica gel is almost independent of the pH [19], so the retention seems to be unchanged.

With eluents containing 0.05–0.25 *M* of sodium chloride and 30% of methanol, the retentions of the barbiturates did not change on silica gel layers impregnated with 0.1 *M* TCMA. There was no difference between the retentions measured as a function of the salt concentration at pH 2 and 10. The diameter of the spots decreased an in parallel the efficiency of the chromatographic process became better with increasing salt concentration in the eluent.

Separation of barbituric acid derivatives

On the basis of the above results, it was found that on silica gel layers impregnated with TCMA the retention is controlled by the surface concentration of TCMA adsorbed on the silica gel. It is controlled directly via the concentration of the impregnating methanolic TCMA solution (adsorption), and indirectly via the methanol content of the eluent (desorption).

The results of the best separations on silica gel impregnated with 0.05 *M* TCMA, with an eluent containing 30% of methanol and 0.25 *M* of NaCl, are given in Table I. The R_s values (resolution) are <1 in several instances, but barbituric acid can be separated from proxibarbal (R_s = 2.1) and hexobarbital from cyclobarbital (R_s = 1.6) with an eluent containing 10% of methanol and 0.25 *M* of NaCl on silica gel impregnated with 0.05 *M* TCMA. The other derivatives which have R_s values <1 in Table I cannot be separated.

REFERENCES

1 S. H. Hansen, *J. Chromatogr.*, 209 (1981) 203.
2 S. H. Hansen, P. Helboe, M. Thomsen and U. Lund, *J. Chromatogr.*, 210 (1981) 453.
3 S. H. Hansen, P. Helboe and U. Lund, *J. Chromatogr.*, 240 (1982) 319.
4 P. Helboe, *J. Chromatogr.*, 245 (1982) 229.
5 S. H. Hansen, P. Helboe and U. Lund, *J. Chromatogr.*, 260 (1983) 156.
6 S. H. Hansen, P. Helboe and U. Lund, *J. Chromatogr.*, 270 (1983) 77.
7 S. H. Hansen, P. Helboe and M. Thomsen, *J. Chromatogr.*, 368 (1986) 39.
8 G. Szepesi, Z. Végh, Zs. Gyulai and M. Gazdag, *J. Chromatogr.*, 290 (1984) 127.
9 M. Gazdag, G. Szepesi, M. Hernyes and Z. Végh, *J. Chromatogr.*, 290 (1984) 135.
10 E. Tyihák, E. Mincsovics and H. Kalász, *J. Chromatogr.*, 174 (1979) 75.

11 E. Mincsovics, E. Tyihák and H. Kalász, *J. Chromatogr.*, 191 (1980) 293.
12 E. Tyihák, E. Mincsovics, H. Kalász and J. Nagy, *J. Chromatogr.*, 211 (1981) 45.
13 K. Kovács-Hadady and K. Barna-Katona, *J. Planar Chromatogr.*, 2 (1989) 133.
14 C. J. Cotzee and H. Freiser, *Anal. Chem.*, 40 (1968) 2071.
15 C. J. Cotzee and H. Freiser, *Anal. Chem.*, 41 (1969) 1128.
16 N. Ishibashi, A. Jyo and K. Matsumoto, *Chem. Lett.*, (1973) 1297.
17 K. K. Choi and K. W. Fung, *Anal. Chim. Acta*, 138 (1982) 385.
18 K. Kovács-Hadady and J. Szilágyi, *J. Chromatogr.*, 553 (1991) 459.
19 K. Kovács-Hadady, and J. Szilágyi, *J. Planar Chromatogr.*, 4 (1991) 194.
20 Zs. Budvári-Bárány, G. Radeczky, A. Shalaby and Gy. Szász, *Acta Pharm. Hung.*, 59 (1989) 49.
21 M. Gazdag, G. Szepesi and M. Hernyes, *J. Chromatogr.*, 316 (1984) 267.
22 G. P. Tomkinson, I. D. Wilson and R. J. Ruane, *J. Planar Chromatogr.*, 2 (1989) 224.

Journal of Chromatography, 589 (1992) 307–313
Elsevier Science Publishers B.V., Amsterdam

CHROM. 23 734

Binary buffers for indirect absorption detection in capillary zone electrophoresis

Tiansong Wang and Richard A. Hartwick*

Department of Chemistry, State University of New York at Binghamton, Binghamton, NY 13902 (USA)

(First received May 28th, 1991; revised manuscript received September 11th, 1991)

ABSTRACT

The displacement processes in binary buffers (two acids and one base) were studied theoretically and experimentally. An equation that correlates the concentration change of buffer ingredients in the sample zone with their electrophoretic mobility was derived. According to the equation, when the mobility of a sample is between those of the two buffer components, the sample will mainly displace the species to which its mobility is closest. This displacement is termed mobility-selective displacement. Several binary buffers with different mobilities were studied, and the experimental results agreed semi-quantitatively with the theory.

INTRODUCTION

The development of improved detection methods in capillary electrophoresis is essential for the continued growth of applications. In principle, capillary zone electrophoresis (CZE) is well suited for direct analyses for compounds such as aliphatic carboxylic acids, amino acids and inorganic acids. However, many of these classes of compounds lack chromophores at useful wavelengths, or have such low molar absorptivities as to prevent reasonable sensitivity by absorption detection. Instead, conductivity detectors [1–7] and amperometric detectors [7–9] have been developed for the CZE of these compounds. The performance of conductivity and amperometric detectors is generally excellent, with detection limits of 10^{-6}–10^{-7} M for carboxylic acids and amino acids. The problems with these detectors are that they are more difficult to fabricate than absorption detectors and are not yet commercially available.

Another strategy for the detection of UV-transparent compounds in CZE is that of indirect fluorescence or indirect absorption detection. To achieve such indirect detection, an ion with either fluorescence or UV absorption properties, which is called the visualization agent, is added to the mobile phase in order to create a high background signal. The analyte ions that have the same sign of charge as the visualization agent are observed from the reduction of the background signal. Indirect fluorescence detection was first introduced to CZE by Kuhr and Yeung [10], and has been applied to the analysis of amino acids, nucleotides, inorganic anions and sugars [10–13]. Impressive detection limits can be achieved, with concentration limits of $2 \cdot 10^{-7}$ M for $H_2PO_4^-$ being reported [12].

Indirect UV detection in CZE was first reported by Hjertén *et al.* [14]. Foret *et al.* [15] presented more details and observed the effect of ion mobility on the peak shape, indicating that high sensitivity could be obtained by selecting visualization agents which have high molar absorptivities and effective mobilities similar to those of sample ions. More recently, indirect UV detection has been applied successfully to the detection of 30 anions separated by CZE [16].

For indirect absorption detection in CZE, the selection of buffers is critical. Currently, most

0021-9673/92/$05.00

indirect absorption and indirect fluorescence detection have been performed with monobuffers (*i.e.*, one acid and one base), because the displacement process in monobuffer is simple. However, monobuffers have several shortcomings: limited pH range because the pH is restricted by the pK of the acid or the base, not ideal for broad mobility ranges of sample ions because the peak shape will be very poor with increasing mobility difference between the sample and visualization agent [15,17] and limited selection in concentration and molar absorptivity of the visualization agent because of the requirements of buffer capacity and linear range of the detector.

It is expected that binary buffers (*i.e.*, two acids and one base) can be used to overcome several of these limitations, but little work has been done on applications of binary buffers [10]. In this paper, a theoretical analysis and experimental study of binary buffer systems are presented. The effects of ion mobility on the displacement and on the peak shape are discussed.

THEORETICAL

In CZE, each ion migrates according to its own mobility under an electric field. The fundamental electrical property that must be satisfied along the path of the capillary is that the electrical current be constant throughout the capillary length. The relationship of current I_i to ion i is [18]

$$I_i = Z_i C_i \mu_i E A F \tag{1}$$

where Z_i is the value of the charge, C_i is the concentration, μ_i is the ion mobility, E is the applied electric field strength, A is the cross-sectional area of solution and F is the Faraday constant. The total current I is

$$I = \sum I_i \tag{2}$$

In Fig. 1, zone B contains only the buffer with anion 1, anion 2 and cation, thus

$$I_b = (Z_1 C_1 \mu_1 + Z_2 C_2 \mu_2 + Z_+ C_+ \mu_+) E_b A F \tag{3}$$

Zone S contains buffer and sample anion 3 and they share the same cation; the concentration of anion 1 and anion 2 will be different from that in zone B, hence

$$I_s = (Z_1 C_1' \mu_1 + Z_2 C_2' \mu_2 + Z_3 C_3 \mu_3 + Z_+ C_+' \mu_+) E_s A F \tag{4}$$

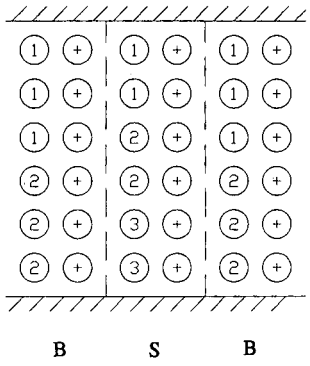

Fig. 1. Representation of two zones in CZE. S, sample zone; B, buffer zone. 1 = Buffer anion 1; 2 = buffer anion 2; 3 = sample anion; + = cation.

It is obvious that $I_s = I_b$, and provided that $C_3 \ll C_1 + C_2$, it is assumed that

$$E_s = E_b \tag{5}$$

Therefore,

$$Z_1 C_1 \mu_1 + Z_2 C_2 \mu_2 + Z_+ C_+ \mu_+ = Z_1 C_1' \mu_1 + Z_2 C_2' \mu_2 + Z_3 C_3 \mu_3 + Z_+ C_+' \mu_+ \tag{6}$$

Let $\Delta C_i = C_i - C_i'$, then eqn. 6 becomes

$$Z_1 \Delta C_1 \mu_1 + Z_2 \Delta C_2 \mu_2 + Z_+ \Delta C_+ \mu_+ = Z_3 C_3 \mu_3 \tag{7}$$

As electroneutrality must hold, then

$$Z_+ C_+ = -(Z_1 C_1 + Z_2 C_2) \tag{8}$$

$$Z_+ C_+' = -(Z_1 C_1' + Z_2 C_2' + Z_3 C_3) \tag{9}$$

Hence

$$Z_+ \Delta C_+ = -(Z_1 \Delta C_1 + Z_2 \Delta C_2 - Z_3 C_3) \tag{10}$$

Combining eqns. 7 and 10, after rearrangement, yields

$$\frac{Z_1 \Delta C_1}{Z_2 \Delta C_2} = \frac{Z_3 C_3 (\mu_3 - \mu_+)}{Z_2 \Delta C_2 (\mu_1 - \mu_+)} - \frac{\mu_2 - \mu_+}{\mu_1 - \mu_+} \tag{11}$$

Assuming that the displacement is in 1:1 ratio in terms of electric charge, then

$$Z_3 C_3 = Z_1 \Delta C_1 + Z_2 \Delta C_2 \tag{12}$$

Combining eqns. 11 and 12, one obtains

$$\frac{Z_1 \Delta C_1}{Z_2 \Delta C_2} = \frac{\mu_3 - \mu_2}{\mu_1 - \mu_3} \tag{13}$$

Eqn. 13 correlates the concentration changes of

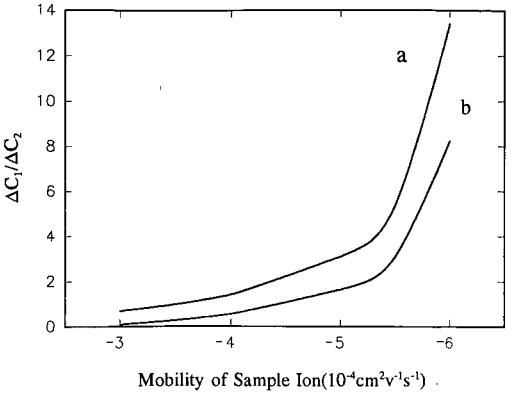

Fig. 2. Relationship between concentration change and ion mobility (eqn. 13). $Z_1 = Z_2 = Z_3$. (a) $\mu_1 = -6.4 \cdot 10^{-4}$, $\mu_2 = -0.64 \cdot 10^{-4}$; (b) $\mu_1 = -6.4 \cdot 10^{-4}$, $\mu_2 = -2.7 \cdot 10^{-4}$.

different buffer components in the sample zone with their mobility and is suitable for Z_1, Z_2 and Z_3 having the same sign and $|\mu_1| > |\mu_3| > |\mu_2|$. This relationship is illustrated in Fig. 2.

EXPERIMENTAL

A Spectra Phoresis 1000 with an SP4400 integrator (Spectra Physics, Reno, NV, USA) was used. The column temperature was 25.0°C, the detector rise time was 0.5 s and sample was injected by a 1.0-s hydrodynamic injection. A laboratory-made PEG bonded capillary and a bare fused-silica capillary (Polymicro Technologies, Phoenix, AZ, USA) were used, both being 75 μm I.D. × 360 μm O.D. with a effective length of 35 cm and a total length 43 cm.

Stock solutions of 10 m*M* 1,3,5-benzenetricarboxylic acids (BTA) and 2 m*M* 1-naphthylacetic acid (NAA) were prepared by dissolving the acids in boiling distilled water. Solutions of lower concentration were obtained by dilution. Buffers of pH 8 were prepared by adding Tris solution.

Sample solutions (malonic acid, tartaric acid, citric acid, propionic acid, hexanoic acid and sodium chloride) of 0.01 *M* were prepared and adjusted to pH 8.0 with Tris solution in order to keep sample pH close to the buffer pH, then diluted to the desired concentration with distilled water. Just before injection, sample solutions were further diluted with buffer in a 1:1 ratio, and the final concentrations were 1.0×10^{-5} *M* for malonic acid and tartaric acid and 2.0×10^{-5} *M* for propionic acid, hexanoic acid and sodium chloride.

The mobilities of BTA and NAA were measured in 1 m*M* phosphate buffer at pH 7.25 and other compounds in 0.5 m*M* BTA–Tris at pH 8.08.

BTA, NAA and hexanoic acid were obtained from Aldrich (Milwaukee, WI, USA), malonic acid and DL-tartaric acid from Sigma (St. Louis, MO, USA), Tris from Bio-Rad Labs. (Richmond, CA, USA) and all other chemicals from Fisher (Fair Lawn, NJ, USA).

RESULTS AND DISCUSSION

One-visualization-agent binary buffer

In this kind of buffer system, the pH is controlled by a secondary non-UV-absorbing component. Hence the disassociation constant of the visualization agent can varied over a broad range, and its concentration can be minimized without a decrease in buffer capacity.

When using a one-visualization-agent binary buffer, competitive displacement between the visualization agent and the pH-controlling ingredient is the problem. There are two cases, as follows.

(1) The mobility of the pH-controlling component is close to that of the visualization agent, and the sample mobility is out of the mobility range of the buffer ingredients. In this instance, common competitive displacement (*i.e.*, no obvious discrimination among the ions to be displaced) takes place, and the sensitivity will obviously be reduced. Two such binary buffers (BTA–citric acid and NAA–hexanoic acid, with the mobilities listed in Table I) were studied and the results are tabulated in Table II. When a binary buffer is used, the sensitivity decreases by 83–90% as the result of competitive

TABLE I

ION MOBILITIES

Compound	μ (10^{-4} cm^2 V^{-1} s^{-1})
NAA	−2.55
Hexanoate	−2.68
Propionate	−3.34
Tartrate	−5.63
Malonate	−6.11
Citrate	−6.20
BTA	−6.39
Chloride	−7.40

TABLE II

COMPARISON OF UNIFORMED PEAK AREA IN MONOBUFFER WITH THAT IN BINARY BUFFER WITH CLOSE MOBILITIES OF BOTH COMPONENTS

Compound	Uniformed peak area (10^3)[a]			
	0.5 m*M* BTA	1.0 m*M* CA[b]–0.1 m*M* BTA	0.3 m*M* NAA	1.0 m*M* HA[c]–0.1 m*M* NAA
Chloride	2.72	0.34	4.13	0.59
Malonate	2.06	–	4.00	0.32
Tartrate	2.15	0.29	3.38	0.38
Propionate	1.30	0.23	4.39	0.56

[a] Uniformed peak area = area/counts retention time.
[b] Citric acid.
[c] Hexanoic acid.

displacement, whereas the noise is reduced only by about 30%. Therefore, this type of binary buffer is generally poor.

(2) The mobility of the pH-controlling component is very different from that of the visualization agent and the sample mobility is in the mobility range of the buffer components. In this instance, mobility-selective displacement will take place. According to eqn. 13, the sample will mainly displace the species to which its mobility is closest, and this process is independent of the concentration of both buffer ingredients. For instance, using BTA–hexanoic acid binary buffer, $\mu_1 = -6.39 \times 10^{-4}$ (BTA), $\mu_2 = -2.68 \times 10^{-4}$ (hexanoate), and when the sample mobility is -6.11×10^{-4} (malonic acid), the concentration change of BTA will be 12.2 times that of hexanoic acid. In other words, the decrease in sensitivity is only 7.6%. The experimental results are given in Table III. Using 1.5 m*M* hexanoic acid–0.5 m*M* BTA binary buffer, the uniformed peak areas of malonate and tartrate are not much different from those in 0.5 m*M* BTA monobuffer, and the uniformed peak areas of these two compounds in 1.5 m*M* hexanoic acid–0.05 m*M* BTA binary buffer are even slightly higher than those in 0.5 m*M* BTA monobuffer, which may be caused by the variation of injection and by the reduction of noise. Generally, the data in Table III are in semi-quantitative agreement with eqn. 13, in that the competitive displacement of hexanoate is supressed in the zones of malonate and tartrate which have mobilities close to that of BTA, and this situation is obviously not affected by the concentration ratio of the pH-controlling component to the visualization agent in the range 3:1–30:1.

TABLE III

COMPARISON OF UNIFORMED PEAK AREA IN MONOBUFFER WITH THAT IN BINARY BUFFER WITH VERY DIFFERENT MOBILITIES OF BOTH COMPONENTS

Compound	Uniformed peak area (10^3)[a]		
	0.5 m*M* BTA	1.5 m*M* HA[b]–0.5 m*M* BTA	1.5 m*M* HA[b]–0.05 m*M* BTA
Chloride	2.72	1.40	1.06
Malonate	2.06	1.83	2.68
Tartrate	2.15	2.19	2.78
Propionate	1.30	no peak	no peak

[a] Uniformed peak area = area/counts retention time.
[b] Hexanoic acid.

When the sample mobility is out of the mobility range of the buffer components, common competitive displacement will dominate again; the higher the concentration of non-UV-absorbing ions, the greater is the decrease in sensitivity, as indicated by chloride in Table III.

Other evidence of mobility-selective displacement is provided by the peak shape. Fig. 3 presents two electropherograms, one obtained from 1.0 m*M* hexanoic acid–0.1 m*M* NAA buffer and the other from 1.5 m*M* hexanoic acid–0.05 m*M* BTA buffer. Although both buffers contain the same pH-con-

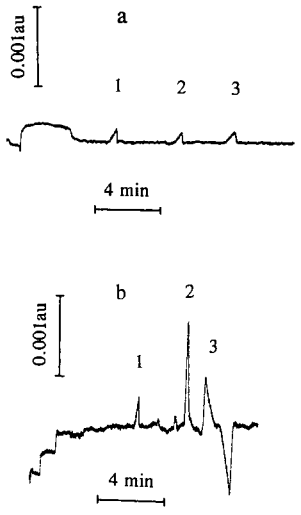

Fig. 3. Comparison of peak shape in one-visualization-agent binary buffers. (a) 1.0 m*M* hexanoic acid – 0.1 m*M* NAA–Tris (pH 8.08); (b) 1.5 m*M* hexanoic acid–0.05 m*M* BTA–Tris (pH 8.09). PEG bonded capillary. Peaks: 1 = chloride; 2 = malonate; 3 = tartrate ($1 \cdot 10^{-5}$–$2 \cdot 10^{-5}$ *M* each).

trolling component, the peak shape is very different. In hexanoic acid–NAA buffer, all peaks are obviously fronting, because the sample ions have much higher mobilities than either hexanoate or NAA. If common competitive displacement was dominant, the replacement of a small amount of NAA with BTA would obviously not affect the peak shape. However, in hexanoic acid–BTA buffer, the peak of malonate becomes symmetrical and the peak of tartrate changes to tailing, similarly to those in BTA monobuffer. Therefore, it is believed that the displacement takes place mainly between BTA and sample (malonate and tartrate), the effect of hexanoate being supressed.

Two-visualization-agent binary buffer

Because of the mobility-selective displacement in binary buffer, the peak shape can be controlled by either of the buffer components. When a buffer is prepared from two visualization agents with different mobilities, good peak shape for ions over a broad mobility range is expected. The experimental results using such a binary buffer can be seen from Table IV and Fig. 4. In BTA monobuffer, the fast ion (malonate) yields a good peak, whereas the slow ion (hexanoate) gives a poor peak. In NAA monobuffer, the situation reversed, *i.e.*, the fast ion generates a poor peak whereas the slow ion generates a good peak. When using BTA–NAA binary buffer, poor peaks seem to disappear and only the good peaks remain. For tartrate, there is no improvement in peak shape, because its mobility is not close enough to that of any visualization agent. In order to improve the peak shape of tartrate, a third visualization agent may be necessary. From this general behavior, it is evident that multi-visualization agents with small (or, ideally, continuous) mobility intervals will be ideal for analyses for ions with broad mobility ranges.

Disturbance peak in binary buffer

In the analysis using BTA–hexanoic acid buffer, a positive peak always appears (Fig. 3b), and peaks with retention times longer than the positive peak disappear, such as propionic acid (Table III). The retention time of the positive peak varies with the concentration ratio of the two buffer components.

TABLE IV

COMPARISON OF PEAK SHAPE AND EFFICIENCY IN MONOBUFFER WITH THOSE IN BINARY BUFFER

Compound	0.3 m*M* BTA		1.0 m*M* NAA		0.25 m*M* BTA–0.25 m*M* NAA	
	N (10^4)[a]	b/a[b]	N (10^4)	b/a	N (10^4)	b/a
Hexanate	4.56	0.29	7.75	0.76	8.06	1.2
Tartrate	3.74	0.18	2.41	7.8	3.02	0.16
Malonate	4.43	0.56	1.37	12	4.10	0.50

[a] Theoretical plate number measured at half-height.
[b] Asymmetry factor measured at 10% of peak height.

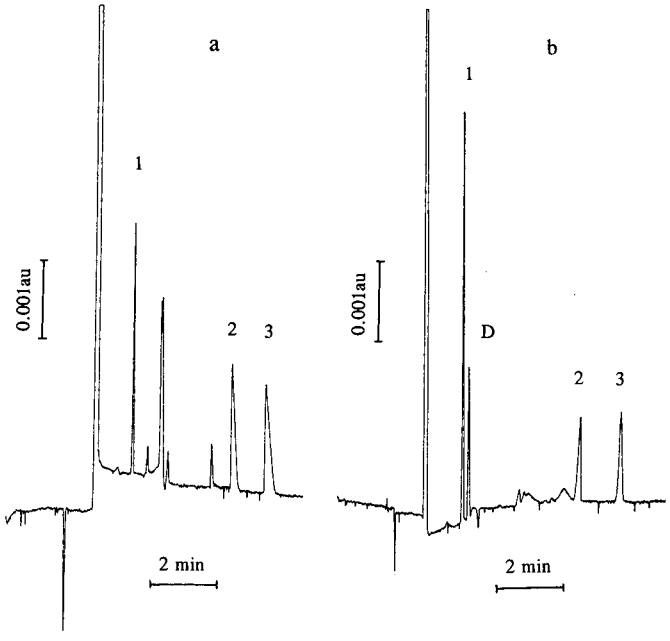

Fig. 4. Comparison of peak shape in monobuffer and in binary buffer. (a) 1.0 m*M* NAA–Tris (pH 8.09); (b) 0.25 m*M* NAA–0.25 m*M* BTA–Tris (pH 8.09). Bare fused-silica capillary. Peaks: 1 = hexanoate; 2 = tartrate; 3 = malonate; D = disturbance peak.

In two-visualization-agent binary buffer, a disturbance peak is also found, but is of negative response. This disturbance peak causes the disappearance of the acetate peak. At present, the disturbance peak is an unsolved problem.

CONCLUSIONS

In binary buffers, there are two kinds of displacement: common competitive displacement which causes a severe decrease in sensitivity, and mobility-selective displacement, which does not lead to obvious decreases in sensitivity. The dominant displacement depends on the mobilities of each species. Theoretical analysis (eqn. 13) indicates that, when the mobility of a sample ion lies between the mobilities of the two buffer components, the sample will mainly displace the species to which its mobility is closest. The experimental results for sensitivity and peak shape support this theory.

In mobility-selective displacement, the peak shape depends on the mobility of the buffer component that dominates the displacement. An improvement in peak shape for both fast and slow ions is observed using the two-visualization-agent binary buffer.

ACKNOWLEDGEMENTS

This research was supported by Spectra-Physics Autolab Division and by the Center for Biotechnology at Stonybrook.

REFERENCES

1 F. E. P. Mikkers, F. M. Everaerts and Th. P. E. M. Verheggen, *J. Chromatogr.*, 169 (1979) 11.
2 P. Gebauer, M. Deml, P. Boček and J. Janak, *J. Chromatogr.*, 267 (1983) 455.
3 J. L. Beckers, Th. P. E. M. Verheggen and F. M. Everaerts, *J. Chromatogr.*, 452 (1988) 591.
4 X. Huang, T. J. Pang, M. J. Gordon and R. N. Zare, *Anal. Chem.*, 59 (1987) 2747.
5 X. Huang, J. A. Luckey, M. J. Gordon and R. N. Zare, *Anal. Chem.*, 61 (1989) 766.
6 X. Huang, M. J. Gordon and R. N. Zare, *J. Chromatogr.*, 480 (1989) 285.
7 X. Huang, R. N. Zare, S. Sloss and A. G. Ewing, *Anal. Chem.*, 63 (1991) 189.
8 R. A. Wallingford and A. G. Ewing, *Anal. Chem.*, 60 (1988) 1972.

9 T. M. Olefirowicz and A. G. Ewing, *J. Chromatogr.*, 499 (1990) 713.
10 W. G. Kuhr and E. S. Yeung, *Anal. Chem.*, 60 (1988) 1832.
11 W. G. Kuhr and E. S. Yeung, *Anal. Chem.*, 60 (1988) 2642.
12 L. Gross and E. S. Yeung, *J. Chromatogr.*, 480 (1989) 169.
13 T. M. Garner and E. S. Yeung, *J. Chromatogr.*, 515 (1990) 639.
14 S. Hjertén, K. Elenbring, F. Kilar, J. L. Liao, A. J. C. Chen, C. J. Siebert and M. D. Zhu, *J. Chromatogr.*, 403 (1987) 47.
15 F. Foret, S. Fanali, L. Ossicini and P. Boček, *J. Chromatogr.*, 470 (1989) 299.
16 W. R. Jones, P. Jandik and R. Pfeifer, *Am. Lab.*, 23, No. 8 (1991) 40.
17 F. E. P. Mikkers, F. M. Everaerts and Th. P. E. M. Verheggen, *J. Chromatogr.*, 169 (1979) 1.
18 P. W. Atkins, *Physical Chemistry*, W. H. Freeman, New York, 4th ed., 1990, p. 756.

Journal of Chromatography, 589 (1992) 315–319
Elsevier Science Publishers B.V., Amsterdam

CHROM. 23 677

Radial pH distribution during capillary electrophoresis with electroosmotic flow

Analysis with high ionic strength buffers

Anders Vinther*

**Novo Nordisk A/S, Department of Fermentation Physiology, Hagedornsvej 1, DK-2820 Gentofte, and Technical University of Denmark, Department of Chemical Engineering, Building 229, DK-2800 Lyngby (Denmark)*

Henrik Søeberg

Technical University of Denmark, Department of Chemical Engineering, Building 229, DK-2800 Lyngby (Denmark)

(First received June 18th, 1991; revised manuscript received August 8th, 1991)

ABSTRACT

The surface of a fused-silica capillary contains ionized silanol groups when in contact with a liquid solution at pH >2. Positive counter ions obeying the Boltzmann distribution law, including H^+, are responsible for the electroosmotic flow and a radial pH gradient. The pH value at the capillary wall can be more than 2 pH units lower than the bulk pH at the tube axis. If analysis is performed at a bulk pH slightly above the isoelectric point of analyte, the pH gradient can result in a net positively charged analyte near the wall. Severe analyte peak tailing or even total adsorption on the wall can occur. The pH gradient can be reduced by increasing the ionic strength of the buffer. Results at various pH values and buffer concentrations are presented.

INTRODUCTION

The characterization of polypeptides and proteins is a very promising area of capillary electrophoresis (CE) [1–6]. These substances, however, have a tendency for adsorption on the capillary wall owing to coulombic interactions between positive moieties of the polypeptide/protein and the negatively charged fused-silica capillary surface. Severe peak tailing or even total adsorption can result. There are several ways of minimizing these "chromatographic effects" [1,4,7–10], one of which is to perform the CE analysis at pH values above the isoelectric point (p*I*) of the polypeptide/protein [4].

Above the p*I* the analyte is net negatively charged, thus being repelled from the likewise negatively charged capillary wall. However, at pH values slightly above the analyte p*I* there are two factors that can cause severe peak tailing. First, even though the analyte is net negatively charged, eventual positive moieties of the molecule are still electrostatically attracted by the fused-silica surface. Second, in all capillaries with an electroosmotic flow, a pH gradient is established between the tube axis and the wall. Hence, when analysis is performed only slightly above the polypeptide/protein p*I*, the radial pH gradient can lead to a net positively charged analyte close to the wall and thereby cause analyte adsorption.

Here we present calculations of the pH gradient as a function of electroosmotic flow and temperature. Electropherograms illustrating the use of high ionic strength buffers to suppress the radial pH gradient are also shown.

0021-9673/92/$05.00

THEORY

One of the characteristics of CE in uncoated capillaries is a strong electroosmotic flow under typical experimental conditions. Electroosmosis is usually explained by the Gouy–Chapman model as revised by Stern [11]. At pH values above *ca.* 2 the silanol groups of the fused-silica capillary wall are ionized, thus making the inner surface negatively charged. Hydrated positive counter ions in the bulk solution are responsible for the electroosmotic flow when a voltage is applied. Hence analytes are transported through the capillary tube by the combined action of electroosmosis and electrophoresis.

The positive counter ions, including H^+, are distributed as a function of radial position in accordance with the Boltzmann equation. The Boltzmann distribution of H^+ ions results in a radial pH gradient in the double layer region, hence of the order of a few nanometres from the capillary surface. A maximum concentration of H^+ ions is obtained close to the wall, whereas the maximum pH is at the capillary tube axis.

The concentration ratio of H^+ ions at the tube wall, $[H^+]_0$, to that at the tube axis (bulk pH), $[H^+]$, is calculated as

$$[H^+]_0/[H^+] = \exp(ze\zeta/kT) \tag{1}$$

where z is the number of charges (= 1), e is the elementary charge (= $1.602 \cdot 10^{-19}$ C), k is the Boltzmann constant (= $1.38 \cdot 10^{-23}$ J K^{-1}) and T is the absolute temperature. The zeta potential, ζ, is calculated by using the equation for electroosmotic mobility, μ_{EO}:

$$\mu_{EO} = v_{EO}/E = \zeta\varepsilon_0\varepsilon_r/\eta \tag{2}$$

where v_{EO} is the electroosmotic velocity (cm s^{-1}), E is the electric field strength (V cm^{-1}) and ε_0 is the permittivity of vacuum (= $8.854 \cdot 10^{-12}$ C^2 J^{-1} m^{-1}). The relative permittivity, ε_r, is calculated as [12,13]

$$\varepsilon_r = 309.78\exp(-0.004605T) \tag{3}$$

while the viscosity, η, is approximated by [12]

$$\eta = (1/800)\exp(1958/T) \tag{4}$$

Combining eqns. 1–4 yields the pH gradient from the capillary tube axis to the wall:

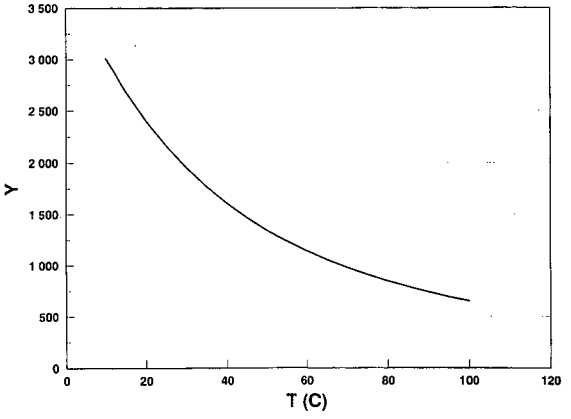

Fig. 1. $Y = \Delta pH/\mu_{EO}$ *vs.* temperature (T, °C). Y is calculated using eqn. 5b. See the text for details.

$$\Delta pH = \log([H^+]_0/[H^+]) = \frac{528.67\exp(1958/T + 0.004605T)}{\ln(10) \cdot T}\mu_{EO} \tag{5a}$$

$$\Longleftrightarrow$$

$$\Delta pH = Y(T)\mu_{EO} \tag{5b}$$

Hence ΔpH is proportional to μ_{EO}, the proportionality constant Y being a function of the temperature, T.

$Y(T)$ is depicted in Fig. 1, and Fig. 2 shows ΔpH *vs.* μ_{EO} at four different temperatures. The pH gradient decreases at decreasing μ_{EO} values (a low bulk pH and/or a high buffer ionic strength suppresses the electroosmotic flow) and increasing

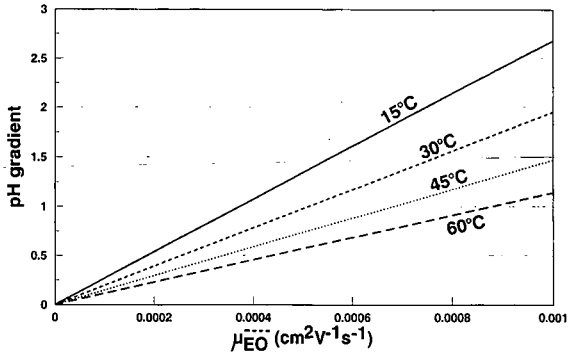

Fig. 2. Radial pH gradient (ΔpH) *vs.* the electroosmotic mobility (μ_{EO}) at four selected temperatures. ΔpH was calculated using eqn. 5a. Under typical experimental conditions such as μ_{EO} = 0.0006 cm^2 V^{-1} s^{-1} at 30°C, ΔpH exceeds unity. See the text for details.

temperatures. It is interesting that pH gradients exceeding unity are often met under typical experimental conditions such as $\mu_{EO} = 0.0006$ cm^2 V^{-1} s^{-1} at 30°C.

EXPERIMENTAL

Biosynthetic human growth hormone (B-hGH) was obtained from Novo Nordisk (Gentofte, Denmark), 2-(N-morpholino)ethanesulphonic acid (MES) from Sigma (St. Louis, MO, USA) and N-[tris(hydroxymethyl)methyl]glycine(tricine) from Fluka (Buchs, Switzerland). A 50 μm I.D. × 192 μm O.D. capillary from Polymicro Technologies (Phoenix, AZ, USA) was cut to a 50-cm total length; the effective length from the introduction end to the detector was 25 cm.

All experiments were performed on an Applied Biosystems Model 270A CE instrument. Except for the electropherogram in Fig. 8, the experimental conditions were as follows. A 0.5 mg/ml B-hGH sample was introduced in 2.0s by means of a 16.8-kPa vacuum; 8 kV was applied during analysis (160 V/cm). Detection was accomplished at 200 nm with a 0.5-s detector rise time. The capillary tube was thermostated at 30°C.

Three experimental series were performed, with different pH values of the MES running buffer. In series 1 the buffer solution had a pH of 6.5 and the MES concentration was varied in the range 12.5–625 m*M*, in series 2 the buffer pH was 6.0 and the MES concentration was varied in the range 25–625 m*M* and in series 3 a 625 m*M* MES buffer at pH 5.5 was used. A 625 m*M* MES stock solution was adjusted to the desired pH by addition of NaOH. The MES concentration was varied by diluting the 625 m*M* MES stock solution with distilled water.

The specific conductivity of the buffer solutions was measured with a CDM 83 conductivity meter (Radiometer, Copenhagen, Denmark) at 21°C. The results are shown in Fig. 3.

RESULTS AND DISCUSSION

Human growth hormone (hGH) is a protein consisting of 191 amino acids [14]. The molecular weight is 22 125 dalton and the isoelectric point (p*I*) is close to pH 5.0.

CE analysis was carried out at three pH values

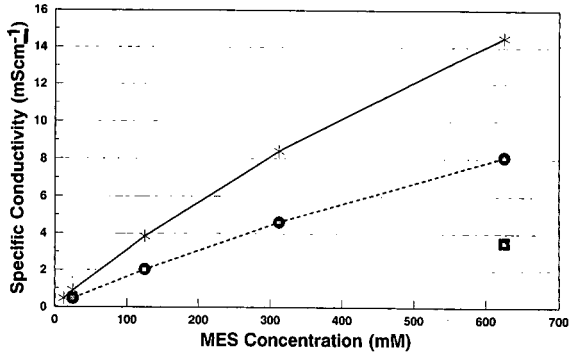

Fig. 3. Measured specific conductivity *vs.* MES concentration in the three experimental series. The pH was adjusted with NaOH, while a 625 m*M* MES stock solution was diluted to the desired final concentration with distilled water. pH: ✳ = 6.5; ● = 6.0; ■ = 5.5.

(5.5, 6.0 and 6.5) above the hGH p*I* and at various MES concentrations (12.5–625 m*M*). Fig. 4 shows the measured μ_{EO} values (eqn. 2) *vs.* the measured specific conductivity (mS/cm) of the buffer solutions. μ_{EO} decreases exponentially with increasing specific conductivity. Further, μ_{EO} increases with increasing pH as a larger proportion of the silanol groups are ionized.

Converting the measured μ_{EO} values to radial pH gradients in accordance with eqn. 5a ($T = 303.15$ K) yielded Fig. 5. At low MES concentrations the pH gradient exceeds unity. When the MES concentration is increased the electroosmotic mobility (and the double layer thickness) decreases, thus decreasing the radial pH gradient.

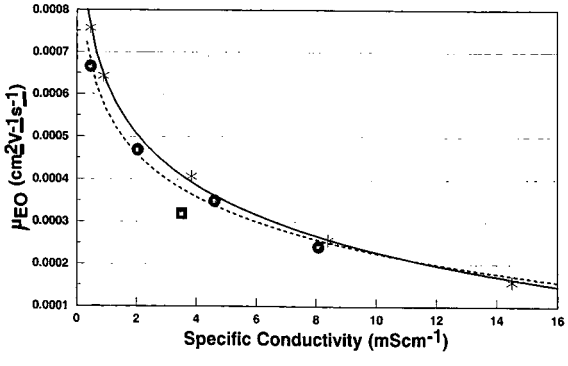

Fig. 4. Measured electroosmotic mobilities (μ_{EO}) *vs.* the measured specific conductivity for each of the buffers used in the experiments. The lines are exponentially fitted to the experimentally obtained values. pH: ✳ = 6.5; ● = 6.0; ■ = 5.5.

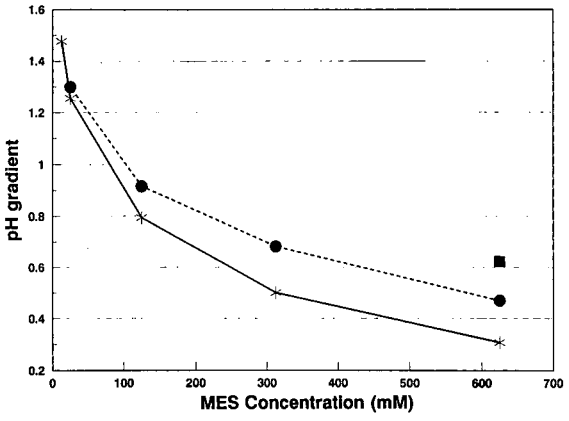

Fig. 5. Calculated radial pH gradient (ΔpH) *vs.* MES concentration for each experiment. ΔpH was calculated by inserting the measured μ_{EO} values in eqn. 5a (T = 303.15 K). pH: ✱ = 6.5; ● = 6.0; ■ = 5.5.

On replacing the pH gradients by the pH values at the capillary wall, Fig. 6 results. In two of the experiments the pH close to the silica surface was calculated to be below the B-hGH p*I* value of *ca.* 5. In those two experiments B-hGH did not elute at all, thus indicating total adsorption on the capillary wall.

All the electropherograms are shown in Fig. 7. With decreasing buffer concentrations the radial pH gradient increases and peak tailing becomes more pronounced. Only at the highest experimental buffer

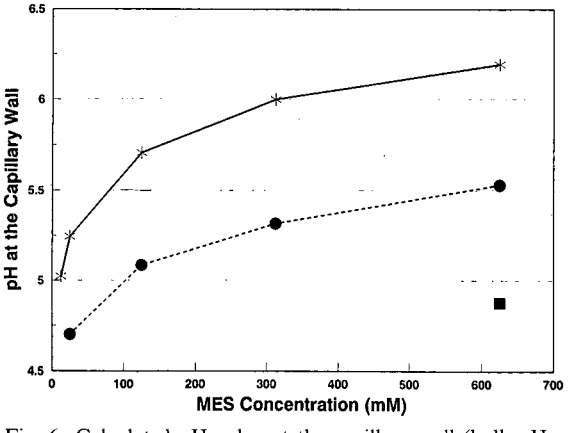

Fig. 6. Calculated pH value at the capillary wall (bulk pH − ΔpH) *vs.* MES concentration for each experiment. In two of the experiments the pH close to the capillary surface was below the hGH p*I* ≈ 5. pH: ✱ = 6.5; ● = 6.0; ■ = 5.5.

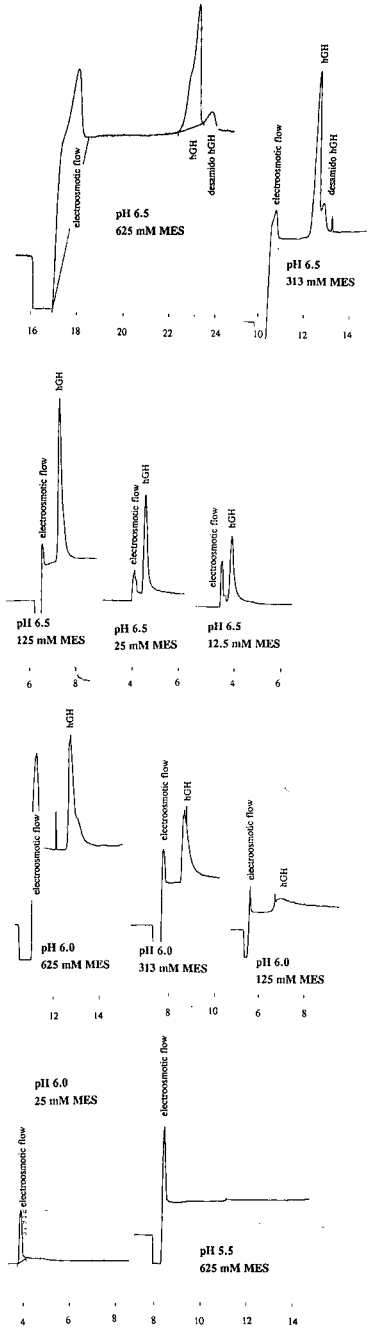

Fig. 7. All the electropherograms obtained during the three experimental series (bulk pH 5.5, 6.0 or 6.5). All retention times are in minutes. Increasing the MES concentration reduces peak tailing. For experimental conditions, see the text.

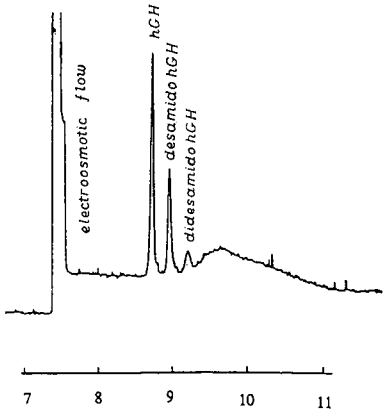

Fig. 8. Electropherogram showing baseline separation of hGH, desamido-hGH and didesamido-hGH [15]. The pH of the running buffer was 8.0. Retention times are in minutes. The experimental conditions were as follows: buffer, pH 8.0, 10 m*M* tricine; sample, 0.1 mg/ml B-hGH (which was allowed to degrade for several weeks at room temperature), introduced in 1.0 s by a 16.8-kPa vacuum; detection at 200 nm, 0.5-s detector rise time; capillary length, 100 cm (total), 75 cm (effective); I.D., 50 μm; 20 kV applied; temperature, thermostated at 27°C.

concentrations and pH values was a separation of hGH and its deamidated form observed, although it is poor. Baseline separation of hGH, desamido-hGH and didesamido-hGH is easily accomplished however, by increasing the buffer pH even further above the analyte p*I*, as shown in Fig. 8. The buffer pH was 8.0.

In addition to suppressing the pH gradient, at increasing buffer concentrations positive moieties in the protein molecule are more effectively shielded, thus decreasing coulombic wall–protein attractions. It is trivial to note that at pH values above the analyte pH increasing the bulk pH increases the capillary wall pH (and the net negative charge on the analyte), which also decreases the wall–protein attraction. Both phenomena contribute to less peak tailing.

CONCLUSIONS

If CE analysis of a polypeptide/protein is performed at a pH value slightly above its isoelectric point, it shows a tendency for adsorption on the fused-silica capillary wall owing to, among other factors, a radial pH gradient. The pH gradient can easily exceed unity under typical experimental conditions. Using high ionic strength buffers suppresses the pH gradient, thus decreasing excessive peak tailing. As an example, in order to keep ΔpH below 0.5, μ_{EO} should not exceed $2.5 \cdot 10^{-4}$ cm^2 V^{-1} s^{-1} at 30°C according to Fig. 2.

ACKNOWLEDGEMENT

The Danish Academy of Technical Sciences is acknowledged for financial support.

REFERENCES

1 A. Vinther, S. E. Bjørn, H. H. Sørensen and H. Søeberg, *J. Chromatogr.*, 516 (1990) 175.
2 P. D. Grossman, J. C. Colburn, H. H. Lauer, R. G. Nielsen, R. M. Riggin, G. S. Sittampalam and E. C. Rickard, *Anal. Chem.*, 61 (1989) 1186.
3 M. V. Novotny, K. A. Cobb and J. Liu, *Electrophoresis*, 11 (1990) 735.
4 H. H. Lauer and D. McManigill, *Anal. Chem.*, 58 (1986) 166.
5 J. Frenz, S.-L. Wu and W. S. Hancock, *J. Chromatogr.*, 480 (1989) 379.
6 H. Lüdi, E. Gassmann, H. Grossenbacher and W. Grossenbacher and W. Märki, *Anal. Chem. Acta*, 213 (1988) 215.
7 S. Hjertén, *J. Chromatogr.*, 347 (1985) 191.
8 R. M. McCormick, *Anal. Chem.*, 60 (1988) 2322.
9 M. M. Bushey and J. W. Jorgenson, *J. Chromatogr.*, 480 (1989) 301.
10 J. S. Green and J. W. Jorgenson, *J. Chromatogr.*, 478 (1989) 63.
11 A. W. Adamson, *Physical Chemistry of Surfaces*, Wiley, New York, Sons, 1982, Ch. 5.
12 A. Vinther and H. Søeberg, *J. Chromatogr.*, 559 (1991) 3.
13 R. C. Weast (Editor), *CRC Handbook of Chemistry and Physics*, CRC Press, Boca Raton, FL, 62nd ed., 1981.
14 T. Christensen, J. J. Hansen, H. H. Sørensen and J. Thomsen, in W. S. Hancock (Editors), *High Performance Liquid Chromatography in Biotechnology*, Wiley, New York, 1990, Ch. 9.
15 A. Vinther, H. H. Sørensen, A. M. Jespersen and H. Søeberg, *Talanta*, in press.

Journal of Chromatography, 589 (1992) 321–327
Elsevier Science Publishers B.V., Amsterdam

CHROM. 23 736

Capillary isoelectric focusing with electroosmotic zone displacement and on-column multichannel detection

Wolfgang Thormann*, Jitka Caslavska, Sarah Molteni and Josef Chmelík☆

Department of Clinical Pharmacology, University of Berne, Murtenstrasse 35, CH-3010 Berne (Switzerland)

(First received July 4th, 1991; revised manuscript received September 12th, 1991)

ABSTRACT

Isoelectric focusing (IEF) of proteins in uncoated, open-tubular fused-silica capillaries of 75 μm I.D. with on-column multiwavelength detection is reported. Small amounts of hydroxypropylmethylcellulose added to the catholyte are shown to provide column conditioning which allows rapid and high-resolution IEF analysis of proteins to be performed in the presence of an electroosmotic flow along the separation axis. The latter process displaces the developing zone pattern towards and across the point of detection. On-column multichannel zone detection is shown to be an efficient method for the simultaneous monitoring of the eluting proteins and carrier ampholytes. The absorbance profiles monitored at one location towards the capillary end and the temporal behaviour of the current under constant voltage conditions are shown to provide information on the degree of focusing at the time of detection.

INTRODUCTION

Traditionally, isoelectric focusing (IEF) has been carried out in gels, requiring tedious, time-consuming preparation and protein staining procedures [1]. In the past few years, however, attention has been given to developing IEF into a more instrumental format. For example, free fluid focusing has been studied in capillaries of rectangular cross-sections [2–6], in glass tubular capillaries [7–9] and in PTFE capillaries [5,10,11]. These approaches operated with minimized electroosmosis in which stationary steady-state zone patterns were established. The zones were detected either by array detection [2,3,5,6] or by UV absorption measurements towards the column end, which required that the proteins were mobilized and swept past a stationary detector after focusing [7–11]. Although these developments did not initiate a widespread use of capillary IEF, they provided an insight into the principles and dynamics of IEF and complemented theoretical descriptions based on computer simulation [2,5,6,12].

Modern capillary-type electrophoretic analysers feature fused-silica capillaries of 25–100 μm I.D. which can exhibit strong electroosmotic flows. Proteins are vulnerable to interactions with the column walls. Not surprisingly, IEF experiments with proteins in untreated fused-silica capillaries cannot, in general, be reproduced, whereas much improved data are obtained in capillaries coated with linear polyacrylamide [13–15] or, alternatively, in PTFE capillaries with minimized electro-osmosis [10,11]. None of these approaches, however, is suitable for routine IEF analysis. The first lacks reproducibility because of the instability of the coatings and the second is too inefficient. Moreover, owing to the mobilization of the zone pattern after focusing, the two procedures are lengthy.

In a recently performed study it was discovered that small amounts of hydroxypropylmethylcellulose (HPMC) added to the buffer allowed high-resolution isotachophoretic analyses of proteins to be performed in untreated, open-tubular fused-silica capillaries, *i.e.* in the presence of an electroosmotic flow [16]. Consequently, the same approach was ap-

☆ Permanent address: Institute of Analytical Chemistry, Czechoslovak Academy of Sciences, CS-611 42 Brno, Czechoslovakia.

0021-9673/92/$05.00

plied to IEF. Independently, Mazzeo and Krull [17,18] investigated a similar method with the addition of methylcellulose. This group used a configuration which required the addition of a strong base to the sample to detect basic proteins. In this paper a fully dynamic approach to capillary IEF in the presence of an electroosmotic flow along the separation axis is reported and capillary IEF analysis with on-column multiwavelength detection is discussed.

EXPERIMENTAL

Chemicals

All chemicals used were of analytical reagent grade. Cytochrome *c* from horse heart [CYTC, molecular weight (MW) 12 384, p*I* 9.3], carbonic anhydrase from bovine erythrocytes (CA, MW 31 000, p*I* 6.18) and HPMC (7509) were from Sigma (St. Louis, MO, USA). Ferritin from horse spleen (FER, MW 450 000, p*I* 4.2–4.5) and equine myoglobin from skeletal muscle (MYO, MW 17 800, p*I* 6.8–7.0) were from Serva (Heidelberg, Germany). Ampholine (pH 3.5–10) was obtained from Pharmacia-LKB (Bromma, Sweden).

Electrolyte systems and sample preparation

For all the experiments presented here 20 m*M* sodium hydroxide and 10 m*M* orthophosphoric acid were used as the catholyte and anolyte, respectively. In most instances 0.06–0.3% HPMC was added to the catholyte. The sample components were dissolved in 2.5 or 5% (w/v) Ampholine without the addition of HPMC. Protein concentrations of 0.06–1 mg/ml were used.

Instrumentation and running conditions

The laboratory-made instrument used in this work has been described previously [16]. It features a 75 μm I.D. fused-silica capillary of about 90 cm length (Polymicro Technologies, Phoenix, AZ, USA) with a fast-scanning multiwavelength detector (Model UVIS 206 PHD) and a capillary detector cell (No. 9550-0155) (Linear Instruments, Reno, NV, USA). The effective separation distance was about 70 cm. No cooling of the capillary was provided. Two 50-ml plastic bottles served as electrode vessels and a VacTorr 150 vacuum pump (CGA/Precision Scientific, Chicago, IL, USA) was used to rinse the capillary tube. Current was applied at constant voltage (20 kV) with a Model HCN 14-20000 power supply (FUG Elektronik, Rosenheim, Germany). Multiwavelength data were read, evaluated and stored using a Mandax AT 286 computer system and running the 206 detector software package version 2.0 (Linear Instruments) with windows 286 version 2.1 (Microsoft, Redmont, WA, USA). Throughout this work the 206 detector was used in the high-speed polychrome mode by scanning from 195 to 320 nm at 5-nm intervals (26 wavelengths). New capillaries were first rinsed with 1 *M* sodium hydroxide solution (20 min) and then 0.1 *M* sodium hydroxide solution containing 0.3% HPMC (10 min). The latter solution was also used to condition the capillary at the beginning of a series of experiments (10-min wash). Before each run the capillary was cleaned with the catholyte for at least 10 min.

Sample application occurred manually via gravity through lifting the capillary end, dipped into the sample vial, some 34 or 65 cm for a specified time interval. With a 4-min injection at 34 cm height and a catholyte with 0.06% HPMC, an initial sample zone of about 5 cm length was obtained. The initial configuration of an experiment, a transient state and the detection phase are shown schematically in Fig. 1.

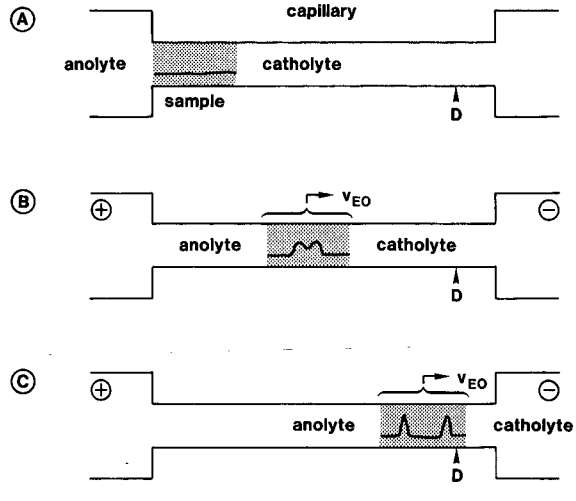

Fig. 1. Schematic representation of (A) the initial configuration, (B) a transient state and (C) detection for capillary IEF in the presence of electroosmosis. D represents the point of detection and v_{EO} the electroosmotic displacement. Carrier ampholytes are represented by the dotted area and the protein distribution by the solid line within that area.

RESULTS AND DISCUSSION

The experimental arrangement used in this work is shown schematically in Fig. 1. Experiments without the addition of HPMC to the catholyte were performed first. It was interesting to find that IEF experiments in the presence of electroosmosis and without proteins (*i.e.* with carrier ampholytes only) were reproducible. However, proteins added to the sample altered the system. Much longer elution times were observed and the experiments became irreproducible. This is similar to the situation reported in the isotachophoresis of proteins [16]. It is presumed that proteins are adsorbed onto the capillary walls, thereby forming a coating which changes the surface charge and thus the electroosmotic flow (reduction or even reversal of net sample flux). The additon of HPMC allowed the IEF analysis of proteins. Fig. 2 shows the focusing of CYTC and CA in 2.5% (w/v) Ampholine and with 0.06% HPMC in the catholyte. The concentrations of the two proteins in the sample were 0.16 and 0.27 mg/ml, respectively, and the initial sample zone length was about 5 cm. Fig. 2A shows the three-dimensional data obtained with on-column fast-scanning polychrome detection. The location of the two proteins is clearly visible as characteristic bands. Owing to the negative surface charge of untreated fused-silica, the entire pattern migrated towards the cathode. Basic proteins, such as CYTC, reach the detector before neutral and acidic proteins. The complex absorption pattern of the carrier ampholytes, seen particularly at low wavelengths, can also be seen (compare with Fig. 3A). The spectra in Fig. 2B represent time slices extracted from the eluting protein peaks. These normalized spectra were corrected for the background absorption of the carrier ampholytes, *i.e.* time slices taken adjacent to the protein zones were subtracted from those obtained within the protein peaks. Fig. 2C and D shows single-wavelength data for 200 and 280 nm, respectively. As a result of the strong absorption of the carrier ampholytes at 200 nm it is difficult to monitor the protein bands at this wavelength. With detection at 280 nm, however, specificity for proteins is obtained. Note that all the data presented in Fig. 2

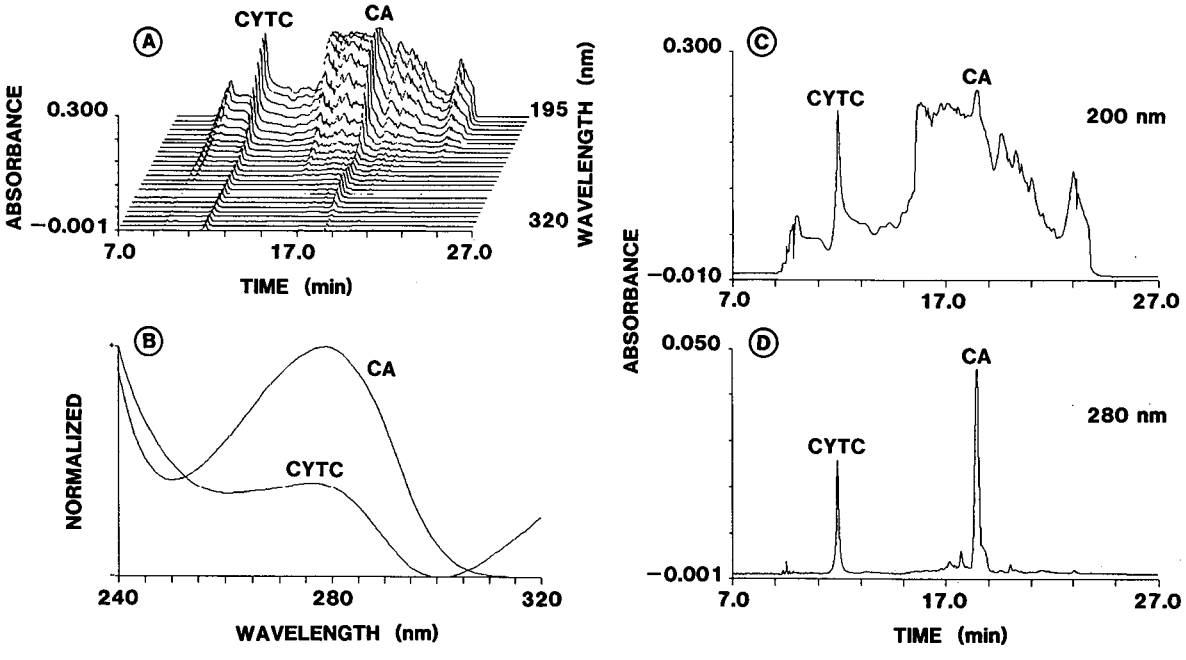

Fig. 2. Capillary IEF of CYTC (0.16 mg/ml) and CA (0.27 mg/ml) in 2.5% Ampholine. The HPMC concentration in the catholyte was 0.06%. Sampling occurred for 4 min at a height of 34 cm. The current values at the beginning, during protein detection and after 30 min of power application were about 25, 2 and 4 μA, respectively. (A) Three-dimensional data plot; (B) background corrected time slices (spectra) for the two proteins; (C) single-wavelength pherogram at 200 nm; (D) pherogram at 280 nm.

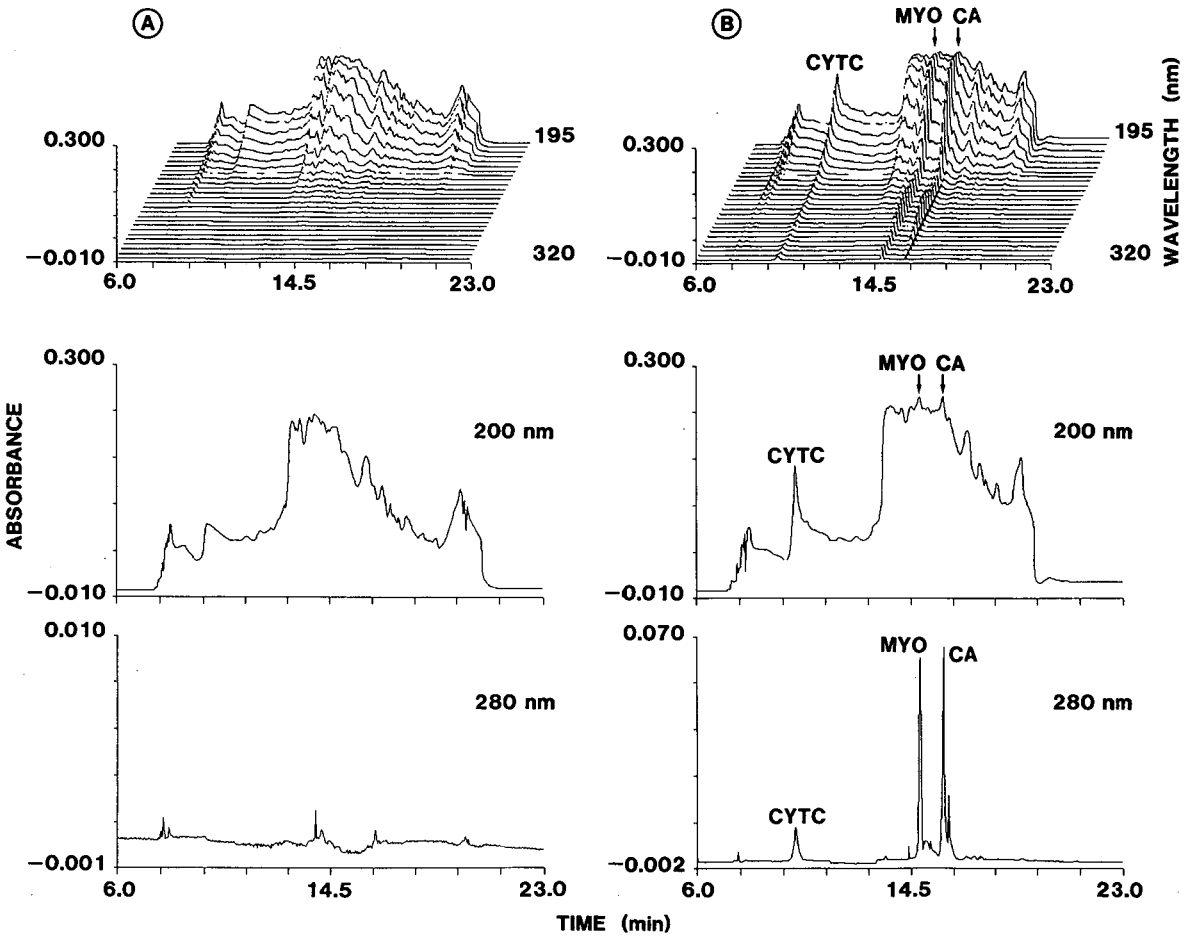

Fig. 3. Capillary IEF of (A) 2.5% Ampholine (blank) and (B) CYTC (0.13 mg/ml), MYO (0.20 mg/ml) and CA (0.22 mg/ml) in 2.5% carrier ampholytes. Other conditions as in Fig. 2.

were extracted from the multichannel data of one run. With multichannel detection the two protein zones and a characteristic IEF pattern of the carrier ampholytes are monitored simultaneously.

The applicability of capillary IEF in the presence of an electroosmotic displacement along the separation axis is further shown by the data presented in Fig. 3. Multichannel and single-wavelength pherograms of a blank (A) and a protein sample (B) are shown. The experimental conditions were essentially the same as in Fig. 2, the exceptions being that MYO was added to the sample as a third protein and that the runs were performed on another day. The pherograms are essentially equal, the retention times, however, are shorter than the previous day. This change is attributed to a different electroosmotic pumping rate, which indicates a slightly different conditioning state of the fused-silica surface. Such a variability is not considered to be a problem as long as an internal standard is used and/or the eluting carrier ampholytes are also monitored. The monitored zones are characterized by comparing time slices, *e.g.* the spectra of the protein zones. Background-corrected, normalized protein time slices of Fig. 3 are shown in Fig. 4A and B. As is shown in Fig. 4C and D, the spectra are in good agreement with those of Fig. 2B.

These simple experiments show that CYTC, MYO and CA can easily be analysed in presence of 0.06% HPMC. Other proteins, including bovine se-

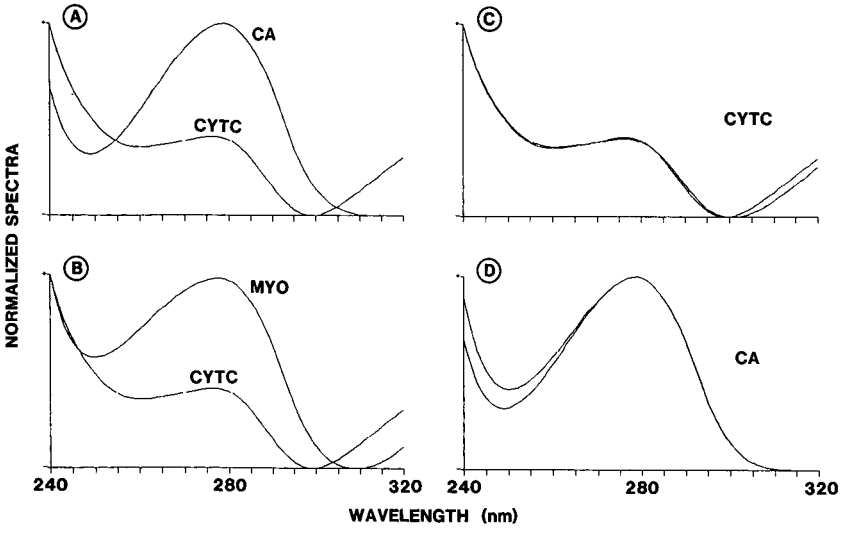

Fig. 4. Background-corrected time slices for (A) CA and CYTC and (B) MYO and CYTC extracted from the data presented in Fig. 3. Panels C and D show the comparison of background corrected normalized spectra of Figs. 2B and 4A for CYTC and CA, respectively.

rum albumin, FER and ribonuclease A, increased the retention times of proteins and carrier compounds, which is considered to be an indication of residual interaction between these proteins and the capillary walls. An increase of the HPMC concentration in the catholyte to 0.3% improved the behaviour of these proteins. With this simple sampling device, however, sample application became difficult. Experiments were therefore continued with 0.1% HPMC. The capillary IEF analysis of a sample containing CYTC, MYO, CA and FER in 2.5% Ampholine and with 0.1% HPMC in the catholyte is shown in Fig. 5A. Sampling occurred for 4 min at a height of 65 cm. All four proteins separated well, as is shown with the single-wavelength pherogram (centre panel) obtained at 280 nm. The trace denoted by S is believed to be a spike originating from particles (protein precipitates) which are transported through the detection cell. Similar spikes were observed in many other experiments.

The experiment was performed at a constant voltage of 20 kV and the current was monitored for the entire run. The temporal change of the current is shown in the bottom graph. It compares well with those published for free solution IEF systems with minimized electroosmosis [4,5]. The slight increase in current after about 15 min of power application was also observed in the experiments reported earlier (see, *e.g.*, the current values of the legend of Fig. 2) and is attributed to the gradual filling of the capillary with the anolyte after focusing has been attained. In all the experiments presented (Figs. 2, 3, 5A), it is assumed that full separation was attained prior to detection of the protein zones.

The risk of protein adsorption onto the capillary wall is not the only fundamental aspect of this IEF technique and experimental configuration used in this work. With a stationary, on-column detector placed towards the capillary end and electroosmotic zone displacement across its location, no complete confirmation of separation can be obtained in a single experiment. This is illustrated with the data shown in Fig. 5B and C. The sample load for the run shown in Fig. 5B was twice that of Fig. 5A; the sample zone lengths at the beginning of the two experiments, however, were equal. Comparison of the monitored absorbance profiles shows that the separation stages at the time of detection were different. Furthermore, the detection time intervals were shorter and the electric current higher with an increased sample concentration, the latter being caused by a smaller resistance across the developing gradient. The higher current produces a larger electroosmotic pump rate such that the characteristic ampholyte pattern could not be completely established prior to detection. The transient IEF data

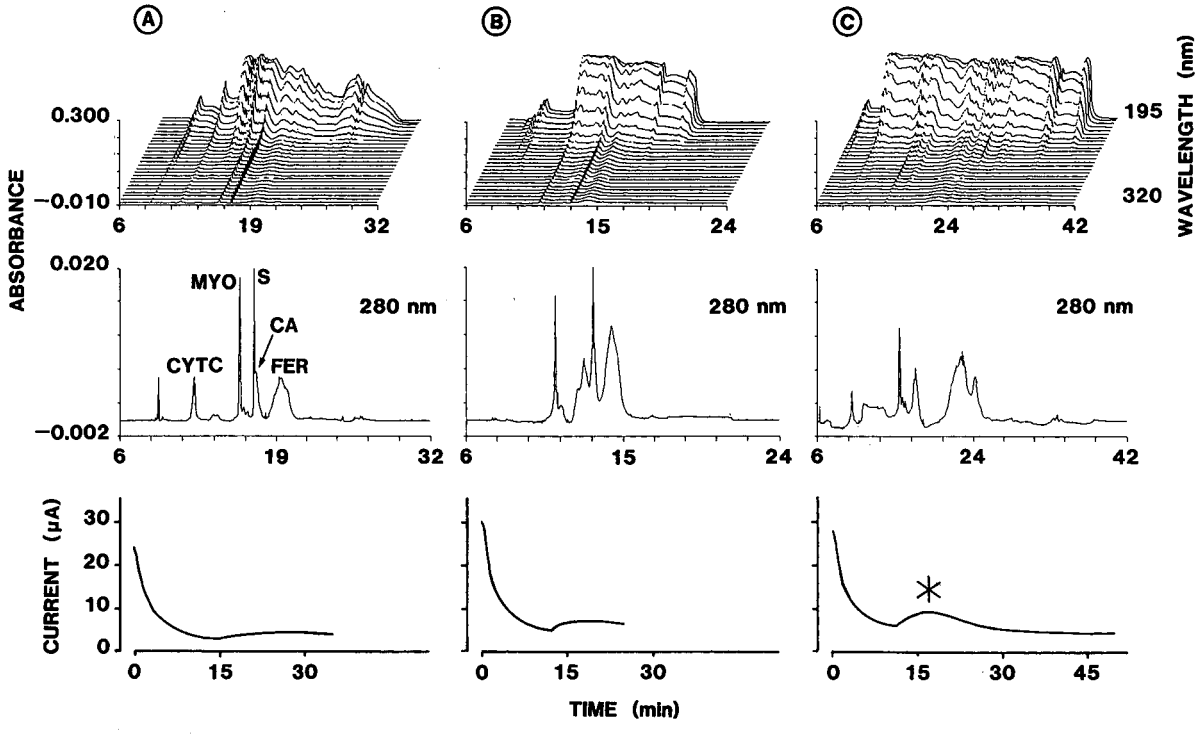

Fig. 5. Focusing of CYTC, MYO, CA and FER with 0.1% HPMC in the catholyte and sampling at a height of 65 cm. S represents a spike from a particle. (A) 4-min sampling of a 2.5% Ampholine solution containing 0.06 mg/ml of each protein. (B) 4-min sampling of a 5% Ampholine solution with 0.12 mg/ml of each protein. (C) 6-min sampling of a 5% Ampholine solution with 0.06 mg/ml of each protein. Three-dimensional pherograms (top panels), single-wavelength pherograms at 280 nm (centre graphs) and temporal behaviour of the current (bottom panels) are shown. Note that the absorbance data for the first 6 min are not depicted, whereas the complete current *versus* time graphs are presented. For other explanations, refer to text.

shown in Fig. 5C were obtained with an even higher sample load than that of Fig. 5B and with a longer initial sample zone. This example clearly illustrates that incomplete focusing is not only seen by the monitored absorbance profiles but also by the temporal behaviour of the current (bottom graph of Fig. 5C). The current–time relationship observed in Fig. 5C, particularly the characteristic current bump marked by the asterisk, was found to be typical for transient states which were not close to complete separation. With the increased sample loads of Figs. 5B and 5C, longer capillaries or capillaries with a reduced surface charge would have to be used to reach complete separation before detection.

CONCLUSIONS

The data presented in this paper prove the feasibility and show the complexity of performing protein IEF in untreated fused-silica capillaries with an electroosmotic flow along the separation axis. HPMC added to the catholyte, with which the capillary is filled prior to sample and power application, is believed to form a dynamic coating and to reduce the interaction between the proteins and the walls. It provides a simple conditioning effect which allows the IEF analysis of many proteins (at the nanogram level) in plain, open-tubular fused-silica capillaries of small I.D. in presence of an electroosmotic flow. The electroosmotic flow is responsible for the transport of the developing zone pattern through the capillary and across the point of detection. Fast-scanning polychrome detection is shown to be an interesting way of characterizing the protein zones and the carrier ampholytes. The absorbance profiles of the carrier ampholytes monitored at one location toward the capillary end and the temporal behaviour of the current provide useful

information on the degree of focusing at the time of detection. However, the confirmation of complete separation in one run can only be obtained with multiple detectors placed along the capillary. Further work has to be performed before this capillary IEF method can be adopted for routine analyses.

ACKNOWLEDGEMENTS

The generous loan of the UVIS 206 detector by its manufacturer, Linear Instruments (Reno, NV, USA), and of the HCN power supply by Mettler-Toledo (Greifensee, Switzerland) is gratefully acknowledged. This work was supported by the Swiss National Science Foundation.

REFERENCES

1 P. G. Righetti, *Isoelectric Focusing: Theory, Methodology and Applications*, Elsevier, Amsterdam, 1983.
2 W. Thormann, R. A. Mosher and M. Bier, *J. Chromatogr.*, 351 (1986) 17.
3 W. Thormann, N. B. Egen, R. A. Mosher and M. Bier, *J. Biochem. Biophys. Methods*, 11 (1985) 287.
4 W. Thormann, A. Tsai, J. P. Michaud, R. A. Mosher and M. Bier, *J. Chromatogr.*, 389 (1987) 75.
5 R. A. Mosher, W. Thormann and M. Bier, *J. Chromatogr.*, 436 (1988) 191.
6 R. A. Mosher, W. Thormann, R. Kuhn and H. Wagner, *J. Chromatogr.*, 478 (1989) 39.
7 S. Hjertén and M. Zhu, *J. Chromatogr.*, 346 (1985) 265.
8 S. Hjertén, J. L. Liao and K. Yao, *J. Chromatogr.*, 387 (1987) 127.
9 S. Hjertén, K. Elenbring, F. Kilàr, J. Liao, J. C. Chen, C. J. Siebert and M. Zhu, *J. Chromatogr.*, 403 (1987) 47.
10 M. A. Firestone and W. Thormann, *J. Chromatogr.*, 436 (1988) 309.
11 W. Thormann and M. A. Firestone, in J. C. Janson and L. Ridén (Editors), *Protein Purification*, VCH, Weinheim, 1989, pp. 469.
12 W. Thormann and R. A. Mosher, *Adv. Electrophoresis*, 2 (1988) 45.
13 F. Kilàr and S. Hjertén, *Electrophoresis*, 10 (1989) 23.
14 F. Kilàr and S. Hjertén, *J. Chromatogr.*, 480 (1989) 351.
15 M. Zhu, D. L. Hansen, S. Burd and F. Gannon, *J. Chromatogr.*, 480 (1989) 311.
16 P. Gebauer and W. Thormann, *J. Chromatogr.*, 558 (1991) 423.
17 J. R. Mazzeo and I. S. Krull, *BioTechniques*, 10 (1990) 638.
18 J. R. Mazzeo and I. S. Krull, presented at the *15th International Symposium on Column Liquid Chromatography, June 3–7, 1991, Basel*, Abstract P226/2.

Journal of Chromatography, 589 (1992) 329–332
Elsevier Science Publishers B.V., Amsterdam

CHROM. 23 722

Influence of poly(vinylpyrrolidone) on isotachophoretic separations of inorganic anions in aqueous electrolyte systems

V. Madajová, E. Turcelová and D. Kaniansky*

Department of Analytical Chemistry, Faculty of Science, Komenský University, Mlynská Dolina CH-2, 84215 Bratislava (Czechoslovakia)

(First received June 21st, 1991; revised manuscript received September 3rd, 1991)

ABSTRACT

Poly(vinylpyrrolidone) (PVP), a water-soluble polymer, was investigated for the use in the isotachophoretic (ITP) separation of a group of eighteen inorganic anions. The polymer (added to the leading electrolyte) was found to influence selectively the effective mobilities of some of the anions. In some instances the resulting differences in these separation characteristics provided ITP separations otherwise impossible in aqueous electrolyte systems. These separations were often associated with changes in the migration orders of the separands (*e.g.*, chlorate and perchlorate; nitrate and sulphate; iodide, chloride and sulphate). The use of PVP in the ITP determination of iodide in mineral water was effective in achieving a complete resolution of this trace constituent from a large excess of matrix anions (chloride, sulphate). Consequently, a $5 \cdot 10^{-6}$ mol/l concentration of iodide could be detected and no sample preparation was needed.

INTRODUCTION

Capillary isotachophoresis (ITP) is a convenient alternative to the separation and determination of inorganic anions in various matrices (*e.g.*, refs. 1–8). Here, separations in aqueous electrolyte systems are preferred in spite of the fact that some organic solvents could provide better ITP differentiations of this group of anions [9,10]. This preference of the aqueous systems can probably be ascribed to limited solubilities of the zones forming constituents in organic solvents.

The ionic mobilities of many inorganic anions are close in aqueous solutions [11,12]. As the pK_a values of the corresponding acids are also low in water (*e.g.*, 11 and 12), there are limited possibilities for optimizing the ITP separations via differences in the ionic mobilities or via different pK_a values [9]. Complex equilibria provide one way to solve these problems [13,14]. In their use, however, disturbances due to precipitations of the separands can occur [10]. In some instances these ITP separands can be resolved when a counter-ionic constituent of appropriate charge number is employed in the leading electrolyte [2,15,16]. It was shown [17] that the effective mobilities of some inorganic anions are influenced in a differentiating manner via the formation of host–guest complexes with cyclodextrins.

It was reported recently [18] that poly(vinylpyrrolidone) (PVP) dissolved in water interacts differentially with halides. These findings, based on NMR measurements, led us to investigate the role of PVP in the ITP separations of a group of inorganic anions when water is used as a solvent. This paper presents the results from this investigation and also shows some practical aspects of the use of this polymer in analytical ITP.

EXPERIMENTAL

Instrumentation

A CS isotachophoretic analyser (VVZ PJT, Spišská Nová Ves, Czechoslovakia) was assembled in the column-coupling configuration of the separation

0021-9673/92/$05.00

unit [19,20] using modules provided by the manufacturer and a preseparation column (7 cm in length) made in this laboratory [20]. The analytical column was provided with an on-column UVD 1 spectrophotometric detector (VVZ PJT) and the detection was carried out at 254 nm.

Chemicals

Chemicals used for the preparation of the leading and terminating electrolyte solutions were obtained from Serva (Heidelberg, Germany), Sigma (St. Louis, MO, USA) and Lachema (Brno, Czechoslovakia). Some of them were purified by conventional methods. Hydroxyethylcellulose 4000 (HEC) obtained from Serva was purified on a mixed-bed ion exchanger (Amberlite MB-1; BDH, Poole, UK). It was used as an anticonvective additive [9] in the leading electrolyte.

PVP was obtained from Fluka (Buchs, Switzerland), Serva and Lachema. Aqueous solutions of the polymer (10%, w/v) were purified in the same way as HEC.

Water delivered by a Rodem-1 two-stage demineralization unit (OPP, Tišnov, Czechoslovakia) was further purified by circulation through laboratory-made polytetrafluoroethylene (PTFE) cartridges packed with Amberlite MB-1 (Serva). Freshly recirculated water was used for the preparation of the electrolyte solutions.

Samples of mineral water were kindly provided by Dr. K. Hyánková (Department of Ground Water, Komenský University, Bratislava, Czechoslovakia).

TABLE I

OPERATIONAL SYSTEMS

Parameter	Electrolyte[a]	
	Leading	Terminating
Anion	Cl^-	MES
Concentration (m*M*)	10	5
Counter ion	HIS	HIS
Anticonvective additive	HEC	–
Concentration (%, w/v)	0.2	–
pH	6.0	*ca.* 6.0
PVP (%, w/v)	0–10%	–

[a] MES = Morpholinoethanesulphonic acid; HIS = histidine; HEC = hydroxyethylcellulose.

RESULTS AND DISCUSSION

Influence of PVP on the effective mobilities of inorganic anions

The electrolyte systems used thoroughout are given in Table I. In experiments aimed at investigating the influence of PVP on the effective mobilities of the anions, the polymer was present in the leading electrolytes at 0–10% (w/v) concentrations. In preliminary experiments we found that PVP from various sources (see Experimental) and of various molecular weights (Fluka, types K30, K60 and K90) have the same influence on the effective mobilities of anions when present in the leading electrolytes at the same concentrations. Small differences were found in the relative step heights (R_{SH}) from the conductivity detector for the same concentrations of various PVP preparations and could be ascribed to different actual concentrations of the polymer rather than to differences, orginating *e.g.*, from their different molecular weights.

The influence of the polymer on the effective mobilities of the anions is clear from Fig. 1. Here, the leading ion (Cl^-) and acetate were taken as reference constituents (ref. 9, p. 307) as they exhibited minimum changes in their step heights with increasing concentration of PVP. It should be noted that the R_{SH} values in PVP containing leading electrolytes were not influenced on addition of HEC (to eliminate disturbances due to electroosmosis as PVP had only a limited capability in this respect). These findings suggest that the distributions of the anions between the soluble polymeric phases [21] did not play a significant role.

From the plots in Fig. 1, it is apparent that PVP retarded the anions in a differentiating manner. A rough classification of the effect of PVP on the effective mobilities leads to the following ordering: I^-, SCN^-, ClO_4^-, $CrO_4^{2-} \gg NO_3^-$, ClO_3^-, NO_2^-, $P_2O_7^{4-}$, Br^-, $S_2O_3^{2-} \gg Cl^-$, SO_4^{2-}, PO_4^{3-}, SeO_3^{2-}, F^-, BrO_3^-, AsO_4^{3-}.

It is known that some organic anions interact with PVP. These interactions have been ascribed to hydrogen bonding, dipole–dipole (Van der Waals–Keesom) and dipole–induced dipole (Van der Vaals–Debye) forces and to hydrophobic effects [22]. Interactions of PVP with halogenides in aqueous solutions are explained via H_2O bridges between the polymer and the anions (the latter replace

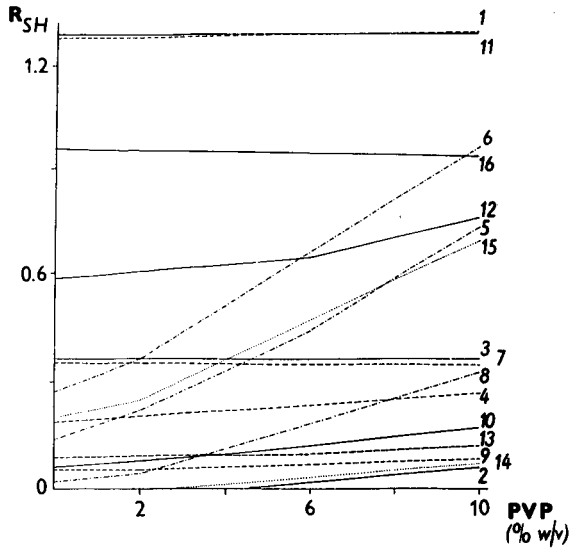

Fig. 1. Dependences of the effective mobilities (expressed in the R_{SH} units) of inorganic anions on the concentration of PVP in the leading electrolyte (for further details, see the text). 1 = AsO_4^{3-}; 2 = Br^-; 3 = BrO_3^-; 4 = ClO_3^-; 5 = ClO_3^-; 6 = CrO_4^{2-}; 7 = F^-; 8 = I^-; 9 = NO_2^-; 10 = NO_3^-; 11 = PO_4^{3-}; 12 = $P_2O_7^{4-}$; 13 = SO_4^{2-}; 14 = $S_2O_3^{2-}$; 15 = SCN^-; 16 = SeO_3^{2-}.

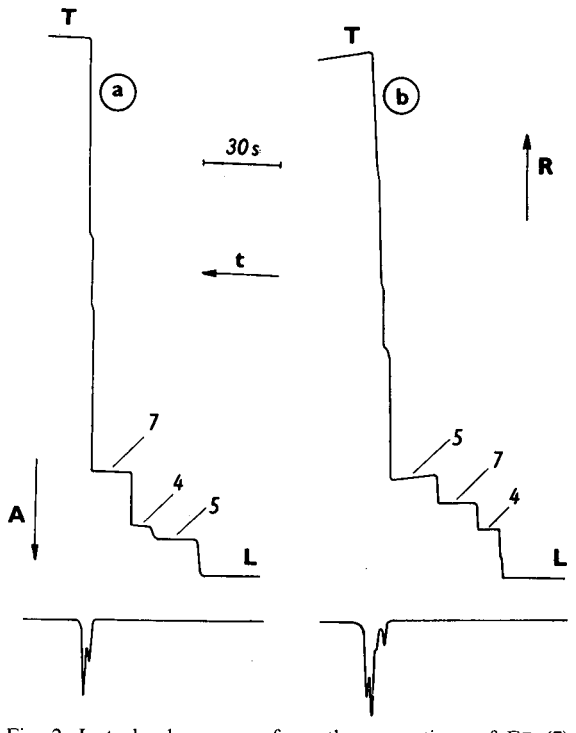

Fig. 2. Isotachopherograms from the separations of F^- (7), ClO_4^- (5) and ClO_3^- (4) by using leading electrolytes (a) without and (b) with PVP [6% (w/v) concentration]. Only the records from the analytical column are given. The driving current in the preseparation column was 250 μA and in the analytical column 50 μA. L, T = leading and terminating zones, respectively; *A*, *R*, *t* = increasing absorption, resistance and time, respectively.

H_2O molecules in the secondary and tertiary hydration spheres of the polymer [18].

Sulphite was found to be unstable in electrolyte systems containing PVP (it was oxidized to sulphate during the ITP run). This behaviour, at least as far as the extent is concerned, was not observed, *e.g.*, for nitrite, thus inducating a certain selectivity of the effect of PVP.

Examples of ITP separations of inorganic anions in water–PVP systems

The plots in Fig. 1 indicate that PVP provides some pratical possibilities for optimizing the separations of inorganic anions unattainable by other means (*e.g.*, pH, complex formation, non-aqueous or mixed solvents). For example, the isotachopherograms in Fig. 2 show that PVP is responsible for an improved separation of chlorate and perchlorate. Here, the effect of polymer can be explained analogously as for halides [18].

A model mixture consisting of anions with very close ionic mobilities in aqueous electrolyte systems (Fig. 3a) could be separated on addition of the polymer (Fig. 3b). From the practical point of view, *e.g.*, a change of the migration order of sulphate and nitrate (Fig. 3b) is worthy of attention. Also, the considerable retardation of I^- relative to Cl^- may have practical analytical utility. A series of isotachopherograms obtained in the determination of I^- in mineral water is given in Fig. 4 as an example.

Here, the spike mode of analysis as introduced by Arlinger [23] was preferred as it provides low detection limits when employed in conjunction with a selective detection method and appropriately chosen spacing constituents [24]. We were able to detect with confidence I^- present in a sample at a concentration of less than $5 \cdot 10^{-7}$ mol/l (for a 30-μl sample injection). This suggests that in mineral water (ten-fold diluted samples were injected) we could detect I^- at a 0.5 ppm concentration while Cl^- was present in the sample at a 10^4–10^5-fold excess. It is obvious that a better choice of the detection wavelength can lead to a further improvement in the detection limits (a 10–100-fold decrease seems feasi-

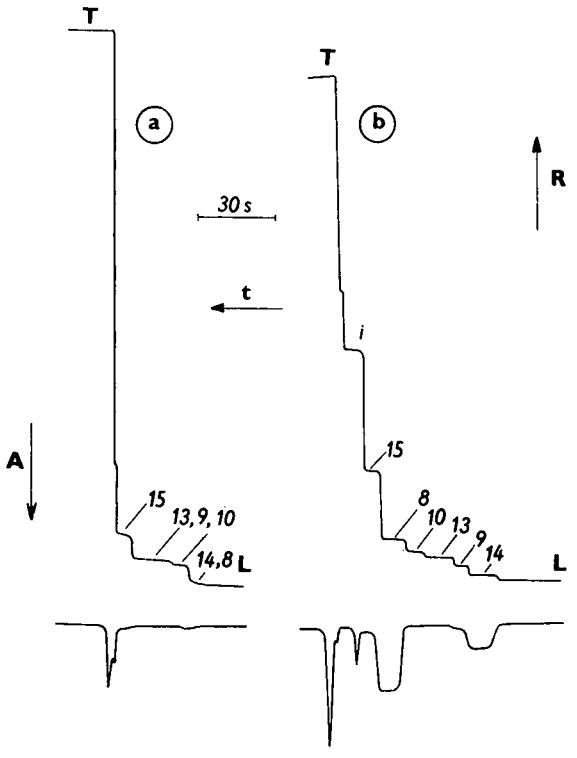

Fig. 3. Isotachopherograms from the separations of a model mixture of inorganic anions (a) without and (b) with the use of PVP [6% (w/v) concentration]. i = Impurities orginating from the electrolyte solutions. Driving currents and symbols as in Fig. 2; zone assignments as in Fig. 1.

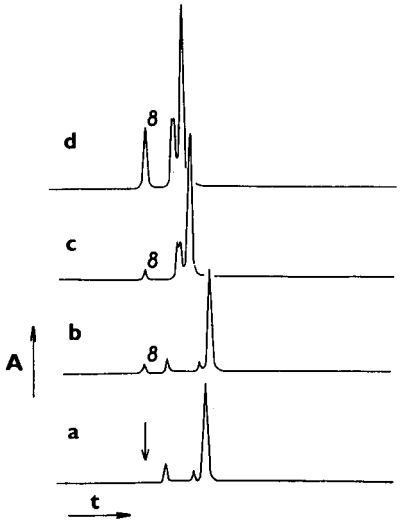

Fig. 4. Isotachopherograms from the determination of I^- (8) in mineral water samples. A 6% (w/v) concentration of PVP in the leading electrolyte was employed. Sulphate and fluoride, added to the samples at 10^{-4} mol/l I^-; concentrations, served as discrete spacers. (a) Blank experiment (only the spacers injected); (b) analysis of a model sample containing 10^{-6} mol/l I^-; (c,d) analysis of samples of mineral water (the samples were diluted 1:10 before the analysis). The arrow indicates the migration position of I^- in the blank experiment. Driving currents and symbols as in Fig. 2.

ble) and thus to a dynamic range of determination unattainable in ITP by other means.

REFERENCES

1 P. Boček and F. Foret, *J. Chromatogr.*, 313 (1984) 189.
2 I. Zelenský, V. Zelenská, D. Kaniansky, P. Havaši and V. Lednárová, *J. Chromatogr.*, 294 (1984) 317.
3 D. Kaniansky, I. Zelenský, P. Havaši and M. Cerovský, *J. Chromatogr.*, 367 (1986) 274.
4 I. Zelenský, E. Šimuničová, V. Zelenská, D. Kaniansky, P. Havaši and P. Chaláni, *J. Chromatogr.*, 325 (1985) 161.
5 T. Yagi, K. Kojima, H. Niariai and I. Motooka, *Bull. Chem. Soc. Jpn.*, 55 (1982) 1831.
6 T. Yagi, K. Kojima and T. Haruki, *J. Chromatogr.*, 292 (1984) 273.
7 H. Yoshida and M. Hida, *J. Chromatogr.*, 351 (1986) 388.
8 I. Matejovič and M. Bieliková, *Collect. Czech. Chem. Commun.*, 53 (1988) 3067.
9 F. M. Everaerts, J. L. Beckers and Th. P. E. M. Verheggen, *Isotachophoresis: Theory, Instrumentation and Applications*, Elsevier, Amsterdam, 1976.
10 M. Koval, *Thesis*, Komenský University, Bratislava, 1981.
11 K. H. Hellwege, A. M. Schäfer and E. Lax (Editors), *Landolt-Börnstein, Zahlenwerte und Funktionen*, Band II, Teil 7, Springer, Berlin, 6. Aufl., 1960.
12 T. Hirokawa, M. Nishino, N. Aoki, Y. Kiso, Y. Sawamoto, T. Yagi and J. Akiyama, *J. Chromatogr.*, 271 (1983) D1.
13 P. Boček, I. Miedziak, M. Deml and J. Janák, *J. Chromatogr.*, 137 (1977) 83.
14 J. Vacík and I. Muselasová, *J. Chromatogr.*, 320 (1985) 199.
15 D. Kaniansky, V. Madajová, I. Zelenský and S. Stankoviansky, *J. Chromatogr.*, 194 (1980) 11.
16 T. Hirokawa, S. Kobayashi and Y. Kiso, *J. Chromatogr.*, 518 (1987) 27.
17 K. Fukushi and K. Hiiro, *J. Chromatogr.*, 518 (1990) 189.
18 Yu. E. Kirsh, S. A. Yakimov, S. A. Sibeldina, T. M. Karaputadze, *Zh. Fiz. Khim.*, 62 (1988) 347.
19 F. M. Everaerts, Th. P. E. M. Verheggen and F. E. P. Mikkers, *J. Chromatogr.*, 169 (1979) 21.
20 D. Kaniansky, *Thesis*, Komenský University, Bratislava, 1981.
21 B. Yu. Zaslavky, L. M. Miheeva, Yu. P. Aleschko-Ozhevskii, A. V. Mahmudov, T. O. Bagirov and E. S. Garaev, *J. Chromatogr.*, 439 (1988) 267.
22 P. Molyneux and S. Vekavakayanondha, *J. Chem. Soc., Faraday Trans. 1*, 82 (1986) 291.
23 L. Arlinger, *J. Chromatogr.*, 91 (1974) 785.
24 D. Kaniansky, V. Madajová, J. Marák, E. Šimuničová, I. Zelenský and V. Zelenská, *J. Chromatogr.*, 390 (1987) 51.

Journal of Chromatography, 589 (1992) 333–338
Elsevier Science Publishers B.V., Amsterdam

CHROM. 23 676

Separation of polycyclic aromatic hydrocarbons by micellar electrokinetic chromatography with cyclodextrins as modifiers

Y. F. Yik, C. P. Ong, S. B. Khoo, H. K. Lee and S. F. Y. Li*

Department of Chemistry, National University of Singapore, Kent Ridge, Singapore 0511 (Singapore)

(First received May 8th, 1991; revised manuscript received August 8th, 1991)

ABSTRACT

The use of α-, β- and γ-cyclodextrins as modifiers to the electrophoretic medium containing sodium dodecyl sulphate and a phosphate–borate buffer in the micellar electrokinetic chromatography of polycyclic aromatic hydrocarbons (PAHs) was investigated. The results showed that the migration behaviour of PAHs could be related to their sizes and the cavity sizes of the cyclodextrins. With the addition of γ-cyclodextrin higher selectivity could be achieved, which consequently resulted in better separation of the seven PAHs investigated.

INTRODUCTION

Micellar electrokinetic chromatography (MEKC) is a separation technique of relatively recent origin. It was developed from capillary zone electrophoresis (CZE), which is based on the differential migration of solutes when a potential field is applied. MEKC employs the same principle as CZE, except that an ionic surfactant is added to the buffer mobile phase. MEKC is able to effect the separation of neutral compounds [1,2] based on the differential distribution of solutes between an electroosmotically pumped aqueous mobile phase and a slower moving electrophoretically retarded micellar phase.

Polycyclic aromatic hydrocarbons (PAHs) are of great environmental concern owing to their carcinogenicity. As they are all neutral, non-ionizable and of similar hydrophobicity, one would not expect a good separation by using conventional CZE or MEKC. Hence it is necessary to extend the concept of employing a mobile phase and a pseudo-stationary phase to the utilization of buffer modifiers [3,4]. Some common buffer modifiers that have been used are derivatized cyclodextrins [5], tetrahexylammonium perchlorate [3], copper(II)–L-histidine complex [6], copper(II)–aspartame complex [4] and organic modifiers [7].

One of the limitations of MEKC is the need for samples to be reasonably soluble in an aqueous mobile phase. Hydrophobic compounds, such as the PAHs, tend to be completely solubilized by the micelles and co-elute with migration times near that of the micelles. This problem is exacerbated by the limited elution range observed in MEKC. These problems can be alleviated by silanizing the capillary column walls [8], coating the walls with polymers [9] or adding modifiers to the electrophoretic buffer [10–13]. Terabe *et al.* [13] reported that PAHs were so hydrophobic that they were almost totally incorporated into the micelle. Although the addition of aqueous organic solvents increased the distribution of PAHs to the aqueous phase, satisfactory resolution was not achieved by this method because of peak tailing. They suggested that the use of γ-cyclodextrin would improve the resolution of PAHs in MEKC. However, only preliminary results were reported [13]. In this work, the use of α-, β-

0021-9673/92/$05.00

and γ-cyclodextrins as modifiers in the MEKC of PAHs was studied. Further, the migration behaviour of PAHs at different concentrations of cyclodextrins (CDs) as modifiers in the electrophoretic media was investigated.

EXPERIMENTAL

A fused-silica capillary tube (Polymicro Technologies, AZ, USA) 580 mm × 0.05 mm I.D. (500-mm effective length) was used as a separation column. On-column UV detection was carried out with a MicroUVis20 spectrophotometric detector (Carlo Erba, Milan, Italy) at 254 nm. Data were recorded using a Model 252A/MM chart recorder (Linear Instruments, CA, USA).

The chromatographic solutions were prepared by dissolving the modifiers and sodium dodecyl sulphate (SDS) in 0.05 *M* phosphate–0.1 *M* borate buffer solution (pH 7.0). All the solutes were first dissolved in the minimum amount of dimethylformamide (DMF) before diluting further with methanol. In our system, sample introduction was carried out via gravitational feed: sample solution was introduced into one end of the capillary tube by siphoning from the sample solution at a higher level than the electrophoretic solution in which the other end of the tube was immersed. A sample mixture consisting of seven PAHs at a concentration of 100 ppm was injected. The injection time and height were 3 s and 50 mm, respectively.

All reagents were of the purest grade available. The seven PAHs studied were acenaphthene, benz[*a*]anthracene, benzo[*a*]pyrene, chrysene, fluoranthene, perylene and phenanthrene. All the PAHs except benz[*a*]anthracene were obtained from Aldrich (Milwaukee, WI, USA). Benz[*a*]anthracene, α-, β- and γ-cyclodextrins, Sudan III and SDS were purchased from Fluka (Buchs, Switzerland). Methanol was obtained from Carlo Erba and dimethylformamide from Merck (Darmstadt, Germany). The buffer solution was prepared by dissolving sodium dihydrogenphosphate and sodium tetraborate (Fluka) in water purified with a Millipore Alpha-Q system.

RESULTS AND DISCUSSION

Previous work by Terabe and co-workers [14,15] has demonstrated that the selectivity can be improved in open-tubular high-performance capillary electrophoresis (HPCE) by including ionic surfactants in the electrophoretic medium. The effects of varying the SDS concentration on the separation of the seven PAHs are depicted in Fig. 1 and the migration times are given in Table I. It was observed that, in general, as the concentration of SDS increased, the migration times of the solutes increased. This can be attributed to the increase in the micelle concentration, which consequently retains the electrically neutral PAHs longer. The plot shows that 10 m*M* SDS provides the optimum se-

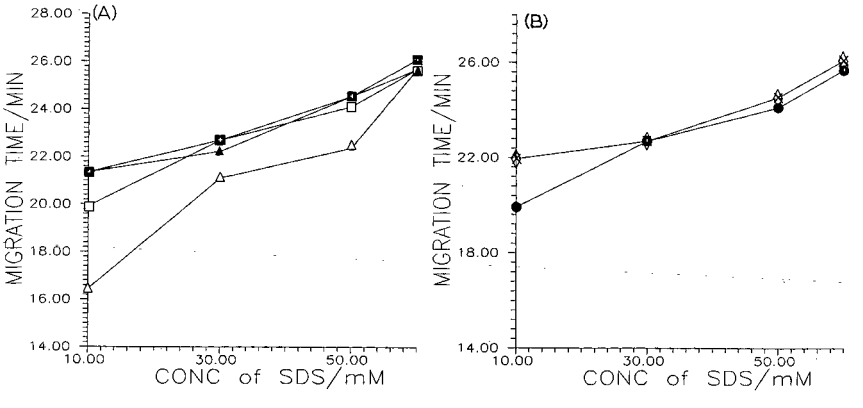

Fig. 1. Plots of migration time *vs.* concentration of SDS. Electrophoretic solution, SDS in 0.05 *M* phosphate–0.1 *M* borate buffer (pH 7.0); separation tube, 500 mm × 0.05 mm I.D. fused-silica capillary; voltage, 15 kV; detection wavelength, 254 nm. (A) △ = Acenaphthene; ▲ = phenanthrene; □ = perylene; ◘ = benzo[*a*]pyrene. (B) ◇ = Chrysene; × = benz[*a*]anthracene; ○ = fluoranthene.

TABLE I

MIGRATION TIME (min) OF PAHs OBTAINED USING SDS AND CD

PAH	SDS (m*M*)[a]				α-CD(m*M*)[b]		β-CD (m*M*)[c]			γ-CD (m*M*)[d]		
	10	30	50	60	2	5	1	2	5	1	2	3
Acenaphthene	16.44	21.10	22.37	25.69	12.90	12.36	14.04	12.30	8.13	12.63	9.60	9.00
Phenanthrene	21.35	22.22	24.54	25.69	16.80	15.90	17.70	17.55	15.18	16.77	12.68	11.10
Perylene	19.92	22.70	24.11	25.69	21.18	19.65	19.74	19.80	19.95	18.54	14.78	12.21
Benzo[*a*]pyrene	21.35	22.70	24.54	26.10	21.00	19.65	19.74	19.68	19.44	18.77	15.30	12.30
Chrysene	21.95	22.70	24.54	26.10	19.80	18.30	19.20	19.50	19.05	18.41	15.90	12.60
Benz[*a*]anthracene	21.95	22.70	24.54	26.10	19.80	18.30	19.20	19.65	19.44	19.26	16.44	13.05
Fluoranthene	19.92	22.70	24.11	25.69	19.20	18.30	19.20	18.60	18.18	18.80	16.80	13.20

[a] Operating buffer contains SDS only.
[b] Operating buffer contains 10 m*M* SDS and α-CD as modifier.
[c] Operating buffer contains 10 m*M* SDS and β-CD as modifier.
[d] Operating buffer contains 10 m*M* SDS and γ-CD as modifier.

lectivity. However, satisfactory separation of all the PAHs could not be achieved by varying the SDS concentration alone.

Cyclodextrins are neutral oligomers with different units of D-(+)-glucopyranose and the most commonly used CDs in chromatographic separation techniques [16] are α-, β- and γ-CD with six, seven and eight glucose units, respectively. The structure of CDs forms a cavity and hence can offer the possibility of behaving similarly to SDS, *i.e.*, providing the partition between CD and solutes.

The effects of the addition of various concentrations of the three different types of CDs to 10 m*M* SDS buffer were investigated at pH 7.0. The migration times of the compounds studied are given in Table I. Plots of migration time *vs.* concentration of CD are depicted in Figs. 2–4.

The general trend observed is that as the number of D-(+)-glucopyranose units of the CD decreased, the migration times increased. This is a consequence of the competition between the CD cavity and SDS micelles for PAH solutes. As the size of the CD cavity decreases, the larger PAH solutes would tend to be solubilized by SDS rather than entering the CD cavity. Hence longer migration times were observed.

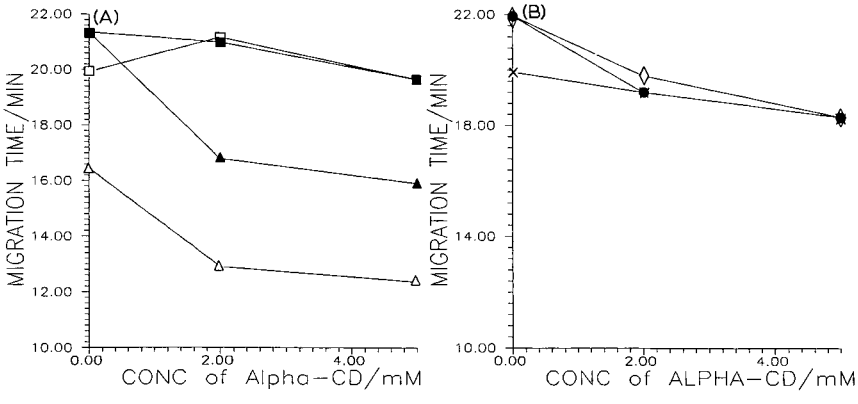

Fig. 2. Plots of migration time *vs.* concentration of α-CD with 10 m*M* SDS in 0.05 *M* phosphate–0.1 *M* borate buffer (pH 7.0). Separation tube, 500 mm × 0.05 mm I.D. fused-silica capillary; voltage, 15 kV; detection wavelength, 254 nm. (A) Symbols as in Fig. 1. (B) ◇ = Chrysene; ● = benz[*a*]anthracene; × = fluoranthene.

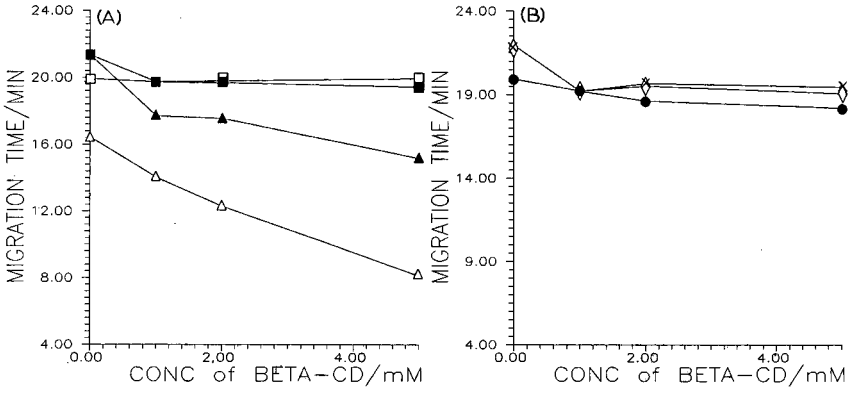

Fig. 3. Plots of migration time *vs.* concentration of β-CD with 10 m*M* SDS in 0.05 *M* phosphate–0.1 *M* borate buffer (pH 7.0). Other conditions as in Fig. 2. Symbols as in Fig. 1.

Fig. 2 depicts the effects of changing the concentration of α-CD on the separation of the seven PAHs. The general trend observed was that when the concentration of CD increased, the migration times of the PAHs decreased. This behaviour may be attributed to the nature of the CD. Unlike SDS micelles, CD is neutral, and hence it is expected to have no electrophoretic velocity and to migrate faster than SDS. Further, at higher concentrations of CD, the tendency of these PAHs to be solubilized in the cavity increases. Hence, as the concentration of CD increases, solubilization increases and consequently a decrease in migration time would be expected. An exception to this trend was observed for perylene, which showed a slight increase in migration time at low α-CD concentration (0–2 m*M*). The difference in behaviour can be attributed to the fact that perylene is the largest among the PAHs investigated, and α-CD has a relatively small cavity size consisting of only six D-(+)-glucopyranose units.

A similar investigation was carried out on β-CD, which has a cavity size intermediate between those of α-CD and γ-CD. The migration times obtained for the PAHs at different concentrations of β-CD are shown in Fig. 3. Six peaks were observed at a concentration of 5 m*M* β-CD. A further increase in β-CD concentration resulted in a decrease in selectivity. Fig. 3 depicts a trend of decreasing migration times with increasing concentration of β-CD for the same reason as cited earlier for α-CD. However, the decrease in migration times is not very prominent for the larger PAHs such as benz[*a*]anthracene,

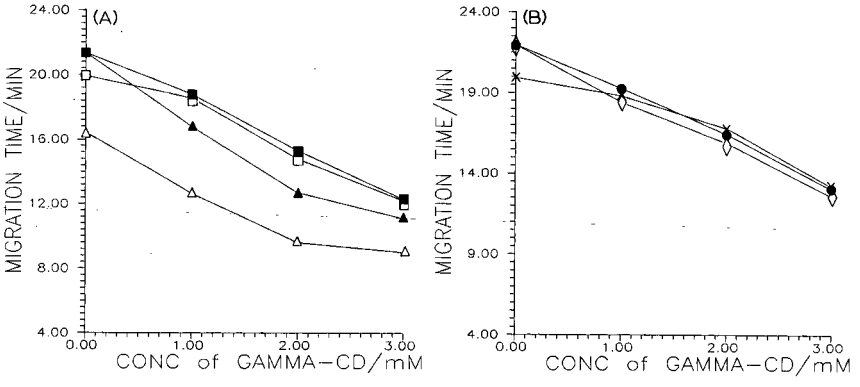

Fig. 4. Plots of migration time *vs.* concentration of γ-CD with 10 m*M*of SDS in 0.05 *M* phosphate–0.1 *M* borate buffer (pH 7.0). Other conditions and symbols as in Fig. 2.

chrysene, benzo[*a*]pyrene and perylene. This could be due to the difficulty in fitting these large solutes into the cavity of β-CD.

Results of experiments on varying the concentration of γ-CD are shown in Fig. 4. A similar trend to that for β-CD was observed for γ-CD, except that the decrease in migration times is now greater. The shorter migration times observed at higher concentrations of CD could be explained by the tendency of the PAH molecules to stay out of the micelle under these conditions. With increase in the concentration of γ-CD, a decrease in selectivity was also observed. As the concentration increased to 3 m*M* γ-CD, the selectivity was found to decrease to an unacceptable level, the last two peaks corresponding to benz[*a*]anthracene and fluoranthene were not being completely resolved.

Nevertheless, a concentration of 2 m*M* γ-CD and 10 m*M* SDS gives a satisfactory resolution of the seven PAHs, as shown in Fig. 5. The analysis was carried out in only 18 min. The improved selectivity compared with α- and β-CD could be attributed to the more effective interaction of the larger cavity size provided by γ-CD, which consists of eight glucopyranose units. The larger PAHs were therefore able to fit into the cavity more readily.

Solute migration in this investigation is dependent on a number of factors, the most important of which are probably hydrophobic retention and partitioning in the CD cavity. The principle of separation is based on the host–guest interaction between the SDS, γ-CD and solutes. The solutes partition between the pseudo-stationary phase (SDS) and the mobile phase (phosphate–borate buffer and γ-CD). This interaction operates as the distribution process. Here, selectivity towards the shape and size of the solutes plays an important role. The usual trends of increasing retention as a function of size are observed for PAHs. Exceptions to these trends are not uncommon, however, and it is clear that solute shape also influences migration behaviour.

With regard to the migration order in Fig. 5, it was noted that fluoranthene, although small, migrated last. There is reason to believe that the rigidity of the cyclopentane ring of fluoranthene caused a poor interaction with the CD cavity, whereas the other PAH solutes possess the ability to "bend" to suit the cavity. Hence the compromising effects of fluoranthene solubilizing into the SDS micelles, which is the dominating factor, and partitioning into the CD cavity explain its migration order.

Finally, it is worth noting that among the seven PAHs, perylene and benzo[*a*]pyrene and also chrysene and benz[*a*]anthracene are two pairs of structural isomers. As complete separation is achieved using γ-CD as modifier in the electrophoretic medium, we can conclude that this technique is very promising for resolving mixtures of PAH isomers.

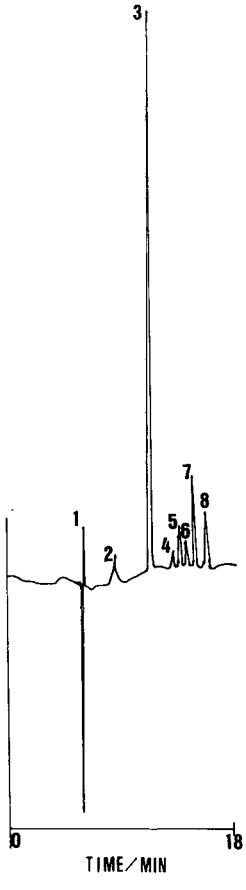

Fig. 5. Electropherogram showing the resolution of (1) methanol, (2) acenaphthene, (3) phenanthrene, (4) perylene, (5) benzo[*a*]pyrene, (6) chrysene, (7) benz[*a*]anthracene and (8) fluoranthene. Electrophoretic solution, 10 m*M* SDS and 2 m*M* γ-CD in 0.05 *M* phosphate–0.1 *M* borate buffer (pH 7.0); separation tube, 500 mm × 0.05 mm I.D. fused-silica capillary; voltage, 15 kV; current, 36 μA; detection wavelength, 254 nm.

ACKNOWLEDGEMENT

Thanks are due to the National University of Singapore for financial support.

REFERENCES

1 K. Otsuka, S. Terabe and T. Ando, *J. Chromatogr.*, 332 (1985) 219.
2 H. Nishi, N. Tsumagari and T. Kakimoto, *J. Chromatogr.*, 465 (1989) 331.
3 Y. Walbroehl and J. W. Jorgenson, *Anal. Chem.*, 58 (1986) 479.
4 P. Gozel, E. Gassmann, H. Michelsen and R. N. Zare, *Anal. Chem.*, 59 (1987) 44.
5 S. Terabe, H. Ozaki, K. Otsuka and T. Ando, *J. Chromatogr.*, 332 (1985) 211.
6 E. Gassmann, J. E. Kuo and R. N. Zare, *Science*, 230 (1985) 813.
7 S. Fujiwara and S. Honda, *Anal. Chem.*, 59 (1987) 487.
8 A. T. Balchunas and M. J. Sepaniak, *Anal. Chem.*, 59 (1987) 1466.
9 S. Terabe, H. Utsumi, K. Otsuka, T. Ando, T. Inomata, S. Kuze and Y. Hanalka, *J. High Resolut. Chromatogr. Chromatogr. Commun.*, 9 (1986) 666.
10 A. S. Cohen, S. Terabe, J. A. Smith and B. L. Karger, *Anal. Chem.*, 59 (1987) 1021.
11 J. G. Dorsey, M. J. DeEchegaray and J. S. Landy, *Anal. Chem.*, 55 (1983) 924.
12 J. Gorse, A. T. Balchunas, D. F. Swaile and M. J. Sepaniak, *J. High Resolut. Chromatogr. Chromatogr. Commun.*, 11 (1988) 554.
13 S. Terabe, Y. Miyashita, O. Shibata, E. Barnhart, L. Alexander, D. Patterson, B. L. Karger, K. Hosoya and N. Tanaka, *J. Chromatogr.*, 516 (1990) 23.
14 S. Terabe, K. Otsuka, K. Ichikawa, A. Tsuchiya and T. Ando, *Anal. Chem.*, 56 (1984) 111.
15 S. Terabe, K. Otsuka and T. Ando, *Anal. Chem.*, 57 (1985) 834.
16 S. Fanali, *J. Chromatogr.*, 474 (1989) 441.

Journal of Chromatography, 589 (1992) 339–345
Elsevier Science Publishers B.V., Amsterdam

CHROM. 23 684

Study of isotachophoretic separation behaviour of metal cations by means of particle-induced X-ray emission

II. Separation efficiency of lanthanoid model mixture

Jian-Ying Hu, Takeshi Hirokawa*, Fumitaka Nishiyama and Yoshiyuki Kiso

Applied Physics and Chemistry, Faculty of Engineering, Hiroshima University, Kagamiyama 1, Higashi-hiroshima 724 (Japan)

(First received June 26th, 1991; revised manuscript received August 13th, 1991)

ABSTRACT

The isotachophoretic (ITP) separation behaviour of fourteen lanthanoid cations coexisting with α-hydroxyisobutyric acid was studied in relation to the separation efficiency. It was confirmed that the stimulated separation efficiencies using approximate equations agreed well with the observed values, except for Eu–Gd. It was found that the separation efficiency of equimolar amounts of neighbouring lanthanoids varied discontinuously but periodically, forming four different groups ("tetrad effect"). The effect of the component ratio on the separation efficiency of minor lanthanoids from major components was studied by means of ITP fractionation and subsequent off-line analysis by particle-induced X-ray emission. It was confirmed that the separation efficiency of multi-component mixtures decreased with decrease in the abundance of the sample. For binary mixtures of neighbouring lanthanoids, however, the separability was almost independent of the abundance, as for strong electrolytes.

INTRODUCTION

The separation of lanthanoid cations is a typical application of isotachophoresis (ITP), where complex-forming equilibria with α-hydroxyisobutyric acid (HIB) were utilized [1]. The principle of the separation was clarified theoretically later [2] and the optimum separation conditions for equimolar amounts of fourteen lanthanoid cations were studied in relation to the pH of and the concentration of HIB in the leading electrolyte [1,2]. From the experimental results [1], the separation efficiency of Pr–Nd and Eu–Gd was calculated as *ca.* 30 nmol/C. They were the least separable pairs in the mixture of fourteen lanthanoid cations.

A knowledge of the separation efficiency is important not only from the preparative but also from the analytical viewpoint, because overloading of the sample is fatal for an ITP separation. As far as we know, there has been no further discussion concerning the separation efficiency of the lanthanoids even for equimolar binary mixtures.

The difference in effective mobility between the separands [3,4] is the most important factor affecting the separation efficiency. On the other hand, the composition of the sample solution is also an important factor, as discussed in previous papers [5,6]. A theoretical elucidation of the composition effect has been given, but it was for the strong electrolytes.

In contrast to the sample system treated previously [5,6], the complex-forming equilibria in isotachophoretic lanthanoid (Ln) zones were very complicated owing to the formation of multi-coordinated ion pairs such as $Ln(HIB)_n$ (n = 1–4). In addition, multi-coordinated ion pairs with acetic acid coexisted to a considerable extent [2]. Acetic acid was added to the leading electrolyte as a pH buffering agent.

For the study of the separation behaviour of metal cations, previous universal detectors such as the

0021-9673/92/$05.00

potential gradient detector are no longer convenient, especially when the sample contains a considerable number of separands and they are not equimolar. A more specific detection method is necessary to distinguish the individual separands. For this purpose, we developed a coupled isotachophoresis–particle-induced X-ray emission (ITP–PIXE) method: The sample zones were fractionated using a preparative ITP analyser [7] and the fractions were analysed off-line by PIXE. In a previous paper [8], the recovery, migration order and separation efficiency of twenty metal cations were studied using ITP–PIXE. The recovery of the isotachophoretic separation of four lanthanoids (La, Ce, Gd and Lu) was 100% under the electrolyte conditions used.

In this work, first the separation efficiency of equimolar binary mixtures of lanthanoids were measured using a potential gradient detector. The separation behavior of minor lanthanoids from a major lanthanoid was then studied by means of ITP–PIXE in order to clarify the effect of composition on the separation efficiency in such a complex-forming system. The experimental results were compared with theoretical values.

THEORETICAL

Efficiency of separation of binary mixtures

The efficiency of separation of component A in a binary mixture of ions A and B, *i.e.* the separable molar amount of ions A per unit amount of electricity, can be defined in a similar manner to that reported by Boček *et al.* [9] and Mikkers *et al.* [10] as follows:

$$\frac{dN_A}{dQ} = \frac{N_A}{It_{res,AB}} = \frac{N_A(V_{ITP} - V_{A/AB})}{Il_A} = \frac{N_A(E_A m_A - E_{AB} m_{B,AB})}{Il_A} = C^t_{A,AB}(E_A m_A - E_{AB} m_{B,AB})/J \quad (1)$$

where N_A is the molar amount of the first migrating sample ion A, Q is the amount of electricity, I the migration current, $t_{res,AB}$ the resolution time of the mixed zone AB, V_{ITP} the isotachophoretic velocity, $V_{A/AB}$ the boundary velocity between zone A and mixed zone AB, l_A the zone length of zone A, E_A and E_{AB} the potential gradient of zone A and mixed zone AB, respectively, m_A the effective mobility of ion A at the steady state, $m_{B,AB}$ that of the second sample ion B at the transient state, $C^t_{A,AB}$ the concentration of ion A in the mixed zone AB and J the current density. A different expression of eqn. 1 can be derived for ion B:

$$\frac{dN_B}{dQ} = C^t_{B,AB}(E_{AB} m_{A,AB} - E_B m_B)/J \quad (2)$$

The efficiency of separation of a binary mixture, S_{eff}, can be calculated as

$$S_{eff} = (N_A + N_B)/Q \quad (3)$$

As the complex-forming equilibria in the lanthanoid zones are very complicated, simulation of the mixed zone to evaluate exactly E_{AB}, $m_{A,AB}$, etc., is not practical: the simulation program SIPSR [5,6] for transient-state analysis cannot be applied to complex-forming equilibria at present.

In order to permit numerical calculation, several assumptions were introduced. When the amount of ion B is negligibly small in comparison with that of ion A, $C^t_{A,AB}$ can be replaced with C^t_A and E_{AB} with E_A as a first approximation. Eqns. 1 and 3 can then be rewritten as

$$\frac{dN_A}{dQ} = C^t_A E_A(m_A - m_{B,A})/J = C^t_A(m_A - m_{B,A})/k_A \quad (4)$$

$$S_{eff,A} \approx N_A/Q = C^t_A(m_A - m_{B,A})/k_A \quad (5)$$

where $m_{B,A}$ is the effective mobility of ion B in zone A and k_A is the conductivity of zone A. A similar expression for ion B can be written as

$$S_{eff,B} \approx N_B/Q = C^t_B(m_{A,B} - m_B)/k_B \quad (6)$$

where $m_{A,B}$ is the effective mobility of ion A in zone B and k_B is the conductivity of zone B. The meaning of $m_{A,B}$ and $m_{B,A}$ has been discussed in detail in relation to the "zone stability" [11].

Numerical calculation of eqns. 5 and 6 is possible using our simulation program SIPS after minor modification and the simulation results are given later.

EXPERIMENTAL

Chemicals

Lanthanoid chlorides ($LnCl_3 \cdot 6H_2O$), α-hydroxyisobutyric acid (HIB) and carnitine hydrochloride

were obtained from Katayama Kagaku (Osaka, Japan). Two cationic dyes, toluidine blue (TB) and astrazon pink (AP), and hydroxypropylcellulose (HPC) were obtained from Tokyo Kasei (Tokyo, Japan). The lanthanoid chlorides and HPC were of extra-pure grade and HIB and carnitine hydrochloride were of guaranteed-reagent grade. The viscosity of the 2% HPC aqueous solution was 1000–4000 cP at 20°C according to the specification.

Samples

Lanthanoid stock solutions were prepared by dissolving the chlorides in high-purity water obtained by treatment with an ion-exchange resin (Puric-R; Japan Organo, Tokyo, Japan). In order to study the efficiency of separation of lanthanoid, thirteen equimolar binary mixtures were prepared using the stock solutions. Each mixture contained only two neighbouring lanthanoids, *e.g.*, La and Ce, and the concentration of each component was 5 m*M*. For La and Ce, binary mixtures with molar ratios of 5:1 (15.82 m*M*) and 10:1 (19.7 m*M*) were also prepared in order to study the effect of composition on the separation efficiency.

Multi-component mixtures containing fourteen lanthanoid cations [Z = 57–71 except Z = 61 (Pm)] were prepared for the same purpose, where La was the major component and the other thirteen cations of equimolar lanthanoids were minor components. The molar ratio of La to each of the individual minor components in the mixture was varied as 10:1, 20:1, 30:1, 40:1, 60:1, 80:1 and 500:1, and the total concentration of the model mixtures was 7.822, 9.948, 11.70, 13.14, 15.37, 17.01 and 25.00, respectively. Small amounts TB and AP were added to the mixtures to monitor the separation process and to determine the timing of fractionation.

Standard lanthanoid solutions (1000 ppm, for atomic absorption spectrometry) were used as analytical standards for PIXE analysis.

Electrolyte system

The electrolyte system used is summarized in Table I. The leading electrolyte was 20 m*M* ammonia solution containing 10 m*M* HIB and the pH of the electrolyte was adjusted to 4.80 by adding acetic acid. The pH measurements were carried out using a Horiba (Tokyo, Japan) Model F7ss expanded pH meter. The terminating electrolyte was a 10 m*M* solution of carnitine hydrochloride. The actually migrating terminator was H^+. HPC was added to the leading and the terminating electrolytes (0.2%) in order to suppress electroendosmosis.

TABLE I

ELECTROLYTE SYSTEM USED IN ISOTACHOPHORETIC SEPARATION

HIB = α-Hydroxyisobutyric acid; CARH = carnitine hydrochloride; HPC = hydroxypropylcellulose.

Leading electrolyte	20 m*M* ammonia solution
Complexing agent	10 m*M* HIB
pH buffer	Acetic acid
pH of leading electrolyte	4.80
Terminating electrolyte	10 m*M* CARH
Additive	0.2% HPC

Preparative isotachophoretic analyser

The preparative analyser and the method of fractionation used were reported in a previous paper [7]. The sample migration in the apparatus can be divided into three stages (preseparation, separation and fractionation stages). The preseparation stage for large amounts of sample was not used in this work. The sample mixture was separated from the separation stage, which was designed for the complete separation of the preseparated samples or the separation of the relatively small amounts of samples of the order of 10^2 nmol or less. The separated zones were fractionated dropwise (5 μl) by a counter flow of leading electrolyte through a nozzle. The fractions were collected drop by drop on Nuclepore filters for PIXE analysis.

In order to obtain the amount of electricity in the electrophoretic process, the migration current was integrated using a microcomputer with an analog-to-digital conversion interface (sampling rate = 2.070 s per datum).

PIXE analysis

For the measurement of PIXE spectra, a Van der Graaff accelerator (Model AN-2500; Nisshin High Voltage, Tokyo, Japan) at the Faculty of Engineering, Hiroshima University, was used. The energy of the H^+ beam was 2.0 MeV and the beam current was 20 nA. The detector used was a high-purity Ge detector (ORTEC Model GLP-10180) and the multi-

channel analyser used was a Model AMS-1000 (Laboratory Equipment, Tokyo, Japan). A typical single run took 250 s to measure the PIXE spectrum of a fraction.

The Nuclepore filter used as the target backing was 5 μm thick and with a pore size of 0.1 μm, mounted on an aluminium flame. The impurities in the Nuclepore filter were mainly Cr and Fe and the abundance of Fe was one tenth of that of Cr, although the amounts were not the same from one unit to another. The PIXE spectrum was measured for each fraction after drying in a desiccator. The diameter of the fraction spot was *ca.* 3 mm. The sample amount was in the range 2.08–2.62 μg (29.4–37.1 μg cm^{-2}). As the volume of one fraction was *ca.* 5 μl, a few or more lanthanoids were contained in a fraction when the abundances were small. The PIXS data reduction software developed previously [12] was used to analyse the PIXE spectra. All the calculations were carried on an NEC (Tokyo, Japan) PC-9801RA microcomputer (CPU = 80 386, co-processor = 80 387, clock = 16 MHz).

RESULTS AND DISCUSSION

Binary equimolar mixture of lanthanoids

The efficiency of separation of binary mixtures of neighbouring lanthanoids was simulated and compared with the experimental results. Table II shows the theoretical separation efficiency of the binary mixture of neighbouring lanthanoids simulated by the use of eqns. 5 and 6, respectively. As discussed before, $S_{eff,A}$ (eqn. 5) gives the separation efficiency per unit amount of electricity for the binary mixture in which the first migrating component is the major component of the mixture. In contrast, $S_{eff,B}$ (eqn. 6) gives the necessary value where the second migrating component is the major component of the mixture. The electrolyte conditions used in the present simulation are given in Table I. Apparently from Table II, the separation efficiency of binary mixtures of neighbouring lanthanoids is almost independent of the ratio of the sample components, because the difference between the mobility differences $m_A - m_{B,A}$ and $m_{A,B} - m_B$ is small. For example, for La–Ce, $m_A - m_{B,A} = (31.7\text{–}28.7) \cdot 10^{-5}$ cm^2 V^{-1} s^{-1} and $m_{A,B} - m_B = (32.2\text{–}29.2) \cdot 10^{-5}$ cm^2 V^{-1} s^{-1}, *i.e.*, the differences are both $3 \cdot 10^{-5}$ cm^2 V^{-1} s^{-1}. For Yb–Lu, the corresponding values are $(17.1\text{–}15.8) \cdot 10^{-5}$ and $(17.7\text{–}16.5) \cdot 10^{-5}$ cm^2 V^{-1} s^{-1}, *i.e.* the differences are almost identical at $1.3 \cdot 10^{-5}$ and $1.2 \cdot 10^{-5}$ cm^2 V^{-1} s^{-1}. Table II also shows the average values of the separation efficiencies, $(S_{eff,A} + S_{eff,B})/2$, which might represent the efficiency of separation of an equimolar binary mixture.

TABLE II

SIMULATIONAL AND EXPERIMENTAL SEPARATION EFFICIENCY OF A BINARY MIXTURE OF NEIGHBOURING LANTHANOIDS

For electrolyte conditions, see Table I.

Lanthanoide pair	Separation efficiency (nmol C^{-1})				Difference (%)
	$S_{eff,A}$ (sim.)	$S_{eff,B}$ (sim.)	$(S_{eff,A} + S_{eff,B})/2$		
			Sim.	Obsd.	
La–Ce	261	298	280	262	+7
Ce–Pr	136	143	140	180	−22
Pr–Nd	100	104	102	123	−17
Nd–Sm	337	376	357	364	−2
Sm–Eu	216	216	216	161	+34
Eu–Gd	163	157	160	27	+493
Gd–Tb	337	359	348	309	+13
Tb–Dy	230	236	233	245	−5
Dy–Ho	169	176	173	197	−12
Ho–Er	255	261	258	279	−8
Er–Tm	177	186	182	234	−22
Tm–Yb	193	202	198	228	−13
Yb–Lu	212	213	213	198	+8

In order to evaluate this simulation, the separation efficiencies of binary mixtures were determined: the separable amount of sample was determined by repeated analyses of equimolar binary mixtures, increasing the amount of sample injected until the step of the mixed zone was found in the potential gradient detector trace. A coupled separation tube was used (16 cm × 1 mm I.D. × 2 mm O.D. and 30 cm × 0.5 mm I.D. × 1 mm O.D.). A typical single run took about 50 min. The migration current was 300 μA for the first 22 min, then it was decreased to 150 μA. The separation efficiency, S_{eff}, was evaluated using the equation

$$S_{eff} = \frac{\text{separable amount of the mixture (nmol)}}{\text{applied amount of electricity (C)}} \quad (7)$$

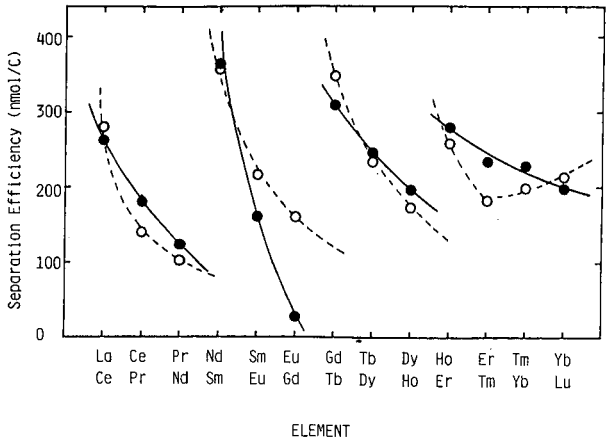

Fig. 1. Experimental (solid lines) and simulational (dashed lines) separation efficiencies of binary mixtures of neighbouring lanthanoids. For the electrolyte system used, see Table I. Migration current = 150 μA.

The observed separation efficiencies are shown in Fig. 1 and Table II. The agreement between the approximately evaluated values and the observed values was good except for the Eu–Gd mixture. If the Eu–Gd mixture was not considered, the average difference was 13%, which is good enough for the calculation of the sample load in the ITP separation. The minimum separation efficiency of 30 nmol C^{-1} for Eu and Gd was the same as in previous work, although the electrolyte conditions used were different.

It was noticeable in Fig. 1 that the separation efficiency changed discontinuously but periodically with the atomic number, suggesting that the so-called "tetrad effect" of lanthanoids was also valid for the separation efficiency [13]. Such a periodic change of separation efficiency is apparently due to the periodic change of the difference in effective mobility, which was caused by similar changes in the stability constants of the ion pairs formed [14].

Table III shows the separation efficiencies simulated for all combinations of fourteen lanthanoid cations. Table III shows a square matrix where the rows and columns correspond to the components of binary mixtures. The diagonal values are zero, which means that the sample is not a binary mixture. The upper triangle of the matrix corresponds to $S_{eff,A}$ and the lower triangle to $S_{eff,B}$. Apparently from Table III, when the difference between the mobility differences $m_A - m_{B,A}$ and $m_{A,B} - m_B$ is large, *e.g.*, for La–Lu, $S_{eff,A}$ and $S_{eff,B}$ differ significantly. In such a case, the separation efficiency depends on the molar ratio of the components.

Effect of composition on the efficiency of separation of lanthanoids

As discussed previously for multi-component

TABLE III

SIMULATED SEPARATION EFFICIENCY (nmol C^{-1}) FOR ALL COMBINATIONS OF FOURTEEN LANTHANOIDS

Assuming this table to be a matrix, the rows and columns correspond to the components of binary mixtures. The upper triangle matrix corresponds to $S_{eff,A}$ and the lower to $S_{eff,B}$. For the electrolyte conditions, see Table I.

	La	Ce	Pr	Nd	Sm	Eu	Gd	Tb	Dy	Ho	Er	Tm	Yb	Lu
La	0	298	454	580	1041	1317	1472	1934	2212	2483	2883	3171	3477	3871
Ce	261	0	143	254	668	918	1072	1499	1765	2013	2382	2652	2937	3302
Pr	381	136	0	104	495	732	882	1287	1543	1777	2124	2380	2651	2991
Nd	466	232	100	0	377	609	758	1152	1404	1430	1967	2217	2480	2809
Sm	745	543	425	337	0	216	367	733	975	1183	1493	1725	1972	2272
Eu	916	731	620	538	216	0	157	517	758	962	1247	1473	1736	2030
Gd	1051	878	771	693	381	163	0	359	602	805	1111	1335	1578	1871
Tb	1287	1145	1048	982	706	503	337	0	236	425	713	923	1155	1429
Dy	1426	1303	1214	1156	906	715	550	230	0	177	450	650	872	1131
Ho	1510	1403	1320	1268	1041	862	699	394	169	0	261	453	669	917
Er	1709	1621	1544	1499	1290	1113	942	644	418	255	0	186	397	638
Tm	1775	1701	1629	1590	1402	1238	1071	790	571	418	177	0	202	430
Yb	1851	1790	1723	1690	1523	1371	1207	942	729	588	361	193	0	213
Lu	2030	1987	1927	1899	1747	1594	1420	1157	941	800	537	407	212	0

sample mixtures [5], the efficiency of separation of a pair of separands of interest is affected not only by the difference in the mobilities of the separands but also by the amount of the coexisting component. Further, the difference among the mobilities of components of interest and other coexisting components also affects the separation efficiency. Such an effect was called the composition effect [5,6].

The composition effect was studied for the mixture of lanthanoids, where La was assumed to be the major component and the other thirteen cations of equimolar lanthanoids were the minor components. In this instance, the separation of Ce, which was adjacent to the La zone, will be very difficult, although the separation efficiency between Eu and Gd is the poorest in the equimolar case. Hence La and Ce were separated under the conditions used (Table I) and the separation efficiency was evaluated by eqn. 7.

As examplified in ref. 6, the potential gradient detector signal of the mixed zone between the minor and the major component resembles that of the steady-state zone of the major component. In such a case, the separable amount could not be determined from mixed zone formation as in the equimolar case, but it should be determinable from the calibration line for the minor component. When the component ratio of the sample was 10:1, 20:1 or 30:1, potential gradient detection was still useful: Fig. 2 shows the observed zone length of Ce based on time. In Fig. 2, a bend was found in each calibration line, suggesting that the injected amount at the bend was a separable amount. In the case of the 10:1 mixture, two bends were found. The reason is unclear but it might be related to mixed zone formation among the matrix La and the minor components Ce and Pr.

When the component ratio was increased, the amount of minor components (Ce–Lu) decreased and it became difficult to detect the zone lengths accurately by means of a potential gradient detector. Therefore, the separated minor zone was fractionated with the preparative isotachophoretic analyser [8] and the fractions were analysed by PIXE.

Fig. 3 shows the PIXE results when the component ratio was varied as 40:1, 60:1 and 80:1. Bends were also found in calibration lines and the separation efficiency was evaluated similarly.

Fig. 4 summarizes the dependence of the component ratio on the efficiency of separation of

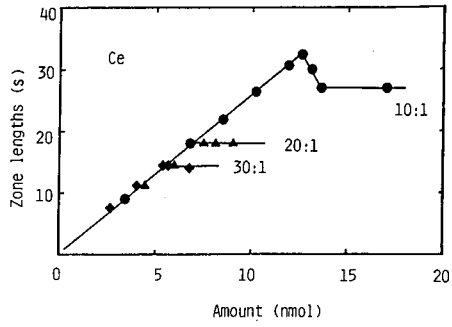

Fig. 2. Observed time-based zone length *vs.* injected amount of Ce with the use of a potential gradient detector. The samples were mixtures of fourteen lanthanoid cations where La was the major component and the other thirteen equimolar lanthanoids were the minor components. The ratio of La to the individual minor components was varied as 10:1, 20:1 and 30:1. For operational conditions, see Fig. 1.

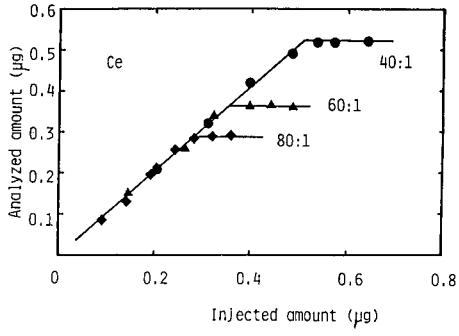

Fig. 3. Analysed amount by IP–PIXE *vs.* injected amount of Ce. The ratio of the sample components (see caption of Fig. 2 for definition) was varied as 40:1, 60:1 and 80:1. For the operational conditions and the composition of the sample see Figs. 1 and 2, respectively.

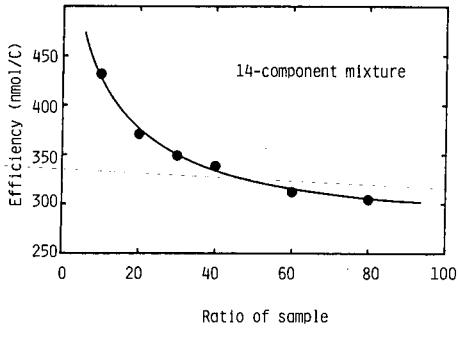

Fig. 4. Dependence of separation efficiency on the ratio of the sample components (see caption of Fig. 2 for definition). For the operational conditions and the composition of the sample see Figs. 1 and 2, respectively.

lanthanoid mixtures. The separation efficiency decreased with increase in the ratio and gradually the effect of the component ratio became smaller and the separation efficiency approached the limiting value of $S_{eff,La}$.

The efficiency of separation of La and Ce contained in the fourteen-component mixture can be calculated from the observed separation efficiency ($S_{eff,Ln}$) shown in Fig. 4 considering the composition of the mixture as follows:

$$S_{eff} = \frac{R+1}{R+13} \cdot S_{eff,Ln} \quad (8)$$

where R is the molar ratio of the major component (La) to the individual minor component.

Evaluated S_{eff} values for La and Ce are shown in Fig. 5 (curve 2). It is interesting that the efficiency of separation of La and Ce contained in the fourteen-component mixture increased with increase in the component ratio, which is just opposite of the tendency observed for the total amounts in Fig. 4. In fact, the phenomenon has been explained by the effect of coexisting components on the separation efficiency of isotachophoresis [5]. The total amount of twelve coexisting lanthanoids except for La and Ce is also shown in Fig. 5. Apparently the increase in the efficiency of separation of La and Ce with increase in the component ratio depends on the decrease in the coexisting amount.

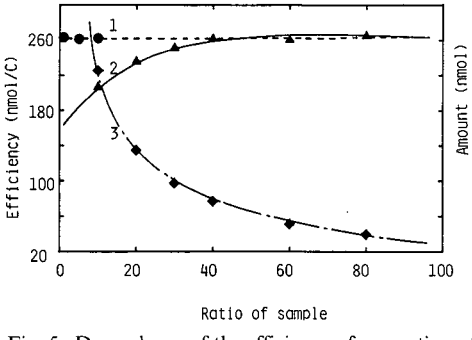

Fig. 5. Dependence of the efficiency of separation of La and Ce on the amount of coexisting component. (1) Two-component mixture of La and Ce; (2) La and Ce in a fourteen-component mixture (for the composition of the sample, see Fig. 2); (3) coexisting composition amount. For the operational conditions, see Fig. 1.

On the other hand, Fig. 5 also shows the observed efficiency of separation of binary mixtures of La and Ce, where La was selected as the major component. Apparently the separation efficiency is independent of the component ratio, which is in agreement with the simulational results in Table II. As the component ratio increases, the efficiency of separation of the fourteen-component mixture agreed with that of the binary equimolar mixture of La and Ce.

In conclusion, the separation of minor components is not difficult if the amount of electricity is appropriate. However, if it is not, it causes a major error in the determination. In a subsequent paper, we shall present the application of the present basic study to the separation of minor heavy lanthanoids from crude rare earth chlorides [15].

REFERENCES

1 I. Nukatsuka, M. Taga and H. Yoshida, *J. Chromatogr.*, 205 (1981) 95.
2 T. Hirokawa, N. Aoki and Y. Kiso, *J. Chromatogr.*, 312 (1984) 11.
3 F. M. Everaerts, J. L. Beckers and Th. P. E. M. Verheggen, *Isotachophoresis —Theory, Instrumentation and Applications*, Elsevier, Amsterdam, 1976.
4 P. Boček, M. Deml, P. Gebauer and V. Dolnik, *Analytical Isotachophoresis*, VCH, Weinheim, 1988.
5 T. Hirokawa, Y. Yokota and Y. Kiso, *J. Chromatogr.*, 545 (1991) 267.
6 T. Hirokawa, A. Omori, Y. Yokota, J.-Y. Hu and Y. Kiso, *J. Chromatogr.*, 585 (1991) 297.
7 T. Hirokawa, J.-Y. Hu, K. Umeda, G. Kimura, H. Ikeda, F. Nishiyama and Y. Kiso, *J. Chromatogr.*, 513 (1990) 297.
8 T. Hirokawa, J.-Y. Hu, S. Eguchi, F. Nishiyama and Y. Kiso, *J. Chromatogr.*, 538 (1991) 413.
9 P. Boček, M. Deml, B. Kaplanova and J. Janak, *J. Chromatogr.*, 160 (1978) 1.
10 F. E. P. Mikkers, F. M. Everaerts and J. A. F. Peek, *J. Chromatogr.*, 168 (1979) 293.
11 P. Boček and P. Gebauer, *Electrophoresis*, 5 (1984) 338.
12 T. Hirokawa, F. Nishiyama and Y. Kiso, *Nucl. Instrum. Methods Phys. Res.*, B31 (1988) 525.
13 L. J. Nugent, *J. Inorg. Nucl. Chem.*, 32 (1970) 3485.
14 Y. Suzuki and M. Mikado, in *Proceedings of the 8th Rare Earth Research Conference, Reno, NV, 1970*, p. 266.
15 J.-Y. Hu, T. Hirokawa, F. Nishiyama, Y. Kiso, K. Ito and E. Shoto, *J. Chromatogr.*, 594 (1992) in press.

Journal of Chromatography, 589 (1992) 346–348
Elsevier Science Publishers B.V., Amsterdam

CHROM. 23 733

Short Communication

Optical resolution of 2-chloro-3-phenylmethoxypropanoic acid after derivatization with (*S*)-2-octanol by high-performance liquid chromatography

Pier Lucio Anelli, Carlo Tomba* and Fulvio Uggeri

Bracco SpA, Research and Development Division, Via E. Folli 50, 20134 Milan (Italy)

(First received June 27th, 1991; revised manuscript received September 10th, 1991)

ABSTRACT

A simple chromatographic method is described to resolve the enantiomers of 2-chloro-3-phenylmethoxypropanoic acid. The optical resolution is achieved by applying a silica phase with 0.4% tetrahydrofuran in *n*-hexane as eluent, after derivatization of the sample with (*S*)-2-octanol in the presence of dicyclohexylcarbodiimmide.

INTRODUCTION

2-Chloro-3-phenylmethoxypropanoic acid [$C_6H_5CH_2OCH_2CH(Cl)COOH$ (**1**)] is a key intermediate in the synthesis of polyaminopolycarboxylic ligands, like diethylenetriamine-N,N,N′,N″,N″-pentaacetic acid (linear) [1,2] and 1,4,7,10-tetraazacyclododecane-1,4,7,10-tetraacetic acid (cyclic) [3,4], whose gadolinium-complexes are used as contrast agents for magnetic resonance imaging (MRI) [5]. The presence of the phenylmethoxymethyl group in the structure makes these gadolinium complexes particularly attractive for imaging of the hepatobiliary system and the myocardium.

The chemical resolution of **1** by formation of the diastereoisomeric salts with enantiomerically pure 1-phenylethylamine has recently been reported [6]. The optical purity of (+)- and (−)-**1** cannot be precisely determined by polarimetry owing to the very low specific rotation values shown by the pure enantiomers in all common solvents.

This paper describes a chemical derivatization method that allows the high-performance liquid chromatographic (HPLC) separation of the optical isomers of **1**. The mixture of enantiomers of **1** was derivatized with (*S*)-2-octanol using the esterification conditions [N,N′-dicyclohexylcarbodiimide, 4-(N,N-dimethylamino)pyridine, chloroform] reported by Felder *et al.* [7].

EXPERIMENTAL

Chemicals

N,N′-Dicyclohexylcarbodiimide, 4-(N,N-dimethylamino)pyridine, analytical-reagent grade chloroform, chromatographic grade *n*-hexane and tetrahydrofuran (THF) were obtained from E. Merck (Darmstadt, Germany) and (*S*)-2-octanol from Aldrich (Milwaukee, WI, USA). (*S*)- and (*R*)-2-chloro-3-phenylmethoxypropanoic acid were synthesized as described previously [6].

0021-9673/92/$05.00

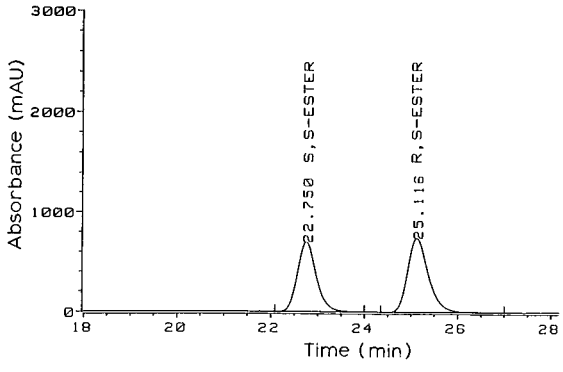

Fig. 1. Resolution of 2-chloro-3-phenylmethoxypropanoic acid after derivatization with (*S*)-2-octanol.

High-performance liquid chromatography

A Hewlett-Packard HP 1090M liquid chromatograph, equipped with an autosampler, a diode-array detector set at 210 nm and a Merck LiChrosorb Si 60 (5 μm) column (250 × 4 mm I.D.) thermostated at 37°C, was used. The column was eluted with 0.4% THF in *n*-hexane at a flow rate of 1 ml min^{-1}.

Procedure

An exactly weighed sample of **1** (about 25 mg; 0.116 mmol) was placed in a 10-ml volumetric flask containing (*S*)-2-octanol (100 μl; 82.7 mg; 0.635 mmol), N,N′-dicyclohexylcarbodiimide (500 μl of a 0.762 *M* solution in chloroform) and 4-(N,N-dimethylamino)pyridine (100 μl of a 0.123 *M* solution in chloroform). The mixture was sonicated for 1 h at 25°C and then diluted to 10 ml by addition of *n*-hexane. The precipitated N,N′-dicyclohexylurea was filtered through an HV 0.45-μm Millipore filter and a sample (15 μl) of the solution was injected for HPLC analysis.

RESULTS AND DISCUSSION

Preliminary attempts to obtain a good resolution of diastereoisomeric mixtures of **1**, esterified with optically active alcohols [*e.g.*, (*S*)-2-butanol, (*S*)-2-octanol, (−)-menthol], by either gas chromatography or reversed-phase failed, despite the wide range of achiral stationary phases tested. As emphasized by other workers [8,9] we obtained much better results using HPLC with a normal silica phase. The use of (*S*)-2-octanol for the preparation of diastereoisomeric derivatives for analytical purposes has already been reported [10].

TABLE I

CALCULATED *vs.* EXPERIMENTAL (*S,S*)-ESTER CONTENT IN NON-RACEMIC MIXTURES OF (*R*)- and (*S*)-2-CHLORO-3-PHENYLMETHOXYPROPANOIC ACID AFTER DERIVATIZATION WITH (*S*)-2-OCTANOL

Sample composition (mg)		(*S,S*)-Ester (%)	
(*R*)-Acid	(*S*)-Acid	Calculated	Found
24.494	0.225	0.91	0.89
21.953	3.396	13.40	14.31
20.122	6.187	23.52	22.86
16.557	8.050	32.71	32.17
13.568	11.924	46.78	46.30
10.005	15.519	60.80	60.03
7.141	18.900	72.64	72.34
5.581	19.122	77.41	76.80
2.538	22.347	89.80	89.50
0.356	22.219	98.49	98.52

The resolution of the two diastereoisomeric esters of **1** with (*S*)-2-octanol, under our experimental conditions, is shown in Fig. 1. The (*S,S*)- and the (*R,S*)-esters elute with retention times of 22.75 and 25.12 min, respectively, and the chromatographic resolution is always better than 2.

Ten suitable samples of (*R*)- and (*S*)-**1** mixtures were analysed and the experimental enantiomeric percentages are reported, together with the calculated values, in Table I. The derivatization procedure proved to be very easy and highly reproducible. Modifying the reaction conditions, *i.e.*, temperature (within the range 20–40°C), concentration of the reagents and time (up to 24 h) did not result in any detectable racemization of either the acids **1** or their corresponding esters. It is noteworthy that even when the derivatization was performed at temperatures up to 40°C we did not observe the formation of any N-acylurea as a side-product [11]. The method described provides a reliable and practical means for the determination of the optical purity of **1**.

REFERENCES

1 E. Felder, L. Fumagalli, F. Uggeri and G. Vittadini, *Eur. Pat. Appl.*, EP 230893 (1987); *Ital. Pat. Appl.* (1986).
2 G. Vittadini, E. Felder, P. Tirone and V. Lorusso, *Invest. Radiol.*, 23 (1988) S246.

3 E. Felder, L. Fumagalli, C. Musu and F. Uggeri, *PCT Int. Appl.*, WO 8905802 (1989); *Ital. Pat. Appl.*, 87/23217 (1987).
4 C. Musu, E. Felder, L. Fumagalli, P. Tirone and G. Vittadini, presented at the *7th Annual Meeting of the Society of Magnetic Resonance in Medicine, San Francisco, CA, August 22–26, 1988.*
5 R. B. Lauffer, *Chem. Rev.*, 87 (1987) 901.
6 S. Aime, P. L. Anelli, M. Botta, M. Grandi, P. Paoli and F. Uggeri, *Inorg. Chem.*, submitted for publication.
7 E. Felder, U. Tiepolo and A. Mengassini, *J. Chromatogr.*, 82 (1973) 291.
8 L. R. Snyder and J. J. Kirkland, *Introduction to Modern Liquid Chromatography*, Wiley-Interscience, New York, 2nd ed., 1979, pp. 359-360.
9 L. R. Snyder, K. Glajch and J. J. Kirkland, *Practical HPLC Method Development*, Wiley-Interscience, New York, 1988, p. 8.
10 B. Halpern, in K. Blau and G. S. King (Editors), *Handbook of Derivatives for Chromatography*, Heyden, London, 1978, p. 482.
11 B. Helferich and H. Böshagen, *Chem. Ber.*, 92 (1959) 2813.

Journal of Chromatography, 589 (1992) 349–352
Elsevier Science Publishers B.V., Amsterdam

CHROM. 23 771

Short Communication

Sensitive fluorescence detection of some nitrosamines by precolumn derivatization with dansyl chloride and high-performance liquid chromatography☆

Zhi Wang☆☆, Hongda Xu and Chengguang Fu*

Research Centre of Physical and Chemical Analysis, Hebei University, Baoding 071002 (China)

(First received June 6th, 1991; revised manuscript received September 24th, 1991)

ABSTRACT

A fluorescence detection method for the determination of some nitrosamines by precolumn derivatization with dansyl chloride and high-performance liquid chromatography was developed. The separation, derivatization and detection conditions were optimized. The sample is first denitrosated by hydrobomic acid–acetic acid to produce secondary amines, which are then subjected to reaction with dansyl chloride to form dansyl derivatives. The reaction mixtures are injected and separated on a C_{18} column with acetonitrile–water (73:27, v/v) as mobile phase with fluorimetric detection at 530 nm (excitation at 350 nm). The method shows high sensitivity and precision. The detection limits are 0.06 ng for N-nitrosodimethylamine and N-nitrosodiethylamine, 0.09 ng for N-nitrosodipropylamine and 0.16 ng for N-nitrosodibutylamine, with relative standard deviations of 2.1, 1.9, 2.1 and 1.5%, respectively. The linearity of the calibration graphs covers more than two orders of magnitude of concentration of the compounds, and the correlation coefficients are 0.9995.

INTRODUCTION

The investigation of nitrosamines is a topic of growing importance because of their carcinogenicity. High-performance liquid chromatography (HPLC) is powerful technique for the analysis of this type of compound, and several HPLC methods [1–5] for the detection and determination of N-nitroso compounds have been reported. Reversed-phase HPLC with UV detection [1] has been used for the quantitative detection of some nitrosoamines. However, this technique lacks both the sensitivity and selectivity necessary for trace analyses of environmental samples. In an attempt to solve the selectivity problem, Singer *et al.* [2] developed a specific method in which a postcolumn reaction detection system is used for HPLC. This reaction detector is useful for those compounds which can be hydrolysed in a dilute acidic solution to give the nitrite ion. This method involves the use of Griess reagent in the postcolumn reactor for the production of chromophores from the N-nitrosamines. The theoretical detection limit for this method was reported to be 0.5 nmol and it is specific for all N-nitroso compounds cleaved by dilute hydrochloric acid. However, owing to the slow reaction kinetics of some nitroso compounds, this technique requires both an air segmentation system and a high-temperature reactor.

☆ Presented at the First Changchun International Symposium on Analytical Chemistry, Changchun, China, August 7–11, 1990.

☆☆ Present address: Department of Basic Courses, Hebei Agricultural University, Boading 071001, China.

0021-9673/92/$05.00

HPLC–thermal energy analysis methods [3,4] have been reported for the determination analysis of some nitrosamines. However, in order to operate continuously, this techniqe requires the use of cold traps for the removal of the eluent and the by-products of pyrolysis and the employment of microbore columns, which limits the use of the method. Lee and Field [5] reported a selective fluorescence detection method for the determination of some N-nitrosamines after postcolumn reaction. The nitrosamines eluted from the column are first hydrolysed to produce the nitrite anion, which is then oxidized with Ce^{4+} to give fluorescent Ce^{3+}. The detection limit for this method is at the ppb level. However, this method also requires a complex postcolumn reactor system with a heating bath.

We report here a sensitive precolumn derivatization method for some nitrosamines, which is based on the following reaction:

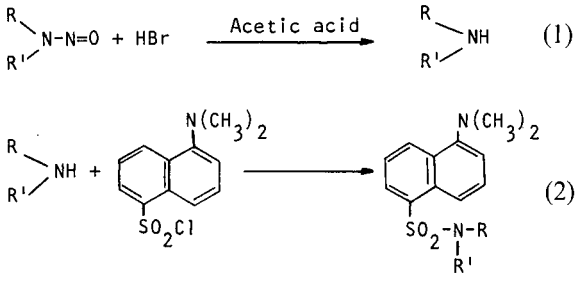

The sensitivitiy and the precision of the method are satisfactory and, as it involves only the use of conventional instrumentation and reagents, it is easy to employ.

EXPERIMENTAL

Apparatus

The HPLC system consisted of a constant-flow pump (Shanghai Chemical Industry Training School, Shanghai, China), an RF-535 fluorescence HPLC monitor (Shimadzy, Kyoto, Japan), a Perkin-Elmer Model 56 recorder and a Rheodyne (Berkeley, CA, USA) Model 7105 injection valve. The separation was carried out on a Perkin-Elmer C_{18} column (12.5 cm × 4.6 mm I.D.).

Chemicals

N-nitrosodimethylamine (NDMA), N-nitrosodiethylamine (NDEA), N-nitrosodipropylamine (NDPA) and N-nitrosodibutylamine (NDBA) were prepared by conventional procedures. All other reagent were of analytical-reagent grade. High-purity water was obtained by double distillation. A mixed standard solution containing 0.1 mg of each of the four N-nitrosoamines in 1 ml of dichloromethane was first prepared, and dilution was made as required. Hydrobromic acid–acetic acid reducing reagent was prepared by adding 5 ml of of acetic anhydride to 4 ml of 47% hydrobromic acid. Dansyl chloride solution was prepared by weighing 28 mg of dansyl chlorid (E. Merck) into a 10-ml volumetric flask, diluting to the mark with acetone and mixing well.

Preparation of dansyl derivatives

A 100-μl volume of the standard solution was mixed with 5 μl of reducing reagent in a graduated test-tube with stopper. After denitrosation reaction for 10 min at 40°C, the stopper was removed in a hood and the dichloromethane solvent was evaporated. About 60 μl of 1 mol/l NaOH solution were added to adjusted the pH to about 9, followed by the addition of 0.5 ml of 0.2 mol/l $NaHCO_3$ buffer and 0.5 ml of dansyl chloride solution. After 30 min at 40°C, the derivatives were diluted with water to 2 ml for HPCL analysis. A blank was run at the same time.

Analytical conditions

The mobile phase was acetonitrile–water (73:27, v/v) at a flow-rate of 0.8 ml/min. The injection volume was 20 μl and the chart speed was 5 mm/min. The fluorescence excitation wavelength was 350 nm and the emission wavelength was 530 nm.

RESULTS AND DISCUSSION

Selection of excitation and emission wavelengths

Stopped-flow scanning was applied to the peak of each of the derivatives to obtain both the emission and excitation spectra. The results obtained showed that the excitation and emission maxima of the NDEA, NDPA and NDBA were at 350 and 530 nm, respectively, but the fluorescence emission maximum of the NDMA derivative was at 540 nm. This is perhaps caused by the hyperconjugation effect in the structure of the NDMA derivative. Con-

sidering the sensitivity as a whole, an emission wavelength of 530 nm and an excitation wavelength of 350 nm were selected for the detection.

Separation of derivatives

Acetonitrile–water mixtures were tested as the mobile phase. When the content of acetonitrile in the mobile phase was increased, the capacity factors (k') of all four derivatives decreased. On the basis of both resolution and separation time, the optimum acetonitrile content was chosen as 73%. A typical chromatogram is shown in Fig. 1, indicating a good separation.

Denitrosation reaction time

The peak heights of the derivatives were measured for denitrosation reaction times from 5 to 40 min at 40°C, other conditions being identical. The peak heights for the derivatives remained almost constant. A denitrosation reaction time of 10 min was adopted.

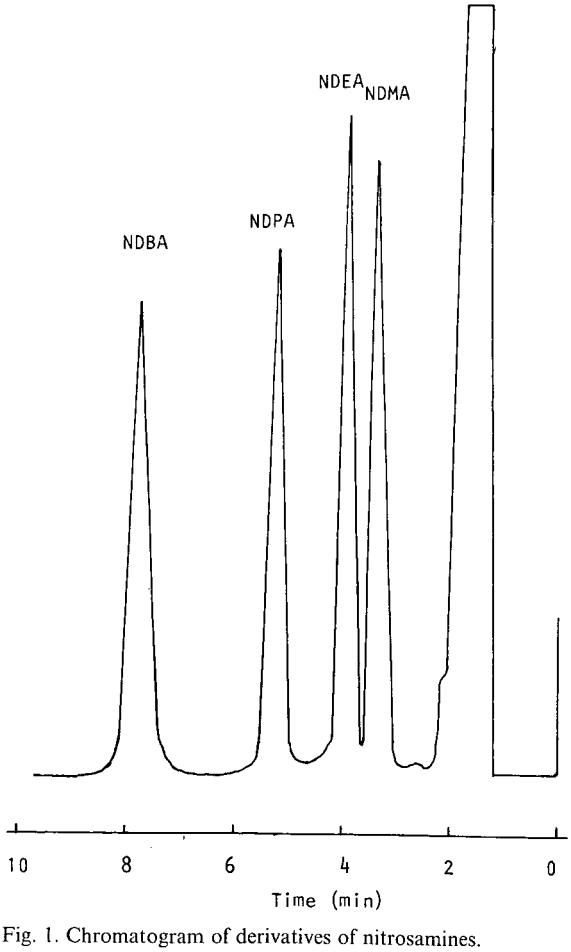

Fig. 1. Chromatogram of derivatives of nitrosamines.

Effect of amount of reducing reagent on signal

With other conditions were fixed, the peak heights of the derivatives were measured with various amounts of the reducing agent. The results showed that with between 1 and 15 μl of the reducing agent, the peak height of the derivatives remained almost unchanged, but above 15 μl the peak height decreased and fluctuated. This effect can be explained as follows. As the amount of reducing agent added is increased, adjustment of the pH to 8.5, which is necessary for the subsequent dansylation reaction, will result in the electrolytes in the reaction media being increased considerably. When the amount of reducing agent added is more than 15 μl, the amount of electrolytes formed will be large sufficient to interfere with the dansylation reaction and therefore make the signal irregular. Owing to the high concentration of the reducing agent, even 1 μl can suffice for the denitrosation reaction. The addition of 5 μl of the reducing agent was selected for subsequent experiments.

Effect of dansylation time on signal

The results showed that the peak height of the derivatives increased rapidly up to 20 min, and then remained constant as the reaction time increased. A derivatization time of 30 min was chosen for subsequent work.

Effect of amount of dansyl chloride on signal

The effect of the amount of dansyl chloride in the range 0–600 μl on the peak heights was investigated. The results showed that the peak height of the derivatives increased markedly as the amount of dansyl chloride was increased from 0 to 200 μl, but above 200 μl it remained almost unchanged. As a result, 500 μl of the dansyl chloride were selected for subsequent experiments.

Calibration and detection limits

A regression analysis was made for all four calibrations, and the relative standard deviations were obtained from seven replicate measurements. The results showed that the correlation coefficients for the

four nitrosamines exceed 0.9995 in the range 1–100 ng (linearity outside this range was not investigated); the detection limits (signal-to-noise ratio = 2) with this technique were between 0.06 and 0.16 ng, depending on the compound; the relative standard deviations for NDMA, NDEA, NDPA and NDBA (peak height) were 2.1, 1.9, 2.1 and 1.5%, respectively.

The sensitivity of this method is good, and the detection limit is lower than those reported for other methods [2,5]. The proposed method also does not require the complex postcolumn reaction apparatus needed for previous methods and can be readily used with conventional instrumentation and reagents. Such advantages suggest wide applicability, and the method provide a good approach for the detection of trace nitrosamines in environmental samples. Pretreatment of the samples would, of course, be required before the precolumn derivatization.

REFERENCES

1 S. S. Hecht, R. M. Ornag and D. Hoffman, *Anal. Chem.*, 47 (1975) 2046.
2 G. M. Singer, S. S. Singer and D. G. Schmidt, *J. Chromatogr.*, 133 (1977) 59.
3 R. C. Massey, C. Crews, D. J. McWeeny and M. E. Knowles, *J. Chromatogr.*, 236 (1982) 527.
4 C. Ruhl and J. Reusch, *J. Chromatogr.*, 328 (1985) 362.
5 S. H. Lee and L. R. Field, *J. Chromatogr.*, 386 (1987) 137.

Journal of Chromatography, 589 (1992) 353–357
Elsevier Science Publishers B.V., Amsterdam

CHROM. 23 779

Short Communication

Resolution of lipolysis mixtures from soybean oil by a solid-phase extraction procedure

W. E. Neff*

National Center for Agricultural Utilization Research, Agricultural Research Service (ARS), US Department of Agriculture, Peoria, IL 61604 (USA)

M. A. M. Zeitoun

Alexandria University, Faculty of Agriculture (Saba Basha), Dept. of Food Science, Alexandria (Egypt)

D. Weisleder

National Center for Agricultural Utilization Research, Agricultural Research Service, ARS, US Department of Agriculture, Peoria, IL 71704 (USA)

(Received July 30th, 1991)

ABSTRACT

A solid-phase extraction procedure was developed to rapidly resolve the lipolysis mixtures of free fatty acids, mono- and diacylglycerols from lipase (E.C. 3.1.1.3) cleavage of soybean oil triacylglycerols. Accuracy of the lipolysis procedure against standard mixtures of triacylglycerols showed coefficients of variance of 5% between known and observed fatty acid composition at glycerol carbon 2. An average coefficient of variance of 5% was obtained between results of the lipolysis procedure, fatty acid composition by gas chromatography, and the results by ^{13}C nuclear magnetic resonance stereospecific analysis for fatty acid composition at glycerol carbons 1;3 and 2 of intact triacylglycerol mixtures.

INTRODUCTION

Recently, we conducted a survey of the oxidative stabilities of the triacylglycerol (TAG) obtained from crude oils of many soybeen varieties [1]. Oxidative stability was correlated statistically with triacylglycerol structure or location of particular fatty acids on the glycerol primary and secondary carbons. This survey of many samples required a convenient and rapid TAG structural determination method.

Two methods are available for regiospecific analyses of vegetable oil TAG. One method involves ^{13}C nuclear magnetic resonance (^{13}C NMR) analyses of the chemical shifts of fatty acid carbonyl and olefinic carbons with glycerol carbon location of the acid [2–5]. The ^{13}C NMR procedures are equipment intensive, require lengthy analysis times and do not differentiate between saturated fatty acids on the glycerol moiety of the TAG.

The second method uses lipase (EC 3.1.1.3) directed cleavage of fatty acids at the glycerol 1,3 car-

bons [6–19]. The lipolysis procedures involve treatment of the TAG with lipase in Trizma buffer pH 8.0, bile salts and calcium chloride at 37–40°C [6] or by streaking the TAG solution over a band of lipase solution in Trizma impregnated on a thin-layer chromatography (TLC) plate [7,17]. These procedures give mixtures of free fatty acids (FFAs), 2-mono acylglycerol (MAG), 1,2(2,3)-di-acylglycerol (DAG) and unreacted TAG. Separate procedures of lipolysis have involved TLC [6,7,12,17–19,27], low-pressure liquid chromatography [8,13]; and high-performance liquid chromatography (HPLC) [20,21] and gas chromatography (GC) [22–24].

We report here a simple separation procedure of lipolysis products on a commercially available silica solid-phase extraction cartridge. Further, accuracy of the procedure is compared to lipolysis of standard mixtures of TAG (by weight) and to ^{13}C NMR regiospecific analysis of intact soybean oil TAG.

EXPERIMENTAL

Materials[a]

Soybeans (Glycine Max (L) Merr.) were commercial cultivars or plant introductions (PI). All solvents were HPLC grade. The solid-phase extraction columns (6.5 ml volume, loaded 2.0 g silica) used for removal of non-TAG components from crude soybean oils were purchased from Baxter Health Care (Muskegon, MI, USA). The solid-phase extraction columns (Bond Elut, 3 ml volume, loaded 0.2 g silica) used for resolution of lipolysis mixtures were purchased from Analytichem (Harbor City, CA, USA). Pancreatic lipase (EC 3.1.1.3, type 2, crude from porcine pancreas, activity 220 units/mg protein with olive oil at pH 7.7) and bile salts or sodium cholate were purchased from Sigma (St. Louis, MO, USA). TLC plates (7.5 × 2.5 cm, 250-μm layer of silica gel A, UV 254 nm indicator) were obtained from Whatman (Fairfield, NJ, USA). The GC direct injection column (182.9 × 0.3 cm I.D.) was packed with 1.8 g of 10% SP 2330 on 100/120 mesh Chromosorb W AW, obtained from Supelco (Bellefonte, PA, USA). Standard TAG and GC reference standard mixture 15A were purchased from NuChek Prep (Elysian, MN, USA).

Crude soybean oils (1.2–2.0 g) were obtained by sonification of ground soybeans with hexane for 5 min. Non-TAG components were removed from the crude oil by mixing with activated carbon (weight of carbon equal to 35% of oil weight) in hexane. The oil–carbon mixture was transferred to a 2.0-g silica solid-phase extraction cartridge. Elution of the oil components was as follows: 1.5 ml hexane, fraction 1, non-polar components; 15 ml of diethyl ether–hexane (10:90, v/v), fraction 2, TAG; and 15 ml methanol, fraction 3, polar components. Purity of the TAG fraction was quickly evaluated using TLC with diethyl ether–hexane (20:80, v/v) eluens and visualization by I_2 or sulfuric/chromic acid charring. Confirmation of the TAG purity was by reversed-phase HPLC with UV detection at appropriate wavelengths [1]. Fatty acid composition of the crude and chromatographed oils obtained by GC analysis [1] was within 5% coefficient of variance [25]. Oxidation level of the chromatographed oil was zero as confirmed by analytical reversed-phase HPLC with UV detection at 232 nm, as previously described [23,24].

Procedure

For statistical studies of oxidative stability, the oil was extracted in duplicate from each soybean variety and chromatographed as described above to recover TAG. Duplicate samples from each TAG fraction were lipolyzed by a modification of the procedure of Awl *et al.* [20] for regiospecific analysis. Briefly, 30-mg samples of TAG in 2 ml Trizma buffer (pH 8), containing 70 μl of 0.1% (w/w) calcium cholate and 120 μl of 22% (w/w) calcium chloride in water were vortexed. Lipase (30 mg) was added to the solution. The mixture (in a screw cap test tube) was incubated at 37°C with shaking using an orbital shaker for 10 min. The reaction mixture was extracted with diethyl ether. The ether extracts were washed with distilled water, dried over sodium sulfate, filtered and evaporated, using a stream of nitrogen at 30°C. The lipolysis reaction was 90–98% complete, as estimated, by TLC [diethyl ether–hexane–acetic acid (50:50:1, v/v/v) eluent], when compared to the starting material before lipolysis. The lipolysis products (15–20 mg) were dissolved in

[a] The mention of firm names or trade products does not imply that they are endorsed or recommended by the US Department of Agriculture over other firms or similar products not mentioned.

0.5 ml hexane and transferred to the top of the 0.2-g solid-phase extraction cartridge. Four fractions were eluted from the solid-phase extraction cartridge, as follows (weight applied: 16.1 mg): 5.0 ml diethyl ether–hexane (10:90, v/v), fraction 1, unreacted TAG 0.5 mg; 18:0 ml diethyl ether–hexane (10:90, v/v), fraction 2, fatty acids cleaved from glycerol carbons 1,3, 7.5 mg; 6 ml diethyl ether–hexane–acetic acid (50:50:1, v/v/v), fraction 3, 1,2(2,3)-DAG, incomplete lipolysis products, 2.0 mg; and 4 ml methanol, fraction 4, MAG, complete lipolysis products, 4.5 mg. Completion of the lipolysis was 97% based on wieght of unreacted TAG. Purity and identification of each fraction was determined by TLC against TAG, FFA, DAG and MAG standards. For GC analysis, the MAG and DAG were transmethylated by 0.5 *M* potassium hydroxide methanol at 50°C. GC analysis of each transmethylated sample was performed in triplicate using a Hewlett-Packard Model 5700 gas chromatograph equipped with flame ionization detectors (Avondale, PA, USA). The packed column was operated at 160°C with a helium carrier gas flow-rate of 20 ml/min. Sample injection was at 200°C with a 1-μl sample [0.5% (w/v) solute in diethyl ether]. Methyl ester identification and quantitation was calibrated against NuChek Prep soybean methyl ester standard 15-A. GC peaks were integrated by computer [26]. GC analysis of the transmethylated MAG fraction gave the average fatty acid composition at the 2 position of the TAG. These data plus GC analysis of the transmethylated TAG allowed the

TABLE I

REGIOSPECIFIC ANALYSIS OF CHROMATOGRAPHED SOYBEAN OILS BY LIPOLYSIS

Soybean variety	Glycerol acyl position	Fatty acid composition Area %					Average C.V.[a]
		16:0	18:0	18:1	18:2	18:3	
PI A-16	1,2,3[b]	10.2	4.8	27.0	54.8	3.2	
(Low linolenic acid)	2[b,c]			27.4	69.7	2.9	
	1,2(2,3)[b]	7.5	3.6	25.7	60.0	3.2	
	1,2(2,3)[d]	7.8	3.7	27.2	58.3	3.1	2.6
	1,3[e]	15.1	7.1	26.9	47.5	3.4	
PI 506.722B	1,2,3[b]	9.7	2.7	19.5	59.4	8.7	
(Low oleic acid, high linoleic acid	2[b,c]			19.2	73.6	7.2	
and linolenic acid)	1,2(2,3)[b]	7.0	2.0	17.8	64.1	9.1	
	1,2(2,3)[d]	7.4	2.1	19.4	62.7	8.4	4.1
	1,3[e]	14.4	4.1	19.7	52.3	9.5	
PI 507.319	1,2,3[b]	10.8	4.0	30.7	47.9	6.7	
(Low linoleic acid and	2[b,c]			30.1	63.8	6.1	
high oleic acid)	1,2(2,3)[b]	8.1	2.8	29.3	52.9	6.8	
	1,2(2,3)[d]	8.2	3.0	30.6	51.7	6.6	2.5
	1,3[e]	16.0	6.0	31.0	40.3	7.0	
Century-84							
Average	1,2,3[d]	10.7	3.5	22.8	56.0	7.0	
composition	2[b,c]			23.0	70.2	6.8	
	1,2(2,3)[b]	7.5	2.5	24.0	59.5	6.5	
	1,2(2,3)[d]	8.0	2.6	22.4	60.0	7.0	3.1
	1,3[e]	15.8	5.2	22.9	48.9	7.2	

[a] Coefficient of variance [25] between experimental and calculated 1,2(2,3)-diacylglycerol positions.
[b] Experimentally determined by GC analysis in triplicate. Standard deviation for average of four lipolysis samples per variety ± 0.1–0.6.
[c] Values for saturated acids less than 1%.
[d] Values calculated by [3 (area % triacyl) + (area % monoacyl)]/4 [17].
[e] Values calculated by [3 (area % triacyl) − (area % monoacyl)]/2 [17].

TABLE II

COMPOSITIONAL ANALYSIS OF 2-MONOACYL GLYCEROLS OBTAINED BY LIPOLYSIS FROM SYNTHETIC TRAICYLGLYCEROL MIXTURES

Synthetic triacyl mixture	Fatty acid composition					Average C.V.[a]
	16:0	18:0	18:1	18:2	18:3	
1	21.8[b]	19.3	21.5	19.5	17.9	
	19.6[c]	19.9	21.9	20.5	17.1	3.1
2	5.5[b]	8.4	32.5	29.1	24.5	
	5.4[c]	7.0	33.3	28.6	25.7	5.2
3	9.7[b]	2.1	18.9	51.9	17.4	
	9.2[c]	2.2	18.1	54.7	15.8	4.1
4	11.7[b]	8.4	29.4	46.7	3.8	
	11.1[c]	8.7	30.3	45.6	4.3	3.7

[a] Coefficient of variance [25].
[b] Weight percent fatty acid composition of triacylglycerol mixtures. Mixtures prepared by weight from trihexadecanoin, trioctadecanoin, trioctadecenoin, trioctadecadienoin and trioctadecatrienoin.
[c] Area percent fatty acid composition on carbon-2 of triacylglycerol synthetic mixtures after lipolysis. GC analysis of fatty acid methyl esters in triplicate.

calculation of the average fatty acid composition at the 1,3 positions of the TAG [17]. To determine if the fatty acids of the MAG were representative of the acids at the 2 position of the intact TAG, fatty acid composition determined by GC for the DAG was compared with that obtained by calculation [17]. For representative samples, these fatty acid values should agree within an average co-efficient of vairance (C.V.) [25] of 5% or less for the data to be used in the study of oxidative stability [1]. Accuracy of the above regiospecific method was compared against lipolysis of a standard mixture of TAG prepared by weight. Also, accuracy of the fatty acid composition by glycerol carbon location was compared against ^{13}C NMR regiospecific analysis on intact TAG [5].

RESULTS AND DISCUSSION

This regiospecific analysis procedure was developed for use in statistical studies to evaluate the effect on oxidative stability of unsaturated fatty

TABLE III

STEREOSPECIFIC ANALYSIS OF CHROMATOGRAPHED SOYBEAN OILS

Comparison of ^{13}C NMR to lipolysis (GC) analyses.

Oil	Carbon number		Fatty acid composition			
			16:0+18:0	18:1	18:2	18:3
1	2	NMR[a]	0.0	24.4	65.2	10.4
		GC[b]	0.0	24.6	64.3	11.1
		CV[c]		0.6	1.0	4.6
	1,3	NMR[a]	24.4	22.2	43.8	9.6
		Calculated[d]	24.6	22.9	43.6	8.9
		CV[c]	0.6	2.2	0.3	5.4
2	2	NMR[a]	0.0	31.9	63.5	4.6
		GC[b]	0.0	31.0	65.2	4.4
		CV[c]		2.0	1.9	3.1
	1,3	NMR[a]	27.2	29.3	39.3	4.2
		Calculated[a]	25.9	30.5	39.7	3.9
		CV[c]	3.5	2.8	0.7	5.2
3	2	NMR[a]	0.0	23.4	68.4	8.2
		GC[b]	0.0	22.3	70.0	7.7
		CV[c]		3.4	1.6	4.5
	1,3	NMR[a]	23.9	23.8	43.5	8.8
		Calculated[d]	22.7	24.7	44.4	8.2
		CV[c]	3.6	2.6	1.5	5.0
4	2	NMR[a]	0.0	23.5	68.1	8.4
		GC[b]	0.0	23.0	69.2	7.8
		CV[c]		1.5	1.1	5.4
	1,3	NMR[a]	24.0	24.3	43.2	8.4
		Calculated[d]	23.2	24.9	43.9	8.0
		CV[c]	2.4	1.7	1.1	3.4

[a] ^{13}C NMR analysis of oil [5].
[b] GC analysis of lipolyzed oil monoglycerides.
[c] Coefficient of variance [25].
[d] Fatty acid composition at 1,3 position calculated from GC analysis of lipolyzed oil monoglycerides.

acid location at the 1,3 and 2 positions of the TAG [1].

The regiospecific analysis of duplicate samples of each oil obtained by duplicate extraction of each soybean variety studied, required 11 h. The time phasing of the analysis was: lipolysis and sample work up: 2 h; solid-phase extraction and sample work up: 2 h; transmethylation of MAG and DAG: 1 h; triplicate GC analysis of samples: 6 h.

This method provided a standard deviation of ± 0.1–0.6 for samples, as shown in Table I for the regiospecific analysis for each of several soybean varieties. Fatty acid compositions of the TAG and of the MAG were experimentally determined. The average fatty acid distribution at the 1,3 positions was obtained by calculation [17].

The 1,2(2,3)-DAG fatty acid distributions were obtained experimentally and by calculation [17]. The observed agreement in fatty acid composition obtained by these two methods for the DAG indicates that the MAG and Dag compositions are representative of the composition of the original TAG [7,17]. Lipolysis analyses of the oil samples in Table I shows a C.V. range of 0.9 to 5.9%. For unsaturated fatty acids, the C.V. was usually less than 5%, which was satisfactory for oxidative stability studies.

The data presented in Table I shows that linoleic acid is in higher concentration at the 2 position, while oileic and linolenic acids have a higher concentration at the 1,3 positions. Also, the saturated fatty acids occur almost entirely at the 1,3 positions. These fatty acid distributions are in agreement with other investigations of soybean oil [18–19, 28–29].

Statistical studies on soybean oil stability with respect to fatty acid location require confidence in the accuracy of the solid-phase extraction lipolysis method. As presented in Table II, the average of the fatty acid composition obtaned by GC compared to weight percent, ranged from 3.1 to 5.2% for synthetic triacyl mixtures. Moreover, comparison of results obtained by an independent analytical method, ^{13}C NMR, for regiospecific analysis of intact TAG with those obtained by GC analysis of lipolysis products from the same TAG gave C.V. values of 0.6–3.4%, oleic; 1.0–1.9%, linoleic; and 3.1–5.4%, linolenic acids at the 2 position of TAG as shown in Table III. The calculated composition for the 1,3 positions of TAG, obtained from lipolysis of TAG and GC analysis of MAG, compared to ^{13}C NMR of intact TAG showed CV values of 0.6–3.6%, palmitic + stearic; 1.7–2.8%, oleic; 0.3–1.5%, linoleic; and 3.4–5.4%, linolenic acids.

ACKNOWLEDGEMENT

We wish to thank W. Rinsch for technical assistance and Dr. E. N. Frankel for useful discussions.

REFERENCES

1 W. E. Neff, E. Selke, T. L. Mounts, W. Rinsch, E. N. Frankel and M. A. M. Zeitoun, *J. Am. Oil Chem. Soc.*, (1991), in press.
2 S. Ng, *J. Chem. Soc., Chem. Commun.*, (1983) 179.
3 S. Ng, *Lipids*, 20 (1985) 778.
4 R. A. Awl, E. N. Frankel, D. D. Brooks and D. Weisleder, *Chem. Phys. Lipids*, 41 (1986) 65.
5 K. F. Wollenberg, *J. Am. Oil Chem. Soc.*, 67 (1990) 487.
6 F. E. Luddy, R. A. Barford, S. F. Herb, P. Magidman and R. W. Riemenschneider, *J. Am. Oil Chem. Soc.*, 41 (1964) 693.
7 J. Dutta, A. K. Das and S. Saha, *J. Chromatogr.*, 154 (1978) 39.
8 F. H. Mattson and R. A. Volpenhein, *J. Lip. Res.*, 2 (1961) 58.
9 H. Yoshida, *Lipids*, 19 (1984) 936.
10 I. A. De La Roche, E. J. Weber and D. E. Alexander, *Lipids*, 6 (1971) 537.
11 H. Brockerhoff, *J. Lip. Res.*, 8 (1967) 167.
12 E. J. Weber, I. A. De La Roche and D. E. Alexander, *Lipids*, 6 (1971) 525.
13 F. H. Mattson and L. W. Beck, *J. Biol. Chem.*, 214 (1955) 115.
14 G. Benzonana and P. Desnuelle, *Biochim. Biophys. Acta*, 105 (1965) 121.
15 F. D. Gunstone, J. L. Hardwood and F. B. Padlex (Editors), *The Lipid Handbook*, Chapman & Hall, London, 1986, p. 267.
16 W. W. Christie, *Lipids Analysis*, Pergamon, Oxford, 2nd ed., 1982, p. 155.
17 H. Yoshida, K. Murata and G. Kajimoto, *Nutr. Rep. Int.*, 32 (1985) 707.
18 J. N. Roehm and O. S. Privett, *Lipids*, 5 (1970) 353.
19 S. H. Fatemi and E. G. Hammon, *Lipids*, 12 (1977) 1032.
20 R. A. Awl, E. N. Frankel, D. D. Brooks and D. Weisleder, *Chem. Phys. Lipids*, 41 (1986) 65.
21 K. Payne-Wahl, G. F. Spencer, R. D. Plattner and R. O. Butterfield, *J. Chromatogr.*, 209 (1981) 61.
22 W. H. Tallent, R. Kleiman and G. C. Cope, *J. Lipid Res.*, 7 (1981) 531.
23 W. E. Neff, E. N. Frankel and K. Miyashita, *Lipids*, 25 (1990) 33.
24 E. N. Frankel, W. E. Neff and K. Miyashita, *Lipids*, 25 (1990) 40.
25 R. G. D.Steel and J. H. Torrie, *Principles and Procedures of Statistics*, McCraw Hill, New York, 2nd edn., 1960.
26 R. O. Butterfield, W. K. Rohwedder, E. D. Bitner, J. O. Ernst, D. J. Wolf and H. J. Dutton, *Progr. Lipid Res.*, 17 (1978) 93.
27 R. A. Awl, E. N. Frankel and D. Weisleder, *Lipids*, 24 (1989) 866.
28 W. P. Pan and E. G. Hammond, *Lipids*, 18 (1983) 882.
29 A. Kuksis, J. J. Myher and L. Marai, *J. Am. Oil Chem. Soc.*, 61 (1984) 1582.

Journal of Chromatography, 589 (1992) 358–361
Elsevier Science Publishers B.V., Amsterdam

CHROM. 23 739

Short Communication

Simultaneous ion chromatographic determination of chloride and calcium contained in Ringer's injection using a chelating agent as eluent

Wei Zhou, Wenying Liu and Dengkui An*

Department of Pharmaceutical Analysis, China Pharmaceutical University, Nanjing, Jiangsu 210009 (China)

(First received June 11th, 1991; revised manuscript received August 26th, 1991)

ABSTRACT

A single-column ion chromatographic system with conductivity detector is described for the simultaneous determination of chloride and calcium contained in Ringer's injection. The separation was achieved by using a polymethacrylate-based anion-exchange column and 0.8 m*M* ethylenediaminetetraacetic acid (pH 5.5) as eluent. Good results were obtained by both the calibration plot approach and the single-point calibration approach. For chloride and calcium, the average recoveries of the two methods were 100.5% and 100.1%, respectively.

INTRODUCTION

Ringer's injection is a sterile solution of sodium chloride, potassium chloride and calcium chloride in water for injection. The chloride and calcium components are usually determined by the argentimetric method and chelatometric titration, respectively [1,2].

Ion chromatography, introduced by Small *et al.* [3], has become one of the most important methods for the rapid separation and highly sensitive measurement of analyte ions [4]. However, with a conventional ion chromatographic system, anions and cations cannot be separated simultaneously on the same column. Because a metal cation can form a chelate anion immediately on contact with a chelating agent such as ethylenediaminetetraacetic acid (EDTA) [5–10], the eluent containing the chelating agent was investigated for the separation of several anions and metal cations on a single anion-exchange column.

In this work, chloride and calcium could be separated in 25 min by ion chromatography with EDTA as eluent. The calibration plot approach and the single-point calibration approach could be used to determine chloride and calcium contained in Ringer's injection. The two methods are not only accurate and sensitive, but also simple and rapid.

EXPERIMENTAL

Reagents and solutions

All reagents were of analytical-reagent grade. Standard and sample solutions were prepared from a stock solution (chloride 467.7 μg ml^{-1}, calcium 8.213 μg ml^{-1}), which was obtained by dissolution of corresponding sodium chloride and calcium chloride, and Ringer's injection, respectively. The

0021-9673/92/$05.00

eluent was prepared by dissolving 0.8 mmol of EDTA in 1 l of deionized water followed by adjustment of the pH to 5.5 with sodium hydroxide solution. Before use the eluent was filtered through a 0.45 μm membrane filter.

Apparatus and procedure

Ion chromatographic studies were performed on a Waters ILC-1 ion/liquid chromatograph (Millipore, Milford, MA, USA), which consists of a Model 590 programmable solvent-delivery module, an ILCI six-channel injection valve equipped with a 100-μl sample loop, a Model 430 conductivity detector and a Model 740 data module.

A 75 × 4.6 mm I.D. stainless steel IC-Pak A HR column with a 6-μm polymethacrylate-based quaternary ammonium packing (Millipore) was employed for the separation. The flow rate of the eluent was kept at 0.7 ml min^{-1}. The sensitivity of conductivity detector was set at 2.5 μS full-scale. Each injection was 100 μl.

In order to determine the content of a sample by the calibration plot approach, the regression equation of the calibration graph of peak height *versus* concentration of test ion must first be set up. From this equation, the amount of test ion in a sample solution could then be obtained easily from its peak height. For the single-point calibration approach, a standard solution should be analysed before a sample solution. The calculation of the concentration of test ion in the sample solution is then based on the concentration of the standard and the ratio of the peak heights of the sample and standard.

RESULTS AND DISCUSSION

Eluent and solvent

The EDTA ion has a high affinity for the anion exchanger, leading to a high eluting power for the separation of anions. As a chelating agent, EDTA can chelate with alkaline earth metal ions to form metal chelate anions, which can be separated together with other test anions on the anion-exchange column. In addition, EDTA is less mobile than inorganic anions and therefore has a lower equivalent conductance. EDTA has been found to be a generally applicable eluent for the simultaneous ion chromatographic separation of anions and alkaline earth metal ions on a single anion-exchange column with conductivity detection.

The active species of EDTA as the eluent is its anions, which are directly dependent on the pH and concentration of the eluent [5]. During the experiments on the ion chromatographic determination of chloride and calcium contained in Ringer's injection, when the pH of the eluent (0.8 m*M* EDTA) was adjusted to 5.5 with sodium hydroxide solution, good separation and satisfactory results were obtained. A typical chromatogram is shown in Fig. 1.

The solvent used for the test solutions can have a considerable effect on chromatographic separations. The eluent was selected as the solvent instead of water for the preparation of test solutions in order to improve the peak shape and increase the resolution of peaks between solvent and chloride.

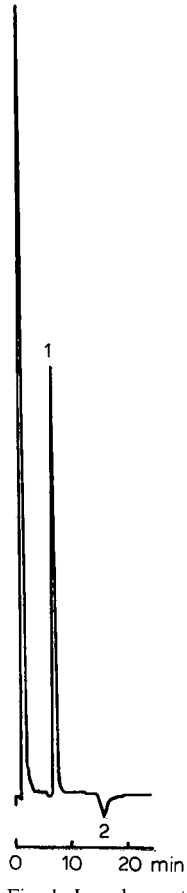

Fig. 1. Ion chromatogram of (1) chloride and (2) calcium in a sample solution prepared by diluting 0.15 ml of Ringer's injection to 100.0 ml. For chromatographic conditions, see Experimental.

TABLE I

COMPARISON OF RESULTS OBTAINED BY THE PROPOSED CHROMATOGRAPHIC METHODS AND THE US PHARMACOPEIA METHOD [2]

Method	Chloride		Calcium	
	Concentration (μg ml^{-1})	R.S.D. (%) (n = 3)	Concentration (μg ml^{-1})	R.S.D. (%) (n = 3)
Calibration plot	5791	0.38	85.08	2.4
Single-point calibration	5554	0.77	87.11	1.7
US Pharmacopeia method	5669	0.04	88.92	0.3

Linearity and detection limit

Volumes of stock solutions of 0.50, 1.00, 1.50, 2.00, 2.50 ml were diluted to 50.0 ml to prepare a series of working standard solutions. Each working standard solution was analysed five times consecutively. The linear relationship between the concentration of each component (c, μg ml^{-1}) and its peak height [h, μV; average of five measurements, relative standard deviation (R.S.D.) < 3.2%] could be described by the regression equation of the calibration graph:

$h = 3064c + 2658$ ($r = 0.9998$; $n = 5$) (chloride)

$h = 5674c + 275.4$ ($r = 0.9902$; $n = 5$) (calcium)

The results indicated that the calibration graphs were linear over the ranges 5.0–25 μg ml^{-1} of chloride and 0.08–0.40 μg ml^{-1} of calcium and the detection limits were 0.2 μg ml^{-1} of chloride and 0.04 μg ml^{-1} of calium under the recommended conditions.

Recovery

The recovery of added ions was studied [11]. A 0.10-ml volume of Ringer's injection, used as a fixed amount of the pre-analysed sample, was taken and standard ions were added at four different levels as 0, 0.50, 1.00 and 1.50 ml of the stock solutions, then each solution was diluted to 50.0 ml. With the calibration plot approach the recovery of the added standard was 99.11% for chloride and 98.05% for calcium, and with the single-point calibration approach 101.9% for chloride and 102.2% for calcium.

Assay

In addition to the two proposed methods, the US Pharmacopeia volumetric method [2] was used to determine the amounts of chloride and calcium in Ringer's injection for comparison. The results obtained by the three methods (Table I) are in good agreement. Although the precision of the US Pharmacopeia method is better than that of the proposed chromatographic methods, the latter methods are simple, rapid and sensitive.

CONCLUSIONS

As the standard and sample solutions were analysed consecutively in the approximately the same chromatographic environment, the experimental conditions of the single-point calibration approach need not be controlled very strictly. Compared with the calibration plot approach, the single-point calibration approach is more practical for the simultaneous determination of chloride and calcium contained in Ringer's injection by ion chromatography.

REFERENCES

1 Chinese Pharmaceutical Association, Shanghai Branch, *Handbook of Preparations Used in the Hospitals of Shanghai*, Shanghai Science and Technical Publishing, Shanghai, 2nd ed., 1988, p. 386.
2 *United States Pharmacopeia XXII Revision and National Formulary XVII*, US Pharmacopeial Convention, Rockville, MD, 1990, p. 1228.
3 H. Small, T. S. Stevens and W. C. Bauman, *Anal. Chem.*, 47 (1975) 1801.
4 D. T. Gjerde and J. S. Fritz, in W. Bertsch, W. G. Jennings and R. E. Kaiser (Editors), *Ion Chromatography*, Hüthig, Heidelberg, 2nd ed., 1987, p. 253.

5 S. Matsushita, *J. Chromatogr.*, 312 (1984) 327.
6 M. Yamamoto, H. Yamamoto, Y. Yamamoto, S. Matsushita, N. Baba and T. Ikushige, *Anal. Chem.*, 56 (1984) 832.
7 S. Matsushita, *Anal. Chim. Acta*, 172 (1985) 249.
8 A. F. Geddes and J. G. Tarter, *Anal. Lett.*, 21 (1988) 857.
9 G. Schwedt and B. Kondratjonok, *Fresenius' Z. Anal. Chem.*, 332 (1989) 855.
10 D. Yan and G. Schwedt, *J. Chromatogr.*, 516 (1990) 383.
11 R. T. Sane, G,. S. Sadana, G. J. Bhounsule, M. V. Gaonkar, A. D. Nadkarni and V. G. Nayak, *J. Chromatogr.*, 356 (1986) 468.

Journal of Chromatography, 589 (1992) 362–367
Elsevier Science Publishers B.V., Amsterdam

CHROM. 23 777

Short Communication

Solvent system for the counter-current purification of hydrophobic bombesin analogues

Luisa Rusconi* and Mauro Galantino

Farmitalia Carlo Erba srl, Biotechnological Research and Development, Peptide Chemistry Department, Via dei Gracchi 35, 20146 Milan (Italy)

(First received January 23rd, 1991; revised manuscript received June 6th, 1991)

ABSTRACT

A two-phase solvent system has been developed for the fractionation of some highly hydrophobic bombesin analogues prepared by solid-phase peptide synthesis. The solvent system, composed of toluene, ethyl acetate, dichloromethane, methanol and aqueous triethylammonium acetate, has been proven useful for the purification of these water-insoluble peptides.

INTRODUCTION

The tetradecapeptide bombesin (BN), orginally isolated from frog skin, exerts a series of physiological effects in humans [1,2], and BN-like peptides have been shown to act as autocrine growth factors in cell lines of a malignant tumour, the small cell lung carcinoma (SCLC) [3]. This finding greatly stimulated the search for BN antagonists, and several classes of peptides with antagonistic properties have since been described [4,5]. We have prepared a series of analogues having a hybrid structure between that of BN itself and [D-Pro^2]-spantide, an antagonist of substance P, which is also a weak BN antagonist [6].

Peptides I and IV (see Table I) are two analogues in this series, which appeared heterogeneous by reversed-phase high-performance liquid chromatography (RP-HPLC), as obtained by solid-phase synthesis. Both of them are N- and C-terminal blocked peptides, spanning a highly hydrophobic sequence. Similar BN-related, water-insoluble peptides have recently been purified by counter-current chromatography in horizontal flow-through coil planet centrifuge, using the aqueous phase of a chloroform–acetic acid–water (2:2:1) system as the mobile phase [7]. Preliminary partition tests in this system, and also in other systems of relevance for peptide counter-current purification [8,9], showed that they were not suitable in this instance. In this

TABLE I

AMINO ACID SEQUENCES OF BN ANALOGUES I–V

<Glu = pyroglutamic acid; [ ] = deleted residue.

No.	Amino acid sequence
I	Boc-D-Gln-Trp-Ala-D-Trp-Phe-D-Trp-Leu-Nle-NH_2
II	D-<Glu——[ ]——NH_2
III	Boc——[ ]——NH_2
IV	Boc——-D- His——NH_2
V	Boc——[ ] -D- His——NH_2

0021-9673/92/$05.00

paper, the particular counter-current conditions developed for the purification of such peptides in a classical apparatus are described.

EXPERIMENTAL

All reagents were of analytical-reagent grade and solvents were of analytical-reagent or HPCL grade. N,N-Dimethylformamide (DMF) was distilled over ninhydrin and stored in the dark over 4 Å molecular sieves. Trifluoroacetic acid (TFA) was of Sequanal grade from Pierce (Rockford, IL, USA). The amino acid derivatives were obtained from Bachem Feinchemikalien (Bubendorf, Switzerland) or Peninsula Labs. (Belmont, CA, USA) and Merrifield resin (0.88 mequiv./g) from Bio-Rad Labs. (Richmond, CA, USA).

Synthesis

The bombesin analogues I and IV were synthesized in a semi-automatic laboratory-made apparatus starting with N^{α}-*tert*-.-butyloxycarbonyl (Boc)–Nle–OCH_2 resin (0.56 mmol/g), prepared by esterification of Merrifield resin by Gisin's method [10]. The protocol of the synthesis involved the following steps: washing with dichloromethane (DCM); deprotection with 40% TFA in DCM or, following the insertion of Trp, with 40% TFA in DCM containing 2.5% anisole and 2.5% 2-mercaptoethanol; washing; neutralization with 10% N-methylmorpholine in DCM; washing; double coupling in DCM or DMF for 1 h with the preformed symmetrical anhydride of the Boc-amino acid or, in the case of Boc-D-glutamine, with the 1-hydroxybenzotriazole (HOBt) ester in DMF for 4 h, then washing with DCM (or DMF and DCM), 2-propanol and again DCM. The imidazole ring of Boc-D-histidine was protected as the 4-toluenesulphonyl (Tos) derivative. The peptides were cleaved from the resin by treatment with saturated anhydrous ammonia in methanol–DMF (1:1, v/v) at 4°C for 4 days. After evaporation of the filtrate, the product was precipitated from methanol solution with diethyl ether. The yield of crude product was 1.35 g for I and 0.91 for IV.

Counter-current chromatography

A Craig-type apparatus (Labortec, Bubendorf, Switzerland) consisting of 120 distribution tubes (volume of the phase = 25 ml) was employed. Crude peptides were dissolved in methanol and the solution was evaporated to an oil, which was taken up with 25 ml of the lower phase obtained by partitioning at room temperature of the following mixture: toluene–ethyl acetate–DCM–methanol–triethylammonium acetate (0.1 *M* triethylamine adjusted to pH 4 with glacial acetic acid) (10:3:5:12:6). The solution was charged into the first tube of the apparatus filled with the lower phase, and distribution was allowed to proceed over the whole series of tubes. Usually, the fractions were analysed by thin-layer chromatography (TLC) on silica gel plates (Merck, Darmstadt, Germany) with the eluent benzene–ethyl acetate–acetic acid–water (5:5:2:0:75), upper phase, or *n*-butanol–acetic acid–water (4:1:1) and detection with Ehrlich's reagent [11]), and peak tubes were combined and evaporated under vacuum. The products were finally recovered by precipitation with water (I–III) or diethyl ether (IV and V) from methanol solution.

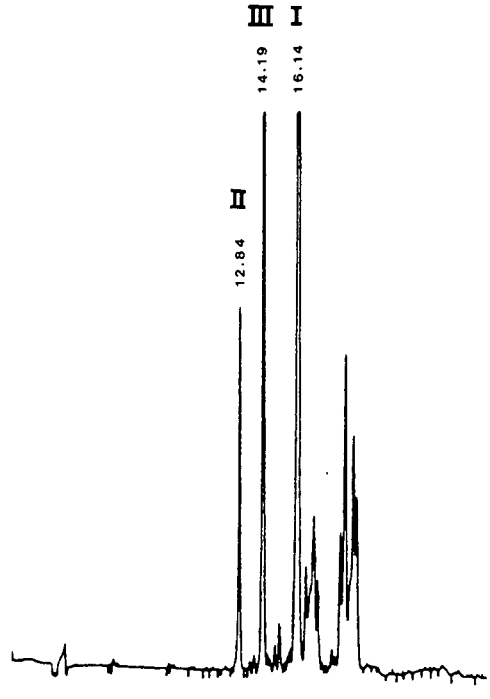

Fig. 1. RP-HPLC profile of crude I. Conditions: eluent A = 0.05% TFA in water, eluent B = 0.05% TFA in acetonitrile gradient from 20% to 70% B over 15 min; sample size, *ca.* 20 μg; detection wavelength, 230 nm at 0.4 a.u.f.s. Arabic numbers at peaks indicate retention times in min.

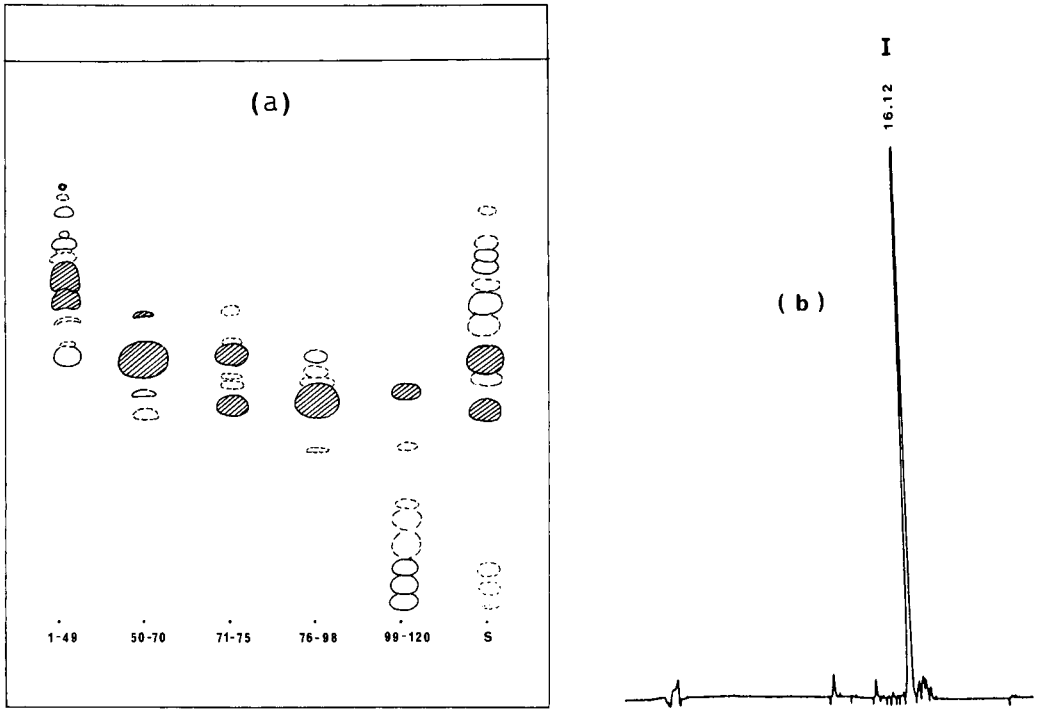

Fig. 2. (a) TLC of fraction pools from the counter-current distribution (CCD) of crude analogue I. Eluent, benzene–ethyl acetate–acetic acid–water (5:5:2:0.75), upper layer; detection, with Ehrlich's reagent [11]; sample size, *ca.* 80 μg. (b) RP-HPLC profile of fractions 50–70 from the same CCD run. Conditions as in Fig. 1, except sample size, *ca.* 8 μg.

Analysis

The purified peptides were analysed for homogeneity by HPLC using a Hewlett-Packard (Avondale, PA, USA) Model 1084 apparatus equipped with a variable-wavelength detector (HP 79875A) and a Model HP79850B LC terminal, on a LiChrosorb RP-18 column (25 × 0.4 cm, I.D. particle diameter 5 μm) (Merck) at 1 ml/min (for other conditions, see the legends of the figures). Amino acid analysis was performed on a 3 *M* mercaptoethanesulphonic acid hydrolysate. The structure of each of the purified peptides was confirmed by fast atom bombardment mass spectrometry (FAB-MS).

RESULTS AND DISCUSSION

BN-antagonist I was obtained as heterogeneous material, as shown in Fig. 1, which reproduces the HPLC trace of the crude product. The major peak

TABLE II

PARTITION COEFFICIENTS, K_n[a], OF BN ANALOGUES IN DIFFERENT SOLVENT SYSTEMS

Solvent composition	Volume ratio	K_n
Chloroform–acetic acid–water	2:2:1	25
Toluene–ethyl–acetate–DCM–methanol–0.1 *M* hydrochloric acid	10:3:5:12:6	4.1
Toluene–ethyl acetate–DCM–methanol–0.1 *M* acetic acid	10:3:5:12:6	2.7
Toluene–ethyl acetate–DCM–methanol–triethyl–ammonium acetate[b]	10:3:5:12:6	1.05; 0.12[c]

[a] K_n = solute concentration in the non-aqueous phase/solute concentration in the aqueous phase.
[b] 0.1 *M* triethylamine adjusted to pH 4 with glacial acetic acid.
[c] The frist value refers to peptide I and the second to peptide IV.

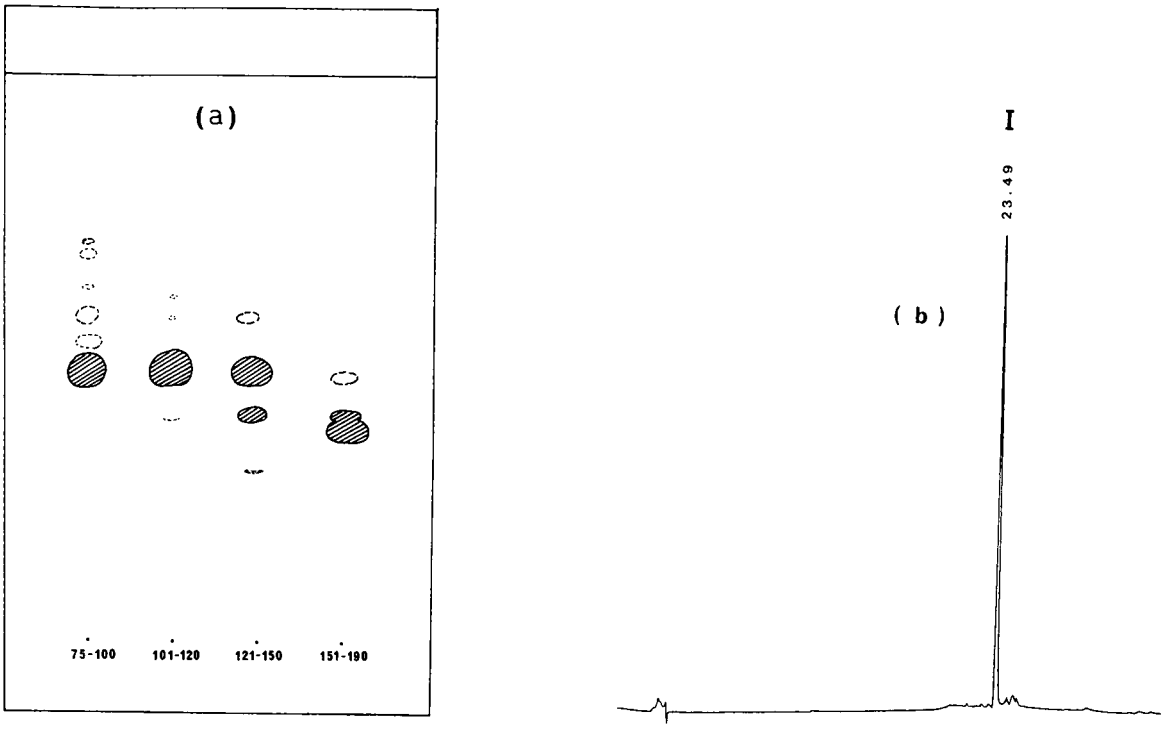

Fig. 3. (a) TLC of fraction pools from the CCD of semi-purified analogue I. Conditions as in Fig. 2a. (b) RP-HPLC profile of fractions 101–120 from the same CCD run. Conditions: eluent A = 20 m*M* KH_2PO_4 (pH 3.5)–acetonitrile (9:1), eluent B = 20 m*M* KH_2PO_4 (pH 3.5)–acetonitrile (3:7), isocratic elution with 30% B for 1 min, then gradient from 30% to 90% B over 20 min; sample size, *ca.* 5 μg; detection wavelength, 210 nm at 0.4 a.u.f.s.

in this chromatogram accounts for *ca.* 41% of the mixture. For the counter-current purification of this synthetic peptide, the usual polar *n*-butanol solvent systems proved totally inadequate. To select a suitable solvent system, the partition coefficient of the sample (defined here as K_n, the solute concentration in the non-aqueous phase divided by that in the aqueous phase) was measured by a traditional micro shake-flask test coupled with HPLC. The screening of relatively non-polar systems started with chloroform–acetic acid–water (2:2:1), which has already been found useful for the purification of similar water-insoluble peptides [7]. In contrast, in this instance the partition coefficient of the sample in that system was very high (Table II), thus rendering its use impractical.

Several other systems that have been suggested for poorly polar peptides were tried [8,9]: they were composed of toluene, and/or DCM (or chloroform), optionally ethyl acetate, methanol and an acidic aqueous component such as dilute hydrochloric or acetic acid, in a range of proportions. The K_n value of peptide I was considerably lowered in some of these systems containing ethyl acetate (see Table II), but still high, considering the large amount of heterogeneous more hydrophobic material which had to be removed in this purification (see Fig. 1). The introduction of triethylammonium acetate as an aqueous component resulted in a critical adjustment of the partition coefficient, which approached unity (see Table II). The whole crude could then be purified by counter-current chromatography with an optimized solvent system, consisting of toluene–ethyl acetate–DCM–methanol–aqueous triethylammonium acetate (10:3:5:12:6, v/v).

After 120 transfers, fractions 50–70 were found to contain the peak of the main product and were pooled, yielding 0.61 g of I with a degree of purity of 84% by HPLC (Fig. 2). The material obtained

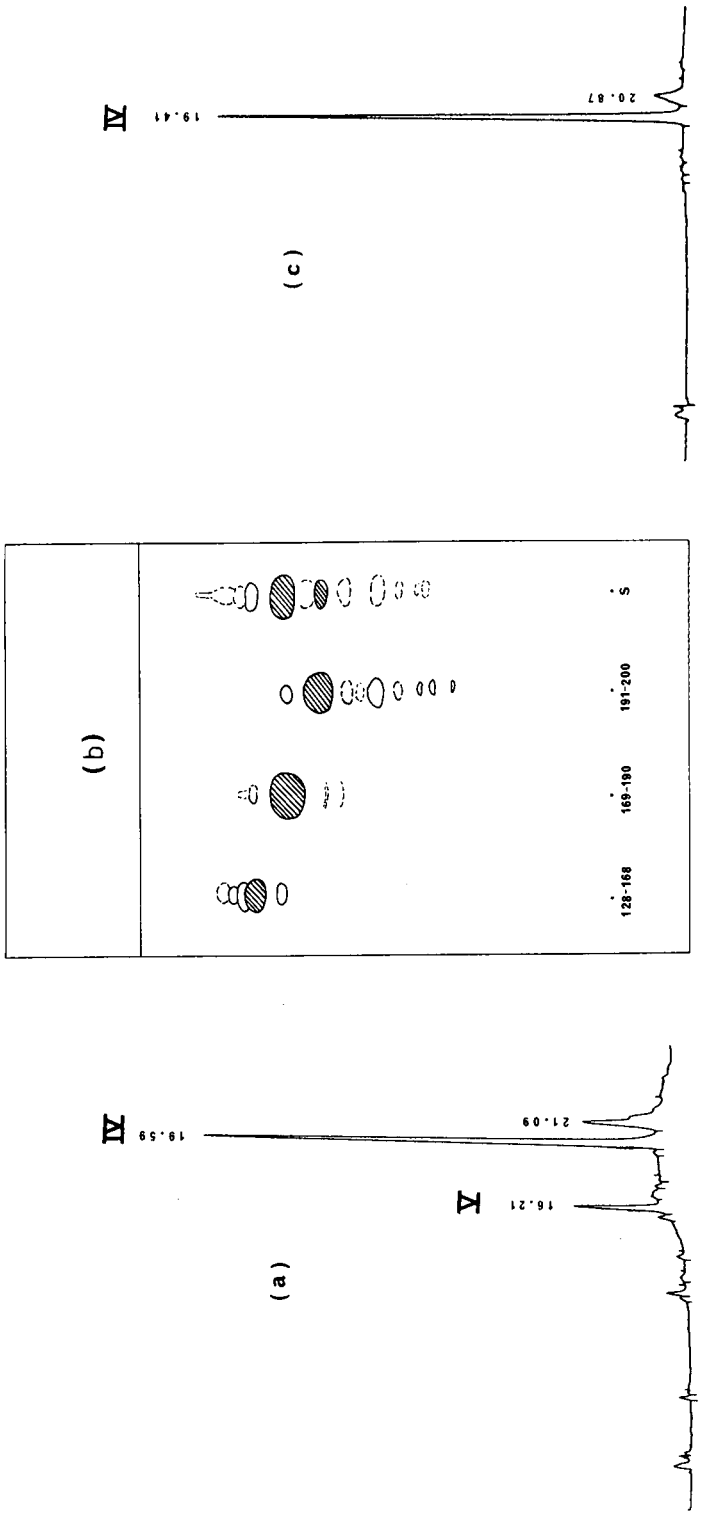

Fig. 4. RP-HPLC profiles of (a) crude IV and (c) fractions 169–190 from CCD performed on this product. Conditions: sample size, (a) *ca.* 10 μg and (c) *ca.* 5 μg; eluents as in Fig. 3b, gradient from 30% to 70% B over 15 min, followed by isocratic elution with 70% B for 10 min; detection wavelength, 210 nm at 0.4 a.u.f.s. (b) TLC of fraction pools from the same CCD. Eluent, *n*-butanol–acetic acid–water (4:1:1); other conditions as in Fig. 2a.

from fractions 76–98 (0.28 g) was also analysed by HPLC and it consisted of the two side-products, II and III, detected in Fig. 1 as peaks with retention times of 12.8 and 14.2 min, respectively. Interestingly, these products were both identified by amino-acid analysis as deletion peptides lacking Phe[5]. FAB-MS analysis enabled us to ascertain that II, the earlier eluting side-product, bore an additional structural modification,consisting of the presence of a D-pyroglutamic residue at the amino terminus instead of the starting Boc-protected D-glutamine. This product may have been formed during the cleavage treatment, performed by prolonged ammonolysis, owing to a sequence-specific lability of the Boc group in the deletion heptapeptide. The pool from fractions 71–75, which was found to be a 1:1 mixture of peptides I and III, the later eluting deletion peptide, yielded a very small amount of material (22 mg).

Hence a single counter-current run with the selected solvent system turned out to be very effective in resolving such products, bearing slight structural modifications. In addition, peptide I could be further purified by subjecting the semi-purified material (0.53 g) to a second counter-current distribution in the same solvent system (Fig. 3a). In this instance, 95 fractions of the head effluent were collected in external tubes, so that a total of 215 transfers was performed. Fractions 101–120 were combined, yielding 0.25 g of fairly pure peptide I (Fig. 3b). In addition, 0.14 g of 75% pure product was recovered from head and tail fractions, possibly to be recycled.

The same solvent system as successfully used for analogue **I** was tried for the purification of analogue **IV**, which also appeared as a composite crude on HPLC analysis (Fig. 4a). The partition coefficient of the product was much lower in this instance (see Table II), owing to the presence of a basic residue (D-His[6]) in the molecule. The crude product was submitted to a total of 200 transfers (80 fractions of the effluent were collected in external tubes), after which (Fig. 4b) fractions 169–190 were found to contain the peak of the main product and pooled, yielding 0.34 g of IV with a degree of purity near 90% (Fig. 4c). The peptide was still contaminated with more hydrophobic material, but had been completely resolved from the main impurity, V (peak which retention time 16.2 min in Fig. 4a). This side-product was isolated from fractions 191–200, and, similarly to what was found with analogue I, it was identified as the deletion peptide lacking Phe[5]. This may reflect a particular difficulty in coupling this amino acid to the tripeptidyl resin, namely H–D-Trp–Leu–Nle–OCH_2 resin for peptide I and H–D-His(Tos)–Leu–Nle–OCH_2 resin for peptide IV.

The results obtained in the counter-current chromatography of the two analogues show that the solvent system containing triethylammonium acetate as an aqueous component can be very helpful for fractionating water-insoluble peptides. In particular, it enabled us to achieve effectively the purification both of peptide I, which displays a strongly hydrophobic structure and had a negligible solubility in the aqueous phase of a number of solvent systems, and peptide IV, which is also water insoluble but contains a residue bearing a dissociable group in the side-chain. In addition, for hydrophobic peptides containing other dissociable functions, one might take advantage of the possibility of adjusting the pH of the aqueous component over a wide range of values, while maintaining its ability to sulubilize the peptides efficiently, and thus possibly conferring on them a suitable partition coefficient.

ACKNOWLEDGEMENTS

We thank Mr. F. Ciprandi and Mr. P. Pelizza for skilful technical assistance.

REFERENCES

1 V. Erspamer and P. Melchiorri, *Pure Appl. Chem.*, 35 (1973) 463–494.
2 V. Erspamer and P. Melchiorri, in E. E. Müller and R. M. MacLeod (Editors), *Neuroendocrine Perspectives*, Vol. 2, Elsevier Biomedical Press, Amsterdam, 1983, pp. 37–106.
3 F. Cuttitta, D. N. Carney, J. Mulshine, T. W. Moody, J. Fedorko, A. Fischler and J. D. Minna, *Nature (London)*, 316 (1985) 823–826.
4 R. T. Jensen and D. H. Coy, *Trends Pharmacol. Sci.*, 12 (1991) 13–19.
5 R. De Catiglione, L. Gozzini, M. Galantino, F. Corradi, M. Ciomei and I. Molinari, in J. E. Rivier and G. R. Marshall (Editors) *Peptides: Chemistry, Structure and Biology*, Escom, Leiden, 1990, pp. 168–170.
6 L. Rusconi, R. de Castiglione, L. Gozzini, M. Ciomei, I. Molinari, L. Basilico, T. Rubino, R. Vinayek and J. D. Gardner, *Farmaco*, 46 (1991) 725–742.
7 M. Knight, J. D. Pineda and T. R. Burke, *J. Liq. Chromatogr.*, 11 (1988) 119–131.
8 K. Hostettmann, *Planta Med.*, 39 (1980) 1–18.
9 M. Knight, in N. B. Mandava and Y. Ito (Editors), *Countercurrent Chromatography*, Marcel Dekker, New York, 1986, pp. 583–616.
10 B. F. Gisin, *Helv. Chim. Acta*, 56 (1973) 1476–1482.
11 J. M. Stewart and J. D. Young, *Solid Phase Peptide Synthesis*, Pierce, Rockford, IL, 1984, p. 122.

Journal of Chromatography, 589 (1992) 368–374
Elsevier Science Publishers B.V., Amsterdam

CHROM. 23 743

Short Communication

Study of dihydroxy-substituted saturated urushiol crown ether as a stationary phase in capillary gas chromatography

Zhao-Rui Zeng, Cai-Ying Wu* and Xiao-Hong Fang

Department of Chemistry, Wuhan University, 430072 Wuhan (China)

Zai-Fu Huang and Yu-Ting Wang

Department of Environmental Science, Wuhan University, Wuhan (China)

(First received January 8th, 1991; revised manuscript received September 6th, 1991)

ABSTRACT

A new way of cross-linking glass capillary columns with dihydroxy-substituted saturated urushiol crown ether stationary phase is described. The columns were evaluated by determining the column efficiency, phase transition temperature, thermal stability and polarity. It was shown that they have good chromatographic characteristics and unique selectivity in separating phenols, nitro compounds and monsaccharides. The average polarity of these columns was comparable to those of SE-52 and FFAP. The mechanism of separation is discussed.

INTRODUCTION

As most crown ethers have a polar ring formed by heteroatoms, they are useful as chromatographic stationary phases because of the good selectivity resulting from the cavity structure and the strong electronegative effect of heteroatoms on the crown ether ring [1–5]. However, their poor column efficiency and thermal stability prevent the practical usage of small crown ethers, and many attempts have therefore been made to increase their molecular weights [3–5]. Two approaches have been used. One is the synthesis of crown ether-substituted polysiloxane stationary phases. In 1988, Rouse *et al.* [3] first substituted 18-crown-6 onto a polysiloxane backbone with a polymer spacing of 3. Later, we developed an 18-crown-6-substituted polysiloxane with a polymer spacing of 11 [5]. The crown ether–polysiloxane gave a good performance as a stationary phase in capillary gas chromatography and it has sufficient efficiency to achieve many separations, such as those of alcohols, ketones and aromatic hydrocarbons, and especially some polar positional isomers.

The other approach is to cross-link the crown ether directly with SE-54 inside a column [4]. This crown ether–polymer phase also gave good results. However, all these methods are carried out by free-radical cross-linking.

In this work, a new crown ether, dihydroxy-substituted saturated urushiol crown ether (DHSU14C4), shown in Fig. 1, was investigated. It

0021-9673/92/$05.00

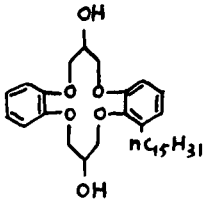

Fig. 1. Structure of dihydroxy-substituted saturated urushiol crown ether.

not only has a long polar alkyl, easily polarizable benzene ring and a polar polyether ring, but also two hydroxyl groups which are convenient for condensation reactions. Capillaries were coated with a mixture of DHSU14C4, OH-terminal silicone oil (GY-202) and γ-chloropropyltriethoxysilane (as coupling agent), and then heated at 60–110°C, so that the crown ether formed a high-molecular-weight immobilized phase on the wall of the glass capillary column by the condesation reaction of the OH-terminated phase on the silica surface [6–8].

Test made with these immobilized crown ether columns showed that the moderately polar phase has a high operating temperature and good selectivity for polar compounds.

EXPERIMENTAL

Apparatus and materials

An SC-7 gas chromatograph (Sichuan Analytical Instrument Factory) equipped with a capillary split injection system and flame ionzation detector, was used with nitrogen as the carrier gas. Capillaries were prepared with a Model GDM glass-drawing machine (Shimadzu).

DHSU14C4 (m.p. 77–78°C) was kindly provided by the Department of Environment Science, Wuhan University). GY202 OH-terminal silicone oil was obtained from the Chendu Centre for Applied Reasarch of Silicone (Ministry of Chemical Industry) and γ-chloropropyltriethoxysilane from Wuhan University Chemical Factory).

Synthesis of DHSU14C4

The dihydroxy-substituted saturated urushiol crown ether was prepared by reaction of saturated urushiol with 1,1′-(*O*-phenyl) bis (2,3-epoxypropyl) ether (Fig. 2). The structure of the new compound was determined by IR, ^{1}H NMR and mass spectrometry and elemental analysis [9].

Capillary column preparation

Glass tubes (7.5 mm O.D, 2.4 mm I.D.) were drawn into capillary columns (0.3 mm I.D.). The columns were filled with 20% hydrochloric acid to 92% of their volume and heated at 180°C for 12 h. They were then rinsed with water and acetone and dried with nitrogen at 150°C for 3 h. The capillaries were statically coated with 0.5% (w/v) mixed stationary phase (DHSU14C4 with GY-202 in different proportions) and γ-chloropropyltriethoxysilane [1% (w/w) of the stationary phase] in methylene chloride. On completion of coating, the column were purged with nitrogen for 5 min, then both ends of the column were flame sealed under vacuum and heated in a gas chromatographic oven at 60°C for 15 h. Finally, the ends were opened and the column was conditioned at 250°C for 8 h. The columns were tested for efficiency. Subsequently, they were rinsed with ten column volumes of methylene chloride and reconditioned at 300°C for 10 h.

RESULTS AND DISCUSSION

When DHSU14C4 was directly coated on a glass capillary column it was found that the capacity factor did not remain constant ($k' = 2.1$–3.4) and the efficiency was especially low ($N < 100$), because the crown ether has poor wettebility on the surface of

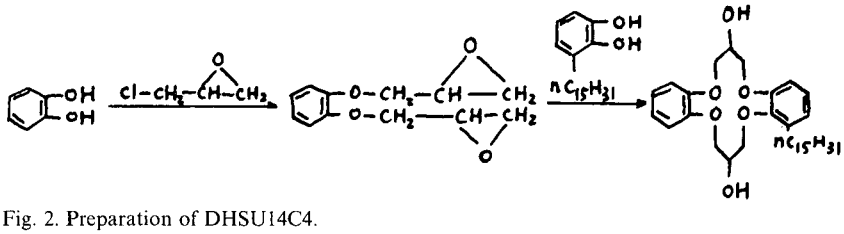

Fig. 2. Preparation of DHSU14C4.

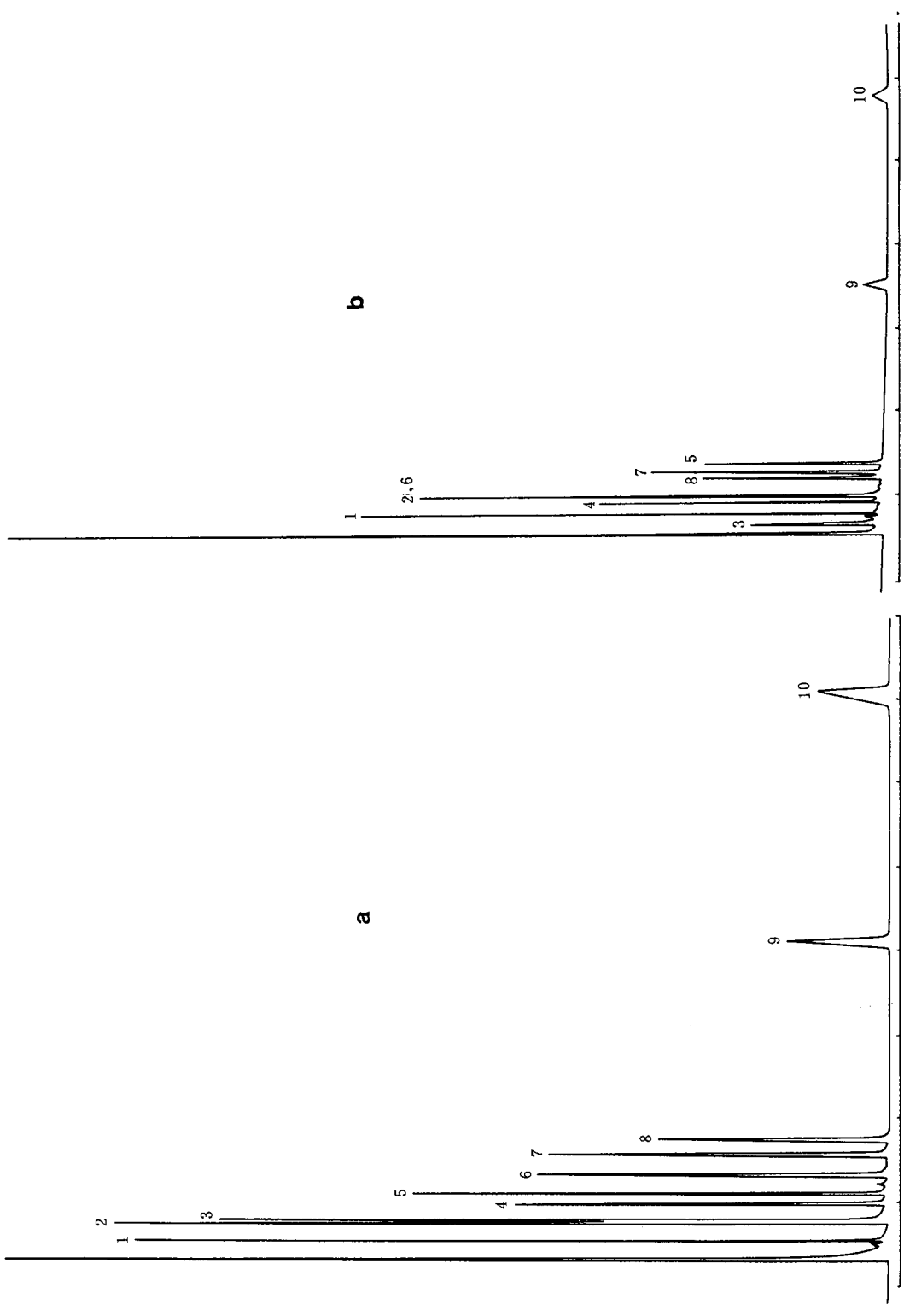

Fig. 3. Chromatogram of the Grob test mixture. (a) On DHSU14C4–GY202 column 2; (b) on GY202 column 5. Temperature, 120°C; flow rate, 13 cm/s. Peaks: 1 = *n*-decane; 2 = *n*-undecane; 3 = 1,3-butanediol; 4 = octanol; 5 = *n*-dodecane; 6 = 2,6-dimethylphenol; 7 = naphthalene; 8 = 2,4-dimethylaniline; 9 = methyl undecanoate; 10 = methyl dodecanoate.

TABLE I

CHARACTERISTICS OF DHSU14C4–GY202 AND GY202

Column No.	Column dimensions [length (m) × I.D. (mm)]	Stationary phase	Capacity factor, k'[a] (naphthalene at 120°C)	Efficiency (plates/m)
1	14 × 0.30	DHSU14C4–GY202	4.1	2141
2	17 × 0.30	DHSU14C4–GY202	3.8	2614
3	17 × 0.30	DHSU14C4	3.9	2185 (3002)[b]
4	18 × 0.30	DHSU14C4–GY202	4.3	2280 (3200)[b]
5	15 × 0.30	GY202	2.1	2950

[a] $k' = (t_r - t_0)/t_0$; t_0 was determined directly with methane.
[b] After use at 300°C for 1 month.

an untreated glass capillary. The mixing of a OH-terminal silicone oil (GY202) can help to spread the stationary phase on the glass surface. However, even at a ratio of DHSU14C4 to GY202 of 50:50, the column efficiency is not high ($N = 1000$), but at 30:70 the theoretical plate number increased to 2000–3000, which is better than that with similar urushiol crown ethers [10]. The chromatographic characteristics of these crown ether columns (DHSU14C4–GY202) are summarized in Table I.

The selectivity and polarity of DHSU14C4–GY202, GY202, SE-52 and FFAP, represented by McReynolds constants and b (the slope of the curve obtained when the logarithms of the adjusted retention times of n-alkanes are plotted against the number carbon atoms), are listed in Table II. The results indicate that DHSU14C4–GY202 has a medium polarity which is higher than that of GY202 and SE-52. However, the b value for the DHSU14C4–GY202 is higher than that of GY202, owing to long apolar alkyl groups of DHSU14C4.

Fig. 3a shows that the Grob test mixture is separated well on DHSU14C4–GY202, in contrast to GY202 (Fig. 3b). The relative retentions of the polar compounds 1,3-butanediol, 1-octanol, naphthalene, 2,6-dimethylphenol and 2,4-dimethylaniline on DHSU14C4–GY202 are about twice those on GY202 (see Table III). The results show that DHSU14C4–GY202 has a higher selectivity for polar compounds.

The glass transition temperature is shown in Fig. 4. A change in the slope is not apparent compared with the column directly coated with a similar crown ether [6]. This indicates that the thermodynamic properties of DHSU14C4–GY202 are very similar in the two states at the transition point of the glass transition temperature.

The thermal stability of the DHSU14C4–GY202

TABLE II

SELECTIVITY (McREYNOLDS CONSTANTS) AND POLARITY OF DHSU14C4–GY202

Test temperature, 120°C.

Stationary phase	Benzene	Butanol	1-Pentanone	Nitropropane	Pyridine	Mean	b
DHSU14C4–GY202 (30:70)	41	137	209	130	180	140	0.275
DHSU14C4–GY202 (50:50)	86	214	216	220	238	195	0.284
GY202	17	64	203	34	119	87	0.254
SE-52	32	72	65	98	67	67	0.249
FFAP	340	580	397	602	627	509	0.222

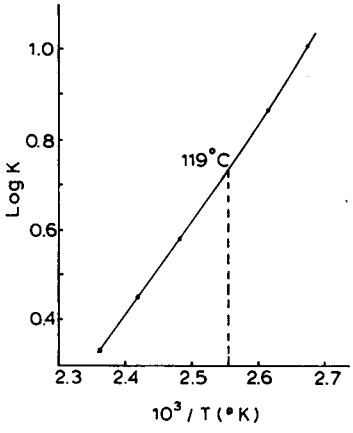

Fig. 4. Plots of log k' (capacity factor) against inverse of absolute temperature for naphthalene on DHSU14C4–GY202.

TABLE III

RELATIVE RETENTION VALUES OF SOME TEST COMPOUNDS

Compound	DHSU14C4–GY202	GY202
n-Decane	0.30	0.31
n-Undecane	0.53	0.55
n-Dodecane	1.00	1.00
Methyl undecanoate	4.88	3.49
Methyl dodecanoate	8.82	6.10
1,3-Butanediol	0.57	0.15
1-Octanol	0.84	0.46
Naphthalene	1.60	0.88
2,6-Dimethylphenol	1.28	0.55
2,4-Dimethylaniline	1.82	0.79

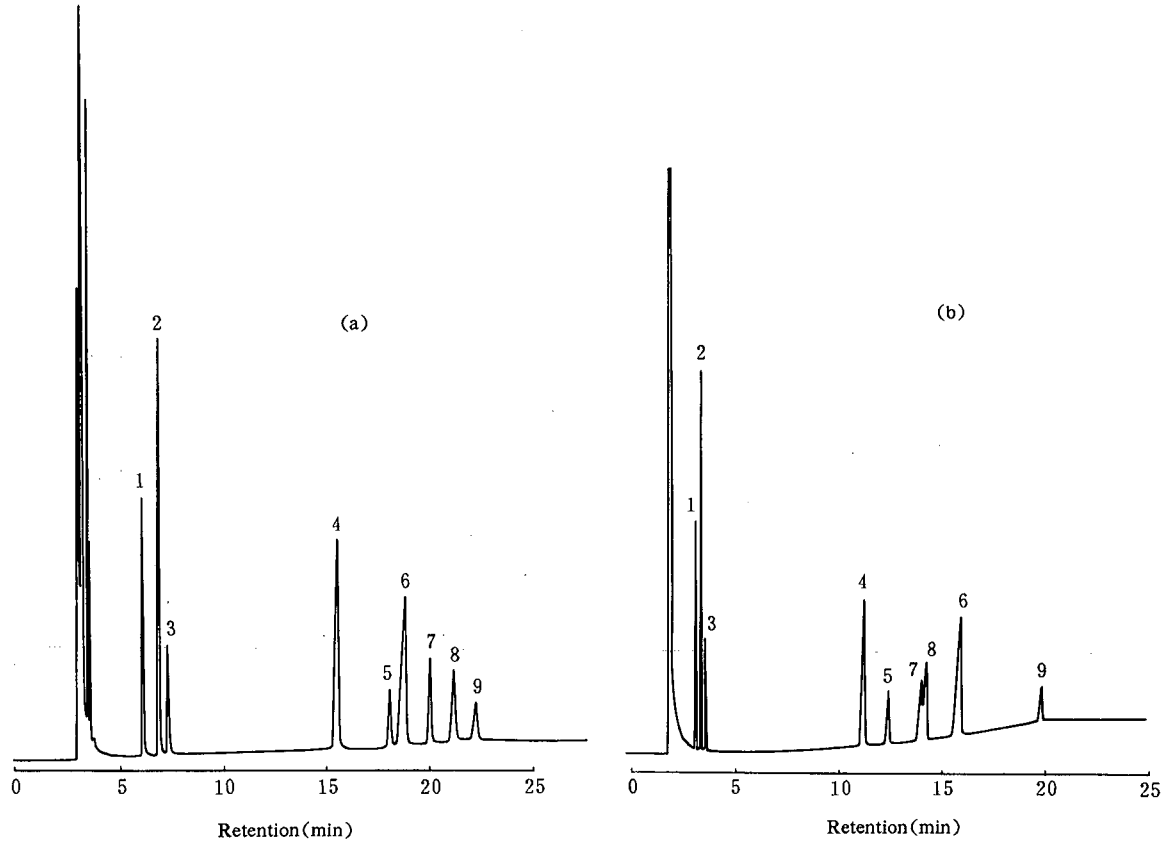

Fig. 5. Separation of a mixture of isomeric nitro compounds, (a) on DHSU14C4–GY202 column 4 and (b) on FFAP. Column temperature, programmed from 150 to 190°C at 2°C/min; flow-rate, 13 cm/s. Peaks: 1 = *o*-MNT; 2 = *m*-MNT; 3 = *p*-MNT; 4 = 2,6-DNT; 5 = 2,5-DNT; 6 = 2,3-DNT; 7 = 2,4-DNT; 8 = 3,5-DNT; 9 = 3,4-DNT (MNT = mononitrotoluene; DNT = dinitrotoluene).

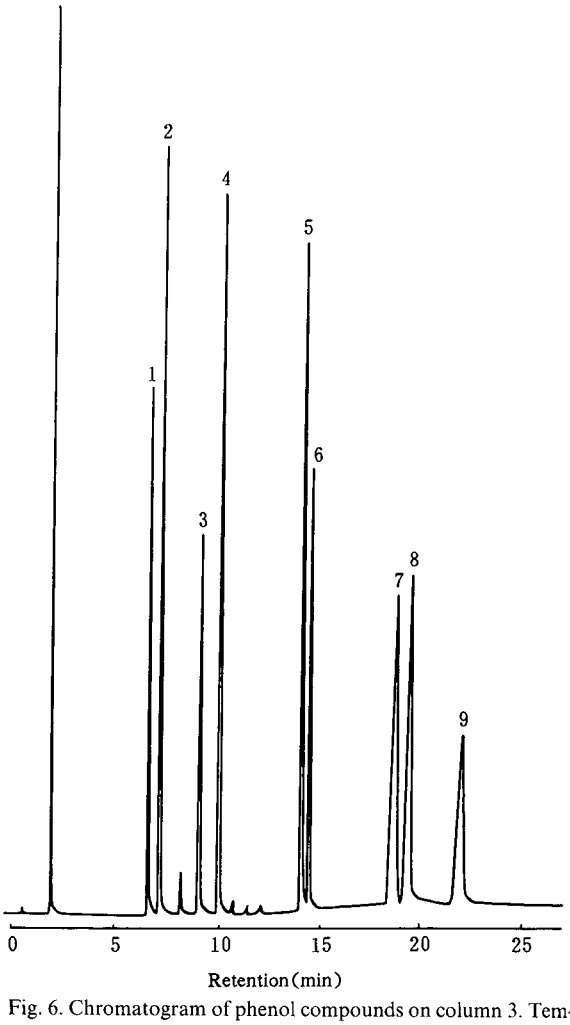

Fig. 6. Chromatogram of phenol compounds on column 3. Temperature, programmed from 90 to 210°C at 8°C/min. Peaks: 1 = *o*-chlorophenol; 2 = phenol; 3 = *o*-nitrophenol; 4 = 2,4-dimethylphenol; 5 = *p*-bromophenol; 6 = 2,4,6-trichlorophenol; 7 = 2,4-dinitrophenol; 8 = *m*-nitrophenol; 9 = *p*-nitrophenol.

column was determined by measuring the column bleed. The results show that the column begins to bleed at 210°C and the baseline drift is $1 \cdot 10^{-12}$ A at 300°C, that is, it has a high thermal stability. When the columns 3 and 4 were used at 300°C for 1 month, the capacity factor did not change and the column efficiencies tended to increase from 2100–2200 to 3000–3200 (Table I). This demonstrates that the crown ether phases have excellent thermal stability.

The DHSU14C4–GY202 column shows high selectivity, especially for nitrotoluene isomers. As shown in Fig. 5, although the polarity of DHSU14C4–GY202 is lower than that of FFAP, its separation properties are better. It is interesting that on the DHSU14C4–GY202 column, the elution of the solutes was not only dependent on the dipole–dipole reaction, but also on the steric hindrance. The sequence of dipole–dipole forces is 2,5-DNT < 2,4-DNT < 2,3-DNT < 2,6-DNT < 3,5-DNT < 3,4-DNT, but the retention times decrease in the order 2,6-DNT < 2,5-DNT < 2,3-DNT < 2,4-DNT < 3,5-DNT < 3,4-DNT (DNT = dinitrotoluene). This differential elution is possibly caused by the steric hindrance of the 2,6- and 2,3-DNT molecules.

The column coated with the crown ether stationary provided good resolution of phenol compounds (see Fig. 6). This selectivity depends on the availability of hydrogen bonding between the hydroxylic hydrogens and the crown ether ring oxigen atoms. For instance, in Fig. 6, *p*-nitrophenol was eluted much later than *o*-nitrophenol, because the *ortho*-substituted compound forms intramolecular hydrogen bonds between the nitro oxygen atom and the phenolic hydrogen atoms, which diminishes the hydrogen-bonding interaction to crown ether oxygens, so that it elutes earlier.

Application of DHSU14C4–GY202 phase to the analysis of monosaccharides in *Mycobacterium tuberculosis* is shown in Fig. 7.

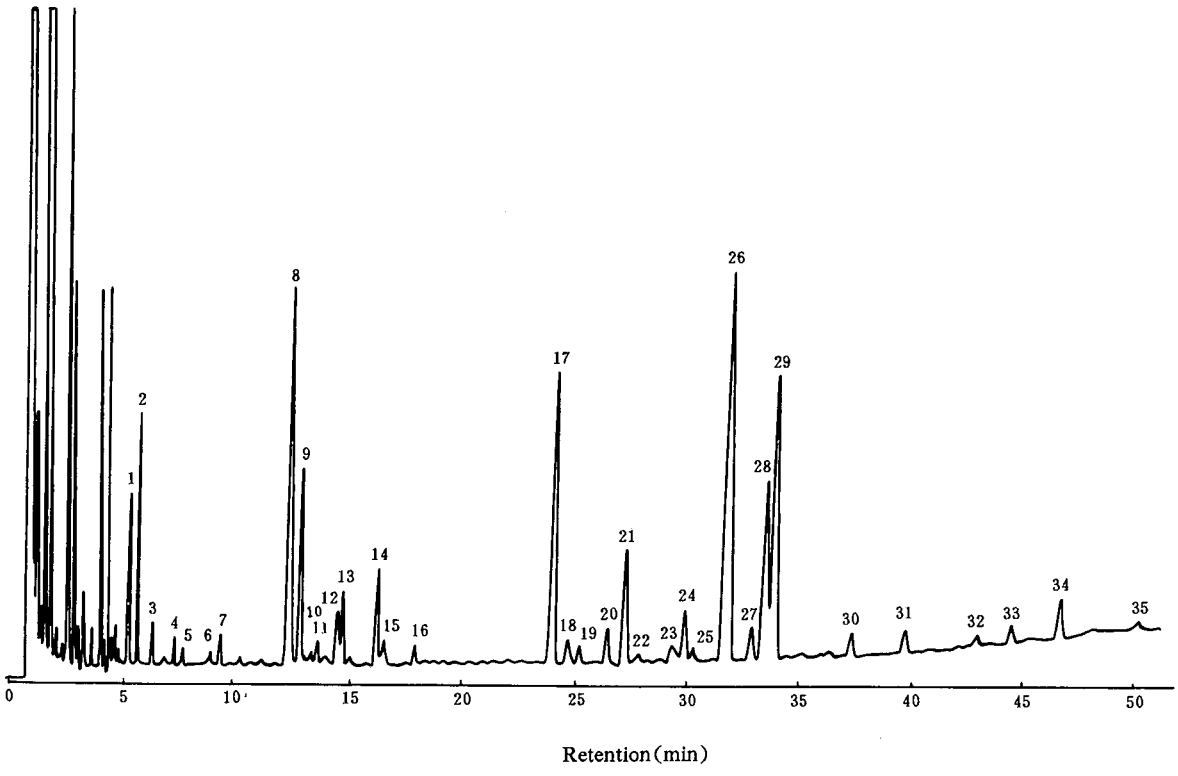

Fig. 7. Chromatogram of monosaccharides in *Mycobacterium tuberculosis* on column 2, separated as trimethylsilyl ether derivatives. Temperature, programmed from 150 to 220°C at 2°C/min. Peaks: 10,14 = ribose; 13 = rhamnose; 17 = mannose; 21 = fructose; 26 = galactose; 27,28,30 = glucose; 29 = mannitol (internal standard); 34 = myo-inositol.

REFERENCES

1 R.-S. Li, *Sepu*, 4 (1986) 304.
2 D. D. Fine, H. L. Gearhart and H. A. Mottola, *Talanta*, 32 (1985) 751.
3 C. A. Rouse, A. C. Finlinson, B. J. Tarbet, J. C. Pixton, N. M. Djordjevic, K. E. Markides, J. S. Bredshaw and M. L. Lee, *Anal. Chem.*, 60 (1988) 901.
4 C.-Y. Wu, H.-Y. Li, Y.-Y. Chen and X.-R. Lu, *J. Chromatogr.*, 504 (1990) 279.
5 C.-Y. Wu, C.-M. Wang, Z.-R. Zeng and X.-R. Lu, *Anal. Chem.*, 62 (1990) 968.
6 W. Blum, *J. High Resolut. Chromatogr. Chromatogr. Commun.*, 9 (1986) 350.
7 W. Blum, *J. High Resolut. Chromatogr. Chromatogr. Commun.*, 11 (1988) 140.
8 W. Blum, *J. High Resolut. Chromatogr. Chromatogr. Commun.*, 9 (1985) 718.
9 Y.-T. Wang, J.-J. Zhou, H.-J. Wan, Z.-S. Xie and Z.-F. Huang, *Chem. J. Chin. Univ.*, 11 (1990) 1292.
10 Y.-H. Jin, R.-N. Fu and Z.-F. Huang, *J. Chromatogr.*, 469 (1989) 153.

Journal of Chromatography, 589 (1992) 375–379
Elsevier Science Publishers B.V., Amsterdam

CHROM. 23 745

Short Communication

Direct gas chromatographic analysis of O,O-dimethyl- and O,O-diethyldithiophosphoric acids and identification of their by-products

Solomon E. Massil*, Itshak Ezra and Lambert Fuss

Department of Analytical Research, Research and Development Division, Makhteshim Chemical Works Ltd., P.O. Box 60, Beer-Sheva 84100 (Israel)

(First received April 29th, 1991; revised manuscript received September 16th, 1991)

ABSTRACT

Direct gas chromatographic methods for the quantitative analysis of O,O-dimethyl- and O,O-diethyldithiophosphoric acids using a 5% SE-30 column and flame ionization detection are described. The separation and identification of by-products were performed by spiking with known standards. The minimum detectable levels were 17.5 ppm for O,O-dimethyl- and 15.5 ppm for O,O-diethyldithiophosphoric acids.

INTRODUCTION

The commercial applications of O,O-dialkyldithiophosphoric acids as raw materials for producing pesticides, lubricant additives and plastic stabilizers are widely known. In spite of these applications, limited information is available regarding their analyses. Methods of analysis which have been applied include acidimetric titration [1–3], colour comparison after alkali decomposition [4,5] and infrared and NMR spectrometry [6,7]. Moreover, two publications have described gas chromatography (GC) after esterification by either diazoalkane [8,9] or trialkyl phosphites [10], since the acids could not be analysed owing to their decomposition at high temperatures.

As we are involved in the synthesis of O,O-dimethyldithiophosphoric acid (DMDTPA) by the reaction of methanol with phosphorus pentasulphide, efforts were directed to developing a GC method for the assay of DMDTPA after distillation. Since our objective was to develop a simple and fast GC method for analysing direct DMDTPA test samples, we carried out thermal stability studies on DMDTPA and O,O-diethyldithiophosphoric acid (DEDTPA) in normal air and in inert helium under fixed time and temperature conditions; these studies indicated they are safe and stable materials. The stationary liquid phase SE-30 was selectively found to be suitable for the separation and identification of by-products of DMDTPA and DEDTPA by spiking, after priming the column for optimization [11].

The GC determinations of DMDTPA and DEDTPA with flame ionization detection (FID) gave reproducible results. To our knowledge, this is the first report on the direct GC analysis of intact, underivatized O,O-dialkyldithiophosphoric acids. The method described here is rapid, sensitive and convenient for monitoring.

0021-9673/92/$05.00

EXPERIMENTAL

Materials

Analytical-grade dichloromethane and absolute ethanol were obtained from Frutarom, Israel. Standard and technical grades of DMDTPA, DEDTPA and by-products, such as O,O,O-trimethylphosphorothioate (TMPT), O,O,S-trimethylphosphorodithioate (TMPDT), O,O-diethylphosphoroite (DEPT) and O,O,S-triethylphosphorodithioate (TEPDT) were supplied by Makhteshim Chemical Works; O,O-dimethylphosphoroite (DMPT) was supplied by Cheminova, Lenwig Denmark. All stationary liquid phases and supports used in this investigation were obtained from Alltech Assoc. All other chemicals were of analytical grade.

Chromatographic conditions

A Varian Model 3700 gas chromatograph with a flame ionization detector equipped with a 4 ft. × 3 mm I.D. glass column packed with a 5% SE-30 on Gas Chrom Q (80–100 mesh) support was used. The column temperature was maintained at 75°C for DMDTPA and at 85°C for DEDTPA, the injector port at 120°C and the detector at 240°C. The carrier gas was helium at a flow-rate of 65 ml/min. A 5-μl sample was injected each time by means of a 10-μl Hamilton syringe. Chromatograms and peak areas were recorded on a Spectra-Physics Model 4290 integrator. For the titrimetric method, a Metrohm Model E-415 semiautomatic titrator and Model 691 pH meter were used.

Titrimetric method

Weigh accurately about 4–5 g of DMDTPA or DEDTPA sample into a 100-ml beaker containing a magnetic stirrer and add 10 ml of absolute ethanol. Titrate with 1 *M* sodium hydroxide solution to pH 3.5.

DMDTPA or DEDTPA (%) = [ml of 1 *M* sodium hydroxide × mol.wt. of DMDTPA (or DEDTPA)]/(weight of sample × 10)

Stability studies

About 10–12 g of technical-grade DMDTPA (or DEDTPA) were placed in a 100-ml, two-neck, round-bottom, quick-fit flask fitted with a condenser carrying a calcium chloride drying tube on the top. A helium gas bubbling tube was fixed to the second neck of the flask. After flushing the helium through the system for 5 min, the flask was immersed in a water bath preheated to 95°C and heating continued. At intervals of 10 and 30 min, the flask was removed and cooled in ice-water and the sample was removed for weighing. The concentration of this sample was determined by the titrimetric method described above. Similar experiments were carried out without bubbling the helium gas. The results obtained are shown in Table I.

Column priming for optimization

First set all the GC conditions as described above. Before starting the routine analysis, load the column by injecting large quantities (10–15 × 5 μl) of a concentrated solution (15%) of DMDTPA (or DEDTPA). Continue operating the system until the baseline reaches its normal position, which takes about 30–40 min.

Using this treatment, optimization is expressed in terms of the ability of the stationary phase to elute free acids with good peak symmetry.

TABLE I

TITRIMETRIC RESULTS OF STABILITY STUDIES ON DMDTPA AND DEDTPA IN AIR AND HELIUM

Average values obtained from duplicate analyses.

Dithiophosphoric acid	Original concentration (%)	Concentration at 95°C (%)		
		In normal air For 10 min	In inert helium	
			For 10 min	For 30 min
DMDTPA	97.33	96.91	97.10	97.06
DEDTPA	98.70	98.37	98.43	98.08

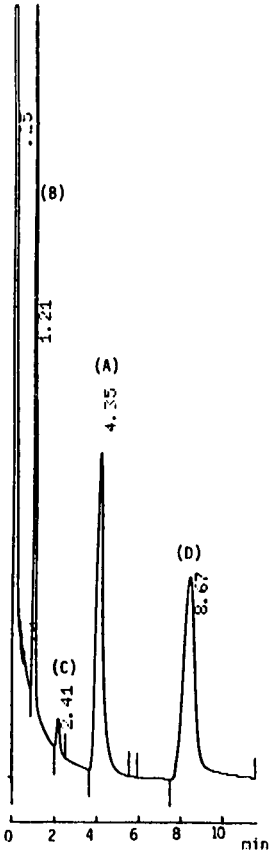

Fig. 1. Chromatogram for comparison with Fig. 2 after spiking with known standards of by-products such as: (A) DMDTPA, (B) O,O-dimethylphophorothioite (DMPT) [$(CH_3O)_2PSH$], (C) O,O,O-trimethylphosphorothioate (TMPT) [$(CH_3O)_3PS$] and (D) O,O,*S*-trimethylphosphorodithioate (TMPDT) [$(CH_3O)_2PS \cdot SCH_3$].

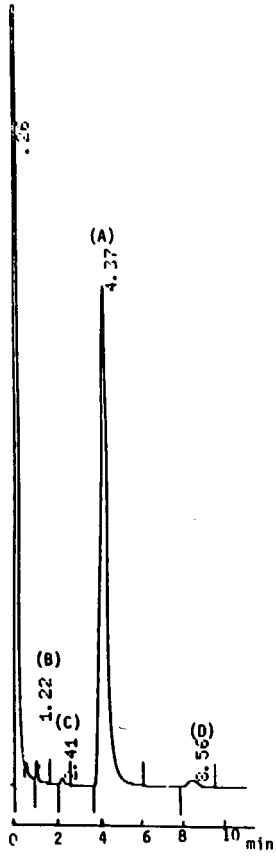

Fig. 2. Chromatogram showing the separation of O,O-dimethyldithiophosphoric acid (DMDTPA) [$(CH_3O)_2PS \cdot SH$], peak A, which contains small impurities of by-products B, C and D in standard material.

Calibration curves

Standard solutions for linearity six different concentrations in the range 50–450 mg for DMDTPA and 50–405 mg for DEDTPA were prepared, dispensed into 100-ml volumetric flasks and dissolved in dichloromethane.

Sample preparation for GC assaying

For regular analysis, duplicate weights of standard (*ca.* 250 mg) and sample (*ca.* 300 mg) were placed in 100-ml volumetric flasks and dissolved in dichloromethane. Injections of 5 μl each were made in the sequence standard then sample.

Identification of by-products by spiking

A 5-ml sample of a 0.1% solution in dichloromethane of each known by-product, such as TMPT, TMPDT and DMPT, was spiked with 25 ml of 0.3% DMDTPA in dichloromethane and injected to detect the elution of spiked peaks. Fig. 1 shows the general profile of the three by-products obtained, and their identity was confirmed by comparison with known samples in Fig. 2.

Similar attempts were made to indentify two by-products observed in DEDTPA, which appeared to be DEPT and TEPDT, as shown in Fig. 3.

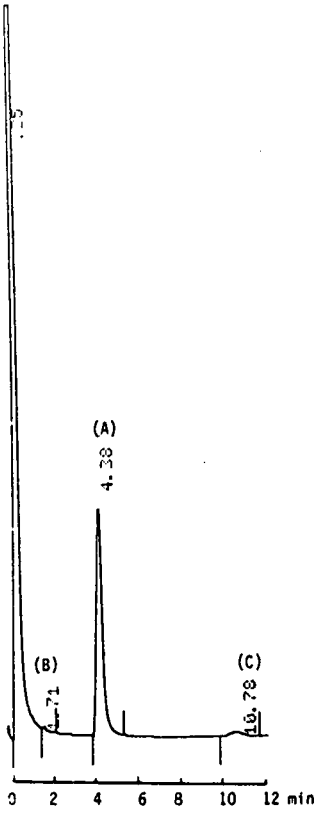

Fig. 3. Chromatogram showing the separation of standard (A) O,O-diethyldithiophosphoric acid (DEDTPA) [$(C_2H_5O)_2PS \cdot SH$] from the two small by-product impurities which were confirmed by spiking as (B) O,O-diethylphosphorothioite (DEPT) [$(C_2H_5O)_2PSH$] and (C) O,O,*S*-triethylphosphorodithoate (TEPDT) [$(C_2H_5O)_2PS \cdot SC_2H_5$].

RESULTS AND DISCUSSION

Information on stability studies by Cheminova [3] has revealed that DMDTPA decomposes by 50% and DEDTPA by 10% upon storing at 50°C for three weeks. For our purpose, it was imperative that the products could be distilled under vacuum as stable materials in order to analyse them by GC as stable materials if heated for a short time inert helium. Accordingly, the results of our stability studies also indicated that no significant changes in the concentrations of DMDTPA and DEDTPA were observed on heating at 95°C in air for 10 min and in helium for up to 30 min (Table I). These finding encouraged us to proceed to the direct GC analysis of DMDTPA and DEDTPA in inert helium under fixed time and temperature conditions for peak elutions.

TABLE II

COMPARISON BETWEEN RESULTS OBTAINED BY GC AND TITRIMETRIC METHODS

Average values obtained from duplicate analyses.

Sample No.	Concentration (%)	
	GC	Titration
DMDTPA		
1	92.81	94.53
2	91.84	94.71
3	93.27	95.02
4	97.42	96.93
5	96.02	96.48
6	96.24	96.86
DEDTPA		
1	98.43	98.51
2	98.13	98.43
3	97.87	98.27

Various stationary liquid phases for GC were examined for the separation of by-products contained in the technical DMDTPA and DEDTPA samples, for example DEGS, DC-550, OVs-17/101/210 and SE-30. Of these, the last column (5% SE-30 on Gas Chrom Q support) gave the most satisfactory separations with a good symmetry in all the peaks in less than 10–12 min, but only after the optimization of the stationary phase as described above. Using this procedure, multiple determinations of commercial DMDTPA and DEDTPA samples gave reproducible results; some of them are shown in Table II.

Since the GC method was found to be very efficient at separating the by-products from the main peaks of DMDTPA and DEDTPA, the assay results were compared with those of the titrimetric method (Table II). Most of results obtained by GC are slightly lower than those obtained by titrimetry, indicating that there was no interference from the by-products present, whereas the titrimetric results are the combined values of free acids such as DMDTPA and DMPT (or DEDTPA and DEPT) and the hydrolysis products of any included esters. The correlation coefficients for DMDTPA and DEDTPA were 0.9984 and 0.9972, respectively, and the relative standard deviations were ± 0.7% (n =

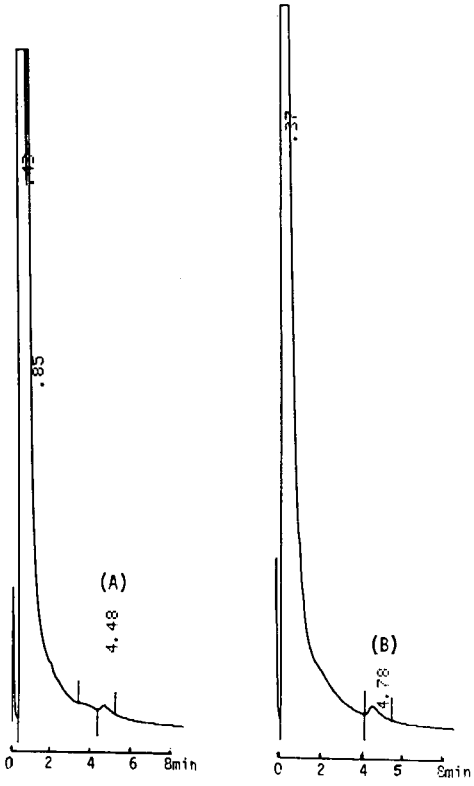

Fig. 4. Chromatogram showing the minimum detectable limit of DMDTPA (A) at 17.5 ppm ($8.5 \cdot 10^{-6}$ mg) and DEDTPA (B) at 15.5 ppm ($7.5 \cdot 10^{-6}$ mg) levels.

8) and ± 0.9% ($n = 9$), respectively, indicating that the GC method is precise and reproducible.

Tentative identification of the by-products of DMDTPA was accomplished by spiking the samples with known compounds and comparing the peaks obtained with those of the original impurities, as shown in Figs. 1 and 2. Similarly, two by-products in DEDTPA were also tentatively identified, as described in Fig. 3.

Determinations of DMDTPA and DEDTPA at the ppm level were achieved using FID at a sensitivity of 10^{-11}. At this sensitivity, it was possible to detect (signal-to-noise ratio > 3) 17.5 ppm ($8.5 \cdot 10^{-6}$ mg) DMDTPA and 15.5 ppm ($7.5 \cdot 10^{-6}$ mg) DEDTPA, as shown in Fig. 4, and to quantitatively analyse samples containing ppm amounts by comparing peak height measurements with standards.

In conclusion, the present GC method is reproducible and rapid, and the availability of the direct GC technique in analytical laboratories represents a valuable alternative to titrimetric and esterification procedures.

REFERENCES

1 M. I. Kabachuik and T. A. Mastryukova, *Otdel. Khim. Nauk.*, (1952) 727; *C.A.*, 47 (1953) 9909a.
2 P. F. Hu and W. Y. Chen, *Hua Hsueh Hsueh Pao*, 22 (1956) 215; *C.A.*, 52 (1958) 7186c.
3 *Commercial Data Sheets on MP-1 and EP-1*, Cheminova, Lemvig, 1980.
4 S. D. Upham, *J. Assoc. Off. Agric. Chem.*, 43 (1960) 360.
5 M. T. H. Regab, *J. Assoc. Off. Agric. Chem.*, 50 (1967) 1088.
6 N. Oi and H. Tadeka, *Bunseki Kagaku*, 16 (1967) 257, *C.A.*, 54 (1967) 96659d.
7 A. E. Lippman, *J. Org. Chem.*, 31 (1966) 471.
8 L. Nebbia and V. Belloti, *Chim. Ind.*, 52 (1970) 369, *C.A.*, 73 (1970) 72854m.
9 Z. Frobe, B. Stengl, V. Drevenkar and A. Deljac, *J. Chromatogr. Sci.*, 28 (1990) 269.
10 K. Imamura and T. Arai, *Bunseki Kagaku*, 19 (1970) 653, *C.A.*, 73 (1970) 72855n.
11 D. M. Ottenstein and W. R. Supina, *J. Chromatogr.*, 91 (1971) 119, and references cited therein.

Journal of Chromatography, 589 (1992) 380–384
Elsevier Science Publishers B.V., Amsterdam

CHROM. 23 797

Short Communication

Monitoring 4-methoxy-2,3,6-trimethylbenzenesulphonyl deprotection of arginine-containing synthetic peptides using capillary zone electrophoresis

Francis Mulholland* and Gordon R. Hague☆

Department of Biotechnology and Enzymology, AFRC Institute of Food Research, Reading Laboratory, Shinfield, Reading RG2 9AT (UK)

(First received July 16th, 1991; revised manuscript received October 11th, 1991)

ABSTRACT

A rapid method has been devised to monitor the deprotection of 4-methoxy-2,3,6-trimethylbenzenesulphonyl (Mtr) groups from an arginine-containing synthetic peptide using capillary zone electrophoresis. Unlike the usual reversed-phase high-performance liquid chromatographic method, ether extractions to remove interfering reagents prior to analysis are not required. For the peptide, Ser–Pro–Arg–Gly, capillary zone electrophoretic conditions of 30 kV at 45°C for 8 min in 20 m*M* sodium citrate buffer, pH 2.5, on a 72-cm capillary gave clear separation of the Mtr-protected (mobility 7.2 min) and the deprotected peptide (mobility 3.5 min). During deprotection of an octapeptide containing two arginines, two transient species occurred corresponding to the two possible partially Mtr-deprotected peptides that could form. These ran predictably at intermediate mobilities of 4.8 and 5.0 min compared to the final free peptide (mobility 3.3 min) and the fully protected species (mobility 8.7 min).

INTRODUCTION

Arginine-containing peptides, synthesized using N^{α}-Fluoroenylmethoxycarbonyl (Fmoc) amino acids, commonly use 4-methoxy-2,3,6-trimethylbenzenesulphonyl (Mtr) as the protecting group on the guanidino side chain of arginine. Following synthesis, the cleavage of this protecting group with trifluoroacetic acid (TFA)–phenol is significantly slower than the peptide-resin cleavage and the other side chain deprotection reactions, normally based on butyl groups [1]. To ensure complete deprotection it is necessary to monitor the cleavage of this group from the peptide. This has previously been accomplished by a reversed-phase high-performance liquid chromatographic (HPLC) method which involves preparation of the sample, extracting several times with ether to remove the phenol from the reaction mixture prior to analysis [2].

Capillary zone electrophoresis (CZE) is an ideal method for analyzing small polar molecules such as peptides and is commonly used to assess the purity of synthesized peptides [3]. This paper describes a method for the rapid monitoring, by CZE, of the deprotection of arginine-containing peptides that involves no significant sample preparation.

MATERIALS AND METHODS

Synthesis of peptides

Ser–Leu–Leu–Leu–Ser–Pro–Arg–Gly, Ser–Arg–

☆ Present address: Biochemistry Department, University of Bath, Claverton Down, Bath BA2 7YA, UK.

0021-9673/92/$05.00

Leu–Leu–Ser–Pro–Arg–Gly, Leu–Leu–Ser–Pro–Arg–Gly and Ser–Pro–Arg–Gly were synthesized on a Pepsynth II semi automatic continuous-flow peptide sunthesizer (CRB, Cambridge, UK) using Pepsyn KA resin with Fmoc-glycine attached (0.5 g resin/column; 0.1 mmol/g substitution; Milligen/Biosearch, Watford, UK) in peptide synthesis-grade dimethylformamide (DMF) (Applied Biosystems, Warrington, UK). Following deprotection with piperidine (20%, v/v, in DMF) the subsequent amino acids were added using the Fmoc-amino acid-pentafluorophenyl esters of Arg(Mtr), Pro and Leu, and the 3,4-dihydro-4-oxobenzotriazin-3-yl ester of Ser(But) (Milligen/Biosearch) in a 4 molar excess and in the presence of hydroxybenzotriazole (0.88 mmol). Prior to each deprotection the resin was analyzed using the test by Kaiser *et al.* [4] to determine the presence of free amino groups. Following deprotection of the final amino acids, the peptide-resins were removed from the columns, filtered on a sintered glass filter and washed with DMF, *tert.*-amyl alcohol, glacial acetic acid, *tert.*-amyl alcohol and diethyl ether before drying overnight in a vacuum desiccator.

Cleavage of peptide-resins; analysis of Mtr deprotection

The dried peptide resins were each mixed with 12.5 ml TFA–phenol (95:5, v/w) and periodically stirred. At intervals of 10 min, 30 min and every hour thereafter, 25-μl aliquots were removed. The TFA was blown off under a gentle nitrogen stream before adding 250 μl 20 m*M* sodium citrate buffer, pH 2.5. This was then analyzed using a Model 270A capillary electrophoresis apparatus (Applied Biosystems) on a 72-cm capillary equilibrated with 20 m*M* sodium citrate buffer, pH 2.5. Electrophoresis conditions in this buffer were 30 kV at 45°C, on a 3-s sample injection by vacuum, monitoring the electrophoretic mobility by absorbance at 200 nm. Initially 30-min runs were performed to ensure complete analysis of the reaction mixture and show the elution of the neutral species. Subsequent run times were 10 min. The CZE data were collected and analyzed using a Roseate chromatography data analysis package (Drew Scientific, London, UK) with a 100 mV input and collecting data at 2 Hz.

RESULTS

For the Ser–Pro–Arg–Gly peptide, the CZE traces (Fig. 1) show three peaks (electrophoretic mobilities; 3.6, 6.9 and 7.2 min), which change in time during the concurrent peptide-resin cleavage and side chain deprotection reactions. These peaks correspond to the three possible products that could be formed for this peptide. Although no standards were used to confirm the electrophoretic mobility of the different species, the CZE traces obtained fit both the expected reaction products over time and the expected electrophoretic mobilities of these products. The guanidino group of the arginine has a high pK_a (12.5) and will be strongly protonated in pH 2.5 buffer used in the electrophoresis. The Mtr-protected guanidino group, however, cannot protonate and makes no contribution to the overall charge of the peptide. The free peptide, Ser–Pro–Arg–Gly (P1), having two protonated groups at pH 2.5 and a lower mass, will clearly separate using CZE from the larger protected species which ony have the N-terminal α-amino group protonated. Under these conditions P1 had, and would be expected to have, the greatest electrophoretic mobility; running at 3.6 min. Thus at 14 h (Fig. 1e), only one peak at 3.6 min was observed which corresponded to the fully deprotected peptide. Further work-up on the peptide was then able to proceed.

For this tetrapeptide the two protected peptide species that can be formed during the peptide-resin cleavage/deprotection reaction are the Mtr-arginine-only protected peptide, Ser–Pro–Arg(Mtr)–Gly (P2) and the double side chain protected peptide, Ser(But)–Pro–Arg(Mtr)–Gly (P3). It is extremely unlikely that the butyl-serine-only protected species, Ser(But)–Pro–Arg–Gly, would be formed in significant quantities as the Mtr deprotection proceeds substantially more slowly than the butyl deprotection [1]. The two possible protected species are seen in the 10 min and 30 min electropherograms, running at 6.9 and 7.2 min, respectively (Fig. 1a and b). P3, having a slightly greater mass for the same charge would be expected to have a slightly slower electrophoretic mobility than P2. The disappearance within 2 h of the slowest running species at 7.2 min confirmed this to be due to P3, the faster butyl deprotection allowing conversion to P2 with increased electrophoretic mobility at 6.9 min. The

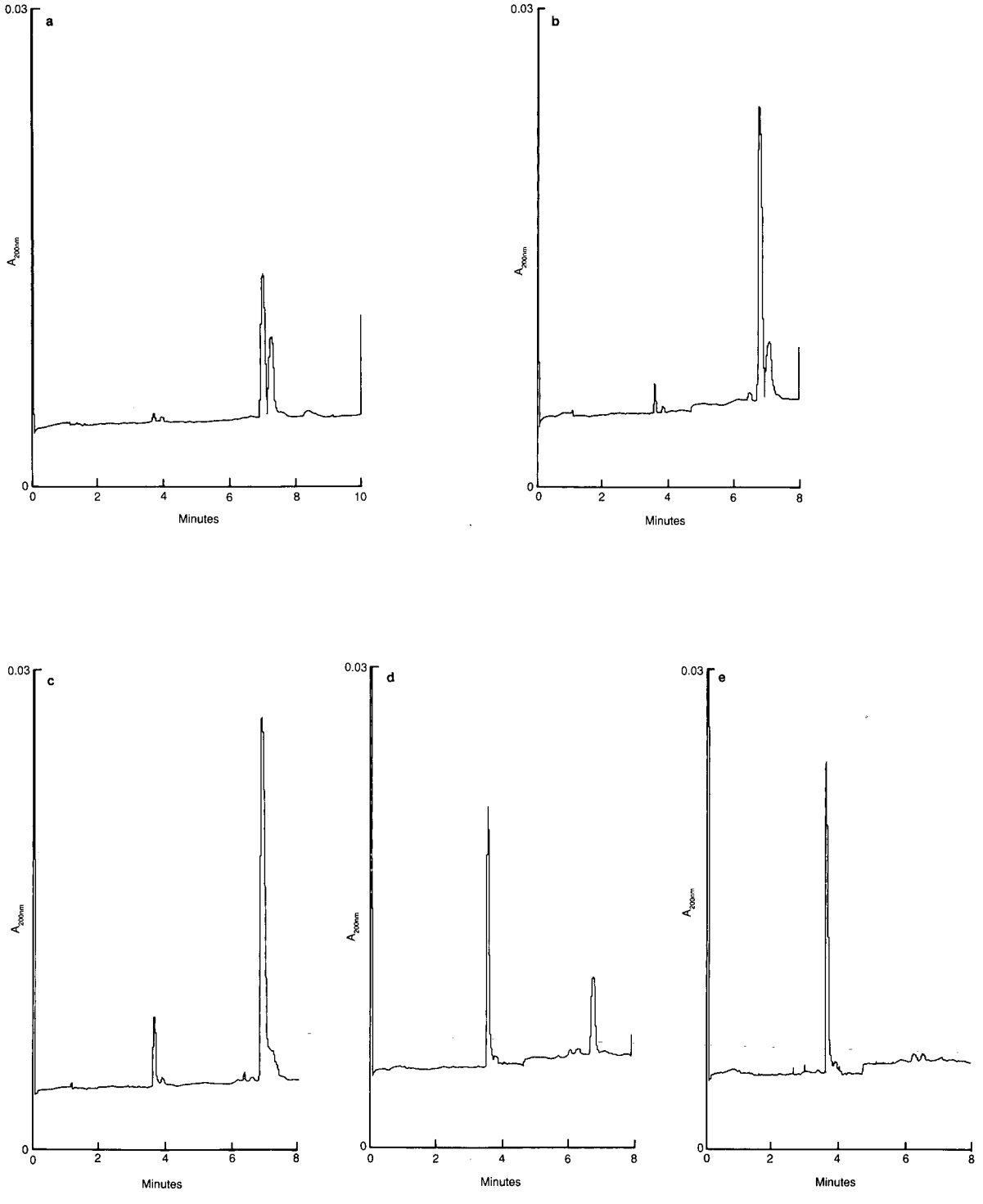

Fig. 1. Capillary zone electropherogram of the Mtr deprotection of Ser–Pro–Arg–Gly reaction over time: (a) 10 min reaction, (b) 0.5 h reaction, (c) 1.0 h reaction, (d) 5.5 h reaction and (e) 14.0 h reaction.

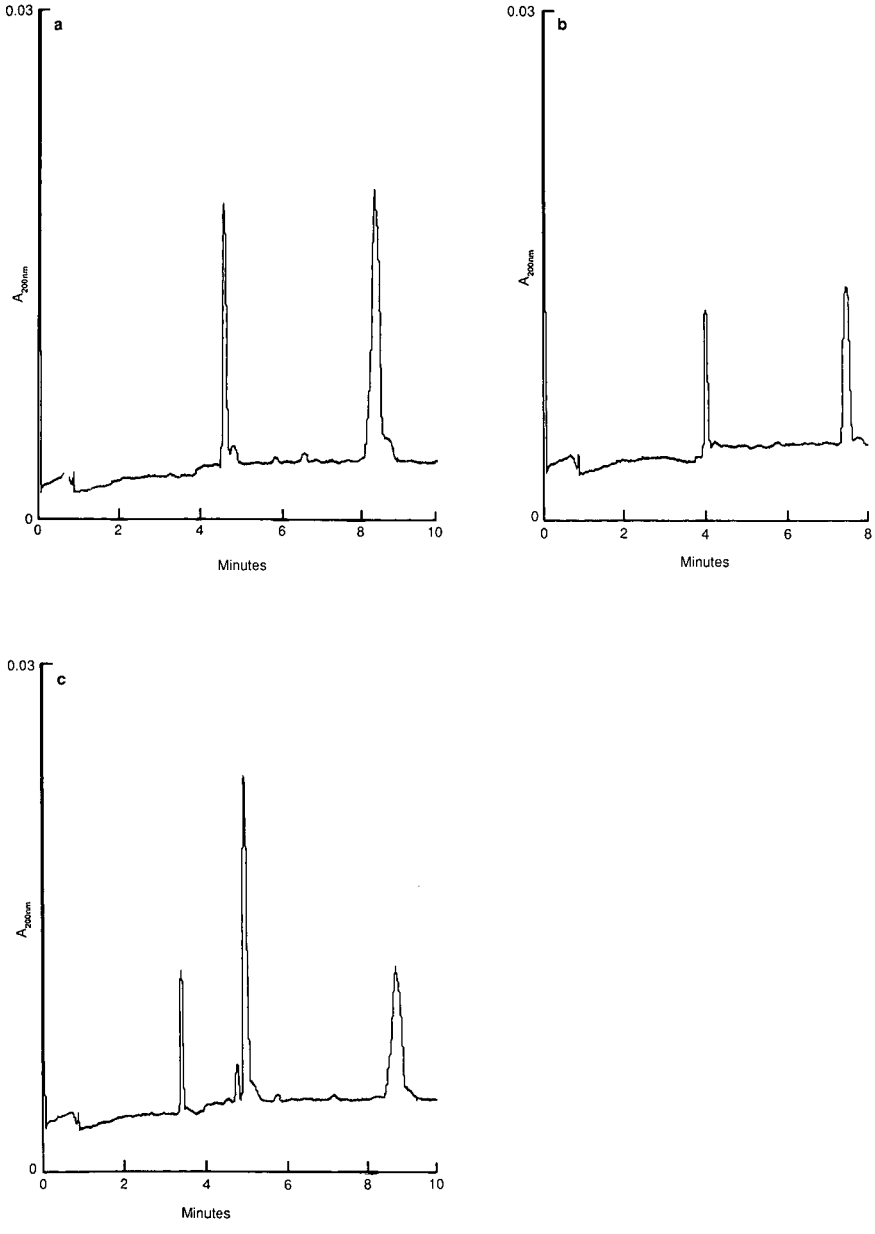

Fig. 2. Capillary zone electropherogram of the Mtr deprotection reaction for synthesized peptides at 2 h: (a) Ser–Leu–Leu–Leu–Ser–Arg–Pro–Gly, (b) Leu–Leu–Ser–Arg–Pro–Gly, (c) Ser–Arg–Leu–Leu–Ser–Arg–Pro–Gly.

later electropherograms (Fig. 1c–e) show the slower Mtr deprotection proceeding, requiring 14 h before complete deprotection of the peptide was achieved. With the larger peptides synthesized, separation of the equivalent PII and PIII species was not observed.

For the other larger peptides, Fig. 2a–c shows the electropherograms for the deprotection reaction at 2 h. The di-arginine-containing octapeptide, Ser–Arg–Leu–Leu–Ser–Pro–Arg–Gly, with three positive charges migrated faster at 3.41 min (see Fig. 2c)

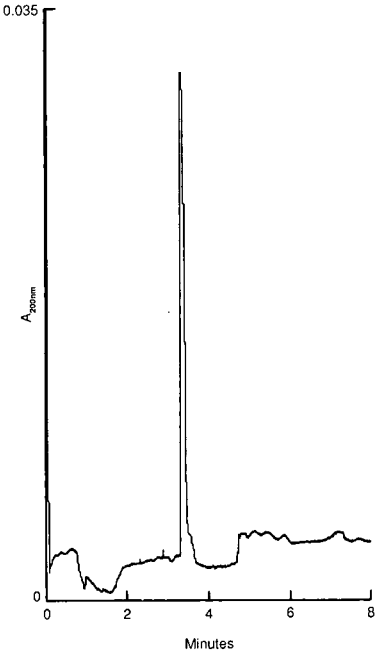

Fig. 3. Capillary zone electropherogram of the Mtr deprotection reaction for Ser–Arg–Leu–Leu–Ser–Arg–Pro–Gly at 22 h.

compared with the octapeptide, Ser–Leu–Leu–Leu–Ser–Pro–Arg–Gly, with only two positive charges and running at 4.56 min (see Fig. 2b). Where only one arginine was present the electropherograms (Figs. 1e, 2a and b) showed that the deprotected peptides ran according to size, the smaller peptide running fastest. Fig. 2c also shows that during the deprotection the di-arginine-containing peptide formed two other species which ran at an intermediate time between the free peptide and the Mtr-blocked peptide. These correspond to the partially Mtr-deprotected peptides, Ser–Arg(Mtr)–Leu–Leu–Ser–Pro–Arg–Gly and Ser–Arg–Leu–Leu–Ser–Pro–Arg(Mtr)–Gly, the intermediates formed prior to the complete deprotection which took place overnight, Fig. 3 showing the formation of the final free peptide.

DISCUSSION

The main advantage of this CZE procedure is the ease of sample preparation, just blowing off TFA with nitrogen and dissolution in electrophoresis buffer, with none of the ether extractions of the reaction mixture that are required by the HPLC procedure [2]. Using CZE the potentially interfering phenol and Mtr groups, with no charge at pH 2.5, run predictably at the neutrality point, clearly separated from the charged peptide species, passing the detector by electroendosmosis at 22 min under the conditions described (data not shown).

This procedure should be able to monitor clearly the deprotection of any arginine-containing synthetic peptide, with the free peptide theoretically being the species with the greatest electrophoretic mobility, provided no other factors such as capillary interactions interfere during electrophoresis.

REFERENCES

1 E. Atherton, R. C. Sheppard and J. D. Wade, *J. Chem. Soc. Commun.*, (1983) 1060.
2 A. X. Eberle, E. Atherton, A. Dryland and R. C. Sheppard, *J. Chem. Soc., Perkin Trans. I*, (1986) 361.
3 P. D. Grossman, J. C. Colburn, H. H. Lauer, R. G. Nielsen, R. M. Riggin, G. S. Sittampalam and E. C. Rickard, *Anal. Chem.*, 61 (1989) 1186.
4 E. Kaiser, R. L. Colescott, C. D. Bossinger and P. I. Cook *Anal. Biochem.*, 34 (1970) 595.

Journal of Chromatography, 589 (1992) 385–389
Elsevier Science Publishers B.V., Amsterdam

CHROM. 23 778

Short Communication

Protection of terpenes against oxidative and acid decomposition on adsorbent cartridges

Ann-Margret Strömvall and Göran Petersson*

Department of Chemical Environmental Science, Chalmers University of Technology, 412 96 Göteborg (Sweden)

(First received July 19th, 1991; revised manuscript received September 30th, 1991)

ABSTRACT

Sampling of monoterpenes from air on Tenax porous polymer may introduce analytical errors owing to oxidation and acid rearrangements on the adsorbent. Particularly terpenes which react rapidly with ozone, *e.g.* myrcene and limonene, are partially lost when sampling air with high photooxidant levels. On acidified adsorption cartridges, α-pinene and β-pinene may be converted into camphene, limonene, *p*-cymene and several minor monoterpenes. Pretreatment of the adsorbent cartridges with thiosulphate as an antioxidant and hydrogencarbonate as a buffer were found to prevent decomposition and rearrangements. Applications to monoterpenes emitted from the kraft, thermo-mechanical and sulphite pulp industries are presented.

INTRODUCTION

Sampling of organic air pollutants on adsorbent cartridges is a widely applied technique because of its simplicity and versatility. It suffers, however, from the inherent disadvantage that adsorbed compounds may react with each other and with active species from the air passing through the cartridge [1]. The very front of the adsorbent column is particularly susceptible to reactions because of elevated levels of all compounds adsorbed. Reactive agents in air may also affect the adsorbent, and thiosulphate treatment was introduced to protect Tenax cartridges [1,2].

Among the hydrocarbons, the terpenes are exceptionally reactive towards air pollutants such as photooxidants [3]. The atmospheric chemistry and the environmental impact of terpenes are subjects of great current interest. A favoured technique for sampling of terpenes in air is adsorption on Tenax porous polymer. Our contributions include studies of monoterpenes from pine forests [4], logging operations [5] and pulp industries [6]. This study is based on analytical results for terpenes emitted into the air from the alkaline sulphate or kraft pulping process, from the acid sulphite pulping process and from thermo-mechanical pulp (TMP) production. Reliable results were found to depend on the techniques reported here for avoiding decomposition and rearrangements in the adsorption cartridges.

EXPERIMENTAL

Basic analytical system

The adsorption cartridges were 80 × 2.2 mm I.D. glass liners filled with 0.1–0.2 ml of Tenax adsorbent (60–80 mesh). Field samples were taken by connecting the cartridges to conventional portable air-sampling pumps [2]. The air volumes were typically in the range 0.2–2 l.

In the laboratory, thermal desorption was effected in the injector of a conventional gas chromato-

0021-9673/92/$05.00

graph [2]. The oven temperature was kept below 0°C during desorption and raised at 2°C/min during analysis. The analytical column was a 25 m × 0.33 mm I.D. fused-silica capillary with the cross-linked methylsilicone BP-1 as the stationary phase. Detection was by flame ionization and the same response factor was used for all monoterpenes [5,6].

Treatments of adsorbent cartridges

The Tenax adsorbent was kept in place by two glass pellets made from fritted glass filters, with a minimum amount of silanized glass-wool providing the required friction between the pellets and the wall of the glass liner.

A 5% aqueous solution of $Na_2S_2O_3$ was used for antioxidant treatment. A droplet (10–20 μl) was introduced on to the front of the adsorbent layer using a micropipette. The water was evaporated cautiously at an elevated temperature and the cartridge was preconditioned in the gas chromatographic injector at 250°C with helium [2] before sampling. Pretreatment with $NaHCO_3$ as a buffer against acids was made in an analogous manner with a 5% aqueous solution.

RESULTS AND DISCUSSION

Oxidative decomposition

In Table I, results are given for air samples taken at ground level several hundred metres downwind of two pulp mills. The kraft mill was Gruvöns Bruk, northwest of lake Vänern, with terpene emissions mainly from processed Scots pine. The thermomechanical pulp (TMP) mill was Bravikens Pappersbruk, in Norrköping on the east coast, with terpene emissions almost exclusively from processed Norway spruce. The samples taken on Tenax cartridges pretreated with thiosulphate correctly reflect the monoterpene composition, as confirmed by comparisons with many other samples. The different compositions of monoterpenes from the two mills reflect the characteristic differences between Norway spruce, with large proportions of α- and β-pinene, and Scots pine, with large proportions of α-pinene and 3-carene [5].

For duplicate samples, taken with untreated cartridges, the percentage oxidative losses given in Table I were determined. It is seen that β-pinene and the terpene-related alkylbenzene *p*-cymene are not affected, whereas the acyclic triene myrcene is lost completely. The other major monoterpenes were lost to various extents from the fairly stable α-pinene to the reactive limonene. The same order of reactivity was observed on other occasions for several different untreated duplicate cartridges, although the degree of losses varied. The greatest losses were observed during daytime in the summer, in periods of fine weather favouring high levels of photooxidants.

Ozone is a major photooxidant which may cause

TABLE I

OXIDATIVE DECOMPOSITION OF MONOTERPENES ON TENAX ADSORPTION CARTRIDGES AND REACTION RATE WITH OZONE IN AIR

Parallel air samples taken *ca.* 500 m downwind from pulp mills, on thiosulphate-treated cartridges (correct results) and on untreated cartridges (results reflecting oxidative losses).

Compound	Kraft mill, Scots pine, 17/8/90, 10.15–12.15		TMP mill, Norway spruce, 21/8/90, 11.15–13.00		Reaction rate with ozone in air [3], $k \times 10^{17}$ (cm^3 $molecule^{-1}$ s^{-1})
	$Na_2S_2O_3$-treated (μg/m^3)	Untreated (% loss)	$Na_2S_2O_3$-treated (μg/m^3)	Untreated (% loss)	
p-Cymene	0.75	0	0.28	0	<0.005
β-Pinene	6.4	0	10.6	0	1.5
α-Pinene	33.9	6	23.8	6	9.7
3-Carene	13.9	34	2.3	33	5.2
β-Phellandrene	0.80	55	1.2	63	17
Limonene	1.70	76	1.7	80	21
Myrcene	0.33	100	0.22	100	49

losses owing to the high reactivity of ozone with branched alkenes such as terpenes. From Table I, it is evident that the gas-phase reactivity of terpenes with ozone correlates fairly well with the sampling losses of different terpenes. Accordingly, sampling of monoterpenes with and without an ozone scrubber [7] results in differences similar to those observed with and without thiosulphate treatment. It should be remembered, however, that terpenes also react rapidly with other photooxidants, and that decomposition in the front of the adsorption cartridges is not a gas-phase reaction.

Freshly thiosulphate-treated cartridges normally permitted a satisfactory recovery of myrcene, thus

TABLE II

ACID REARRANGEMENTS OF MONOTERPENES ON TENAX ADSORPTION CARTRIDGES

Composition (%) of monoterpenes emitted from processed wood of Norway spruce, for parallel air samples taken on neutral cartridges (correct results) and on acid-treated cartridges (results reflecting acid rearrangements).

Compound	Structure	TMP process		Pulpwood chipping	
		Correct	Acidic	Correct	Acidic
α-Pinene	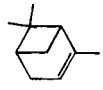	58	55	58	46
β-Pinene	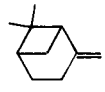	26	14	23	12
Camphene		1.7	6.1	1.8	9.0
3-Carene	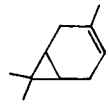	3.5	3.3	4.9	4.2
β-Phellandrene	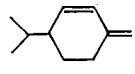	3.0	2.9	3.1	2.3
Limonene	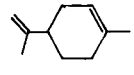	5.1	9.9	6.2	9.3
Terpinolene	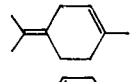	0.25	1.3	0.40	2.2
γ-Terpinene	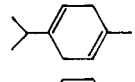	0.10	0.6	0.11	1.1
α-Phellandrene	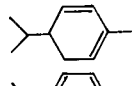	0.05	0.5	0.07	0.5
α-Terpinene	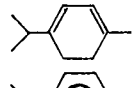	0.04	0.6	0.06	1.1
p-Cymene	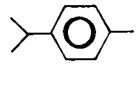	0.8	3.3	0.9	8.6

ensuring that no oxidative losses of the less reactive monoterpenes were obtained. The minor monoterpenes terpinolene, α-terpinene and α-phellandrene are even more reactive than myrcene with ozone [3], but they are often absent from ambient air owing to their high gas-phase reactivity. Near conifers and man-made monoterpene emissions, they act as oxidant scavengers and may be sampled without oxidative losses [5].

Oxidative reactions during sampling also affect the Tenax adsorbent and cause the formation of artifacts such as benzaldehyde and acetophenone [2]. The thiosulphate treatment prevents this decomposition and therefore often provides additionally improved analytical quality.

Acid rearrangements

Man-made terpene emissions from the forest industry and other sources are often accompanied by emissions of sulphur dioxide, nitrogen oxides and organic acids. In these instances, acidification of the adsorbent front during sampling is an obvious consequence. However, even the acidity of ambient air in general might have a limited impact. The character of the acidic terpene reactions on the adsorbent cartridges was found to be well elucidated by parallel sampling on untreated and artificially acidified cartridges.

In Table II, the percentage monoterpene composition is given for emission samples from the processing of spruce pulpwood. The first sample corresponds to TMP refiner steam emissions passed through fresh chips before venting to air at the Braviken mill. The sample from industrial pulpwood chipping was taken at the Billerud sulphite pulp mill west of lake Vänern. It is seen that the percentage compositions are very similar. In Fig. 1, the chromatographic separation is illustrated. The total monoterpene concentrations were as high as 7 mg/m^3 for the TMP sample and 60 mg/m^3 for the chipping sample, resulting in a depletion of oxidants from the air. As a consequence, even the most easily oxidized hydrocarbon monoterpenes could be determined without oxidative losses. With the attenuation chosen for Fig. 1, the minor species α-phellandrene and α-terpinene are just visible in front of 3-carene and *p*-cymene, respectively.

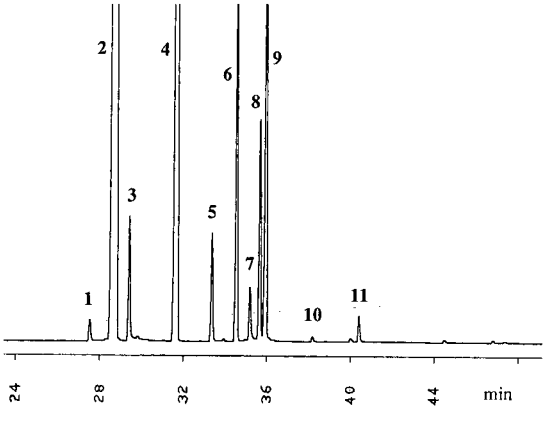

Fig. 1. Gas chromatographic separation of monoterpenes emitted into the air during industrial chipping of pulpwood from Norway spruce. Peaks: 1 = tricyclene; 2 = α-pinene; 3 = camphene; 4 = β-pinene; 5 = myrcene; 6 = 3-carene; 7 = *p*-cymene; 8 = β-phellandrene; 9 = limonene; 10 = γ-terpinene; 11 = terpinolene.

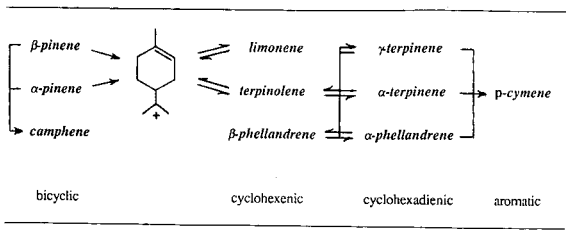

Fig. 2. Scheme of sequential acid-catalysed rearrangements of monoterpenes.

The duplicate samples in Table II were taken on cartridges acidified with trace amounts of sulphuric acid. No significant decrease in the total amount of monoterpenes was observed, but the composition was very different, indicating acid rearrangements in the acidified cartridges. The proportions of α-pinene and particularly β-pinene were greatly lowered and those of β-phellandrene and 3-carene were slightly lowered. The percentages of camphene, limonene, terpinolene and the alkylbenzene *p*-cymene were increased. The minor cyclohexadienic components γ-terpinene, α-terpinene and α-phellandrene increased considerably compared with their true proportions in the emissions. Other samples taken on acidified cartridges were found to give qualitatively the same errors, although the magnitude and proportions of the deviations varied.

The basic acidic rearrangement reactions of monoterpenes, as outlined in Fig. 2, are compatible with the deviations observed for acidified cartridges.

The acid rearrangements of α- and β-pinene to camphene, and via the depicted carbonium ion to isomerizing monocyclic terpenes, are known from terpene chemistry [8,9]. The formation of *p*-cymene in high yield from monoterpenes is also known from the acid sulphite pulping process [10]. The deviations for limonene and other terpenes which appear as reaction intermediates were found to be irregular in magnitude for different acidic samples. Weakly acidified samples tended to give rearrangements without any significant dehydrogenation to *p*-cymene. The risk of overlooking more or less subtle analytical errors resulting from acid rearrangements is obvious.

The pretreatment of the adsorption cartridges with buffering hydrogencarbonate prevented acid rearrangements without affecting the analytical performance. After this treatment, the previously acidified cartridges worked perfectly well again. Reproducible results could be obtained even for digester emissions from the acid sulphite pulp mill. It is concluded that the pretreatment of adsorption cartridges with a buffer may offer an improved analytical quality for a wide range of applications.

REFERENCES

1 J. E. Bunch and E. D. Pellizzari, *J. Chromatogr.*, 186 (1979) 811.
2 M. Mattsson and G. Petersson, *Int. J. Environ. Anal. Chem.*, 11 (1982) 211.
3 R. Atkinson, D. Hasegawa and S. M. Aschmann, *Int. J. Chem. Kinet.*, 22 (1990) 871.
4 G. Petersson, *Atmos. Environ.*, 22 (1988) 2617.
5 A.-M. Strömvall and G. Petersson, *Scand. J. For. Res.*, 6 (1991) 253.
6 A.-M. Strömvall and G. Petersson, *Holzforschung*, 44 (1990) 449.
7 F. Jüttner, *J. Chromatogr.*, 442 (1988) 157.
8 S. Coffey (Editor), *Rodd's Chemistry of Carbon Compounds*, Vol. IIc, Elsevier, Amsterdam, 1969.
9 G. N. Valkanas, *J. Org. Chem.*, 41 (1976) 1179.
10 A. Waller, *Sven. Papperstidn.*, 44 (1941) 427.

Journal of Chromatography, 589 (1992) 390–393
Elsevier Science Publishers B.V., Amsterdam

CHROM. 23 737

Short Communication

Determination of diacetoneketogulonic acid in water samples by high-performance thin-layer chromatography

Adriana Eisenbeiss

Central Analytical Laboratory, E. Merck, Darmstadt 1 (Germany)

Sabine Reuke

Reagents Research Department —Chromatography, E. Merck, Darmstadt 1 (Germany)

Michael Türck*

Central Analytical Laboratory, E. Merck, P.O. Box 4119, W-6100 Darmstadt 1 (Germany)

(First received May 23rd, 1991; revised manuscript received September 12th, 1991)

ABSTRACT

A fast and efficient method for the determination of diacetoneketogulonic acid (DAG) —a substance relevant as contaminant in drinking water— is described. The method is characterized by enrichment of the analyte by solid-phase extraction using a innovative adsorbent and consecutive separation and quantitation by high-performance thin-layer chromatography. The method can be applied to the determination of diacetoneketogulonic acid in waste water, ground water and drinking water. The solid-phase extraction described may also be useful as sample preparation method for other separation techniques.

INTRODUCTION

Over the years, diacetoneketogulonic acid (DAG) (Fig. 1), the penultimate stage in the synthesis of ascorbic acid [1], was discharged in large amounts into surface waters by chemical manufacturers. From there the salts infiltrated the ground water. As DAG sodium salt inhibits the growth of grasses [2], the 1986 European Drinking Water Regulations restrict the concentration of this substance in drinking water to 0.1 μg/l, despite the fact that the substance has no apparent toxicity ($LD_{50_{rat,oral}}$ = 18 000 mg/kg) [3].

There are few tried and tested analytical methods capable of measuring the pesticides listed in the Regulations down to the stipulated limit of 0.1 μg/l individually and 0.5 μg/l *in toto*. The pesticides,

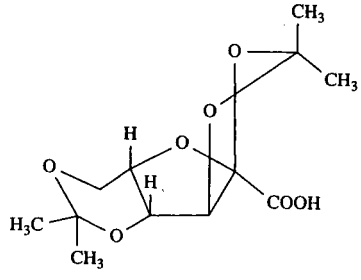

Fig. 1. Structure of DAG.

0021-9673/92/$05.00

mostly lipophilic substances, can be concentrated by solid-phase extraction on C_{18}-bonded silica gel and then determined selectively by high-performance liquid or gas chromatography.

In principle, the same procedure may be used to determine DAG. At an acidic pH DAG occurs as the free acid and can be adsorbed on C_{18}-bonded silica gel. However, in an acidic environment the substance is rapidly hydrolysed, resulting in poor recoveries.

This paper describes a method of sample preparation which avoids decomposition of DAG and provides good recoveries. Virtually any chromatographic method can then be used to separate DAG from impurities and determine it quantitatively. We chose high-performance thin-layer chromatography (HPTLC) as a rapid and cost-efficient method.

EXPERIMENTAL

Materials

All of the chemicals and TLC plates used were of "GR" or "for residue analysis" grade from E. Merck (Darmstadt, Germany). 4-Methoxybenzaldehyde was obtained from Schuchardt (Hohenbrunn, Germany) and membrane filters were Sartorius Type SM. The C_{18}-modified silica gel adsorbent was obtained from E. Merck and other suppliers, and the polymer adsorbent was Polyspher RP-18 (35 μm) from E. Merck.

Sample preparation (optimized method)

Filter the water sample over a membrane filter (only if it is not clear) and adjust the pH to 4.0 with 2.5% sulphuric acid. Pack an empty cartridge with 0.2 g of Polyspher RP-18 (35 μm) and condition the column: rinse it twice with 1 ml of ethyl acetate (leaving it to act for 10 min), twice with 1 ml of methanol (leaving it to act for 10 min) and twice with 1 ml of water (adjusted to pH 4.0 with sulphuric acid, DAG-free). Aspirate 20 ml–1 l of the sample through the column, dry the column in a stream of nitrogen for 30 min and elute with two 1-ml volumes of ethyl acetate. Add one drop of 25% ammonia solution to the eluate and evaporate it in a stream of nitrogen at a maximum temperature of 40°C to leave 0.5 ml. Apply an aliquot to the HPTLC plate. For DAG concentrations of < 5 μg/l, evaporate the eluate to leave a small drop. Apply all of this to the plate, rinse the dish with one drop of methanol and apply this to the plate also.

Thin-layer chromatography

Silica gel 60 F_{254} HPTLC precoated plates (10 × 20 cm) were used with (A) chloroform–methanol (80:20) and (B) chloroform–methanol–glacial acetic acid (80:20:2) as eluents under conditions of chamber saturation and spot or streak application. The sample volume was up to 20 μl, depending on the concentration. One-dimensional development (> 5 μg/l) was for 8 cm with eluent A, followed by drying, and then for 6.5 cm with eluent B. Two-dimensional development (< 5 μg/l) was for 8 cm with eluent A, followed by drying, turning the plate through 90°, application of a calibration series and then for 6.5 cm with eluent B.

For detection, the plates were immersed in 4-methoxybenzaldehyde solution (3 ml of 4-methoxybenzaldehyde dissolved in 80 ml of ethanol, 3 ml of concentrated sulphuric acid added and diluted to 100 ml with ethanol), heated at 130°C for 2–3 min and evaluate after 1 h. Red fluorescent spots with $R_F \approx 0.4$ were visible under long-wavelength UV light (366 nm). Chromatograms were evaluated with a TLC scanner.

RESULTS

Sample preparation

Concentration of DAG by adsorbtion on C_{18}-modified silica gel must take place at a highly acidic pH, otherwise DAG shows insufficient affinity to the adsorbent. The optimum pH is *ca.* 2. However, at this pH DAG losses due to hydrolysis are considerable, so that even with rapid operation the recovery is at best *ca.* 60% (Table I). For quantitative determinations such low recoveries require a standardized time schedule. Additionally, a standard dilution series (used to calibrate the method) has to receive the same treatment.

The use of a polymeric adsorbent with C_{18} sidechains instead of the modified silica gel does not improve recoveries significantly at pH 2. However, this material shows sufficient affinity to DAG at higher pH values, which allows adsorption at pH 4 with a recovery of virtually 100%. In comparision, the recovery at pH 4 using C_{18}-bonded silica gel is only about 40%.

TABLE I

COMPARISON OF RECOVERIES OF DAG IN DRINKING WATER: INFLUENCE OF SOLID-PHASE ADSORBENT AND SAMPLE pH

Adsorbent[a]	pH	Amount of DAG added to 500 ml of water (μg)	Amount of DAG found (μg)	Mean recovery (%)[b]
Adsorbent A, C_{18} silica gel (40–63 μm)	2	180	110	61
Adsorbent B, C_{18} silica gel (25 μm)	2	10	6.0	60
Adsorbent C, C_{18} silica gel (25 μm)	2	10	4.8	48
Adsorbent D, C_{18} silica gel (40 μm)	2	25	15.4	61
Adsorbent D, C_{18} silica gel (40 μm)	4	25	10.0	40
Adsorbent E, C_{18} polymer (35 μm)	2	25	17.1	68
Adsorbent E, C_{18} polymer (35 μm)	4	25	24.0	96

[a] Adsorbents: A = LiChroprep RP-18; B = RP-Select B; C = LiChrospher RP-18; E = Polyspher RP-18 (all from E. Merck); D = bonded-phase C_{18} (J.T. Baker).
[b] The relative standard deviation was <5% (n = 3–10) in all experiments.

During optimization, attention was given to the effect of the displacement medium on recoveries. Methanol and acetone yielded poor recoveries of *ca.* 60%. This can be improved by adding ammonia solution, although the formation of acetone condensation products and the larger number of side components adversely affect evaluation. Elution with ethyl acetate is both selective and efficient. DAG shows virtually 100% recovery and interfering impurities are mostly retained by the adsorbent. Addition of a small amount of ammonia solution prior to evaporation of the eluate has proved to be advantageous. At alkaline pH the stability of DAG is preserved.

Determination

When testing water for DAG, it is important to expect the presence of a number of substances similiar to DAG. Often seen is diacetoneketogluconic acid, a diastereomer of DAG, and diacetonesorbose. Good separations and a good limit of detection are obtained on extra-thin HPTLC pre-coated plates (Fig. 2).

Under the conditions selected, as little as 0.125 μg of DAG still produces a clear signal. This amount (obtained from 500 ml of sample) represents a concentration of 0.25 μg/l. To permit the detection of extremely small levels of DAG, the HPTLC plate must be developed two-dimensionally. DAG is thus better resolved from the interfering background,

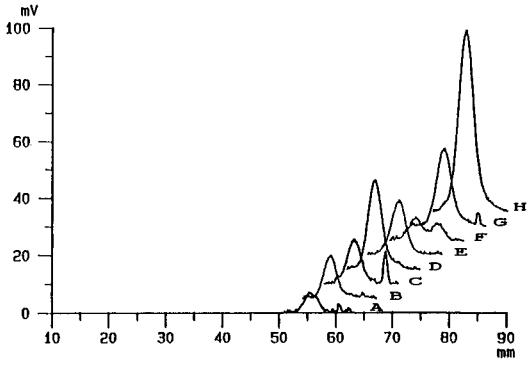

Fig. 2. Signals from a scanned HPTLC plate with calibration series from 0.25 to 2.0 μg of DAG and three samples of drinking water. Lane A, 0.25 μg of DAG; lane B, water sample containing *ca.* 1 μg/l of DAG; lane C, 0.5 μg of DAG; lane D, water sample containing *ca.* 2.5 μg/l of DAG; lane E, 0.75 μg of DAG; lane F, water sample containing *ca.* 0.5 μg/l of DAG and *ca.* 0.4 μg/l of the diastereomeric diacetoneketogluconic acid; lane G, 1.0 μg of DAG; lane H, 2.0 μg of DAG. The method is described in the text.

caused by impurities worked up concomitantly. Two-dimensional development is recommended in all instances when samples contain <5 μg/l DAG. For higher concentrations one-dimensional development suffices.

Owing to virtually 100% recovery following work-up, a directly prepared dilution series can be used for calibration purposes. The calibration graph is linear within the range 0.125–1.5 μg, with evaluation by peak area being slightly favourable over evaluation by peak height.

At higher concentrations application must be streakwise, so as to obtain a linear signal-to-concentration ratio. By careful matching of the application and development procedures, DAG can be measured in drinking water at concentrations from 0.25 to 250 μg/l with consistent accuracy.

The method is simple and ensures both good accuracy and repeatability. This is due mainly to the fact that samples are prepared at a pH at which DAG is stable, thus ensuring complete recovery with a precision of better than 2%. Consequently, the crucial step of sample preparation is no longer critical.

DISCUSSION

The solid-phase adsorbent used for sample work-up is a polystyrene–divinylbenzene polymer with C_{18} chains on the benzene rings. In this material it seems that both the C_{18} alkyl chains and the aromatic component contribute to the adsorption, leading to a concentration effect which is superior to that obtained on C_{18}-modified silica gel. An additional advantage of this adsorbent is that it can be reused without apparent loss of activity following a simple regeneration schedule (washing with 1 *M* sulphuric acid, 1 *M* sodium hydroxide solution, water and methanol). This method of sample preparation offers significant advantages for the determination of DAG by other chromatographic methods (*e.g.*, gas chromatography–mass spectrometry following methylation) and in samples of higher concentration (*e.g.*, industrial effluents). The determination of very small concentrations of DAG is even possible with the naked eye under a long-wavelength UV lamp without apparent loss of accuracy. This makes the method especially suitable for screening purposes or for less well equipped laboratories.

ACKNOWLEDGEMENTS

We thank Dr. F. Eisenbeiss and Dr. M. Wotschokowsky for their expert advice during this work.

REFERENCES

1 T. Reichstein and A. Grüssner, *Helv. Chim. Acta*, 17 (1934) 311.
2 P. F. Bocion, W. H. de Silva, G. A. Hüppi and W. Szkrybalo, *Nature (London)*, 258 (1975) 142.
3 D. V. Sweet (Editor), *Registry of Toxic Effects of Chemical Substances (RTECS), 1985–86 Edition*, Vol. 3, US Department of Health and Human Services, Washington, DC, 1987, p. 2658.

Author Index

PUBLICATION SCHEDULE FOR 1992

Journal of Chromatography and *Journal of Chromatography, Biomedical Applications*

MONTH	O 1991	N 1991	D 1991	J	F	M	
Journal of Chromatography	585/1	585/2 586/1 586/2 587/1	587/2 588/1 + 2	589/1 + 2 590/1 590/2	591/1 + 2 592/1 + 2 593/1 + 2	594/1 + 2 595/1	The publication schedule for further issues will be published later
Cumulative Indexes, Vols. 551–600							
Bibliography Section						610/1	
Biomedical Applications				573/1 573/2 574/1	574/2	575/1 575/2	

INFORMATION FOR AUTHORS

(Detailed *Instructions to Authors* were published in Vol. 558, pp. 469–472. A free reprint can be obtained by application to the publisher, Elsevier Science Publishers B.V., P.O. Box 330, 1000 AH Amsterdam, The Netherlands.)

Types of Contributions. The following types of papers are published in the *Journal of Chromatography* and the section on *Biomedical Applications:* Regular research papers (Full-length papers), Review articles and Short Communications. Short Communications are usually descriptions of short investigations, or they can report minor technical improvements of previously published procedures; they reflect the same quality of research as Full-length papers, but should preferably not exceed five printed pages. For Review articles, see inside front cover under Submission of Papers.

Submission. Every paper must be accompanied by a letter from the senior author, stating that he/she is submitting the paper for publication in the *Journal of Chromatography*.

Manuscripts. Manuscripts should be typed in double spacing on consecutively numbered pages of uniform size. The manuscript should be preceded by a sheet of manuscript paper carrying the title of the paper and the name and full postal address of the person to whom the proofs are to be sent. As a rule, papers should be divided into sections, headed by a caption (*e.g.*, Abstract, Introduction, Experimental, Results, Discussion, etc.). All illustrations, photographs, tables, etc., should be on separate sheets.

Introduction. Every paper must have a concise introduction mentioning what has been done before on the topic described, and stating clearly what is new in the paper now submitted.

Abstract. All articles should have an abstract of 50–100 words which clearly and briefly indicates what is new, different and significant.

Illustrations. The figures should be submitted in a form suitable for reproduction, drawn in Indian ink on drawing or tracing paper. Each illustration should have a legend, all the *legends* being typed (with double spacing) together on a *separate sheet*. If structures are given in the text, the original drawings should be supplied. Coloured illustrations are reproduced at the author's expense, the cost being determined by the number of pages and by the number of colours needed. The written permission of the author and publisher must be obtained for the use of any figure already published. Its source must be indicated in the legend.

References. References should be numbered in the order in which they are cited in the text, and listed in numerical sequence on a separate sheet at the end of the article. Please check a recent issue for the layout of the reference list. Abbreviations for the titles of journals should follow the system used by *Chemical Abstracts*. Articles not yet published should be given as "in press" (journal should be specified), "submitted for publication" (journal should be specified), "in preparation" or "personal communication".

Dispatch. Before sending the manuscript to the Editor please check that the envelope contains four copies of the paper complete with references, legends and figures. One of the sets of figures must be the originals suitable for direct reproduction. Please also ensure that permission to publish has been obtained from your institute.

Proofs. One set of proofs will be sent to the author to be carefully checked for printer's errors. Corrections must be restricted to instances in which the proof is at variance with the manuscript. "Extra corrections" will be inserted at the author's expense.

Reprints. Fifty reprints of Full-length papers and Short Communications will be supplied free of charge. Additional reprints can be ordered by the authors. An order form containing price quotations will be sent to the authors together with the proofs of their article.

For Superior Chiral Separation From Analytical To Preparative.

The finest from DAICEL……

Why look beyond DAICEL? We have developed the finest CHIRALCEL, CHIRALPAK and CROWNPAK with up to 17 types of HPLC columns, all providing superior resolution of racemic compounds.

NEW CHIRALPAK AS

● CHIRALPAK AS

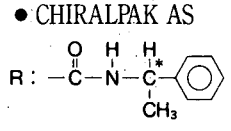

for β-Lactam antibiotics

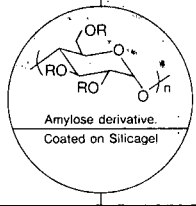

4-Acetoxy-2-azetidine

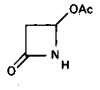

Eluent : Hexane/Ethanol = 8/2
Flow rate : 1.0mℓ/min
Temperature : r.t.
Detection : UV254nm

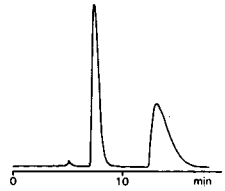

Ofloxacine methyl ester

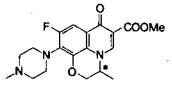

Eluent : Hexane/EtOH = 8/2
Flow rate : 1.2mℓ/min
Temperature : 40°C
Detection : UV254nm

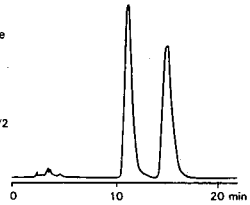

NEW CHIRALPAK AD

● CHIRALPAK AD

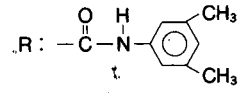

Oxyphencyclimine

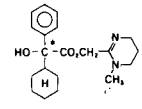

Eluent : Hexane/2-Propanol = 9/1
Flow rate : 1.0mℓ/min
Temperature : r.t.
Detection : UV254nm

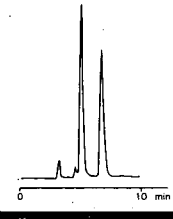

Verapamil

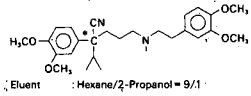

Eluent : Hexane/2-Propanol = 9/1
Flow rate : 1.0mℓ/min
Temperature : r.t.
Detection : UV254nm

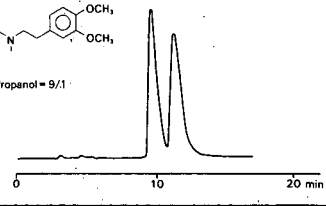

Analytical column 0.46cm×25cm(10μm)

CHIRALCEL OA
OB
OC
OD
OJ
OF
OG
OK

CHIRALPAK AS
AD

Normal Phase

Semi-preparative column 2cm×25cm(10μm)

You can have Pure enantiomer quickly!!

■Separation Service

- A pure enantiomer separation in the amount of 100g~10kg is now available.
- Please contact us for additional information regarding the manner of use and application of our chiral columns and how to procure our separation service.

DAICEL CHEMICAL INDUSTRIES, LTD.

chiral chemicals division.
8-1, Kasumigaseki 3-chome, Chiyoda-ku, Tokyo 100, Japan Phone: 03 (507) 3151 FAX: 03 (507) 3193

DAICEL(U.S.A.), INC.
Fort Lee Executive Park
Two Executive Drive, Fort Lee,
New Jersey 07024
Phone: (201) 461-4466
FAX: (201) 461-2776

DAICEL(U.S.A.), INC.
23456 Hawthorne Blvd.
Bldg. 5, Suit 130
Torrance, CA 90505
Phone: (213) 791-2030
FAX: (213) 791-2031

DAICEL(EUROPA)GmbH
Oststr. 22
4000 Düsseldorf 1, F.R. Germany
Phone: (211) 369848
Telex: (41) 8588042 DCEL D
FAX: (211) 364429

DAICEL CHEMICAL(ASIA)PTE. LTD.
65 Chulia Street #40-07
OCBC Centre, Singapore 0104
Phone: 5332511
FAX: 5326454